Electromagnetic Transient Analysis *and* Novel Protective Relaying Techniques *for* Power Transformer

Xiangning Lin • Jing Ma
Qian Tian • Hanli Weng

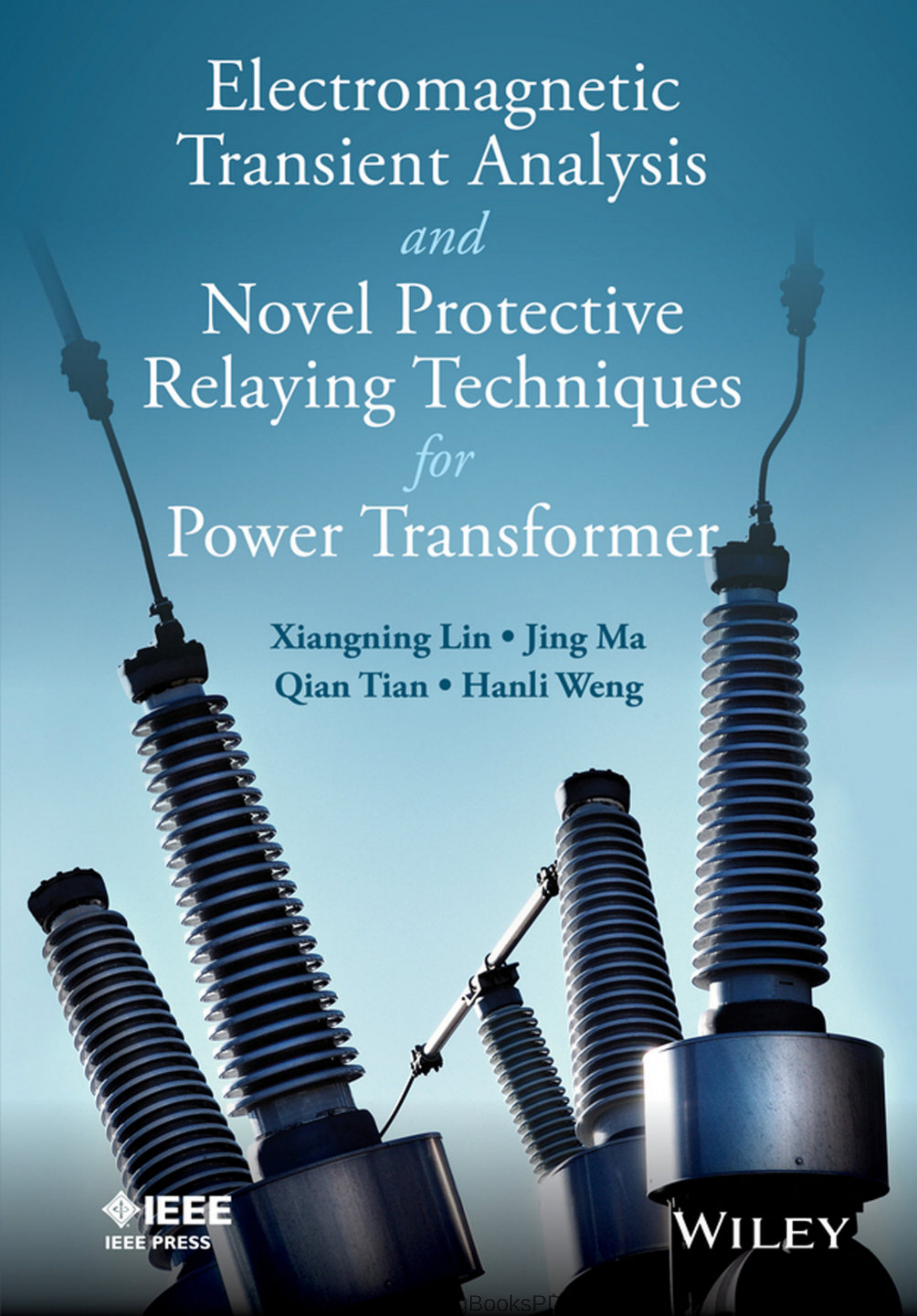

IEEE
IEEE PRESS

WILEY

ELECTROMAGNETIC TRANSIENT ANALYSIS *AND* NOVEL PROTECTIVE RELAYING TECHNIQUES *FOR* POWER TRANSFORMER

ELECTROMAGNETIC TRANSIENT ANALYSIS *AND* NOVEL PROTECTIVE RELAYING TECHNIQUES *FOR* POWER TRANSFORMER

Xiangning Lin

State Key Laboratory of Electromagnetic Engineering
School of Electrical and Electronic Engineering
Huazhong University of Science and Technology

Jing Ma

State Key Laboratory of Alternate Electrical Power System with Renewable Energy Sources
School of Electrical and Electronic Engineering
North China Electric Power University

Qing Tian

Chief Dispatching Center
Southern China Power grid

Hanli Weng

College of Electrical Engineering & New Energy,
China Three Gorges University.

IEEE

WILEY

This edition first published 2015

Registered office
John Wiley & Sons Singapore Pte. Ltd., 1 Fusionopolis Walk, #07-01 Solaris South Tower, Singapore 138628.

For details of our global editorial offices, for customer services and for information about how to apply for permission to reuse the copyright material in this book please see our website at www.wiley.com.

Library of Congress Cataloging-in-Publication Data

Lin, Xiangning.
Electromagnetic transient analysis and novel protective relaying techniques for power transformer / Xiangning Lin, Jing Ma, Qing Tian, Hanli Weng.
pages cm
Includes bibliographical references and index.
ISBN 978-1-118-65382-1 (hardback)
1. Electric relays. 2. Electric transformers – Protection. 3. Transients (Electricity) I. Title.
TK2861.E4233 2014
621.31′4 – dc23

2014021807

Typeset in 10/12pt TimesLTStd by Laserwords Private Limited, Chennai, India

1 2015

Contents

About the Authors

Professor Xiangning Lin has been working in this area since 1996. His research is mainly concentrated in the areas of power system protection/operation/control/modelling/simulation/analysis and smart grids. He has carried out very systematic research and practiced on power transformer electromagnetic transient simulation and protective relaying, especially approaches on operating characteristic analysis and studies on the novel principle of the transformer differential protection, for more than 18 years. He was the first to discover the ultra-saturation phenomenon of the power transformer and then designed appropriate operating characteristics analysis planes to make clear the advantages and disadvantages of the existing differential protection of power transformers. On the basis of this, he invented a variety of novel protection algorithms for the main protection of the power transformer. A series of papers were published in authoritative journals such as the *IEEE Transactions on Power Systems* and *IEEE Transactions on Power Delivery*. The work has been widely acknowledged and cited by international peers. Part of his research results have been used in many practical engineering projects. He is also a pioneer to the introduction of modern signal processing techniques to the design of the protection criteria for power transformers.

In recent years, Professor Lin has undertaken many major projects in China. For example, he guided a project of the National Natural Science Foundation of China to study the abnormal operation behaviour analysis and appropriate countermeasures of power transformers. Then he set up an advanced simulation and protection laboratory for the main equipment of power systems and pioneered the design and implementation of the corresponding protection techniques. He was also responsible for several projects from governments and enterprises on the study of the power transformer protection and monitoring. In addition, Professor Lin is a major member of the National Basic Research Program of China (973 Program) on the study of the interaction between large-scale electric power equipment characteristics and power system operation. He cooperated with the China Electric Power Research Institute to guide the study on the main protection for wind farms, including different types of power transformer. He has been teaching courses on *Power system protective relaying* and *Power system analysis* for many years. Much of the material covered in this book has been taught to students and other professionals.

Professor Jing Ma has been working in this area since 2003. His research is mainly concentrated in the areas of power system protection/control, modelling/simulation/analysis and smart grids. He has carried out very systematic research and practiced on power system protection, especially approaches concerning power transformer protection, for more than 10 years. He was the first to apply the two-terminal network algorithm to the areas of power system protection. A series of papers were published in authoritative journals such as the *IEEE Transactions on Power Delivery*. The work has been widely acknowledged and cited by international peers. He also proposed an approach based on the grille fractal to solve the Transient Analysis saturation problem, and the related paper has been published in the *IEEE Transactions on Power Delivery*. His research results have been used in many practical engineering projects.

In recent years, Dr Ma has undertaken many major projects in China. For instance, he participated in a key project of the National Natural Science Foundation of China to study the wide-area protection. He was also responsible for a project of the National Science Foundation project on the study of the power system smart protection and control. He is a major member of the National Basic Research Program of China (873 Program) on the study of the utilization of large-scale renewable energy with high security and efficiency, and was responsible for the design of the Power System Protection and Control Simulation Platform. Professor Ma has been teaching courses of *Power System Protection Theory* and *Power System Automation* for many years. He is also a key member of National Prime Course – *Power System Protection Theory*. Much of the material covered in this book has been taught to students and other professionals.

Dr Qing Tian is a senior engineer with the Chief dispatching centre, Southern Power grid, Guangzhou, China. He has been working in this area since 1998. His main research fields include power system protection, operation and control, together with the operation and maintenance technologies in HVDC and UHV AC transmission projects. He has published some well cited papers in authoritative international and Chinese journals. In particular, he has many experiences in solving practical engineering problems concerning UHVAC and UHVDC protections.

Dr Hanli Weng is a senior engineer with College of Electrical Engineering & New Energy, China Three Gorges University. She has been working in this area since 2004. Her main research fields include protective relaying of power transformer. She has published some well cited papers in the authoritative international and Chinese journals. In particular, she has many experiences in solving practical engineering problems concerning main equipment protection of large-scale hydro power station.

Preface

As the heart of the power system, the power transformer is crucial for the safety and stability of the power system, and the reliability of the protection arranged for the power transformer becomes a critical factor in guaranteeing the security of the system. Nevertheless, according to existing fault reports in the power industry, it is accidental event for the differential protection to mal-operate under some operating conditions. With the growing complexity of the power system structure and its components, the differential protection mal-operation events revealed have become an area of intense investigation in order to eliminate potential uncertainty and danger. Moreover, the electric circuit and the magnetic circuit, coupling in conjunction with each other, make the above phenomena even more intricate, as transformer switching events may cause electromagnetic transients. These phenomena remain an open issue and comprehensive studies are needed. However, while it is clearly essential to find out the origin of the abnormal operational behaviour in the power transformer, basic theory about electromagnetic transients in the power transformer is currently lacking. This book is published to address this problem directly.

The content of this book is arranged as follows: Chapter 1 defines the fundamental principle of the power transformer differential protection and some problems in this background. Second harmonic restraint based differential protection of Ultra High Voltage (UHV) power transformers is also investigated in this chapter. Chapter 2 attempts to study the unusual mal-operation of the differential protection of the transformer caused by ultra-saturation phenomena. In Chapter 3, appropriate theoretical bases for the existing protection method are discussed, preliminary comparative studies between phase current based and superimposed current based differential criteria are conducted and the results are compared. The main focus of Chapter 4 is on inrush identification by means of several novel schemes. Chapter 5 deals with the problems revealed in Chapter 4, with new methods put forward to eliminate the magnetizing inrush. Simulation verifications for the methods are also proposed.

The book is intended for graduate students in electric power engineering, for researchers in correlative fields or for anyone who wishes to keep an eye on the power transformer and the power system. We also gratefully acknowledge the technical assistance of *State Key Laboratory of Electromagnetic Engineering, School of Electrical and Electronic Engineering, Huazhong University of Science and Technology*. The work was also partly supported by the *National Natural Science Foundation of China (project numbers 50177011, 50407010, and 50777024)*. The authors are continuing their research in this field and would welcome contact with new ideas or if there is any confusion generated.

Xiangning Lin
Wuhan, China
2014

1

Principles of Transformer Differential Protection and Existing Problem Analysis

1.1 Introduction

With the development of the electric power industry, large capacity power transformers are more and more widely applied in power systems. As the heart of the whole power system, the performance of the transformer directly affects the continuous and stable operation of the whole power system. In particular, once a modern transformer of large capacity, high voltage, high cost and complicated structure is destroyed by a fault, a series of problems will emerge, such as wide-ranging impact, difficult and lengthy maintenance, and great economic loss. Statistics show that during the years 2001–2005, the average correct operating rate of transformers 220 kV and above is only up to 79.97%, far below the correct operating rate of line protection (more than 99%).

Differential protection is one of the foremost protection schemes used in the power transformer. The theoretical foundation of differential protection is Kirchhoff's current law (KCL), which is applied successfully in the protection of transmission lines and generators. However, there are many problems when it is necessary to identify transformer internal faults under various complicated operation conditions [1]. From the perspective of an electric circuit, the transformer's primary and secondary windings cannot be treated as the same node, with the voltage on each side being unequal. Besides, the two sides are not physically linked. In terms of basic principle, transformer differential protection is based on the balance of the steady magnetic circuit. However, this balance will be destroyed during the transient process and can only be rebuilt after the transient process is finished. Therefore, many unfavourable factors need to be taken into account in the implementation of transformer differential protection:

- Matching and error of the current transformer (CT) ratio.
- Transformer tap change.
- Transfer error of the CT increases during the transient process of the external fault current.
- Single-phase earth fault on the transformer's high voltage side via high resistance.
- Inter-turn short circuit with outgoing current.
- The magnetizing inrush.

With respect to the scenarios listed above, solutions to the first five mainly rely on the features of the differential protection. The tripping resulting from the inrush current needs to be blocked for the purpose

Electromagnetic Transient Analysis and Novel Protective Relaying Techniques for Power Transformer,
First Edition. Xiangning Lin, Jing Ma, Qing Tian and Hanli Weng.

of preventing mal-operation. In this section, various problems in current differential protection principles and inrush current blocking schemes are firstly studied and discussed. Then, some novel principles for transformer main protection are proposed and analyzed. Simulation and dynamic tests are carried out to verify the validity and feasibility of the novel principles. By comparative research, the development route of the transformer main protection technology is given.

Compared with EHV (Extra High Voltage) power systems, the electromagnetic environment of UHV (Ultra High Voltage) systems is more complex. Meanwhile, the configuration and parameters of an UHV transformer differ from an EHV transformer. In this case, the preconditions of applying transformer differential protection correctly rest with the modelling of the UHV power transformer reasonably and appropriate analysis of corresponding electromagnetic transients. The autotransformer is the main type of UHV transformer. However, the model of the autotransformer is not available in most simulation software. An ordinary countermeasure is to replace the autotransformer by the common transformer when executing electromagnetic transient simulations. In this case, the effect of magnetic coupling can be included but the electric relationship between the primary side and the secondary side cannot be involved. One of the existing models adopts the flux linkage as the state variable and includes the nonlinearity of the transformer core. It is clear in terms of concept but too complex to perform in many cases. In contrast, a new transient simulation model of the three-phase autotransformer is described, in which the controlled voltage and current sources are developed with the modified damping trapezoidal method, which is engaged to form the synthetic simulation model. In this case, both the efficiency and the precision of simulations are improved. However, this type of model will be more reasonable if it takes into account the nonlinearity of magnetizing impedance. Furthermore, the electromagnetic transient simulations in the UHV electromagnetic environment are new challenges, especially when including the UHV transmission line with distributed parameters.

Differential protection is usually the main protection of most power transformers. The key problem for the differential protection is how to distinguish between the inrush caused by unwanted tripping or clearing the external fault and fault currents rapidly [2–4]. The traditional methods of identifying the inrush are based on the theories of second harmonic restraint and dead angle. The flux saturation point becomes lower with the improvement of iron materials. The percentage of the second harmonic in the three-phase inrush current is probably lower than 15% in the case of higher residual magnetism and initial fault current satisfying certain constrains; the lowest might be under 7% with the relative dead angle smaller than 30°. The transformer differential protection cannot avoid the mal-operation regardless of whether second harmonic restraint and dead angle based blocking schemes are adopted. The theory of identifying the inrush using currents and voltages faces the problem of low sensitivity because of the difficulty of acquiring precisely the parameters of transformers. On the other hand, if the percentage of the second harmonic within the fault current is greater than 15%, this will cause a time delay in tripping of the protection based on the second harmonic criterion. This is due to the long-distance distributed capacitance and series compensation capacitance resonance in the high voltage power systems. The percentage of the harmonic will be larger if the characteristic of CT is not good (easy to saturate) and the differential protection cannot operate with the restraint ratio of 15%. Therefore, it is necessary to find a new criterion to identify the inrush for optimizing the characteristic of the differential protection of the power transformers.

1.2 Fundamentals of Transformer Differential Protection

1.2.1 Transformer Faults

Transformers are used widely in a variety of applications, from small-size distribution transformers serving one or more users to very large units that are the essential parts of the bulk power system. Moreover, a power transformer has a variety of features, including tap changers, phase shifters, and multiple windings, which requires special consideration in the protective system design.

Transformer faults are categorized into two classes: external faults and internal faults.

External faults are those that occur outside the transformer. These hazards present stresses on the transformer that may be of concern and may shorten the transformer life. These faults include: overloads; overvoltage; underfrequency; and external system short circuits. Most of the foregoing conditions are often ignored in specifying transformer relay protection, depending on how critical the transformer is and its importance in the system. The exception is protection against overfluxing, which may be provided by devices called 'volts per hertz' relays that detect either high voltage or underfrequency, or both, and will disconnect the transformer if these quantities exceed a given limit, which is usually 1.1 per unit.

Internal faults are those that occur within the transformer protection zone. This classification includes not only faults within the transformer enclosure but also external faults that occur inside the current transformer (CT) locations. Transformer internal faults are divided into two classifications for discussion; incipient faults and active faults.

Incipient faults are those that develop slowly but which may develop into major faults if the cause is not detected and corrected. They are of three kinds – transformer overheating, overfluxing, or overpressure – and usually develop slowly, often in the form of a gradual deterioration of insulation due to some causes. This deterioration may eventually become serious enough to cause a major arcing fault that will be detected by protective relays. If the condition can be detected before major damage occurs, the needed repairs can often be made more quickly and the unit placed back into service without a prolonged outage. Major damage may require shipping the unit to a manufacturing site for extensive repair, which results in an extended outage period.

Active faults are caused by the breakdown in insulation or other components that create a sudden stress situation that requires prompt action to limit the damage and prevent further destructive action. They occur suddenly and usually require fast action by protective relays to disconnect the transformer from the power system and limit the damage to the unit. For the most part, these faults are short circuits in the transformer, but other difficulties can also be cited that require prompt action of some kind. The following classifications of active faults are considered:

1. Short circuits in Y-connected windings
   (a) Grounded through a resistance
   (b) Solidly grounded
   (c) Ungrounded.
2. Short circuits in Δ-connected windings.
3. Phase-to-phase short circuits (in three-phase transformers).
4. Turn-to-turn short circuits.
5. Core faults.
6. Tank faults.

1.2.2 *Differential Protection of Transformers*

The most common method of transformer protection uses the percentage differential relay as the primary protection, especially where speed of fault clearing is considered important. The trend in standards for reduced fault-withstand time in power transformers requires that fast clearing of transformer faults be emphasized.

As shown in Figure 1.1, $\dot{I}_1, \dot{I}_2$ represent the transformer primary currents and $\dot{I}'_1, \dot{I}'_2$ represent the corresponding secondary currents. Differential current in the relay KD can be given by:

$$\dot{I}_r = \dot{I}'_1 + \dot{I}'_2 \tag{1.1}$$

The operating criterion is as follows:

$$I_r \geq I_{set} \tag{1.2}$$

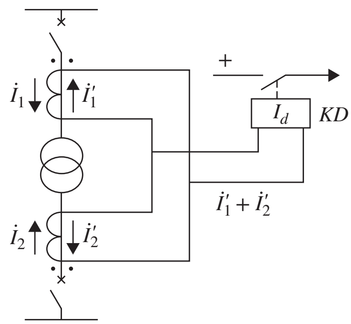

Figure 1.1 The wiring diagram of differential protection for a double winding transformer

I_{set} means the operation current and $I_r = |\dot{I}_1' + \dot{I}_2'|$ represents the root mean square (RMS) value of the differential current.

If setting transformer ratio $n_T = U_1/U_2$, Equation (1.1) can be rewritten as:

$$\dot{I}_r = \frac{\dot{I}_2}{n_{TA2}} + \frac{\dot{I}_1}{n_{TA1}} \tag{1.3}$$

$$\dot{I}_r = \frac{n_T \dot{I}_1 + \dot{I}_2}{n_{TA2}} + \left(1 - \frac{n_{TA2} n_T}{n_{TA2}}\right) \frac{\dot{I}_1}{n_{TA1}} \tag{1.4}$$

If $\frac{n_{TA2}}{n_{TA1}} = n_T$, we can know that $\dot{I}_r = \frac{n_T \dot{I}_1 + \dot{I}_2}{n_{TA2}}$. Having ignored the transformer loss, the differential current $\dot{I}_r$ will be zero during normal operation or when experiencing transformer external faults. In this case, the protection will not activate. When an internal fault exists, it will produce an additional fault current, which makes the differential protection operate.

We always use three-winding transformers in the real power system, usually with Y/Δ-11 connection (Figure 1.2).

In Figure 1.2, i_a, i_b, i_c represent the currents on the windings and i_A, i_B, i_C represent the currents on the Y-windings; u_a, u_b, u_c represent the voltages of the windings and u_A, u_B, u_C represent the voltages of the Y windings; i_{La}, i_{Lb}, i_{Lc} represent line currents of phase A, B, C on the windings.

For the winding differential protection principle, the differential current between the two sides can be calculated according to Figure 1.2:

$$\begin{bmatrix} I_{da} \\ I_{db} \\ I_{dc} \end{bmatrix} = \begin{bmatrix} 1 & 0 & 0 \\ 0 & 1 & 0 \\ 0 & 0 & 1 \end{bmatrix} \begin{bmatrix} I_a \\ I_b \\ I_c \end{bmatrix} + K \begin{bmatrix} 1 & 0 & 0 \\ 0 & 1 & 0 \\ 0 & 0 & 1 \end{bmatrix} \begin{bmatrix} I_A \\ I_B \\ I_C \end{bmatrix} \tag{1.5}$$

In Equation (1.5), $K = \frac{U_Y}{\sqrt{3}U_D} = \frac{w_Y}{w_D}$.

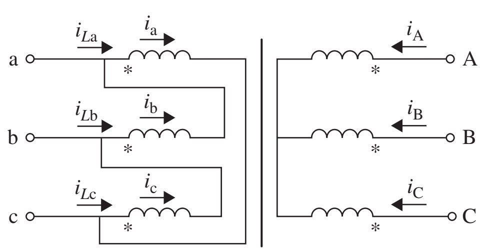

Figure 1.2 Three-phase transformer with Y/Δ-11 connection

1.2.3 The Unbalanced Current and Measures to Eliminate Its Effect

Due to differences in transformer ratios and CT accuracy, unbalanced current may exist in the CT secondary currents during external faults which could influence differential protection's correct operation.

There are three sources of error that tend to cause unbalanced currents:

1. Tap changing in the power transformer
2. Mismatch between CT currents and relay tap ratings.
3. Differences in accuracy of the CTs on either side of the transformer bank.

As illustrated, the unbalanced current produced by the difference of transformation ratio and transformer error is related to the through current caused by transformer external faults. With an increase in the through current, the unbalanced current also increases. This feature is the basis of the operating principle of the differential relay with restrained characteristics. When a restraint current, which can reflect the size of transformer, is introduced, the operating current of the relay will not be set to avoid the maximum through current ($I_{k\cdot\max}$) but will be automatically adjusted according to the restraint current. For a two-winding transformer, since $\dot{I}_2 = -\dot{I}_1$ (when an external fault occurs), it can be concluded that $I_{res} = I_1$. Besides, we have $I_{unb} = f(I_{res})$, since the unbalanced current is related to the fault current. Hence, the operation equation of the differential relay with restrained characteristics is given by $I_r > \mathrm{K_{rel}} f(I_{res})$, where $\mathrm{K_{rel}}$ is the reliability coefficient.

The relationship between the differential current (I_r) and restraint current (I_res) is demonstrated in Figure 1.3. Obviously the differential relay will act only when the differential current is above the curve of $\mathrm{K_{rel}} f(I_{res})$. So the curve of $\mathrm{K_{rel}} f(I_{res})$ is defined as the restrained characteristic of the differential relay. The area above the curve is the action area while the area below is the restraint area.

Figure 1.3 shows that the curve $\mathrm{K_{rel}} f(I_{res})$ is a monotonously rising function. When I_{res} is small, the transformer is unsaturated, therefore the curve $\mathrm{K_{rel}} f(I_{res})$ is in proportion to I_{res}. As I_{res} increases and becomes large enough to set the transformer saturated, the changing rate of curve $\mathrm{K_{rel}} f(I_{res})$ will increase, thus the curve becomes nonlinear.

Since the transformer saturation depends on many factors, the nonlinear part of the restrained characteristic is difficult to measure. Hence, the actual restrained characteristic must be simplified. Generally in differential protection, the 'two broken line' characteristic is widely used, with a straight line parallel to the coordinate axis and an oblique line represented by $I_{set.r}$. In Figure 1.3, the oblique line intersects with the horizontal line at point g and with the curve $\mathrm{K_{rel}} f(I_{res})$ at point a. In correspondence to point g, the action current is the minimum action current; the restraint current corresponding to the action current is defined as the inflection point current. When $I_{res} < I_{res.\max}$, $I_{set.r}$ is less than $\mathrm{K_{rel}} f(I_{res})$ permanently, this ensures that the differential relay will not mal-operate under any external fault. However, this leads to decrease of the protection sensitivity under internal faults. The unbalanced current, such as the excitation current and noise caused by the restraint current in measurement circuit, also requires the setting

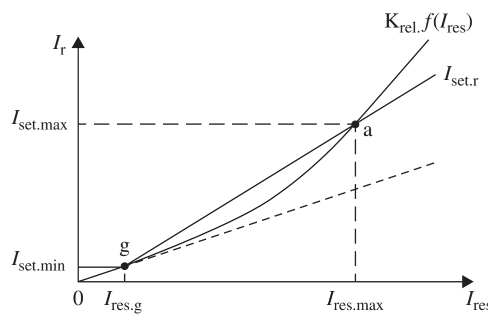

Figure 1.3 The restrained characteristic of relay

of a minimum action current. Otherwise mal-operation may result. The mathematical expression of the restrained characteristic is:

$$I_{set.r} = \begin{cases} I_{set.\min} & I_{res} < I_{res.g} \\ K\left(I_{res} - I_{res.g}\right) + I_{set.\min} & I_{res} \geq I_{res.g} \end{cases}$$

where K represents the slope of the restrained characteristic:

$$K = \frac{I_{set.\max} - I_{set.\min}}{I_{res.\max} - I_{res.g}}$$

Apart from the restraint current, the transformer inrush current will also cause unbalanced current, which also calls for discussion.

When a transformer is first energized, there is a transient inrush of current that is required to establish the magnetic field of the transformer. The mechanism of inrush generation can be seen in Figure 1.4. The reason rests with the transient saturation of flux of the transformer core due to appropriate inception angle and residual flux. This is not a fault condition and should not cause protective relays to operate. However, under certain conditions, depending on the residual flux in the transformer core, the magnitude of inrush current can be as much as 8–10 times normal full load current and can be the cause of false tripping of protective relays. This is rather serious, since it is not clear that the transformer is not internally faulted. The sensible response is, therefore, to thoroughly test the transformer before making any further attempts at energizing. This will be expensive and frustrating, especially if the tests show that the transformer is perfectly normal. Since this is such an important concept, it will be examined in some detail in order to understand the reason for high inrush current and to learn what steps can be used in protective relays to prevent their tripping due to magnetizing inrush.

There are several factors that control the magnitude and duration of the magnetizing inrush current:

- Size of the transformer bank.
- Strength of the power system to which the bank is connected.
- Resistance in the system from the equivalent source to the bank.
- Type of iron used in the transformer core.
- Prior history of the bank and the existence of residual flux.
- Conditions surrounding the energizing of the bank, for example,
  (a) Initial energizing
  (b) Recovery energizing from protective action
  (c) Sympathetic inrush in parallel transformers.

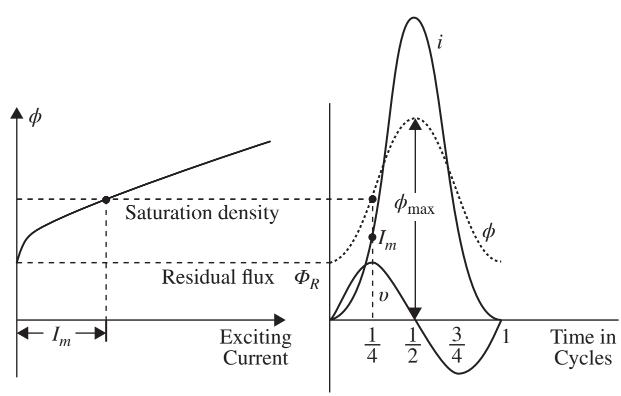

Figure 1.4 Derivation of the inrush current wave from the excitation saturation curve

There are several methods that have been used to prevent the tripping of a sound transformer due to large inrush currents that accompany initial energizing of the unit. The common methods used are:

1. Desensitize the relay during start-up.
2. Supervise the relay with voltage relays.
3. Add time delay.
4. Detect magnetizing inrush by observing the current harmonics.

These methods can be further described, as follows:

1. Methods have been devised to desensitize the differential relay and prevent tripping during start-up. One method parallels the operating coil with a resistor, with the resistor circuit being closed by an undervoltage relay contact. When the transformer bank is de-energized, the undervoltage relay resets, thereby closing the resistor bypass circuit. On start-up, the operating coil is bypassed until the undervoltage relay picks up, which is delayed for a suitable time.
2. Another method uses a fuse to parallel the differential relay operating coil. The fuse size is selected to withstand normal start-up currents, but internal fault currents are sufficient to blow the fuse and divert all current to the operating coil.
3. The voltage supervised relay measures the three-phase voltage as a means of differentiating between inrush current and a fault condition, a fault being detected by a depression in one of the three-phase voltages. This concept is usable for either fast or slow relays, it constitutes an improvement in the method.
4. Simply adding time delay to the differential relays during energizing the transformer is effective but must be accompanied by some method of overriding the time delay if an actual fault occurs during start-up. Usually, time delay is used in conjunction with other relay intelligence.
5. Harmonic current restraint is another method that is used. It was noted earlier that the second harmonic of the total current is almost ideal for determining whether a large inrush of current is due to initial energizing or to a sudden fault. Most differential relays use filters to detect the second, and sometimes the fifth, harmonic current and restrain tripping when this current is present.

1.3 Some Problems with Power Transformer Main Protection

1.3.1 Other Types of Power Transformer Differential Protections

1.3.1.1 Inter-Phase Differential Protection Principle

There are still some problems that exist in the winding differential protection:

- The winding current of transformers with Y/Δ-connection cannot be obtained.
- Cooperation with overcurrent protection is difficult, which will produce a protection dead zone.

Similar to the phase differential protection, the differential current of inter-phase current differential protection can be obtained:

$$\begin{bmatrix} I_{da} \\ I_{db} \\ I_{dc} \end{bmatrix} = \begin{bmatrix} 1 & -1 & 0 \\ 0 & 1 & -1 \\ -1 & 0 & 1 \end{bmatrix} \begin{bmatrix} I_a \\ I_b \\ I_c \end{bmatrix} + K \begin{bmatrix} 1 & -1 & 0 \\ 0 & 1 & -1 \\ -1 & 0 & 1 \end{bmatrix} \begin{bmatrix} I_A \\ I_B \\ I_C \end{bmatrix} \tag{1.6}$$

The disadvantage of inter-phase differential protection principle is as follows: for a three-phase transformer with Y/Δ-11 connection, when a Y-side single-phase grounding occurs, protection sensitivity will decrease. As a solution to this problem, a zero-sequence differential protection scheme is put forward in this section.

1.3.1.2 Zero-Sequence Differential Protection Principle

For single-phase high voltage large transformers, the main type of short-circuit fault is between winding to the iron core (when ground insulation is damaged), that is, single-phase grounding. Inter-phase short-circuit (in-box fault) seldom happens. Thus, single-phase grounding is carefully studied.

The constitution of zero-sequence differential protection is shown in Figure 1.5. On the Y-side of the transformer, the secondary sides of the CTs are connected to form a zero-sequence filter. Together with the secondary side of the neutral CT, the zero-sequence differential protection is formed.

Advantages of zero-sequence differential protection are:

- Relatively high sensitivity to single-phase grounding faults on the Y-side;
- The operation current is not affected by the transformer tap.
- Not directly influenced by the magnetizing inrush current.
- All CTs apply the same ratio, which is not related with the transformer ratio.

Disadvantages of zero-sequence differential protection are:

- Low (zero) sensitivity to inter-phase faults and faults on the low voltage side.
- Low sensitivity to high resistance grounding faults.
- Examination of wiring error on the secondary side is more complicated.

1.3.1.3 Split-Side Differential Protection

For phase differential protection schemes, the problem of mal-operation caused by inrush current or overexcitation always exists. Therefore, it is necessary to develop a novel transformer differential protection scheme that is not affected by either inrush current or overexcitation current. The new protection scheme is called transformer split-side differential protection in this section, the wiring diagram of which is shown in Figure 1.6.

For transport considerations, modern large capacity transformers are commonly made up of three single-phase transformers. The terminals of the windings are all led out of the shell, which facilitates the implementation of the proposed spilt-side differential protection. Advantages of this protection scheme are:

- Relatively high sensitivity to single-phase grounding faults.
- Not affected by the transformer tap.
- Not directly affected by the inrush current.

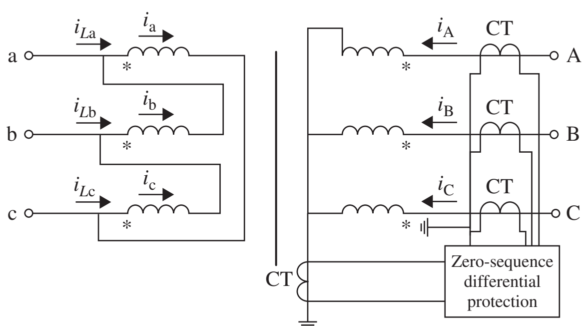

Figure 1.5 Connecting diagram of zero-sequence current differential protection

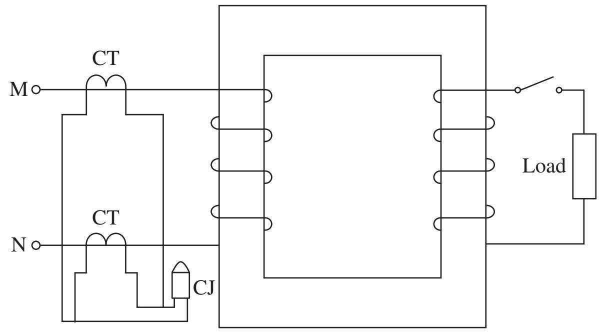

Figure 1.6 Connecting diagram of split-side differential protection

- The spilt-side differential protection being applied to large power transformers can simplify the device.
- Simple protection principle, reliable device, and convenient debugging.

Disadvantages of split-side differential protection are:

- Low (zero) sensitivity to common inter-turn faults.
- Applicable only when each winding has two terminals led out.
- The number of protection relays needed doubles.

From the above analysis, it is obvious that zero-sequence differential protection and spilt-side differential protection schemes are both superior to inter-phase differential protection in certain aspects. However, in view of the actual connection modes of transformers and the protective relaying characteristics, the inter-phase differential protection, especially longitudinal differential protection, is still most commonly used as the main protection for transformers. In longitudinal differential protection, the impact of inrush current has long been a problem that requires special measures to deal with it.

1.3.2 Research on Novel Protection Principles

With the rapid development of microcomputer technology and the wide application of the transformer main-backup-integrated protection scheme, it has become possible to conduct complex calculations within the transformer protection device using multiple electric variables. Since the transformer is a nonlinear and time-varying system, the voltage and current are two independent variables, not linearly correlated. Thus, by using both the voltage and current variables to describe the operation state of transformer, the information is more complete. Furthermore, it facilitates the search for new protection criteria of higher sensitivity and better reliability. Currently, transformer protection principles that use both the voltage and current variables mainly include: the magnetic flux characteristic principle, sequence impedance principle, loop equation principle, power differential principle and so on.

The magnetic flux characteristic principle is based on the nonlinearity of the excitation branch and has a promising application future. However, currently it is applicable only to single-phase transformer groups. For three-phase transformers with Y/Δ connection, since the internal circulation current on the Δ-side winding is difficult to measure, how the magnetic flux characteristic can be applied in this case to reflect the nonlinear characteristics of the excitation branch remains to be studied.

In the following sections, the advantages and disadvantages of the sequence impedance principle, loop equation principle and power differential principle are discussed, on the basis of which some novel principles of transformer main protection are put forward.

1.3.2.1 Sequence Impedance Principle

The sequence impedance principle is based on the changes of the transformer positive and negative sequence equivalent networks before and after the fault. With the variation of the positive and negative sequence voltage and current, the positive and negative sequence impedances felt by the relay points on both sides of the transformer can be calculated. Then, according to the direction of the calculated impedances, it can be decided whether the transformer fault is internal or external. For a convenient illustration, a two-winding transformer is taken as an example, the system model of which is shown in Figure 1.7. The protective relays are installed on both sides of the transformer and the positive direction for current is set as in the figure.

For transformer external faults, suppose a fault occurs at F1 on the transmission line. According to the positive sequence equivalent network before and after the fault, the following expression can be obtained:

$$\Delta V_{x1}/\Delta I_{x1} = -Z_{Gx1}, \Delta V_{y1}/\Delta I_{y1} = -(Z_{Gy1} + Z_{\text{Line1}}) \tag{1.7}$$

where ΔV_{x1}, ΔI_{x1}, ΔV_{y1} and ΔI_{y1} represent the variation of positive sequence voltage and current on both sides of the transformer before and after the fault; Z_{Gx1} and Z_{tran1} are the positive sequence equivalent impedance of the system on the X-side and the transformer, respectively.

Similarly, according to the negative sequence equivalent network before and after the fault, the following can be obtained:

$$\Delta V_{x2}/\Delta I_{x2} = -Z_{Gx2}, \Delta V_{y2}/\Delta I_{y2} = +(Z_{Gy2} + Z_{tran2}) \tag{1.8}$$

where ΔV_{x2}, ΔI_{x2}, ΔV_{y2} and ΔI_{y2} represent the variation of negative sequence voltage and positive sequence current on both sides of the transformer before and after the fault; Z_{Gx2} and Z_{tran2} are the negative sequence equivalent impedance of the system on the X-side and the transformer respectively.

For transformer internal faults, suppose a fault occurs at F2. Similarly, the positive and negative sequence impedances on both sides of the transformer can be calculated as shown in the following:

$$\Delta V_{x1}/\Delta I_{x1} = -Z_{Gx1}, \Delta V_{y1}/\Delta I_{y1} = -(Z_{Gy1} + Z_{\text{Line1}}) \tag{1.9}$$

$$\Delta V_{x2}/\Delta I_{x2} = -Z_{Gx2}, \Delta V_{y2}/\Delta I_{y2} = -(Z_{Gy2} + Z_{\text{Line2}}) \tag{1.10}$$

where Z_{Gy1}, Z_{Line1}, Z_{Line2} and Z_{Gy2} are the positive and negative sequence equivalent impedances of the system on the Y-side and the transmission line respectively.

It can be seen from Equations (1.7) and (1.8) that, when a transformer external fault occurs, the positive and negative sequence impedances felt by both sides of the transformer are different in direction – one positive and the other negative. And from Equations (1.9) and (1.10) it can be seen that, when a transformer internal fault occurs, the positive and negative sequence impedances felt by both sides of the transformer are the same in direction – both negative. Based on this fact, a method is put forward to distinguish between internal and external faults of the transformer (referred to as the 'quadrant division method' hereinafter): if the positive and negative sequence impedances on both sides of the transformer are different in direction – one located in first quadrant on the image plane and the other in the third quadrant – then the fault can be identified as an external fault; otherwise, if the positive and negative

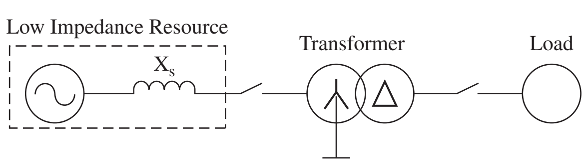

Figure 1.7 System model of a two-winding transformer

sequence impedances on both sides of the transformer are the same in direction – both in the third quadrant on the image plane – then the fault can be identified as an internal fault. On the basis of the 'quadrant division method', the division of the image plane is revised by extending the regional boundary to the second and fourth quadrants. Simulation results show that this revision improves the reliability and sensitivity of identification to a certain degree. However, neither the 'quadrant division method' nor the revised method can counteract the negative influence of inrush current. Therefore, other criteria should be added to form an effective protection scheme. Furthermore, for transformer protection principles based on sequence impedance, the correct identification between the conditions of normal no-load switching and no-load switching at internal faults remains to be studied.

1.3.2.2 Loop Equation Principle

Microcomputer transformer main protection based on the loop equation principle is very different from traditional differential protection. The interference of inrush current is avoidable with this method, since it does not distinguish inrush current from the internal fault current according to the waveform characteristics of the inrush current. Moreover, this method is not affected by the connection mode of the transformer. Take a single-phase transformer as an example. The system model is shown in Figure 1.8, which can be described by the two differential equations in Equation (1.11). By eliminating the nonlinear item $d\Psi_m/dt$ in Equation (1.11), which reflects the transformer's core flux, the two equations in Equation (1.12) are obtained.

$$\begin{cases} u_1 = i_1 r_1 + L_1 \dfrac{di_1}{dt} + \dfrac{d\psi_m}{dt} \\ u_2 = i_2 r_2 + L_2 \dfrac{di_2}{dt} + \dfrac{d\psi_m}{dt} \end{cases} \tag{1.11}$$

$$\begin{cases} u_{12} = L_1 \dfrac{di_1}{dt} - L_2 \dfrac{di_2}{dt} \\ u_{12} = u_1 - u_2 - i_1 r_1 + i_2 r_2 \end{cases} \tag{1.12}$$

In Equations (1.11) and (1.12), u_1 and u_2 are the voltages of the primary and secondary windings; i_1 and i_2 are the currents on the primary and secondary windings; L_1 and L_2 are the leakage inductances of the primary and secondary windings; Ψ_m is the mutual inductance flux between the primary and secondary windings; r_1 and r_2 are the resistances of the primary and secondary windings.

When the transformer operates in the normal state, $r_1 + r_2 = r_k$ and $L_1 + L_2 = {}^{x_k}/_{w}$, where r_k and x_k are the winding resistance and short-circuit reactance, respectively. By applying these two formulas to

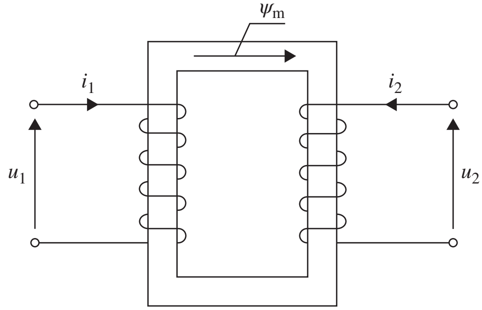

Figure 1.8 Two-winding single-phase transformer

Equation (1.12), two equivalent loop balance equations can be obtained:

$$u_1 - u_2 + i_2 r_k + \frac{x_k}{w}\frac{di_2}{dt} = (i_1 + i_2)r_1 + L_1\frac{d(i_1 + i_2)}{dt} \tag{1.13}$$

$$u_1 - u_2 - i_1 r_k - \frac{x_k}{w}\frac{di_1}{dt} = -(i_1 + i_2)r_2 - L_2\frac{d(i_1 + i_2)}{dt} \tag{1.14}$$

Since Equation (1.12) is based on the normal operation state of the transformer, it is applicable for any circumstance except for a transformer internal fault. Therefore, the validity of Equation (1.12) can be used as a criterion to direct the action of the protective relay. However, this method needs improving in the following two aspects:

1. Currently no feasible method is available to obtain the leakage inductance of each winding in real-time.
2. Even if the leakage inductance parameters can be obtained, it is still dependent on accurate internal fault data to determine the protection scheme, protection criterion and the sensitivity check methods.

Addressing the above problems, the following measures for improvement are proposed.

Based on the transformer loop equation, the equivalent instantaneous leakage inductance of each winding is established; this can reflect the variation status of the transformer leakage magnetic field. The equivalent instantaneous leakage inductance bears similar changing characteristics to the actual leakage inductance. Thus, firstly each equivalent instantaneous leakage inductance is obtained in the cases of inrush current, excessive excitation or external fault, which is a constant value. Secondly, when a fault occurs to the transformer winding, the equivalent instantaneous leakage inductance of the fault phase will change significantly, rendering an obvious difference in value from the normal leakage inductance. Such difference or variation in the value of the equivalent instantaneous leakage inductance can be used to form new transformer main protection criteria.

Establishment of Equivalent Instantaneous Leakage Inductance Parameter

Equation (1.13) contains two unknown parameters (r_1 and L_1), so it cannot be solved directly. However, by establishing two independent equations using data measured at different moments, it can be solved. To this end, two adjacent moments, t_1 and t_2, are chosen to establish the equations:

$$u_{121}(t_1) = r_1 i_d(t_1) + L_1\frac{di_d(t_1)}{dt} \tag{1.15}$$

$$c(t_2) = r_1 i_d(t_2) + L_1\frac{di_d(t_2)}{dt} \tag{1.16}$$

where $u_{121} = u_1 - u_2 + i_2 r_k + \left(\frac{x_k}{w}\right)\left(\frac{di_2}{dt}\right)$, $i_d = i_1 + i_2$.

In implementation, current difference can be used instead of current differential in Equations (1.15) and (1.16). To this end, three adjacent sample values (three continuous points after the digital filtering) are chosen. Suppose that u_{k-1}, u_k and u_{k+1} represent the voltage samples at t_{k-1}, t_k and t_{k+1}, and that i_{k-1}, i_k and i_{k+1} represent the current samples at t_{k-1}, t_k and t_{k+1}. Set t_1 to be in the midst of t_{k-1} and t_k, and t_2 in the midst of t_k and t_{k+1}, with a sampling interval between t_1 and t_2. Then $u_{121}(t_1)$, $u_{121}(t_2)$, $i_d(t_1)$, $i_d(t_2)$, $di_d(t_1)/dt$ and $di_d(t_2)/dt$ in Equations (1.15) and (1.16) can be expressed by interpolation of the samples:

$$u_{121}(t_1) = \frac{u_k + u_{k-1}}{2}, u_{121}(t_2) = \frac{u_k + u_{k+1}}{2} \tag{1.17}$$

$$i_d(t_1) = \frac{i_k + i_{k-1}}{2}, i_d(t_2) = \frac{i_k + i_{k+1}}{2} \tag{1.18}$$

$$D_1 = \frac{di_d(t_1)}{dt} = \frac{i_k - i_{k-1}}{T_s}, D_2 = \frac{di_d(t_2)}{dt} = \frac{i_{k+1} - i_k}{T_s} \tag{1.19}$$

Combining Equations (1.15) and (1.16), the instantaneous leakage inductance L_1 at t_1 can be obtained, as shown in Equation (1.20). Thus, calculated instantaneous leakage inductance is based on the normal operating model of the transformer. In the case of an internal fault, since the loop equation is no longer valid, the calculated leakage inductance is not the actual measuring value but, rather, an equivalent one. Therefore, it is defined as the equivalent instantaneous leakage inductance.

$$L_1 = \frac{u_{121}(t_1)i_d(t_2) - u_{121}(t_2)i_d(t_1)}{i_d(t_2)D_1 - i_d(t_1)D_2} \tag{1.20}$$

Similarly, the equivalent instantaneous leakage inductance L_2 at t_1 can be obtained:

$$L_2 = \frac{u_{122}(t_1)i_d(t_2) - u_{122}(t_2)i_d(t_1)}{i_d(t_2)D_1 - i_d(t_1)D_2} \tag{1.21}$$

where $u_{122} = -(\mathrm{u}_1 - \mathrm{u}_2 - \mathrm{i}_1\mathrm{r}_k - (x_k/w)(di_1/dt))$.

Design of the Protection Scheme

Main criterion:

After the protection starts, calculate on-line the equivalent instantaneous leakage inductance of each phase and use a 1/4 cycle length sliding data window to calculate the real-time average value of the leakage inductance. Compare the average equivalent instantaneous leakage inductances of different phases, then the protection criterion can be formed. It should be noted that the average equivalent instantaneous leakage inductance of the non-pick-up phase is represented by the normal leakage inductance of that phase.

Take the Δ-side of a three-phase Y/Δ-connected transformer as an example. The difference among the average equivalent instantaneous leakage inductances of the phases is described by ${\sigma_1}^2$ in Equation (1.22). When ${\sigma_1}^2 > {\sigma_{zd}}^2$, it can be identified as an internal fault and the protection should operate.

$${\sigma_1}^2 = \frac{1}{3}((L'_{lae} - L'_{lbe})^2 + (L'_{lbe} - L'_{lce})^2 + (L'_{lce} - L'_{lae})^2) \tag{1.22}$$

where L'_{lae}, L'_{lbe} and L'_{lce} represent the average equivalent instantaneous leakage inductance of each phase on the Δ-side. If there is any phase not switched on (un-started), then its average equivalent instantaneous leakage inductance should be replaced by L'_{lie} $(i = 1, 2, 3)$, the normal leakage inductance of the phases on the Δ-side.

Auxiliary criterion:

When a serious internal fault occurs in the transformer, the differential current will be very large, so that the calculated leakage inductances will be small in value and minor in their differences. In this case, using only the main criterion may lead to operation failure of the protection. Therefore, the conventional differential current instantaneous break protection can be introduced as an auxiliary criterion for comprehensive identification.

Scheme Verification

Considering the influence of different switching moments, 20 measurements are conducted for each operation state. The calculation results of each group of 20 data are listed in Table 1.1.

As shown in the σ_2^2 column of Table 1.1, the minimum value of σ_2^2 under fault conditions (except inter-phase faults) is 80.65 times the maximum value of σ_2^2 under normal no-load switching conditions. If σ_{zd}^2 is set to be $10 \times (10^{-4}\,H)^2$, then according to the main criterion, it is possible to effectively distinguish between inrush current and internal fault current (except inter-phase faults). Furthermore, with the cooperation of the auxiliary criterion, correct and reliable operation of the protective relay under various internal fault conditions can be guaranteed.

Table 1.1 Calculation results of σ_2^2 under various situations

Operation states			$\sigma_2^2(\times 10^{-4}\ \mathrm{H})^2$	Serial number
Drop	Normal dropping		0.9538–1.2152	1
In star side fault	Inter-turn	A9%	112.7443–125.3236	2
		B18%	216.7854–223.7382	3
		C18%	220.8367–231.1159	4
	Grounding	A	197.2485–222.1532	5
		B	148.5279–160.2373	6
	Inter-phase	AB	1.9634–3.1248	7
		BC	1.5586–3.0747	8
Star side fault under operation	Inter-turn	A9%	98.0825–111.3468	9
		B18%	205.4478–218.4637	10
		C18%	161.2256–172.6055	11
	Grounding	A	212.6494–223.1037	12
		B	155.3819–160.6530	13
	Inter-phase	AB	1.7832–2.9875	14
		BC	1.6329–2.8321	15

1.3.2.3 Power Differential Principle

Transformer microcomputer main protection based on the power differential principle considers the voltage and current information synthetically based on the law of energy conservation. When the transformer operates in the normal state, little active power is consumed; but when the transformer insulation is damaged, the sparkling electrical arc will consume large amounts of active power. Therefore, by detecting the amount of active power consumed, it can be decided when an internal fault occurs. The power differential principle does not rely on the waveform characteristics of the inrush current and is a novel main protection scheme. However, there are still some problems about the scheme that remain to be solved:

- This scheme is not totally free from the negative influence of the inrush current. By avoiding the charging process in the first cycle when there is inrush current, the protection judgment will be delayed.
- When there is inrush current, the copper loss is difficult to calculate accurately and the iron loss will increase, which make the value setting complicated.
- For transformers with Y/Δ connection, the current on windings of the Δ-side cannot be obtained, thus the copper loss cannot be determined, which reduces the sensitivity of protection.

In view of the above questions, based on the normal operation state loop equation of the transformer, a two-terminal network containing only the leakage inductance and winding resistance is formed in this section. By analysing the input generalized instantaneous reactive power, the essential difference between the inrush current and internal fault is further revealed.

Design of the Two-Terminal Network

Taking the double-winding single-phase transformer as an example, the two-terminal network based on the voltage and current information can be designed.

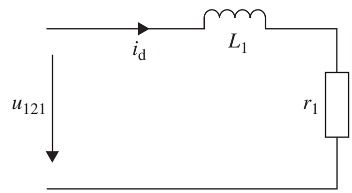

Figure 1.9 Two-terminal network of the primary side

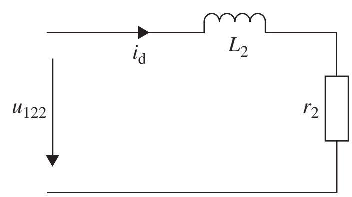

Figure 1.10 Two-terminal network of the secondary side

According to Equations (1.13) and (1.14), two two-terminal networks can be formed. The one containing only r_1 and L_1 is shown in Figure 1.9, which is defined as the primary side two-terminal network. The other, containing only r_2 and L_2, is shown in Figure 1.10 and is defined as the secondary side two-terminal network.

The terminal voltage of the network in Figure 1.9 is:

$$u_{121} = u_1 - u_2 + i_2 r_k + \frac{x_k}{w}\frac{di_2}{dt} \tag{1.23}$$

The terminal voltage of the network in Figure 1.10 is:

$$u_{122} = -\left(u_1 - u_2 - i_1 r_k - \frac{x_k}{w}\frac{di_1}{dt}\right) \tag{1.24}$$

In both Figures 1.9 and 1.10, the arrow represents the direction of voltage drop and the current injected into the two-terminal network is: $i_d = i_1 + i_2$.

In the case of no-load switching, suppose that the secondary side of the transformer is not loaded, then a two-terminal network similar to that in Figure 1.9 can be formed according to Equation (1.12). In this case the terminal voltage is: $u_{121} = u_1 - u_2$ and the current injected into the two-terminal network is i_1.

Take the two-terminal network in Figure 1.9 for illustration. Although i_d(t) and u_{121}(t) of the input terminal are not correspondently related in the actual system, their product has the nature of instantaneous power. Thus, it can be defined as the generalized instantaneous power, that is, $S_{gy1} = u_{121}(t)i_d(t)$, or in another form: $\backslash S_{gy1}(t) = \overline{S}_{gy1} + \widetilde{S}_{gy1}(t)$, where the DC part $\overline{S}_{gy1}$ is the generalized instantaneous power absorbed by the primary side. Similarly, the generalized instantaneous power absorbed by the secondary side $\overline{S}_{gy2}$ can obtained. On this basis, define the difference between $\overline{S}_{gy1}$ and the active power consumed by the normal winding resistance r_1 to be P_1, and the difference between $\overline{S}_{gy2}$ and the active power consumed by the normal winding resistance r_2 to be P_2. Formulas to calculate P_1 and P_2 are:

$$\begin{cases} P_1 = \dfrac{1}{T}\displaystyle\int_0^T \left(u_{121}(t)\, i_d(t) - i_d^2(t) r_1\right) dt \\ P_2 = \dfrac{1}{T}\displaystyle\int_0^T \left(u_{122}(t)\, i_d(t) - i_d^2(t) r_2\right) dt \end{cases} \tag{1.25}$$

It can be seen from Equation (1.25) that, in the cases of the normal operating state (including no-load switching and external faults), the generalized active power absorbed by the two-terminal network is all consumed by the winding resistance, thus P_1 and P_2 are both zero (not considering various kinds of errors). But in the case of internal faults, due to the power loss of the fault branch and the fact that P_1 and P_2 are calculated with the voltage and current after the fault and the winding resistance before the fault, P_1 and P_2 will no longer be zero. By setting an appropriate threshold value, it is possible to effectively distinguish between normal operation state and fault condition.

Principle Verification

The dynamic simulation results of the power differential principle and the novel principle applied in various cases are shown in Table 1.2. P_m represents the maximum active power in three phases. Considering the influence of different closing moments, the calculation result under every operation state is the comprehensive analysis of 20 measurements.

Table 1.2 Calculation results of the power differential method and the novel method when the transformer is energized

Operation states				Pc/W	Pm/W	Serial number
Normal state	Normal switching on			854–1 393	0.76–2.2	1
	Normal operation			309–348	0.53–0.96	2
Dropping fault with faults	Star side fault	Inter-turn	A2.4%	1 161–1 484	27–36	3
			A6.1%	1 659–1 827	48–58	4
			A9%	2 471–2 539	62–69	5
			B18%	8 363–8 432	104–115	6
			C18%	8 016–8 109	112–124	7
		Grounding	A	14 142–14 275	1 032–1 087	8
			B	16 057–16 148	651–734	9
		Inter-phase	AB	23 814–23 906	2 212–2 320	10
			BC	25 689–25 762	2 146–2 199	11
	Angle side inter-turn fault		A1.8%	1 123–1 415	25–32	12
			A4.5%	1 582–1 737	38–46	13
Fault state under operation	Star side fault	Inter-turn	A2.4%	1 098–1 217	26–31	14
			A6.1%	1 769–1 895	53–61	15
			A9%	2 471–2 539	62–69	16
			B18%	8 363–8 432	104–115	17
			C18%	8 016–8 109	124–135	18
		Grounding	A	13 986–14 095	876–892	19
			B	14 260–14 363	535–568	20
		Inter-phase	AB	22 381–22 476	2 054–2 139	21
			BC	23 905–24 019	1 963–2 017	22
	Angle side inter-turn fault		A1.8%	1 112–1 228	25–29	23
			A4.5%	1 594–1 703	42–51	24

It can be seen from Table 1.2 that, for the differential active power principle, if the threshold value is set to be 2100 W (i.e. 1.5 times the maximum value of P_c in the normal operation state), there will be eight cases (serial numbers 3, 4, 12, 13, 14, 15, 23 and 24) that cannot be identified.

For the proposed novel principle, the maximum value of P_m in normal operation state and the minimum value of P_m under fault condition are more than 10 times apart. Therefore, if the threshold value of P_m is set to be 4 W (i.e. the maximum value of P_m in the normal operation state), then all kinds of faults can be identified with a good redundancy.

It is thus obvious that the proposed novel principle is superior to the existing power differential principle in reliability and sensitivity.

Concerning the technology development route of transformer main protection, the principle is to 'aim at old problems and come up with new ideas'. On one hand, with no better protection schemes coming forth, the focus should be on summarizing effective solutions and experience in the identification of inrush current and fault current, while at the same time exploring the application of new theories and new technology, in an effort to improve the performance of the current differential protection. The study topics involved in this aspect mainly include:

- Explore novel principles of transformer differential protection.
- Research on the identification of inrush current and fault current.
- Study on the recognition of CT saturation.
- Application of CT transient transfer characteristic in the differential protection.

On the other hand, attention should be paid to finding new protection principles that are completely different from the differential protection scheme and which no longer rely on the recognition of the inrush current and fault current to form the protection criteria. This should be a goal in constant pursuit by relay protection researchers. Three new principles totally different from the differential protection have been analysed: (i) the sequence impedance principle; (ii) the equivalent instantaneous leakage inductance principle; and (iii) the generalized instantaneous power principle. Dynamic simulation results verify the validity of the new principles.

The rapid development of electronic technology, computer technology and communication technology facilitates the development of transformer protection. Besides, with the idea of 'main and backup protection integration' and new principles and technology widely applied, transformer protection and operating performance will be greatly enhanced. In the near future, transformer protection will use the digital current and voltage signals from OCT (optical current transformer) and OVT (optical voltage transformer) to form the protection scheme, thus avoiding the problems in a traditional current transformer (CT) and potential transformer (PT). Transformer protection will move rapidly toward informationization, integration and intelligence.

1.4 Analysis of Electromagnetic Transients and Adaptability of Second Harmonic Restraint Based Differential Protection of a UHV Power Transformer

PSCAD/EMTDC is typical simulation software applied in various fields of power systems. In particular, it is suitable for electromagnetic transient simulations. According to the equivalent circuit of a three-winding autotransformer, a UHV autotransformer model and its internal faults model were set up by means of a UMEC (Unified Magnetic Equivalent Circuit) transformer model provided by EMTDC software. This new model takes into account both the particularity of the UHV transformer and the nonlinearity of the transformer core. Based on this model, a variety of simulation tests were carried out, including energizing, inter-turn short-circuit faults, phase-to-ground short-circuit faults and phase-to-phase short-circuit faults. Finally, the current waveforms were analysed and the issues of the transformer differential protection using the second harmonic blocking scheme applied in UHV transformer protections were evaluated.

1.4.1 Modelling of the UHV Power Transformer

1.4.1.1 Basic Configuration of the UHV Power Transformer

An autotransformer is applied widely in 220 kV and higher systems due to many merits, such as low cost, high efficiency, low exciting power and so on. The tremendous capability and the high requirement for insulation lead to the huge bulk and prodigious weight of UHV transformers, as the single-phase capability of UHV transformers is up to 1000 MVA. In view of the need for convenient transport, single-phase configuration is necessary. The UHV transformer produced in China is the single-phase autotransformer [5]. The three-phase configuration is implemented with a single-phase transformer bank.

The autotransformer has a tertiary winding, namely the low voltage winding. The tertiary winding is not loaded. Instead, its functionality rests with the circulation of the third harmonic. Three phases of the tertiary winding are connected by delta-type and earthed through a low voltage reactor.

To meet the demand of electric isolation, the nonexciting voltage regulation from the neutral terminal is adopted and the voltage regulator and compensation transformer are set separately by the UHV transformer. The principle is illustrated in Figure 1.11.

SV, CV, LV, TV, EV, LE and LT represent, respectively, series winding, common winding, low voltage winding, voltage regulation winding, magnetizing winding, low voltage magnetizing winding and low voltage compensation winding. Due to this special type of coupling of windings, the short-circuit impedance of the UHV transformer is much bigger than that of the ordinary transformer.

Since the currents of all sides of the UHV transformer are the main concerns, the main transformer and the corresponding voltage-regulating compensation transformer are equivalent to a three-winding autotransformer.

1.4.1.2 The Equivalent Circuit of Three-Winding Autotransformer

No matter how the windings are arranged, the three-winding autotransformer can be studied by means of a Y-type equivalent circuit. In the following, the equivalent circuit of the UHV transformer based on the series, common and tertiary winding are modelled.

As seen in Figure 1.12, converting electrical quantities to common winding side, $\dot{U}'_c$ and $\dot{I}'_c$, are the voltage and the current respectively of the series winding. The voltage and the current of the common winding are denoted by $\dot{U}_Q$ and $\dot{I}_Q$. $\dot{U}'_B$ and $\dot{I}'_B$ represent the voltage and the current of the tertiary winding.

Similar to the ordinary three-winding transformer, the following equation can be deduced when the exciting current is ignored:

$$\begin{cases} \dot{U}'_C - \dot{U}_Q = \dot{I}'_C Z_C{}' + \dot{I}_Q Z_Q \\ \dot{U}'_C - \dot{U}'_B = \dot{I}'_C Z_C{}' + \dot{I}'_B Z'{}_B \end{cases} \tag{1.26}$$

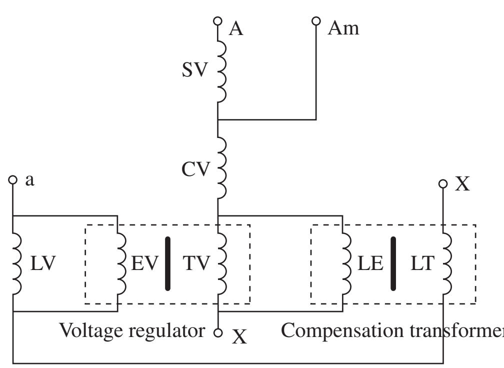

Figure 1.11 The principle of UHV transformer voltage regulation

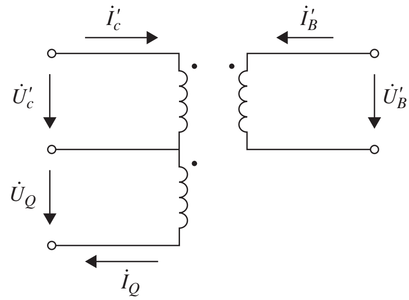

Figure 1.12 Three-winding autotransformer theory diagram

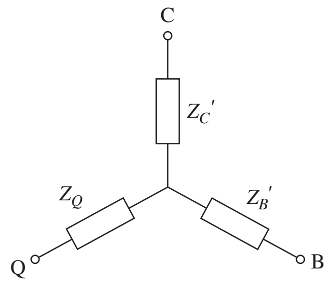

Figure 1.13 Three ports Y-type equivalent circuit

where $Z_C{}'$ is the leakage impedance converted from the series winding, Z_Q is the leakage impedance of the common winding and $Z_B{}'$ is the leakage impedance converted from the low voltage winding.

According to Equation (1.26), its Y-type equivalent circuit can be deduced as seen in Figure 1.13.

The parameters of the equivalent circuit can be obtained from the tests of the ordinary three-winding transformer. By this arrangement, the three-winding autotransformer can be simulated based on the ordinary three-winding transformer.

1.4.1.3 Models of the UHV Transformer for Simulation

Modelling of the UHV transformer and simulation of electromagnetic transients are both carried out by virtue of EMTDC. However, EMTDC does not provide the three-winding autotransformer models directly. According to the above analysis, and in view of the 'electric' relationship between the series winding and the common winding of autotransformer, two windings of the UMEC three-winding transformer model are connected to form the high voltage winding and the medium voltage winding. In this way, the UHV transformer model can be obtained.

As seen in Figure 1.14, #1 winding, #2 winding and #3 winding denote the low voltage winding, the series winding and the common winding, respectively. The validation of the equivalence is to guarantee the leakage impedances of corresponding windings are equal between the equivalent model and the original model. Significantly, the parameters of the UHV transformer should be converted to the side of the tertiary winding.

The UMEC transformer model is built primarily based on the core geometry. Unlike the classical transformer model, the magnetic coupling between windings of different phases is taken into account in the UMEC model, in addition to coupling between windings of the same phase. The piecewise technique

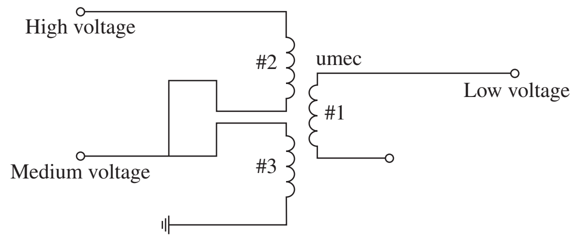

Figure 1.14 Model of the UHV transformer

is used to control the conductance of equivalent branch. The nonlinearity characteristic of the core is input directly into the model as a piecewise U–I curve, which makes full use of the interpolation algorithm for the calculation of exact instants when the state changes.

Internal faults of the transformer include inter-turn short-circuit faults, turn-to-ground faults, lead-out phase-to-phase short-circuit faults and lead-out phase-to-ground faults. The modelling of internal winding faults is the main concern of this section.

When an inter-turn fault occurs on the dual-winding transformer, the faulty turns of the faulty winding can be regarded as a tertiary winding. Based on this concept, the faulty turns of the three-winding transformer can be simulated by a fourth winding (Figure 1.15).

In Figure 1.15, #2 winding denotes the faulty turns; the fault types can be controlled by the breakers. The leakage reactance X_2 of #2 winding and the leakage reactance X_3 of #3 winding can be calculated by:

$$\begin{cases} X_2 + X_3 = X_c \\ X_2/X_3 = \left(N_2/N_3\right)^2 \end{cases} \tag{1.27}$$

In Equation (1.27), X_c is known as the leakage reactance of the series winding. N_2 and N_3 are, respectively, the turn quantities of #2 winding and #3 winding. Practically, N_2/N_3 nearly is equal to the ratio of #2 winding's rated voltage to #3 winding's rated voltage.

1.4.2 Simulation and Analysis

Due to the nonlinearity of the transformer core, the magnetizing inrush possibly occurs when a transformer is energized, which easily leads to the mal-operation of the differential protection if no blocking

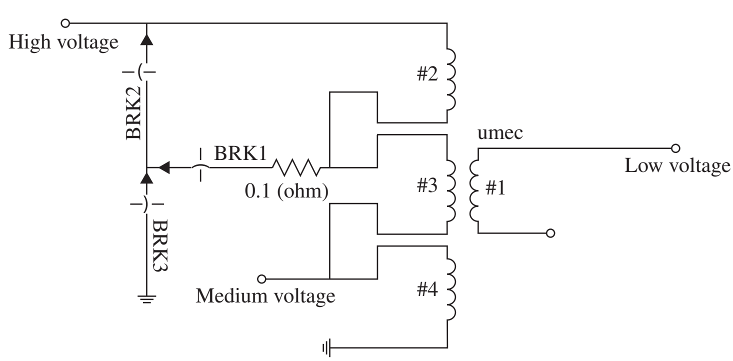

Figure 1.15 Internal faults model of a transformer

strategy is included. Therefore, identification of the inrush current is the premise of the correct operation of the differential protection. In the following, the above two models are used to simulate the energizing and internal faults of a UHV transformer. In this way, the operating behaviour of the protection can be investigated rationally.

1.4.2.1 System Model and Correlative Parameters

The system model comes from Jindongnan–Nanyang–Jingmen 1000 kV AC test and demonstration project in China, and all the parameters in the model system are from the real UHV project.

The transmission line parameters are:

Jindongnan–Nanyang: length = 363 km. Positive sequence resistance $R_1 = 0.00758\ \Omega$/km, positive sequence reactance $X_1 = 0.26365\ \Omega$/km, positive sequence capacitance $C_1 = 0.01397\ \mu$F/km. Zero sequence resistance $R_0 = 0.15421\ \Omega$/km, zero sequence reactance $X_0 = 0.7821\ \Omega$/km, zero sequence capacitance $C_0 = 0.008955\ \mu$F/km.

Nanyang–Jingmen: length = 291 km. Positive sequence resistance $R_1 = 0.00801\ \Omega$/km, positive sequence reactance $X_1 = 0.2631\ \Omega$/km, positive sequence capacitance $C_1 = 0.013830\ \mu$F/km. Zero sequence resistance $R_0 = 0.1563\ \Omega$/km, zero sequence reactance $X_0 = 0.8306\ \Omega$/km, zero sequence capacitance $C_0 = 0.009296\ \mu$F/km.

The parameters of the UHV autotransformer are:

Rated capabilities of the high voltage side, the medium voltage side and the low voltage side are 1000, 1000 and 334 MVA, respectively.

The voltage ratings of the high voltage side, the medium voltage side and the low voltage side are 1050, 525 and 110 kV, respectively.

The parameters of the short-circuit impedances (based on rated capabilities of the high voltage side) are:

The short-circuit impedance is 18% in the high–medium side, 62% in the high–low side and 40% in medium–low side.

No-load loss is 0.07%; magnetizing loss is 155 kW.

The rated capability of the high voltage reactors are:

The rated capability is 960 MVA in the Jindongnan side of Jindongnan–Nanyang transmission line and 720 MVA in Nanyang side. The rated capability is 720 MVA in Nanyang side of the Nanyang–Jingmen transmission line and 600 MVA in Jingmen side.

In view of the influences that result from the energizing transient of the transmission lines and high voltage reactors, the energizing position is at the high voltage side of UHV transformer at Jingmen side.

The configuration of the system model is shown in Figure 1.16.

As seen in Figure 1.16, the UHV source is connected to the high voltage side of the UHV transformer via UHV transmission lines. The medium voltage side is linked with an equivalent load, while low voltage winding is connected in delta-type and is grounded through a reactor and a capacitor for compensation.

Actually, the source of the UHV project is provided by the medium voltage side of the UHV transformer at Jindongnan. It is no harm to replace Jindongnan by an equivalent source since the emphasis rests with the energizing at Jingmen. The reactors are modelled by the parallel inductances and the capacitors are modelled by capacitances. The remnant flux is modelled by the DC source, which is put on the high voltage side of the UHV transformer.

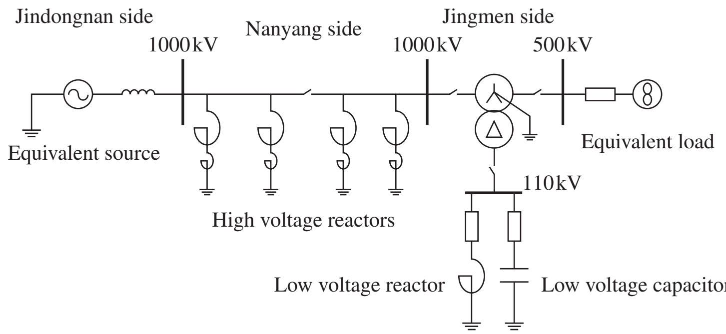

Figure 1.16 Jindongnan–Nanyang–Jingmen system model

1.4.2.2 Simulation and Analysis of Energizing

Energizing simulations are carried out in terms of diverse initial angles and remnant fluxes. A scenario of typical inrush waveforms of three phases is shown in Figure 1.17. As seen, the harmonics of the inrush is more abundant than the transformer's in EHV and lower level systems, leading to the more abnormal waveforms.

The UHV transformer adopts Y/Δ-11 type. Therefore, the concern focuses on the differential current, which determines whether the differential protection can operate correctly or not. The differential current is the summation of three-side incoming currents. Therefore, the phase and magnitude compensation should be carried out instead of summation directly. Namely, if the incoming currents of the high, medium and low voltage sides of phase A are $\dot{I}_{ah}$, $\dot{I}_{am}$ and $\dot{I}_{al}$, and the incoming currents of the high, medium and low voltage sides of phase B are $\dot{I}_{bh}$, $\dot{I}_{bm}$ and $\dot{I}_{bl}$, in view of the phase compensation and magnitude compensation, the differential current of phase A should be $(\dot{I}_{ah} - \dot{I}_{bh}) + \frac{525/\sqrt{3}}{1050/\sqrt{3}}(\dot{I}_{am} - \dot{I}_{bm}) + \frac{110}{1050/\sqrt{3}}\dot{I}_{al}$.

Because the transformer is energized at the high voltage side, there are no currents in the other two sides. Therefore, the differential current of phase A is $(\dot{I}_{ah} - \dot{I}_{bh})$ exactly. Table 1.3 shows the harmonic ratios of the three-phase differential currents in various energizing conditions.

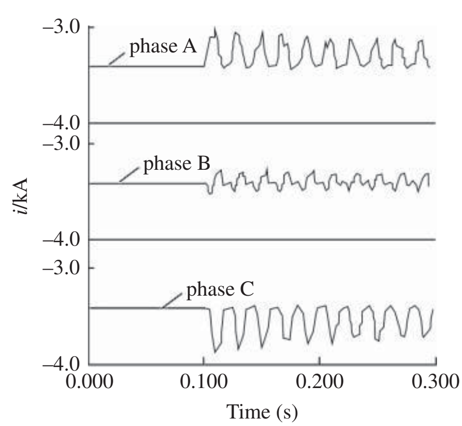

Figure 1.17 Magnetic inrush currents in typical energizing, initial angle of phase A is 0°; remnant flux densities of the three phases are all 0

Table 1.3 Harmonic analysis of inrush currents

Remnant flux density	Initial angle of phase A (°)	Second harmonic ratio (%)		
		Phase A	Phase B	Phase C
Phase A: $0B_m$	0	30.4	40.4	15.1
Phase B: $0B_m$	30	31.8	22.6	14.8
Phase C: $0B_m$	60	37.0	23.7	34.3
Phase A: $0.7B_m$	0	16.0	18.9	10.1
Phase B: $-0.5B_m$	30	17.0	15.4	1.9
Phase C: $-0.5B_m$	60	30.3	15.0	3.7
Phase A: $0.9B_m$	0	12.8	17.7	4.0
Phase B: $0B_m$	30	9.8	6.9	6.1
Phase C: $-0.9B_m$	60	17.0	17.0	7.8

According to Table 1.3, when the initial angle of phase A is 30°, the harmonic ratio of one phase will be under 15%, even if no remnant flux exists. If the remnant flux is taken into account, the harmonic ratio of phase C will fall below 1.9%, as shown in fifth row of Table 1.3. This indicates that it is unrealistic to only adjust the harmonic restraint ratio to avoid the mal-operation of the differential protection. The mal-operation above cannot be avoided unless the following blocking strategy is adopted, that is, set the threshold of harmonic restraint ratio as 15% and implement the blocking while the second harmonic ratio of the differential current of any phase exceeds the threshold. Furthermore, when the remnant fluxes of the three phases are 0.9, 0 and $-0.9B_m$ and the initial angle of phase A is 30°, the second harmonic ratios of the three-phase differential currents are all under 10%, of which the corresponding waveforms are shown in Figure 1.18. In this case, even the above strict countermeasure will not allow the protection to survive.

In this scenario, mal-operation is unavoidable even though the above-mentioned blocking strategy is adopted and the harmonic restraint ratio is regulated to 15%.

The higher order harmonics, especially the odd harmonic of the inrushes of the UHV transformer, are more abundant than in an ordinary transformer. This possibly has some impact on the methods used to identify inrush by means of waveform characteristic.

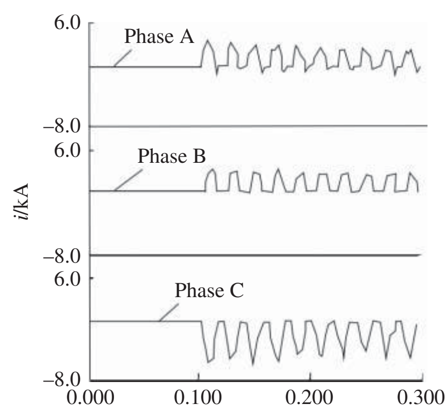

Figure 1.18 Magnetic inrushes leading to the mal-operation of differential protection

It is impossible to simulate all the conditions involving the diverse initial angles, remnant flux densities and different operation states of systems to validate the existing schemes for differential protection. However, the simulation results presented in this section at least suggest that the second harmonic characteristic of the inrush of the UHV transformer is weaker than that in EHV and lower voltage systems.

This scenario should be paid attention to when commissioning the differential protection of the UHV transformer.

1.4.2.3 Simulation and Analysis of Internal Faults

The simulations of inter-turn short-circuit faults, turn-to-ground fault of various short-circuit turns ratios have been carried out. For simplicity, all the faulty phases are designated phase A.

Moreover, several lead-out short-circuit faults are simulated by means of the FAULTS module provided by EMTDC, including phase A to ground faults, phase A–B short-circuit faults and phase A–B to ground faults.

Several phase current waveforms of phase A in different fault conditions are shown in Figure 1.19.

As seen, for inter-turn short-circuit faults or for phase to ground faults, more turns are short-circuited the smaller the primary current is. When the lead-out fault occurs, the fault current is high and distorted.

Accordingly, in order to investigate the operation of the differential protection, the three-side incoming currents of the transformer should be phase compensated to form the differential current. The second harmonics of differential currents in manifold fault conditions were analysed; some results are given in Table 1.4, the data window length is one cycle. Due to the phase compensation, phase B has no differential current when the fault occurred in phase A.

Table 1.4 Harmonic analysis of fault currents

(a) Internal winding short-circuit fault

Fault type	Fault turns ratio (%)	Second harmonic ratio (%)	
		Phase A	Phase B
Inter-turn short-circuit	2	22.6	22.9
	5	8.0	8.0
	10	3.7	3.3
	30	2.7	2.2
Turn-to-ground	2	4.6	4.6
	5	3.8	3.6
	10	3.6	3.3
	30	3.1	2.9

(b) Lead-out short-circuit faults

Fault type	Second harmonic ratio (%)		
	Phase A	Phase B	Phase C
Phase A to ground	3.3	–	3.3
Phase A–Phase B	3.7	3.3	4.1
Phase A–B to ground	3.1	2.4	3.0

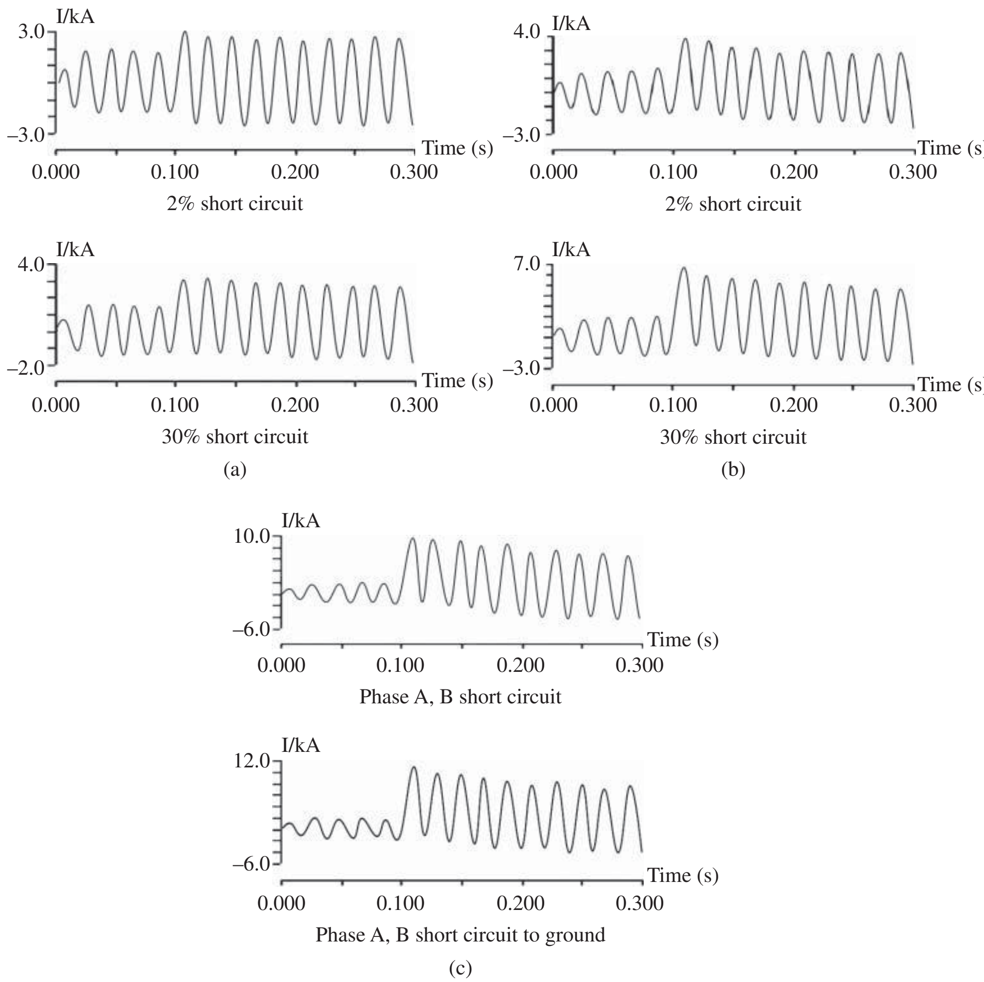

Figure 1.19 Phase currents in the case of internal faults: (a) Inter-turn short circuit; (b) short circuit to ground; (c) lead-out short circuit

According to Table 1.4, due to the effect of the distributed capacitance of the UHV transmission line and the particularity of the UHV transformer, abundant harmonics exist within the fault currents. However, except for a 2% inter-turn fault, the ratios of the second harmonic of the differential currents in the case of diversified faults are under 15%. The most adverse scenario is a 5% inter-turn fault, of which the second harmonic is 8%. Combined with the analysis of inrush currents, the mal-operation probability may be evidently reduced if the second harmonic restraint ratio declines properly, for example, declining to 10%. Meanwhile, it will not influence the operating speed of the differential protection in a mass of fault conditions.

The case of a 2% inter-turn fault is an exception. In this case, the second harmonic of the differential current of the faulty phase is 22.6%, which exceeds the conventional setting value of second harmonic restraint ratio. The differential current waveform in this scenario is shown in Figure 1.20.

Furthermore, the change of the second harmonic content in this condition is investigated, referring to Figure 1.21.

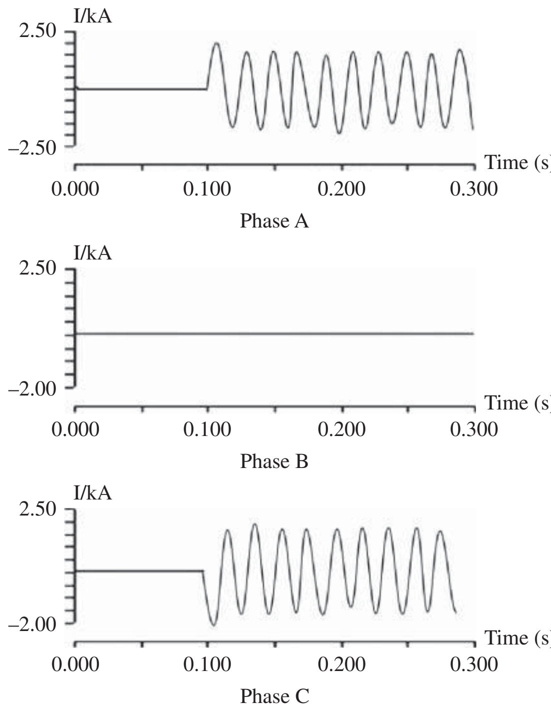

Figure 1.20 Differential current in the case of a 2% inter-turn fault

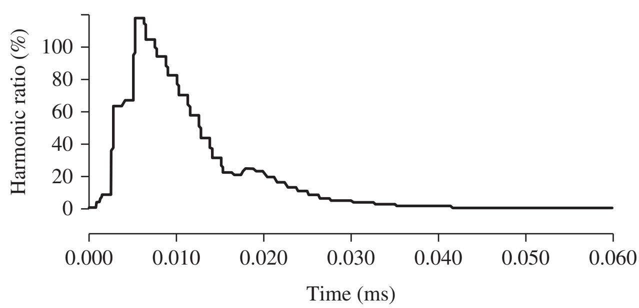

Figure 1.21 Second harmonic curve in the case of a 2% inter-turn fault

As seen, the second harmonic of the differential current declines rapidly. The second harmonic ratio is 22.6% after the first post-fault cycle elapses. After that, it decreases to 19% at 21 ms, to 15.3% at 22 ms, to 12.4% at 23 ms, to 10% at 25 ms and to 7.4% at 26 ms. The time delay is only 6 ms even if the threshold of restraint ratio is set to be 10%.

According to the simulation results, the second harmonic based blocking scheme can, on the whole, distinguish between inrush and fault current. The protection can be reliably blocked during the energizing of the UHV transformer if the second harmonic restraint ratio is set below 10%. However, it may lead to some time delay in the response of the differential protection to some scenarios of internal faults.

In this sense, the discrimination between the inrush and the fault current of the UHV transformer is still valuable.

A great many beneficial works for identifying the inrush from fault current have been reported [6–9]. Their adaptability to the UHV transformer base can be assessed on the models of energizing and internal fault of the UHV transformer proposed in this section and chose a satisfactory one. Accordingly, the operational level of the differential protection of the UHV transformer can be improved further.

In summary, based on the benchmark model of the transformer provided by EMTDC, the energizing and internal fault models of UHV transformer are established in this section in terms of autotransformer mode. The corresponding electromagnetic transient simulations in a UHV environment are carried out, and reasonable preconditions for investigating the operating performance of the UHV transformer protection are offered. These models are especially suitable for evaluating the applicability of the existing main protection systems of transformers to the UHV test and demonstration project in China. The emphasis of this section rests with evaluating the operation reliability of the differential protection based on second harmonic blocking. It is proven with the simulation results that the harmonic characteristic of the inrush of the UHV transformer is weaker than that of the transformer in EHV and lower voltage grade systems. The second harmonic ratios of three-phase differential currents may be all under 10% in some extreme conditions. On the other hand, in the fault conditions, the second harmonic ratios of differential currents all exceed 10%, except some light inter-turn faults. In terms of comprehensive analysis of the inrush and fault current obtained from the simulation tests, the differential protection with the second harmonic blocking scheme still has redundancy when applied to UHV transformer protection. As for the light inter-turn fault, although the second harmonic ratio is higher than 15% by the end of the first post-fault cycle, this ratio decreases to 15% below at 23 ms and goes below 10% at 26 ms. Therefore, the time delay of the protection is not serious in the case of internal faults.

1.5 Study on Comparisons among Some Waveform Symmetry Principle Based Transformer Differential Protection

Recently, a type of criteria based on so-called 'symmetry waveform', which identify the inrush by comparing the first half cycle and the second half cycle of a signal, are proposed. Because this theory makes full use of the shape, size and changing ratio of the waveform, it is worth being studied further. Some references identified three criteria based on the symmetrical waveform from different aspects and made some simulations and dynamic simulation tests to validate them. However, the analysis of this is not comprehensive because of the diversity of the inrushes and fault currents. Therefore, the performance of symmetrical waveform based methods for identifying the inrushes and fault currents was investigated. Useful conclusions were gained after the test and comparison of the three criteria.

1.5.1 The Comparison and Analysis of Several Kinds of Symmetrical Waveform Theories

1.5.1.1 The Theory of Integral-Type Symmetrical Waveform and its Analysis

The main idea of the theory using the integral-type symmetrical waveform is shown in Figure 1.22. Divide the sampling signals A B C of a whole cycle into two half cycles AB and BC with the same length, B′C′ can be obtained by flipping the second half cycle BC with symmetry in the X-axis. Then quadrilateral ABCD can be formed using DE that is translated forward by B′C′ and the first half cycle AB. Denote the area of this quadrilateral as S, the area of straight ladder as Sti, the area overlapped by AB and the X-axis as S+, and the area overlapped by BC and X-axis S. Also, denote the factor of symmetry waveform as:

$$K_{sym} = \frac{|S - S_{ti}|}{\max(\mathrm{S}_{+}, \mathrm{S}_{-})} \tag{1.28}$$

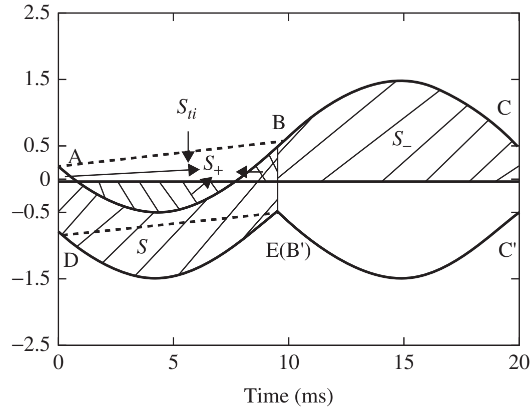

Figure 1.22 Fault current and its waveform transform

The periodic component of signals AB and DE can be offset with each other. In this case, $S_i = S_{ti}$ can be obtained for the ideal periodic sinusoidal signal containing only the DC component. S, S_{ti} are equal to zeros for a pure sine signal. K_{sym} is equal to zero under the above premise. For the inrush, the value of K_{sym} fluctuates around a positive value, of which the maximum value is 1.4 and the minimum value is larger than zero. The fault and the inrush can be identified using this method [10]. Fuzzy recognition is used for practical implementations. The Trip Counter is designed using different ways of counting due to different K_{sym}. When the accumulated value of the Trip Counter is larger than the threshold, the inrush is identified and this phase is then blocked. This scheme is denoted criterion 1.

The speed of the protection output is faster than conventional methods in the case of a low percentage of the fault current harmonic component. However, long time delay will occur in the case of serious distortion of fault currents. Figure 1.23 shows the waveform comparison between fault current and three-phase inrushes recorded by the dynamic simulation laboratory of Huazhong University of Science and Technology.

The fault is set as the B–C short-circuit occurring on the transformer with load and long-distance line connected. The sample rate is 12 points per cycle. The waveform obtained from the disturbance recorder includes two cycles before the fault and five cycles after the fault. From this figure it can be seen that the distortion is serious because of the influence caused by the capacitive current of the long line and the bad characteristic of CT.

To make the figure easy to understand, Figure 1.24 only shows how K_{sym} changes with the fault current and the inrush in C-phase. Figure 1.25 shows how the Trip Counter changes with the fault current and inrush. The X-axis represents the time duration of post-fault. The bold solid lines represent how K_{sym} or Trip Counter change, and the normal solid lines represent how K_{sym} or Trip Counter changes.

The rules of changing of the fault current K_{sym} and the inrush are similar to each other in five cycles; meanwhile, the counting of the trip counter of the inrush in C phase is always smaller than that of the fault current; it is difficult to identify the inrush from the fault current. Therefore, it is not appropriate to use criterion 1 in the case of serious distortion on the fault current waveform. Further study needs to be done to make this scheme adapt to the complex contingencies occurring in the high voltage system.

1.5.2 The Theory of Waveform Symmetry of Derivatives of Current and Its Analysis

A waveform symmetry method is proposed based on comparing the symmetry of the first half waveform and the second half waveform of the current derivative. The main idea is that, in a time window of one

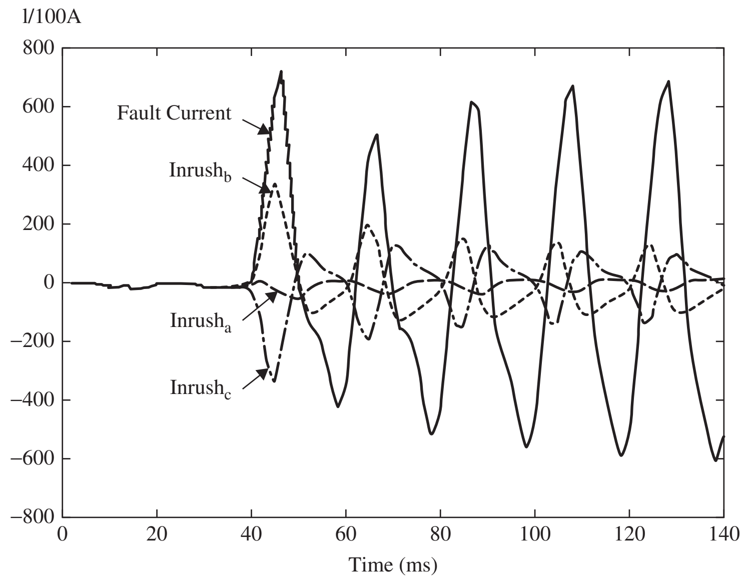

Figure 1.23 The waveform comparison between fault current and three-phase inrushes

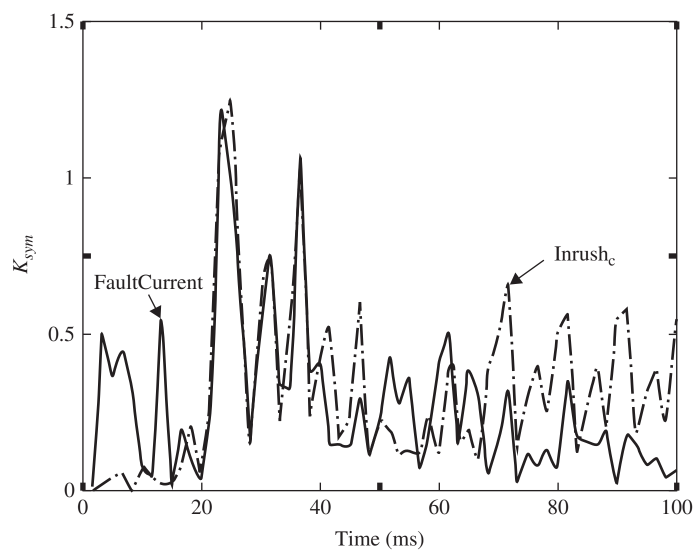

Figure 1.24 Change of K_{sym} with respect to the currents in Figure 1.23

cycle plus one point, the derivatives of differential current with one cycle time window are obtained using the forward differentiation operation. Then, the derivative series of the first half cycle are compared with that of the second half cycle. Denote the value of one point in first half cycle of derivative current as I'_i and denote the value of the second half as $I'_{i+180°}$. If the value satisfies Equation (1.29), the waveform is

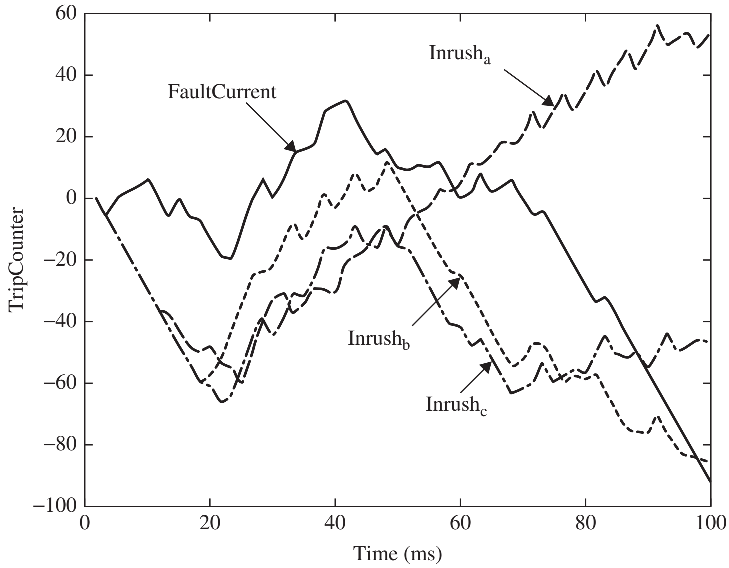

Figure 1.25 Change of Trip Counter with respect to K_{sym} in Figure 1.24

regarded as symmetrical. Otherwise, the waveform is asymmetrical.

$$\left|\frac{I'_i + I'_{i+180°}}{I'_i\text{-}I'_{i+180°}}\right| \le K_{sym} \tag{1.29}$$

It declares that in the whole half cycle (180°), the angle satisfying the inrush characteristic could reach as much as 60°, while that of the fault current could reach 150°.

Therefore, this scheme needs two setting values. One is the symmetrical factor K_{sym}, the other is symmetrical range K_{anlge}. If the sampling rate is N points per cycle, the symmetrical range can be expressed as

$$K_m = K_{angle} \times N/360 \tag{1.30}$$

Denote Equations (1.29) and (1.30) criteria 2, where K_m is relative, with the sampling points satisfying the symmetrical condition (1.29) in one cycle. For example, if the angle satisfying the symmetry condition at most is $K_{angle} = 60°$ and there are 12 sample points per cycle, $K_m = \mathrm{N}/6 = 2$. For the inrush current waveform, there are at least two points satisfying the symmetry condition.

The above analysis focuses on the primary side waveform of the inrush under a certain value of K_{sym}. If the setting value is set on the basis of secondary waveform of inrush current, K_{sym} should be reduced to guarantee the symmetry constraints of 60°. The symmetry range will be reduced under 150° with the reduced K_{sym}. Under some serious conditions, the time delay may be very long before the setting value of 60° is reached. This situation is analysed here.

Figure 1.26 shows the three phase magnetizing inrushes from the secondary side of CTs. The wiring type of $Y_0/\Delta - 11$ is applied in the transformer. The iron is Type-96 material, that is, the nonlinear inductance model with hysteresis loops. The saturation magnetic density is $B_s = 1.15B_m$, and residual magnetism of each phase $B_{ra} = 0.9B_m$, $B_{rb} = B_{rc} = -0.9B_m$. The inception angle is 30°. The B–H curve of the CT adopts the characteristic of a tangent, the sampling rate is 120 points per cycle.

The symmetry factor can be calculated after deriving the inrush waveform. For the scenario in Figure 1.26, the symmetry degrees of the first half and the second half waveform of the three phase

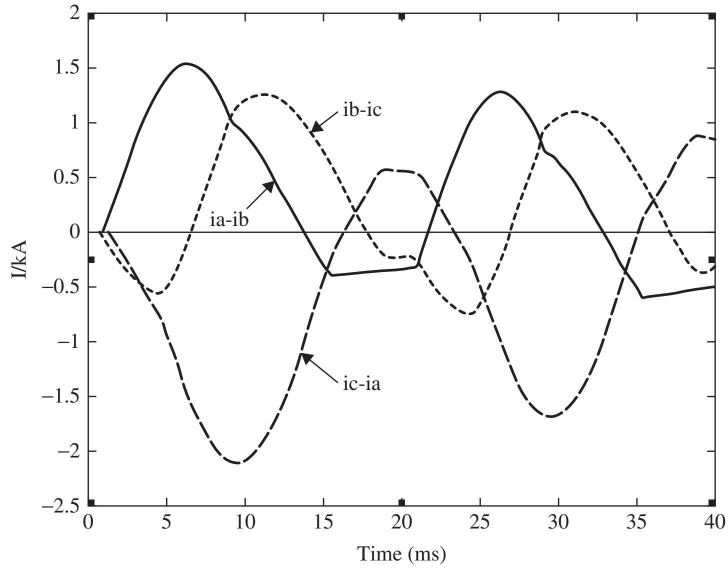

Figure 1.26 Three-phase magnetizing inrushes on the secondary side

Table 1.5 The relationship between waveform symmetrical coefficients and the number of sample points satisfying the symmetrical condition

K_{sym} I	0.10	0.11	0.12	0.13	0.14	0.15
I_{2a}	10	12	13	14	14	15
I_{2b}	7	8	8	9	9	10
I_{2c}	14	15	17	18	20	21

inrushes are all quite high. The number of points of the three-phase inrush current satisfying constrains of symmetry are calculated and shown in Table 1.5.

As shown in the table, in order to reach the requirements of inrush, which only have 60° symmetric range, the value of symmetric coefficient K_{sym} should not be too high. When K is equal to 0.15, the phase C secondary inrush has reached 21(63°). Evidently, in order to ensure that the symmetric range is not greater than 60°, the value of symmetric coefficient K_{sym} can only be taken as 0.15 if taking the secondary transforming into account. At this time, take the fault current in Figure 1.23 to analyse the tripping speed of this criterion. Choose $K_m = 2$, $K_{sym} = 0.15$, the fault current K_m is less than or equal to two in five cycles after the fault occurrence. In this case, the protection cannot trip. Increase K_{sym} gradually until K_{sym} is equal to 0.2. By this means, the fault current cannot lead to $K_m = 3 > 2$ until 93.3 ms after the fault occurrence. In this case, the protection will trip with a very long time delay. Thus, under low sampling rate conditions it is found that, to ensure that the mal-trip due to inrush is reliably blocked, there is no obvious advantage for this scheme compared with the second harmonic restraint principle. In the case of high harmonic content within the fault current, the protection would also trip with a long time delay.

Take K_{sym} as the basic symmetry coefficient and $K_m{*}K_{sym}$ as global setting value K'_{sym}. Improving K'_{sym} means that mal-operation may occur due to inrush, and reducing K'_{sym} makes the delay longer when the fault occurs.

There exists another implementation of this scheme, that is, let $S_{+} = \sum_{1}^{N/2} \left| I'_i + I'_{i+N/2} \right|$, $S_{-} = \sum_{1}^{N/2} \left| I'_i - I'_{i+N/2} \right|$, and therefore $K_{sym} = S_{+}/S_{-}$. When $K_{sym} > K_{symset}$, it will be judged as the inrush, otherwise it will be judged as the fault. The greater the value of K_{sym}, the higher the degree of asymmetry. This scheme is named criterion 3. The transformer protection adopting criterion 3 is produced by Nanzi and has been commissioned. For the true waveform, S_{+} is 0 and S_{-} is a positive real number. For the magnetizing inrush, no matter whether there is dead angle or not, S is always nonzero as long as the first half wave and the second half wave do not strictly satisfy the symmetry conditions ($S = S_{ti} = 0$ in Section 1.5.1). This scheme is similar to the percentage differential principle to some extent, among which S_{+} can be regarded as the differential quantity and S_{-} can be regarded as the restraint quantity. Furthermore, calculating the three-phase inrush symmetric coefficients in Figure 1.25 applying based on criterion 3, the values are 0.35, 0.53 and 0.21, respectively. In order to compare with criterion 2, taking $K_{symset} = 0.21$, the sensitivity is analysed based on the waveform in Figure 1.23.

At the beginning of the fault, K_{sym} is much greater than K_{symset}. Along with the attenuation of the harmonic with the differential current, K_{sym} continues to reduce. At the time of 98.3 ms post-fault, $K_{sym} = 0.20$, the protection trips while criterion 2 fails to trip. Obviously, any comparison should be conducted on the same basis. As shown in the above analysis, based on the waveform in Figure 1.26, and 60° as the maximum symmetry of the inrush (corresponding $K = 0.15$), in the case of Figure 1.23, criterion 1 fails to trip within five cycles after the fault occurrence. Only in the case of K increasing to 0.2, can criterion 1 operate with five cycles time delay. To facilitate the following comparison, criterion 1 will take the condition of $K_{sym} = 0.20$ in the following discussion. For the other criteria which take Figure 1.26 as the setting base, in order to compare with criterion 1 using $K_{sym} = 0.20$, the waveform symmetry coefficient must be adjusted correspondingly. Assume that the original waveform symmetry coefficient being set entirely based on Figure 1.22 is K'_{symset}, and the protection trips when waveform symmetry coefficient is less than the setting, the new setting value K_{symset} should be:

$$K_{symset} = K'_{symset} \times 0.20/0.15 \tag{1.31}$$

If the protection trips when the waveform symmetry coefficient is less than the setting, the new setting value K_{symset} should be:

$$K_{symset} = K'_{symset} \times 0.15/0.20 \tag{1.32}$$

After performing the above adjustments, the comparison between every new criterion and criterion 1 are taken under the same condition that the K_{symset} of the criterion is 0.2. Here, the above approach is used to maintain the same reliable discrimination margin for all criteria.

Therefore, increasing the K_{symset} of criterion 2 to $0.21 \times 0.2/0.15 = 0.28$, K_{sym} drops to 0.207 and the protection trips in 83.3 ms after the fault occurred. In this case the operating time of criterion 2 is 93.3 ms. Therefore, under the premise of the same sampling rate, criterion 3 is slightly better than criterion 2.

1.5.3 Principle and Analysis of the Waveform Correlation Method

The basic idea of the waveform analysis method to identify the inrush is to divide the waveform of one cycle data window into two parts using appropriate methods and compare the correlation of these two parts to identify the inrush and the fault current. The key problem of the wave correlation algorithm is how to determine these two waveforms. A so-called maximum area method is illustrated in Figure 1.27. One cycle sampling signal is extended to two periods. Intercept the half cycle signal point by point and calculate the projection area of this waveform on the time axis. Denote the sampling period as N points in one period, thus giving N values. The corresponding starting point of maximum area is taken as the start of waveform comparison (t = 5 ms) in Figure 1.27. One period sampling signal is intercepted from

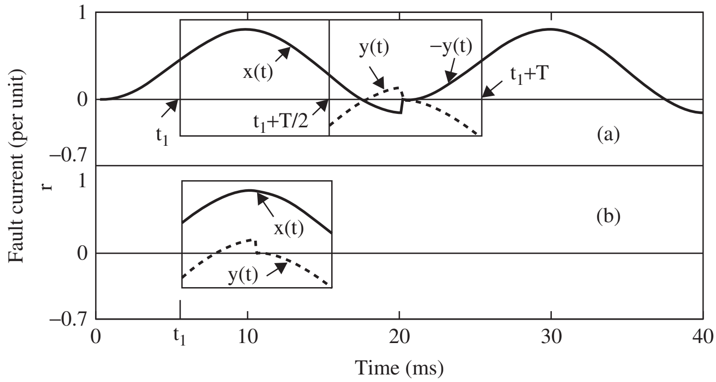

Figure 1.27 Internal fault current extended periodically

this point, as show in Figure 1.27 using major gridlines. The second half wave is reversed, that is, −y. The first half wave is x, then −y and x are compared using the modified waveform factor as given by Equation (1.33):

$$J = \frac{Cov(X, Y)}{\sigma^2(X)} \tag{1.33}$$

where $Cov(X, Y)$ is the covariance coefficient of X and Y, $\sigma^2(X)$ is the variance of x. Then, for the fault current that only contains the DC component, it is clear that waveform of the first half wave is completely consistent with that of the negative second half wave, that is, they are completely correlative ($J=1$). Reorganize the waveform of the inrush according to the above principle, its correlation between the first half wave and the second half wave becomes worse. Hereby, the inrush can be identified. The waveform correlation method is called criterion 4. Denote J_{set} as a fixed value. When the result is $J < J_{set}$, the current is regarded as inrush, otherwise it is fault current.

Correspondingly, the three-phase inrushes in Figure 1.26 are calculated using criterion 4, and the waveform factors are $J_{a\text{-}b} = 0.6513$, $J_{\text{b-c}} = 0.2107$ and $J_{\text{c-a}} = 0.8038$, respectively. Set the modified waveform factor as $J_{zd} = 0.80$ due to generally adopting phase-separating blocking, protection cannot trip until 95 ms after fault occurrence (4.75 periods). Comparing criterion 2 with criterion 3 in the same reliability margin, the setting value will be decreased to 0.6. Meanwhile, the fault will be tripped with a time delay of 60 ms, which is better than criteria 2 and 3, and the tripping speed is also faster than the second harmonic restraint criterion that has 15% restraint ratio (81.6 ms).

1.5.4 Analysis of Reliability and Sensitivity of Several Criteria

It can be seen from the analysis above that for criterion 3 the waveform is more symmetrical when the symmetrical coefficient is smaller. For criteria 2 and 4 the scenario is different. To investigate the maximum degree of the inrush to reach symmetrical condition and analyse the reliability of the criterion quantitatively during the practical energizing operation, sufficient switching-on experiments should be made. The symmetrical coefficient is calculated according to the recorded data. The minimum symmetrical coefficient should be used when criterion 3 is investigated, and the maximum waveform (symmetrical) coefficient should be calculated when criteria 2 and 4 are studied. In addition, the basic symmetrical coefficient K_{sym} should be determined firstly when calculating the symmetrical coefficient K'_{sym} in criterion 2. The inrush is still considered in the maximum symmetrical range of 60° (two sampling points in terms of 600 Hz sampling rate). It increased from 0.2 to K_{sym} gradually. When the inrush increases to 0.3, there

Table 1.6 The minimum ratios of second harmonic to fundamental in the case of some inrushes recorded by digital device and the corresponding

Inrush number	Min (I_2/I_1)(%)	Criterion 2 (J_{max})	Criterion 3 (J_{min})	Criterion 4 (J_{max})
1	47	0.58	0.65	0.5
2	56	0.58	0.54	0.5
3	46	0.58	0.65	0.5
4	43	0.58	0.55	0.55
5	58	0.58	0.58	0.55
6	39*	0.58	0.64	0.41
7	42	0.58	0.66	0.44
8	42	0.58	0.62	0.51
9	50	0.58	0.57	0.48
10	49	0.58	0.53	0.55

Waveform coefficients with criteria 2, 3 and 4 under the most adverse judging conditions.

are three sampling points of the inrush (Table 1.6) satisfying the symmetrical condition. Therefore, the largest basic symmetric coefficient that can be adopted as 0.29 in criterion 2, and the corresponding symmetric coefficient K'_{sym} is 0.58.

In Table 1.6, faults 1–4 are the transformer energizing without long line, faults 5–9 are the transformer energizing with long line. Fault 10 is the inrush current caused by the voltage recovery when the external fault is removed.

The minimum or maximum symmetric coefficient of each inrush is analysed during energizing in five cycles. To compare with the second harmonic restrained method, the proportion of second harmonic in three-phase inrushes and the fundamental harmonics are calculated point-by-point. The maximum value in three phases is taken as an element of the second harmonic restrained ratio sequence. Then the percentage of the second harmonic ratio for five cycles is calculated and the minimum value taken as the minimum second harmonic ratio of actual inrush. The analysis of 10 classical inrush groups is listed in Table 1.6.

It can be seen from the table that the minimum value of second harmonic ratio is 39% and the normal setting value is 15%. To ensure the same reliable discrimination margin, the setting value in criterion 2 should be the maximum value in the table and it should be divided by the coefficient 39/15. The setting value in criterion 3 should be the minimum value in the table and it should be divided by the coefficient 39/15. The setting value in criterion 4 should be the maximum value in the table and it should be multiplied by the coefficient 39/15. Then the operation times of criteria 2–4 are calculated respectively when the comparability to the second harmonic restrained method is guaranteed. The setting value for criterion 2 is 0.23, 0.204 for criterion 3 and 1.43 for criterion 4. The waveform coefficient is 1 when the waveform is completely correlated, the setting value in criterion can be taken as 0.8 as in the inrush current shown in Figure 1.26.

The classic faults of the transformer in Table 1.7 are analysed based on the above settings. The non-operation times of the second harmonic restrained method and criteria 2–4 are listed in Table 1.7.

Cases 1–18 in Table 1.7 are classic transformer faults and cases 19–27 are transformer energizing faults. Cases 1–4 represent phase B to ground fault. The operation condition is with load and long line, with load but without long line, without load but with long line, without load and long line, respectively. The following are studied by considering four cases as one group. Among them cases 5–8 are BC inter-phase short-circuit on the high voltage side; cases 9–12 are AB inter-phase short-circuit on the low voltage side; 13–16 are 4.38% inter-turn short-circuit, 17–18 are 2.18% inter-turn short-circuit. In faults 19–27, two situations are combined as one group. Cases 19 and 20 are B phase short-circuit

Table 1.7 Nonoperation times in milliseconds for the second harmonic restraint scheme and for criteria 2, 3 and 4 under typical fault conditions

Fault number	I_2/I_1 (ms)	Criterion 2 (ms)	Criterion 3 (ms)	Criterion 4 (ms)
1	81.6	NOP	NOP	95
2	60	93.3	75	68.3
3	58.3	83.3	61.6	46.6
4	18.3	31.6	18.3	18.3
5	93.3	NOP	NOP	48.3*
6	63.3	98.3	75	43.3
7	78.3	NOP	95	83.3
8	60	NOP	75	40
9	58.3	NOP	75	38.3
10	20	70	35	28.3
11	73	NOP	90	40*
12	58.3	NOP	70	36.6
13	31.6	33.3	31.6	30
14	31.6	33.3	31.6	31.6
15	20	21.6	21.6	18.3*
16	25	26.6	25	25
17	20	18.3	20	21.6
18	26.6	28.3	26.6	23.3
19	NOP	NOP	NOP	81.6
20	NOP	NOP	75	60
21	NOP	NOP	NOP	50
22	NOP	95	75	40
23	NOP	NOP	76.6	25*
24	NOP	96.6	71.6	40
25	NOP	31.6	26.6	25
26	NOP	45	26.6	25
27	NOP	26.6	20	23.3

NOP: nonoperation, that is, fail-to-trip.

accompanied by transformer energizing; cases 21 and 22 are inter-phase short-circuit between phase B and phase C on the high voltage side accompanied by transformer energizing; cases 23 and 24 are inter-phase shor-circuit between phase A and phase B on the low voltage side accompanied by transformer energizing; cases 25 and 26 are 4.38% inter-turn short-circuit accompanied by transformer energizing; case 27 is 2.18% inter-turn short-circuit without long line accompanied by transformer energizing.

Figure 1.28 illustrates the tripping times of 27 kinds of classic fault calculated by the second harmonic restrained method and by criteria 2–4. The abscissa shows fault number and the ordinate shows the tripping time. The threshold of protection fail-to-trip is set as 300 ms.

It can be seen by combining Table 1.7 and Figure 1.28 that:

1. The operation speeds are the same in the case of single-phase short-circuit and inter-turn short-circuit(1–4, 13–18).
2. The operation speed from slow to fast is: criterion 2 → criterion 3 → criterion 4 in the case of inter-phase short-circuit faults except the inter-phase short-circuit between phase B and phase C without load but with long line. And the performance of criterion 4 is the best.

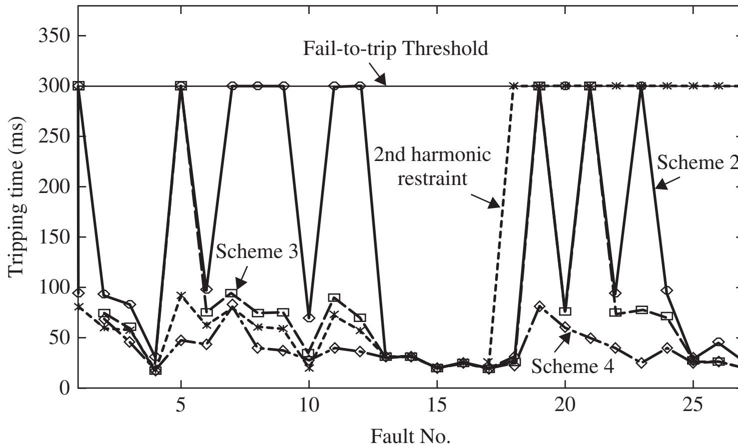

Figure 1.28 Non-operation time of scheme 2 to scheme 4 with the same reliability

3. The performance of criterion 4 is the best when the fault accompanied by transformer energizing occurs, it always can operate correctly. These always exist the scenarios of fail-to-trip for other criteria.
4. The operation speed is not ideal when the fault waveform distortion becomes bigger in the three criteria ($t > 90$ ms).

In summary, the three criteria by waveform symmetry principle for transformer differential protection, the reliability and sensitivity of the criteria are analysed. The Alternative Transients Program (ATP) is used to simulate the inrush scenario, which is critical to validate the waveform symmetry based methods so that the reliability of this type of method can be tested. The sensitivity is verified by the distorted fault current waveform resulting from the dynamic simulation experiment. It can be seen from the comparison that the sensitivity of criterion 4 is higher than that of the other two criteria when those criteria have the same reliability margin under the circumstances of transformer energizing and external fault removal. The faults can be tripped correctly even when the fault waveform distorts greatly or is accompanied by the transformer energizing. Criterion 2 and criterion 3 may fail to trip for some fault cases. Criterion 4 is the best among all waveform symmetry based methods. However, when the waveform is distorted seriously, the operation speed of criterion 4 is still slow. To achieve a better effect in large-scale transformer protection, existing methods should be further optimized.

1.6 Summary

With large capacity transformers being put into operation continuously, the demand for high reliability, rapidity and sensibility are on the increase. It is imperative to consummate transformer differential protection and bring forward novel transformer main protection schemes. In this section, various problems in current differential protection principles and inrush current blocking schemes have been studied and discussed. By comparative research, the development route of the transformer main protection technology is given.

References

[1] Wang, W.J. (2002) *Principles and Applications of Main Electrical Equipment Protection*, China Electric Power Press, Beijing.

[2] Guzman, A., Zochol, S., Benmouyal, G. *et al.* (2001) A current-based solution for transformer differential protection. Part I: problem statement. *IEEE Power Engineering Review*, **21** (8), 61.
[3] Saleh, S.A. and Rahman, M.A. (2005) Modeling and protection of a three-phase power transformer using wavelet packet transform. *IEEE Transactions on Power Delivery*, **20** (2), 1273–1282.
[4] Kasztenny, B. and Rosolowski, E. (2008) Modeling and protection of hexagonal phase-shifting transformers-part II: protection. *IEEE Transactions on Power Delivery*, **23** (3), 1351–1358.
[5] Sun, S., Fang, M. and Zhong, J. (2007) Development and design of 1000 kV autotransformer. *Electrical Equipment*, **4**, 002.
[6] Rahman, M.A. and Jeyasurya, B. (1988) A state-of-the-art review of transformer protection algorithms. *IEEE Transactions on Power Delivery*, **3** (2), 534–544.
[7] Guzman, A., Zocholl, S., Benmouyal, G. *et al.* (2002) A current-based solution for transformer differential protection. II. Relay description and evaluation. *IEEE Transactions on Power Delivery*, **17** (4), 886–893.
[8] Hayder, T., Schaerli, U., Feser, K. *et al.* (2008) Universal adaptive differential protection for regulating transformers. *IEEE Transactions on Power Delivery*, **23** (2), 568–575.
[9] Faiz, J. and Lotfi-Fard, S. (2006) A novel wavelet-based algorithm for discrimination of internal faults from magnetizing inrush currents in power transformers. *IEEE Transactions on Power Delivery*, **21** (4), 1989–1996.
[10] Polycarpou, M.M. and Helmicki, A.J. (1995) Automated fault detection and accommodation: a learning systems approach. *IEEE Transactions on Systems, Man, and Cybernetics*, **25** (11), 1447–1458.

2

Malfunction Mechanism Analysis due to Nonlinearity of Transformer Core

2.1 Introduction

Differential relay has served as the fast protection for transformers for many years [1]. However, it is prone to mal-operate in the presence of transformer inrush currents. The magnetizing inrush is a transient phenomenon that occurs primarily when a transformer is energized [2].

Various schemes have been proposed to address this problem. Most of them are the current-based methods, which fall into two groups: those using harmonics to restrain or block [3, 4] and those based on wave-shape identification [5].

All the methods mentioned above come from the following assumptions:

The transformer core is the nonlinear element that could partially saturate during energizing. In this case, the wave-shape of the inrush will be distorted from the sinusoidal waveform. The inrush occurs as the very low current in the linear transforming region whereas it occurs as the surge with high peak value in the saturation region. Meanwhile, the linear transformation dominates within each fundamental cycle.

The above claim originates from the analysis of unloaded transformer energizing. Actually, most existing theoretical analyses concerning power transformer energizing are based on the one order equivalent circuit suitable for the study of no-load transformer energizing. If so, the main flux consists of the steady-state flux and an exponentially decaying DC flux.

The core saturation and, therefore, the inrushes should be induced by this superimposed DC flux. In this case, the mal-operation of the differential protection due to inappropriate restraining ratio setting is supposed to occur at the very beginning of energizing, as the most severe saturation takes place at this moment. The saturation will fade with the decaying of the DC flux. Then the harmonics and the dwell-time of the low current of the inrush will increase accordingly. However, the above analysis cannot explain the mal-operation of differential protection highlighted in the next paragraph, which was reported on 19 December 2000, by HongXi substation, Chifeng city, Inner Mongolia province, China.

A loaded transformer switched on the system after a fault occurring on the transmission line was cleared. The differential protection using a 15% second harmonic restraining ratio and cross-blocking scheme was stable for the duration of the first five cycles after energizing. Afterwards, the differential protection operated although the transformer was proven to be healthy. The waveforms of the inrushes

Electromagnetic Transient Analysis and Novel Protective Relaying Techniques for Power Transformer,
First Edition. Xiangning Lin, Jing Ma, Qing Tian and Hanli Weng.

were not captured due to the limited buffer of the fault recorder. A satisfactory explanation has not been provided yet.

Moreover, some mal-operations of transformer differential protection during external fault clearance are reported each year by the East China and North China grid companies, several of them have operation time sequences similar to the above scenario. Several national meetings in China aimed at verifying the origin of such mal-operations have been held. However, no reasonable explanations have been reached until now.

For the purpose of studying this phenomenon and reinforcing the theory system of transformer transient analysis, a preliminary loaded transformer energizing model is put forward. Using this model, the delayed mal-operation of differential protection can be explained. What is more, the possible 'ultra-saturation' phenomenon during the loaded transformer energizing is revealed, which will result in the inevitable mal-operation during switching on of the loaded transformer.

Due to the nonlinearity of transformer core, the magnetizing inrush possibly occurs when a transformer is energized. In this case, the security of the differential protection will be challenged. To solve this problem, many criteria have been proposed to prevent differential protection from mal-operation due to inrush. Among these, second harmonic restraint criterion is the most prevalent [6–13]. The effectiveness of this criterion has been verified with significant industrial application in past decades. However, the stability of this protection is challenged due to the increase of the complexity and the time-changing operating modes of the power system, for example, the rapid increase of nonlinear industrial load. Therefore, a higher requirement for the transformer protection is required.

In recent years, several cases of abnormal mal-operation of transformer differential protection have been reported. For instance, three mal-tripping accidents of the differential protection of the #3 transformer in Qing-he Substation of Tie-ling Power Supply Company, Northeast China Power Grid, occurred in July and August 2001. The fault recorder showed that the differential protection did not trip instantaneously after a disturbance was detected. After a time delay of dozens of cycles tripping operation occurred but no fault was detected. The recorded bias current and differential current were intermediate but within the operating region. Also, the second harmonic ratio decreased to a value lower than threshold 15% from a quite high quantity, resulting in the differential protection failing to block. The reason has not been ascertained yet. However, according to the analysis related to the event records, all these mal-operation cases occurred during the course of the adjacent steelmaking furnace switching-in, and the differential protection adopted the second harmonic restraint principle.

It is known that in the above-mentioned cases the transformer was involved in the system with two nonlinear components, and experienced several switching operations. Therefore, the interaction between the electrical quantities complicates the analysis. Because the transformer contains not only electric circuits but also the core magnetic circuit, which is coupling with electric circuits, together with the introducing of the nonlinear load the interaction between the two nonlinear components may cause one or both of them to enter the extreme saturation state, which is accompanied by a complex electromagnetic transient course. To interpret this phenomenon reasonably, an accurate model should be established.

It was reported that there existed two types of abnormal mal-operation of transformer differential protection similar to the scenario described above. Both models established in these references are second order equivalent circuits and only include one nonlinear component. According to the existing analysis, the amplitude of the magnetizing inrush should be very high when the transformer experiences 'ultra-saturation state'. In this case, the protection will detect a quite high bias current and differential current, which does not coincide with the situation mentioned above. A phenomenon, named CT (current transformer) local transient saturation, resulting in a big measuring angle error and relative smooth waveform, was used to interpret the mal-operation of the protection. However, the CT local transient saturation results from the through current changing from a heavy fault current with a high value to a normal load current. This transition state is not applicable to the above scenario. According to the fault recorder, the currents on both sides of the transformer of the situation mentioned above were intermediate, which will not lead to CT transient saturation. Therefore, models in these two references are not suitable for illustrating the phenomenon mentioned.

Furthermore, few investigations have been conducted in discussing the transient course of transformer involved in the system with two nonlinear components. According to existing analysis, the sympathetic interaction between the transformers that takes place during the inrush transient is analysed on the basis of system configurations with transformers in parallel and in series. It is pointed out that the sympathetic interaction is triggered by the voltage drop across the system resistance produced by the inrush current. Furthermore, it may lead to the mal-operation of the transformer differential protection and cause temporary harmonic overvoltages. It is reported that the phenomenon of sympathetic inrush current in the cases of the transformers connected in parallel and in series is investigated using nonlinear-transient field-circuit coupled finite element formulation. The study of factors affecting the magnitude and duration of the sympathetic inrush current is also presented. However, the initial conditions leading to the phenomenon mentioned above cannot be located by virtue of modelling and analyses in the above-mentioned references. Here the equivalent model is described by means of the analytic method and the problem solved by using the numerical analysis method. In this case, the qualitative and quantitative analyses results of the flux linkage and inrush can be obtained in order to disclose the real causes of the mal-operation of the transformer differential protection.

Therefore, a model for analysing the transient course of the nonlinear load switching-in to a system with a power transformer is proposed. The characteristics of the saturation of transformer core and the nonlinear load are taken into account in this model. Together with the analytic and numerical analyses, the waveform characteristics of the inrushes are analysed. On the basis of the analyses of the transient characteristics of the inrushes, the reason that second harmonic restraint criterion fails to block the transformer differential protection during nonlinear load switching-in be explained rationally.

The magnetizing inrushes possibly occur when a transformer is energized or an external fault isolated. In this case, the security of the differential protection will be challenged. Therefore, many criteria have been proposed to prevent differential protection from mal-operation. Among these, second harmonic restraint criterion is the most prevalent. The effectiveness of this criterion has been verified with significant industrial applications in past decades. However, some differential protections equipped with second harmonic restraint mal-operate under some abnormal disturbances or operations. For instance, some mal-operations of the transformer differential protections due to the removal of external fault have been reported recently.

The data from the field fault recorder disclose this sort of unusual mal-operation. One of the cases is shown in Figure 2.1. The operating point is located at the nonrestraint region in the percentage biased characteristic plane, and the operating current was only somewhat higher than the threshold. In this case, the second harmonic component within the differential current is too low (6%) to block the differential protection. Therefore, the occurrence of mal-operation is inevitable.

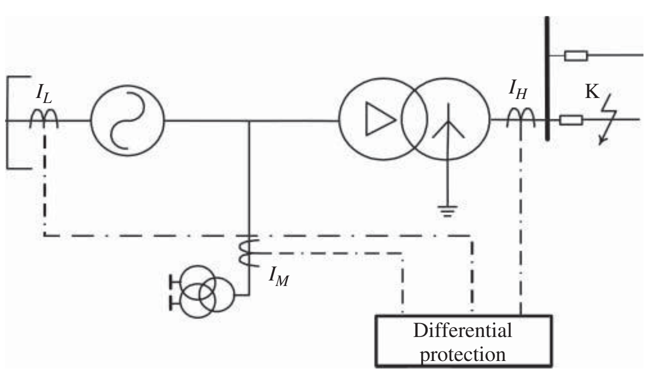

Figure 2.1 The connection of a generator and transformer unit corresponding to a case of mal-operation of differential protection due to removal of an external fault

Conventionally, there are two chief causes responsible for the mal-operation of transformer differential protection, namely, the magnetizing inrush with high amplitude caused by the nonlinearity of transformer core and the CT transient saturation caused by the high fault current. The reasons of inrush emergence due to the transformer switching-in, including a loaded transformer switching-in, and removal of serious external fault are essentially the same, namely the sudden rise of the terminal voltage of power transformer. A concept named as the 'ultra-saturation state' is put forward to explain the mal-operation of differential protection with second harmonic restraint due to a loaded transformer switching-in. However, according to the existing analysis, the amplitude of the magnetizing inrush should be very high when the transformer experiences the 'ultra-saturation state'. In this case, the protection will detect a quite high biased current, a high operating current and low second harmonic of differential current; it therefore mal-operates at the biased operation region. Similarly, in the case of the CT transient saturation caused by the high through-fault current, the false differential current and corresponding biased current are both high in the event of mal-operation of the transformer differential protection. Obviously, these two point of views are not suitable to explain scenarios illustrated in Figure 2.2. Therefore, a mathematic model for analysing the transient course including inception and isolation of an external fault, together with the CT model involving the magnetic hysteresis effect, is proposed. On the basis of detailed analysis, a novel explanation for this sort of mal-operation of transformer differential protection is disclosed.

High voltage direct current (HVDC) transmission possesses many advantages that alternating current (AC) transmission cannot achieve. Therefore, it is extensively applied in power systems gradually. As the most important equipment in converting stations, the converter transformer plays a very vital role and its protection is extremely important to the normal operation of the whole system.

The principal discussion of the transformer differential protection has, for a long time, mainly concentrated on how to discriminate between magnetizing inrushes and internal faults. Many criteria have been proposed to prevent the transformer differential protection from mal-operation caused by the magnetizing inrush. Among these the second harmonic restraint criterion is the most prevalent; it can be used to effectively discriminate between magnetizing inrushes and fault currents. However, even though the differential protection of the converter transformer is equipped with second harmonic restraint function, some instances of mal-operations caused by magnetizing inrushes during transformer energizing still occur. For example, a case was reported by Tianguang HVDC transmission system in China on 28 January 2007. During the course of manipulating pole 1 from the stand-by state to the blocking state,

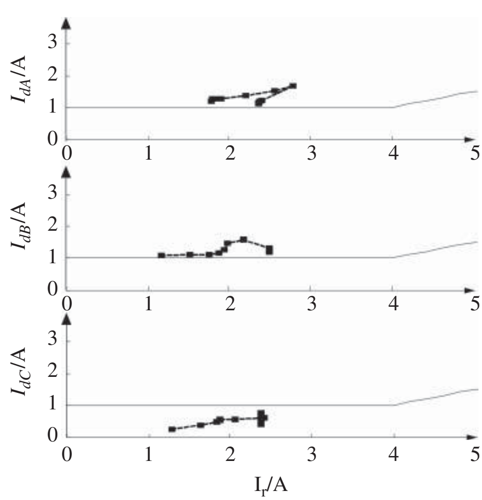

Figure 2.2 Operation analysis of differential protection on the operation plane

the differential protection of the converter transformer on pole 1 mal-operated and the circuit breaker was opened after the converter transformer was energized. According to the subsequence of event (SOE), it is a typical mal-operation of the differential protection of the converter transformer resulting from the magnetizing inrush. The mal-operation of the second harmonic restraint based transformer protection postponed the restoration of the HVDC transmission system. By virtue of the phenomenon of above field report and the characteristics of converting stations, it is conjectured that the inrush waveform of the converter transformer may change compared to that of the conventional transformer, owing to the existence of AC and DC filters in addition to the influence of the core saturation. In this case, the second harmonic characteristic may be impaired and it is much easier for mal-operation of the converter transformer to occur. This point of view is verified by the simulation analyses in the following.

On the other hand, due to the particularity of the operating environment of the converter transformer, the differential current may contain a quite high second harmonic component in the case of asymmetric internal faults. It is guessed that by virtue of the interaction between AC and DC systems, the negative sequence component in the AC voltage may produce the second harmonic component in the AC power network side of converting valves, which may consequently result in the unnecessary blocking of the differential protection. However, this assumption has not been verified by tests. All in all, it is still necessary to further verify the effectiveness of the second harmonic restraint criterion applied to the differential protection for the converter transformer in the HVDC system.

The models of unloaded energizing and internal faults of the converter transformer are established by virtue of the HVDC benchmark test system I of CIGRE (the International Council on Large Electric Systems). Based on these models, the characteristics of the differential currents during unloaded transformer energizing and internal faults are analysed. Furthermore, the operation performance of the second harmonic restraint based differential protection for the converter transformer is evaluated. By virtue of simulation analyses based on EMTDC software, it can be confirmed that the second harmonic restraint criterion is not completely appropriate when it is applied to the differential protection for the converter transformer. For the purpose of achieving reliable protection for the converter transformer, a novel criterion using the time difference between the superimposed phase voltage and differential current to discriminate between magnetizing inrushes and fault currents is proposed. The effectiveness of the proposed criterion is validated with extensive simulation tests.

2.2 The Ultra-Saturation Phenomenon of Loaded Transformer Energizing and its Impacts on Differential Protection

2.2.1 Loaded Transformer Energizing Model Based on Second Order Equivalent Circuit

2.2.1.1 Energizing of the Single-Phase Transformer

The model of single-phase loaded transformer energizing can be described as a second-order equivalent circuit illustrated by Figure 2.3, where U_s is the EMF of the source, L_1 and R_1 are the inductive and the resistive components of the equivalent impedance comprising of system impedance and leakage impedance of transformer primary winding, and R_2 and L_2 denote the total loop resistance and inductance of the secondary side of the transformer. The magnetizing branch is represented by an equivalent inductance, L_μ, if the iron loss is neglected. Based on Figure 2.3, the loop equation set can be given by

$$\begin{cases} R_1 i_1(t) + L_1 \dfrac{di_1(t)}{dt} + \dfrac{d\psi(t)}{dt} = U_s(t) \\ i_1(t) = i_2(t) + i_\mu(t) \\ \dfrac{d\psi(t)}{dt} = R_2 i_2(t) + L_2 \dfrac{di_2(t)}{dt} \end{cases} \tag{2.1}$$

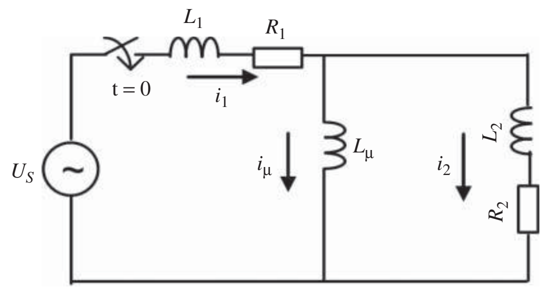

Figure 2.3 Circuit model for analysing the transient phenomenon when switching on a loaded transformer

Eliminating i_1 and i_2, Equation (2.1) can be deduced to be:

$$(L_1 + L_2)\frac{d^2\psi(t)}{dt^2} + (R_1 + R_2)\frac{d\psi(t)}{dt} + L_1L_2\frac{d^2 i_\mu(t)}{dt^2} +$$
$$(L_1R_2 + R_1L_2)\frac{di_\mu(t)}{dt} + R_1R_2 i_\mu(t) = L_2\frac{dU_s(t)}{dt} + R_2U_s(t) \tag{2.2}$$

Equation (2.2) is difficult to solve due to the existence of the second derivative term of $i_\mu(t)$ and the nonlinear relationship between $\psi(t)$ and $i_\mu(t)$. There is no harm to set $L_2 = 0$, that is, the load of the transformer is resistive; therefore:

$$\frac{L_1}{R_2}\frac{d^2\psi(t)}{dt^2} + \left(1 + \frac{R_1}{R_2}\right)\frac{d\psi(t)}{dt} + L_1\frac{di_\mu(t)}{dt} + R_1 i_\mu(t) = U_s(t) \tag{2.3}$$

$L_1\frac{di_\mu(t)}{dt} + R_1 i_\mu(t)$ can be regarded as the equivalent voltage drop, which is produced by the inrush $i_\mu(t)$ and acts on the system impedance. This equivalent voltage should be smaller than the real voltage drop $L_1\frac{di_1(t)}{dt} + R_1 i_1(t)$ since $i_\mu(t)$ is part of $i_1(t)$. Also, $L_1\frac{di_1(t)}{dt} + R_1 i_1(t)$ is much smaller than $\frac{d\psi}{dt}$. As a consequence, $L_1\frac{di_\mu(t)}{dt} + R_1 i_\mu(t)$ is small enough compared with $\frac{d\psi}{dt}$.

Based on the above analysis, a virtual equivalent constant reactance, $L_{\mu v}$, can be introduced as follows:

$$i_\mu(t) = \frac{\psi(t)}{L_{\mu v}} \tag{2.4}$$

The simplified $i_\mu(t)$ depicted by Equation (2.4) is capable of producing the average voltage drop equivalent to $L_1\frac{di_\mu(t)}{dt} + R_1 i_\mu(t)$ in a certain time duration. As analysed above, this simplification will not cause obvious unbalance of Equation (2.3) according to the comparison between $L_1\frac{di_\mu(t)}{dt} + R_1 i_\mu(t)$ and $\frac{d\psi}{dt}$.

Using Laplace's transformation and differential theorem, Equation (2.3), can be represented by:

$$\frac{L_1}{R_2}[s^2\psi(s) - s\psi(0) - \psi'(0)] + \left(1 + \frac{R_1}{R_2}\right)[s\psi(s) - \psi(0)] + L_1[sI_\mu(s) - I_\mu(0)] + R_1 I_\mu(s) = U_s(s) \tag{2.5}$$

$\psi(0)$ should be equal to the remnant flux ψ_r. In addition, $\psi'(0) = 0$, $I_\mu(0) = 0$. Combined with Equation (2.4):

$$\frac{L_1}{R_2}s^2\psi(s) + \left(1 + \frac{R_1}{R_2}\right)s\psi(s) + L_1 s\frac{\psi(s)}{L_{\mu v}} + R_1\frac{\psi(s)}{L_{\mu v}} = U_s(s) + \frac{sL_1 + R_1 + R_2}{R_2}\psi_r \tag{2.6}$$

that is:

$$s^2\psi(s) + \left(\frac{R_1 + R_2}{L_1} + \frac{R_2}{L_{\mu v}}\right) s\psi(s) + \frac{R_1R_2}{L_1L_{\mu v}}\psi(s) = \frac{R_2}{L_1}U_s(s) + \left(s + \frac{R_1 + R_2}{L_1}\right)\psi_r \tag{2.7}$$

Equation (2.7) can be expressed as:

$$\left(s + \frac{1}{T_1}\right)\left(s + \frac{1}{T_2}\right)\psi(s) = \frac{K_R}{T_0}U_s(s) + \left[s + \frac{1}{T_0}\left(1 + K_R\right)\right]\psi_r \tag{2.8}$$

among which, $K_R = \frac{R_2}{R_1}$, $T_0 = \frac{L_1}{R_1}$.

In addition, Equations (2.9) and (2.10) can be given as:

$$\frac{1}{T_1} = \frac{1}{T_0} \times \frac{1 + K_R + \dfrac{K_R}{K_L} + \sqrt{(1 + K_R)^2 + \left(\dfrac{K_R}{K_L}\right)^2 - \dfrac{2K_R(1 - K_R)}{K_L}}}{2} \tag{2.9}$$

$$\frac{1}{T_2} = \frac{1}{T_0} \times \frac{1 + K_R + \dfrac{K_R}{K_L} - \sqrt{(1 + K_R)^2 + \left(\dfrac{K_R}{K_L}\right)^2 - \dfrac{2K_R(1 - K_R)}{K_L}}}{2} \tag{2.10}$$

if letting $K_L = \frac{L_{\mu v}}{L_1}$.

Suppose the EMF of the source is:

$$U_s(t) = U_m \sin(\omega t + \alpha)u(t) \tag{2.11}$$

Laplace's transformation of Equation (2.11) is, therefore, given by:

$$U_s(s) = \frac{s\sin\alpha + \omega\cos\alpha}{s^2 + \omega^2} \tag{2.12}$$

Substituting Equation (2.12) into Equation (2.8) and performing the inverse Laplace's transformation, the time-domain expression of the flux link can be given by:

$$\psi(t) = \psi_0(t) + \psi_1(t) + \psi_2(t) = \psi_{0m}\sin(\omega t + \alpha - \delta_0) - \psi_{1m}e^{-t/T_1} + \psi_{2m}e^{-t/T_2} \tag{2.13}$$

among which,

$$\psi_{0m} = \frac{K_R}{T_0\sqrt{\left(\omega^2 + \dfrac{1}{T_1^2}\right)\left(\omega^2 + \dfrac{1}{T_2^2}\right)}}U_m \tag{2.14}$$

$$\delta_0 = tg^{-1}\frac{\omega(T_1 + T_2)}{1 - \omega^2 T_1 T_2} \tag{2.15}$$

$$\psi_{1m} = \frac{\psi_{0m}\sqrt{\omega^2 + \dfrac{1}{T_2^2}}\sin(\delta_1 - \alpha) - \left[\dfrac{1}{T_1} - \dfrac{1}{T_0}\left(1 + K_R\right)\right]\psi_r}{\left(\dfrac{1}{T_1} - \dfrac{1}{T_2}\right)} \tag{2.16}$$

$$\psi_{2m} = \frac{\psi_{0m}\sqrt{\omega^2 + \dfrac{1}{T_1^2}}\sin(\delta_2 - \alpha) - \left[\dfrac{1}{T_2} - \dfrac{1}{T_0}\left(1 + K_R\right)\right]\psi_r}{\left(\dfrac{1}{T_1} - \dfrac{1}{T_2}\right)} \tag{2.17}$$

$$\delta_1 = tg^{-1}\omega T_1,\ \delta_2 = tg^{-1}\omega T_2 \tag{2.18}$$

As seen in Equation (2.13), the main flux comprises of a steady-state flux and two exponential decaying DC fluxes. Among them, a DC offset decays exponentially with time constant T_1 whereas the other decays with time constant T_2. Both time constants are related to the parameters of primary side and secondary side apart from the parameters of transformer core.

As seen in Equations (2.16) and (2.17), ψ_{m1} and ψ_{m2} are all possibly much greater than ψ_{m0} when the system parameters satisfy certain conditions. Meanwhile, the time constants T_1 and T_2 are possibly big but different. In this case, these two transient fluxes may offset each other at the beginning of energizing if ψ_{m1} has the approximate magnitude and same sign when compared with ψ_{m2}. In this moment, the main flux should be within the linear transforming region and no inrush occurs. Thereafter, the main flux will experience three successive statuses, that is, nonsaturation only, the alternate occurrence between nonsaturation and saturation, and ultra-saturation (where the term ‘ultra-saturation’ is used to describe such a phenomenon that no dead angle occur within a complete cycle of the inrush). The transformer possibly stays at the ultra-saturation region for a period of time if T_2 is quite big. Only if all the DC offsets decay thoroughly can the core revert to the linear transforming region. The inrush will, however, lose characteristics such as the dead angle and high percentage of second harmonics ratio during the period of ultra-saturation. The differential protections that take advantage of the features the inrush waveform abnormity, for example, the asymmetry, dead angle, harmonic or the flux change between saturation and nonsaturation, as their blocking schemes will lose the stability.

2.2.1.2 Energizing of the Three-Phase Transformer

In this section the scenarios of the energizing of the three-phase transformer are discussed. Generally, energizing the transformer mainly originates from two aspects: the clearance of external faults and switching on the system. As a whole, the external faults of the transformer are mostly single-phase grounded ones and the voltages of the healthy phases are only subject to a small change during the external fault or after clearance of the fault. Therefore, most scenarios for mal-operation of the differential protection due to the clearance of external fault can be explained using the aforementioned theory with regard to single-phase loaded transformer energizing. Admittedly, most three-phase transformers adopt Y/Δ-connection so that the differential currents should occur on two of the three phases. Both inrushes, however, have the same wave-shape characteristic, since they are actually generated by the same inrush.

The more complicated scenario is the switching on of the loaded three-phase transformer. In general, the inception angles of the three-phase driving voltages should be balanced if the circuit breakers are closed reliably in the same time. However, the inception angles may deviate slightly from the balanced condition due to the diversity of the switching-on scenarios. Taking the universal scenarios into account, there is no harm to suppose the expected inception time instant be $t = 0$ and the expected inception angle be α, while the inception time instant of reliable connection is $t = t_0$. Hence, the driving voltage during energizing will be:

$$U_s(t) = U_m \sin(\omega t + \alpha) u(t - t_0) \tag{2.19}$$

Performing the coordinate transformation to the time axis:

$$t' = t - t_0 \tag{2.20}$$

The driving voltage can be expressed as:

$$U_s(t') = U_m \sin[\omega t' + \alpha + \omega t_0] u(t') \tag{2.21}$$

The inception angle should be $\alpha + \omega t_0$ actually.

Substituting Equation (2.21) into Equation (2.3) and following the same equation-solving strategy as above, the main flux can be evaluated by

$$\begin{aligned}\psi(t') = \psi_0(t') + \psi_1(t') + \psi_2(t') &= \psi_{0m} \sin[\omega t' + \alpha + \omega t_0 - \delta_0] u(t') \\ &\quad - \psi'_{1m} e^{-t'/T_1} u(t') + \psi'_{2m} e^{-t'/T_2} u(t')\end{aligned} \tag{2.22}$$

where T_1, T_2 and the amplitude of the steady state are still the same as those in Equations (2.9), (2.10), and (2.14). The peak values of the transient fluxes are given by:

$$\psi'_{1m} = \frac{\psi_{0m}\sqrt{\omega^2 + \frac{1}{T_2^2}}\sin(\delta_1 - \alpha - \omega t_0) - \left[\frac{1}{T_1} - \frac{1}{T_0}\left(1 + K_R\right)\right]\psi_r}{\left(\frac{1}{T_1} - \frac{1}{T_2}\right)} \tag{2.23}$$

$$\psi'_{2m} = \frac{\psi_{0m}\sqrt{\omega^2 + \frac{1}{T_1^2}}\sin(\delta_2 - \alpha - \omega t_0) - \left[\frac{1}{T_2} - \frac{1}{T_0}\left(1 + K_R\right)\right]\psi_r}{\left(\frac{1}{T_1} - \frac{1}{T_2}\right)} \tag{2.24}$$

where T_0 and K_R are the same as those in Equations (2.9) and (2.10), and δ_1 and δ_2 are the same as those in Equation (2.18). Substituting Equation (2.20) into Equation (2.22) gives:

$$\begin{aligned}\psi(t) &= \psi_0(t) + \psi_1(t) + \psi_2(t)\\ &= \psi_{0m}\sin(\omega t + \alpha - \delta_0)u(t - t_0) - \psi'_{1m}e^{-(t-t_0)/T_1}u(t - t_0) + \psi'_{2m}e^{-(t-t_0)/T_2}u(t - t_0)\end{aligned} \tag{2.25}$$

On the basis of the above analysis, assume phase A of the transformer closing at t = 0, phase B closing at $t = t_b$ and phase C closing at $t = t_c$. The driving voltages of three phases should be:

$$\begin{cases} U_a(t) = U_m\ \sin(\omega t + \alpha)u(t)\\ U_b(t) = U_m\ \sin(\omega t + \alpha - 120^\circ)u(t - t_b)\\ U_c(t) = U_m\ \sin(\omega t + \alpha + 120^\circ)u(t - t_c)\end{cases} \tag{2.26}$$

With these driving voltages and the same equation-solving strategy, the main fluxes of three phases can be deduced from Equation (2.27); the amplitudes of the fluxes are shown in Equations (2.28) and (2.29). Note that the residual fluxes in Equations (2.28) and (2.29) are denoted by the residual flux of each phase, that is ψ_{ra}, ψ_{rb} and ψ_{rc}.

$$\begin{cases} \psi_a(t) = \psi_{0a}(t) + \psi_{1a}(t) + \psi_{2a}(t) = \psi_{0m}\ \sin(\omega t + \alpha_a - \delta_0)u(t) - \psi'_{1ma}e^{-t/T_1}u(t) + \psi'_{2ma}e^{-t/T_2}u(t)\\ \psi_b(t) = \psi_{0b}(t) + \psi_{1b}(t) + \psi_{2b}(t)\\ \qquad = \psi_{0m}\sin(\omega t + \alpha_b - \delta_0)u(t - t_b) - \psi'_{1mb}e^{-(t-t_b)/T_1}u(t - t_b) + \psi'_{2mb}e^{-(t-t_b)/T_2}u(t - t_b)\\ \psi_c(t) = \psi_{0c}(t) + \psi_{1c}(t) + \psi_{2c}(t)\\ \qquad = \psi_{0m}\sin(\omega t + \alpha_c - \delta_0)u(t - t_c) - \psi'_{1mc}e^{-(t-t_c)/T_1}u(t - t_c) + \psi'_{2mc}e^{-(t-t_c)/T_2}u(t - t_c)\end{cases} \tag{2.27}$$

where

$$\begin{cases} \psi'_{1ma} = \dfrac{\psi_{0m}\sqrt{\omega^2 + \frac{1}{T_2^2}}\sin\left(\delta_1 - \alpha_a\right) - \left[\frac{1}{T_1} - \frac{1}{T_0}\left(1 + K_R\right)\right]\psi_{ra}}{\left(\frac{1}{T_1} - \frac{1}{T_2}\right)}\\ \psi'_{1mb} = \dfrac{\psi_{0m}\sqrt{\omega^2 + \frac{1}{T_2^2}}\sin(\delta_1 - \alpha_b - \omega t_b) - \left[\frac{1}{T_1} - \frac{1}{T_0}\left(1 + K_R\right)\right]\psi_{rb}}{\left(\frac{1}{T_1} - \frac{1}{T_2}\right)}\\ \psi'_{1mc} = \dfrac{\psi_{0m}\sqrt{\omega^2 + \frac{1}{T_2^2}}\sin(\delta_1 - \alpha_c - \omega t_c) - \left[\frac{1}{T_1} - \frac{1}{T_0}\left(1 + K_R\right)\right]\psi_{rc}}{\left(\frac{1}{T_1} - \frac{1}{T_2}\right)}\end{cases} \tag{2.28}$$

$$\begin{cases} \psi'_{2ma} = \dfrac{\psi_{0m}\sqrt{\omega^2 + \dfrac{1}{T_1^2}}\sin\left(\delta_2 - \alpha_a\right) - \left[\dfrac{1}{T_2} - \dfrac{1}{T_0}\left(1 + K_R\right)\right]\psi_{ra}}{\left(\dfrac{1}{T_1} - \dfrac{1}{T_2}\right)} \\ \psi'_{2mb} = \dfrac{\psi_{0m}\sqrt{\omega^2 + \dfrac{1}{T_1^2}}\sin(\delta_2 - \alpha_b - \omega t_b) - \left[\dfrac{1}{T_2} - \dfrac{1}{T_0}\left(1 + K_R\right)\right]\psi_{rb}}{\left(\dfrac{1}{T_1} - \dfrac{1}{T_2}\right)} \\ \psi'_{2mc} = \dfrac{\psi_{0m}\sqrt{\omega^2 + \dfrac{1}{T_1^2}}\sin(\delta_2 - \alpha_c - \omega t_c) - \left[\dfrac{1}{T_2} - \dfrac{1}{T_0}\left(1 + K_R\right)\right]\psi_{rc}}{\left(\dfrac{1}{T_1} - \dfrac{1}{T_2}\right)} \end{cases} \tag{2.29}$$

$$\alpha_a = \alpha,\ \alpha_b = \alpha - \frac{2}{3}\pi,\ \alpha_c = \alpha + \frac{2}{3}\pi \tag{2.30}$$

With the above flux expressions, the inrush of each phase can be evaluated. Thereafter, the actual differential current, that is the difference between two phase inrushes in the case of the Y/Δ-connection of the three-phase transformer windings, are available accordingly.

2.2.2 *Preliminary Simulation Studies*

The appropriate depiction of the magnetizing curve of the transformer core is crucial for the simulation. The accurate saturation curve should be depicted as a multivalue curve if taking the hysteresis into account. However, it is believed that the accuracy of saturation curve will not affect the approximate shape of inrush waveform, for example, the peak value of the surge and the dead angle too much. In this sense, the magnetization curve can be simplified to be a broken line comprising of three lines, as illustrated in Figure 2.4. The harmonics content and dead angle of the inrush investigated with this core model should still be believable.

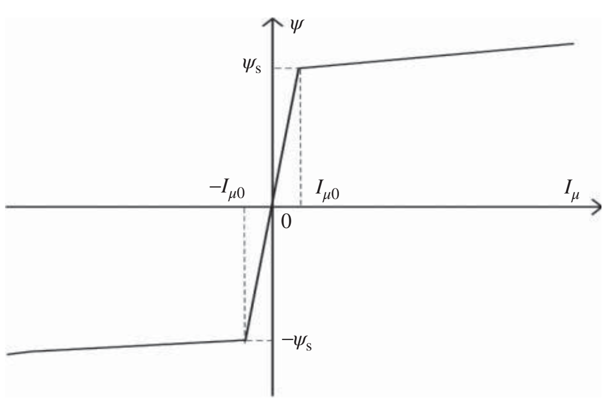

Figure 2.4 Simplified saturation characteristic of the transformer core

2.2.2.1 Energizing of the Single-Phase Transformer

A variety of simulations have been carried out to investigate the delayed mal-operation of the protection and the ultra-saturation of the core. Two cases (Scenarios 2.1 and 2.2) are given in terms of the illustrations. In addition, some typical scenarios are presented in terms of tables.

Scenario 2.1 Protection mal-operation due to ultra-saturation case A
$T_1 = 0.055$ s, $T_2 = 90$ s, $\psi_s = 1.2$ p.u., $\psi_r = 0.0$ per unit (p.u.), inception angle $\alpha = 82°$. In this case, $\psi_{1m} = 1.41$, $\psi_{2m} = 2.40$.

With this arrangement, the ultra-saturation of the transformer can be retrieved.

The flux waveform within 20 cycles of post-energizing is presented in Figure 2.5 and the corresponding magnetizing inrush waveform is illustrated in Figure 2.6. As seen in Figure 2.5, the instantaneous main flux rises from 0 to a quite high offset level in several cycles after the transformer is switched on. As the energizing time exceeds 0.2 s, the instantaneous flux is completely lifted beyond the saturation point and stays at the saturation area for several cycles. Accordingly, the surges of the inrush in Figure 2.6 will occur consecutively but no dead angle exists between two surges anymore.

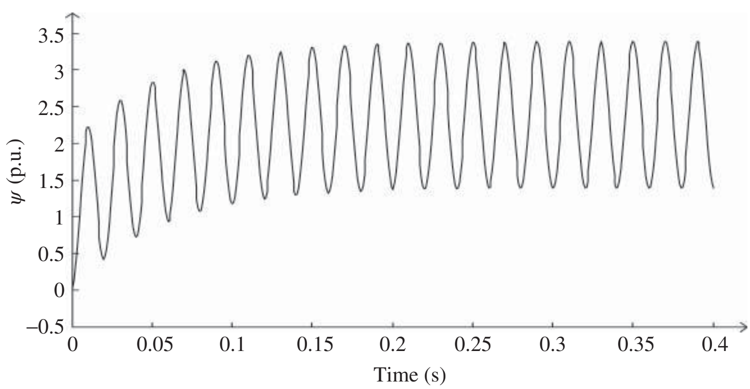

Figure 2.5 The changing flux curve with respect to the time after switching on the transformer

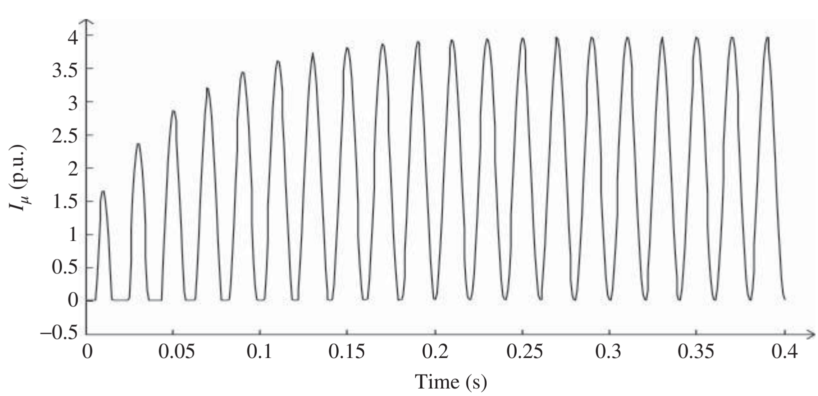

Figure 2.6 The changing inrush curve with respect to the time after switching on the transformer

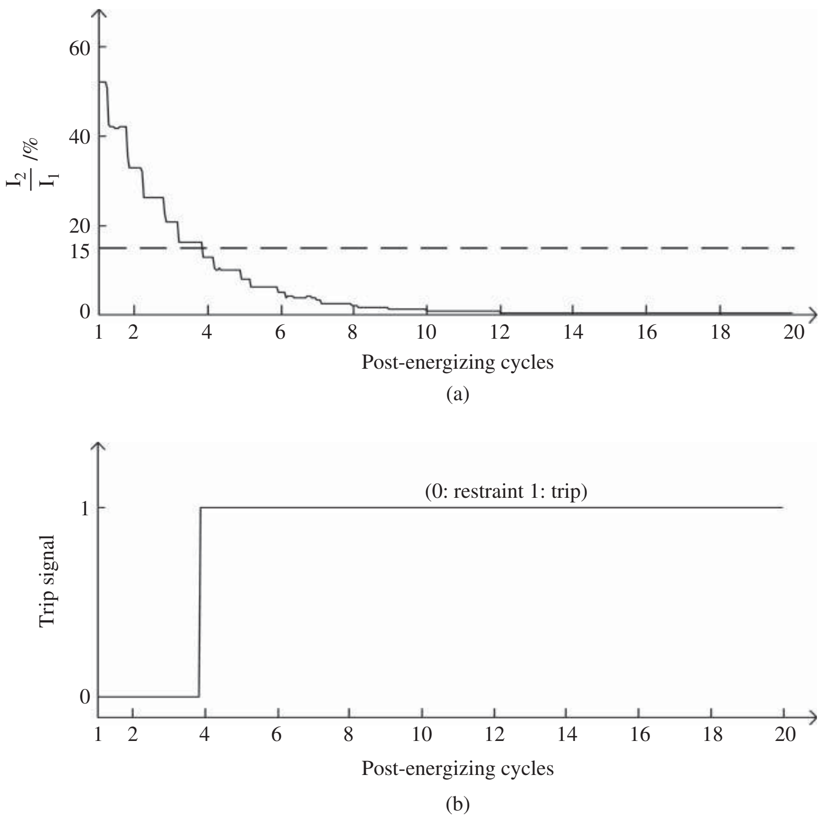

Figure 2.7 (a) The changing curve of the ratio between second harmonic and fundamental with respect to the cycles after switching on the transformer and (b) the response of the relay using 15% second harmonics restraint

Figure 2.7 shows the ratio change of second harmonic to fundamental of the inrush in Figure 2.6 analysed with the differential DFT (Discrete Fourier Transform) algorithm. The relay response is presented as well.

As seen in Figure 2.7a, the second harmonic ratio is at a maximum immediately after energizing. Afterwards, the second harmonic content decreases gradually. Approximately four cycles after switching on, the ratio of second harmonic becomes lower than 15%. Therefore, differential protection using 15% as the restraint ratio will trip by mistake. Additionally, the second harmonic content will nearly decrease to zero 10 cycles after energizing. This status is called 'ultra-saturation'. As seen, both the delayed mal-operation of differential protection during transformer energizing and ultra-saturation can be explained using this new model.

Scenario 2.2 Protection mal-operation due to ultra-saturation case B
$T_1 = 0.055$ s, $T_2 = 0.9$ s, $\psi_s = 1.2$ p.u., $\psi_r = -0.25$ p.u, $\alpha = 82°$. In this case, $\psi_{1m} = 1.56$, $\psi_{2m} = 2.31$.

The flux, inrush waveform and the ratio change of second harmonic to fundamental together with the response of the relay using 15% restraint ratio within 20 cycles after transformer energizing are illustrated in Figures 2.8–2.10.

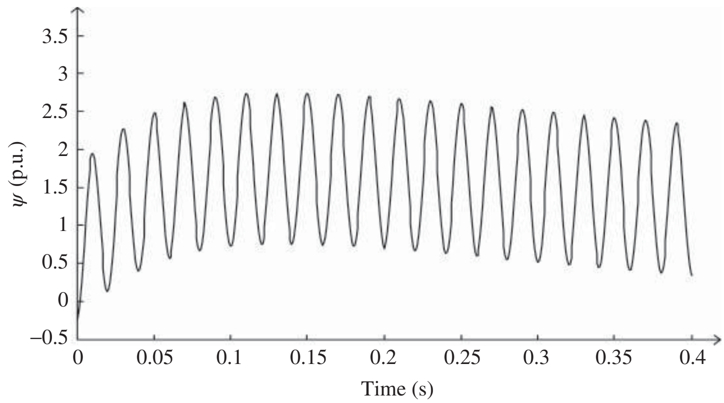

Figure 2.8 The changing flux curve with respect to the time after switching on the transformer

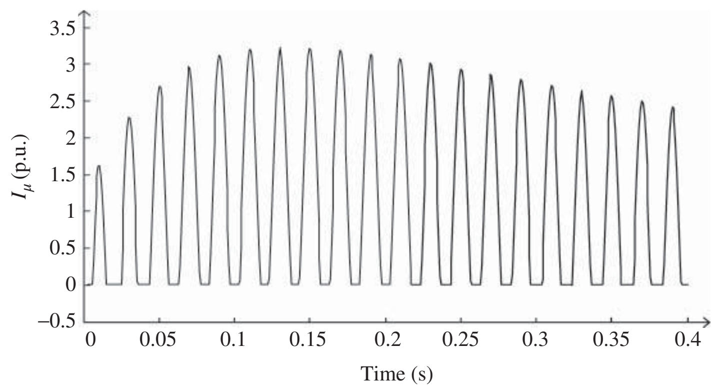

Figure 2.9 The changing inrush curve with respect to the time after switching on the transformer

As seen, the protection can be correctly blocked for the first five cycles post-energizing. However, the flux tends to saturate more deeply during this period of time. Correspondingly, the dead angle and the ratio of second harmonic to fundamental decrease step by step. By the end of the fifth cycle, the ratio of I_2/I_1 becomes lower than 15%, which results in the mal-operation of the protection. The status of I_2/I_1 lower than 15% continues for six cycles, which is long enough for mal-operation of the protection.

By adjusting each parameter of energizing, a variety of mal-operation scenarios can be simulated. Some typical delayed mal-operations are listed in Table 2.1. As shown, the occurrence of the delayed mal-operation of the differential protection depends on a variety of factors, such as T_1, T_2, knee point of the saturation curve, residual flux, inception angle and so on. The mal-operations shown in Table 2.1 usually occur at inception angles around ±90°. However, the universal rule of the mal-operation still needs to be investigated.

2.2.2.2 Energizing of the Three-Phase Transformer

The switching-on model is a three-phase transformer bank of Y/Δ-11 connection. Various simulations tests were carried out. Among which, two typical cases below are illustrated for detailed reference. The first simulation scenario is that three phases of the transformer switch on simultaneously.

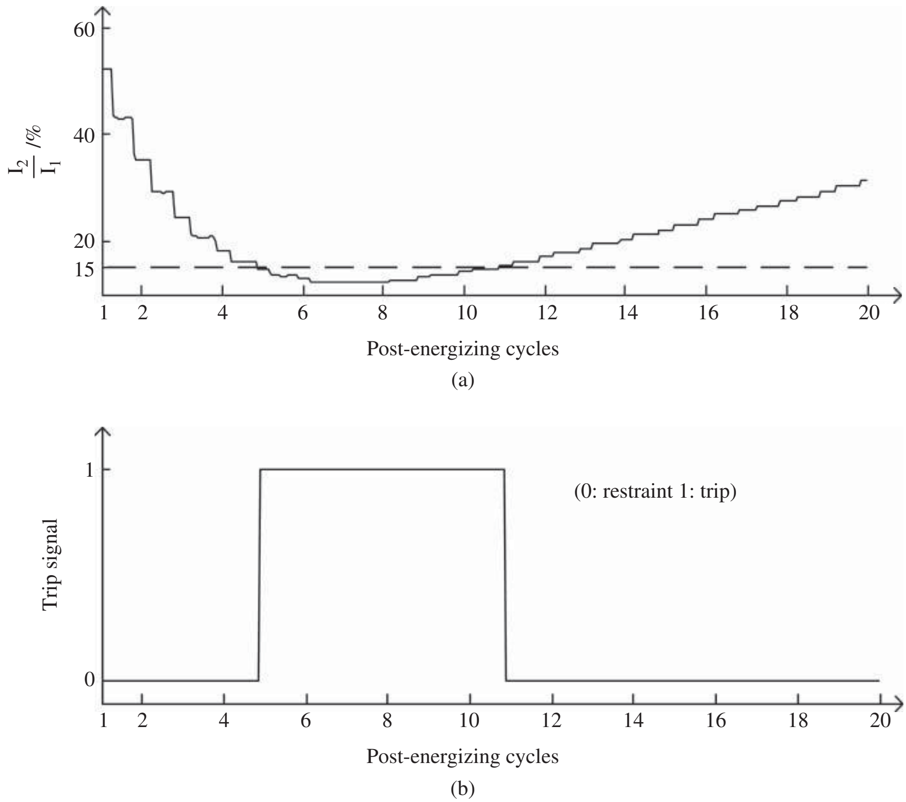

Figure 2.10 The changing curve of the ratio between second harmonic and fundamental with respect to the cycles after switching on the transformer and the response of the relay using 15% second harmonics restraint. (a) The ratio of second harmonic to fundamental and (b) the response of the relay

Table 2.1 Some scenarios of typical delayed mal-operations

Case	T_1 (s)	T_2 (s)	ψ_s (p.u.)	ψ_r (p.u.)	α (°)	Operation (time/ms)
1	0.055	0.9	1.2	−0.25	−75	47
2	0.055	0.9	1.2	0.25	82	38
3	0.055	0.9	1.4	0.25	82	60
4	0.055	0.5	1.4	0.25	82	78
5	0.07	0.5	1.4	0.25	82	45
6	0.03	0.08	1.4	−0.8	60	38
7	0.03	0.9	1.4	−0.8	85	38
8	0.1	2.0	1.4	−0.8	93	260
9	0.1	2.0	1.4	−0.8	92	128
10	0.055	0.9	1.15	0.5	82	22

The switching-on parameters are listed in Table 2.2.

For simplicity, only the ratio of second harmonic to fundamental of the inrushes together with the relay response is demonstrated in Figure 2.11.

The second harmonic contents of the inrushes decrease continuously after the transformer is switched on (Figure 2.11a). This is because one of the transient fluxes decays much faster than the other.

Table 2.2 The parameters of simulation case I

Parameter	T_1 (s)	T_2 (s)	ψ_{ra} (p.u.)	ψ_{rb} (p.u.)	ψ_{rc} (p.u.)
Value	0.01	0.5	−0.8	0.0	−0.2
Parameter	ψ_s (p.u.)	α (°)	K_L (p.u.)	t_b (ms)	t_c (ms)
Value	1.2	20	1.2	0	0

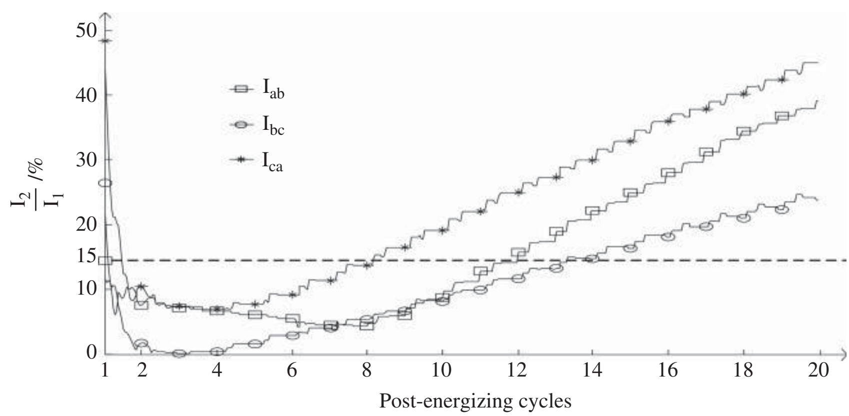

(a)

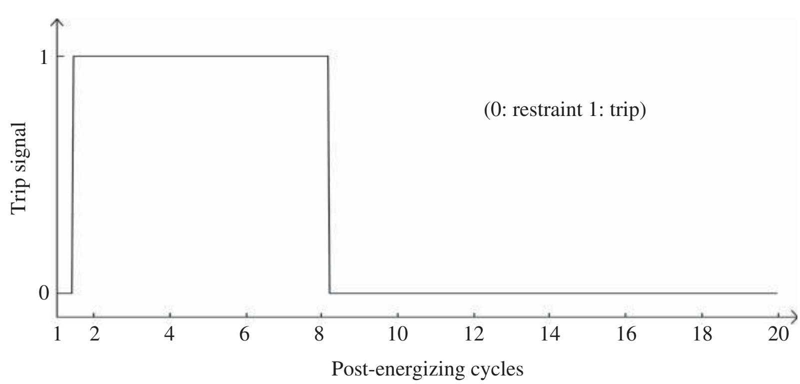

(b)

Figure 2.11 (a) The change of the ratios of second harmonics to fundamentals of three-phase inrush differences and (b) the relay response of the differential protection using 15% harmonic ratio and cross-blocking scheme with respect to the cycles post-energizing

The remnant DC flux with a big decay time constant makes the composition flux rise beyond the saturation point. Accordingly, the second harmonic contents of the inrushes become lower. The characteristics of the inrushes take over again after an adequate time for the other transient DC flux to decay. Then, the contents of second harmonics will increase correspondingly. As for the second harmonic restraint scheme, the time spent below the threshold for several cycles is enough to fail to block the protection (Figure 2.11b).

The final simulation case is an attempt to retrieve the mal-operation scenario of differential protection depicted in beginning of this chapter. The unsynchronized switching-on model is utsed for this purpose. The parameters are listed in Table 2.3.

Phase A of the transformer switches on the system at $t = 0$ while phase B and phase C close 6.5 and 3.3 ms later, respectively. The changes of three phase main fluxes are shown in Figure 2.12.

Figure 2.13 illustrates the changes of the three phases of inrush. As seen, the ultra-saturation phenomenon occurs on the phase B inrush.

With the Y/Δ-11 transformer type transformation, the differential currents used by the differential protection are demonstrated in Figure 2.14. As seen, both phase A and phase B lose the characteristics

Table 2.3 The parameters of simulation case II

Parameter	T_1 (s)	T_2 (s)	ψ_{ra} (p.u.)	ψ_{rb} (p.u.)	ψ_{rc} (p.u.)
Value	0.05	0.92	−0.26	−0.35	0.0
Parameter	ψ_s (p.u)	α (°)	K_L (p.u.)	t_b (ms)	t_c (ms)
Value	1.35	82	2.06	6.5	3.3

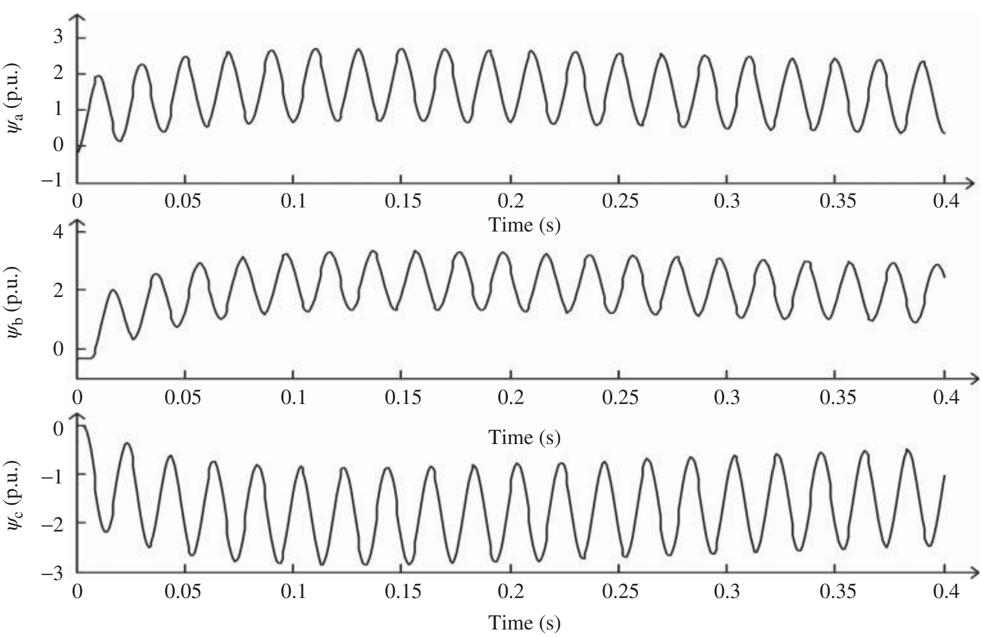

Figure 2.12 The change of three-phase main fluxes with respect to the time after energizing

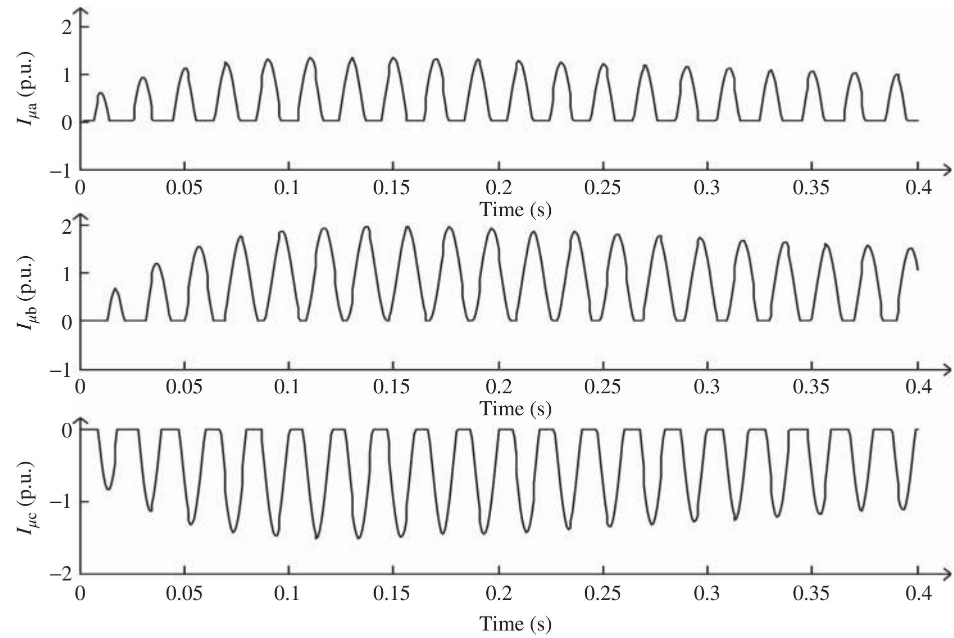

Figure 2.13 The change of three phases of inrush with respect to the time after energizing

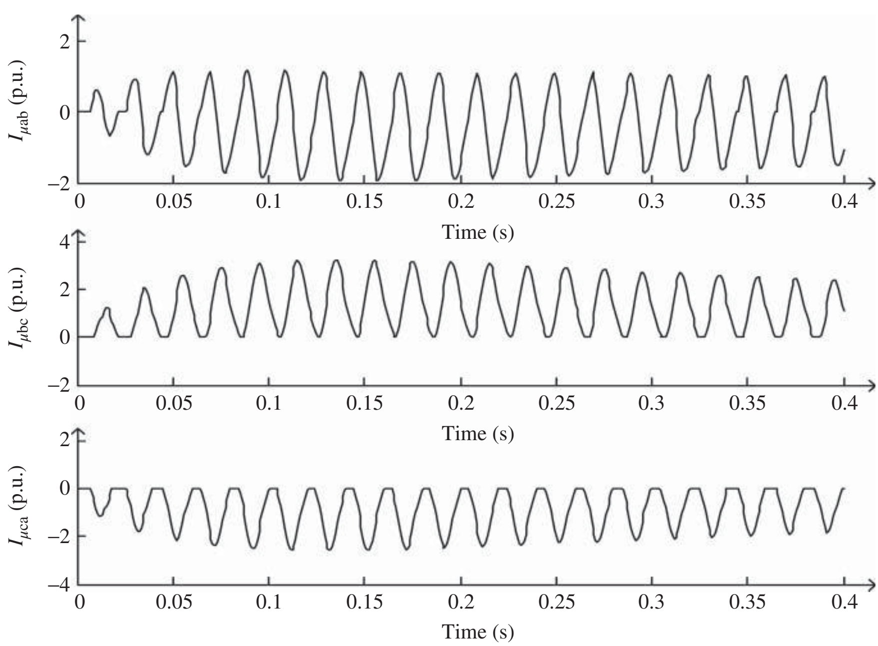

Figure 2.14 The change of three phases of inrush differences with respect to the time after energizing

of the typical inrushes. Moreover, phase A loses the DC offset. The inrush of phase C has a very small dead angle, although its DC offset exists, which will make it lose the characteristic of second harmonic content.

Accordingly, the changes of the ratio of second harmonic to fundamental of the three phases of inrush in Figure 2.14 are shown in Figure 2.15, together with the response of the relay. As shown, the relay can be blocked in the first five cycles of energizing. Notwithstanding, the protection mal-operates at the beginning of the sixth cycle.

With the proposed universal model of three-phase loaded transformer energizing, a variety of mal-operation scenarios of the differential protection, for example various mal-operation time instants, various transformer connection types, various restraint schemes and so on can be retrieved.

As analysed above, the possibility of ultra-saturation seems considerable. The differential protection using the characteristics of the inrush as the restraining scheme will be prone to mal-operate during the

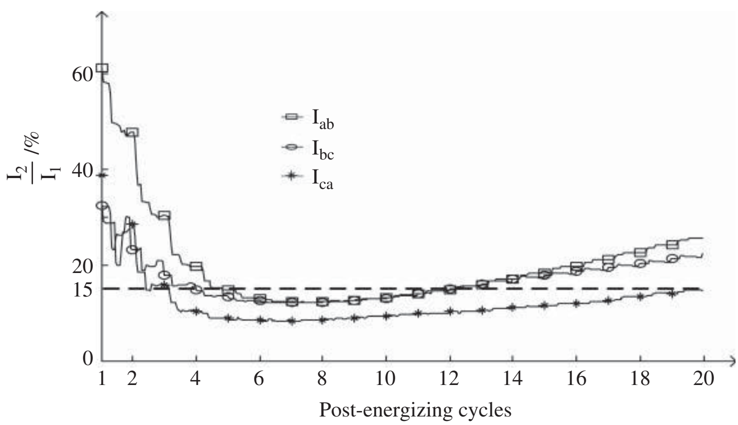

(a)

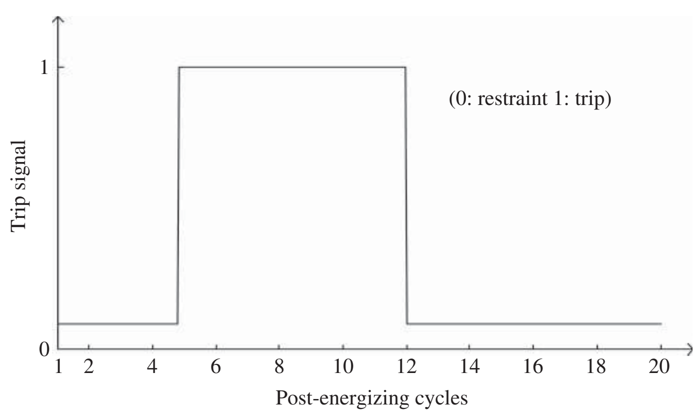

(b)

Figure 2.15 (a) The change of the ratios of second harmonic to fundamental of three phases of inrush differences and the relay response of the differential protection using 15% harmonic ratio and cross-blocking scheme with respect to the cycles of post-energizing loaded transformer energizing. However, the actual statistics on the mal-operation of transformer protection is much less than the theoretical cases. Indeed, the risk of the differential protection mal-operation during the switching on of a loaded transformer is overestimated due to the following simplifications during the simulations:

- Taking the magnetizing reactance of time-variant characteristic as an equivalent inductance so that the model of switching on the loaded transformer can be based on the ordinary differential equation.
- The core model of the transformer neglecting the smoothing effect of real magnetization curve and the local hysteresis loop.
- Without considering the transferring effect of CT to the primary inrush.
- Only the resistive loaded is concerned.

The detailed evaluation of such type of mal-operation is difficult since so many factors are involved. The probability of ultra-saturation should be much lower than the theoretically expected cases when the above factors are involved. However, it cannot be denied that ultra-saturation and delayed mal-operation of the transformer are the real physical phenomena that did possibly occur.

It can be observed as above that the DC component of at least one phase of inrush is considerable during the ultra-saturation. Therefore, the cross-blocking scheme using the DC component [14] is promising to improve the stability of the differential protection. The alternative solutions should be the model-based algorithms [15, 16]. These schemes are independent of the inrush waveform and can operate with high speed. The existing difficulty of these schemes is to obtain accurate transformer parameters, otherwise the accuracy of the protection operation is lowered. However, this problem can be solved with other techniques, for example the adaptive threshold. In this sense, more attention should be paid to schemes that are independent of the inrush waveform.

In summary, the energizing of a loaded transformer is a peculiar electromagnetic phenomenon that differentiates to the case of no-load transformer energizing. It causes some mal-operation of the differential protection that cannot be explained with the classic theory of the transformer switching-on. A second order equivalent circuit model is therefore proposed to investigate this phenomenon. With rational assumptions, the analytical solution of the main flux is obtained by use of Laplace's transform. With the deduced flux expression, a relatively rational explanation of the delayed mal-operation of the differential protection can be reached. In addition, the 'ultra-saturation' phenomenon of the core of the energized transformer is demonstrated. A variety of simulation tests were carried out to validate the proposed model. It is proved that delayed mal-operation and ultra-saturation will occur if appropriate conditions are satisfied. This disclosure enhances the system of the transient analysis theory of transformer energizing. Furthermore, it will possibly advance the research of fast main protection of transformer immune to the impact of inrush.

2.3 Studies on the Unusual Mal-Operation of Transformer Differential Protection during the Nonlinear Load Switch-In

2.3.1 Simulation Model of the Nonlinear Load Switch-In

The transient course of the nonlinear load switching-in to the system with a transformer involved can be illustrated by the equivalent circuit. When a nonlinear load is switched-in to a system with a power transformer, there are two optional switch-in positions. One is for the switch on the secondary side of the transformer; the switch position is shown in Figure 2.16a, where the switch K being closed means the nonlinear load being switched-in. The other case is for the switch on the primary side of transformer; the switch position is shown as Figure 2.16b. In both cases, the transformer magnetizing branch and the nonlinear load are illustrated as nonlinear components. For different switch-in positions, the corresponding meanings of the components will be different. To explain this phenomenon with a uniform model, a

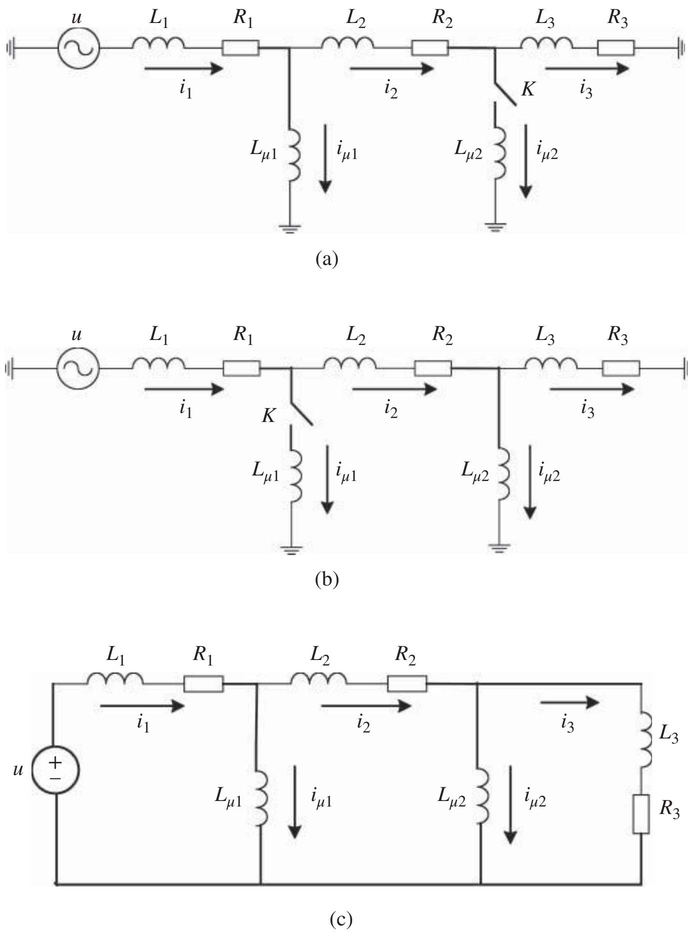

Figure 2.16 The circuit of the nonlinear load switch-in: (a) the switch position when the nonlinear load is switched-in on the side of transformer load; (b) the switch position when the nonlinear load is switched-in on the source side of the transformer; (c) the circuit of the nonlinear load switch-in of both switch-in positions

model consisting of two nonlinear components is established and illustrated in Figure 2.16c. The parameters in this figure can be defined in different ways to depict the different switch-in positions of the nonlinear load, which is detailed in the following.

The system power supply is a sine voltage source *u*. Other parameters in Figure 2.16c can be explained as follows depending on the position of load switching-in. When the nonlinear load is switched-in on the side of transformer load, $R_1 + j\omega L_1$ is the impedance of the source side of transformer combining the leakage impedance with the source impedance, through which the current flows is i_1, and the induced flux linkage is ψ_1; the transformer magnetizing branch is supposed to be a pure inductance $L_{\mu 1}$, the magnetizing current is $i_{\mu 1}$ and the induced flux linkage is $\psi_{\mu 1}$; $R_2 + j\omega L_2$ is the equivalent impedance of the side of transformer load from the transformer to the point of nonlinear load switching-in, through which the current flows is i_2, and the induced flux linkage is ψ_2; $R_3 + j\omega L_3$ is impedance of the basic load of transformer, through which the current flows is i_3, and the induced flux linkage is ψ_3; $L_{\mu 2}$ is the inductance of the nonlinear load (such as furnace), through which the current flows is $i_{\mu 2}$, and the induced flux linkage is $\psi_{\mu 2}$.

In contrast, when the nonlinear load is switched-in on the source side of transformer, $R_1 + j\omega L_1$ can be considered as the equivalent impedance from the point load switching-in to the system supply; $L_{\mu 1}$ is the inductance of the nonlinear load, through which the current flows is $i_{\mu 1}$, and the induced flux linkage is $\psi_{\mu 1}$; $R_2 + j\omega L_2$ is the equivalent impedance from the point of load switching-in to the source side of transformer (including the leakage impedance of transformer primary side); $R_3 + j\omega L_3$ is the total impedance of the side of transformer load; the transformer magnetizing branch is supposed to be a pure inductance $L_{\mu 2}$, the magnetizing current is $i_{\mu 2}$ and the induced flux linkage is $\psi_{\mu 2}$.

By virtue of the Kirchoff principle, the equations relevant to the equivalent circuit can be given by:

$$\begin{cases} u = \dfrac{d\psi_1}{dt} + R_1 i_1 + \dfrac{d\psi_{\mu 1}}{dt} \\ \dfrac{d\psi_{\mu 1}}{dt} = R_2 i_2 + \dfrac{d\psi_2}{dt} + R_3 i_3 + \dfrac{d\psi_3}{dt} \\ \dfrac{d\psi_{\mu 2}}{dt} = R_3 i_3 + \dfrac{d\psi_3}{dt} \\ i_1 = i_{\mu 1} + i_2; i_2 = i_3 + i_{\mu 2} \end{cases} \tag{2.31}$$

As for the linear branch, $i_1 = \frac{\psi_1}{L_1}$, $i_2 = \frac{\psi_2}{L_2}$ and $i_3 = \frac{\psi_3}{L_3}$ come into existence. With regard to the transformer magnetizing branch and the nonlinear load, the relationships between currents and magnetic linkages are nonlinear. It is no harm to let $i_{\mu 1} = f_1(\psi_{\mu 1})$ and $i_{\mu 2} = f_2(\psi_{\mu 2})$, which means that $i_{\mu 1}$ and $i_{\mu 2}$ are functions of $\psi_{\mu 1}$ and $\psi_{\mu 2}$, respectively. The accurate curves of $\psi_{\mu 1}$–$i_{\mu 1}$ and $\psi_{\mu 2}$–$i_{\mu 2}$ should be depicted as multivalued curves if taking the saturation factors into account. For the convenience of solving the differential equations, the transformer magnetizing branch and the nonlinear load can be simplified as piecewise lines, as illustrated in Figures 2.17 and 2.18, respectively. The saturation points are $(\psi_{s1}, i_{\mu 01})$ and $(\psi_{s2}, i_{\mu 02})$, the inductances in saturation region are L_{s1} and L_{s2}, and the inductances outside saturation region are $L_{\mu 1}$ and $L_{\mu 2}$.

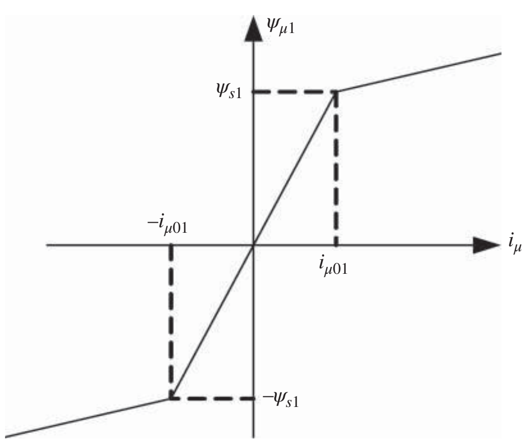

Figure 2.17 The characteristics of the nonlinear component 1

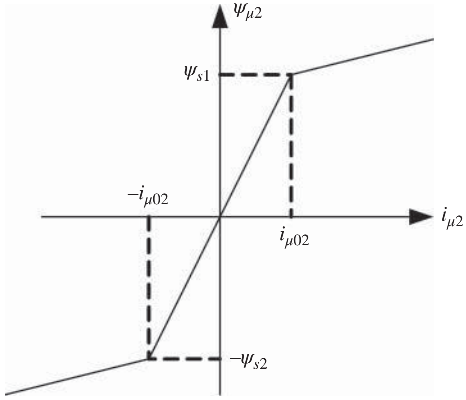

Figure 2.18 The characteristics of the nonlinear component 2

As a result, the expressions of $f_1(\psi_{\mu 1})$ and $f_2(\psi_{\mu 2})$ can be written respectively as:

$$f_1(\psi_{\mu 1}) = \begin{cases} \dfrac{\psi_{\mu 1}}{L_{\mu 1}} & , \left|\psi_{\mu 1}\right| \leq \psi_{s1} \\ \dfrac{\psi_{\mu 1} - \psi_{s1}}{L_{s1}} + i_{\mu 01}, & \psi_{\mu 1} > \psi_{s1} \\ \dfrac{\psi_{\mu 1} + \psi_{s1}}{L_{s1}} - i_{\mu 01}, & \psi_{\mu 1} < -\psi_{s1} \end{cases} \tag{2.32}$$

$$f_2(\psi_{\mu 2}) = \begin{cases} \dfrac{\psi_{\mu 2}}{L_{\mu 2}} & , \left|\psi_{\mu 2}\right| \leq \psi_{s2} \\ \dfrac{\psi_{\mu 2} - \psi_{s2}}{L_{s2}} + i_{\mu 02}, & \psi_{\mu 2} > \psi_{s2} \\ \dfrac{\psi_{\mu 2} + \psi_{s2}}{L_{s2}} - i_{\mu 02}, & \psi_{\mu 2} < -\psi_{s2} \end{cases} \tag{2.33}$$

By virtue of Equations (2.31)–(2.33) and the relationships between currents, eliminating i_1, i_2, i_3, ψ_2 and ψ_3, the deduced equations can be expressed in terms of state space matrixes and then the final result of the mathematic model can be obtained. $f_1(\psi_{\mu 1})$ and $f_2(\psi_{\mu 2})$ are divided into three segments respectively. Therefore, the final result is illustrated in nine cases, given by:

1. $|\psi_{\mu 1}| \leq \psi_{s1}$ and $|\psi_{\mu 2}| \leq \psi_{s2}$;
2. $|\psi_{\mu 1}| \leq \psi_{s1}$ and $\psi_{\mu 2} > \psi_{s2}$;
3. $|\psi_{\mu 1}| \leq \psi_{s1}$ and $\psi_{\mu 2} < -\psi_{s2}$;
4. $\psi_{\mu 1} > \psi_{s1}$ and $|\psi_{\mu 2}| \leq \psi_{s2}$;
5. $\psi_{\mu 1} > \psi_{s1}$ and $\psi_{\mu 2} > \psi_{s2}$;
6. $\psi_{\mu 1} > \psi_{s1}$ and $\psi_{\mu 2} < -\psi_{s2}$;
7. $\psi_{\mu 1} < -\psi_{s1}$ and $|\psi_{\mu 2}| \leq \psi_{s2}$;
8. $\psi_{\mu 1} < -\psi_{s1}$ and $\psi_{\mu 2} > \psi_{s2}$;
9. $\psi_{\mu 1} < -\psi_{s1}$ and $\psi_{\mu 2} < -\psi_{s2}$.

According to different cases, state equations can be deduced correspondingly. Taking case a for instance, the corresponding state equations are:

$$\dot{\psi}_1 = \frac{C1 + \frac{R_1}{L_1}B1}{A1 - B1}\psi_1 + \frac{D1}{A1 - B1}\psi_{\mu 1} + \frac{E1}{A1 - B1}\psi_{\mu 2} - \frac{B1}{A1 - B1}U \tag{2.34}$$

$$\dot{\psi}_{\mu 1} = -\frac{\frac{R_1}{L_1}A1 + C1}{A1 - B1}\psi_1 - \frac{D1}{A1 - B1}\psi_{\mu 1} - \frac{E1}{A1 - B1}\psi_{\mu 2} + \frac{A1}{A1 - B1}U \tag{2.35}$$

$$\begin{aligned}\dot{\psi}_{\mu 2} = &\left[-\frac{L_2}{L_1}\frac{C1 + \frac{R_1}{L_1}B1}{A1 - B1} - \left(1 + \frac{L_2}{L_{\mu 1}}\right)\frac{\frac{R_1}{L_1}A1 + C1}{A1 - B1} - \frac{R_2}{L_1}\right]\psi_1\\
&+ \left[-\frac{L_2}{L_1}\frac{D1}{A1 - B1} - \left(1 + \frac{L_2}{L_{\mu 1}}\right)\frac{D1}{A1 - B1} + \frac{R_2}{L_{\mu 1}}\right]\psi_{\mu 1}\\
&+ \left[-\frac{L_2}{L_1}\frac{E1}{A1 - B1} - \left(1 + \frac{L_2}{L_{\mu 1}}\right)\frac{E1}{A1 - B1}\right]\psi_{\mu 2}\\
&+ \left[\frac{L_2}{L_1}\frac{B1}{A1 - B1} + \left(1 + \frac{L_2}{L_{\mu 1}}\right)\frac{A1}{A1 - B1}\right]U\end{aligned} \tag{2.36}$$

where

$$\mathrm{A1} = \frac{-(L_{\mu 2} + L_3)(L_2 + L_3) + L_3L_3}{L_{\mu 2}L_1}$$

$$\mathrm{B1} = \frac{(L_{\mu 2} + L_3)(L_{\mu 1} + L_2 + L_3) - L_3L_3}{L_{\mu 1}L_{\mu 2}}$$

$$\mathrm{C1} = \frac{(L_3 + L_{\mu 2})(R_2 + R_3) - R_3L_3}{L_1L_{\mu 2}}$$

$$\mathrm{D1} = \frac{-(L_3 + L_{\mu 2})(R_2 + R_3) + R_3L_3}{L_{\mu 1}L_{\mu 2}}$$

$$\mathrm{E1} = -\frac{R_3}{L_{\mu 2}}$$

The voltage source is defined as $U = U_m\sin(\omega t + \theta)$.

Results corresponding to the other eight cases can be expressed similarly but are not listed here for lack of space.

The flux linkage of each branch during the nonlinear load switch-in can be obtained by selecting appropriate parameters and using a four-order Runge–Kutta algorithm to solve the nonlinear differential equations above. By virtue of the relationships of flux linkages and currents, the current waveforms can be obtained correspondingly.

It should be pointed out that a nonlinear load being switched-in to a system with a power transformer is different from a loaded transformer energizing. The difference mainly rests with the initial conditions for the calculation. For the loaded transformer energizing, the initial magnetizing linkage of each inductive branch can be dealt with arbitrarily in theory; for example, the magnetizing linkage of the transformer magnetizing branch is defined as the residual magnetizing linkage, the absolute value of which is less than 0.8 on the basis of per unit system. In contrast, for the nonlinear load being switched-in, the initial value of the magnetizing linkage of each inductance branch, including the linear inductance on the primary side of transformer, must be calculated in virtue of the steady-state equations of the circuit before the nonlinear load branch is closed. In the event of steady-state calculations, the transformer magnetizing branch can be regarded as a linear branch with unsaturated high inductance, and hence the corresponding expressions of the magnetizing current and linkage can be established, and the initial magnetizing linkage values of the inductance branches for the purpose of nonlinear load being switched-in to a system can be figured out.

2.3.2 Simulation Results and Analysis of Mal-Operation Mechanism of Differential Protection

There is no harm in assuming that the nonlinear load is switched-in at 0 s.

Source parameters: $U_m = 110$ kV, $\omega = 100\,\pi$rad. The rated capacity of the transformer is 315 MVA, ratio k = 110/35 kV, then the primary rated current of the transformer is 1653 A. Transformer core: $\psi_m = U_m/\omega$, the saturation multiple: $\psi_s/\psi_m \approx 1.2$.

Scenarios of the nonlinear load switch-in on both sides of transformer are discussed here (Scenarios 2.3 and 2.4). In the simulation results, the flux linkages are expressed as the reduced nominal values on the basis of the primary system. The currents are represented by per unit system taking the primary rated current of the transformer as the base.

Scenario 2.3 Protection mal-operation case due to nonlinear load being switched-in on the side of the transformer load

The nonlinear load is switched-in on the side of transformer load; the corresponding simulating parameters are:

$L_1 = 0.06$ H, $R_1 = 15\ \Omega$; $L_2 = 0.05$ H, $R_2 = 15\ \Omega$; $L_3 = 1.5$ H, $R_3 = 5\ \Omega$; for the transformer magnetizing branch: $L_{\mu 1} = 700$ H, $\psi_{s1} = 420$ Wb, $L_{s1} = 0.2$ H, $i_{\mu 01} = \psi_{s1}/L_{\mu 1}$; for the nonlinear load: $L_{\mu 2} = 700$ H, $\psi_{s2} = 350$ Wb, $L_{s2} = 0.15$ H, $i_{\mu 02} = \psi_{s2}/L_{\mu 2}$.

By virtue of the second-order circuit in Figure 2.16a before K is closed, the steady-state magnetizing linkages of the inductances on each branch can be calculated. In the simulation, it is assumed that the nonlinear load is switched-in when the magnetizing linkage of the transformer magnetizing branch is just crossing zero; this time is regarded as 0 s. Correspondingly, the initial angle of the voltage source is $\theta = -90°$ and the initial value of the magnetizing linkage of L_1 is 0.53 Wb. The initial magnetizing linkages of other branches can be evaluated correspondingly. Based on the initial value and Figure 2.16a, the case of the nonlinear load being switched-in on the side of transformer load is investigated.

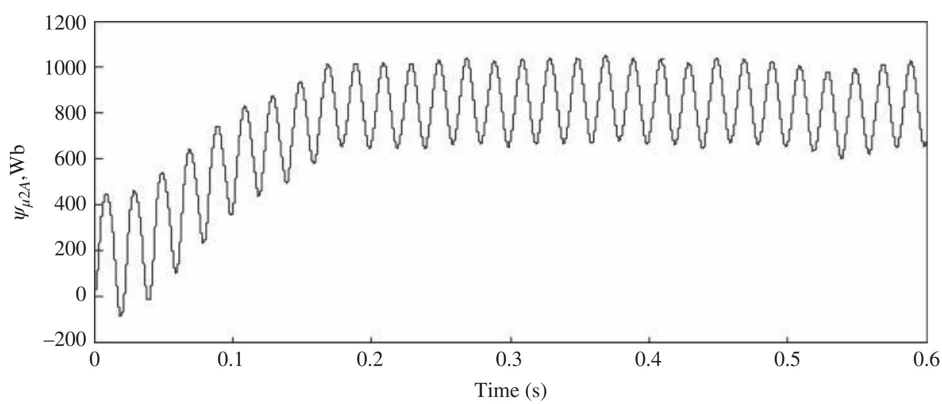

Figure 2.19 The waveform of the flux linkage of the nonlinear load of phase A

The waveform of the flux linkage of the nonlinear load of phase A is shown in Figure 2.19. In the initial stage of the nonlinear load switch-in, the nonlinear load is within the unsaturated state, which means that the corresponding inductance is relatively high. Therefore, the current flowing through the nonlinear load is low. However, the flux linkage of the nonlinear load probably contains a high aperiodic component because of some factors, such as inception angle, while the voltage source has relatively high amplitude. Therefore, the flux linkage enters the saturated portion of the nonlinear characteristic and, correspondingly, the inductance decreases rapidly in a certain half cycle. However, the voltage source, which is a periodic component, reduces the flux linkage to the normal operating value in the opposite half cycle, leading to an increase of equivalent impedance in the nonlinear branch.

Consequently, the high aperiodic component in the flux linkage of the nonlinear load means the flux linkage of transformer magnetizing branch is superimposed with a corresponding aperiodic component. After a while, as the flux linkage enters the saturated portion of the magnetizing characteristic, the inductance of the transformer core decreases rapidly and considerable current at the source side of transformer flows through the magnetizing branch. While, the flux linkage is reduced to the normal operating value during the successive half cycle, the value of the voltage source is opposite to the aperiodic component (Figure 2.20). Then the inrush fades rapidly. To illustrate this case, the complete course of inrush $i_{\mu 1A}$ is shown in Figure 2.21.

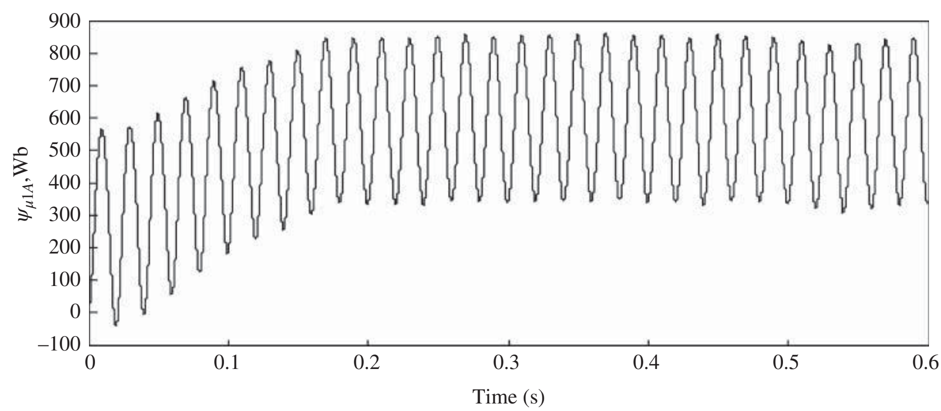

Figure 2.20 The waveform of the flux linkage of the transformer magnetizing branch of phase A

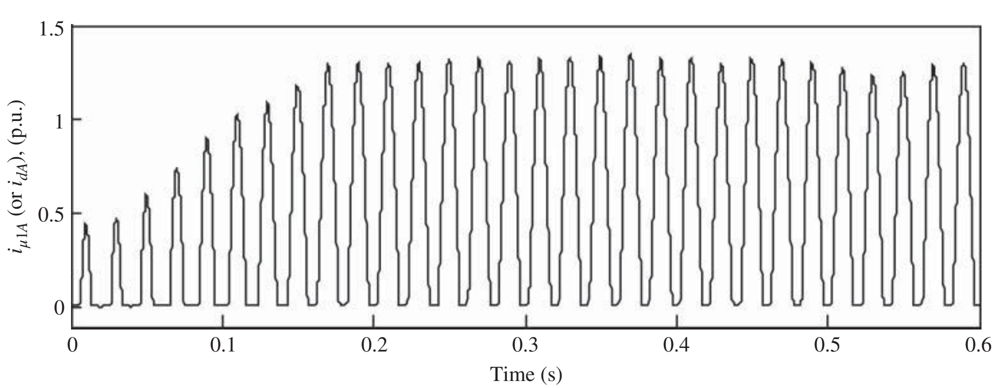

Figure 2.21 The waveform of the current of the transformer magnetizing branch (differential current) of phase A

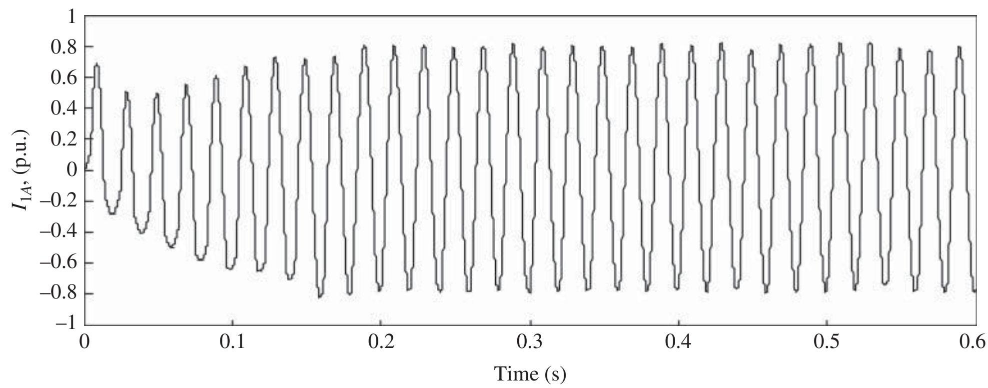

Figure 2.22 The waveform of the current at the source side of the transformer of phase A

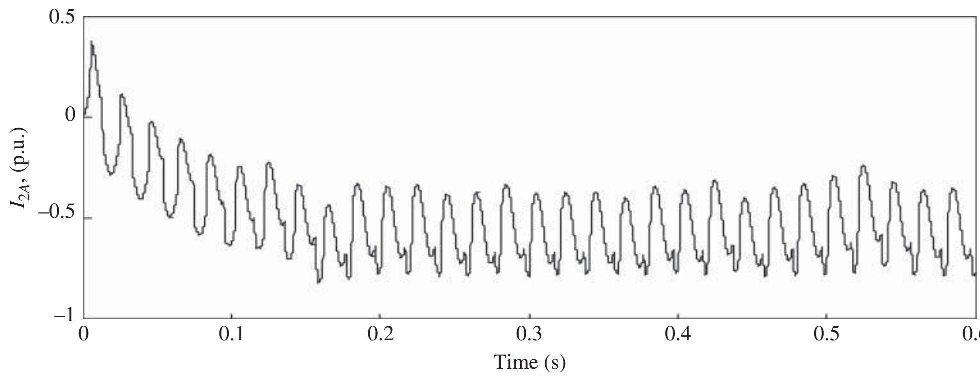

Figure 2.23 The waveform of the current at the side of transformer load of phase A

The current waveforms of phase A of both sides of the transformer are shown in Figures 2.22 and 2.23. As considerable current at the source side of transformer flows through the magnetizing branch because of the flux linkage entering the saturation state, and the magnetizing current deviates to one side of the horizontal axis, the current at the side of transformer load is distorted and deviates to the other side of the horizontal axis. It can be seen as well that the currents at both sides of the transformer are lower than the rated current; therefore, CTs on both sides of the transformer can transform the current linearly. Regardless of the transforming error of the CT, the magnetizing current $i_{\mu 1A}$ can be regarded as the differential current (i_{dA}) in Figure 2.21.

Figure 2.24 shows the changes of the magnitude of the fundamental component of i_{dA} in Figure 2.21, which is evaluated with the DFT algorithm. The steady-state magnitude of i_{dA} stabilizes above 0.3 p.u. after the nonlinear load switch-in exists for 0.1 s. If the setting of operating threshold is below 0.3, mal-operation of phase A differential protection will occur. Certainly, the mal-operation cannot occur unless the ratio of second harmonic to fundamental of the differential current of phase A is lower than the threshold, which is generally set at 15–20%. Figure 2.25 shows the ratio change of second harmonic

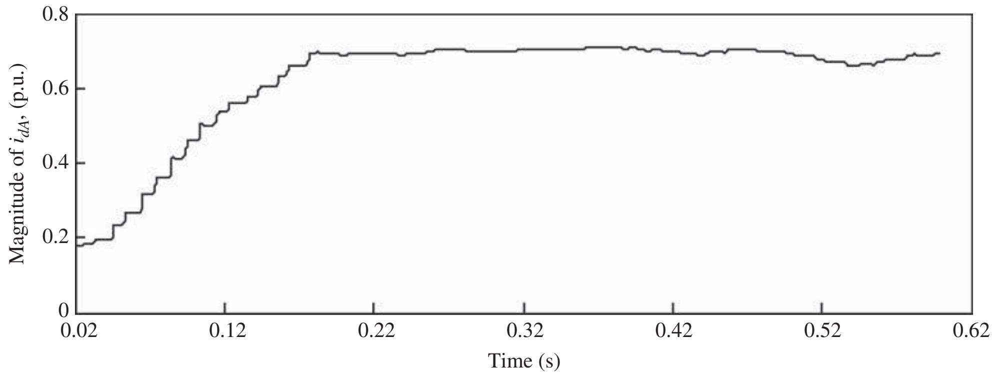

Figure 2.24 The magnitude of the fundamental component of the differential current of phase A

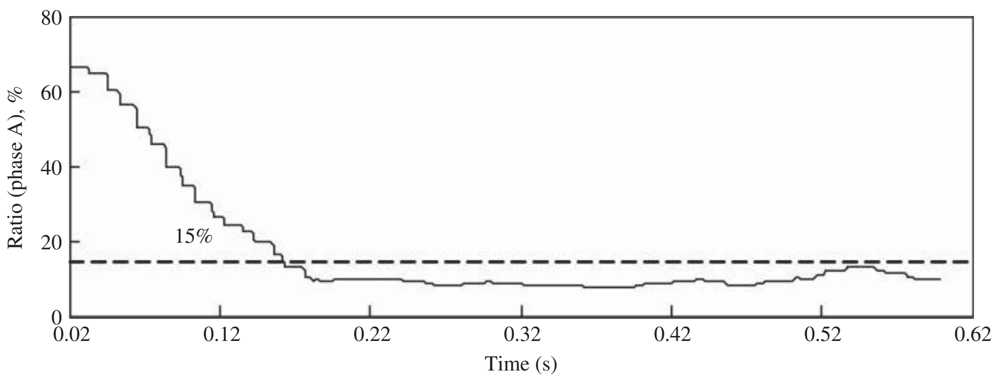

Figure 2.25 The ratio of second harmonic to fundamental of the differential current of phase A

to fundamental of the differential current of phase A after the nonlinear load switch-in. As the switch-in time exceeds 0.15 s, the ratio of the second harmonic to fundamental of phase A stabilizes below 15%.

Generally, in China, if the second harmonic component of any phase differential current rises over threshold, the differential protection that uses such a blocking scheme will be blocked. Therefore, the scenarios of phases B and C must be investigated as well. The transformer differential currents of phases B and C, as well as the analyses of the characteristics of the fundamental component and the second harmonic of the differential currents, are shown in Figures 2.26–2.31, respectively.

As seen in Figures 2.27 and 2.30, the steady state magnitudes of i_{dB} and i_{dC} both stabilize above 0.3 p.u. after the nonlinear load switches in and this state lasts for 0.12 s. Analysing the ratio changes of second harmonic to fundamental of the differential current of phases B and C (Figures 2.27 and 2.31), it can be seen that the ratios stabilize below 15% as the state of post-switch-in lasts for 0.25 and 0.27 s, respectively. Together with the above analyses of phase A, as the switch-in time exceeds 0.27 s the differential protections of the three phases will all operate and the second harmonic restraint criteria of three phases will all fail to block. Therefore, mal-operation of the transformer differential protection is inevitable.

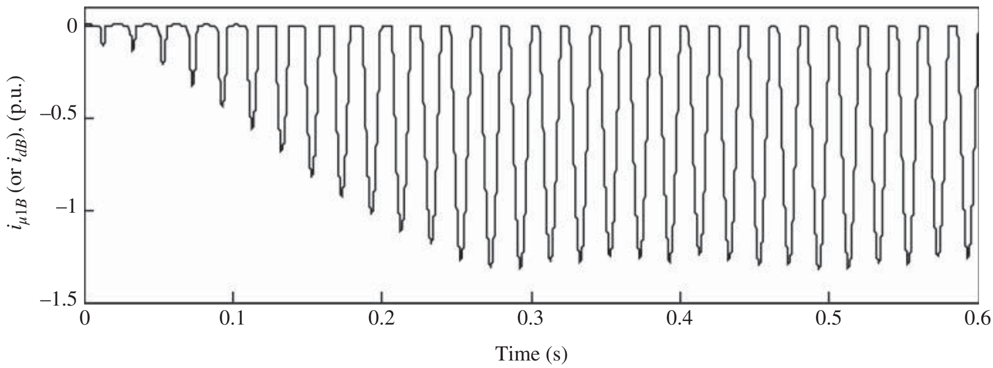

Figure 2.26 The waveform of the differential current of phase B

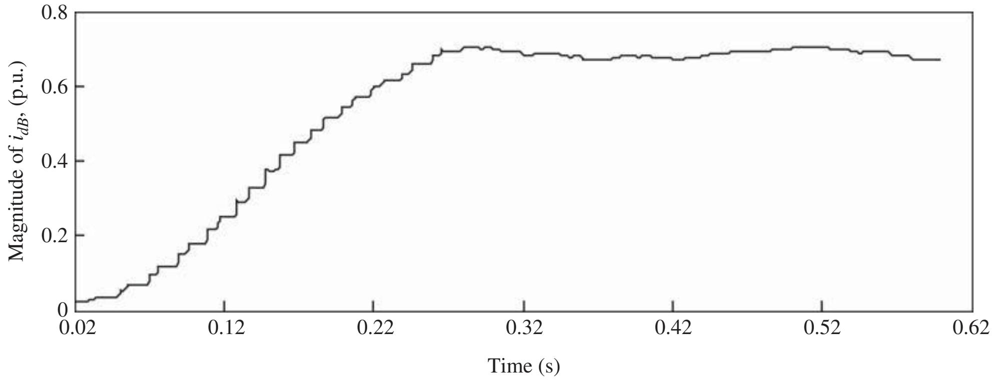

Figure 2.27 The magnitude of the fundamental component of the differential current of phase B

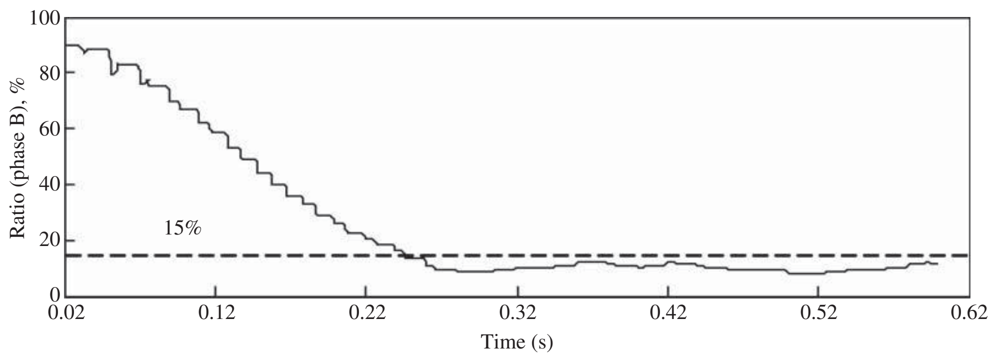

Figure 2.28 The ratio of second harmonic to fundamental of the differential current of phase B

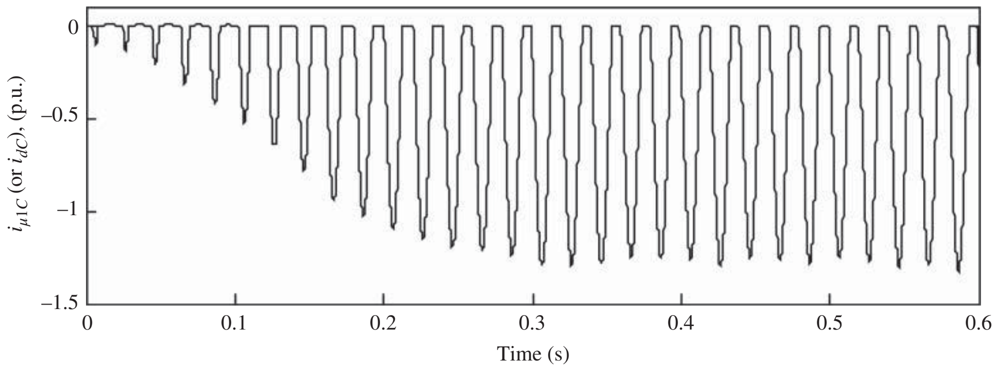

Figure 2.29 The waveform of the differential current of phase C

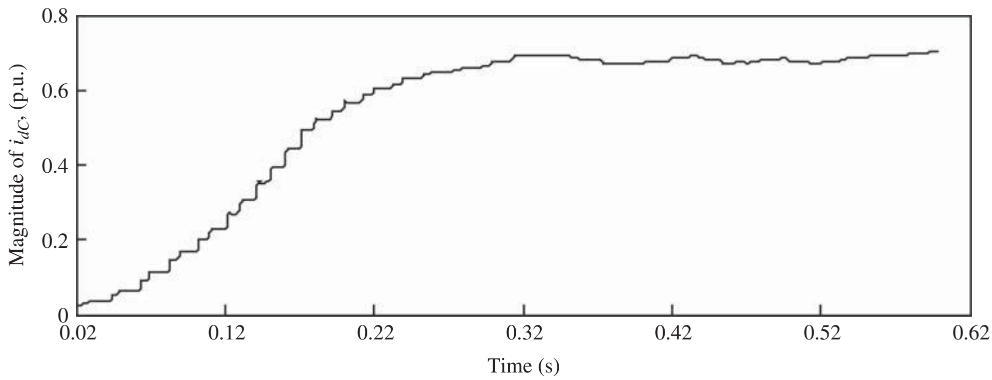

Figure 2.30 The magnitude of the fundamental component of the differential current of phase C

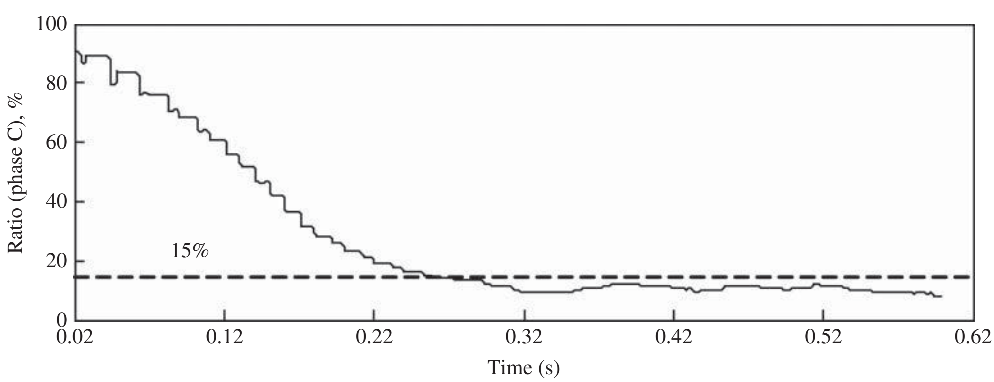

Figure 2.31 The ratio of second harmonic to fundamental of the differential current of phase C

Scenario 2.4 Protection mal-operation case due to nonlinear load being switched-in on the source side of the transformer

The nonlinear load is switched-in on the source side of transformer, the corresponding simulating parameters are:

$L_1 = 0.05$ H, $R_1 = 5\ \Omega$; $L_2 = 0.01$ H, $R_2 = 10\ \Omega$; $L_3 = 1.55$ H, $R_3 = 7.5\ \Omega$; for the nonlinear load: $L_{\mu 1} = 1000$ H, $\psi_{s1} = 350$ Wb, $L_{s1} = 0.3$ H, $i_{\mu 01} = \psi_{s1}/L_{\mu 1}$; for the transformer magnetizing branch: $L_{\mu 2} = 700$ H, $\psi_{s2} = 420$ Wb, $L_{s2} = 0.2$ H, $i_{\mu 02} = \psi_{s2}/L_{\mu 2}$;

Similar to Scenario 2.3, according to the second-order circuit in Figure 2.16b before K is closed, the steady-state magnetizing linkages of the inductances on each branch can be calculated. Still assume that the nonlinear load is switched-in when the magnetizing linkage of the transformer magnetizing branch is just crossing zero and this time is regarded as 0 s. Correspondingly, the initial angle of the voltage source is $\theta = -90°$ and the initial value of the magnetizing linkage of L_1 is 0.035 Wb. The initial magnetizing linkages of other branches can be evaluated correspondingly. Based on the initial value and Figure 2.16b, the case of the nonlinear load being switched-in on the source side of transformer is investigated.

As the nonlinear simplifications adopted for the transformer core and the nonlinear load are similar, the transient course of the nonlinear load switch-in on the source side of transformer is similar to that of the nonlinear load switch-in on the side of transformer load. The changes of the magnitude of the fundamental component and second harmonic ratio results of the differential currents of the three phases are illustrated in Figures 2.32–2.37.

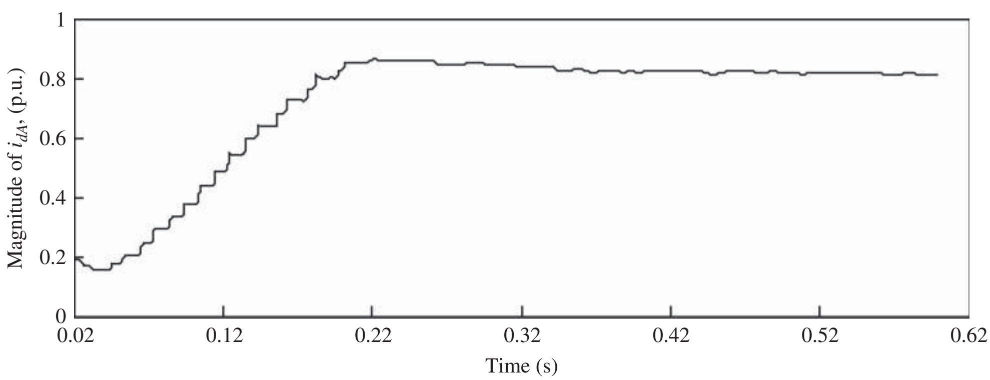

Figure 2.32 The magnitude of the fundamental component of the differential current of phase A

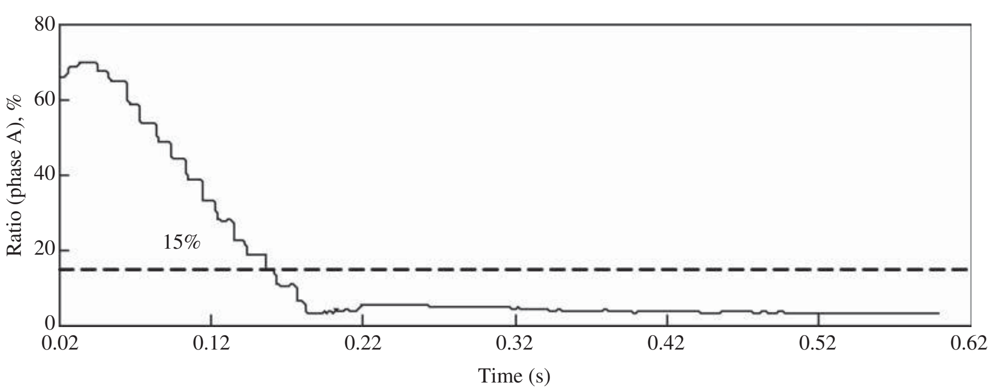

Figure 2.33 The ratio of second harmonic to fundamental of the differential current of phase A

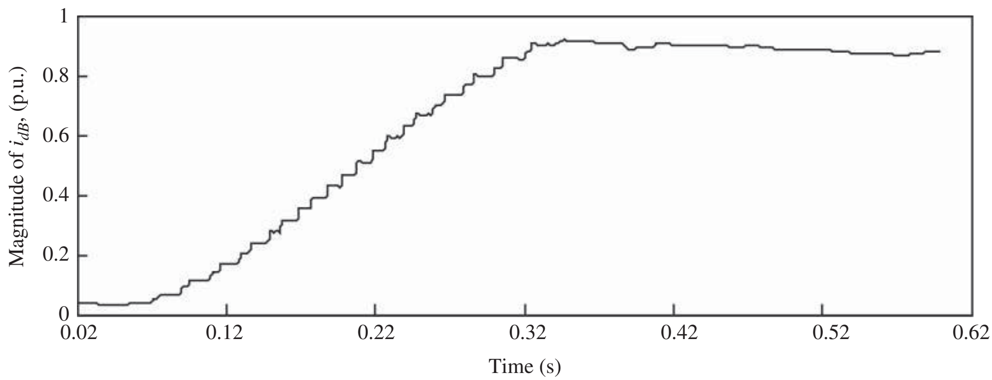

Figure 2.34 The magnitude of the fundamental component of the differential current of phase B

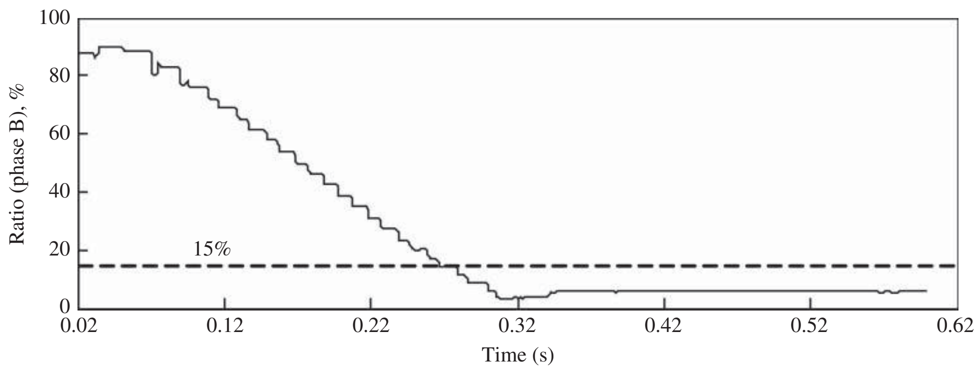

Figure 2.35 The ratio of second harmonic to fundamental of the differential current of phase B

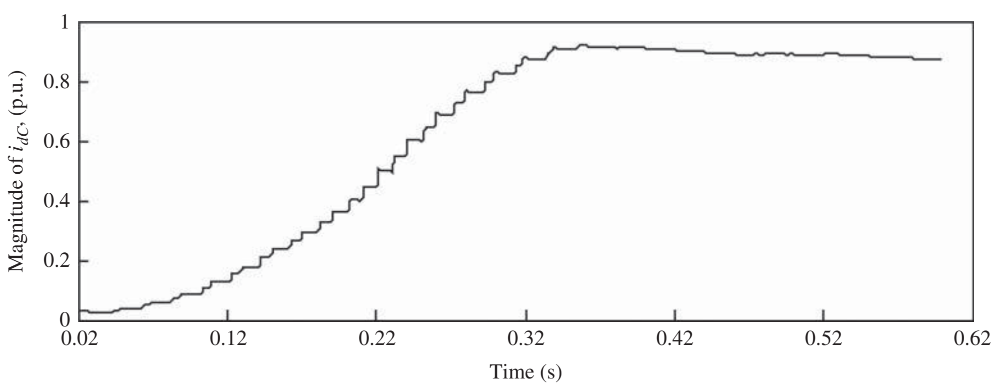

Figure 2.36 The magnitude of the fundamental component of the differential current of phase C

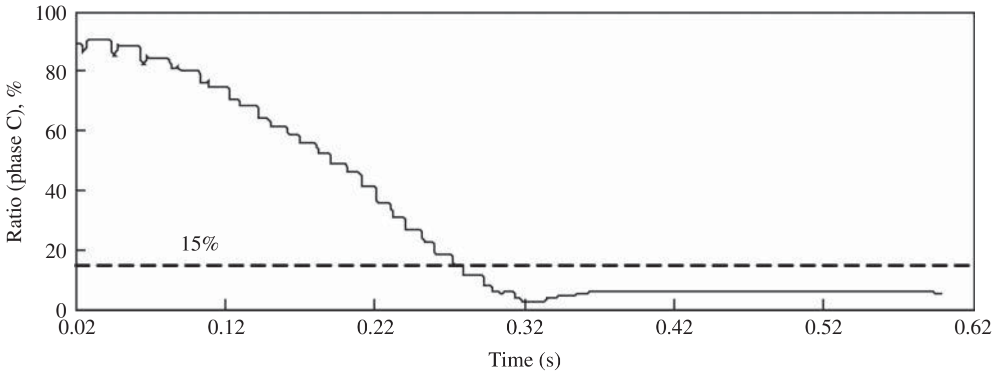

Figure 2.37 The ratio of second harmonic to fundamental of the differential current of phase C

For phase A, the magnitude of the fundamental component of the differential current stabilizes above 0.3 p.u. after approximately 0.1 s post-switch-in (Figure 2.32), while the ratio of the second harmonic to fundamental stabilizes below 15% as the switch-in time exceeds 0.15 s (Figure 2.33); For phase B, the magnitude of the fundamental component of the differential current stabilizes above 0.3 p.u. after nearly 0.15 s post-switch-in (Figure 2.34), while the ratio of the second harmonic to fundamental stabilizes below 15% as the switch-in time exceeds 0.27 s (Figure 2.35). For phase C, the magnitude of the fundamental component of the differential current stabilizes above 0.3 p.u. after 0.17 s post-switch-in (Figure 2.36), while the ratio of second harmonic to fundamental stabilizes below 15% as the switch-in time exceeds 0.28 s (Figure 2.37). Therefore, the transformer differential protection, which is based on the second harmonic restraint criterion with the threshold as 15%, will mal-operate as the switch-in time exceeds 0.28 s.

By virtue of the above analyses, in the cases of two different switch-in positions of the nonlinear load, the second harmonic restraint criteria of the three phases will all fail to block and, as a result, the transformer differential protection mal-operates.

In summary, the mechanism of a type of abnormal mal-operation of the differential protection during the nonlinear load switch-in to the transformer involved system has been analysed in this section. It is concluded that the extreme saturation state may occur because of the mutual enhancement effects between the transformer core and the nonlinear load. In this case, the degree of saturation of the transformer core becomes greater and, finally, the flux linkage stays within the area near the saturation point for several or dozens of cycles. Therefore, the current at transformer magnetizing branch (differential current) is relatively high and with a relatively smooth waveform. In this case, the differential current of the protection possibly exceeds the threshold and the ratio of second harmonic to fundamental is low, which leads to the mal-operation of the differential protection.

2.4 Analysis of a Sort of Unusual Mal-operation of Transformer Differential Protection due to Removal of External Fault

2.4.1 Modelling of the External Fault Inception and Removal and Current Transformer

2.4.1.1 Model of the External Fault Inception and Removal

The model of external fault inception and removal is illustrated by Figure 2.38. T means the ideal transformer. R_1 and L_1 are the resistance and the inductance of the primary side, respectively, and R_2 and L_2

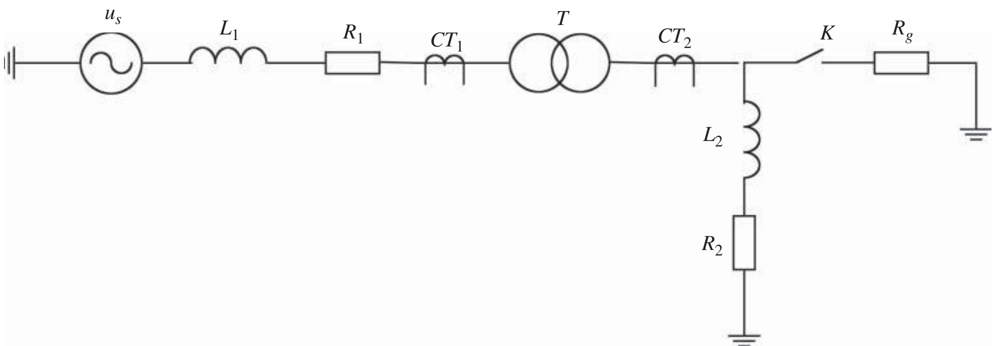

Figure 2.38 The circuit model of external fault inception and removal

are the resistance and the inductance of the secondary side; R_g means the fault resistance of the external fault. CT_1 and CT_2 are the current transformers on both sides of the transformer, respectively.

K denotes the switch that is used to simulate the occurrence and isolation of the external fault. Inception of the fault is simulated by closing the switch K, while the removal of fault is simulated by opening the switch K.

The voltage source is defined in Equation (2.37):

$$u_s = U_m \sin(\omega t + \theta) \tag{2.37}$$

Selecting appropriate parameters and simulating the above model by means of applying the ATP software, the through current of external fault inception and removal can be obtained.

2.4.1.2 CT Modelling

An accurate model of a CT suitable for transient analysis is necessary apart from the above primary model of power transformer. The equivalent circuit of the CT model is shown in Figure 2.39, in which i_1 and i_2 are the currents through the primary side and the secondary side of the CT, respectively, i_μ is the current of the CT magnetizing branch and ψ_μ is the induced magnetic linkage corresponding to i_μ.

By virtue of the Kirchoff principle, the equations relevant to the equivalent circuit can be given by:

$$i_1 = i_2 + i_\mu \tag{2.38}$$

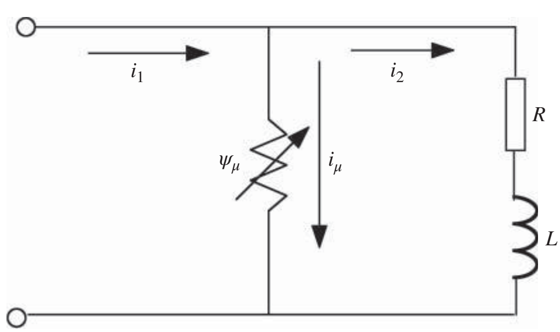

Figure 2.39 The equivalent circuit of the CT model

$$\frac{d\psi_\mu}{dt} = Ri_2 + L\frac{di_2}{dt} \tag{2.39}$$

Equation (2.38) can be changed into:

$$i_2 = i_1 - i_\mu \tag{2.40}$$

Substituting Equation (2.40) into Equation (2.39), Equation (2.41) is obtained:

$$\left(\frac{d\psi_\mu}{dt} + L\right)\frac{di_\mu}{dt} + Ri_\mu = Ri_1 + L\frac{di_1}{dt} \tag{2.41}$$

It is no harm letting $\psi_\mu = f(i_\mu)$ express the relationship between ψ_μ and i_μ.

The main difficulty in illustrating the magnetizing curve rests with the simulation of the hysteresis loop. A proposed multivalued curve of $\psi - I$ is adopted in modelling the CT.

The modified arc tangent function is adopted to fit the limit hysteresis loop, which can describe the basic contour of the hysteresis. Pro rata compression of the limit hysteresis loop allows the rising and falling loci of the dynamic hysteresis loop to be simulated approximately (Figure 2.40).

Then, a four-order Runge–Kutta algorithm is used to solve the differential equations. The arithmetic solutions of the magnetizing current, the secondary current and the magnetic linkage can be obtained by means of applying the iterative computation. Figure 2.41 shows a simulated dynamic magnetizing course of the CT core caused by an external fault.

By virtue of the model of external fault inception and removal, the currents injected into the CTs located on the primary and secondary sides of the power transformer can be obtained. Then, using the above CT model, the secondary currents for both sides of the transformer differential protection zone can be obtained as well allowing analysis of the protection.

2.4.2 Analysis of Low Current Mal-operation of Differential Protection

In this section, it is preferred to reproduce the mal-operation of differential protection due to low differential current by virtue of simulation tests. If successful, the mechanism of this sort of mal-operation can be disclosed.

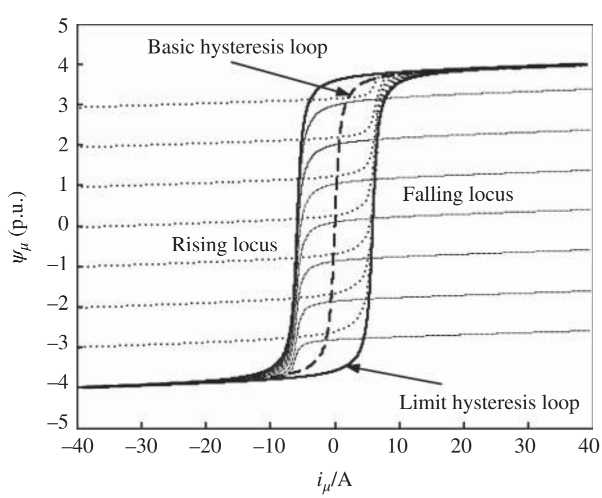

Figure 2.40 Dynamic magnetizing curve of the CT core

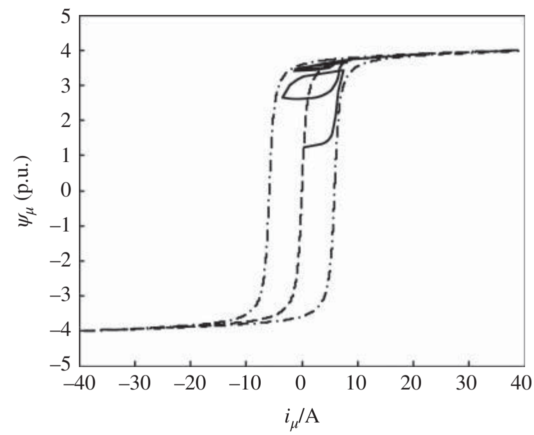

Figure 2.41 A simulated dynamic magnetizing curve of the CT core

With respect to the simulation model illustrated in Figure 2.38, the source parameters can be given by:

$$U_m = 110\text{ kV},\ \omega = 100\ \pi\text{rad},\ \text{inception angle } \theta = 20^\circ.$$

The parameters for the primary circuit in Figure 2.38 can be given by:

$$\text{Ratio of the transformer } k = 110/35\text{ kV};\ L_1 = 0.04\text{ H},\ R_1 = 2.5\ \Omega,$$
$$L_2 = 0.12\text{ H},\ R_2 = 12.5\ \Omega,\ R_g = 0.1\ \Omega.$$

Parameters for the CT1 on the high voltage side of the transformer can be given by:

$$\text{Transforming ratio } k = 600/5\text{ A},\ l = 0.68\text{ m},\ S = 23.2\text{ cm}^2,\ R = 1\ \Omega,$$
$$\text{saturation flux densities of the magnetizing branch } B_s = 1.5\text{ T};$$

Parameters for the CT2 on the low voltage side of the transformer can be given by:

$$\text{Transforming ratio } k = 2000/5\text{ A},\ l = 0.5\text{ m},\ S = 44.2\text{ cm}^2,\ R = 1\ \Omega,\ B_s = 1.5\text{ T}.$$

The saturation points of the magnetizing branch of CTs for both sides are determined by $\Psi_s/\Psi_m = 3.9$. It can be assumed that the fault occurs at $t = 0.057$ s and is removed at $t = 0.215$ s.

The fault current is much higher than the load current when a serious external short-circuit fault occurs. Sometimes the fault current is 10–20 times as high as the rated current. In the initial stage of the external fault occurrence, the fault current probably contains high aperiodic component because of factors such as inception angle. After a while, with the decay of the aperiodic component, the current presents a symmetrical waveform. Provided that the fault is removed, the fault current decreases suddenly to the level of load current (Figure 2.42).

Taking i_1 as the input of the CT model, we can obtain the transforming characteristic (Figure 2.43) and the dynamic magnetizing course (Figure 2.44) of CT1. As shown in Figure 2.43, i_{11}, i_{12} and $i_{1\mu}$ are the primary, secondary and magnetizing currents of CT1, respectively.

As seen in Figure 2.43, before the fault occurs the primary current is within normal range and the core of CT1 works at the linear region. It means that the corresponding magnetizing inductance is relatively high. Therefore, the magnetizing current is almost zero.

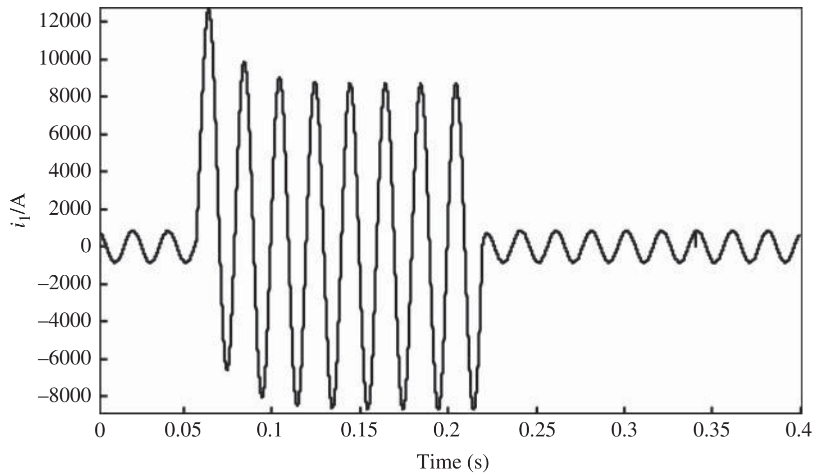

Figure 2.42 The current waveform of the primary side of the transformer of external fault inception and removal

However, during the existence of external fault, the amplitude of i_{11} far exceeds its steady-state level and contains a high aperiodic component. The flux densities of the magnetizing branch of CTs during the existence of external fault can be calculated according to Equation (2.42):

$$B = B_r + B_m[C\omega T_1(1 - e^{-t/T_1}) - \sin \omega t] \tag{2.42}$$

where $B_m = \frac{RI_m{}'}{\omega kS}$. Among them, $I_m{}'$ is the amplitude of the primary current during the existence of external fault, B_r is the remnant flux density of CT, T_1 is the time constant of the primary system and C is the coefficient expressing ratio of aperiodic component to periodic component of fault current at the beginning of the fault occurrence.

By virtue of Equation (2.42) it is found that about 0.025 s after the fault occurs, the flux density of CT1 turns into the saturated state for the first time. However, the flux density will be pulled back to the unsaturated region owing to the presence of the periodic component. Due to the accumulation effect of the aperiodic component, the saturation degree of flux density is growing. However, owing to the relative high periodic component, the flux density will be pulled back to the unsaturated region periodically. In this case, the waveform of the magnetizing current becomes irregular, as shown in Figure 2.43. After CT1 turns into the saturated state, $\psi_{1\mu}$ and $i_{1\mu}$ vary with the route of the hysteresis loop, that is, the rise and fall of the flux linkage is governed by the physical law mentioned in Section 2.2, as seen in Figure 2.44.

After the fault is removed, the amplitude of i_{11} is restored suddenly to its steady state. Note that at this time the magnetic linkage of the CT1 core has been pushed into the region near to the saturation point by the previous high fault current. In contrast, the magnetic linkage resulting from the low load current has relatively low amplitude. Therefore, $\psi_{1\mu}$ probably stays within the limit hysteresis loop and cannot return to the normal operation region immediately. As a consequence, the inductance of the magnetizing branch may maintain a relatively low value during an entire period of power frequency. And this phenomenon may last for a period of time. Consequently, considerable primary current will be forced to pass through the magnetizing branch, causing serious measuring error. This case is shown clearly in Figure 2.44.

The same CT model is used to analyse behaviour of CT2. Based on Equation (2.42) as mentioned previously, it is found that the maximum of B of CT2 is 0.79 T during the period of the external fault, which is lower than the saturation flux density. Therefore, the flux density of the magnetizing branch of CT2 always stays within the linear operation region throughout the entire process, which means the

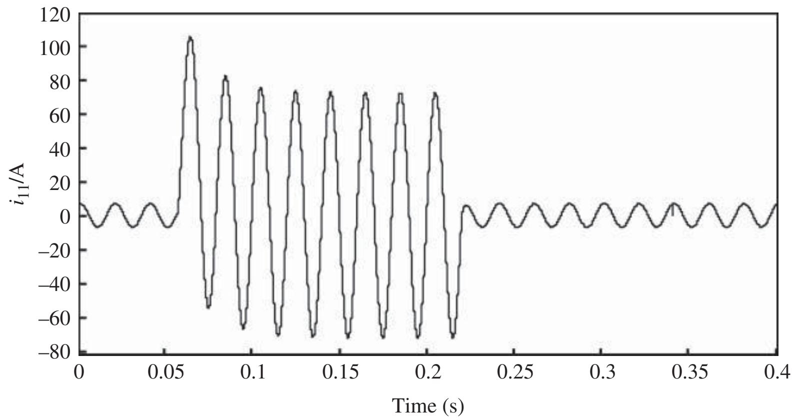

(a)

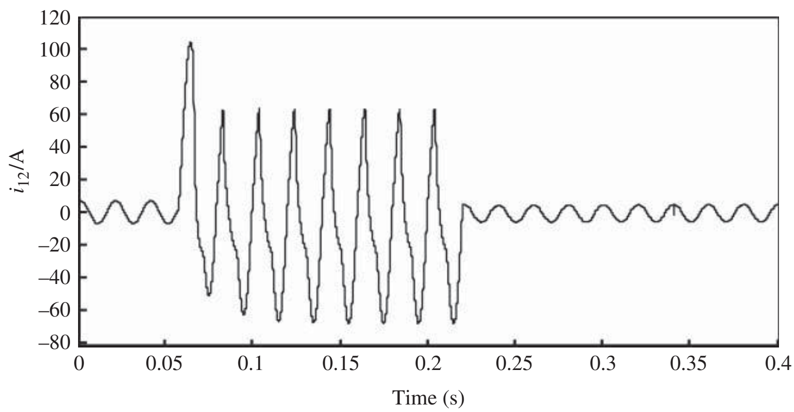

(b)

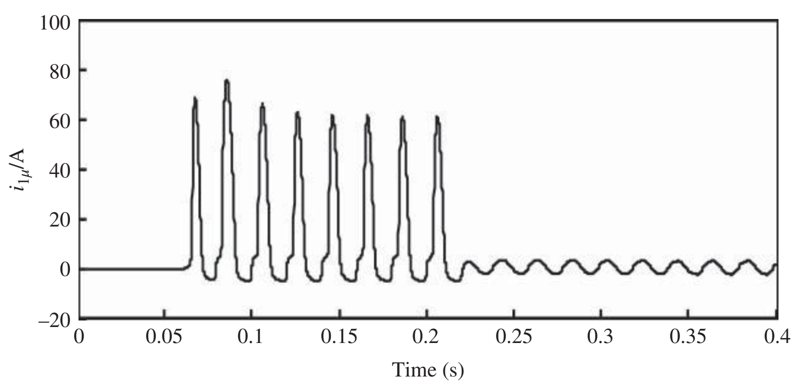

(c)

Figure 2.43 The transforming characteristic of CT1: (a) the primary current i_{11}; (b) the secondary current i_{12}; (c) the magnetizing current $i_{1\mu}$

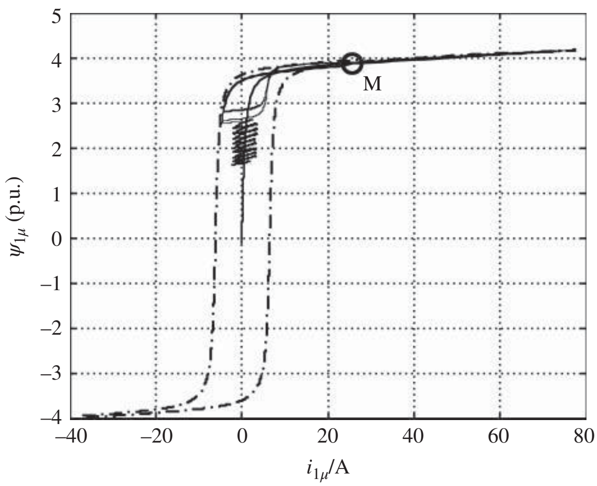

Figure 2.44 The dynamic magnetizing curve of CT1

corresponding inductance of the magnetizing branch may maintain a relatively high value. As a result, the secondary current of CT2 is nearly equal to the primary current. The secondary current of the CT i_{22} can be obtained, as seen in Figure 2.45.

By virtue of i_{12} and i_{22} (Figures 2.43b and 2.45b, respectively), the differential current can be obtained (Figure 2.46). As analysed above, CT1 works in the nonlinear region for most of the time after a given period of time post-fault, while CT2 can always transform the current linearly. Therefore, the false differential current basically results from the nonlinear transformation of CT1.

As seen in Figure 2.46, it can be noticed that the differential current is noticeably distorted during the period the external fault exists. This distortion, resulting in the high second harmonic content of false differential current, is due to the nonlinear transforming caused by the saturation state of the CT1 core. After the fault is removed, the phenomenon of CT local transient saturation leads to a big angle error and amplitude error of CT1, resulting in a false differential current that exhibits a relatively smooth waveform lacking in second harmonic content. This point of view can be verified by the following harmonic analysis.

According to the setting parameters and Figure 2.42, the rated value of the steady-state current of CT1 is 600 A, and the ratio of CT1 is 600/5 A. There is no loss of generality in assuming that the primary rating current of this side is 600 A, the secondary rating current is 5 A.

Figure 2.47 shows the changes of the magnitude of the fundamental component of i_d, which is evaluated with the DFT algorithm. Applying the per unit system to denote the differential current and bias current and taking 5 A as the base, the steady-state magnitude of i_d stabilizes above 0.25 after fault inception (Figure 2.47). If the setting of operating threshold is below 0.25, the mal-operation possibly occurs. Certainly, the mal-operation cannot occur unless the ratio of second harmonic to fundamental of the differential current is lower than the threshold, which is generally set at 15–20%. Figure 2.48 shows the ratio change of second harmonic to fundamental of the differential current after fault occurs. During the existing period of external fault, the ratio of the second harmonic is quite high, far exceeding the threshold. Therefore, mal-operation cannot occur although the magnitude of the fundamental component is high. However, after the fault is removed, the ratio of the second harmonic stabilizes below 15% and the magnitude of the fundamental component stabilizes above 0.25. Provided the differential protection uses 0.25 as the operating threshold and 15% as the second harmonic restraint ratio, mal-operation will definitely occur. The tripping signal of the differential protection will be issued accordingly (Figure 2.49).

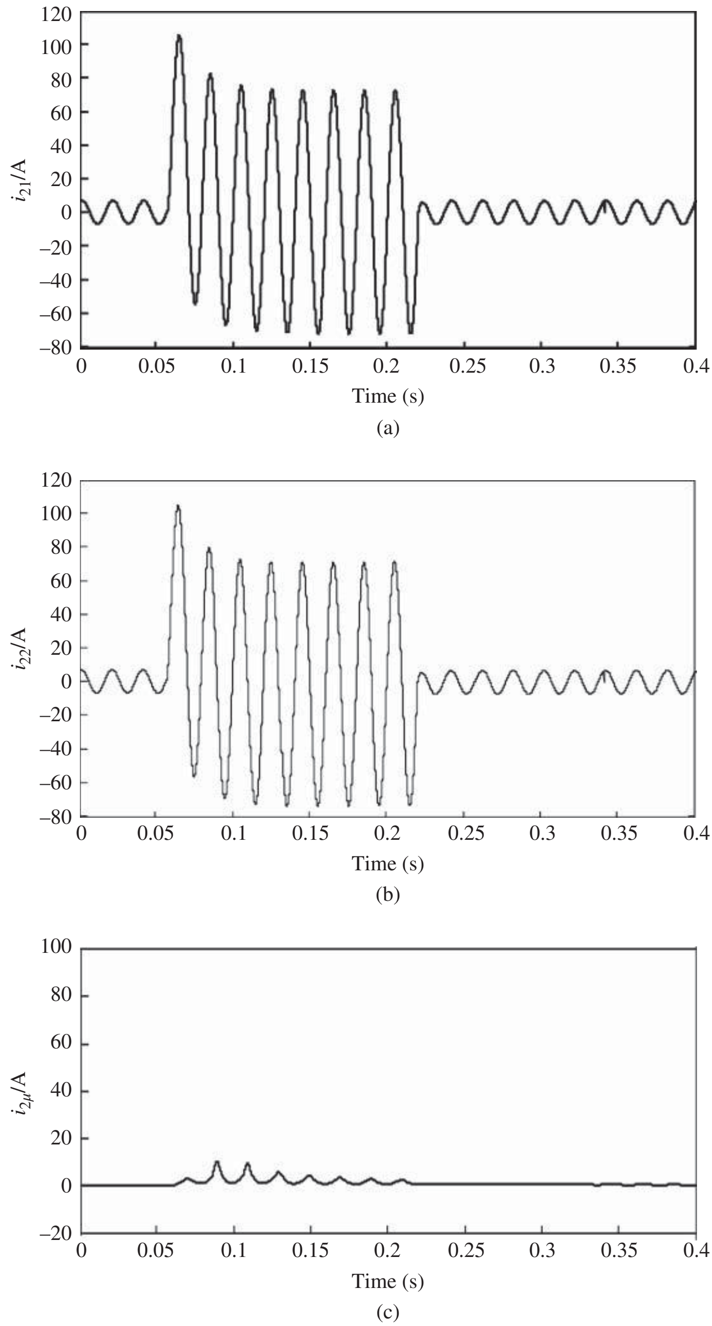

Figure 2.45 The transforming characteristic of the CT2: (a) the primary current i_{21}; (b) the secondary current i_{22}; (c) the magnetizing current $i_{2\mu}$

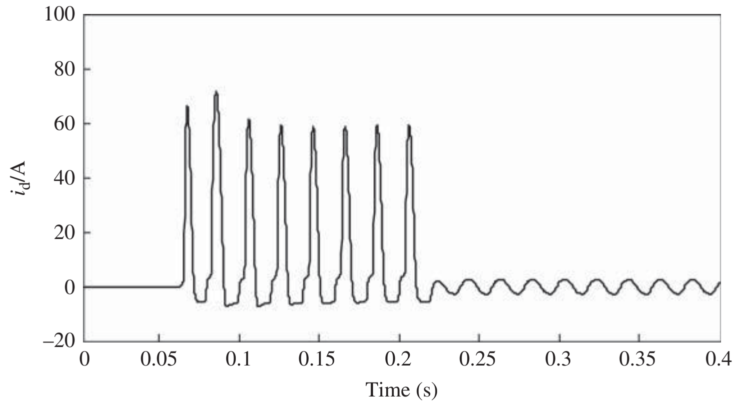

Figure 2.46 The waveform of the differential current between both side CTs

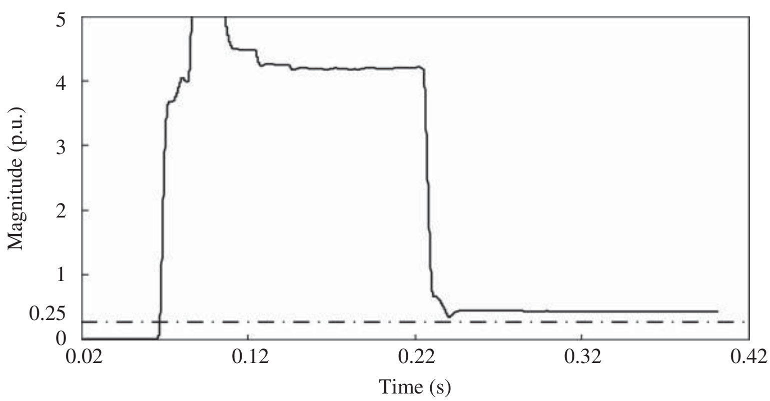

Figure 2.47 The magnitude of the fundamental component of the differential current

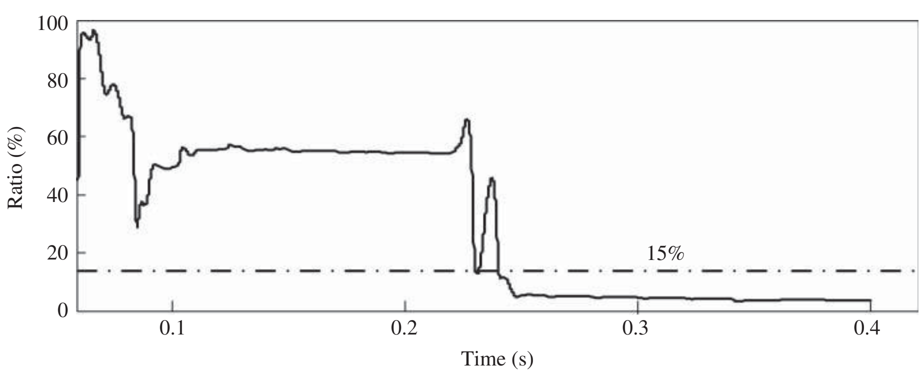

Figure 2.48 The ratio of second harmonic to fundamental of the differential current

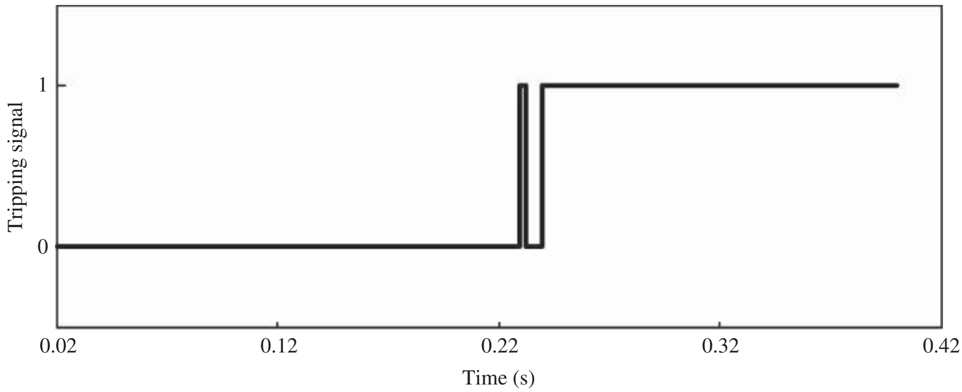

Figure 2.49 The tripping signal of the differential protection

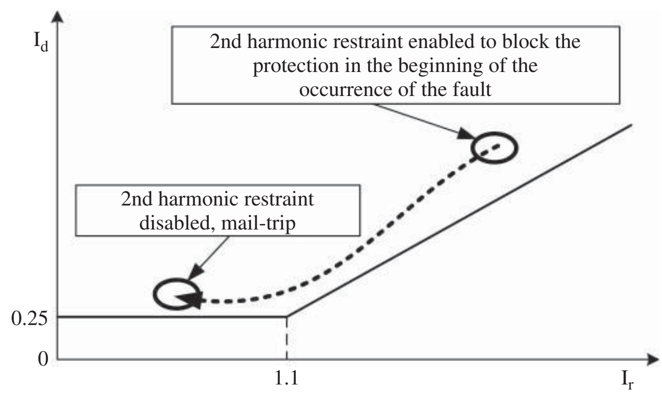

Figure 2.50 The state locus of the mal-operation of the differential protection

Furthermore, Figure 2.50 shows the state locus of the mal-operation of the differential protection. The second harmonic of the differential current is high during the period of the fault. Therefore, the differential protection is blocked reliably. As the fault is removed, the operating point of the CT of one side enters into the region of local transient saturation. In this case, both the amplitude of the differential current and the ratio of its second harmonic component to fundamental component possibly satisfy the tripping conditions of the differential protection, which makes the protection mal-operate.

As seen in Figure 2.49, the differential protection outputs tripping signal continuously less than 0.04 s (two cycles) after the fault is removed.

In summary, a preliminary explanation of one type of unusual mal-operations of the differential protection after the removal of external fault is proposed in this section. The reason is that the saturation states of the CTs on each side of the transformer are different after an external fault occurs. The concept of 'local transient saturation of the CT' is put forward to explain such strange phenomenon. According to this concept, the CT on the primary side of the transformer has entered the saturated state sometime before the fault is removed. The high fault current with aperiodic component pushes the magnetic linkage of the CT into the saturation region. As the fault is removed, due to the dynamic magnetizing characteristic and load current with low amplitude, the CT enters into local transient saturation. In this case, considerable current will flow through the magnetizing branch of this CT, which leads to significant measuring error. On the other hand, the CT on the secondary side of the transformer never enters the saturated state due to different parameters of the CT and, hence, can basically transform linearly throughout the entire process. The secondary currents of both side CTs will form a false differential current with relatively smooth waveform. In this case, the differential current may exceed the minimum operation threshold together with low second harmonic content, leading to the above-mentioned unusual mal-operation of the differential protection. Engineers in the field of protective relaying should recognize this phenomenon and propose corresponding solutions.

2.5 Analysis and Countermeasure of Abnormal Operation Behaviours of the Differential Protection of the Converter Transformer

2.5.1 Recurrence and Analysis of the Reported Abnormal Operation of the Differential Protection of the Converter Transformer

2.5.1.1 Simulation Model of the HVDC System

The magnetizing currents and internal fault currents of the converter transformer in the HVDC system are investigated by virtue of HVDC benchmark test system I of CIGRE (namely Benchmark I). This model was put forward by the DC Links Committee of CIGRE in 1991 and is the first standard model applied to the research of the HVDC control system.

The main circuit structure of the model is shown in Figure 2.51; the values labelled in the figure are all nominal values, the units of which are respectively Ω, H, and F. The whole HVDC system mainly consists of two DC converting stations, DC transmission lines and basic valve control systems. Both sides of the system are connected with AC power systems and the inverting side is a weak system. The short-circuit ratios of rectifiers and inverters are all 2.5 and the basic pulse count is 12. The rated voltage and current of the DC line are 500 kV and 2 kA, respectively. The resistance of the DC line is 2.5 Ω and the converting reactance of the inverter and converter are, respectively, 9.522 and 21.4245 Ω. The reactive power compensation device is a fixed capacitor and the filter is a damping filter.

The Y_0/Δ-1 connected transformer on the converting side is investigated and the parameters of the transformer are:

The rated power is 603.73 MVA and the rated voltages on both sides are 345 kV/213.4557 kV. The positive sequence leakage reactance and the air-gap reactance are respectively 0.18 and 0.2 p.u. The saturation point is 1.25 p.u. and the magnetizing current is 1%. Following the conventional setting criterion, the operation threshold of the differential protection is set as 0.25 p.u., and the ratio of second harmonic restraint is set as 15%.

Adopting the usual operating mode of differential protection in China, the protection will not operate unless the protection elements of three phases are capable of issuing the tripping signal. Unloaded transformer energizing, single-phase-to-earth faults, two-phase(to earth) short-circuit faults and three-phase (to earth) short-circuit faults on the secondary side of the converter transformer are simulated by virtue of the PSCAD/EMTDC software. DC current sources are adopted to simulate the remanence of the transformer core in the case of simulations of magnetizing inrushes; various internal faults on the secondary side of the transformer are simulated by means of adding fault modules.

2.5.1.2 Analysis of Mal-operation of Differential Protection during Unloaded Energizing of the Converter Transformer

Unloaded transformer energizing with various inception angles and remanences are simulated in this part. In view of the length limit, only one of the scenarios of the second harmonic restraint criterion fail-to-block is illustrated.

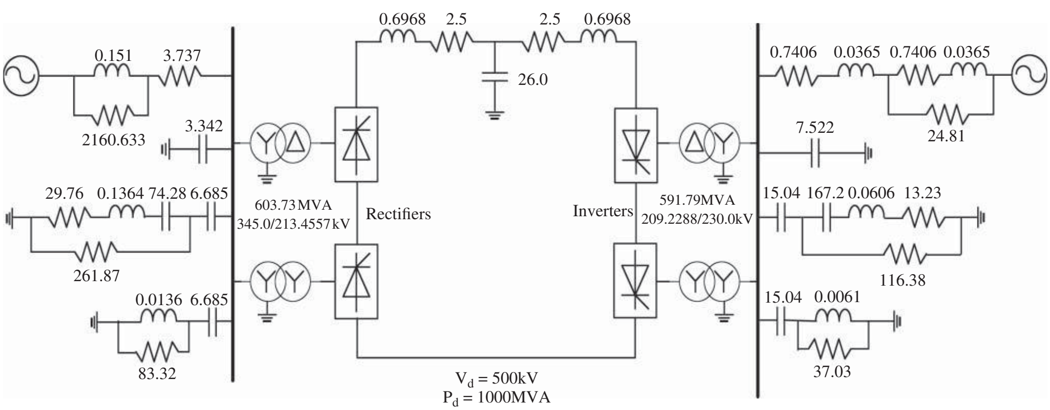

Figure 2.51 Simulation model of the HVDC system

Suppose that the simulation lasts for 0.6 s and the transformer is energized at $t = 0.2617$ s, which means the inception angle of phase A is 30°. The remanences of three phases of transformer core are 0.7 , 0 and −0.7 p.u., respectively. The waveforms, magnitudes of the fundamental components, percentages of second harmonic of the differential currents and the tripping signals of the differential protections of three phases are shown in Figures 2.52–2.55, in which the currents are denoted in terms of per-unit system.

As seen in Figure 2.53, the steady-state magnitudes of differential currents of the three phases all are above 0.25 stably after energizing, which possibly enables the differential protections of the three phases to trip. Furthermore, the percentages of second harmonic to fundamental of differential currents are analysed, as seen in Figure 2.54. It can be seen that percentages of second harmonic to fundamental of differential currents of the three phases are below 15% at, respectively, 0.01, 0.015 and 0.02 s after energizing, and the state of the three percentages simultaneously below 15% lasts for 3/4 cycle. Together with the above analyses of the magnitudes of the fundamental components of differential currents, the

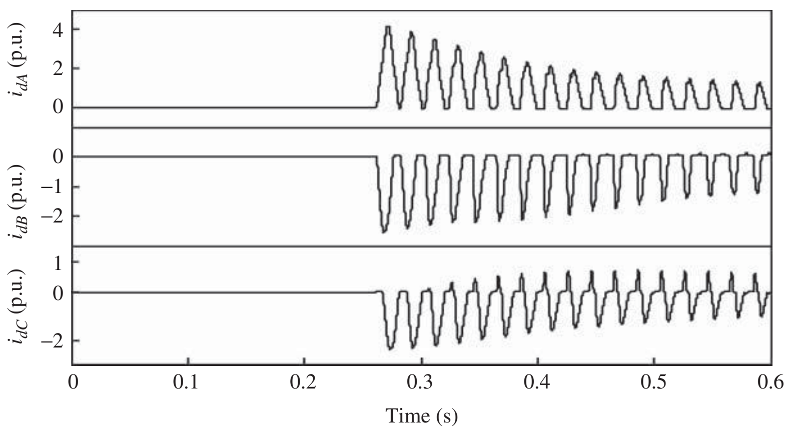

Figure 2.52 Waveforms of differential currents during the energizing of the unloaded transformer

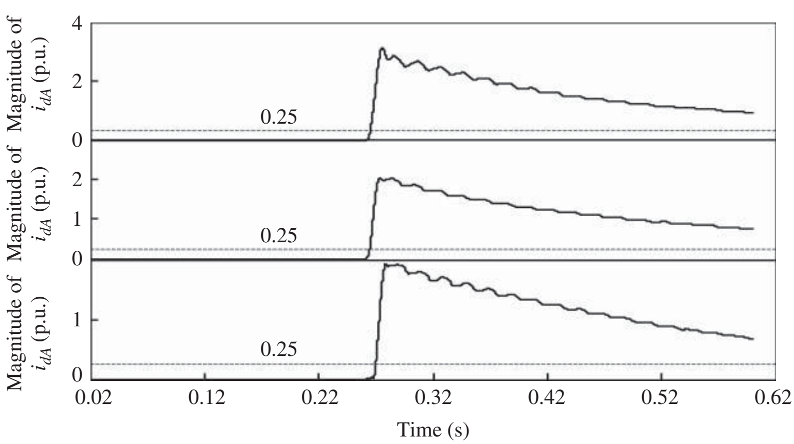

Figure 2.53 Magnitudes of the fundamental component of differential currents

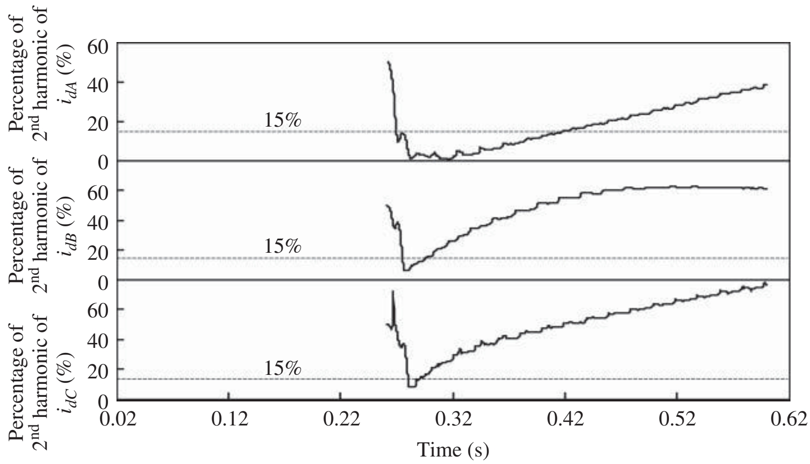

Figure 2.54 Percentages of second harmonic to fundamental of differential currents

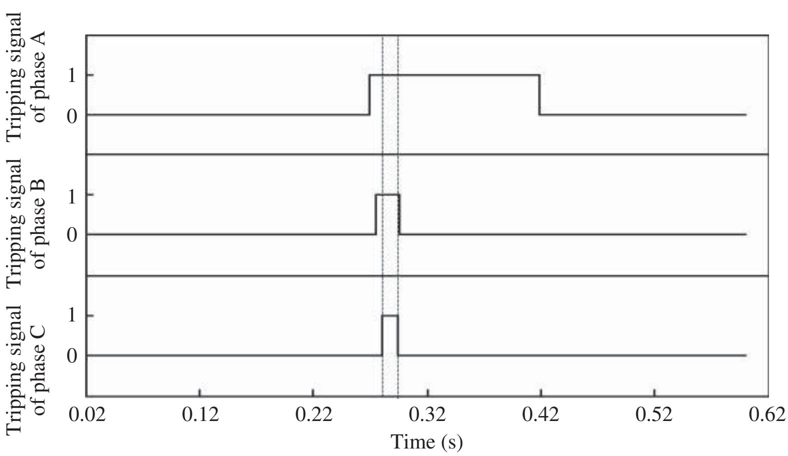

Figure 2.55 Tripping signals of the differential protections of the three phases

tripping of differential protections of three phases is inevitable, as shown in Figure 2.55. It means that the differential protections of three phases will all operate and second harmonic restraint criteria of three phases will all fail to block after about one cycle of the unloaded transformer energizing. Therefore, mal-operation of the transformer differential protection cannot be avoided.

2.5.1.3 Analysis of the Fail-to-Trip of Differential Protection during Internal Faults of the Converter Transformer

The internal fault on the secondary side of the converter transformer actually leads to the short-circuit fault of the converting valves. In this case, the fault current is high during one half cycle, while it is small during the other half cycle owing to the unilateral conduction of the valves, which results in the differential current containing a relatively high second harmonic component. In this case, the differential protection of the converter transformer may fail to trip because of the increase of the second harmonic component in the differential current. For the purpose of investigating the influence of the second harmonic restraint criterion on internal faults of the converter transformer, single-phase-to-earth faults, two-phase short circuit (to earth) faults and three-phases short-circuit (to earth) faults on the secondary side of converter transformer are simulated respectively. Each of simulations lasts for 0.6 s and each fault occurs at 0.2 s. Some scenarios of unnecessarily blocking of the second harmonic restraint criterion are illustrated here, in which the currents are denoted in terms of per-unit system (Scenarios 2.5 and 2.6).

Scenario 2.5 Single phase to earth fault (phase A)

The waveform, magnitude of the fundamental component and the percentage of second harmonic of the differential current of phase A in the case of phase A-to-earth fault on the secondary side of the converter transformer are shown in Figures 2.56 and 2.57, respectively.

It can be seen from Figure 2.57 that the percentage of the second harmonic of the differential current of phase A is always above the restraint threshold after the fault occurs, although the magnitude of the differential current exceeds the operation threshold as well. In this case, the differential protection is unnecessarily blocked and the fault cannot be removed in time.

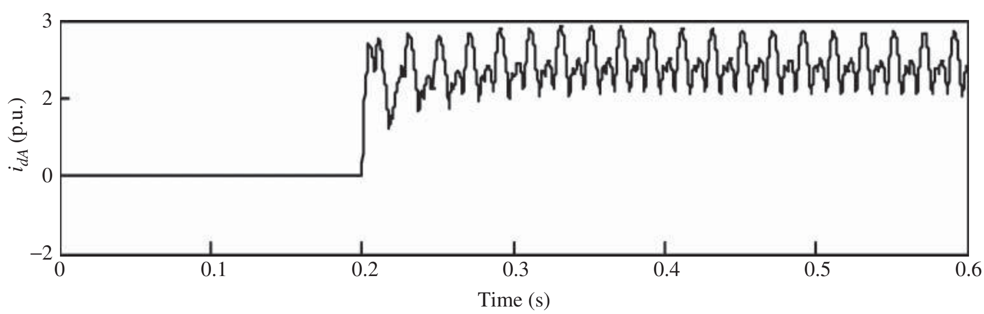

Figure 2.56 Waveform of the differential current of phase A

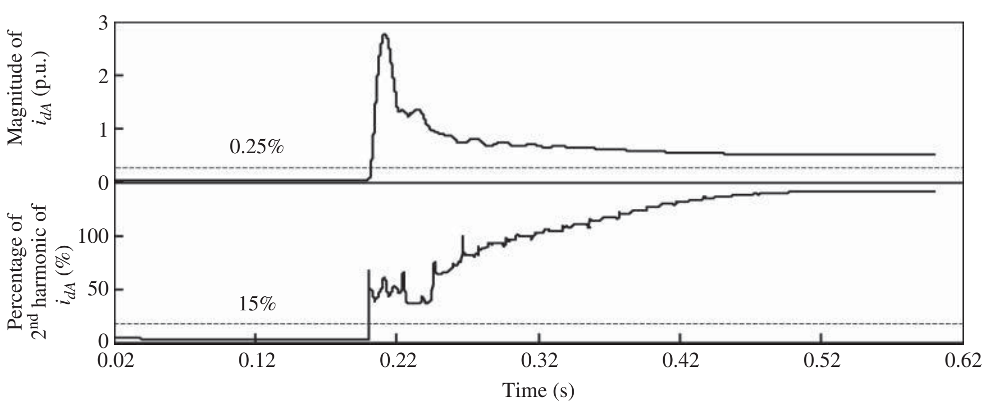

Figure 2.57 Magnitude of the fundamental component and percentage of second harmonic to fundamental of differential current of phase A

Scenario 2.6 Two phase to earth fault (phases A and B)
The waveforms, magnitudes of the fundamental component and the percentages of second harmonic of the differential currents of phases A and B in the case of a A-B-G fault occurring on the secondary side of converter transformer are respectively shown in Figures 2.58–2.61.

As seen in Figures 2.59 and 2.61, the magnitudes of the differential currents of both phases A and B exceed the operation threshold after the fault occurrence, which should lead to the operation of the differential protections of these two phases. However, the percentage of second harmonic of the differential current of phase B is stably above the restraint threshold. As a result, even though the protection of phase A can operate correctly, the differential protection of the converter transformer is still wrongly blocked by the second harmonic restraint criterion of phase B.

It is proven with the above analyses that the decrease of second harmonic component in the differential current due to the impacts of inception angle and remanence may result in the mal-operation of the differential protection during energizing of the unloaded converter transformer. On the other hand, the increase of second harmonic component in the differential current may lead to the wrong blocking of the differential protection in the case of some internal faults on the secondary side of the converter transformer. Consequently, the second harmonic restraint criterion is not completely appropriate when it is applied to discriminating between magnetizing inrushes and fault currents of the converter transformer. Therefore, it is necessary to find a novel criterion that is immune to the impacts of the core saturation

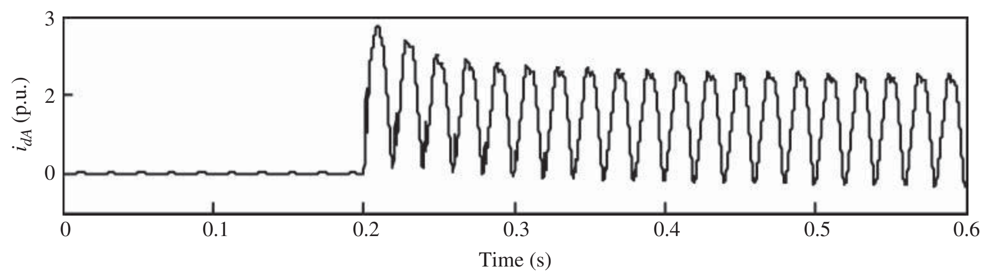

Figure 2.58 Waveform of differential current of phase A

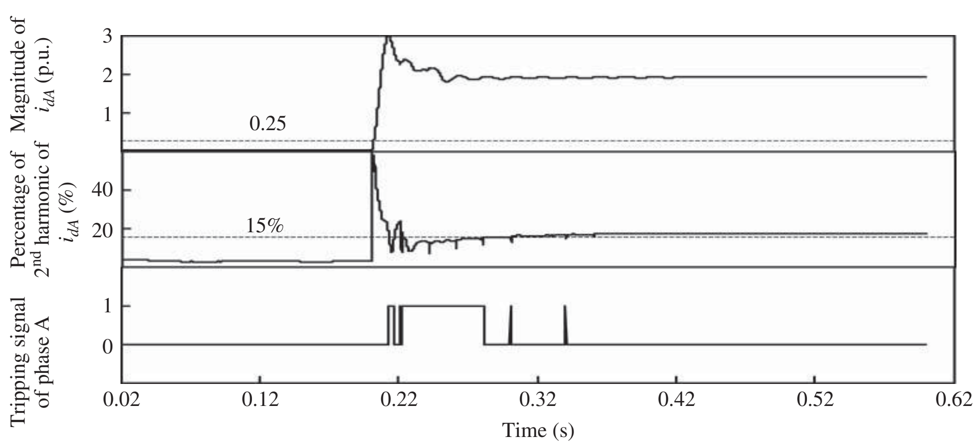

Figure 2.59 Magnitude of fundamental component, percentage of second harmonic to fundamental of differential current and tripping signal of differential protection of phase A

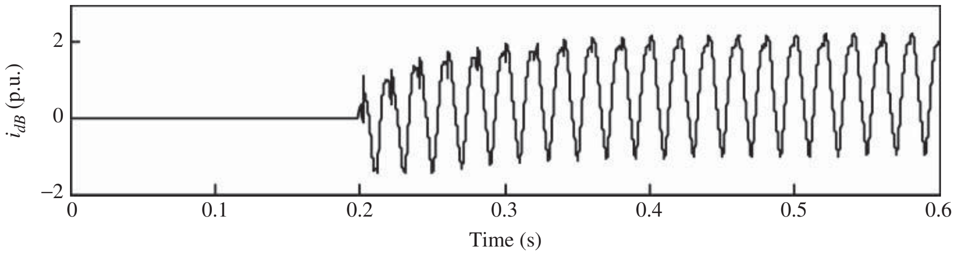

Figure 2.60 Waveform of differential current of phase B

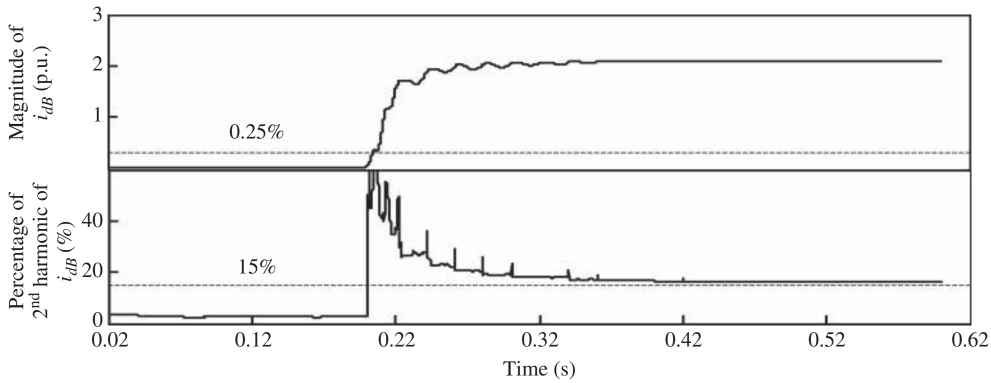

Figure 2.61 Magnitude of fundamental component and percentage of second harmonic to fundamental of differential current of phase B

and harmonic characteristics to discriminate between internal faults and magnetizing inrushes of the converter transformer.

As it must take a certain time for the transformer core to enter saturation in the case of unloaded transformer energizing, the appearance of the differential current caused by the magnetizing inrush always lags behind the occurrence of the disturbance for a time difference. For internal faults, the occurrences of the differential current and the fault are theoretically simultaneous, which means that such a time difference does not exist. Therefore, if the time difference can be located by means of an effective method, it can be applied to discriminate between internal faults and magnetizing inrushes at the beginning of disturbances.

2.5.2 Time-Difference Criterion to Discriminate between Faults and Magnetizing Inrushes of the Converter Transformer

2.5.2.1 Existing Time-Difference Methods and their Limitation Applied to Discriminating between Faults and Magnetizing Inrushes of the Converter Transformer

For the purpose of simplifying protection schemes, most of the existing time-difference methods are based on the time difference between the change of line current of one side of the transformer and the occurrence of differential current to avoid introducing voltage quantity. In this case, a method to locate the time difference between the fault occurrence and the appearance of the differential current implemented with mathematical morphology was presented as reference. The time difference can be used to identify the external fault from internal faults in the case of CT saturation. A method to identify the synchronization of the change of line current and differential current was proposed in reference. Based on the method, the sympathetic inrush and the internal and external faults during sympathetic inrush occurring can be identified. The line current on the Y-side of the transformer and the differential current are adopted as the reference quantities for both of the two time-difference methods mentioned above.

However, the methods cannot be applied to identify unloaded transformer energizing. This is because the differential current is exactly the line current on the energizing side of the transformer in the case of unloaded transformer energizing. Therefore, the time difference impossibly exists between the change of line current and the appearance of differential current.

When the transformer experiences various disturbances, the voltage always changes relatively instantaneously at the time the disturbance occurs. As it takes a certain length of time to enter saturation of the transformer core in the case of unloaded transformer energizaing, the appearance of the differential current caused by the magnetizing inrush consequentially lags behind the voltage change for a time difference. Therefore, the phase voltage and the differential current can be used to form a novel time-difference method in order to discriminate between magnetizing inrushes and internal faults. In this case, the shortage of the exiting time-difference methods mentioned above can be overcome.

2.5.2.2 The Novel Criterion Using the Time Difference between Superimposed Phase Voltage and Differential Current to Discriminate between Internal Faults and Transformer Energizing

Actually, the differential current is the magnetizing inrush caused by the transformer core saturation in the event of unloaded transformer energizing and the emergence of the magnetizing inrush lags behind the change of the phase voltage. On the other hand, the differential current is the fault current in the case of internal faults of the transformer and the change of the phase voltage is theoretically simultaneous with that of the differential current. The time difference between the change of the phase voltage and that of the differential current can be identified. If the time difference is greater than a certain threshold, the differential current should be the normal magnetizing inrush and the protection will be blocked. According to the field experience and results of extensive simulation tests, the threshold of the time difference can be set as 3 ms.

The superimposed components of the phase voltage and differential current are used as the reference quantities for the criterion to locate the times of sudden changes of phase voltage and differential current. In theory, if there is no disturbance in the system, the superimposed components of the phase voltage and the differential current are always zero, or they are quantities with quite small random fluctuant values. However, the captured superimposed component will appear as a waveform of a one-cycle power-frequency component containing some harmonic components once a disturbance occurs. This waveform always emerges from zero value to a nonzero series. This phenomenon always exists no matter how the inception angle of the disturbance changes. Therefore, the detection of the emergence time of this series should be quite easy. A detailed description of the time locating method is given here.

Firstly, the superimposed components of the phase voltage and the differential current are extracted by means of the real-time calculation of the superimposed quantity that is relative to the corresponding point of the previous cycle. Then, the differential calculation is performed on these two superimposed components and two difference sequences relating to the superimposed components of the phase voltage and the differential current are obtained; these are stored in the circulatory buffer. On this basis, the floating threshold used to locate the change times of the difference sequences, described as: the maximum of the absolute values of the sequence within a one-cycle time window, whose end is one-cycle leading to the current point, is extracted. The absolute value of the current point and the extracted maximum are

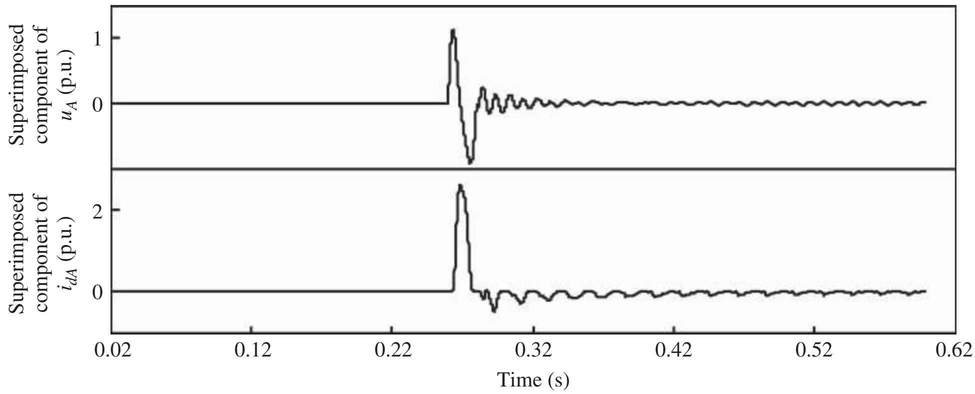

Figure 2.62 Superimposed components of the voltage and the differential current of phase A (Scenario 2.7)

compared. If the former exceeds a specified multiple of the latter, the first extremum after the current point should be captured. This multiple is temporarily set as 5 and it can be adjusted according to actual operating conditions. After that, the time corresponding to the point having the value of 30% of the captured extremum is back traced, and this time is regarded as the time that the sudden change of the phase voltage or differential current occurs.

The criterion is enabled when the differential current exceeds the threshold, and then the time difference between the sudden changes of the phase voltage and the differential current is located. If this time difference exceeds 3 ms, the differential protection is blocked. Otherwise, it is unblocked. In this case, the disturbance can be identified as a fault or an energizing.

2.5.2.3 Simulation Tests of the Time-Difference Criterion

The simulation model is shown in Figure 2.51; unloaded energizing and various internal faults of the converter transformer are simulated to validate the proposed time-difference criterion. The simulation results of several representative scenarios are illustrated here (Scenarios 2.7–2.13), in which the superimposed components of the phase voltage and the differential current are denoted in terms of per-unit system.

Scenario 2.7 Transformer energizing with phase A 0° inception angle and all phases with zero remanence

The simulation duration is 0.6 s and the transformer is energized at $t = 0.26$ s, which means the inception angle of phase A is 0°. The remanences of three phases of transformer core are all 0.

The waveforms and located occurrence times of superimposed components of phase voltages and differential currents of three phases are shown in Figures 2.62–2.67 respectively.

As seen in Figures 2.63, 2.65 and 2.67, the time differences between the superimposed components of phase voltages and differential currents of three phases are 5.2, 4.2 and 4.6 ms, respectively, all of which exceed the restraint threshold of 3 ms. Therefore, the disturbance is identified as the one due to magnetizing inrush and the differential protections of the three phases are all reliably blocked.

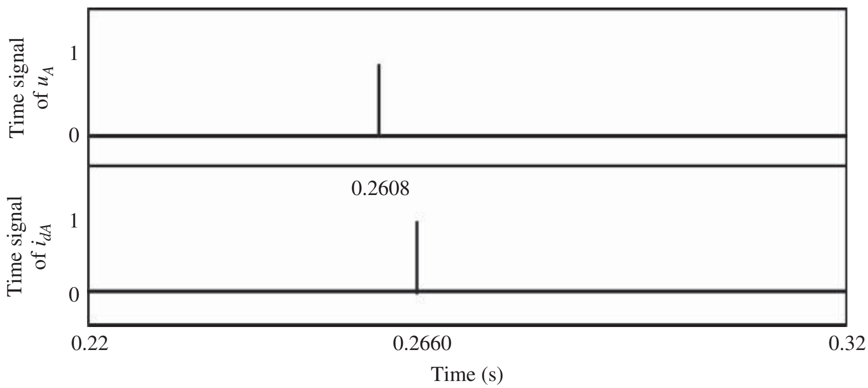

Figure 2.63 Occurrence times of superimposed components of the voltage and the differential current of phase A (Scenario 2.7)

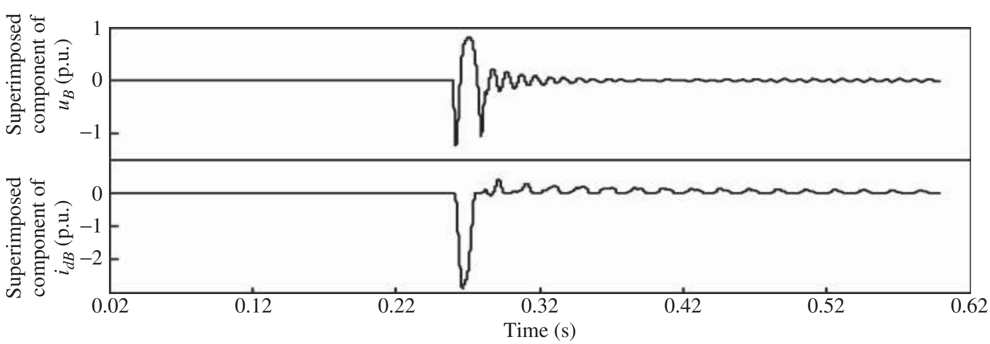

Figure 2.64 Superimposed components of the voltage and the differential current of phase B (Scenario 2.7)

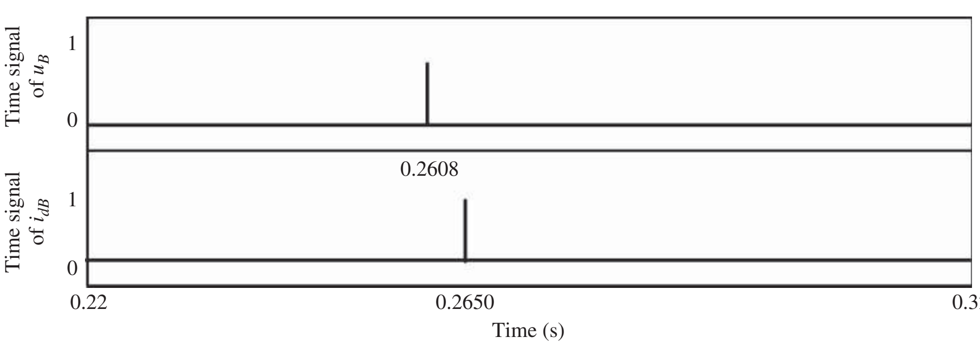

Figure 2.65 Occurrence times of superimposed components of the voltage and the differential current of phase B (Scenario 2.7)

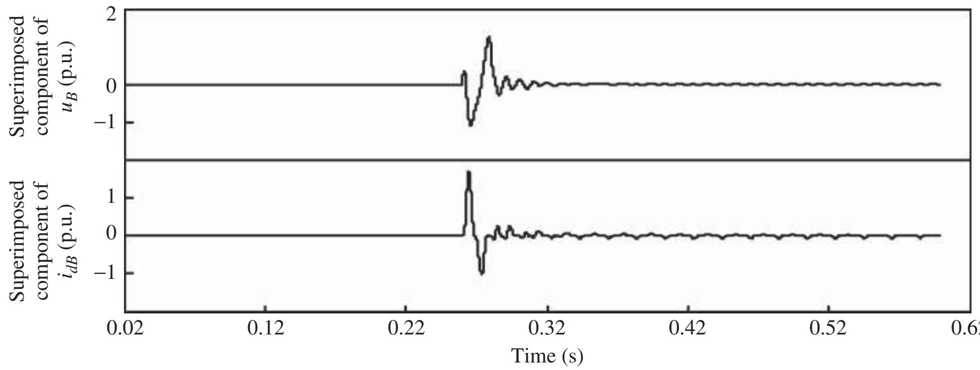

Figure 2.66 Superimposed components of the voltage and the differential current of phase C (Scenario 2.7)

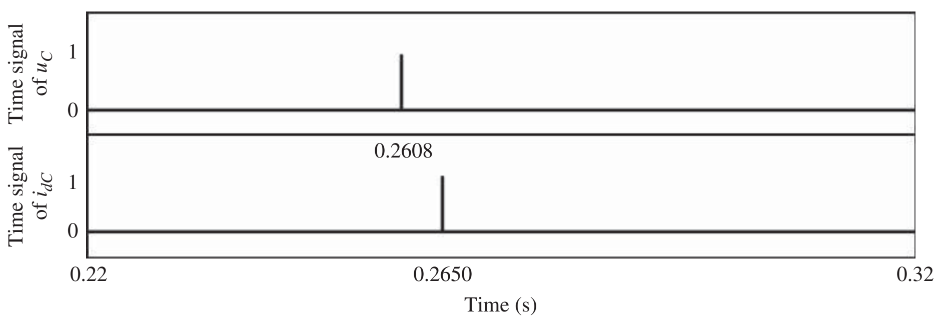

Figure 2.67 Occurrence times of superimposed components of voltage and differential current of phase C (Scenario 2.7)

Scenario 2.8 Transformer Energizing with phase A 30° inception angle and remanences of phases A, B and C being 0.7, 0 and −0.7 p.u., respectively

The simulation duration is 0.6 s and the transformer is energized at $t = 0.2617$ s, which means the inception angle of phase A is 30°. The remanences of three phases of the transformer core are 0.7, 0 and −0.7 p.u. respectively.

According to the analyses in Section 2.2, the second harmonic restraint based differential protection mal-operates for this scenario. The occurrence times of superimposed components of phase voltages and differential currents of three phases, which are located by means of the proposed method, are shown in Figures 2.68–2.70, respectively.

It can be seen that the sudden changes of the three differential currents lag behind those of three phase voltages for 3.8, 5.0 and 4.2 ms, respectively. The three time differences all exceed the restraint threshold and, hence, the differential protections of three phases can be reliably blocked. Therefore, it is proven that the application of the proposed time-difference criterion can prevent the differential protection from the mal-operations analysed in Section 2.2.

The effectiveness of the proposed criterion in the case of internal faults of the converter transformer is validated by means of the simulation tests of Scenarios 2.9–2.13. The fault conditions are similar to

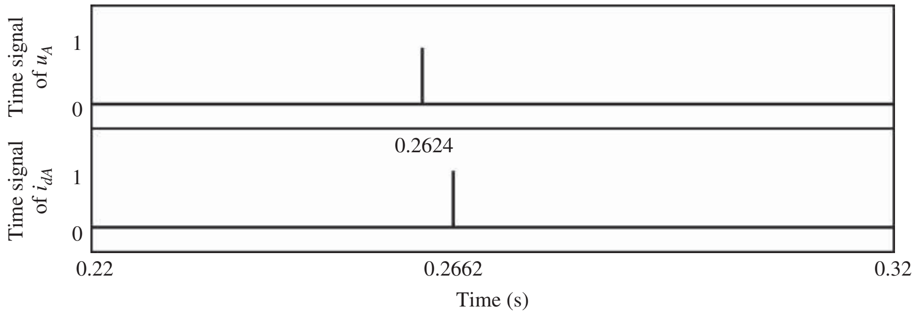

Figure 2.68 Occurrence times of superimposed components of the voltage and the differential current of phase A (Scenario 2.8)

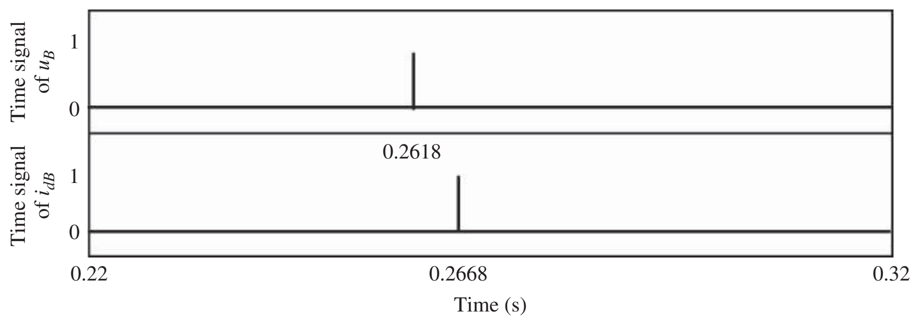

Figure 2.69 Occurrence times of superimposed components of the voltage and the differential current of phase B (Scenario 2.8)

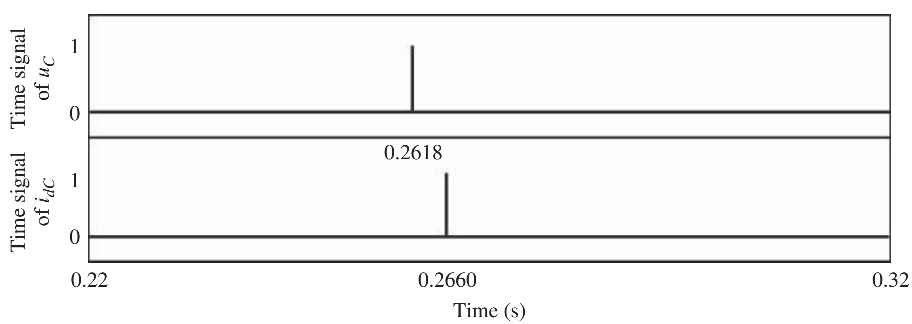

Figure 2.70 Occurrence times of superimposed components of the voltage and the differential current of phase C (Scenario 2.8)

those in Section 2.2, that is, the simulation duration of each case lasts for 0.6 s and each fault occurs at 0.2 s.

Scenario 2.9 Fail-to-trip case due to Phase A to earth fault on the secondary side of the converter transformer

The fail-to-trip case due to phase A to earth fault on the secondary side of the converter transformer, that is, Scenario 2.1 in Section 2.1.

The waveforms and located occurrence times of superimposed components of phase voltage and differential current of phase A are shown in Figures 2.71 and 2.72, respectively. It can be seen that the detected change times of the phase voltage and the differential current are 0.2014 and 0.2016 s, respectively. As seen, the time difference is only 0.2 ms. In this case, the disturbance is identified as an internal fault by means of the proposed criterion and the protection can operate correctly.

Scenario 2.10 Fail-to-trip case due to Phases A and B to earth fault on the secondary side of the converter transformer

The fail-to-trip case due to phases A and B to earth fault on the secondary side of converter transformer that is, Scenario 2.2 in Section 2.1.

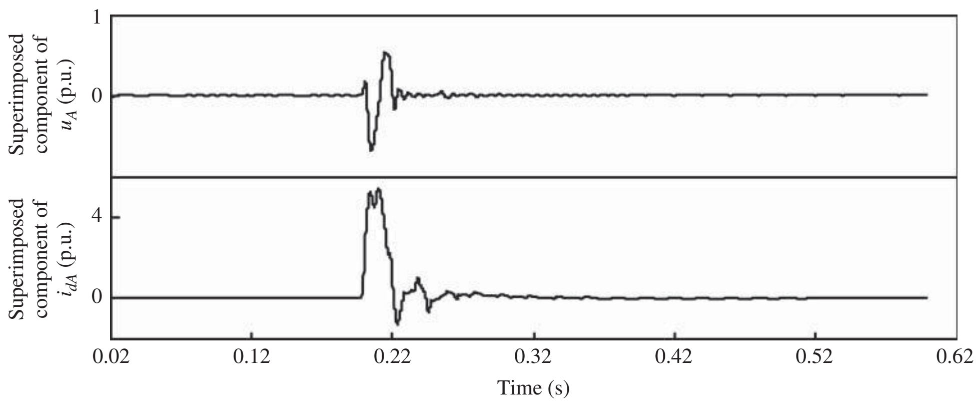

Figure 2.71 Superimposed components of voltage and the differential current of the phase A (Scenario 2.9)

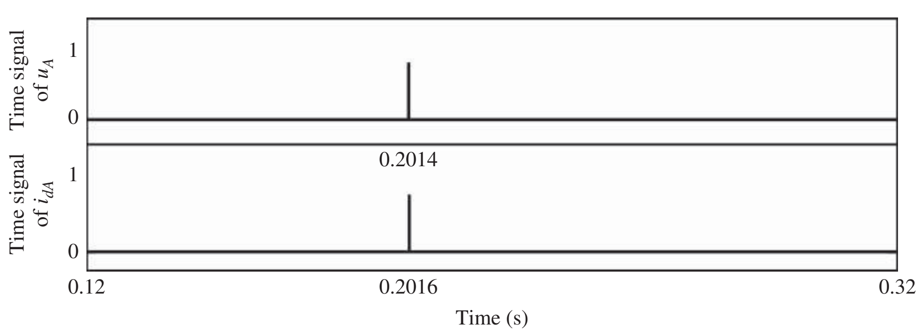

Figure 2.72 Occurrence times of superimposed components of voltage and differential current of phase A (Scenario 2.9)

The waveforms and the location of the occurrence times of superimposed components of phase voltages and differential currents of phases A and B are shown in Figures 2.73 and 2.74 and Figures 2.75 and 2.76 respectively.

According to Figures 2.74 and 2.76, the time differences between the sudden changes of phase voltages and differential currents of phases A and B are 0.4 and 1.0 ms, respectively, both of which are less than

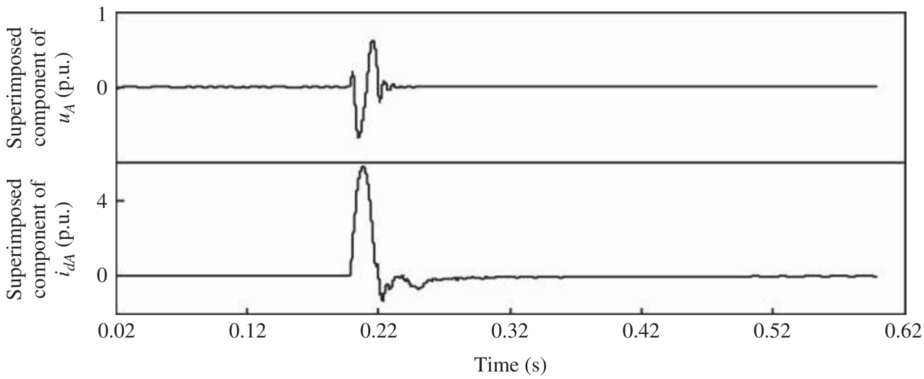

Figure 2.73 Superimposed components of the voltage and the differential current of phase A (Scenario 2.10)

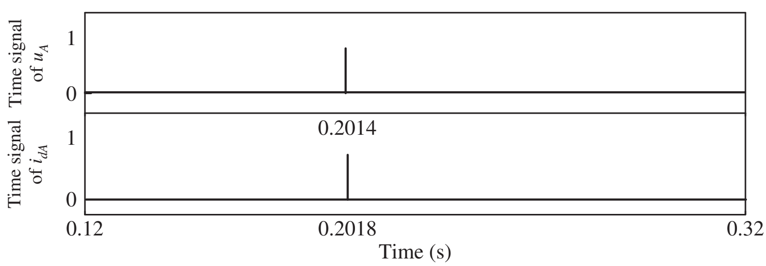

Figure 2.74 Occurrence times of superimposed components of the voltage and the differential current of phase A (Scenario 2.10)

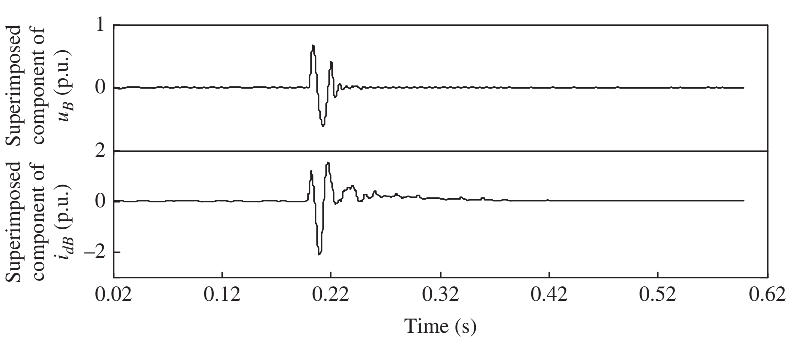

Figure 2.75 Superimposed components of the voltage and the differential current of phase B mbox(Scenario 2.10)

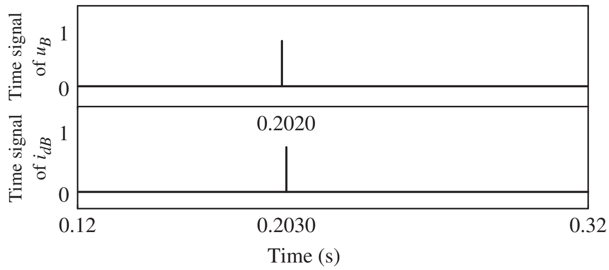

Figure 2.76 Occurrence times of superimposed components of the voltage and the differential current of phase B (Scenario 2.10)

the restraint threshold. As a result, the disturbance is identified as an internal fault and both protections of phases A and B can operate correctly.

In virtue of the analyses in Section 2.2, the second harmonic restraint based differential protection are unnecessarily blocked for the above two scenarios. In contrast, the application of the proposed time-difference criterion can prevent the differential protection from being wrongly blocked in these cases.

Simulation results of the time differences between sudden changes of phase voltages and differential currents for Scenarios 2.11–2.13 are presented in Table 2.4. The descriptions of Scenarios 2.11–2.13 are:

Scenario 2.11 Protection response to a phase to phase (AB) short-circuit fault occurring on the secondary side of the converter transformer

Scenario 2.12 Protection response to a three-phase short-circuit fault occurring on the secondary side of the converter transformer

Scenario 2.13 Protection response to a three-phase to earth fault on the secondary side of the converter transformer

Table 2.4 Simulation results of the time differences between sudden changes of phase voltages and differential currents for Scenarios 2.11–2.13

Scenario number	Faulty phase	Occurrence time of superimposed components		Time difference (ms)	Operation of the protection
		Voltage	Current		
2.11	A	0.2012	0.2020	0.8	Operates
	B	0.2014	0.2020	0.6	Operates
2.12	A	0.2014	0.2020	0.6	Operates
	B	0.2016	0.2024	0.8	Operates
	C	0.2020	0.2022	0.2	Operates
2.13	A	0.2014	0.2016	0.2	Operates
	B	0.2012	0.2020	0.8	Operates
	C	0.2016	0.2020	0.4	Operates

As seen in Table 2.4, in the case of these faults the time difference between sudden changes of the phase voltage and the differential current of each phase is less than the restraint threshold of 3 ms. Consequently, the faults are all identified as internal faults and the protections can all operate correctly.

It has been proven in hundreds of simulation tests that the criterion using the time difference between the superimposed phase voltage and differential current is effective when identifying unloaded energizing from internal faults of the converter transformer under various conditions.

In summary, the operation performance of the second harmonic restraint based differential protection in the case of unloaded energizing and internal faults of the converter transformer has been investigated. It is demonstrated that the second harmonic restraint criterion may result in both mal-operation and fail-to-trip when it is applied in the differential protection for converter transformers. Therefore, it has been required to design a novel criterion to discriminate between the internal faults and the magnetizing inrushes of the converter transformer. According to the characteristic of transformer core, there exists a time difference between the sudden change of the phase voltage and the emergence of the differential current in the event of unloaded transformer energizing. Based on this phenomenon, a novel criterion using the time difference between the superimposed phase voltage and differential current to discriminate between internal faults and energizing of the converter transformer is proposed. The effectiveness of the proposed criterion in the case of various unloaded energizing and internal faults of the converter transformer is validated by virtue of EMTDC-based simulation tests. Furthermore, the principle of the criterion is quite simple and it is immune to the impacts of any harmonic. This proposed criterion is applicable to not only converter transformers but for common transformers in terms of discriminating between unloaded energizing and internal faults.

2.6 Summary

Several cases of abnormal mal-operation of transformer differential protection have been reported in recent years. This chapter is an attempt to study the unusual mal-operation of the differential protection of the transformer and reinforce the theory system of transformer transient analysis. Based on the non-linearity of transformer core, mathematical models are put forward for analysing the transient course of external fault inception and removal, together with the CT model involving the magnetic hysteresis effect. The effectiveness of model is validated with extensive simulation tests.

References

[1] Mathews, C.A. (1954) An improved transformer differential relay. *Electrical Engineering*, **73** (7), 648–648.

[2] Specht, T.R. (1951) Transformer magnetizing inrush currents. *Electrical Engineering*, **70** (4), 324–324.

[3] Sharp, R.L. and Glassburn, W.E. (1958) A transformer differential relay with second-harmonic restraint. *Transactions of the American Institute of Electrical Engineers Part III: Power Apparatus and Systems*, **77** (3), 913–918.

[4] Kennedy, L.F. and Hayward, C.D. (1938) Harmonic-current-restrained relays for differential protection. *Electrical Engineering*, **57** (5), 262–271.

[5] Lin, X., Liu, P. and Malik, O.P. (2002) Studies for identification of the inrush based on improved correlation algorithm. *IEEE Transactions on Power Delivery*, **17** (4), 901–907.

[6] Einvall, C.H. and Linders, J.R. (1975) A three-phase differential relay for transformer protection. *IEEE Transactions on Power Apparatus and Systems*, **94** (6), 1971–1980.

[7] Wang, Z.P., Xu, Y., Wang, X. *et al.* (2003) Study on the novel transformer protection principle based on the transformer model. *Proceedings of the CSEE*, **23** (12), 54–58.

[8] He, B.H. and Xu, X.D. (1998) The principle of transformer differential protection based on wave comparison. *Proceedings of the CSEE*, **18** (6), 395–398.

[9] Hu, Y.F. and Chen, D.H. (2000) A new method to identify inrush current based on sample values. *Proceedings of the CSEE*, **20** (9), 55–58.

[10] Jiao, S.H. and Liu, W.S. (1999) A novel scheme to discriminate inrush current and fault current based on integrating the waveform. *Proceedings of the CSEE*, **19** (8), 35–38.
[11] Jiao, S.H., Liu, W.S., Liu, J.F. *et al.* (1999) A new principle of discrimination between inrush current and fault current of transformer based on wavelet. *Proceedings of the CSEE*, **19** (7), 1–6.
[12] Li, G.C., Liu, W.S., Jia, Q.Q. *et al.* (2001) A new algorithm to prevent misoperation of transformer differential protection based on principle of wavelet transform. *Power System Technology*, **25**(7), 47–51.
[13] Wang, Z.G., Ren, J., Qiu, X.H. *et al.* (2006) New criteria for harmonic blocking differential protection of transformers. *Automation of Electric Power Systems*, **30** (14), 50–53.
[14] Guzman, A., Zocholl, Z., Benmouyal, G. *et al.* (2001) A current-based solution for transformer differential protection. I. Problem statement. *IEEE Transactions on Power Delivery*, **16** (4), 485–491.
[15] Sidhu, T.S. and Sachdev, M.S. (1992) Online identification of magnetizing inrush and internal faults in three-phase transformers. *IEEE Transactions on Power Delivery*, **7** (4), 1885–1891.
[16] Inagaki, K., Higaki, M., Matsui, Y. *et al.* (1988) Digital protection method for power transformers based on an equivalent circuit composed of inverse inductance. *IEEE Transactions on Power Delivery*, **3** (4), 1501–1510.

3

Novel Analysis Tools on Operating Characteristics of Transformer Differential Protection

3.1 Introduction

Due to the nonlinearity of the transformer core, a magnetizing inrush possibly occurs when a transformer is energized. In this case, the security of the differential protection will be challenged [1]. To solve this problem, many criteria have been proposed [2–4] to prevent differential protection from mal-operation due to inrush. Among these, the second harmonic restraint criterion is the most prevalent. The effectiveness of this criterion has been verified with a considerable number of industrial applications in past decades. However, some differential protections equipped with second harmonic restraint mal-operate under some abnormal disturbances or operations. For instance, some mal-operations of the transformer differential protection during loaded transformer energizing have been reported recently [5]. A concept called 'ultra-saturation state' has been put forward to explain this phenomenon. According to the existing analysis, the amplitude of the magnetizing inrush should be very high when the transformer experiences the 'ultra-saturation state'. In this case, the protection will detect a quite high bias current, a high operating current and a low second harmonic of differential current; therefore, it mal-operates at the biased operation region, since the percentage bias characteristic is employed by most differential protection. However, the data from the field fault recorder show that some mal-operation cases occurred at the non-restraint region in the percentage bias characteristic plane, and the operating current was only somewhat higher than the threshold. Of course, the second harmonic restraint criterion failed to block the differential protection as well in these cases. Obviously, the ultra-saturation model of the transformer is not suitable for explaining such scenarios. Furthermore, the loaded transformer energizing model needs to improve, in that the nonlinear magnetizing inductance of transformer is simplified as an average inductance being a constant, which does not coincide with the real situation. Therefore, a novel model for analysing the transient course of the loaded transformer energizing is proposed. Together with the existing CT (current transformer) models, the waveform characteristics of the primary and secondary inrushes are analysed. On basis of above models, the reported mal-operations can be explained rationally.

The performance of the differential protection is an issue of concern in the field of theoretical analyses of the relay protection. By means of these studies, researchers always try to exploit the potential of the existing criteria, or provide some qualitative and quantitative conclusions for the adoption of certain

Electromagnetic Transient Analysis and Novel Protective Relaying Techniques for Power Transformer,
First Edition. Xiangning Lin, Jing Ma, Qing Tian and Hanli Weng.

criterion as the theoretical bases. In fact, observing the differential protection, which seems uncomplicated, from different angles, some new discoveries can be obtained. In this section, an attempt is made to find out the appropriate theoretical bases for the existing method in the engineering field of relay protection according to the comparative studies on the phase current percentage differential criterion and phase current difference based percentage differential criterion.

There is no doubt that current differential protection has been one of the most popular main protections to secure electrical equipment [6, 7]. The core philosophy of its principle has never changed since it was firstly proposed by C.H. Merz and B. Price in 1904, although the implementations, especially the restraint quantities or bias current, may have different forms [8].

As for the percentage differential criterion, the dependability will be the main concern in the case of isolating an internal fault. Thereby, the restraint current needs to be reduced as much as possible. However, it is preferable to increase the restraint quantity (RQ) when an external fault occurs because the security, in turn, becomes the subject. To resolve the contradiction, a so-called "Complex Percentage Differential" (CPD) criterion has been proposed, which compensates the restraint current with the minus differential current. It is declared that both the reliability and selectivity of protection can be enhanced. Nevertheless, this point of view has to be confirmed by convincing comparative analyses. It is thus necessary to compare the CPD criterion with the Normal Percentage Differential (NPD) criterion. In the classical theory of comparators, there exists a representation of a differential characteristic in the complex plane defined as the alpha or beta plane. With this plane, a certain percentage differential criterion can be investigated with a complex variable that is precisely the ratio of the outgoing current over the incoming current. However, it is not suitable for comparing the overall performances among various criteria, since each criterion has own restraint coefficient settings. It should be determined how the restraint coefficients should be configured for the compared criteria and then the comparison can be based on a rational premise. At present, no applicable baseline is available for such a purpose. A novel reliability evaluation criterion is therefore proposed to compare the performances among various differential protections; this is referred to as 'consistent security' in this chapter. CPD criterion is proved to be better than NPD criterion using the criterion.

It has been proven with the history and progress of protective relaying of power systems, that the use of the superimposed components enhances the performance of protection devices to a great extent. The distinct examples are the applications of superimposed component based distance protection and directional protection of transmission lines. However, there are still some arguments on the applications of superimposed currents to the current differential protections. The discussions on this issue will help to advance the research in this aspect and improve the operating reliability of current differential protections. Although the principles and operating problems of the superimposed current based differential protection have been studied and presented in quite a few textbooks and references, most of them originate from the viewpoint of the protection of specific equipment, such as a generator or transformer, and hence cannot provide sufficient theoretical fundamentals of differential protection for generic electric components. Especially, the literature about comparative studies on differential protection criteria using between phase current directly and superimposed phase current has not come into existence until now. Indeed, comparative study is the most convincing method to testify a novel criterion. Nevertheless, as taking the load current into account complicates the analyses of the phase current based criterion, researchers sometimes consciously or unconsciously avoid investigations of this aspect. However, a determinative conclusion of the performances of the two criteria in various operating modes cannot be obtained without quantitative comparisons.

Therefore, preliminary comparative studies between the phase current based and the superimposed current based differential criteria are conducted in this chapter. Furthermore, on the basis of the comparative studies, an attempt is made to try to find some results that can be used as a guide of the application of percentage differential protections.

3.2 Studies on the Operation Behaviour of Differential Protection during a Loaded Transformer Energizing

3.2.1 Simulation Models of Loaded Transformer Switch-On and CT

3.2.1.1 Model of Loaded Transformer Energizing

Loaded transformer energizing can be illustrated by the equivalent circuit, as shown in Figure 3.1.

In Figure 3.1, the side of the transformer where power is provided is the primary side (also the side of the transformer switch-on) and the side with load connected is the secondary side. R_1 and L_1 are the resistance and the inductance of the primary side, respectively, and R_2 and L_2 are the resistance and the inductance of the secondary side; L_μ means the nonlinear inductance of the magnetizing branch of the transformer.

By virtue of Kirchoff's principle, the equations relevant to the equivalent circuit can be given by:

$$\begin{cases} \dfrac{d\psi_1}{dt} + R_1 i_1 + \dfrac{d\psi_\mu}{dt} = U_1 \\ i_1 = i_\mu + i_2 \\ \dfrac{d\psi_\mu}{dt} = \dfrac{d\psi_2}{dt} + R_2 i_2 \end{cases} \tag{3.1}$$

among which i_1 and i_2 are the currents through the primary side and the secondary side, respectively. ψ_1 and ψ_2 are the induced magnetic linkage corresponding to i_1 and i_2. i_μ is the current of transformer magnetizing branch and ψ_μ is induced magnetic linkage corresponding to i_μ.

As for the linear branch, $i_1 = \frac{\psi_1}{L_1}$ and $i_2 = \frac{\psi_2}{L_2}$ come into existence. With regard to the magnetizing branch, the relationship between current and magnetic linkage is nonlinear. It is acceptable to let $i_\mu = f(\psi_\mu)$.

The second equation of Equation (3.1) can be changed into:

$$i_2 = i_1 - i_\mu \tag{3.2}$$

Substituting $i_1 = \frac{\psi_1}{L_1}$, $i_2 = \frac{\psi_2}{L_2}$, and $i_\mu = f(\psi_\mu)$ into Equation (3.2) gives:

$$\frac{\psi_2}{L_2} = \frac{\psi_1}{L_1} - f(\psi_\mu) \rightarrow \psi_2 = \frac{L_2}{L_1}\psi_1 - L_2 f(\psi_\mu) \tag{3.3}$$

Substituting $i_1 = \frac{\psi_1}{L_1}$ into the first equation of Equation (3.1) gives:

$$\frac{d\psi_1}{dt} + R_1\frac{\psi_1}{L_1} + \frac{d\psi_\mu}{dt} = U_1 \tag{3.4}$$

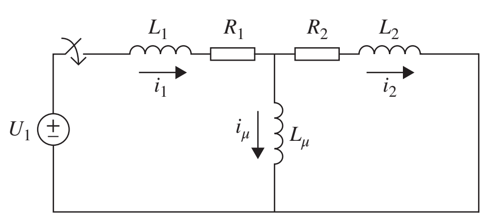

Figure 3.1 The circuit of loaded transformer energizing

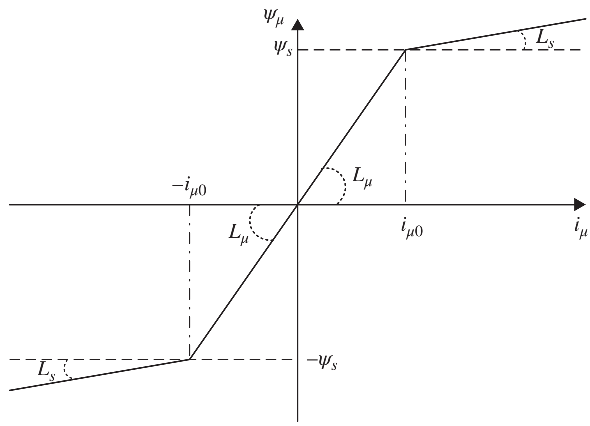

Figure 3.2 The magnetizing characteristics of the transformer core

Substituting Equations (3.2) and (3.3) into the third equation of Equation (3.1) gives:

$$\frac{d\psi_\mu}{dt} = \frac{L_2}{L_1}\frac{d\psi_1}{dt} - L_2\frac{df(\psi_\mu)}{dt} + R_2\frac{\psi_1}{L_1} - R_2 f(\psi_\mu) \tag{3.5}$$

Equations (3.4) and (3.5) can be expressed as:

$$\begin{cases} \dfrac{d\psi_1}{dt} + R_1\dfrac{\psi_1}{L_1} + \dfrac{d\psi_\mu}{dt} = U_1 \\ \dfrac{d\psi_\mu}{dt} = \dfrac{L_2}{L_1}\dfrac{d\psi_1}{dt} - L_2\dfrac{df(\psi_\mu)}{dt} + R_2\dfrac{\psi_1}{L_1} - R_2 f(\psi_\mu) \end{cases} \tag{3.6}$$

In Equation (3.6), i_μ is a function of ψ_μ. The accurate curve of $\psi_\mu - i_\mu$ should be depicted as a multivalued curve if the hysteresis is taken into account. For the convenience of solving the differential equation, the magnetization curve can be simplified to be a stepwise line, as illustrated in Figure 3.2. It can be supposed that the saturation point is $(\psi_s, i_{\mu0})$, the inductance in saturation region is *Ls* and the inductance outside saturation region is L_μ. It should be emphasized that the inductance of the magnetizing branch of transformer is still nonlinear even if above-mentioned simplification is employed.

As a result, the expression of $f(\psi_\mu)$ can be written as:

$$f(\psi_\mu) = \begin{cases} \psi_\mu / L_\mu, & |\psi_\mu| \le \psi_s \\ (\psi_\mu - \psi_s)/L_s + i_{\mu0}, & \psi_\mu > \psi_s \\ (\psi_\mu + \psi_s)/L_s - i_{\mu0}, & \psi_\mu < -\psi_s \end{cases} \tag{3.7}$$

Substituting Equation (3.7) into Equation (3.6), the differential equation for ψ can be expressed in terms of the matrix:

$$\dot{\boldsymbol{\psi}} = \boldsymbol{B}^{-1}\boldsymbol{A}\boldsymbol{\psi} + \boldsymbol{B}^{-1}\boldsymbol{U} \tag{3.8}$$

where $\boldsymbol{\psi} = \binom{\psi_1}{\psi_\mu}$, $\dot{\boldsymbol{\psi}} = \begin{pmatrix} \frac{d\psi_1}{dt} \\ \frac{d\psi_\mu}{dt} \end{pmatrix}$.

Among which

$$\boldsymbol{A} = \begin{pmatrix} R_2/L_1 + \left(1 + L_2/L_\mu\right) R_1/L_1 & R_2/L_\mu \\ R_2/L_1 - L_2 R_1/L_1^2 & -R_2/L_\mu \end{pmatrix} \tag{3.9}$$

$$\boldsymbol{B} = \begin{pmatrix} 1 + L_2/L_1 + L_2/L_\mu & 0 \\ 0 & 1 + L_2/L_1 + L_2/L_\mu \end{pmatrix} \tag{3.10}$$

$$\boldsymbol{U} = \begin{pmatrix} \left(1 + L_2/L_\mu\right) U_1 \\ (L_2/L_1) U_1 \end{pmatrix} \tag{3.11}$$

if $|\psi_\mu| < \psi_s$. Whereas

$$\boldsymbol{A} = \begin{pmatrix} R_2/L_1 + \left(1 + L_2/L_S\right) R_1/L_1 & R_2/L_S \\ R_2/L_1 - L_2 R_1/L_1^2 & -R_2/L_S \end{pmatrix} \tag{3.12}$$

$$\boldsymbol{B} = \begin{pmatrix} 1 + L_2/L_1 + L_2/L_S & 0 \\ 0 & 1 + L_2/L_1 + L_2/L_S \end{pmatrix} \tag{3.13}$$

$$\boldsymbol{U} = \begin{pmatrix} \left(1 + L_2/L_S\right) U_1 - (R_2/L_S)\psi_S + R_2 i_{\mu 0} \\ (L_2/L_1) U_1 + (R_2/L_S)\psi_S - R_2 i_{\mu 0} \end{pmatrix} \tag{3.14}$$

if $\psi_\mu > \psi_s$. Whereas

$$\boldsymbol{A} = \begin{pmatrix} R_2/L_1 + \left(1 + L_2/L_S\right) R_1/L_1 & R_2/L_S \\ R_2/L_1 - L_2 R_1/L_1^2 & -R_2/L_S \end{pmatrix} \tag{3.15}$$

$$\boldsymbol{B} = \begin{pmatrix} 1 + L_2/L_1 + L_2/L_S & 0 \\ 0 & 1 + L_2/L_1 + L_2/L_S \end{pmatrix} \tag{3.16}$$

$$\boldsymbol{U} = \begin{pmatrix} \left(1 + L_2/L_S\right) U_1 + (R_2/L_S)\psi_S - R_2 i_{\mu 0} \\ (L_2/L_1) U_1 - (R_2/L_S)\psi_S + R_2 i_{\mu 0} \end{pmatrix} \tag{3.17}$$

if $\psi_\mu < -\psi_s$.

The voltage source is defined as:

$$U_1/U_m \sin(\omega \mathrm{t} + \theta) \tag{3.18}$$

The current waveform during loaded transformer energizing can be obtained by selecting proper parameters and using a four-order Runge–Kutta algorithm to solve the nonlinear differential equations above.

3.2.1.2 CT Modelling

As supported by the following simulation test results, the loaded transformer energizing model properly satisfies both conditions of differential current in the nonrestraint region and the second harmonic restraint criterion failing to block. An obvious assumption is that the problem with the failure to block stems from the different CT transforming characteristics subjected to primary currents with different aperiodic components. To substantiate this assumption, it is necessary to build an accurate model of a CT suitable for transient analysis. The main difficulty in CT modelling in this frequency range lies in the simulation of the hysteresis loop. Then, a four-order Runge–Kutta algorithm is used to solve the differential equations. The arithmetic solutions of the inrush, the secondary current and the magnetic linkage can be obtained by means of applying the iterative computation.

The through inrush events simulated with the loaded transformer energizing model provide the primary current inputs to the CTs located on the primary and secondary sides of the power transformer. Thus, the secondary current for both sides of the transformer differential protection zone can be arrived at allowing analysis of the protection.

3.2.2 Analysis of the Mal-operation Mechanism of Differential Protection

It can be assumed that the transformer has load connected and is energized from the high voltage side at t = 0 s.

Scenario 3.1

Source parameters: Um = 110 kV, $\omega = 100\,\pi$rad, inception angle $\theta = 20°$, where θ means the phase angle of phase A at the moment that the transformer is connected to the voltage source.

Transformer parameters are:

The windings of both sides: ratio $k = 110/35$ kV, $L_1 = 0.06$ H, $R_1 = 15\,\Omega$, $L_2 = 0.035$ H, $R_2 = 115\,\Omega$
The core: $\Psi_m = U_m/\omega$, saturation point $\Psi_s/\Psi_m = 1.2$, $L_\mu = 500$ H, $L_s = 0.01$ H, $i_{\mu 0} = \Psi_s/L_\mu$;
Parameters for the CT on the high voltage side of the transformer: $k = 600/5$ A, $l = 0.7$ m, $S = 23.2\,\text{cm}^2$, $R = 0.05\,\Omega$; for the CT on the transformer's secondary side: $k = 2400/5$ A, $l = 0.5$ m, $S = 51.2\,\text{cm}^2$, $R = 0.15\,\Omega$; saturation points of the magnetizing branch of the CTs for both sides are determined by $\Psi_s/\Psi_m = 3.9$.

In the initial stage of transformer energizing with load, the core of the transformer is in the unsaturated state, which means that the corresponding magnetizing inductance is relatively high. Therefore, basically the current flows through the primary and secondary windings. However, the magnetic linkage in the core probably contains high aperiodic component because of factors such as inception angle (Figure 3.3).

After a while, as the magnetic linkage enters the highly saturated portion of the magnetizing characteristic, the inductance of the core falls rapidly and considerable current at the primary side of the transformer flows through the magnetizing branch. The voltage source, which is a periodic component with relatively high amplitude, reduces the magnetic linkage to the normal operating value at the opposite half cycle. The inrush then diminishes rapidly. Therefore, i is an offset current as shown in Figure 3.4. This is similar to the scenario of the unloaded transformer energizing.

However, i_1, the current at transformer primary side, is the sum of i_μ and i_2. This is the difference from the situation of energizing an unloaded transformer. When the amplitude of i_μ is similar to the amplitude of i_2, there will be no obvious discontinuity in the waveform of current i_1. The current waveform of i_1 is shown in Figure 3.5 and, accordingly, the current waveform of i_2 is shown in Figure 3.6.

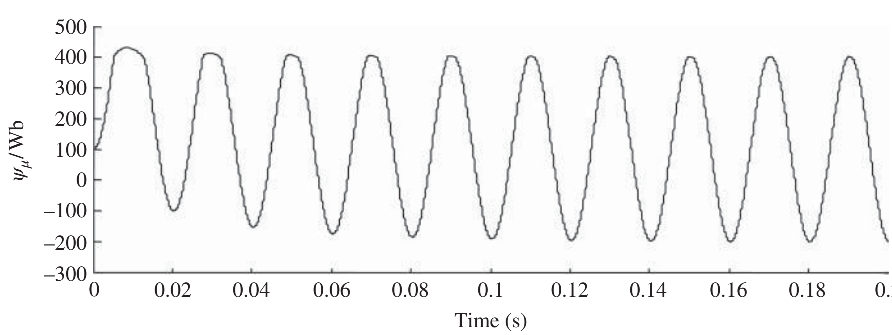

Figure 3.3 The waveform of the magnetic linkage of transformer core

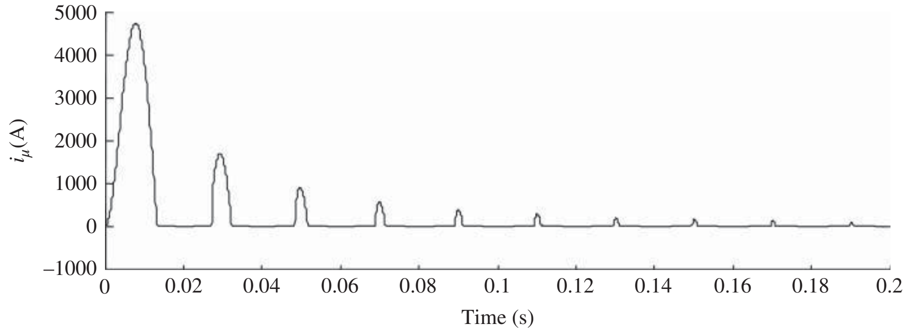

Figure 3.4 The waveform of the current of transformer magnetizing branch

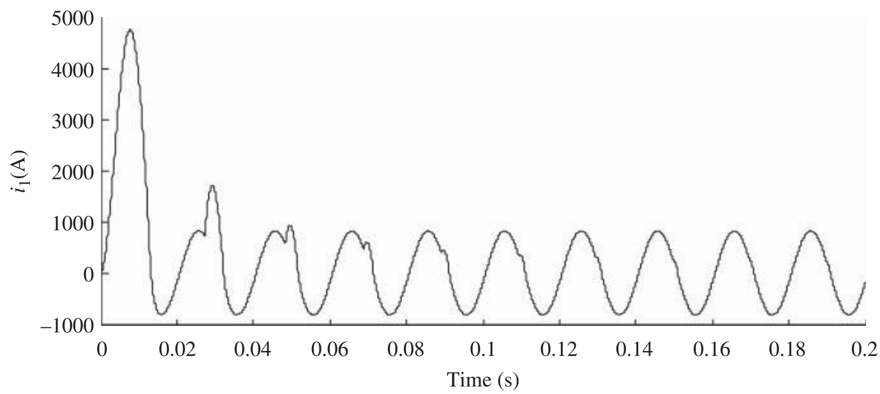

Figure 3.5 The current waveform of the primary side of the transformer

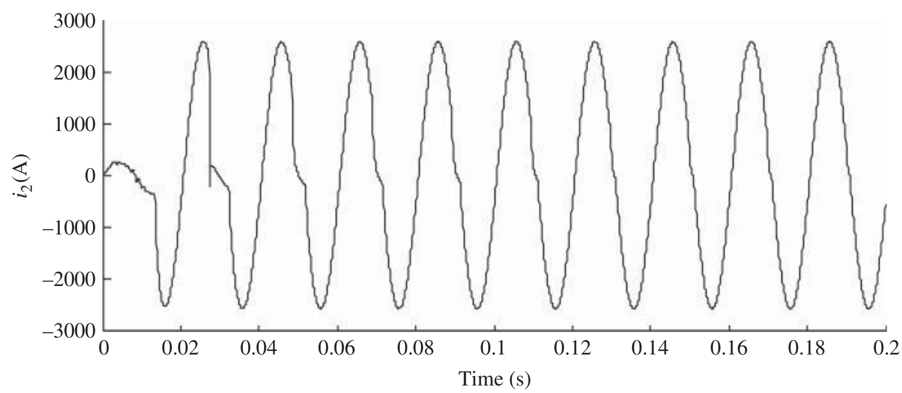

Figure 3.6 The current waveform of the secondary side of the transformer

Regardless of the existing transforming error of the CTs (as evidenced by their i_μ and the resulting differential current in the protection circuit), when the transformer core significantly enters saturation the ratio of second harmonic to fundamental greatly exceeds the typical 15%, allowing the blocking criterion to take effect and prevent differential operation. When the magnetic linkage of the transformer core returns to the linear operation region, the inrush is too small to exceed the minimum operating threshold of the differential protection. It should be noted that the ratio of the second harmonic to fundamental in i_μ greatly exceeds 15%, the common setting of restraint ratio, during the whole process of energizing. In this regard, the mal-operation of the differential protection cannot be explained only with the loaded transformer energizing model.

Note that most of the aperiodic component of i_1 flows through the transformer core because of the inductive character of the core during the transient course of transformer energizing. This results in prominent differences between the aperiodic components of currents at both sides. Comparing Figures 3.5 and 3.6 shows that the aperiodic component of the through current is mainly manifested in the current i_1, while it is hardly noticeable in i_2. In this case, the CTs of both sides differ greatly in the transforming behaviour. It can be shown that the false differential current with significant amplitude and relatively low harmonic contents will likely be formed because of the transforming difference of the CTs. In this scenario, the conditions necessary for mal-operation of the differential protection (differential current exceeding minimum operate threshold and second harmonic content below restraint threshold) can both be satisfied simultaneously. Therefore, the occasional mal-operation of the differential protection under loaded transformer energizing is inevitable. This perspective is substantiated with the following simulation tests.

Taking i_1 as the input of the CT model, the dynamic magnetizing course (Figure 3.7) and the transforming characteristic (Figure 3.8) of the CT on the primary side of transformer can be obtained. As shown in Figure 3.8, i_{11}, i_{12} and $i_{1\mu}$ are the primary, secondary and magnetizing currents of the CT on the primary side of the transformer respectively.

It can be seen from Figures 3.7 and 3.8 that the amplitude of the aperiodic component of i_{11} far exceeds its steady-state level in the first few cycles of energizing. This results in the magnetic linkage of the core being lifted beyond the saturation point; accordingly, a considerable portion of the primary current flows through the magnetizing branch. After CT enters into saturation, ψ_μ and $i_{1\mu}$ vary with the route of the hysteresis loop. As seen in Figure 3.8, due to the resistive load of CT, the aperiodic components

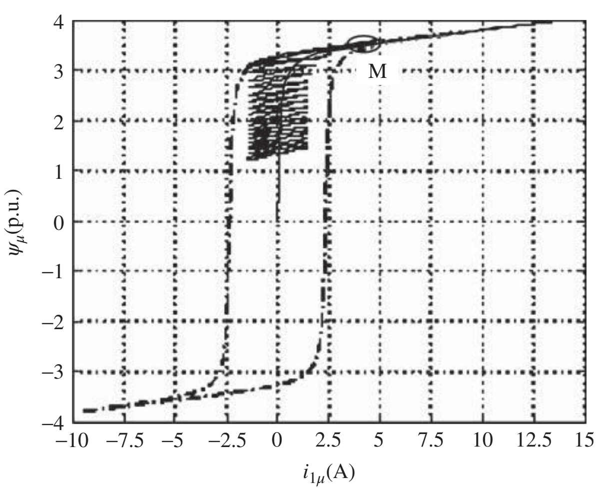

Figure 3.7 The dynamic magnetizing course of the CT on the primary side of the transformer

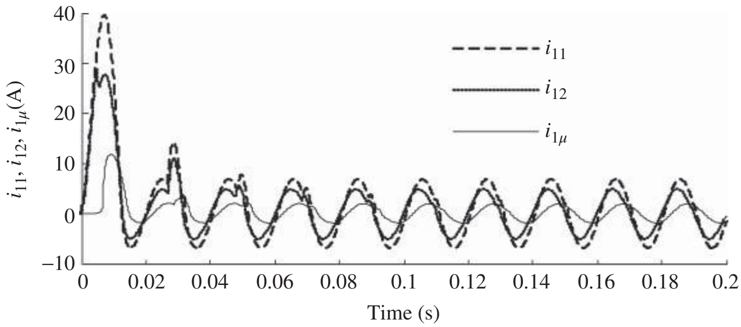

Figure 3.8 The transforming characteristic of the CT on the primary side of the transformer

of all currents decay rapidly during the transforming course. After several cycles, the residual current is mainly composed of the periodic component. Note that at this time the magnetic linkage of the CT core has been pushed into the region near to the saturation point by the previous aperiodic components. In contrast, the periodic component of ψ_μ resulting from the periodic component of i_{11} has relatively low amplitude. Therefore, ψ_μ probably stays within the hysteresis loop limit and cannot return to the normal operation region immediately. As a consequence, the inductance of the magnetizing branch may maintain a relatively low value during an entire period of power frequency with this phenomenon lasting for a period of time. Consequently, considerable primary current will be allowed to pass through the magnetizing branch and cause serious measuring error. This case is shown clearly in Figure 3.8.

The same CT model is used to analyse behaviour of the CT on the secondary side of the transformer. The waveform of i_2 does not contain an aperiodic component and the amplitude of its periodic component is basically equal to the rated value of the CT. As a result, the CT can transform linearly. The secondary current of the CT i_{22} can be obtained.

By virtue of i_{12} and i_{22}, the differential current can be obtained; this is shown in Figure 3.9, from which it can be seen that it is noticeably distorted during the first few cycles of energizing. This distortion is due to the aperiodic component of the current on the primary side of the transformer not having fully decayed yet. After a while, the decay of the aperiodic component is almost complete. However, in this time the magnetic linkage of the CT core has been pushed into the region near to the saturation point (point M in Figure 3.7). Meanwhile, the magnetic linkage formed by the periodic component of the

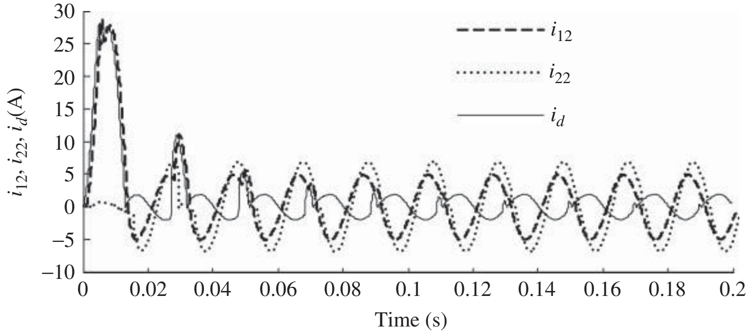

Figure 3.9 The waveforms of the secondary currents of both side CTs and corresponding differential current

current with low amplitude is not enough to pull the operating point of the magnetic linkage back to the linear region. Therefore, this phenomenon of CT local transient saturation leads to the obvious angle error and amplitude error of the CT. The result of the CT local transient saturation is a false differential current that exhibits a relatively smooth waveform lacking in second harmonic content. According to the setting parameters and Figure 3.5, the rated value of the steady-state current of the primary side of the transformer is 600 A, and the ratio of the CT on this side is 600/5 A. It can be assumed that the primary rating current of this side is 600 A, the secondary rating current is 5 A. Figure 3.10 shows the changes of the magnitude of the fundamental component of i_d in Figure 3.9, which is evaluated with the Discrete Fourier Transform (DFT) algorithm. Applying the per unit system to denote the differential current and bias current and taking 5 A as the base, the steady-state magnitude of $\mathrm{i_d}$ stabilizes above 0.25 after five cycles after energizing (Figure 3.10). If the setting of operating threshold is below 0.25, mal-operation will occur. Certainly, the mal-operation cannot occur unless the ratio of second harmonic to fundamental of the differential current is lower than the threshold, which is generally set at 15–20%. Figure 3.11 shows the ratio change of second harmonic to fundamental of the differential current after energizing. As the energizing time exceeds 0.13 s, the ratio of the second harmonic stabilizes below 15% and the magnitude of the fundamental component stabilizes above 0.25. If the differential protection uses 0.25 as the operating threshold and 15% as the second harmonic restraint ratio, mal-operation occurs. The tripping signal of the differential protection is shown in Figure 3.12.

In addition, Figure 3.13 shows the state locus of the mal-operation of the differential protection. The second harmonic of the differential current is high during the initial period of the energizing. Therefore, the differential protection is blocked reliably. As time goes on, the operating point of the CT enters into the region of local transient saturation. In this case, both the amplitude of the differential current and

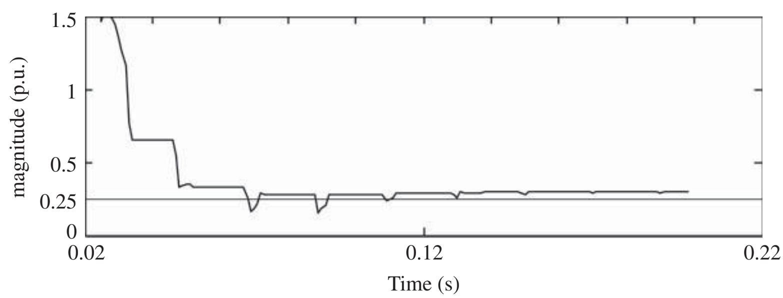

Figure 3.10 The magnitude of the fundamental component of the differential current

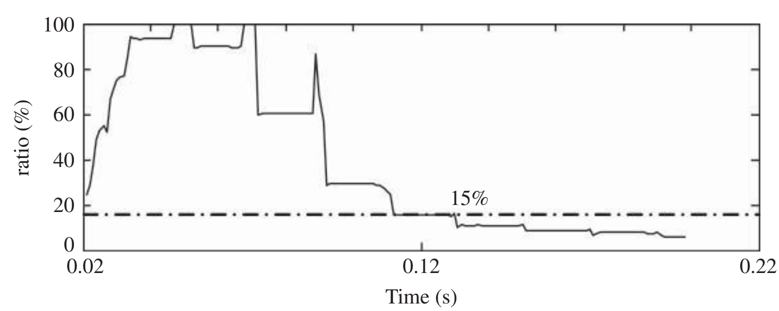

Figure 3.11 The ratio of second harmonic to fundamental of the differential current

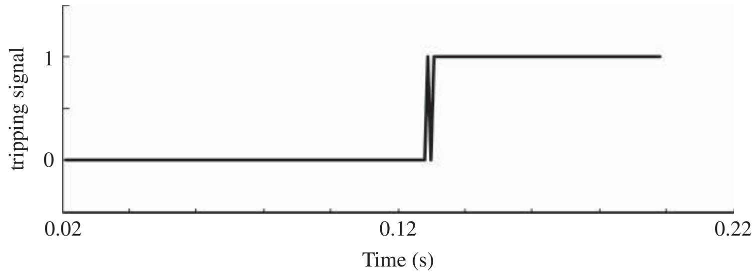

Figure 3.12 The tripping signal of the differential protection

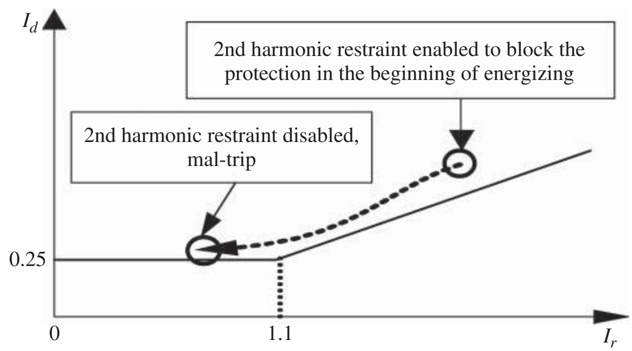

Figure 3.13 The state locus of the mal-operation of the differential protection

the content of the harmonic component possibly satisfy the tripping conditions of the differential protection, which makes the protection mal-operate. Compared with this phenomenon, the above conditions can hardly be satisfied during the unloaded transformer energizing. Because the load is disconnected the current from the CT on the secondary side is always zero, thus the differential current is always equal to the current from the CT on the primary side. In this case, the differential current is always equal to the winding inrush or the linear combination of the winding inrushes depending on the style of winding connection of transformer. In other words, no matter how saturated the CT is, it only results in the distortion of the waveform of differential current when the compensation of the current at the secondary side of transformer cannot be involved. The ratio of second harmonic to fundamental will remain at a high level and the mal-operation can hardly occur in this case.

The different parameters of the primary system lead to a different time of CT initial saturation and then a different time of mal-operation of protection. The following provides a scenario of the mal-operation with a long time delay of the differential protection during the loaded transformer energizing.

Scenario 3.2

Transformer parameters: $L_1 = 0.1$ H, $R_1 = 8.5\,\Omega$, $L_2 = 0.06$ H, $R_2 = 115\,\Omega$, $\Psi_m = Um/\omega$, $\Psi_s/\Psi_m = 1.3$, $L_\mu = 500$ H, $L_s = 0.01$ H, $\theta = 0$ rad, $i_{\mu 0} = \Psi_s/L_\mu$.

CT parameters and the operating threshold of protection are the same as Scenario 3.1.

The simulation results are illustrated in Figures 3.14 to 3.17. Among them, Figure 3.14 shows the waveforms of the secondary currents of both side CTs and corresponding differential current. Figure 3.15

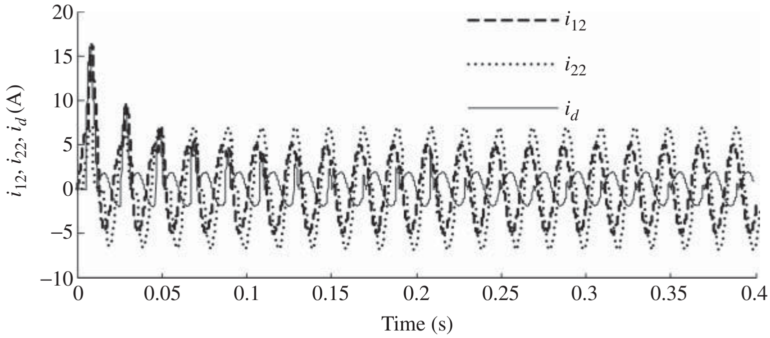

Figure 3.14 The waveforms of the secondary currents of both side CTs and corresponding differential current

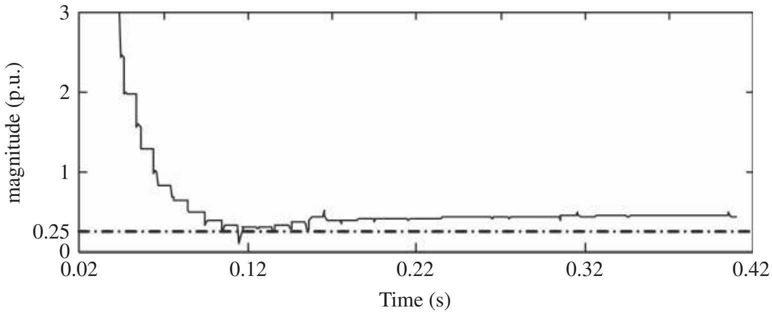

Figure 3.15 The magnitude of the fundamental component of the differential current

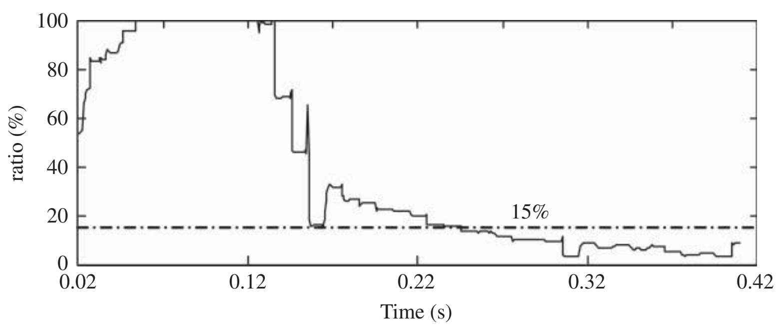

Figure 3.16 The ratio of second harmonic to fundamental of the differential current

shows the magnitude change of the fundamental component of the differential current. Figure 3.16 shows the ratio change of second harmonic to fundamental of the differential current. Figure 3.17 shows the tripping signal of the differential protection.

As seen in Figure 3.17, the differential protection outputs tripping signal continuously as the energizing time exceeds 0.26 s (13 cycles).

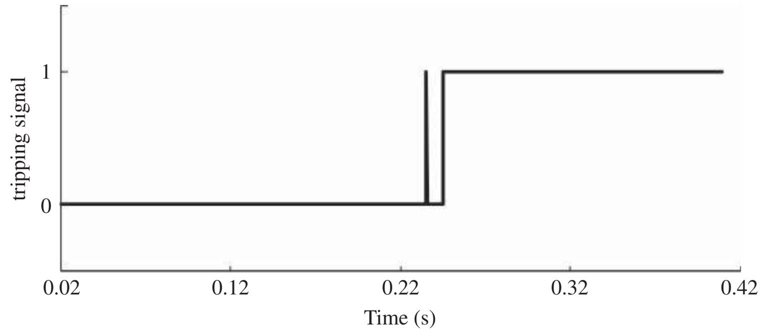

Figure 3.17 The tripping signal of the differential protection

In summary, the mechanism of the mal-operation of the differential protection caused by the low through inrush during the loaded transformer energizing has been studied in this section. The reason is that ratios of the aperiodic components of the currents on each side of the transformer are different during the transient of energizing. The current at the primary side of the transformer contains a much greater aperiodic component, which pushes the magnetic linkage of the CT into the saturation region. Due to the dynamic magnetizing characteristic and the small periodic component of current, the CT enters into local transient saturation after the aperiodic component fully decays. Thus, considerable periodic component current will flow through the magnetizing branch of the CT, which leads to significant measuring error. On the other hand, the aperiodic component of current at the secondary side of the transformer is very low and the CT, therefore, can basically transform linearly. The secondary currents of both side CTs will form the false differential current with a relatively smooth waveform. In this case, the differential current may exceed the minimum operation threshold while also having low second harmonic content, leading to the mal-operation of the differential protection. Researchers in the field of protective relaying should recognize this phenomenon and propose reasonable solutions.

3.3 Comparative Investigation on Current Differential Criteria between One Using Phase Current and One Using Phase–Phase Current Difference for the Transformer using Y-Delta Connection

3.3.1 Analyses of Applying the Phase Current Differential to the Power Transformer with Y/Δ Connection and its Existing Bases

For the differential protection of the power transformer with Y/Δ connection, the secondary currents forming the differential currents are usually revised on amplitudes and phase angles by means of CTs or digital angle changing in order to adapt to the Y/Δ transformation of the primary side of the transformer. In this way, the differential currents are 0 in the cases of normal operating conditions and external faults. At the same time, the sensitivities of the differential protection during internal faults are unaffected. Take the case of Y_0/Δ-11 connection, which is wildly used in China, analyses of this method were conducted as follows (Figure 3.18).

Supposed that the high voltage side and the low voltage side of the transformer adopt Y_0 connection and Δ connection, respectively, the currents in the windings on the high-voltage side are $\dot{I}_A$, $\dot{I}_B$ and $\dot{I}_C$, respectively, and the corresponding phase currents are $\dot{I}_{\mathrm{mL1}} = \dot{I}_A$, $\dot{I}_{\mathrm{mL2}} = \dot{I}_B$ and $\dot{I}_{\mathrm{mL3}} = \dot{I}_C$ respectively. Similarly, the currents in the windings on the low-voltage side are $\dot{I}_a$, $\dot{I}_b$ and $\dot{I}_c$, respectively, and the corresponding phase current differences are $\dot{I}_{\mathrm{nL1}} = \dot{I}_a - \dot{I}_b$, $\dot{I}_{\mathrm{nL2}} = \dot{I}_b - \dot{I}_c$ and $\dot{I}_{\mathrm{nL3}} = \dot{I}_c - \dot{I}_a$, respectively.

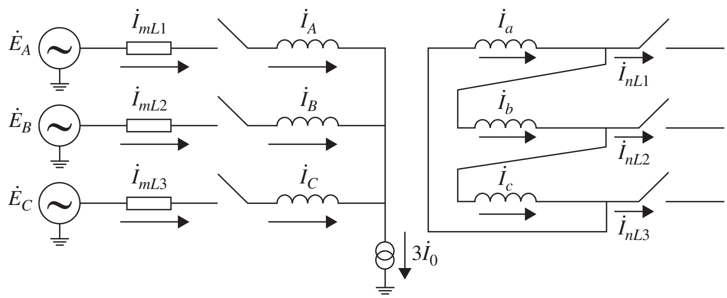

Figure 3.18 The currents of the power transformer with Y_0/Δ-11 connection

In China, the method of setting up the differential protection is as follows: the phase current differences on the low voltage side are directly introduced as the inputs of one side of the differential relay, the phase current differences on the high voltage side are revised in terms of the formation of the phase current differences on the low voltage side, that is:

$$\dot{I}'_{\mathrm{mL1}} = \dot{I}_A - \dot{I}_B,\ \dot{I}'_{\mathrm{mL2}} = \dot{I}_B - \dot{I}_C,\ \dot{I}'_{\mathrm{mL3}} = \dot{I}_C - \dot{I}_A$$

The simplest current differential criterion, for example, for phase A, is given by:

$$I'_{\mathrm{dA}} = |\dot{I}'_{\mathrm{mL1}} + \dot{I}_{\mathrm{nL1}}| > I_0 \tag{3.19}$$

Of course, varied percentage differential criteria can be set up. Some relative detailed discussion is conducted in the following sections.

For the sake of clear expression, the revised current differential criterion mentioned above is called phase current difference based differential criterion in this section.

Some manufacturers claim that the zero-sequence current is removed in the phase current difference based differential criterion and the sensitivity of the protection in the event of single-phase earth fault or inter-turn fault is lowered. Therefore, protections specially responding to earth faults are introduced, for example the zero-sequence current differential criterion. Another method is to revise the two currents forming the differential current in order to enable the influence of the zero-sequence current to be covered.

It should be pointed out that the above conclusion is correct. In other words, comparing with the phase current differential protection, the sensitivity of the phase current difference based differential protection is lowered in the case of an earth fault. However, the argument saying that the sensitivity is lowered because of the zero-sequence current being removed in the phase current difference based differential criterion, is not proper. The analyses are as follows.

For the simple current differential protection for phase A, the corresponding criterion is given by:

$$I_{dA} = |\dot{I}_A + \dot{I}_a| > I_0 \tag{3.20}$$

This criterion is called phase current differential criterion in this section.

Figure 3.19 is used to analyse the instance in the event of internal fault.

An internal fault can be described as the pre-fault network and superimposed fault network by means of the superposition method, as seen in Figure 3.19.

The superimposed fault network can be regarded as a passive network from the fault port. Furthermore, the superimposed fault network in Figure 3.19 can be decomposed to positive, negative and zero-sequence systems according to symmetrical component method, as seen in Figure 3.20. In the figure, the equivalent electric potential sources of the fault port are replaced by equivalent current sources.

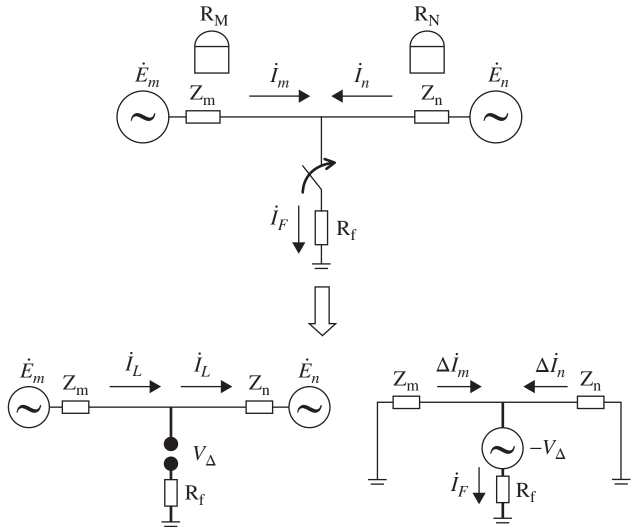

Figure 3.19 The superimposition of the pre-fault network and superimposed fault network describing an internal fault

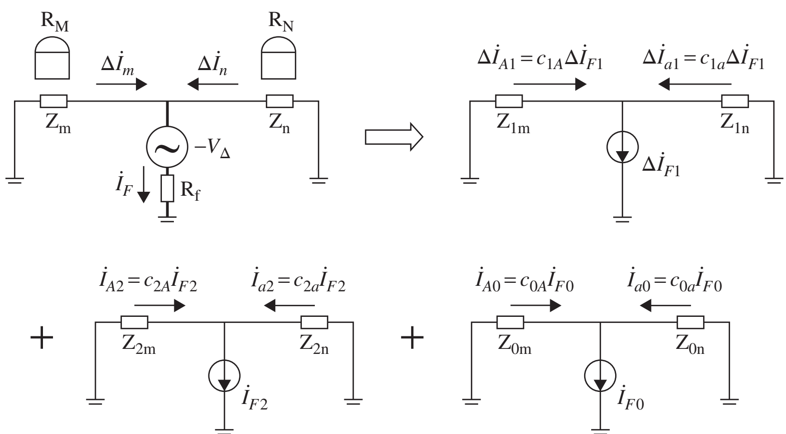

Figure 3.20 Decomposition of the superimposed fault network to positive, negative and zero-sequence systems

By virtue of Figure 3.20, in the superimposed fault network the phase currents on the high voltage side of the transformer are expressed in terms of symmetrical components:

$$\begin{cases} \Delta\dot{I}_A = \Delta\dot{I}_{A1} + \dot{I}_{A2} + \dot{I}_{A0} \\ \Delta\dot{I}_B = a^2\Delta\dot{I}_{A1} + a\dot{I}_{A2} + \dot{I}_{A0} \\ \Delta\dot{I}_C = a\Delta\dot{I}_{A1} + a^2\dot{I}_{A2} + \dot{I}_{A0} \end{cases} \tag{3.21}$$

Similarly, the phase currents on the low voltage side are given by:

$$\begin{cases} \Delta\dot{I}_a = \Delta\dot{I}_{a1} + \dot{I}_{a2} + \dot{I}_{a0} \\ \Delta\dot{I}_b = a^2\Delta\dot{I}_{a1} + a\dot{I}_{a2} + \dot{I}_{a0} \\ \Delta\dot{I}_c = a\Delta\dot{I}_{a1} + a^2\dot{I}_{a2} + \dot{I}_{a0} \end{cases} \tag{3.22}$$

In the case of adopting the phase current differential criterion, the differential current of phase A is expressed as:

$$\dot{I}_{dA} = \Delta\dot{I}_A + \Delta\dot{I}_a = (\Delta\dot{I}_{A1} + \Delta\dot{I}_{a1}) + (\dot{I}_{A2} + \dot{I}_{a2}) + (\dot{I}_{A0} + \dot{I}_{a0}) \tag{3.23}$$

While for the phase current difference based differential criterion, the differential current of phase A is given by:

$$\dot{I}'_{dA} = \Delta\dot{I}_{AB} + \Delta\dot{I}_{ab} \tag{3.24}$$

With respect to Equations (3.21) and (3.22), Equation (3.25) comes into existence.

$$\begin{cases} \Delta\dot{I}_{AB} = \left(1 - a^2\right)\Delta\dot{I}_{A1} + (1 - a)\Delta\dot{I}_{A2} \\ \Delta\dot{I}_{ab} = (1 - a^2)\Delta\dot{I}_{a1} + (1 - a)\Delta\dot{I}_{a2} \end{cases} \tag{3.25}$$

Substituting Equation (3.25) into Equation (3.24), the differential current of phase A in the case of adopting the phase current difference based differential criterion can be expressed by:

$$\dot{I}'_{dA} = (1 - a^2)(\Delta\dot{I}_{A1} + \Delta\dot{I}_{a1}) + (1 - a)(\dot{I}_{A2} + \dot{I}_{a2}) \tag{3.26}$$

It can be seen by comparing Equation (3.23) with Equation (3.26) that $\dot{I}_{dA}$ contains the zero-sequence component but $\dot{I}'_{dA}$ does not. It seems that the former is greater than the latter. However, this is not exact actually. The illustration is as follows.

For any internal fault, Equation (3.27) comes into existence:

$$\begin{cases} \dot{I}_{F1} = \Delta\dot{I}_{A1} + \Delta\dot{I}_{a1} \\ \dot{I}_{F2} = \dot{I}_{A2} + \dot{I}_{a2} \\ \dot{I}_{F0} = \dot{I}_{A0} + \dot{I}_{a0} \end{cases} \tag{3.27}$$

Substituting Equation (3.27) into Equations (3.23) and (3.26) respectively, the differential currents for the two criteria are given by:

$$\dot{I}_{dA} = \dot{I}_{F1} + \dot{I}_{F2} + \dot{I}_{F0} \tag{3.28}$$

$$\dot{I}'_{dA} = (1 - a^2)\dot{I}_{F1} + (1 - a)\dot{I}_{F2} \tag{3.29}$$

Taking the single-phase earth fault, for example, assume that an internal earth fault of phase A occurs; Equation (3.30) comes into existence:

$$\dot{I}_{F1} = \dot{I}_{F2} = \dot{I}_{F0} \tag{3.30}$$

Substituting this into Equations (3.28) and (3.29), it follows that:

$$\dot{I}_{dA} = \dot{I}'_{dA} = 3\dot{I}_{F1} \tag{3.31}$$

On the surface, the differential current for the phase current differential criterion contains the zero-sequence component, but the coefficients of three sequence components are all one in the event of single-phase short-circuit fault. Although the differential current for the phase current difference based differential criterion does not contain the zero-sequence component, the positive-sequence and negative-sequence components are magnified $(1 - a^2)$ and $(1 - a)$ times, respectively. In this instance, the composite differential currents for the two criteria are identical. Obviously, the argument that the sensitivity of the differential protection is lowered due to the zero-sequence current being removed in the phase current difference based differential criterion, is not tenable. In fact, the zero-sequence current assists the phase current differential current via apparent action whereas it assists the phase current difference based differential current via latent action.

Actually, Equation (3.32) comes into existence:

$$\dot{I}_{AB} + \dot{I}_{ab} = (\dot{I}_A + \dot{I}_a) - (\dot{I}_B + \dot{I}_b) \tag{3.32}$$

When an internal fault of phase A occurs, only the through current flows through phase B, $\dot{I}_B + \dot{I}_b = 0$, it follows that:

$$\dot{I}_{AB} + \dot{I}_{ab} = \dot{I}_A + \dot{I}_a \tag{3.33}$$

Consequently, the opinion that the effect of the zero-sequence current is not taken into account in the phase current difference based differential criterion, is not tenable in theory.

3.3.2 *Rationality Analyses of Applying the Phase Current Differential Criterion to the Power Transformer with Y/Δ Connection*

Based on the above analyses, it is hoped to comprehend whether the effects of the two current differential criteria are identical. If adopting simple differential protection, the effects are identical in the case of same settings. However, if adopting the percentage differential criterion, the result is different. The analyses are shown here.

By virtue of the distribution of the currents in Figure 3.20, for the high voltage side:

$$\begin{cases} \Delta\dot{I}_A = c_{1A}\Delta\dot{I}_{F1} + c_{2A}\dot{I}_{F2} + c_{0A}\dot{I}_{F0} \\ \Delta\dot{I}_B = c_{1A}a^2\Delta\dot{I}_{F1} + c_{2A}a\dot{I}_{F2} + c_{0A}\dot{I}_{F0} \\ \Delta\dot{I}_C = c_{1A}a\Delta\dot{I}_{F1} + c_{2A}a^2\dot{I}_{F2} + c_{0A}\dot{I}_{F0} \end{cases} \tag{3.34}$$

For the low voltage side:

$$\begin{cases} \Delta\dot{I}_a = c_{1a}\Delta\dot{I}_{F1} + c_{2a}\dot{I}_{F2} + c_{0a}\dot{I}_{F0} \\ \Delta\dot{I}_b = c_{1a}a^2\Delta\dot{I}_{F1} + c_{2a}a\dot{I}_{F2} + c_{0a}\dot{I}_{F0} \\ \Delta\dot{I}_c = c_{1a}a\Delta\dot{I}_{F1} + c_{2a}a^2\dot{I}_{F2} + c_{0a}\dot{I}_{F0} \end{cases} \tag{3.35}$$

where, c_{1A}, c_{2A}, c_{0A}, c_{1a}, c_{2a} and c_{0a} are the distribution coefficients of the positive, negative and zero-sequence currents on both sides; strictly speaking, they are all complex numbers.

Under common conditions, the ratio of the resistance to the system impedance is quite low. For the convenience of analysing, the resistance can be ignored and, hence, the distribution coefficients of the currents can all be regarded as real numbers. For the analyses of protections, the structures and the parameters of positive and negative sequence networks are generally considered to be equal, that is $c_{1A} = c_{2A}$ and $c_{1a} = c_{2a}$.

Here the comparative analyses are conducted by means of researching two forms of restraint criteria. For the sake of clear depiction, ABC and abc are used to denote the phase sequences of CTs on both sides of the protection.

Take the protection of phase A for instance. For the phase current differential criterion:

$$I_{dP} > K_{resP} I_{HP} \tag{3.36}$$

where

$$I_{dP} = |\dot{I}_A + \dot{I}_a| \tag{3.37}$$

and

$$I_{HP} = |\dot{I}_A - \dot{I}_a| \tag{3.38}$$

For the phase current difference based differential criterion:

$$I_{dL} > K_{resL} I_{HL} \tag{3.39}$$

where

$$I_{dL} = |\dot{I}_{AB} + \dot{I}_{ab}| \tag{3.40}$$

and

$$I_{HP} = |\dot{I}_{AB} - \dot{I}_{ab}| \tag{3.41}$$

For the protections of other phases, similar analyses can be conducted on the basis of rotating the phase sequences. In the following section only the operating behaviours in the event of short-circuit fault of phase A are discussed.

A uniform reference is necessary to compare the two criteria and the reference is the consistent security [9, 10]. It means that in the case of the two criteria having consistent securities during an external fault with CT saturation, the proportion factors of the two criteria to be compared can be determined. On this basis, the comparison of the sensitivities of two criteria during the internal fault can be conducted.

Figure 3.21 illustrates the situation of the differential protection experiencing the external short-circuit fault of phase A.

When a single-phase short-circuit fault occurs, the CT on one side of the faulty phase may saturate and give rise to a false differential current. It may result in the mal-operation of the differential protection. Even though the currents on the sound phases contain the currents induced from the faulty phase, they are relatively low and may not lead to the CT saturation. Therefore, the through currents on phase A (the faulty phase) and phase B (the sound phase) can be supposed to be $\dot{I}_{thA}$ and $\dot{I}_{thB}$, respectively. The CT on phase A saturates and the transformation ratio is $\dot{\delta}$; CTs on phase B, C, a, b and c all transform linearly. According to the assumed positive direction, Equation (3.42) comes into existence:

$$\begin{cases} \dot{I}_A = \dot{I}_{thA} \\ \dot{I}_a = -\dot{\delta}\dot{I}_{thA} \end{cases} \tag{3.42}$$

It is proven by the above analyses that the differential currents of the two criteria are equal for the percentage differential protection. Therefore, the corresponding bias coefficients of the two criteria used for comparison can be determined just by means of investigating the bias currents.

For the phase current differential criterion, the bias current is given by $I_{HP} = |\dot{I}_A - \dot{I}_a| = |(1 + \dot{\delta})\dot{I}_{thA}|$.

For the phase current difference based differential criterion, the bias current is given by $I_{HL} = |\dot{I}_{AB} - \dot{I}_{ab}| = |(1 + \dot{\delta})\dot{I}_{thA} - 2\dot{I}_{thB}|$.

The next thing to do is to solve the expressions of $\dot{I}_{thA}$ and $\dot{I}_{thB}$ quantitatively. Similar to the analyses of the internal fault, the superimposed fault network and its positive, negative and zero-sequence systems in relation to the fault in Figure 3.21 are shown in Figure 3.22. There is no loss of generality in assuming

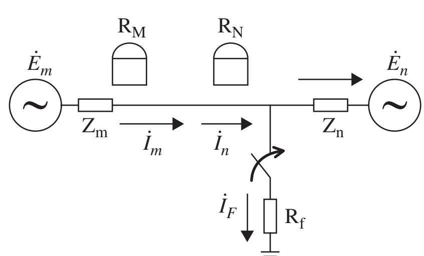

Figure 3.21 The CT saturation due to the external fault

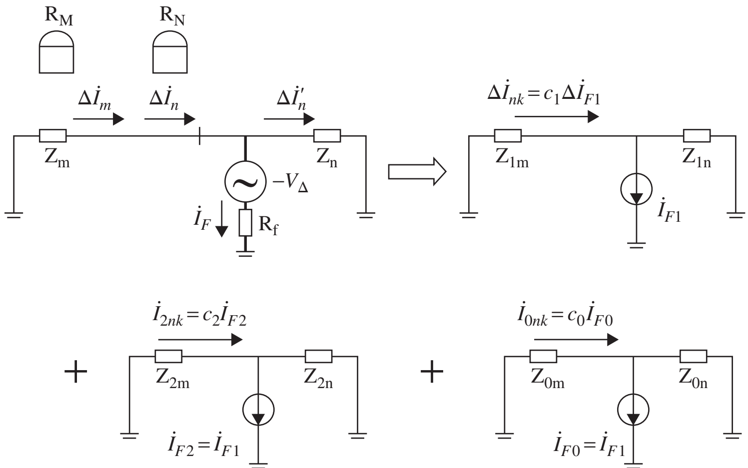

Figure 3.22 Superimposed fault network and its positive, negative and zero-sequence systems in relation to the fault in Figure 3.21

that the current on the faulty branch is $\dot{I}_F$, the corresponding positive sequence current is $\dot{I}_{F1} = \dot{I}_F/3$. In the positive and negative sequence systems, the distribution coefficients of the currents on the side with the differential protection are c_1, c_2 and c_0, where $c_1 = c_2$.

For the sake of simplifying the analyses, the branch with the protection is considered to be unloaded before the fault occurs, the fault components of positive, negative and zero-sequence currents in Figure 3.22 can directly compose the through currents of three phases. It follows that $\dot{I}_{thA} = (2c_1 + c_0)\dot{I}_{F1}$ and $\dot{I}_{thB} = (c_0 - c_1)\dot{I}_{F1}$, where $\dot{I}_{F1} = \dot{I}_F/3$.

It is obvious that the phase angle relationship between $\dot{I}_{thA}$ and $\dot{I}_{thB}$ rests with the values of c_0 and c_1. If $c_0 > c_1$, the two currents are in-phase, the bias current for the phase current difference based differential criterion is lower. In order to ensure that the bias current for the phase current difference based differential criterion is the same as that for the phase current differential criterion, the bias coefficient for the phase current difference based differential criterion should be greater. If $c_0 < c_1$, the bias coefficient for the phase current difference based differential criterion should be smaller to ensure that the two criteria both have the consistent security. In practical systems, probabilities of the two instances above are identical. Therefore, from the statistical point of view, the amplitudes of the bias currents for the two criteria are identical during CT saturation.

If the branch with the protection is loaded before the fault occurs, the directions of the load current and the fault component current are random in theory. From the statistical point of view, its effects on the bias currents for the two criteria are also identical. As a consequence, the two criteria should adopt the same bias coefficients to ensure that the two criteria both have the consistent security

The situation during the internal fault of phase A is analysed according to Figure 3.19. Supposing that the distribution coefficients of the currents on side M are c_{1A}, c_{2A} and c_{0A}, and the distribution coefficients of the currents on side N are c_{1a}, c_{2a} and c_{0a}. Discussed firstly is the unloaded case of the fault; here the two criteria actually become the percentage differential criteria based on fault component.

With the above analyses, it is disclosed that the differential currents of the two criteria are identical and the bias coefficients are also identical. The sensitivities can be evaluated just by means of investigating the bias currents during the internal fault.

Assuming the current on the faulty branch is $\dot{I}_F$, the corresponding positive sequence current is $\dot{I}_{F1} = \dot{I}_F/3$.

In this way, Equations (3.43)–(3.48) come into existence on the basis of the assumed positive direction of the current:

$$\dot{I}_A = (2c_{1A} + c_{0A})\dot{I}_{F1} \tag{3.43}$$

$$\dot{I}_a = (2c_{1a} + c_{0a})\dot{I}_{F1} \tag{3.44}$$

$$\dot{I}_B = (\dot{I}_{0A} - c_{1A})\dot{I}_{F1} \tag{3.45}$$

$$\dot{I}_b = (c_{0a} - c_{1a})\dot{I}_{F1} \tag{3.46}$$

and

$$\dot{I}_{HP} = |\dot{I}_A - \dot{I}_a| = |2\Delta c_1 + \Delta c_0| I_{F1} \tag{3.47}$$

$$I_{HL} = |\dot{I}_{AB} - \dot{I}_{ab}| = |3\Delta c_1| I_{F1} \tag{3.48}$$

where

$$\Delta c_1 = c_{1A} - c_{1a} \tag{3.49}$$

$$\Delta c_0 = c_{0A} - c_{0a} \tag{3.50}$$

Owing to $c_{1A}, c_{1a}, c_{0A}, c_{0a} \in [0, 1]$, it follows that $\Delta c_1, \Delta c_0 \in [-1, 1]$.

Obviously, when Equation (3.51) comes into existence, the sensitivity of the phase current difference based differential criterion is superior to that of the phase current differential criterion. The result is just the reverse under other conditions.

$$|2\Delta c_1 + \Delta c_0| > 3|\Delta c_1| \tag{3.51}$$

As Δc_1 and Δc_0 both vary within the range of $[-1,1]$, it is actually a problem to calculate the area satisfying Equation (3.51) in the $(\Delta c_1, \Delta c_0)$ plane. The result is shown as the shadow region in Figure 3.23, the area of which is $2 \times 1.2 \times 0.5 = 1.2$, and the area that the sample space covers is $2 \times 2 = 4$. Therefore, the probability satisfying Equation (3.51) is $1.2 \times 100\%/4 = 30\%$.

In other words, under varied possible operating conditions, the probability of which the sensitivity of the phase current differential criterion is lower than that of the phase current difference based differential criterion is 30%. Under the other 70% of possible conditions, the sensitivity of the phase current differential criterion is higher than that of the phase current difference based differential criterion.

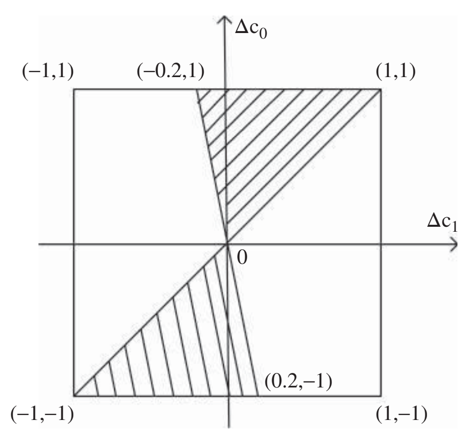

Figure 3.23 The probability of which the sensitivity of phase current difference based differential criterion is higher than that of the phase current differential criterion in the event of a single-phase earth fault

In the case of the load current existing before the fault occurs, as the phase angle of the load current is random relative to the fault component, its effects on the bias currents for the two criteria are also identical from the statistical point of view. These are not analysed in detail here.

In summary, it can be seen from the analyses in this section that, when applying the percentage differential criterion, the integrated sensitivity of the phase current difference based differential criterion is lowered relative to the phase current differential criterion in the case of the earth fault especially the single-phase earth fault. Therefore, adopting some compensation methods, for example the zero-sequence current differential criterion, is reasonable. However, the effect of the phase current difference based differential criterion on the sensitivity of the protection does not rest with the differential current but the bias current. It is quite obvious in the field of applying the differential protection based on fault component.

3.4 Comparative Analysis on Current Percentage Differential Protections Using a Novel Reliability Evaluation Criterion

3.4.1 Introduction to CPD and NPD

The currents related to the differential protection can be always summarized as the incoming current $\dot{I}_{in}$ and outgoing current $\dot{I}_{out}$ as shown in Figure 3.24, which is applicable to all kinds of protected objects.

In theory, $\dot{I}_{in}$ and $\dot{I}_{out}$ will be 180° out of phase with the same magnitudes in the case of an external fault if the direction of positive current flow is assumed to flow toward the protected object. On the other hand, they will be nearly in phase, or all flow toward the protected object, when an internal fault occurs. In this regard, the identification of an internal fault from an external fault is quite easy and the current differential protection will be adequate. However, the above circumstance is rarely tenable in reality due to many complicated factors. That is why the percentage differential protection was proposed. In order to refine of the following discussion, the general expression of percentage differential protection criterion should be presented at first.

The NPD criterion can be illustrated as the comparison between the differential current and the bias current. $|\dot{I}_{in} + \dot{I}_{out}|$ is usually taken as the differential current while the bias current has various constitutions, among which $|\dot{I}_{in}| + |\dot{I}_{out}|$ is one of the common designs. In this circumstance, the NPD criterion can be expressed as:

$$I_{d1} > K_{r1} I_{bias1} \tag{3.52}$$

where, $I_{d1} = |\dot{I}_{in} + \dot{I}_{out}|$, $I_{bias1} = |\dot{I}_{in}| + |\dot{I}_{out}|$ and K_{r1} is the restraint coefficient.

For the CPD criterion, the differential current I_{d2} is also designed as $|\dot{I}_{in} + \dot{I}_{out}|$ whereas the restraint current I_{bias2} is defined as the compensation quantity $I_{bias1} - I$. The criterion can, therefore, be shown as:

$$I_{d2} > K_{r2} I_{bias2} \tag{3.53}$$

where, $I_{d2} = I_{d1}, I_{bias2} = I_{bias1} - I_{d2}$.

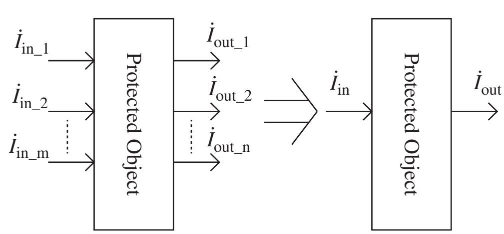

Figure 3.24 General description of current differential protection

Note that the restraint coefficient K_{r1} in Equation (3.52) is different from K_{r2} in Equation (3.53).

Both above-mentioned criteria have the satisfactory reliability, where the reliability is specified to be the dependency and security in terms of protective relaying applications, if the following conditions are satisfied: firstly, all components of a protective relay are sound; secondly, all CTs can transform the primary currents entirely accurately in any case; thirdly, $\dot{I}_{in}$ and $\dot{I}_{out}$ all flow toward the protected object in the occurrence of internal fault. However, the differential criteria rarely achieve their optimal performances in real operation due to many adverse factors, for instance, CT saturation or the current of the shunt branch within the protected zone cannot be measured. Truly, many supplementary criteria [11–13] are available to enhance the stability of differential protection in the condition of CT saturation. It will be, however, the other subject irrespective of the purpose of this section, since the aim is to discuss the reliability, including the stability of the percentage differential criteria themselves.

The investigations will be based on the differential protection of a two-terminal object in accordance with the criteria described in Equations (3.52) and (3.53). Parameter $\dot{\delta} = \delta\angle\alpha$ is introduced for the purpose of clarifying the following demonstrations: it can be considered as a transferring ratio of the CT when evaluating the protective criterion of the relay subject to an external fault. In the case of an internal fault, it can then be regarded as the complex ratio between outgoing current and incoming current.

3.4.2 Performance Comparison between CPD and NPD in the Case of CT Saturation

Suppose that the CT at outgoing current side saturates with the transferring ratio $\dot{\delta} = \delta\angle\alpha$ while the CT at incoming current side can completely transform the primary current during an external fault.

To prevent the protection from mal-operation in this case, the following inequality should naturally be satisfied:

$$\text{NPD criterion}: I_{d1} < K_{r1} I_{bias1} \tag{3.54}$$

$$\text{CPD criterion}: I_{d1} < K_{r2}(I_{bias1} - I_{d1}) \tag{3.55}$$

According to the above-mentioned assumed direction of positive current flow, the outgoing current and incoming current should satisfy Equation (3.56) from the point of view of the CTs secondary side:

$$\dot{I}_{out} = -\dot{\delta}\dot{I}_{in} \tag{3.56}$$

It has been indicated in the Appendix that the δ will be approximately equal to $\cos\alpha$ in the case of CT saturation. In this condition the differential current can be given by:

$$I_d = \sqrt{1-\delta^2} I_{in} \tag{3.57}$$

and the bias current can be given by:

$$I_{bias1} = (1+\delta) I_{in} \tag{3.58}$$

Substituting $I_{d1}(I_d)$, I_{bias1} and Equation (3.56) into Equation (3.54) gives:

$$\delta > \frac{1-K_{r1}^2}{1+K_{r1}^2} = \delta_{01} \tag{3.59}$$

It is shown in Equation (3.59) that the NPD criterion having a certain restraint coefficient K_{r1} will block the protection correctly during an external fault even though the CT saturates, as long as the transferring ratio of the saturated CT δ is greater than δ_{01}. In this sense δ_{01} can be called the CT critical transferring ratio of NPD criterion.

For CPD criterion, substitute $I_{d2}(I_d)$, I_{r2} and Equation (3.56) into Equation (3.55):

$$\delta > \frac{1+2K_{r2}}{1+K_{r2}+K_{r2}^2} = \delta_{02} \tag{3.60}$$

Similarly, δ_{02} can be called the CT critical transferring ratio of CPD criterion.

Comparing Equation (3.59) with Equation (3.60), both criteria have the same restraint effect when the CTs on the outgoing current side have the same transferring ratio δ_0 ($\delta_0 = \delta_{01} = \delta_{02}$). In this case, Equation (3.61) can thus be deduced:

$$K_{r2} = \frac{K_{r1}}{1 - K_{r1}} \tag{3.61}$$

The condition illustrated by Equation (3.61) can be defined that NPD and CPD have the 'consistent security', that is, the CTs on the outgoing current sides have the same critical transferring ratio δ_0 and Equation (3.61) is satisfied with the restraint coefficient pair, K_{r1} of NPD and K_{r2} of CPD.

The concept of consistent security can be explained further as follows.

The protections implemented with NPD or CPD, whose restraint coefficients meet Equation (3.61), will both mal-operate when experiencing such an external fault that the current transferring ratio δ at the outgoing current side is less than δ_0 while the CT at the incoming side can completely transform primary current. Otherwise, the protections can both be blocked reliably.

According to Equation (3.59), the restraint coefficient can be expressed with the critical transferring ratio:

$$K_{r1} = \sqrt{\frac{1 - \delta_0}{1 + \delta_0}} \tag{3.62}$$

To ease the analysis, assume that I_{in} is the base of current per unit. In this way, the differential current can be rewritten as the operation quantity (OQ) of the protection. Thus, Equation (3.57) can be rewritten as:

$$OQ = \sqrt{1 - \delta^2} \tag{3.63}$$

Combining Equations (3.54), (3.58) with Equation (3.62), the RQ of the NPD can be given by:

$$RQ1 = \sqrt{\frac{1 - \delta_0}{1 + \delta_0}}(1 + \delta) \tag{3.64}$$

Combining Equations (3.55)–(3.58) and (3.61) with Equation (3.62), the RQ of the CPD can be given by:

$$RQ2 = \frac{\sqrt{1 - \delta_0}}{\sqrt{1 + \delta_0} - \sqrt{1 - \delta_0}}(1 + \delta - \sqrt{1 - \delta^2}) \tag{3.65}$$

With Equations (3.63)–(3.65), the operation region and the stabilizing area can be illustrated by Figure 3.25.

The X-axis of Figure 3.25 represents the value of δ and Y-axis is labelled with the OQ or RQ calculated by Equations (3.63)–(3.65) (in per unit values). In fact, OQ and RQ are the normalized expressions of differential and restraint currents with δ as their variables. As indicated in Equations (3.54) and (3.55), the OQ of both criteria are equal. It is only necessary to investigate the RQs. In Figure 3.25 the restraint quantities of NPD and CPD are signified as *RQ1* and *RQ2*, respectively. It can be seen from Figure 3.25 that both *RQ1* and *RQ2* pass across the point (δ_0, $1 - \delta_0$) and are all in proportion to δ.

To assess the security of both criteria a term "security margin" can be defined as:

$$K_{secu} = \frac{RQ_{\min}}{OQ_{\max}} \tag{3.66}$$

where $OQ_{\max}$ is defined to be the maximum OQ and $RQ_{\min}$ accordingly is defined to be the minimum RQ in the occurrence of any possible external faults or disturbances. Obviously, the relay is stable if K_{secu} is greater than 1. Otherwise the protection will mal-operate. To clearly evaluate the security margins of CPD and NPD, suppose that δ_1 is the minimum transferring ratio during all possible external faults, and it is greater than δ_0, as seen in Figure 3.25. In this case both CPD and NPD will be within the stabilizing area. Theoretically the relay can be stabilized no matter with NPD or CPD since the K_{secu} of both criteria

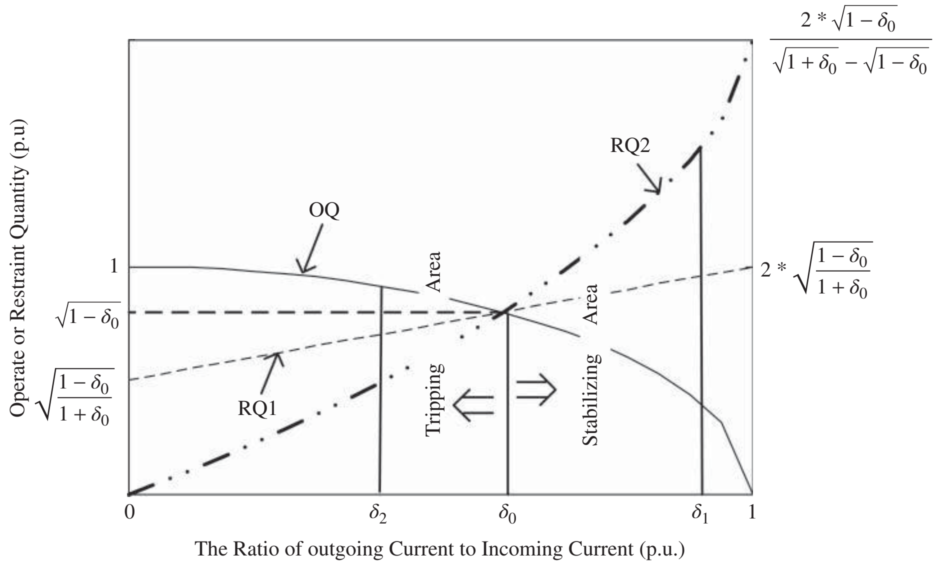

Figure 3.25 The performance comparison between CPD and NPD in accordance with consistent security

will be greater than 1. However, many uncertain factors may result in the accuracy loss of extraction of OQ and RQ. For example, the digital relay usually uses DFT, extracting the fundamental component to evaluate the OQ and RQ. However, the exponential DC offset due to fault transient will bring some measuring error. In this case, the greater the K_{secu}, the higher the redundancy of the criterion immune to any reverse interference. According to Equation (3.54) and the above descriptions, the security margin of NPD can be given by:

$$K_{\sec u-n} = \frac{K_{r1}(1+\delta_1)}{\sqrt{1-\delta_1^2}} \tag{3.67}$$

Similarly the security margin of CPD can be given by:

$$K_{\sec u-c} = \frac{K_{r2}(1+\delta_1-\sqrt{1-\delta_1^2})}{\sqrt{1-\delta_1^2}} \tag{3.68}$$

Combining Equations (3.61), (3.62), (3.67) and (3.68), comparing expression of the criteria is given by:

$$\frac{K_{\sec u-c}}{K_{\sec u-n}} = \frac{1-\sqrt{\frac{1-\delta_1}{1+\delta_1}}}{1-\sqrt{\frac{1-\delta_0}{1+\delta_0}}} \tag{3.69}$$

$\frac{K_{\sec u-c}}{K_{\sec u-n}}$ should be greater than 1 because of $\delta_1 > \delta_0$, that is, the security margin of CPD is higher than NPD, which implies that CPD has more redundancy to withstand CT saturation. For example, in the case of $\delta_1 \approx \delta_0$ CPD is more likely capable of blocking the differential protection correctly even though the ability of filter algorithms, such as DFT, to accurately extract the fundamentals is possibly degraded due to fault transient and DC exponential offset.

It is in vain to discuss the security margin in the condition of $\delta < \delta_0$ because both criteria cannot prevent the protection from mal-operation in this case, as indicated in Figure 3.25 ($\delta = \delta_2 < \delta_0$).

The impacts of the change of the restraint coefficients on the above two criteria in the condition of external fault accompanied by CT saturation can be investigated with two scenarios as below. 0.3 and 0.7 are taken as two restraint coefficients of NPD. In terms of consistent security, the K_{r2} should be selected as 0.43 and 2.33.

The characteristics of NPD and CPD are referred as to Figure 3.26, where the restraint quantities of NPD and CPD are simply replaced by the notation 'NPD' and 'CPD', which is used later. Besides, 'T-Area' in the figure means 'Tripping Area' and 'S-Area' means 'Stabilizing Area'.

The critical transferring ratio, δ_0, will be equal to 0.83 for the case in Figure 3.26a in line with the restraint coefficients. Both criteria will restrain the protection correctly if transforming error of the saturated CT is below 17% and no other errors introduced. In this case, it can be seen from Figure 3.26a that the RQ of CPD is always greater than that of NPD in the stabilizing area, which means higher security for CPD, as discussed above. On the other hand, both criteria will fail to block the protection when $\delta < \delta_0$. Therefore, it is meaningless to discuss and compare the security of the protection between CPD and NPD in this case.

The impacts of restraint coefficients of CPD and NPD are given in Figure 3.26b, where the restraint coefficient pair is selected as (0.7, 2.33). As shown, the change of OQ, *RQ1*, and *RQ2* in Figure 3.26b is similar to Figure 3.26a, except that the critical point, δ_0, moves from 0.83 to 0.34. In this scenario, the CT error allowed can be larger, which coincides with the theory of current percentage differential protection.

As a consequence, the security of CPD is higher than NPD in terms of consistent security.

3.4.3 Performance Comparison between CPD and NPD in the Case of Internal Fault

To further investigate the performance of CPD and NPD, the scenarios of internal faults should be investigated as well. The outgoing current can be still represented with the incoming current, as shown

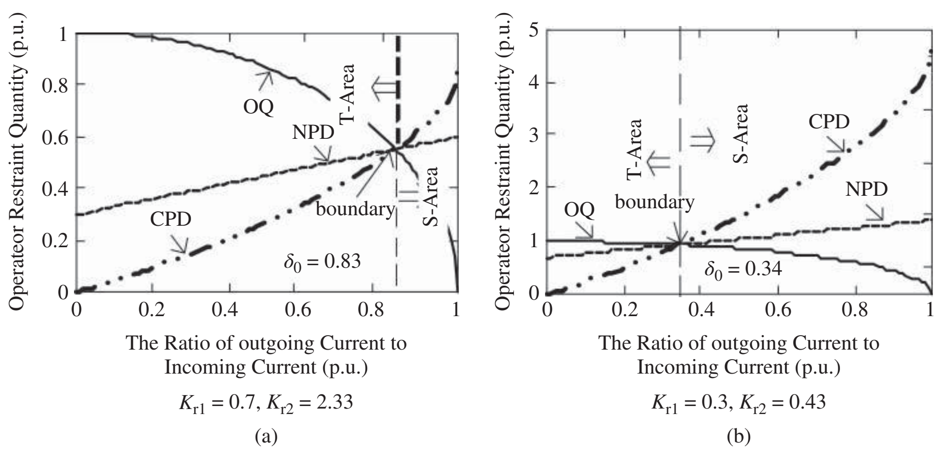

Figure 3.26 The differential or restraint value with the change of the ratio of outgoing current to incoming current for comparing the performance of CPD with NPD during external fault accompanied by CT saturation

in Equation (3.70):

$$\dot{I}_{out} = \dot{\delta}\dot{I}_{in} = \delta\angle\beta\dot{I}_{in} \tag{3.70}$$

where the magnitude ratio of outgoing current to incoming current is independent of the phase angle between the incoming current and outgoing current, which differs from the condition of CT saturation. It is feasible to let $\delta < 1$. But the phase angle β possibly changes from $-180°$ to $180°$ depending on the fault conditions.

In this case, with the definition of differential current and Equation (3.19), the OQ can be given by:

$$OQ = \sqrt{1 + 2\delta\cos\beta + \delta^2} \tag{3.71}$$

Similarly, the restraint quantity *RQ1* and *RQ2* should be given as:

$$RQ1 = 1 + \delta \tag{3.72}$$

$$RQ2 = 1 + \delta - OQ \tag{3.73}$$

As shown in Equations (3.71)–(3.73) the situations of β locating at $[-180°, 0°]$ are identical to those of β locating at $[0°, 180°]$. Thus, only the range of $[0°, 180°]$ is investigated. It should be noted that the choice of restraint coefficients of CPD and NPD still should be in accordance with Equation (3.62) to meet the 'consistent security', so that they can be compared reasonably.

In contrast to the discussions of the external fault accompanied by CT saturation, K_{r1} and K_{r2} are still supposed to be 0.3 and 0.43 respectively. Theoretically, to completely compare the performance of CPD and NPD, the comparison should be developed in a 3D space of axis OQ (RQ), δ and β since δ and β are variables. Nevertheless, it will result in unclear illustrations. It is feasible to let β be a constant. 30° and 150° will be two typical scenarios when the protected object is subject to the internal fault. $\beta = 30°$ indicates all fault currents flow toward the protected object, and the phase difference is induced by the angle difference of the equivalent sources' electromotive force (EMF). On the other hand, there must be a shunt current branch of current not being measured when $\beta = 150°$. The illustrations of these two cases are shown in Figure 3.27, where, 'T-Area' means 'Tripping Area' and 'F-Area" means 'Fail-to-trip Area'.

In the scenario of $\beta = 150°$, the tripping areas of NPD and CPD are all 72% when δ, the outgoing current ratio, changes from 0 to 1. However, the RQ of CPD is less than NPD in the tripping area, denoting higher sensitivity of CPD. Furthermore, Figure 3.27b shows the case of $\beta = 30°$. In this scenario, the protections

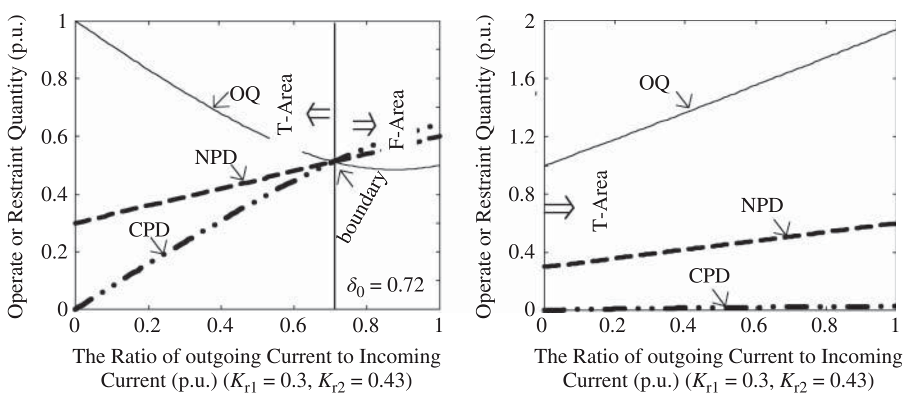

$\beta = 150°$
(a)

$\beta = 30°$
(a)

Figure 3.27 The differential or restraint value with the change of the ratio of outgoing current to incoming current for comparing the performance of CPD with NPD during internal faults

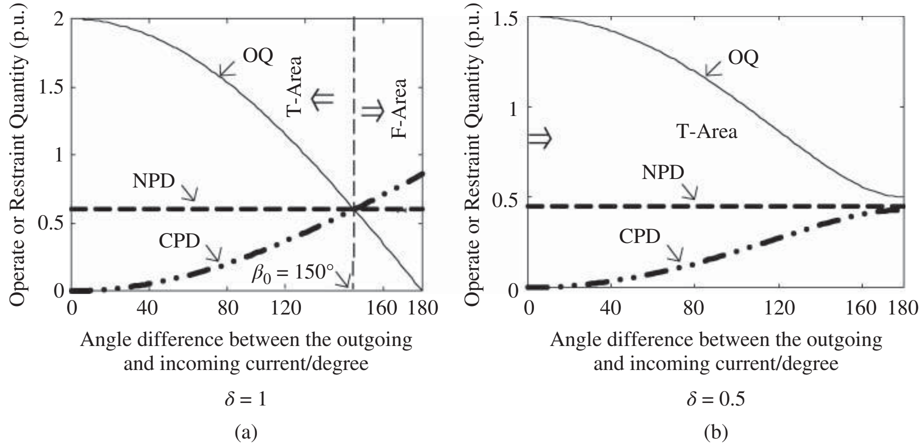

Figure 3.28 The differential or restraint value with the change of the angle difference between the outgoing and incoming current for comparing the performance of CPD with NPD in the occasion of internal faults

implemented with NPD or CPD can always trip irrespective of how δ changes. But there is the difference in terms of the operation sensitivity. As seen in Figure 3.27b, the RQ of CPD is nearly 0 over all variables δ. In contrast, the RQ of NPD is comparable to the OQ although it is smaller. Meanwhile, it is always greater than that of CPD. In this regard, CPD have higher sensitivity.

On the other hand the outgoing current ratio δ can be set to a vector at a fixed magnitude to investigate the influence of phase difference between incoming current and outgoing current. $\delta = 1$ and 0.5 are two of the scenarios presented in Figure 3.28. In this moment β will be the variable changing from 0° to 180°.

As seen in Figure 3.28a the tripping areas of CPD and NPD are all within $0 < \beta < 150°$. In the tripping area, the RQ of CPD is always less than that of NPD, which means CPD has higher sensitivity. The situation is confirmed by Figure 3.28b. The only difference between them is that there is no fail-to-trip area when δ is equal to 0.5.

Based on the above discussions, CPD certainly has higher reliability than NPD in any fault conditions.

In summary, a rational criterion for the comparative reliability analyses among any percentage differential protection criteria will be valuable, although there have been various criteria for evaluating the performance of a certain and individual percentage differential criterion. To clarify the impacts of restraint coefficient and the bias current design, the comparison shall follow a reasonable premise. Such premise is thus proposed in terms of 'consistent security' in this section. Based on this premise, the potential advantages of CPD criterion have been disclosed in contrast to NPD criterion. In addition, any normal differential criteria can also be compared following the 'consistent security'. This novel reliability evaluation criterion will reinforce the evaluation system of differential protection characteristics and provide a benchmark for designing reasonable bias current and, further, a better percentage differential criterion.

3.5 Comparative Studies on Percentage Differential Criteria Using Phase Current and Superimposed Phase Current

3.5.1 The Dynamic Locus of $\frac{\dot{\rho}-1}{\dot{\rho}+1}$ in the Case of CT Saturation

The scenario of CT saturation can be analysed based on a simplified CT model shown in Figure 3.29. As the resistance of the CT core is very small with respect to the magnetizing reactance, it can be neglected here. Further, the secondary leakage reactance of the CT can be combined to the CT load.

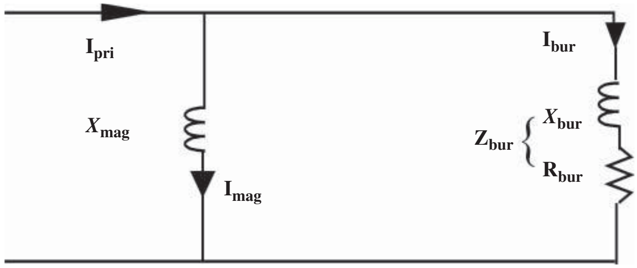

Figure 3.29 Simplified CT model

Normally, the CT load is inductive and, therefore, can be supposed to be $Z_{bur} = |Z|_{bur}\angle\theta_b$, where θ_b ranges from 0° to 90°.

The ratio of the current flowing through the CT load relative to the primary current can be expressed as:

$$\dot{\rho} = \frac{\dot{I}_{bur}}{\dot{I}_{pri}} = \frac{jX_{mag}}{Z_{bur} + jX_{mag}} = \frac{1}{1 - j\dfrac{Z_{bur}}{X_{mag}}} \tag{3.74}$$

and

$$\dot{\rho}' = \frac{\dot{\rho} - 1}{\dot{\rho} + 1} = \frac{j\dfrac{Z_{bur}}{X_{mag}}}{2 - j\dfrac{Z_{bur}}{X_{mag}}} = \frac{A + kB}{C + kD} \tag{3.75}$$

where

$$\begin{aligned} &\mathrm{A} = 0 \\ &\mathrm{B} = e^{j\theta_b + 90°} \\ &\mathrm{C} = 2 \\ &\mathrm{D} = e^{j\theta_b - 90°} \text{ and } k = \frac{|Z_{bur}|}{X_{mag}} \end{aligned}$$

When the impedance of the CT load is determined and the magnetizing reactance varies due to the saturation, A, B, C and D are all constants, while k is a variable real number.

Equation (3.75) denotes a circle, the centre together with the semi-radius of which are expressed as Equations (3.76) and (3.77), respectively:

$$\dot{O} = \frac{\dot{B}}{\dot{D}} + \left(\frac{\dot{A}}{\dot{C}} - \frac{\dot{B}}{\dot{D}}\right)\frac{e^{j(90° - \phi_D + \phi_C)}}{2\sin(\phi_D - \phi_C)} \tag{3.76}$$

$$R = \left|\frac{\dot{A}}{\dot{C}} - \frac{\dot{B}}{\dot{D}}\right| \frac{1}{2|\sin(\phi_D - \phi_C)|} \tag{3.77}$$

Substituting the expressions of A, B, C and D into Equations (3.76) and (3.77), it is possible to obtain the expressions of the centre and semi-radius of the circle as:

$$\dot{O} = -\frac{1}{2} - j\frac{1}{2}tg\theta_b \tag{3.78}$$

$$R = \frac{1}{2\cos\theta_b} \tag{3.79}$$

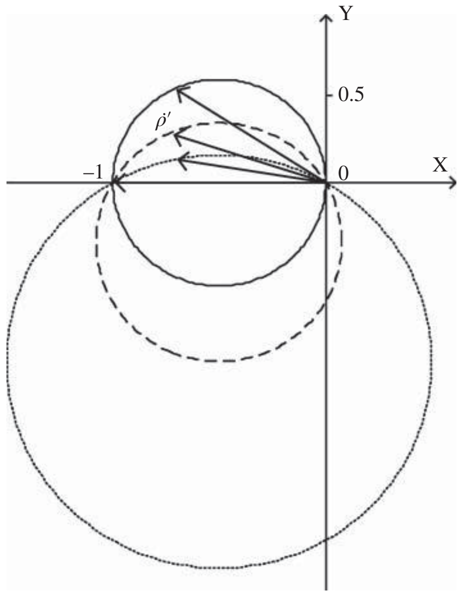

Figure 3.30 The locus of $\dot{\rho}'$ in the phase plane

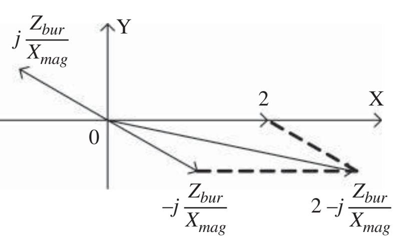

Figure 3.31 The vector chart for studying the phase of $\dot{\rho}'$

When θ_b varies, the locus of $\dot{\rho}'$ form a family of circles with the vector $-1+0\times\mathrm{j}$ as a chord (Figure 3.30).

The locus of $\dot{\rho}'$ that may occur in practice can now be investigated. By virtue of Equation (3.75), the phase angle of $\dot{\rho}'$ is equivalent to the phase angle of $j\frac{Z_{bur}}{X_{mag}}$ leading $2-j\frac{Z_{bur}}{X_{mag}}$. Using the vector graph in Figure 3.31, further analyses can be conducted.

According to the vector triangle, the phase angle of $j\frac{Z_{bur}}{X_{mag}}$ leading $2-j\frac{Z_{bur}}{X_{mag}}$ should be smaller than 180°. Further, it also can be seen that the phase angle $j\frac{Z_{bur}}{X_{mag}}$ leading $2-j\frac{Z_{bur}}{X_{mag}}$ should be larger than 90° in that $j\frac{Z_{bur}}{X_{mag}}$ is always within the quadrant II while $2-j\frac{Z_{bur}}{X_{mag}}$ is always within quadrant IV. As a consequence, the phase angle of $\dot{\rho}'$ should be in quadrant II, that is, the locus of $\dot{\rho}'$ should be the circular arc in quadrant II in Figure 3.30. When θ_b is varying, the locus of $\dot{\rho}'$ always lies within a semicircle which is in quadrant II and takes the vector $-1+0\times\mathrm{j}$ as its diameter. As a result, the module of $\dot{\rho}'$ is less than 1.

3.5.2 Sensitivity Comparison between the Phase Current Based and the Superimposed Current Based Differential Criteria

The sensitivity of the aforesaid criteria can be contrasted based on the system shown in Figure 3.32. It is acceptable to suppose that the protections are equipped at end S and end R, and the fault occurs at point F. Suppose that the phase-separated differential protection is applied in the system and the protection of each phase can be illustrated by virtue of Figure 3.32.

$\dot{I}_s$ and $\dot{I}_r$ are supposed to be the incoming current and outgoing current, respectively, at fault point and the corresponding directions of these currents are shown as Figure 3.32. The differential current is usually defined as $|\dot{I}_s - \dot{I}_r|$. In contrast, the design of the restraint current is more flexible, such as $\frac{|\dot{I}_s|+|\dot{I}_r|}{2}$, $\frac{|\dot{I}_s+\dot{I}_r|}{2}$ and so on, depending on the different requirements on the sensitivity of the differential protections. For the convenient of discussions, the restraint currents all adopt the type of $\frac{|\dot{I}_s+\dot{I}_r|}{2}$ irrespective of the conventional phase current based differential protection or of the superimposed current based differential protection. In this case, the phase current based percentage differential criterion can be described by:

$$|\dot{I}_s - \dot{I}_r| > K_{res}\frac{|\dot{I}_s + \dot{I}_r|}{2} \tag{3.80}$$

Equation (3.80) is denoted as criterion 1 for the convenience of description.

Correspondingly, the percentage differential criterion based on the superimposed current can be given by:

$$|\dot{I}_{sg} - \dot{I}_{rg}| > K_{resg}\frac{|\dot{I}_{sg} + \dot{I}_{rg}|}{2} \tag{3.81}$$

Compared with Equation (3.80), the subscripts of currents in Equation (3.81) are supplemented with 'g', which indicates superimposed components. In this case, criterion 2 can be distinguished from criterion 1.

The sensitivity of the two criteria responding to internal faults from criterion 1 can be discussed first. With a view to facilitating comparison, the restraint coefficients of both criteria are supposed to be 1. The selection and the influence of the restraint coefficient is discussed later.

According to the superposition principle, the faulty power system shown in Figure 3.32 can be decomposed into two conditions – normal load condition and short-circuit additional condition.

The relationships of the phase current, superimposed phase current and the load current of both sides are given by:

$$\dot{I}_s = \dot{I}_L + \dot{I}_{sg} \quad \dot{I}_r = \dot{I}_L + \dot{I}_{rg} \tag{3.82}$$

where $\dot{I}_L$ is the load current, $\dot{I}_{sg}$ and $\dot{I}_{rg}$ are the superimposed phase currents on end S and end R respectively. In this case, the differential currents can be expressed as:

$$\dot{I}_s - \dot{I}_r = \dot{I}_f = \dot{I}_{rg} - \dot{I}_{sg} = \dot{I}_{fg} \tag{3.83}$$

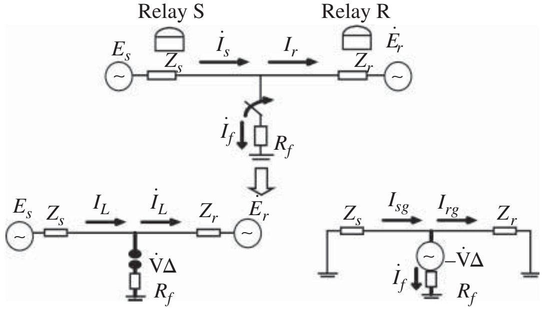

Figure 3.32 Faulty power system equivalent decomposition in the event of an internal fault

It is obvious that the differential current with respect to the phase current is equal to that based on the superimposed phase currents.

In virtue of Figure 3.32, supposing that the parameters in end R are described as $Z_r = \alpha Z_s$ and $\dot{E}_r = \beta \dot{E}_s$, the load current can be expressed as:

$$\dot{I}_L = \frac{\dot{E}_s - \dot{E}_r}{Z_s + Z_r} = \frac{\dot{E}_s(1-\beta)}{Z_s(1+\alpha)} \tag{3.84}$$

The current through the faulty branch is given by:

$$\dot{I}_f = \frac{\dot{U}_{F0}}{R_f + Z_s//Z_r} = \frac{\dot{E}_s(\alpha+\beta)}{R_f(1+\alpha)+\alpha Z_s} \tag{3.85}$$

The superimposed currents through the relay points can be given as:

$$\begin{cases} \dot{I}_{sg} = \dfrac{Z_r}{Z_s+Z_r}\dot{I}_f = \dfrac{\alpha \dot{E}_s(\alpha+\beta)}{[R_f(1+\alpha)+\alpha Z_s](1+\alpha)} \\ \dot{I}_{rg} = -\dfrac{Z_s}{Z_s+Z_r}\dot{I}_f = -\dfrac{\dot{E}_s(\alpha+\beta)}{[R_f(1+\alpha)+\alpha Z_s](1+\alpha)} \end{cases} \tag{3.86}$$

Firstly, the impact of transition resistance on the sensitivity of the protections is discussed. Equation (3.87) is used to express the sensitivity of the protections:

$$K_{sen} = \frac{\dot{I}_f}{\dot{I}_{res}} \tag{3.87}$$

According to Equation (3.80), the restraint current of criterion 1 is given by:

$$\dot{I}_{res} = \frac{\dot{I}_s + \dot{I}_r}{2} = \dot{I}_L + \frac{\dot{I}_{sg}+\dot{I}_{rg}}{2} \tag{3.88}$$

With respect to Equation (3.88), the restraint current of criterion 1 contains not only the superimposed phase currents but also the load current, which will lead to the impacts on the security and the sensitivity of differential protection.

Substituting Equations (3.84)–(3.86) and (3.88) into Equation (3.87), the sensitivity can be expressed by:

$$K_{sen} = \frac{2}{2\left(\dfrac{R_f}{Z_s} + \dfrac{\alpha}{1+\alpha}\right)\dfrac{1-\beta}{\alpha+\beta} + \dfrac{\alpha-1}{1+\beta}} \tag{3.89}$$

When the operating mode of power systems and the fault point are determined, the parameters in Equation (3.89) are all constants. It is easy to understand that the sensitivity becomes lower as R_f increases.

Comparatively, the restraint current of criterion 2 is given by:

$$\dot{I}_{resg} = \frac{\dot{I}_{sg}+\dot{I}_{rg}}{2} \tag{3.90}$$

The expression of sensitivity can be deduced similarly, given by:

$$K_{seng} = \frac{2(\alpha+1)}{1-\alpha} \tag{3.91}$$

The sensitivity of criterion 2 is not subject to transition resistance and the system EMFs of both sides. As the system impedances of both sides are inductive, the locus of α lies within quadrants I and IV. By virtue of the relationship of the vectors, the sensitivity of criterion 2 will always exceeds 2. Further, the sensitivity of criterion 2 becomes infinite if $\alpha = 1$. In this case, the sensitivity of criterion 1 is expressed as following:

$$K_{sen} = \frac{2}{\left(\frac{2R_f}{Z_s} + 1\right)\frac{1-\beta}{\beta+1}} \tag{3.92}$$

It can be seen from Equation (3.92) that the sensitivity of phase current based differential criterion is a finite value subject to the transition resistance.

It can also be perceived from Equation (3.89) that the unequal system EMFs of both ends have adverse influences on the sensitivity of criterion 1. In the event of $\beta \neq 1$, the sensitivity of criterion 1 is probably low, even for the solid-grounded faults under some conditions, such as power swings. The analytical process is described here.

It is acceptable to suppose that the magnitudes of the system EMFs of both sides are equal, and a solid-grounded fault occurs in the case of the phase angle between two sources reaching 180°. In this case, $\beta = -1$ and $R_f = 0$. Substituting $\beta = -1$ and $R_f = 0$ into Equation (3.89), it follows that:

$$K_{sen} = \frac{2}{\frac{4\alpha}{\alpha^2 - 1} + \frac{1-\alpha}{1+\alpha}} \tag{3.93}$$

The sensitivity of criterion 1 will be very low when Z_r is close to Z_s. Especially, the sensitivity drops to zero when $\alpha = 1$. In this case, the protection cannot operate unless the phase angle returns to a relatively small angle. Therefore, if internal faults occur during power swings, the phase current based differential protection may fail to operate for a long time, which may lead to the delayed removal of faults.

As a matter of fact, the maximum restraint coefficient is usually 0.15 when criterion 1 is applied to the differential protections of generators, while the slope of the ascending line in the percentage bias characteristic plane is around 0.3–0.7 when criterion 1 is applied to the differential protections of transformers. Nevertheless, the maximum restraint coefficient of criterion 1 will not exceed 0.7, while the restraint coefficient of criterion 2 is usually adopted as 0.8–1.0. As seen, the restraint coefficient of criterion 1 is obviously smaller than that of criterion 2, which makes the gap of the performances between the two criteria not distinct as analysed above. However, it will not upset the above conclusions and the influences of transition resistance and system EMFs on criterion 1 always exist. For this reason, in the case of common internal faults, the sensitivity of criterion 2 will exceed that of criterion 1.

3.5.3 Security Comparison between the Phase Current Based and the Superimposed Current Based Differential Criteria

Following the below analysis, it will be found that the security of criterion 1 in the case of external faults is not as satisfactory as criterion 2.

Figure 3.33 can be applied for the purpose of discussions on the security of the two criteria in the case of external faults. The distribution of the current on the faulty branch and system ends is the same as that in Figure 3.32, except that the protection on side R is now assumed to be located on side S′.

$\dot{I}_s$ and $\dot{I}_{s'}$ are both through currents from the viewpoint of the protection in the case of an external fault. Hence, in theory the protection should be stable due to the zero differential current. However, it is a different situation when the CT, especially only the CT on single end of the protected equipment, saturates. Suppose that the through current is $\dot{I}_{th}$, the CT on side S can transform linearly, while the CT on side S′ transforms partly and the transforming ratio is $\dot{\rho}$. Then, Equations (3.94)–(3.96) come into existence:

$$\dot{I}_s = \dot{I}_{th} = \dot{I}_{sg} + \dot{I}_L \tag{3.94}$$

$$\dot{I}_{s'} = \dot{\rho}\dot{I}_{th} \tag{3.95}$$

$$\dot{I}_{s'g} = \dot{I}_{s'} - \dot{I}_L = \dot{\rho}\dot{I}_{sg} + (\dot{\rho} - 1)\dot{I}_L \tag{3.96}$$

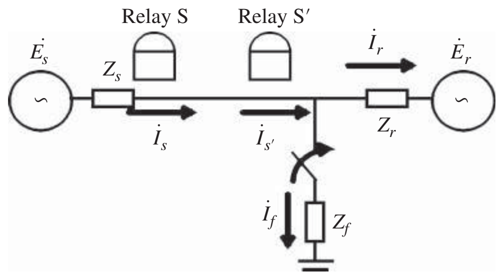

Figure 3.33 System specification of the external fault

The differential currents of criterion 1 and criterion 2 can be given by Equations (3.97) and (3.98), respectively:

$$\dot{I}_f = \dot{I}_s - \dot{I}_{s'} = (1-\dot{\rho})\dot{I}_{th} = (1-\dot{\rho})(\dot{I}_{sg} + \dot{I}_L) \tag{3.97}$$

$$\dot{I}_{fg} = \dot{I}_{sg} - \dot{I}_{s'g} = (1-\dot{\rho})(\dot{I}_{sg} + \dot{I}_L) \tag{3.98}$$

As seen, the differential currents of criterion 1 and criterion 2 are still equal. In this case, a reasonable evaluation of these two criteria can be obtained just by comparing the restraint currents of them. The restraint current of criterion 1 is given by:

$$\dot{I}_{res} = \frac{\dot{I}_s + \dot{I}_r}{2} = \frac{(1+\dot{\rho})}{2}(\dot{I}_{sg} + \dot{I}_L) \tag{3.99}$$

It follows that:

$$I_{res} = \frac{|1+\dot{\rho}|I_L}{2}\left|\frac{\dot{I}_{sg}}{\dot{I}_L} + 1\right| \tag{3.100}$$

Correspondingly, the restraint current of criterion 2 is expressed as:

$$I_{resg} = \frac{|1+\dot{\rho}|I_L}{2}\left|\frac{\dot{I}_{sg}}{\dot{I}_L} + \frac{\dot{\rho}-1}{\dot{\rho}+1}\right| \tag{3.101}$$

It can be seen from Equations (3.100) and (3.101) that the restraint performances of these two criteria can be distinguished just by comparing the magnitudes of vectors between $\frac{\dot{I}_{sg}}{\dot{I}_L} + \frac{\dot{\rho}-1}{\dot{\rho}+1}$ and $\frac{\dot{I}_{sg}}{\dot{I}_L} + 1$. Equation (3.101) can be derived by virtue of Equations (3.84) and (3.86) as below:

$$\frac{\dot{I}_{sg}}{\dot{I}_L} = \frac{\alpha + \dot{\beta}}{\left[\frac{R_f}{Z_s}\left(\frac{1}{\alpha}+1\right)+1\right](1-\dot{\beta})} \tag{3.102}$$

Generally, the saturation of the CT results from the heavy through current of external faults, which is probable only when α is quite large ($\alpha \gg 1$) and the transition resistance is quite small. In this scenario, as R_f is a pure resistance and the impedance angle of Z_s is near to 90°, the argument of vector $\left[\frac{R_f}{Z_s}\left(\frac{1}{\alpha}+1\right)+1\right]$ ranges from −90° to 0°. According to these hypotheses, the magnitude and the argument of vector $\left[\frac{R_f}{Z_s}\left(\frac{1}{\alpha}+1\right)+1\right]$ should approach 1° and 0°, respectively. The magnitude of vector $\dot{\beta}$ is near to 1 and the corresponding argument ranges from −60° to 60° when a fault occurs under normal operating conditions. When the argument varies within the above range, the difference between restraint currents of the two criteria is not quite apparent, especially for the case of a fault occurring in the event of a small phase angle difference between two sources. For instance, if supposing $\beta = 1$, the conditions of

$\alpha + \dot{\beta} \approx \alpha >> 1$ and $1 - \dot{\beta} = 0.52\angle 75°$ come into existence when $\dot{\beta} = 1\angle 30°$. Furthermore, according to the condition of $\left[\frac{R_f}{Z_s}\left(\frac{1}{\alpha}+1\right)+1\right] \approx 1$, Equation (3.103) can be obtained:

$$\left|\frac{\dot{I}_{sg}}{\dot{I}_L}\right| \approx 2\alpha \tag{3.103}$$

In this case, the magnitude of $\frac{\dot{I}_{sg}}{\dot{I}_L}$ will far exceed 1. As analysed in the Section 3.5.1, the actual locus of $\frac{\dot{\rho}-1}{\dot{\rho}+1}$ varies in a semi-circle, which is in quadrant II taking vector $-1+0\times j$ as its diameter, and hence the magnitude of $\frac{\dot{\rho}-1}{\dot{\rho}+1}$ is smaller than 1. Therefore, both $\frac{\dot{\rho}-1}{\dot{\rho}+1}$ and $1\angle 0°$ can be regarded as trivial factors resulting in the saturation of CT compared with $\frac{\dot{I}_{sg}}{\dot{I}_L}$. In this circumstance, the basic restraint currents of the two criteria are approximately equal.

It is clear that the abilities of being immune to CT saturation are similar if the restraint coefficients of the two criteria are equal. In practice, as the restraint coefficient of criterion 2 is apparently greater than that of criterion 1, the stability of criterion 2 in the case of external faults will surpass that of criterion 1 by far.

It is a complex scenario when the magnitude of the superimposed current is near to that of the load current under some fault conditions, which means the magnitude of $\frac{\dot{I}_{sg}}{\dot{I}_L}$ is close to, even less than, 1, accompanied by the argument changing from 0° to 360°. It can be seen from Equations (3.100)–(3.102) that there are too many variable factors. Besides, after taking the restraint coefficients into account, it is difficult to determine whether the restraint current of criterion 1 is greater than that of criterion 2. However, qualitatively, based on the fact that the direction of $\frac{\dot{\rho}-1}{\dot{\rho}+1}$, which is the additional component of the superimposed current based criterion, is basically opposite to the direction of $1\angle 0°$, which denotes the additional component of the phase current based criterion, the operation stability of criterion 1 is higher when the superimposed current is in phase with the load current. On the contrary, criterion 2 has higher stability when the superimposed current is 180° out of phase with the load current. As for other scenarios, a determinative conclusion cannot be drawn until all the factors are available.

3.5.4 Simulation Analyses

Adopting the system configuration of Figure 3.32, the ATP based simulations are carried out. The internal fault shown in Figure 3.32 and the external fault shown in Figure 3.33 are simulated respectively. In order to discuss the situation during CT saturation in the case of an external fault, the CT is modelled based on ATP considering the characteristic of the core. When the CT enters the saturation state in the case of an external fault, the currents on side S and S′ are shown in Figure 3.34. Furthermore, the differential

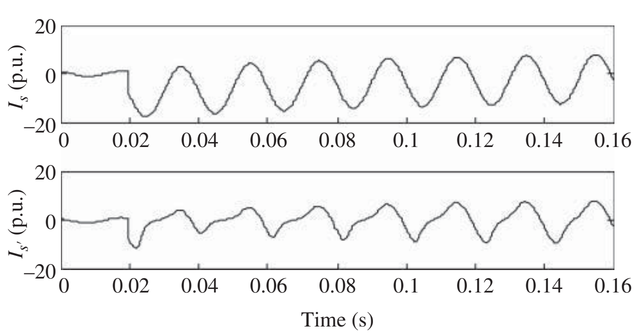

Figure 3.34 CT saturation on only one side during an external fault

currents and restraint currents of criteria 1 and 2 can be obtained. In this case, the operation points of the two criteria in the percentage bias characteristic plane can be investigated (Figure 3.34).

Usually, criterion 1 adopts a bias characteristic with two different slopes. The first section should be a flat line and the threshold is often set as $0.15I_n$, while the slope of the second section is usually 0.3. As for criterion 2, a bias characteristic with a single straight line passing through the original point is adopted, whose slope is usually set to be 1.

It can be seen from Figure 3.35 that the operation points of the two criteria are very close. However, as the characteristics of the two criteria are different, the operation point of criterion 2 keeps away from its operation region and, hence, the protection is stable. In contrast, the operation point of criterion 1 enters its operation region and, hence, the protection mal-operates. Further, the performances of the two criteria in the case of an internal fault are investigated. The fault conditions are supposed to be $\alpha = 0.2$, $\beta = 1\angle-60^\circ$, $R_f = 300\Omega$, and $Z_s = 20\Omega$. The operation points of the two criteria in the percentage bias characteristic plane are shown in Figure 3.36. It is obvious that the protection with criterion 2 can operate correctly and the sensitivity is 3 accordingly. However, the protection with criterion 1 fails to trip.

In summary, the comparative sensitivity and the security of the percentage differential criteria using the phase current and the superimposed phase current have been studied in this section. On the basis of quantitative analyses, it is found that the sensitivity of the superimposed current based differential criterion exceeds that of the phase current based differential criterion in the case of internal faults. In terms

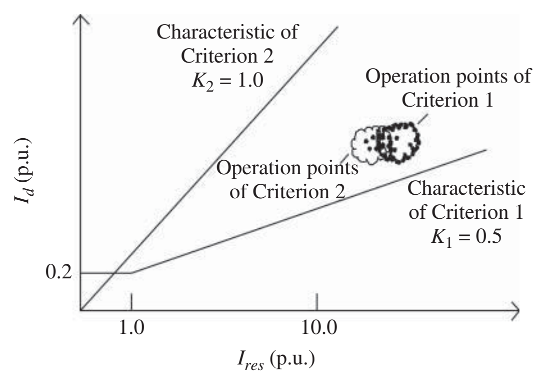

Figure 3.35 Operation points of criteria 1 and 2 during an external fault

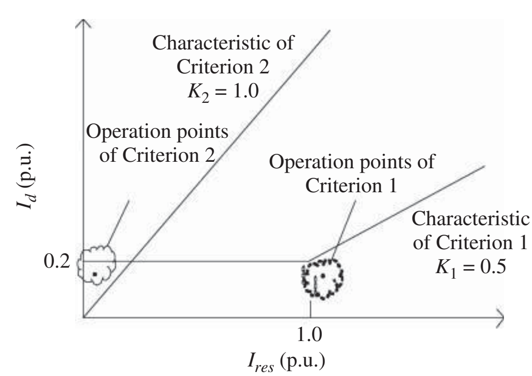

Figure 3.36 Operation points of criteria 1 and 2 during an internal fault with high fault resistance

of the security analysis and based on the existing setting principles, the superimposed current based differential protection is also better than the phase current based differential protection in most cases. Nevertheless, it should also be pointed out that as the system frequency will change after fault occurs, it is difficult to capture the superimposed currents accurately. Generally, the operating correctness of the superimposed current based protection cannot be guaranteed if the fault exists for a long period of time. Under this condition, the phase current based differential criterion is capable of taking over the task of the protection independently. Therefore, these two criteria can complement each other and should not replace each other.

3.6 A Novel Analysis Methodology of Differential Protection Operation Behaviour

3.6.1 The Relationship between Transforming Rate and the Angular Change Rate under CT Saturation

The exact model of the CT is shown in Figure 3.37.

The resistance R_{loss} representing the active power loss of the magnetizing branch is very small compared to the magnetizing reactance. The secondary leakage reactance can be combined into the load of CT. It is convenient if iron loss is neglected when investigating CT saturation.

As shown in Figure 3.37a, the load of the CT is normally inductive. Therefore, suppose $Z_a = |Z_b| \angle p$, $0° < \beta < 90°$. It can be demonstrated that the saturated CT will produce maximum false differential current when load is purely resistant ($\beta = 0°$).

When discussing the influences due to angular error, suppose $|Z_b|$ is constant. For the differential protection, the current through the CT magnetizing branch is the false differential current if the CT on the other side transforms correctly.

Strictly speaking, CT saturation is due to the decaying DC component within the through current. The magnetizing current should be solved by a nonlinear differential equation because of the nonlinearity of

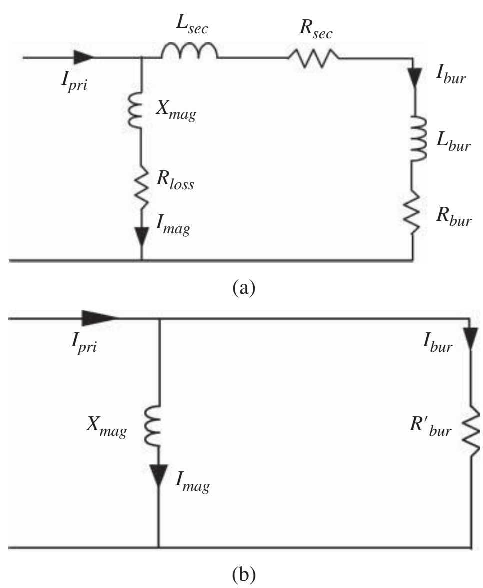

Figure 3.37 Current transformer model: (a) precise model; (b) simplified model

magnetizing reactance. However, no exact analytic expression is available. If the magnetizing reactance is replaced by average reactance, it is possible to evaluate the magnitude and the phase of magnetizing current (differential current) to some extent. This is because that the fundamental frequency component is the primary one within the differential current. An interesting law will be disclosed although the above processing is not very strict; for this purpose, the magnetizing reactance is replaced by the average reactance in the following discussion.

According to Figure 3.37a (ignoring the magnetizing resistance), the current in magnetizing branch is expressed as:

$$\dot{I}_{mag} = \frac{|Z_b|(\cos\beta + j\sin\beta)}{|Z_b|(\cos\beta + j\sin\beta) + jX_{mag}}\dot{I}_{pri} \tag{3.104}$$

The magnitude of the magnetizing current is given by:

$$I_{mag} = \frac{|Z_b|I_{pri}}{\sqrt{|Z_b|^2 + 2|Z_b|\sin\beta X_{mag} + X_{mag}^2}} \tag{3.105}$$

When $|Z_b|$ and X_{mag} are constant, it can easily be understood that Equation (3.105) approaches the maximum value as $\beta = 0°$. In this sense, pure resistance load has the strictest influence in CT saturation. On the premise of CT load being pure resistance, the relationship between transforming rate and angular error can be formed. The model of CT can be simplified in Figure 3.37b. The current through the CT load is expressed as:

$$\dot{I}_{mag} = \dot{I}_{pri}\frac{jX_{mag}}{R'_{bur} + jX_{mag}} = s\dot{I}_{pri}\angle\alpha \tag{3.106}$$

where s represents variable rates and α stands for angular error during the process of current transforming.

According to Equation (3.106):

$$s = \frac{X_{mag}}{\sqrt{(R'_{bur})^2 + X_{mag}^2}} \tag{3.107}$$

$$\alpha = \arccos\frac{X_{mag}}{\sqrt{(R'_{bur})^2 + X_{mag}^2}} \tag{3.108}$$

As shown in Equations (3.107) and (3.108), s and α satisfy the following equation:

$$s = \cos\alpha \tag{3.109}$$

3.6.2 Principles of Novel Percentage Restraint Criteria

As the earliest and the most widely used method of power system protection, the excellent performance of differential protection is universally accepted. Generally, assuming differential current as I_Δ and restraint current as I_H, the protection criterion is usually described in terms of the (I_Δ, I_H) plane. Actually, due to various alternatives on restraint current, the operating behaviour of the protection criteria under various practical operation conditions is hardly evaluated in the (I_Δ, I_H) plane. Therefore, different analysis methods are proposed by means of coordinate transformation. As for any percentage differential criterion, with multiple parameters to be set in the (I_Δ, I_H) plane, it needs to be observed under a multidimensional space to obtain the global characteristics. The selection method of coordinate axis of the multidimensional space is directly related to human intuition when evaluating a certain index of the percentage differential criterion. After selecting the coordinate system of multidimensional space, global evaluation can be done by means of it. In fact, existing methods for evaluating the operation behaviour of the criterion only intercept a sectional view in view of limiting conditions in a multidimensional space. Although incomplete, these analysis methods can indeed effectively investigate the criterion of operation behaviour from a certain aspect. The following novel analysis methodology is actually plane-based as well.

3.6.2.1 The Analysis Methodology of Differential Protection Operating Behaviour Based on through Current and Current Transformer Transferring Ratio Plane

There are two main aspects when evaluating the performance of percentage differential protection criterion: (i) the mal-operation probability when the current transformer saturates due to an external fault and (ii) the operation sensitivity when high outgoing current exists on the occasion of a slight internal fault. As the following analysis shows, evaluating the performance of differential protection criteria by analysing the operation behaviour with the relationship of the through current with respect to the ratio difference between bilateral currents is an effective method.

For the percentage differential protection, the protected object can always be equivalent to a two-terminal network, irrespective of whether it is a real two-terminal network (mostly it would be generator, transformer or transmission line) or a multiport network (mostly it will be a transformer with three or more windings, T-connection transmission line, bus). Assume that the incoming current is $\dot{I}_1$ and the outgoing current is $\dot{I}_2$, the positive direction is shown in Figure 3.38.

Generally, the differential quantity can be formed by $I_\Delta = |\dot{I}_1 + \dot{I}_2|$. Assuming that the CT saturates on the occasion of through fault. In this case, $\dot{I}_p = pI_n\angle 0°$, where p is the through current multiple. The worst scenario rests when one side of the CT saturates accompanied by the other side of the CT fully transferring. Assume the incoming current fully transferring, that is, $\dot{I}_1 = \dot{I}_p$. When the outgoing side of the CT saturates, the ratio difference and angle difference occur. Assuming the transferring ratio is s, the ratio difference will be $1-s$. Actually, s can be regarded as the outgoing current ratio when analysing the sensitivity of the criteria with respect to the internal fault. Let the angle difference be α. According to the positive direction shown in Figure 3.38, the relationship between outgoing current and through current is given by:

$$\dot{I}_2 = -s\dot{I}_p\angle\alpha \tag{3.110}$$

The simple criterion of differential protection is:

$$I_\Delta > I_0 = gI_n \tag{3.111}$$

To illustrate the effectiveness of the method, in view of the anti-CT saturation performance from Equation (3.105), $\dot{I}_1$ and $\dot{I}_2$ are substituted into Equation (3.105) and the relationship given by Equation (3.112) is acquired:

$$\sqrt{1 - 2s\cos\alpha + s^2} > \frac{g}{p} \tag{3.112}$$

From Section 3.6.1, the corresponding false differential current reaches its highest point when the CT load is purely resistive. On this basis, the CT angular difference and transferring ratio should satisfy Equation (3.109). Substituting them into Equation (3.112) gives:

$$s < \sqrt{1 - \left(\frac{g}{p}\right)^2} \tag{3.113}$$

The operating behaviour of the relay in the p–s plane is shown below.

Figure 3.39 illustrates the protection operation region when I_p varies from 0 to ∞. In the p–s plane the shadowed area shows the operation region. Assume the critical action equation, which means the

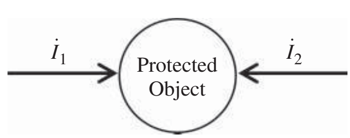

Figure 3.38 Principle illustration of current differential protection

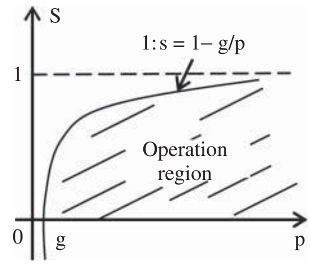

Figure 3.39 Mal-operation region of criterion given by Equation (3.111) in the condition of current transformer saturation

boundary line of the shadowed area is $s = f(g)$. If (p_0, s_0) satisfies this function, a wrong tripping command will be issued while $s < s_0$ and $p = p_0$. Call $1 - s_0$ the CT admissible error of p_0 times through current. As seen in Figure 3.39, there will exist a large mal-operation region if Equation (3.111) is adopted as the single criterion. In particular, the CT admissible error $1 - s_0$ will approach 0 rapidly as I_p grows and it is inevitable that great error comes with high current, which indicates that this criterion may hardly work when I_p is very high.

A new type of restraint criterion outlined below is evaluated to highlight the effectiveness of this method. In fact, this method can be used to analyse various percentage differential criteria.

3.6.2.2 Analysis for Three Product Restrain Criteria Employing the p–s Plane

As mentioned above, the operating quantity of the differential protection is usually $I_\Delta = |\dot{I}_1 + \dot{I}_2|$ but different constructions of the restrained quantity form various percentage differential protection criteria. In the a novel criterion design proposed by the ABB Company, the differential quantity adopts $I_\Delta^2 = |\dot{I}_1 + \dot{I}_2|^2$ and the restraining quantity is $I_H^2 = |\dot{I}_1||\dot{I}_2| \cos\alpha$, where α is the included angle of $\dot{I}_1$ and $-\dot{I}_2$.

The protection criterion is given by:

$$I_\Delta^2 > K_{res}{}' I^2{}_H \tag{3.114}$$

where $K_{res}{}'$ is the restrained coefficient, which theoretically has wide value-taking area because of different setting principles in different applications.

In the ideal scenario, $\dot{I}_1 = \dot{I}_2 = \dot{I}_p$ and $\alpha = 0^0$ if the fault current is the through current. In this case, I_Δ^2 on the left-hand side of Equation (3.114) will be zero. On the right-hand side of Equation (3.114), $K_{res}{}' I^2{}_p$. As long as I_P reaches a certain level, the restrained effect can be achieved. When an internal fault occurs, the scenario $90° < \alpha < 270°$ exists with both sides injected by power supplies and the right-hand side of Equation (3.114) $I_H^2 = -K'_{res} I_1 I_2 |\cos\alpha|$ is negative. The restrained quantity presents as the operating quantity. The operating quantity of the left-hand side is larger than $I_1^2 + I_2^2$, which leads to the sensitive action of the relay. Even though only a single power supply is provided (assume $\dot{I}_2 = 0$), as the restrained quantity is 0 and the operating quantity is $\dot{I}_1$, protection would still take action as long as I_1 can be measured within its detectable range.

All sorts of percentage differential protections of the ABB Company employ the criteria based on this product RQ. The alternative is to ignore the transferring from the restraining quantity to the operating quantity when internal faults occur and setting the RQ as 0 when it turns negative. Therefore, the restrained current can be set as:

$$I_H = \begin{cases} \sqrt{|\dot{I}_1|\,|\dot{I}_2| \cos\alpha} & \cos\alpha \geq 0 \\ 0 & \cos\alpha < 0 \end{cases} \tag{3.115}$$

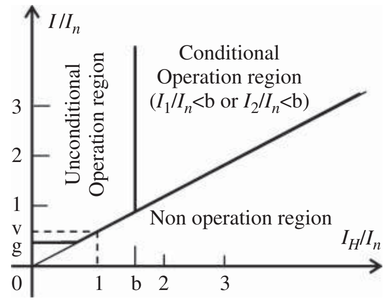

Figure 3.40 Percentage differential characteristics of novel current comparison criteria. g is the fixed threshold and v is the gradient of slope

Assume that the restrained current is still $I_\Delta = |\dot{I}_1 + \dot{I}_2|$. Figure 3.40 shows the action condition of the percentage differential protection, which is called as current phase comparison differential protection.

The most significant difference of this criterion compared to the NPD protection criterion is that the operation region is divided at a certain fixed threshold (usually 1.5 times rated current). The left-hand side is the unconditional operation region. When the restrained current is under the threshold, the protection will take action as long as it meets the requirements of percentage differential action. The right-hand side stands for conditional operation region or restrained region. One choice is at least one side current is under the threshold for protection tripping apart from satisfying percentage differential protection conditions when the restrained current is higher than the threshold; this is criterion 1. Another choice is that the protection will be blocked as long as the restrained current exceeds the threshold and the operation region narrows down to the left area of the division line; this is criterion 2. Obviously, the action performance of criterion 1 or 2 cannot be directly evaluated according to Figure 3.40. However, when changing the coordinate system from (I_Δ, I_H) to (p, s), some interesting phenomenon of the criteria are found. The protection operation behaviour in Figure 3.40 is discussed in the next sections, firstly when there is no vertical limiting condition (conventional product restraint criterion), and based on it the actual performances of two new criteria are correspondingly analysed.

Conventional Product Restraint Criterion

From Figure 3.40, the operation region of conventional product restraint criterion could be solved by the following inequality simultaneously:

$$\begin{cases} I_\Delta = |\dot{I}_1 + \dot{I}_2| > gI_n \\ I_\Delta = |\dot{I}_1 + \dot{I}_2| > vI_H = v\sqrt{|\dot{I}_1||\dot{I}_2|\cos\alpha} \end{cases} \tag{3.116}$$

The coefficients of the inequality are shown in Figure 3.40.

Substituting $\dot{I}_1$, $\dot{I}_2$ and Equation (3.110) into Equation (3.116) gives:

$$\begin{cases} \sqrt{1 - 2s\cos\alpha + s^2}I_p > gI_n \\ \sqrt{1 - 2s\cos\alpha + s^2} > v\sqrt{s\cos\alpha} \end{cases} \tag{3.117}$$

Firstly, the ability of the above criterion to resist CT saturation can be analysed. In the case of a through fault, the angular difference due to CT saturation will fit the definition of this product restraint criterion to α. Similarly, according to Equation (3.109), Equation (3.117) can be transformed as follows:

$$\begin{cases} s < \sqrt{1 - \left(\frac{g}{p}\right)^2} \\ s < \dfrac{1}{\sqrt{1 + v^2}} \end{cases} \tag{3.118}$$

From Equation (3.118), the mal-operation region can be formed when the CT is saturated (Figure 3.41). Point (p_1, p_2), the intersection of the two curves, is given by:

$$\begin{cases} p_{12} = \dfrac{g}{v}\sqrt{1 + v^2} \\ s_{12} = \dfrac{1}{\sqrt{1 + v^2}} \end{cases} \tag{3.119}$$

Figure 3.41 can be analysed as below. The protection will not mal-operate theoretically whether the CT is saturated or not if $p < g$ due to no solution for s. The mal-operation region changes as one covered by the curve $s = \sqrt{1 - (g/p)^2}$ when $g < p < p_{12}$. The value of s changes from 0 up to s_{12}. Correspondingly, the permissible error reduces from 100% to $(1 - s_{12}) \times 100\%$. When $p > p_{12}$, the permissible error will remain $(1 - s_{12}) \times 100\%$. For the convenience of description, s_{12} is called the minimum CT transferring ratio against mal-operation, noting it as s_0. To ensure that mal-operation of criterion never occurs whatever the value of through current, the transferring ratio must be more than this value. Accordingly, call $1 - s_0$ the global most easy mal-operation CT error E_0. Meanwhile, p_{12} is critical through current multiple and identified as p_0. Compared with Equation (3.111), E_0 increases from 0 to $1 - 1/\sqrt{1 + v^2}$. In this case, security has been improved. From Equation (3.119) it is known that s_0 is invariant when the slope v of the percentage restrained straight line is at constant value but p_0 and the low action threshold value g is proportional. When g increases, the critical through current multiple p_0 that leads to mal-operation will increase. Correspondingly, both the possibility of mal-operation and the mal-operation region will decrease. It is thus clear that increasing the value of g will help to improve the security of the protection. From Figure 3.41 and Equation (3.119), the possibility of mal-operation is quite high when the values of v and g are small if there is no other limiting condition. For example, adopting $v = 0.2$ and $g = 0.15$, E_0 cannot exceed 2% in order to ensure protection does not mal-operate when the through current multiple is equal to or more than 0.76 times of the rated current. In the case of a large through current caused by the external short-circuit fault, it is difficult to ensure that the above condition is satisfied. Therefore, additional constraints are needed.

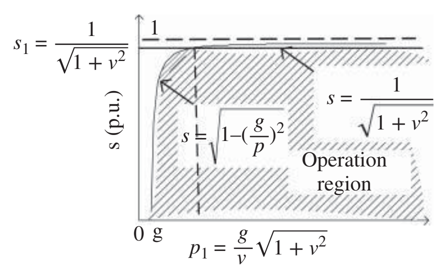

Figure 3.41 Mal-operation region of previous current comparison criterion under the condition of current transformer saturation

New Product Restraint Criterion

1. **Analysis of criterion 1**
   (a) *CT saturated*
   Substituting the condition Equation (3.109) of saturation into Equations (3.110) and (3.115), the incoming current is equal to the restrained current at this time. This means that the condition of the operation region is invalid in the case when CT is saturated because it is clearly impossible to meet the condition:

$$I_1 \geq I_2,\ I_2 = I_H,\ I_1 \text{ or } I_2 < b,\ I_H \geq b$$

The boundary conditions of the criterion are showed in the (p, s) plane with the following straight line or curve:

$$s = \sqrt{1 - \left(\frac{g}{p}\right)^2} \tag{3.120}$$

$$s = \frac{1}{\sqrt{1 + \upsilon^2}} \tag{3.121}$$

$$s = \frac{b}{p} \tag{3.122}$$

The criterion of operation (mal-operation actually) region is surrounded by the three curved (straight) lines and the p axis. Due to the different values of b, g and υ, the shape of the mal-operation region is slightly different. The operation region may be surrounded by two curves and the axis (case 1), that is the region surrounded by Equation (3.120), Equation (3.122) and the p axis (Figure 3.42). It is or surrounded by three curves and the p axis (case 2), that is the region surrounded by the equations from Equation (3.120)–(3.122) and the p axis, as shown in Figure 3.43.

Compared with Figure 3.41, in Figures 3.42 or 3.43 the mal-operation region of the criterion has been limited to some extent. Particularly, in the case of large through current, the allowable CT transferring ratio can be smaller, which allows the CT's transferring error to increase. This is obviously ideal.

   (b) *Internal fault*:
   The outgoing current and differential current are no longer equal under this condition. Now, s represents the ratio of the outgoing current with respect to the incoming current. In addition, α represents the angle offset of the outgoing current with respect to incoming current. When $\alpha = 0$, not only does outgoing current exists but the outgoing current is in phase with the incoming current according to the positive current direction defined by the current comparison criterion.

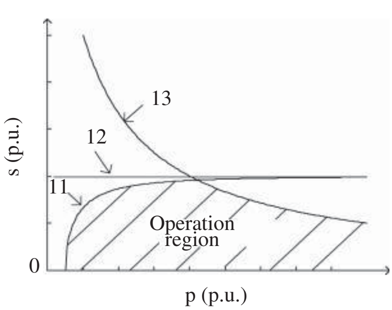

Figure 3.42 Mal-operation region of criterion 1 under the condition of current transformer saturation (case 1)

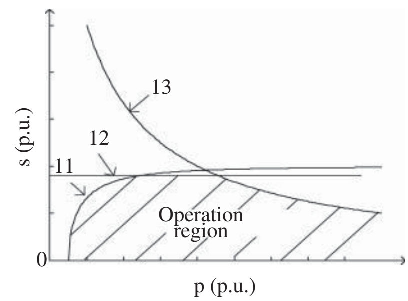

Figure 3.43 Mal-operation region of criterion 1 under the condition of current transformer saturation (case 2)

Under the premise of keeping the same amplitude of the outgoing current, the differential current caused by this case is the least, and the corresponding sensitivity is the lowest. When assessing the sensitivity of the internal fault, the scenario of $\alpha = 0$ can be assessed; this scenario is referred to as the slight internal fault. In this case $I_1 = p$, $I_2 = ps$ and $I_H = p\sqrt{s}$. $I_1 < b$ is still impossible since $s \le 1$ when $I_H > b$. $I_2 < b$ is possible when $I_H < b$ because now $I_2 \le I_H$. The criterion can be expressed as the union of Equations (3.123) and (3.124) in the $p - s$ plane.

$$\begin{cases} s < 1 - \dfrac{g}{p} \\ s < \dfrac{1}{1 + \dfrac{v^2}{2} + \sqrt{\dfrac{v^4}{4} + v^2}} \\ s < \left(\dfrac{b}{p}\right)^2 \end{cases} \tag{3.123}$$

$$\begin{cases} s < \dfrac{b}{p} \\ s \ge \left(\dfrac{b}{p}\right)^2 \end{cases} \tag{3.124}$$

Inequalities in Equations (3.123) and (3.124) can be solved as:

$$s < 1 - \frac{g}{p} \tag{3.125}$$

$$s < \frac{1}{f(v)} \tag{3.126}$$

$$s < \frac{b}{p} \tag{3.127}$$

where

$$f(v) = 1 + \frac{v^2}{2} + \sqrt{\frac{v^4}{4} + v^2} \tag{3.128}$$

Taking equal signs in inequalities Equations (3.125)–(3.127), the boundary of the operation region can be obtained.

The operation region of the criterion is the area surrounded by the three curves and p axis together. The shape of the operation region is similar to the shape of mal-operation

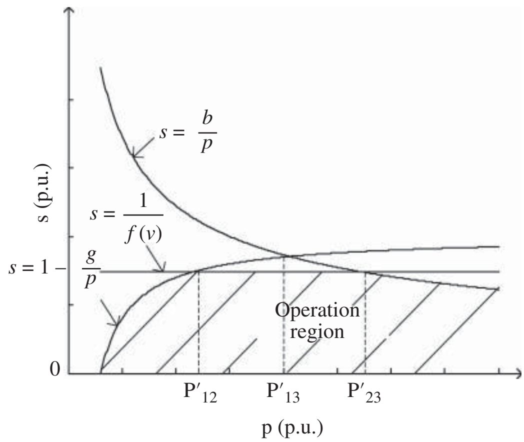

Figure 3.44 Operation area of criterion 1 under the condition of light internal fault (curves defined by Equations (3.119)–(3.121) and the *p* axis)

region in the condition of CT saturation. The operation region is surrounded by the curves defined by Equations (3.119)–(3.121) and the *p* axis (Figure 3.44) or by the curves defined by Equations (3.125), (3.127) and the *p* axis (Figure 3.45).

The operation regions in Figures 3.44 and 3.45 will be the operation regions of the conventional product restraint criterion if the limitations of Equation (3.127) are not taken into account. Apparently, the operation region of the criterion will be reduced with additional conditions. However, the reduced operation region corresponds to a rare fault, the probability of which occurring is very small (e.g. a slight internal fault accompanied by an external fault occurring on the same phase). Taking into account the significant increase in security, this compromise is reasonable and necessary.

2. **Analysis of criterion 2**
   (a) *CT saturation*
   The conditional operation region is unavailable when the CT is saturated. On that occasion, the criterion is equal to criterion 1. The mal-operation region can be represented as shown in Figures 3.42 and 3.43.
   (b) *Slight internal fault*
   When a slight internal fault occurs, the criterion condition can be expressed by Equation (3.123). It is clear in Figure 3.46 that the operation region is confined by Equation (3.123) and the *p* axis, or by the first curve, the third curve and the *p* axis as shown in Figure 3.47. Meanwhile, the limited conditions of criterion 1 as reference, s = b/p, are marked by the dotted line.

   Under the above analysis, the operation region and optimum sensitivity (vertex of the operation region) in Figures 3.46 and 3.47 decrease compared to criterion 1. Therefore, it is questionable on cancelling the conditional operation region.

Next, the sensitivity and the security of these two criteria are investigated by adjusting the proportionality coefficient of the percentage differential criterion and configuring the operation region and mal-operation region.

In summary, by using the relationships between through fault current and the transforming rate of the CT or the rate of outflow current, a new methodology for analysing the operation behaviour of the differential protection is designed in this section, which can be used to evaluate any percentage differential

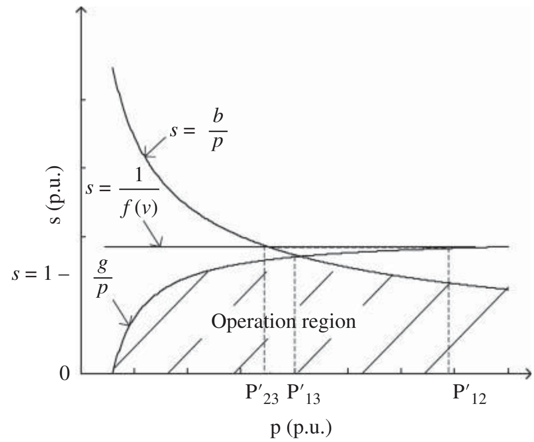

Figure 3.45 Operation area of criterion 1 under the condition of light internal fault (curves defined by Equations (3.125), (3.127) and the p axis)

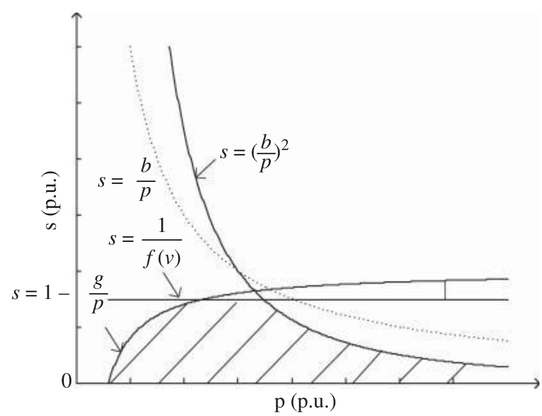

Figure 3.46 Operation area of criterion 2 under the condition of light internal fault (case 1)

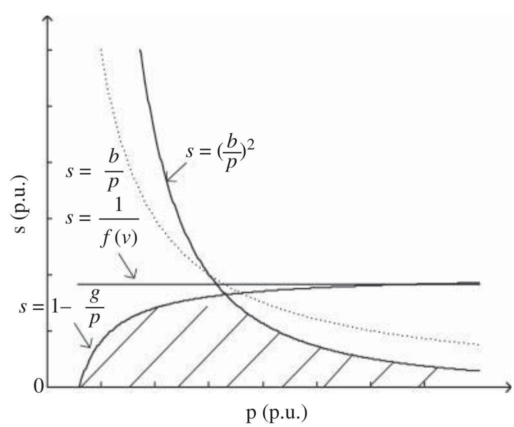

Figure 3.47 Operation region of criterion 2 in the condition of light internal fault (case 2)

criterion in any conditions. The method is helpful in analysing the impacts of CT saturation on protection security when an external fault occurs. The change of CT transforming rate is clear as the through fault current changes. In the same way, when there is an external fault, the protection sensitivity changes according to the severity of fault (especially slight internal fault). Preliminary assessments of three percentage differential protections have been made by this method. As a matter of fact, this method includes but is not limited to assessment of product restraint criterion. Any percentage restrained characteristics could be converted to this plane. It is necessary to replenish and consummate the current differential protection system as the important role of current differential protection in power system relaying system.

3.6.3 Analysis of Novel Percentage Differential Criteria

According to the analysis of Section 3.6.2, the evaluation of the criteria proceeds with a plane with the through current and CT transforming ratio (or the ratio of outgoing current with respect to incoming current) as its coordinate axis. The operation characteristics of above two novel product restraint criteria proposed by ABB Company in the case of the CT saturation and slight internal fault case can be assessed intuitively. In the following sections, the changes of criterion performance when the parameters of the criterion take different values are discussed.

3.6.3.1 The Two Criteria on the p–s Coordinate Plane

Firstly, the characteristics of the two criteria discussed in Section 3.6.2 in the case of CT saturation and operating conditions and the operation region in the p–s plane under a slight fault case are briefly summarized. The specific details can be found in Section 3.6.2. The percentage differential characteristics of novel current comparison are shown in Figure 3.40.

Criterion 1

Taking a certain point, b, of the restraint current as a dividing line in the plane of percentage restraint characteristics, the left-hand side is for the unconditional operation region and the right-hand side is the conditional operation region. In the conditional operation region, protection can take action when at least one of the currents on both sides is greater than the setting value.

Criterion 2

The conditional operation region of the criterion 1 is changed to be the restraint region. When the restraint current is greater than the cut-off point, the protection will be always blocked.

1. **Representations of criterion 1**
   (a) *The scenario of CT saturation*
   The boundary conditions of the criterion in the case of the CT saturation are given by:

$$s = \sqrt{1 - \left(\frac{g}{p}\right)^2} \tag{3.129}$$

$$s = \frac{1}{\sqrt{1 + v^2}} \tag{3.130}$$

$$s = \frac{b}{p} \tag{3.131}$$

The operation region (or mal-operation region) of the criterion is surrounded with the three curved (straight) line and the p axis. According to the different value of the b, g and v, there is a slight difference for the shape of mal-operation regions. It is better to get the expression of the boundary intersection point firstly. Among them, the intersection of the Equations (3.129) and (3.130) are given by:

$$\begin{cases} p_{12} = \sqrt{g^2 + \left(\frac{g}{v}\right)^2} \\ s_{12} = \frac{1}{\sqrt{v^2 + 1}} \end{cases} \tag{3.132}$$

The intersection of Equations (3.129) and (3.132) is given by:

$$\begin{cases} p_{13} = \sqrt{b^2 + g^2} \\ s_{13} = \frac{1}{\sqrt{\left(\frac{g}{b}\right)^2 + 1}} \end{cases} \tag{3.133}$$

The intersection of Equations (3.130) and (3.131) is given by:

$$\begin{cases} p_{23} = \sqrt{(bv)^2 + b^2} \\ s_{23} = \frac{1}{\sqrt{v^2 + 1}} = s_{12} \end{cases} \tag{3.134}$$

It can be determined that the shape of the operation region depends on the location of the minimum vertex. $s_{13} < s_{12} = s_{23}$ when $g/b < v$. The operation region is surrounded by two curves with the p axis (case 1), namely, the area surrounded by Equations (3.129), (3.131) and the p axis (Figure 3.48); the vertex is shown by Equation (3.132).

The vertex means that the protection's ability to withstand the CT saturation becomes the weakest in the case of $\sqrt{b^2 + g^2}$ times through current. To avoid protection mal-operation, there exists the highest requirement for the CT transforming. This transforming ratio is called global biggest anti-malfunction CT transforming ratio s_0. Correspondingly, there exists a CT allowable error $1 - s_0$. In order to guarantee the protection operation correctly, the CT error cannot exceed the value that is called the most easily global malfunction CT error, E_0. In addition, there is a multiple p_0 of through current, which is called the most easily global malfunction through current multiple corresponding to s_0.

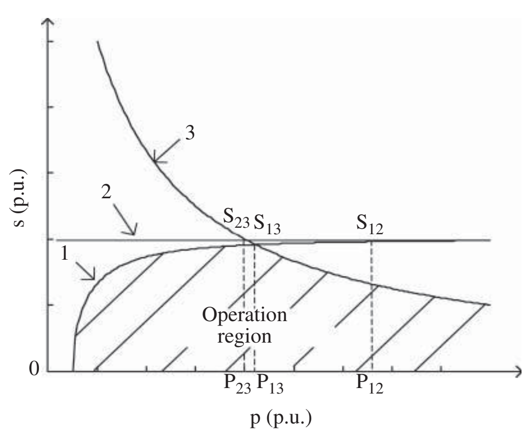

Figure 3.48 Mal-operation region of criterion 1 under the condition of CT saturation (case 1)

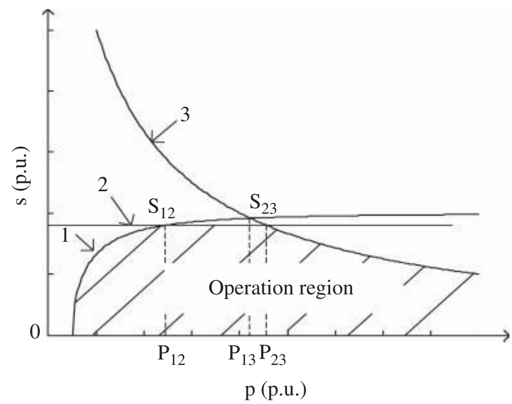

Figure 3.49 Mal-operation region of criterion 1 under the condition of CT saturation (case 2)

The expression $s_{13} > s_{12} = s_{23}$ will be tenable when $g/b \leq v_0$. The operation region is surrounded by three curves with the p axis (case 2), namely, the area surrounded by the curves defined by Equations (3.129)–(3.131) and the p axis (Figure 3.49). Correspondingly, the vertex is shown by Equations (3.132) and (3.134). In this case, $s_0 = s_{12} = s_{23}$. Meanwhile, the most easily global malfunction through current multiple is expanded into an interval $[p_{01}, p_{02}]$, and the upper and lower boundaries are $p_{01} = p_{12}$, $p_{02} = p_{23}$, respectively. When the through current multiple lies within the interval, the protection will mal-operate very easily.

(b) *Internal fault condition*

According to Section 3.6.2, assessment on the internal fault condition can be expressed based on Equations (3.135)–(3.137).

$$s < 1 - \frac{g}{p} \tag{3.135}$$

$$s < \frac{1}{f(v)} \tag{3.136}$$

$$s < \frac{b}{p} \tag{3.137}$$

where,

$$f(v) = 1 + \frac{v^2}{2} + \sqrt{\frac{v^4}{4} + v^2} \tag{3.138}$$

The boundary of the operation region can be obtained through changing the inequalities of Equations (3.135)–(3.137) into equalities. The operation region of the criterion is enclosed by three such curves (straight line) with the p axis (Figure 3.50)

Now the shape of operation region resembles the CT saturation's mal-operation region. Thus, the intersection of the curve is found first, given by:

$$\begin{cases} p'_{12} = \left(\dfrac{1}{2} + \sqrt{\dfrac{1}{4} + \dfrac{1}{v^2}}\right) g \\ s'_{12} = \dfrac{1}{f(v)} \end{cases} \tag{3.139}$$

$$\begin{cases} p'_{13} = b + g \\ s'_{13} = \dfrac{1}{1 + \dfrac{g}{b}} \end{cases} \tag{3.140}$$

$$\begin{cases} p'_{23} = bf(v) \\ s'_{23} = \dfrac{1}{f(v)} = s_{12} \end{cases} \tag{3.141}$$

The operation region is still surrounded by the above curves. The shape of the operation region can be determined depending on the location of the minimum vertex. $s'_{13} > s'_{12} = s'_{23}$ when $\frac{g}{b} \leq \frac{v^2}{2} + \sqrt{\frac{v^4}{4} + v^2}$. The operation region is enclosed by the curves defined by Equations (3.135)–(3.137) and the p axis (Figure 3.50); the vertex is shown by the curves defined by Equations (3.139) and (3.141). Correspondingly, $s'_0 = s'_{12} = s'_{23}$, where s'_0 is the global optimal sensitivity of the criterion when a slight internal fault occurs. Correspondingly, there exists a through current multiple interval $[p'_{01}, p'_{02}]$, called the through current multiple, that satisfies the global optimal sensitivity. The upper and lower bounds are $p'_{01} = p'_{12}$, $p'_{02} = p'_{23}$, respectively. The protection will be the most sensitive when responding to the slight internal fault if the through current is within the above interval.

Without taking the limit given by Equation (3.137) into account, the criterion will turn to the conventional scalar product restrained one, and the operation region will increase, which can be reflected by the increasing sensitivity of the protection in the case of a large incoming current. However, it is found that the increased sensitivity is actually very difficult to achieve. This is because the system should be experiencing overload or an external fault when the incoming current is relatively high. In this scenario, the probability that a slight internal fault of which the incoming current and the outgoing current have the same phase occurs simultaneously will be very low. Furthermore, these two system operating conditions can only exist for a very short duration. Once the system recovers, this operation region will not exist. If the conventional criterion is used to keep the sensitivity that is very difficult to obtain actually, the loss of security is far more than the benefits.

When $\frac{g}{b} > \frac{v^2}{2} + \sqrt{\frac{v^4}{4} + v^2}$, $s'_{13} < s'_{12} <= s'_{23}$. The operation region is surrounded by the curves defined by Equations (3.135) and (3.137) and the p axis (Figure 3.51) and the peak point can be achieved by Equation (3.140). When s_0' changes from s'_{12} to s'_{13}, the multiple of through current that satisfies the global optimal sensitivity also changes from an interval $[p'_{12}, p'_{23}]$ to a point p'_{13}.

2. **Representations of criterion 2**
   (a) *CT saturation*
   According to Section 3.6.2, as the conditional operation region is invalid in the case of CT saturation, criterion 2 is completely equivalent to criterion 1. Its mal-operation operation region can be represented as in Figure 3.48.

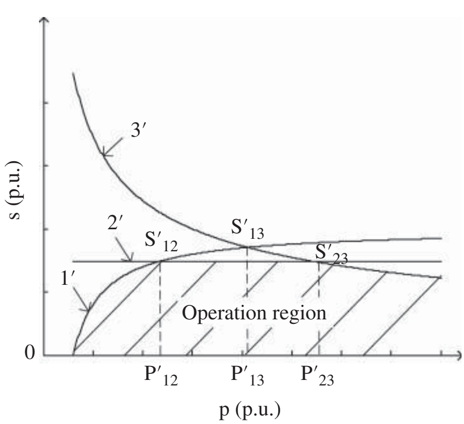

Figure 3.50 Operation region of criterion 1 under the condition of a slight internal fault (case 1)

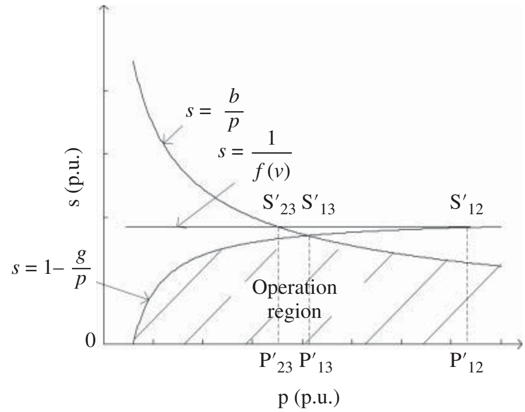

Figure 3.51 Operation region of criterion 1 under the condition of a slight internal fault (case 2)

(b) *Slight internal fault*
According to the Section 3.6.2:

$$\begin{cases} 1' : s < 1 - \dfrac{g}{p} \\ 2' : s < \dfrac{1}{f(v)} \\ 3' : s < \left(\dfrac{b}{p}\right)^2 \end{cases} \tag{3.142}$$

The intersection point of the first and second inequality in Equation (3.142) is still the same as in Equation (3.139), and the intersection point of the first and third inequality is given by:

$$\begin{cases} p'_{13} = \left[\dfrac{1}{2} + \sqrt{\dfrac{1}{4} + \left(\dfrac{b}{g}\right)^2}\right] g \\ s'_{13} = \dfrac{1}{f\left(\dfrac{g}{b}\right)} \end{cases} \tag{3.143}$$

The intersection point of the second and third inequality is:

$$\begin{cases} p'_{23} = b\sqrt{f(v)} \\ s'_{23} = \dfrac{1}{f(v)} \end{cases} \tag{3.144}$$

Similarly, the shape of the operation region can be determined according to the minimum vertex location. $s''_{13} > s''_{12} = s''_{23}$ when $g/b \geq v_0$. The operation region is surrounded by the curves defined by Equation (3.142) and the p axis (Figure 3.52), and the vertex is shown by the curves defined by Equations (3.142) and (3.144). In this case, $s''_{13} = s''_{12} = s''_{23}, p''_{01} = p''_{12}, p''_{02} = p''_{23}$.

$s''_{13} < s''_{12} = s''_{23}$ when $g/b > v$. The operation region is surrounded by the first equation and the third inequality of Equation (3.142) and the p axis (Figure 3.53), and the vertex is shown by the curve defined by Equation (3.143). In this case, $s''_0 = s''_{13}, p''_{01} = p''_{13}$.

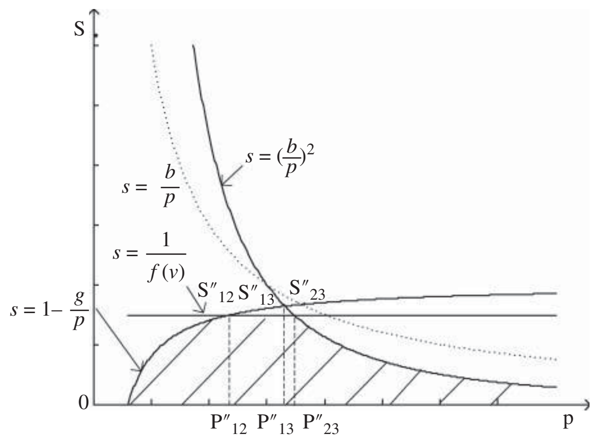

Figure 3.52 Operation region of criterion 2 under the condition of slight internal fault (case 1)

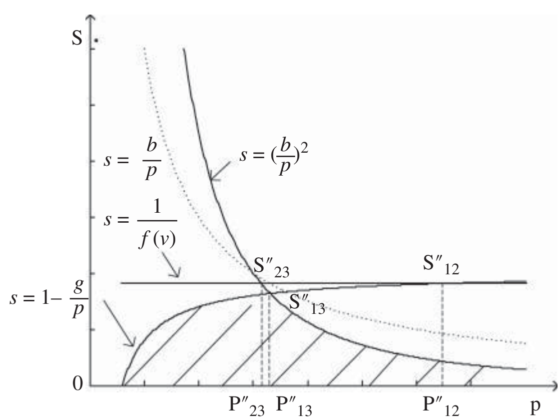

Figure 3.53 Operation region of criterion 2 under the condition of slight internal fault (case 2)

3.6.3.2 Quantization and Comparative Analysis of the Two Criteria

During the analysis, selection of parameters should follow two principles: (i) to maximize the allowable error of saturation and (ii) to maximize the sensitivity of protection in the case of internal fault with outgoing current.

For clarity, the analysis still begins with criterion 1. Some of the conclusions of the analysis process are also applicable to criterion 2.

1. **Criterion 1**
   (a) *The analysis of security and reliability*
   The studies show that investigating with *g/b* as the parameter will be helpful to find some useful conclusions.

The mal-operation region of the protection can be seen in Figure 3.48. $s_0(E_0)$ and p_0 corresponding to the vertex can be obtained from Equation (3.133).

A reasonable milestone for analysis is to firstly determine the index of the error E_0 of the CT that most easily leads to mal-operation, then to analyse a variety of scenarios on this basis. It is easy to know that the through current corresponding to E_0 can be set near the rated current and it is unnecessary to set E_0 at a high value if the proper parameters have been equipped. Take 5% as the example for evaluation. Assume that $E_0 \geq 5\%$, this leads to a value of $s_0 \leq 95\%$ and $\frac{g}{b} \geq 0.313$. The analysis below suggests that the increase of *g/b* will reduce the allowable outgoing current for the internal fault. The sensitivity of the protection is analysed in the case of the internal fault with setting the value $\frac{g}{b} = 0.313$.

When making the analysis in the case of the slight internal fault, there are two cases of the value of *g/b*:

i.
$$v < \frac{g}{b} \leq \frac{v^2}{2} + \sqrt{\frac{v^4}{4} + v^2}$$

The operation region is shown in Figure 3.50, enclosed by the curves defined by the equations from Equations (3.135)–(3.137) and the p axis. The vertexes are expressed as the curves defined by Equations (3.139) and (3.141). In this case:

$$v \geq \sqrt{\frac{bg}{b^2 + g^2}} = 0.273$$

As s'_0 is determined by s'_{12} in Equation (3.135), we can take v to its minimum value 0.273 for the highest sensitivity. Now we have $p'_{12} = p'_{23} = p'_{13}$ and $s'_0 = 0.762$, which means three intersections coincide.

ii.
$$\frac{g}{b} \geq \frac{v^2}{2} + \sqrt{\frac{v^4}{4} + v^2}$$

In this case, the operation region is shown in Figure 3.51, enclosed by the curves defined by Equations (3.135), (3.137) and the p axis. The vertex is expressed by Equation (3.140). Substituting $\frac{g}{b} = 0.313$ into this gives $s'_0 = 0.762$.

Under the conditions of $\frac{g}{b} > v$, the maximum allowable outgoing current can reach 76% on the premise that $E_0 = 5\%$.

When $\frac{g}{b} < v$, the operation region is shown in Figure 3.49 under the condition of CT saturation, which is enclosed by the curves defined by the equations from Equation (3.129)–(3.131) and the p axis. The vertexes are expressed by the curves defined by Equations (3.132) and (3.134). According to these two equations, the slope v of the restraint line should be at least 0.313 to ensure E_0 to be 5%.

As $\frac{g}{b} < \frac{v^2}{2} + \sqrt{\frac{v^4}{4} + v^2}$ can be naturally fulfilled in the condition of internal faults, the operation region at this time is shown in Figure 3.50, enclosed by the curves defined by the equations from Equation (3.135)–(3.137) and the p axis. The vertexes are expressed by Equations (3.139) and (3.141). Substitute $v = 0.313$ into it and we have $s'_0 = 0.732$.

It can be seen that the maximum allowable outgoing current at this time reduces by 3% on the same premise that $E_0 = 5\%$compared to the case of $\frac{g}{b} \geq v$, and the sensitivity decreases. In terms of higher sensitivity, $\frac{g}{b} \geq v$ is the better choice.

(b) *Reasonableness analysis to b = 1.5*

The recommended value of b by the ABB Company is 1.5. However, it can still be debated whether this value is reasonable or not. We can still start to analyse under the condition of CT saturation.

In this condition, choose $\frac{g}{b} = 0.313 > v$ to ensure $E_0 = 5\%$. In this case, $g = 0.47$. Substituting this into Equation (3.133) gives $p_0 = 1.05\ b = 1.57$, which means the error of CT should not exceed 5% with 1.57 times rated current. Generally speaking, this index is acceptable, but it cannot achieve optimization. This is because that the error can be minimized with the rated current through the CT. Therefore, the attempt should be made to limit the vertex of the operation region to the rated value to eliminate the possibility of the error being greater than 5%. Furthermore, the claim that $b = 1.5$ is unreasonable also results from the very high requirement on the capability of CT in suffering the large through current. The analysis is as below. According to Equations (3.129)–(3.131), the critical transforming rate is limited by the equation $s = b/p$. Hence, $s = b/10 = 0.15$ in the case of through current being equal to 10 times rated current. In this case, the tolerance error of CT is 85%. It still can be optimized.

Based on the analysis in Section 3.6.2, under the condition of internal faults, the through currents corresponding to the maximum allowable outgoing current are $p'_{13} = b + g = 1.97$ in both case a and b with $\frac{g}{b} > v$, which means that the through current should be nearly twice rated current to achieve the best sensitivity. However, the through current is supposed to be limited to the rated value (i.e. the normal operation of the system) and the corresponding allowable outgoing current is $s'_1 = 1 - \frac{g}{p} = 53\%$ under this condition, which is not satisfying.

In view of improving the anti-saturation level and the sensitivity to internal faults of the criterion, the value of b ought to be reduced. The analysis below is still on the premise that $\frac{g}{b} = 0.313 > v$.

When the CT becomes saturated, set $p_{13} = \sqrt{b^2 + g^2} = 1$. Then $b = 0.954$, corresponding to $g = 0.299$. This will place the weakest point of the criterion on the rated current point. It is evident that the error of CT will be the minimum when the burden is at the rated current. Thus, this placement is reasonable. Under this condition, the critical transforming rate is $b/10 = 0.095$ with 10 times the rated current and the tolerance is over 90%. It is better than the scenario that $b = 1.5$.

From the analysis above, it can be seen that the maximum allowable outgoing current can be estimated according to the area enclosed by curves defined by Equations (3.135) and (3.137) when evaluating the ability to respond to internal faults. It can be seen from Equation (3.140) that the corresponding through current times is $p'_0 = p'_{13} = b + g = 1.25$ at this time, that is, the sensitivity reaches its best with nearly 1.25 times the rated current. Accordingly, the allowable outgoing current increases to $s'_1 = 1 - \frac{g}{p} = 70.1\%$ when the through current is equal to the rated current. The sensitivity of the criterion to the common slight internal faults is much higher than in the case $b = 1.5$.

Obviously, according to Equation (3.141), b can be adjusted to make the criterion most sensitive to the slight fault when $p'_0 = 1$. Now, the operating point of the protection being able to tolerate 5% CT error (the most vulnerable point) now offsets, since p_0 moves to 0.8. Compared with the scenario of $p_0 = 1$, the probability of CT reaching 5% error increases. In practical application, we can choose parameter b reasonably based on the sensitivity requirements of internal faults and the precise transforming rate range of CT.

2. **Criterion 2:**
The following two cases will be discussed: $g/b > v$ and $g/b < v$. The value of g/b or v is still derived from the CT saturation condition. Then, they are used to discuss the case of internal faults.
(a)

$$g/b > v$$

When the CT saturates, the mal-operation region is enclosed by the curves defined by Equations (3.129) and (3.131) and the p axis in Figure 3.48 and the vertex is defined by Equation (3.133). Keeping $s_0 = 0.95$, we have $g/b = 0.313$.

In the case of internal faults, f(g/b) is greater than f(v) because f(x) is the function of monotonically increasing, which leads to $s''_{13} < s''_{23}$. According to the analysis of Section 1.2, the operation region is shown in Figure 3.53 and the vertex is defined by Equation (3.133). Substituting $g/b = 0.313$ into Equation (3.143), $s''_0 = 73.2\%$ and $p''_0 = p''_{12} = 1.17$b.

(b)

$$g/b < v$$

According to the Section 3.6.1, when the CT saturates, the mal-operation region is enclosed by the curves defined by the equations from Equation (3.129)–(3.131) and the p axis while the vertexes are defined by Equations (3.132) and (3.134). Keeping $s_0 = 0.95$, we have $v = 0.313$.

For internal faults, f(g/b) < f(v) because f(x) is the function of monotonically increasing. According to Section 3.6.2, $s''_{13} > s''_{23}$, the operation region is enclosed by the curve defined by Equation (3.142) and the p axis. The vertexes are defined by Equations (3.139) and (3.144). Substituting $v = 0.313$ into them, gives $s_0'' = 73.2\%$, and the two corresponding critical through currents will be $p''_{01} = p''_{12} = 3.73\, g$, $p''_1 = p''_{23} = 1.17b$.

According to the condition of $g/b < v$, g can be changed from 0 to 0.313b while p''_{01} can be changed from 0 to 1.17b correspondingly. This means that the best sensitivity can also be achieved when through current is very small (light load or no load) during an internal fault. However, g is very small, which may lead to the decrease of the security. The analysis is as follows.

Taking the CT being saturated (it is more appropriate to say that the current is so small that the CT incompletely transforms) into account, the left boundary point of mal-operation region is $p_{01} = p_{12}$. According to Equation (3.132), p_{01} will approach to zero when g is very small. This means that the protection will also mal-operate if the error is above 5% when the through current is very small such as no-load. Due to the restrictions of CT linear transforming area, the CT transforming error approaching to 5% is possible when the current is very small. Therefore, g should not be set to a very small value.

To sum up, the choice of $g/b > v$ and $g/b < v$ can be accepted in criterion 2. Because of on the premise of guaranteeing the same security, they have the same best sensitivity in response to slight internal faults. The choice of $g/b < v$ is more flexible. The multiple of through current globally most vulnerable to mal-operate and the multiple of through current globally optimal sensitivity are all expressed in terms of an interval. Therefore, g/b can be adjusted upon the requirement.

It should be pointed out that criterion 1 can reach the same flexibility as criterion 2 when choosing $g/b < v$. But the best sensitivity also drops to the same compared with the criterion 2. Compared with criterion 2, the only advantage of criterion 1 is that the sensitivity of the protection is slightly higher $\left(\text{it is limited by } s < b/p \text{ rather than } s < \left(\frac{b}{p}\right)^2\right)$ when the slight internal fault occurs during the heavy through current (external fault) process. For example, for the transformer protection, criterion 2 is only able to reflect the fault existing 0.11(11%) outgoing current when the external fault results in three times the through current, while criterion 1 is able to reflect the fault existing 33% outgoing current if the inter-turn short-circuit fault occurs and $b = 1$.

In summary, by means of the through current multiples–CT transforming rate (or the ratio of outgoing current) plane analysis, it is possible to analyse the security and the sensitivity of the two novel scalar product restraint criteria when each parameter of the proportional restraint characteristics changes. Conclusively, the anti-saturation abilities of both criteria are identical. To ensure the same security, criterion 1 has higher operation sensitivity than criterion 2. Under the premise of choosing the correct parameters, criterion 2 can allow the protection achieving the best sensitivity when the through current offsets to some extent. But, at the same time, the security of the protection has to be decreased relatively. If the best sensitivity index of criterion 1 drops to the same as criterion 2, criterion 1 can also achieve the flexibility that the best sensitivity is not influenced by the deviation of through current within a certain interval. Compared with criterion 2, criterion 1 has a higher sensitivity in response to the slight internal fault accompanied by the external fault with large through current. In all, criterion 1 is slightly better.

3.7 Summary

The performance of the differential protection is an issue of concern in the field of theoretical analyses of the relay protection. This chapter is an attempt to find out the appropriate theoretical bases for the existing method in the engineering field of relay protection. Preliminary comparative studies between the phase current based and the superimposed current based differential criteria have been conducted and, on the basis of these, some results can be obtained as the guide of the application of percentage differential protections.

References

[1] Liu, J., Yang, Q., Ren, B. *et al.* (1998) Analysis and discussion on several issues for application of digital transformer protective relays. *Power Systems Technology*, **22**, 18–21.
[2] Specht, T.R. (1951) Transformer magnetizing inrush currents. *Electrical Engineering*, **70** (4), 324–324.
[3] Guzman, A., Zocholl, S., Benmouyal, G. *et al.* (2002) A current-based solution for transformer differential protection. II. Relay description and evaluation. *IEEE Transactions on Power Delivery*, **17** (4), 886–893.
[4] Sidhu, T.S. and Sachdev, M.S. (1992) Online identification of magnetizing inrush and internal faults in three-phase transformers. *IEEE Transactions on Power Delivery*, **7** (4), 1885–1891.
[5] Lin, X.N. and Liu, P. (2005) The ultra-saturation phenomenon of loaded transformer energization and its impacts on differential protection. *IEEE Transactions on Power Delivery*, **20** (2), 1265–1272.
[6] Sidhu, T.S., Bajpai, M., Darlington, A. *et al.* (1998) Bibliography of relay literature, 1996 IEEE Committee Report. *IEEE Transactions on Power Delivery*, **13** (1), 85–95.
[7] Aggarwal, R.K. and Johns, A.T. (1989) A differential line protection scheme for power systems based on composite voltage and current measurements. *IEEE Transactions on Power Delivery*, **4** (3), 1595–1601.
[8] Serizawa, Y., Myoujin, M., Kitamura, K. *et al.* (1998) Wide-area current differential backup protection employing broadband communications and time transfer systems. *IEEE Transactions on Power Delivery*, **13** (4), 1046–1052.
[9] Lin, X.N., He, Z.H., Liu, S.M. *et al.* (2001) Reliability evaluations on complex current percentage differential criterion. *Proceedings of the CSEE*, **21** (7), 98–102.
[10] Lin, X.N., Tian, Q. and Zhao, M.H. (2006) Comparative analysis on current percentage differential protections using a novel reliability evaluation criterion. *IEEE Transactions on Power Delivery*, **21** (1), 66–72.
[11] Kang, Y.C., Ok, S.H. and Kang, S.H. (2004) A CT saturation detection algorithm. *IEEE Transactions on Power Delivery*, **19** (1), 78–85.
[12] Kang, Y.C., Lim, U.J., Kang, S.H. *et al.* (2004) Compensation of the distortion in the secondary current caused by saturation and remanence in a CT. *IEEE Transactions on Power Delivery*, **19** (4), 1642–1649.
[13] Fernandez, C. (2001) An impedance-based CT saturation detection algorithm for busbar differential protection. *IEEE Transactions on Power Delivery*, **16** (4), 468–472.

4

Novel Magnetizing Inrush Identification Schemes

4.1 Introduction

The power transformer functions as a node to connect two different voltage levels. Therefore, the continuity of transformer operation is of vital importance in maintaining the reliability of power supply. Any unscheduled repair work, especially replacement of a faulty transformer, is very expensive and time consuming.

The differential protective relay has been used as the primary protection of most power transformers for many years. Inrush can be generated when an unloaded transformer is switched on the transmission line or an external line fault is cleared. It may result in mal-operation of differential protection if a blocking scheme is unavailable. Therefore, distinguishing between inrush and fault current is the key to improving the reliability of the differential protection.

Three types of schemes are currently in use for this purpose. Some schemes make use of the information obtained from the differential currents of the transformer, such as the method based on the scheme of second harmonic restraint [1]. Some methods make use of the information obtained from the variation of the transformer terminal voltages, such as the method based on the voltage restraint principle [2]. Other alternative schemes make use of the information obtained from both the currents and the voltages of the transformer, such as the method based on the flux characteristic principle and the method based on the equivalent circuit equation of the transformer model [3, 4]. However, the most widely used methods in practice are still those that are based on the principle of the second harmonic restraint. The main drawback of this method is that the harmonics existing in the long Extra High Voltage (EHV) transmission lines can cause the differential relay either not to operate or to operate with a long time delay [5, 6]. Furthermore, according to the current schemes using only a single measurand, no matter whether it is current or voltage, any internal fault with energizing cannot be cleared quickly until the inrush damps below the differential current threshold. Remedial schemes introduced to overcome the problems simply complicate the primary transformer protection. Consequently, they are not too practical in practice. Other techniques have been developed for transformer protection. These techniques include transient signal analysis [7], waveform symmetry and WCS [8], artificial neural networks (ANNs) [9], fuzzy logic [10], the differential active power method [11], the equivalent instantaneous inductance (EII) based method [12] and the transformer model based method [13]. They provide alternatives or improvements to the existing protective relaying functions.

Electromagnetic Transient Analysis and Novel Protective Relaying Techniques for Power Transformer,
First Edition. Xiangning Lin, Jing Ma, Qing Tian and Hanli Weng.

Recently, a so-called 'waveform symmetry', also called 'waveform correlation' scheme (WCS), has been proposed, which compares the symmetry between the first half cycle and the latter half cycle waveform in a total one-cycle evaluating time window span. This scheme deserves to be studied further, since it considers the shape, magnitude and gradient of the current waveform overall. With this scheme, the performance of differential protection is expected to be enhanced further; for example, it is possible to implement the pole-separated restraint for the relay without decreasing the reliability. However, there still are some drawbacks to be overcome, such as the selection of compared signals and the expression of the waveform correlation coefficient. To improve the reliability and sensitivity of these types of schemes further, an enhanced scheme belonging to the family of 'waveform correlation' is presented in this chapter.

With respect to the waveform of the inrush, many state-of-the-art protection schemes are proposed. A new method based on waveform singularity factor (WSF) to distinguish between the magnetizing inrush currents and internal faults in power transformers is presented here. Firstly, the definition and calculation method of the WSF method are explained. How the WSF technique is used to detect the singularity of waveforms and then to implement the discrimination between an internal fault and inrush are proposed. Another new principle to discriminate between an internal fault and a magnetizing inrush current by correlation function principle in Digital Signal Processing (DSP) is proposed and the self-correlation function (SCF) of the sampled data is calculated and compared with the standard self-correlation function formed with sinusoidal current.

As mentioned previously, the inrush current is a result of transformer core saturation. Furthermore, due to the alternating of the iron core between saturation and nonsaturation, waveforms of the exciting inrush currents show singularity characteristics. However, in the internal fault and normal operation states of the power transformer, the iron core is not saturated and the magnetizing current is very small. Owing to the operation in the linear area of the magnetizing characteristic, waveforms of internal fault currents present sinusoidal characteristics. A new sinusoidal proximity factor (SPF) based scheme to distinguish between magnetizing inrush currents and internal faults in power transformers is proposed. Firstly, the basic theories and definitions about the SPF are explained. Then, the SPF technique is used to detect the sinusoidal characteristics of waveforms. The criterion and algorithm to distinguish the internal fault from the inrush current are proposed.

Based on the high nonlinearity in exciting cores of transformers, waveforms of the exciting inrush currents show 'sudden change' characteristics. Therefore, research was concentrated into fault generated transient signals to increase the speed of relay response. Recently, the continuous developments of modem science technology have provided new means to extract transient components using the wavelet transform method. Wavelet transform (WT), as a milestone of the development of the Fourier transform, has attracted great attention and been successfully used in many applications in the past decade. Its application in the power system has also been investigated in recent years. It has been attempted to introduce wavelet transform into power system protective relaying, with the emphasis on the transformer inrush identification.

However, threshold and frequency bands need to be predefined when it comes to energy spectrum analysis, so its flexibility is affected. In contrast with Fourier transformation and Hilbert transformation, the mathematical morphology (MM) is developed from set theory and integral geometry, and is concerned with the shape of a signal waveform in the complete time domain rather than the frequency domain. Therefore, signals being processed by MM are immune to the amplitude decaying and phase shifting. Moreover, since it requires a much shorter data window for calculation, the MM technique can provide a rapid and good performance simultaneously with the signal sudden changes and transient process. Additionally, MM is a nonlinear approach and has been widely used in geometrical analysis and description. The mathematical calculation involved in MM includes only addition, subtraction, maximum and minimum operations without any multiplication and division, so it can be put into a real-time process.

A new MM method to distinguish between the magnetizing inrush and internal faults in power transformers is proposed in this section. Transient current signals are extracted by use of morphological gradient (MG) and morphological opening and closing transform. The proposed technique has stability during symmetrical inrush currents and CT saturation. Moreover, it is immune to both DC components with disturbing signals and random noises.

More advanced inrush identification schemes are also introduced in this chapter. A novel technique to distinguish the inrush currents from the internal faults in power transformers is proposed using the normalized grille curve (NGC). The NGC is an effective tool for transient signal analysis and feature extraction and can be implemented with only a small level of computation. Firstly, the method to calculate the NGC is introduced. Then, the criteria in the time and frequency domains to discriminate between inrush currents and internal faults are respectively presented. The experimental results verify the feasibility of this method.

Another new method focusing on the equivalent instantaneous leakage inductance (EILI) considering B–H curve data and hysteresis is presented in this chapter, which shows the different characteristics between internal faults and inrush currents. Firstly, the basic theory and definition of the EILI of the transformer are explained. Then, the mathematical expressions are obtained to calculate the EILIs of two-winding and three-winding transformers in real time, and their properties and accuracy are analysed. Finally, the proposed methods are verified by the experimental results.

This chapter also presents a technique for discrimination between an internal fault and an inrush current using the two-terminal network. The technique is suitable for situations whether or not it is possible to measure the winding currents. Also, the technique does not make use of the presence of harmonic currents to restrain the relay during the magnetizing inrush. Furthermore, the technique requires neither the data of the B–H curve nor the knowledge of leakage inductances and iron losses. The basic theory about the two-terminal network containing only the winding resistance and the leakage inductance is introduced first. The active powers flowing into the two-terminal network and consumed by the two-terminal network are compared and then are employed to develop the criteria.

4.2 Studies for Identification of the Inrush Based on Improved Correlation Algorithm

4.2.1 Basic Principle of Waveform Correlation Scheme

The WCS to distinguish between inrush and fault current is presented in Figure 4.1 in this section.

This scheme is validated as soon as the protection is initiated and the sampling data window has included one-cycle samplings. This sampled one-cycle data (0–20 ms for 50 Hz power frequency) is extended into a two-cycle sampling (0–40 ms) (Figure 4.1a). From a special point (t_1) new one-cycle data are taken, as shown in the large solid-line frame in Figure 4.1a. Let the first half cycle signal in this

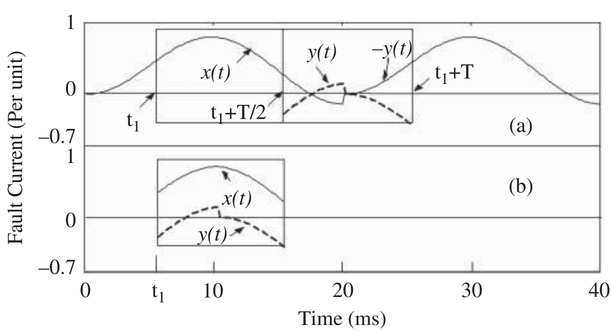

Figure 4.1 Internal fault current extended periodically: (a) a half cycle integral window; (b) the correlativity between *x(t)* and *y(t)*

frame be *x(t)*, which is included in the former small solid line frame, and the signal in the latter one with the same length as the former one be $-y(t)$. The correlation between *x(t)* and *y(t)*, shown as the dotted-line waveform in the latter small frame, was evaluated and the inrush can be identified from the internal fault current with a low value of the correlation coefficient (CC). For illustratively evaluating the degree of correlation between *x(t)* and *y(t)*, *y(t)* can be translated forward one half cycle, then *y(t)* and *x(t)* are located on the same frame (Figure 4.1b). From the above, the determination of t_1 and the constitution of CC are the most important to the performance of the WCS. The exiting scheme adopts maximum area algorithm to determine t_1, as below.

Figure 4.1 shows an internal fault current with a 100% damped DC component, where the sampling rate is N times the fundamental. A half cycle integral window, shown as the small frame including *x(t)* in Figure 4.1a, is shifted from 0 to 20 ms, Consequently, total N area values are calculated by means of the absolute value sum of the current sampling in this time window, shown as Equation (4.1):

$$S(k) = \sum_{j=k}^{k+N/2-1} |i(\mathrm{mod}(j))| \quad \mathrm{k} = 0, 1, 2, \ldots \mathrm{N} - 1 \tag{4.1}$$

where

$$\mathrm{mod}(j) = \begin{cases} j & j < N \\ N - j & j > N - 1 \end{cases} \tag{4.2}$$

Let the origin of the time window corresponding to the maximum among these N area values be t_1, from which a one-cycle signal is sampled and the correlativity between *x(t)* and *y(t)* is evaluated. Seen in Figure 4.1b, the correlativity is rather good for this internal fault. In contrast, the corresponding situations of two types of typical inrushes are shown in Figures 4.2 and 4.3.

It can be seen in Figures 4.2 and 4.3 that *x(t)* is quite different from *y(t)* for both types of inrushes, that is, the relativity between them is weaker than that of the fault current. A revised correlation coefficient, called the waveform coefficient here, is derived from the above analysis:

$$J = \frac{Cov(X, Y)}{\sigma^2(X)} \tag{4.3}$$

In contrast, a normal correlation coefficient is given by:

$$J = \frac{Cov(X, Y)}{\sigma(X)\sigma(Y)} \tag{4.4}$$

where *cov* (*X, Y*) is the covariance of *x(t)* and *y(t)*, and $\sigma(X)$ and $\sigma(Y)$ denote the mean-square deviation of *x(t)* and *y(t)*. The difference between waveform coefficient J and the normal correlation coefficient ρ_{XY} is that $\sigma(X)\sigma(Y)$ in ρ_{XY} is substituted by $\sigma^2(X)$. Criterion 1 is derived according to Equations (4.1)

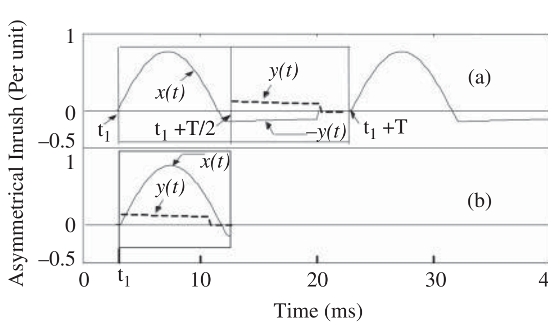

Figure 4.2 The inrush with single peak value extended periodically: (a) a half cycle integral window; (b) the correlativity between *x(t)* and *y(t)*

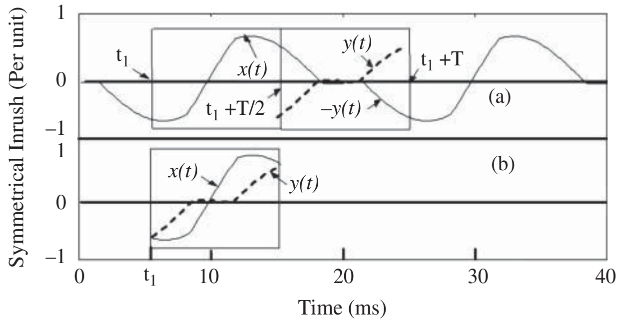

Figure 4.3 The inrush with double peak values extended periodically: (a) a half cycle integral window; (b) the correlativity between *x(t)* and *y(t)*

and (4.3). The value J is calculated as soon as the differential protection is initiated and the protection will operate if J is over a threshold, otherwise the protection will be blocked.

There is no doubt that criterion 1 is somewhat original. However, it is rather hard to set in cases, as in those illustrated by Figures 4.4–4.6. Figures 4.4 and 4.5 show inrushes on the primary and secondary side of the CT, respectively, where the transformer is simulated by ATP software and the CT model with 1 : 1 ratio is introduced.

The simulated transformer model consists of a transformer bank, which is a three-phase two-winding transformer with high voltage side Y-connected and low voltage side delta connected (YNd5), where the magnetization branch is connected to the low voltage side and the neutral terminal on high voltage side is grounded. The apparent power S_{rated} is equal to 750 MVA and the voltage ratio is 420 kV/27 kV. In this simulation the transformer is energized from the low voltage side. The saturation characteristic curve of iron core element adopts type-96 model and the saturation flux density B_s is assumed to be $1.15B_m$. The residual fluxes density of all phases are $B_{ra} = 0.9\ B_m$, $B_{rb} = B_{rc} = -0.9\ B_m$, and the inception angle of phase A voltage source, whose type is sine, is 30°. The hysteresis model of the CT is simulated as a main loop and a set of minor loop trajectory.

For convenient discussion, let I_2/I_1 be the ratio of second harmonic to the fundamental, and J be the waveform coefficient. As shown in Figure 4.5, the evenness of the inrush increases on the secondary in contrast to that on the primary. Correspondingly, the waveform coefficients of three phase inrushes in Figure 4.4 are $J_{a-b} = 0.536$, $J_{b-c} = 0.386$ and $J_{a-b} = 0.714$, respectively, and the relevant values in Figure 4.5 are $J_{a-b} = 0.651$, $J_{b-c} = 0.211$ and $J_{a-b} = 0.804$, respectively. Meanwhile, the ratio of I_2/I_1 of the waveforms in Figure 4.5 are $(I_2/I_1)_{a-b} = 11\%$, $(I_2/I_1)_{b-c} = 9\%$ and $(I_2/I_1)_{a-b} = 6\%$.

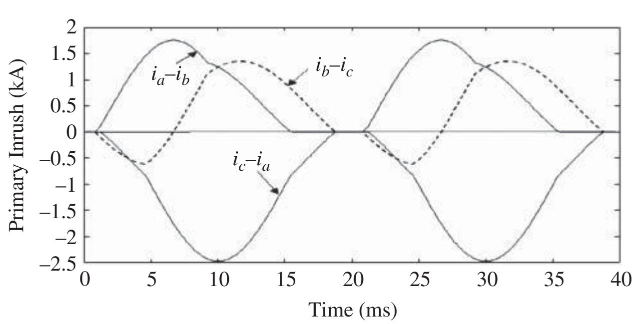

Figure 4.4 Three-phase magnetizing inrushes on the primary of the CT

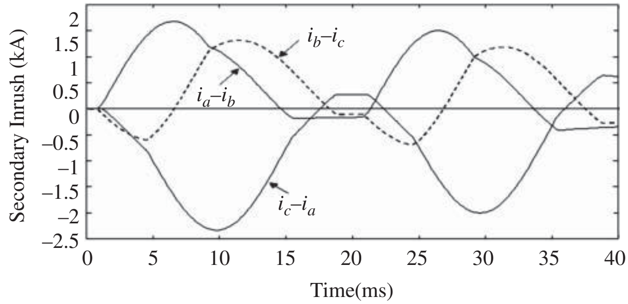

Figure 4.5 Three-phase magnetizing inrushes on the secondary of the CT

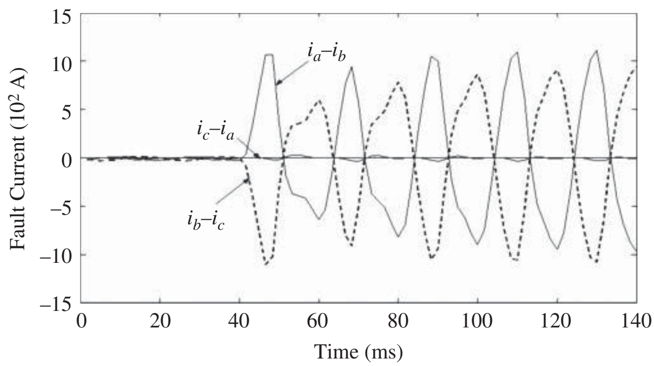

Figure 4.6 'B'-earth fault on primary, with a long transmission line connected

Obviously, the threshold of J should be larger than 0.8 when the implementation of pole-separated tripping is available. Nevertheless, a long time delay is unavoidable using such a high setting value when the internal fault current is distorted seriously. To illustrate this situation, an example of dynamic test is given as below:

Consider a 'B'-earth internal fault on the primary, whose current waveforms captured by the fault recorder installed on the dynamic simulation laboratory of Huazhong University of Science & Technology are shown in Figure 4.6.

In this case, the transformer is linked with a long transmission line and the sampling rate is 600 Hz at 50 Hz fundamental frequency. In these recorded data, the phase currents are scaled up currents from the secondary winding of the delta-connected CTs on the primary terminals of the power transformer. As seen, the differential currents exist in both phase A and B due to the delta connection on the CT's secondary. As shown in Figure 4.6, the waveforms of currents deform due to the CT saturation and the capacitance current of the long transmission line. The changes of waveform coefficients and ratios of second harmonic to the fundamental of the fault currents are illustrated in Table 4.1.

For some special cases, the differential current in response to a transformer internal fault could contain a second harmonic component, which may result in an operation with a long time delay of differential protection with second harmonic restraint. It can be seen from Table 4.1 that the protection will not trip until the fault continues for 95 ms using criterion 1 with threshold 0.8. For the scheme of second harmonic restraint with 15% restraint ratio, the nonoperation time (N.O.T.) for such a fault is 93.3 ms,

Table 4.1 Changes of waveform coefficients and ratios of second harmonic to the fundamental of the fault currents

Post-fault time (ms) / Criteria	90	91.7	93.3	95
$(I_2/I_1)_{a-b}$ (%)	15	15	14	13
$(I_2/I_1)_{b-c}$ (%)	14	14	14	14
J_{a-b}	0.76	0.76	0.79	0.82
J_{b-c}	0.75	0.75	0.79	0.81

that is, the scheme of second harmonic restraint with 15% restraint ratio and criterion 1 with a 0.8 waveform coefficient threshold are approximately equivalent for such heavy fault.

There is no doubt that the relay will operate more quickly if the threshold of J is decreased. However, the reliability may be decreased. Therefore, criterion 1 deserves to be improved in sensitivity without decreasing reliability. Some discussion on how to determine t_1 and improve the constitution of waveform coefficient is given here.

4.2.2 *Design and Test of the Improved Waveform Correlation Principle*

4.2.2.1 Improvement of Compared Signal Selection

As mentioned above, the original maximum area algorithm to separate a one-cycle signal into two most irrelevant parts is not applicable to distinguish real inrush and internal fault. To solve this problem, the formula of area given by Equation (4.1) is revised as below:

$$S(k) = \sum_{j=k}^{k+N/2} |i(\mathrm{mod}(j))| \quad \mathrm{k} = 0, 1, 2, \ldots \mathrm{N} - 1 \tag{4.5}$$

where the integral window is prolonged from $N/2$ to $N/2 + 1$. The ability of the improved maximum area algorithm to separate a signal into two irrelevant parts is weakened. However, this exactly meets the demands for distinguishing between the real inrush and the deformed internal fault current. In contrast to Equations (4.1), Equation (4.5) is insensitive even to the inrush, so the waveform coefficient has no obvious increase. The improved algorithm also is insensitive to the distorted internal fault current, that is, J apparently does not decrease. Obviously, J decreases when using Equation (4.1) to determine t_1, which causes a misjudgement between inrush and internal fault. Thus, Equation (4.5) can effectively improve the sensitivity of identifying the real inrush from the fault current.

Equations (4.5) and (4.3) are combined as criterion 2. The waveform coefficients of three phase inrushes in Figure 4.5 are $J_{a-b} = 0.652$, $J_{b-c} = 0.211$ and $J_{c-a} = 0.804$, that is, the reliability of criterion 2 for inrush is approximately equivalent to that of criterion 1. In contrast to criterion 1, by use of the fault in Figure 4.6 the performance of criterion 2 is evaluated with a 0.8 waveform coefficient threshold. Here, the N.O.T. of criterion 2 is 40 ms, since J_{a-b} increases to 0.83 at $t_{\mathrm{post-fault}} = 40$ ms. At this time, the ratio of I_2/I_1 using the Fourier algorithm is 31% and the differential protection with 15% second harmonic restraint ratio cannot operate. It is clear that criterion 2 can shorten the N.O.T. by about 2.7 cycles.

4.2.2.2 Sensitivity Analysis of Criterion 2

Table 4.2 shows the N.O.T.s of criteria 1 and 2 and of the scheme of second harmonic restraint for all types of typical internal faults, where the fault data came from the above mentioned fault recorder. The pole-separated trip mode is adopted here for WCS and the threshold is set to 0.8, that is, the protection operates as soon as the waveform coefficient of any phase current is over 0.8. The scheme that the transformer differential protection will be blocked when the inrush occurs in one phase alone is applied to second harmonic restraint.

N.O.T. denotes nonoperation time and NOP means nonoperation, that is, the protection still cannot operate even though the fault has been present for five cycles. For convenience, the faults in Table 4.2 are numbered to indicate the fault conditions. For instance, cases 1–4 are ‘B’-earth faults on primary, whose operating conditions are that the transformer is loaded with a long line (PL), loaded without a long line (PUL), unloaded with a long line (UPL) and unloaded without a long line (UPUL). The illustrations of the operating conditions for other faults are similar to the above. Cases 4–8 are ‘B’–‘C’ phase faults on the primary, cases 9–12 are ‘A’–‘B’ phase faults on the secondary, cases 13–16 are ‘B’-phase 4.35% winding faults on the primary, cases 17 and 18 are ‘B’-phase 2.18% winding faults on the primary. Moreover, cases 19–27 are energizing with internal faults.

It should be noted that the above test results for transformer fault and the ones below for transformer energizing are all determined with a variety of random points on wave closures.

Table 4.2 Nonoperation times for 0.8 threshold of waveform coefficient of criterion 1 and criterion 2, and 15% of second harmonic restraint

Case	Fault type and conditions	N.O.T. of criterion 1 (ms)	N.O.T. of criterion 2 (ms)	N.O.T. of I_2/I_1 (ms)
1	BG_PL	95	40	81.6
2	BG_PUL	68.3	21.6	60
3	BG_UPL	46.6	26.6	58.3
4	BG_UPUL	18.3	16.6	18.3
5	BC_PL	48.3	51.6	93.3
6	BC_PUL	43.3	40	63.3
7	BC_UPL	83.3	43.3	78.3
8	BC_UPUL	40	31.6	60
9	ab_PL	38.3	20	58.3
10	ab_PUL	28.3	20	20
11	ab_UPL	4	51.6	73
12	ab_UPUL	36.6	20	58.3
13	BW4_PL	30	30	31.6
14	BW4_PUL	31.6	31.6	31.6
15	BW4_UPL	18	20	20
16	BW4_UPUL	25	25	25
17	BW2_PUL	21.6	18.3	20
18	BW2_UPUL	23.3	23.3	26.6
19	I_BG_L	81.6	55	NOP
20	I_BG_UL	60	20	NOP
21	I_BC_L	50	36.6	NOP
22	I_BC_UL	40	38.3	NOP
23	I_ab_L	25	38.3	NOP
24	I_ab_UL	40	33.3	NOP
25	I_BW4_L	25	25	NOP
26	I_BW4_UL	25	25	NOP
27	I_BW2_UL	23.3	23.3	NOP

The following conclusions can be drawn from Table 4.2:

1. Both criteria 1 and 2 can always trip quite quickly for light winding faults no matter whether accompanied by energizing. The longest time delay is 31.6 ms. However, the protection with the scheme of normal second harmonic restraint cannot trip for cases 19–27 even the internal faults have presented for five cycles.
2. Criterion 2 can operate faster than criterion 1, especially for heavy faults or energizing with heavy faults.
3. In some cases, criterion 1 can operate more quickly than criterion 2 when the harmonics contained in the fault current do not influence the evenness of the current. However, only four cases appear in the above 27 cases, and two of them trip faster by only one or two sampling intervals than ones using criterion 2.
4. For the very heavy faults (cases 5, 19), both criteria operate with a long time delay (at least 50 ms). Of course, the scheme with 15% second harmonic restraint also cannot operate at this moment. Therefore, it is still necessary to improve criterion 2 further.

4.2.2.3 Improvement of the Waveform Coefficient J

It can been observed from Equation (4.3) that the waveform coefficient only uses the information of $\sigma(X)$, that is, the mean square error of 'large area' in Figure 4.2, and the information of $\sigma(Y)$ (small area) is ignored. As the analysis in part II, the $\sigma(Y)$ of the inrush is quite small. For the fault current containing certain damped DC components, $\sigma(Y)$ may be larger than $\sigma(X)$ according to the investigations for various internal fault waveforms. Therefore, an improved waveform coefficient is:

$$J = \frac{Cov(X,Y)}{\sigma^2(X)} \times \frac{\sigma^2(Y)}{\sigma^2(X)} \tag{4.6}$$

Equations (4.5) and (4.6) form criterion 3. With this criterion the waveform coefficient of inrush will decrease due to the introduction of $\sigma(Y)$. For criterion 3, the waveform coefficients of the inrushes in Figure 4.5 are evaluated as $J_{a-b} = 0.523$, $J_{b-c} = 0.181$ and $J_{c-a} = 0.661$. As seen, the maximum J has decreased to 0.661. In fact, the inrushes in Figure 4.5 only indicate the very extreme case. In this case, the maximum ratio of I_2/I_1 is only given by 11% using Fourier algorithm, whereas the accepted ratio in industrial applications in China is 15–20%. Consequently, here the waveform coefficient J can be decreased so that this algorithm can be contrasted with the scheme of second harmonic restraint. The threshold of criterion 3 can be decreased to $0.66 \times 11/15$, that is, 0.48. In order to compare the criteria 1, 2 and 3 with the same thresholds induced from Figure 4.5, the criterion 3 with a threshold of 0.48 is denoted criterion 4. The reliability and sensitivity evaluations of all the above four criteria are described below.

Figure 4.7 illustrates the N.O.T.s in milliseconds for the faults in Table 4.1, where the X-axis is denoted as fault number and the Y-axis is denoted as the N.O.T.

The N.O.T. series for criterion 1 is denoted by the marker '+' and the ones for criterion 2, 3, and 4 by '*', 'o' and 'Δ', respectively. It can be concluded form Figure 4.7 that criterion 2 has nearly the same sensitivity as criterion 3, but criterion 3 has better reliability than criterion 2 when they are applied to identify the inrushes. The maximum waveform coefficients of all types of typical inrushes recorded by the same recorder were investigated. Among them 10 values are given in Table 4.3, of which cases 1–4 are conditions such that the transformer is energized without a long transmission line; in cases 5–9 the transformer is energized with a long line. In the end, the energizing induced by the clearance of external fault is given by case 10. The maximum waveform coefficients of all cases during the five cycles after inrushes occur are indicated in Table 4.3.

It can be seen from Table 4.3 that the maximum J_{max} among the 10 cases are 0.55 or 0.54 and 0.18 for criteria 1, 2 and 3, respectively.

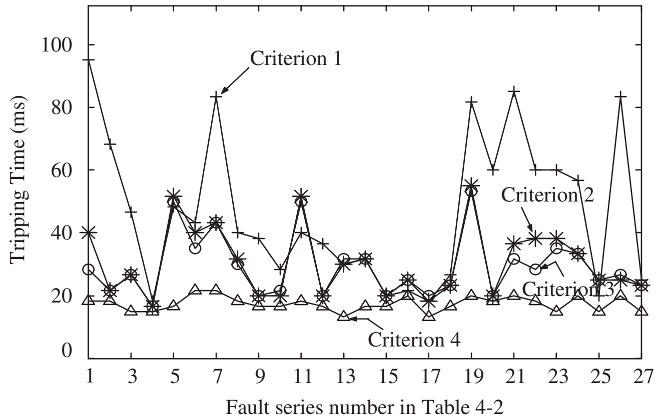

Figure 4.7 Nonoperation times of criterion 1 to criterion 4 with the same reliability

Table 4.3 Maximums of waveform coefficients of real magnetizing inrushes derived by criteria 1, 2 and 3

Case	Inrush condition	J_{max} of criterion 1	J_{max} of criterion 2	J_{max} of criterion 3
1	Inrush_UL1	0.5	0.46	0.11
2	Inrush_UL2	0.5	0.5	0.14
3	Inrush_UL3	0.5	0.46	0.11
4	Inrush_UL4	0.55	0.51	0.16
5	Inrush_L1	0.55	0.54	0.18
6	Inrush_L2	0.41	0.41	0.08
7	Inrush_L3	0.44	0.44	0.10
8	Inrush_L4	0.51	0.5	0.15
9	Inrush_L5	0.48	0.48	0.13
10	External fault	0.55	0.46	0.11

For convenient contrast, a reliability coefficient is defined as:

$$k_{rel} = J_{theomax}/\text{Max}(J_{realmax}) \tag{4.7}$$

where $J_{theomax}$ is the theoretical maximum waveform coefficient induced by the inrushes in Figure 4.5, Max $(J_{realmax})$ is the real maximum waveform coefficient among the values in Table 4.3. It is evident that K_{rel} is 1.45, 1.48, 3.67 and 2.67, for the criteria respectively. The reliability of criteria 3 and 4 is far larger than that of criteria 1 and 2, and criterion 4 is more sensitive than criterion 3 because of a smaller threshold of J.

As seen in Figure 4.7, criterion 4 obviously operates more quickly than the other three criteria. For most faults, the relay can trip within one cycle after a fault occurs. In these 27 cases, the quickest operation time is 13.3 ms, and the longest is 21.6 ms; any winding fault can be cleared with one cycle even though the short circuit is present before the transformer is energized.

To validate the proposed algorithms more thoroughly, some further work should be advanced. For one thing, more types of ATP simulation based transformers, such as three-leg or five-leg Core Type ones, should be considered. Additionally, more dynamic tests in laboratories other than those of Huazhong University of Science & Technology should be carried out. As a prototype, the company that the author is working in has implemented this algorithm in its transformer protection product. Such a protection device will be put into commission as soon as it passes the dynamic simulation tests in the laboratory of Shangdong University, PRC.

In summary, an improved scheme (criterion 4) used for the transformer inrush identification of differential protection has been developed. The proposed scheme is based on improved correlation analysis. Simulation and dynamic test results show that this algorithm is effective in distinguishing inrushes from different types of internal faults of a transformer with or without transmission lines and loads. The scheme has high reliability when the threshold is determined according to the boundary inrush condition. On the other hand, the sensitivity of the scheme also is higher than that of other common schemes with the same reliability. Furthermore, the computation simplicity is such that it can be implemented in real-time applications using the present microprocessor hardware.

4.3 A Novel Method for Discrimination of Internal Faults and Inrush Currents by Using Waveform Singularity Factor

4.3.1 Waveform Singularity Factor Based Algorithm

The sinusoidal waveform $f(t)$ shown in Figure 4.8a can be described as:

$$f(t) = A\sin(\omega t + \theta) \tag{4.8}$$

where A is the amplitude of sinusoidal waveform, ω is the power angular frequency and θ is the initial phase angle.

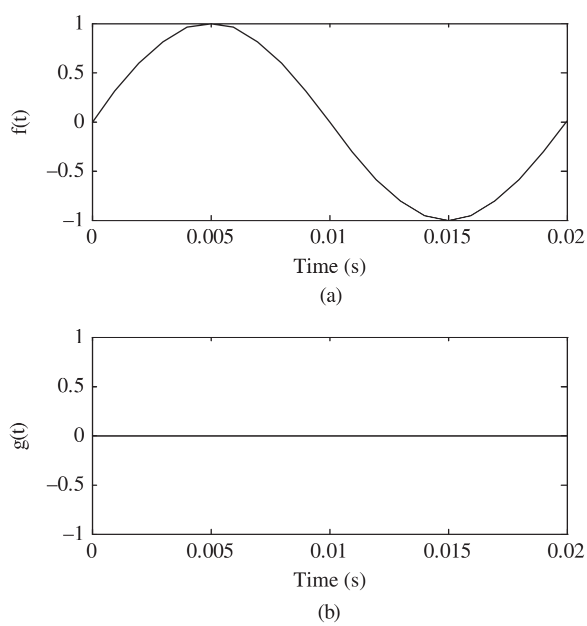

Figure 4.8 (a) The sinusoidal waveform $f(t)$ and (b) the calculated $g(t)$

The time interval of a quarter cycle, Δt, is $0.5\pi/\omega$; the $f(t)$ at $t_k + \Delta t$ instant is given by:

$$\begin{aligned} f(t+\Delta t) &= A\sin(\omega(t+\Delta t)+\theta) \\ &= A\sin(\omega(t+0.5\pi/\omega)+\theta) \\ &= A\cos(\omega t+\theta) \end{aligned} \tag{4.9}$$

$f(t)$ at $t_k + \Delta t/2$ instant is given by:

$$\begin{aligned} f(t+\Delta t/2) &= A\sin(\omega(t+\Delta t/2)+\theta) \\ &= A\sin(\omega(t+0.25\pi/\omega)+\theta) \\ &= A\cos(\omega t+\theta+\pi/4) \end{aligned} \tag{4.10}$$

$g(t)$ is defined as:

$$g(t) = f(t) + f(t+\Delta t) - \sqrt{2}f(t+\Delta t/2) \tag{4.11}$$

For a pure sinusoidal waveform, $g(t)$ is a constant value and equal to zero as shown in Figure 4.8b. However, the actual current waveform usually contains harmonics or noises and cannot be exactly the pure sinusoidal waveform. Therefore, the WSF is defined to calculate the difference between the actual current waveform and the pure sinusoidal waveform:

$$h(t) = \frac{1}{e}\sqrt{\frac{1}{N}\sum_{t=t_k}^{t=t_k+2\Delta t}(g(t)-e)^2} \tag{4.12}$$

$$e = \frac{1}{N}\sum_{t=t_k}^{t=t_k+2\Delta t} g(t) \tag{4.13}$$

where N is the number of samples per power frequency cycle (20 ms in 50 Hz system).

When an internal fault occurs, owing to its operation point in the linear area of the magnetizing characteristic, the waveform of the faulty phase presents an approximate pure sinusoidal feature. So the curve of the calculated $g(t)$ of the faulty phase is very close to zero. And by using Equation (4.12), $h(t)$ of the faulty phase is also close to zero. On the other hand, when the magnetizing current is generated, $g(t)$ of the phase with the inrush current is featured by a drastic variation, which is caused by the high nonlinearity characteristic in exciting core of transformer. Therefore, $h(t)$, also called WSF, is a favourable feature for discriminating between the inrush currents and internal faults.

If the WSF of each phase exceeds the threshold 1.0, the relay will judge that the pick-up is due to inrush current and reject tripping. Or else, the relay judges an internal fault occurs if WSF is less than the threshold. In theory, the threshold is close to zero.

4.3.2 Testing Results and Analysis

To verify the effectiveness of the proposed method, experimental tests have been carried out at the Electrical Power Dynamic Laboratory (EPDL). The experimental system is one machine model with a two-winding three-phase Y/Δ-11 connected transformer bank as shown in Figure 4.9. The parameters of the experimental system are given in Table 4.4. CTs with Y/Y connection are used as transducers to measure the line currents of the transformer bank.

The experiments provide samples of line currents and terminal voltages in each phase when the transformer is energized or when a fault occurs or when both occur simultaneously. A total of 162 cases are divided into four main categories: 56 cases for switching on the transformer with no load, 52 cases for simultaneous internal fault and inrush conditions, and 54 cases for faulty conditions only, to verify the

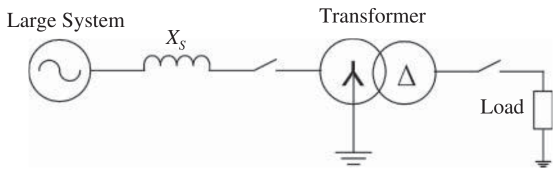

Figure 4.9 Experimental system

Table 4.4 Parameters of the transformer used in the test

Rated capacity (kVA)	30 kVA
Rated voltage ratio (V)	1732.05/380
Rated current ratio (A)	10/45.58
Rated frequency (Hz)	50
No load current (%)	1.45
No load loss (%)	1
Short-circuit voltage (%)	9.0–15.0
Short-circuit loss (%)	0.35
Load (kW)	0.9

proposed algorithm. Different inception and clearing instants for inrush current, as well as different faults and short-circuit turn ratios for the internal fault are considered in the tests.

Figures 4.10–4.15 show some examples of the experimental test results: the line currents and the waveforms of the calculated WSFs along with the resulting analysis.

4.3.2.1 Responses to Inrush Conditions Only

The magnetizing inrush current is often generated when a transformer is energized. A total of 56 cases were tested in this scenario. The inrush current waveform is a function of the different core residual

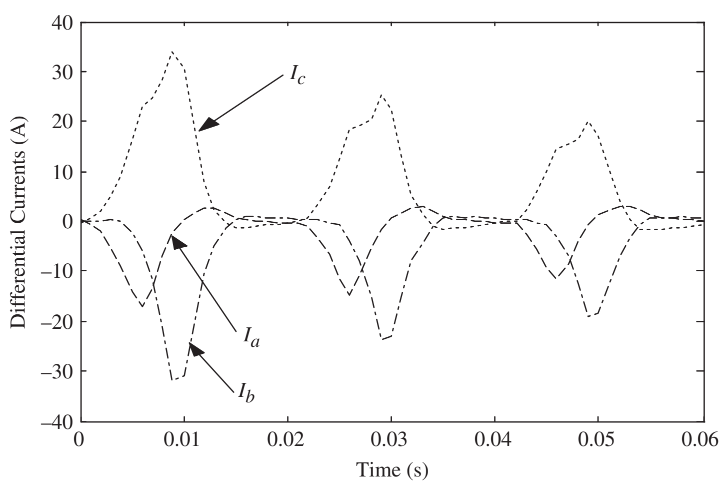

Figure 4.10 Differential currents when the transformer is energized

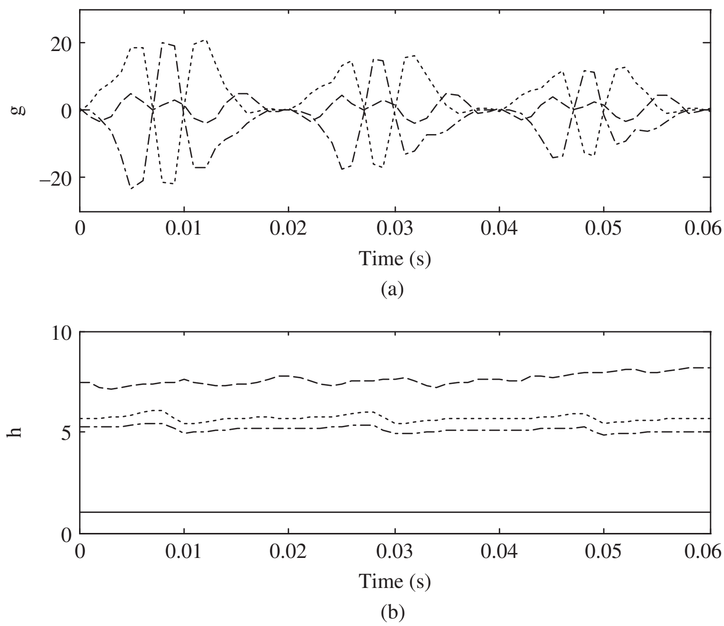

Figure 4.11 Experimental results when the transformer is energized: (a) the *hs* of three phases; (b) the WSFs of three phases

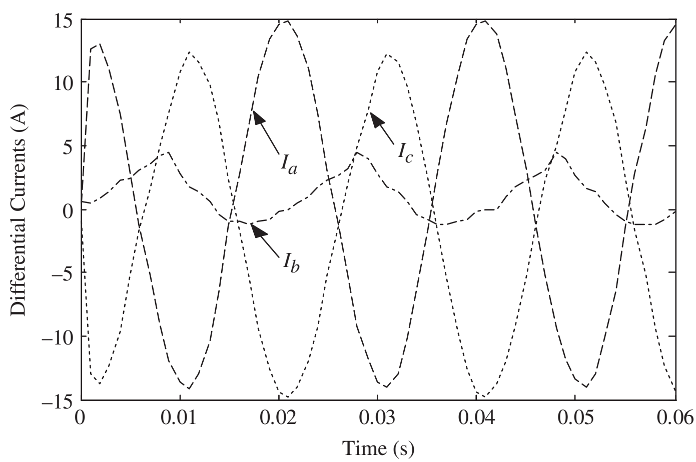

Figure 4.12 Differential currents when the transformer is energized with a 6.2% turn-to-turn internal fault

magnetization and the switching instant. The same feature of the inrush current, just like the previous analysis, is extracted from the data of the 56 cases, although the inrush current waveforms are different from each other.

An example taken from these cases is given in Figures 4.10 and 4.11, of which the three differential currents present the asymmetrical inrush currents shown in Figure 4.10. The calculated *hs* of three

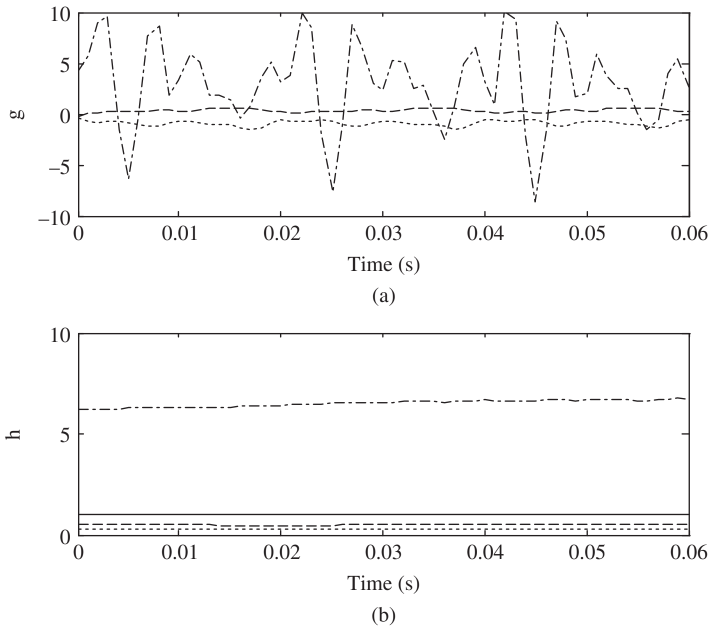

Figure 4.13 Experimental results when the transformer is energized with a 6.2% turn-to-turn internal fault: (a) the *hs* of three phases; (b) the WSFs of three phases

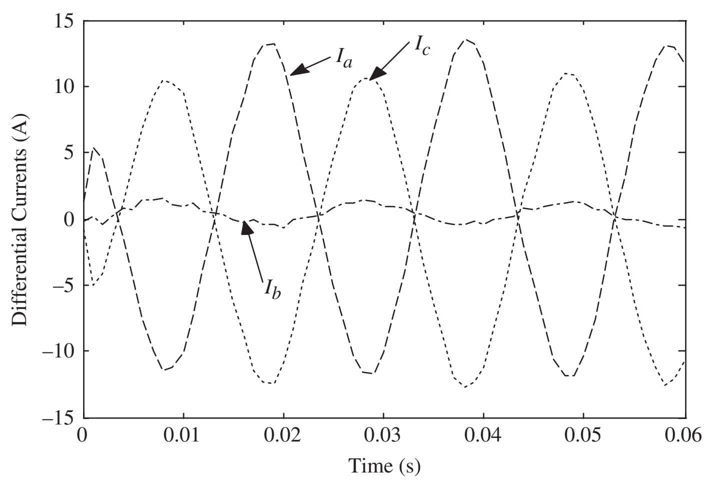

Figure 4.14 Differential currents when a 6.2% turn-to-turn internal fault occurs during normal conditions

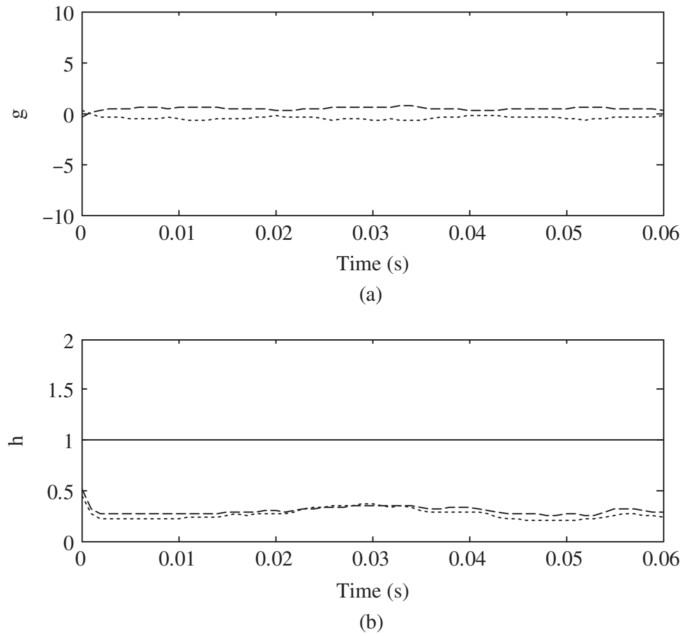

Figure 4.15 Experimental results when a 6.2% turn-to-turn internal fault occurs during normal conditions: (a) the *hs* of three phases; (b) the WSFs of three phases

differential currents are shown in Figure 4.11a. The *h* of each phase presents drastic variation of high amplitude. After calculation using Equations (4.12) and (4.13), the WSFs of three phases are obtained and shown in Figure 4.11b. The WSF of each phase shows a noticeable value. Furthermore, the WSF of each phase is much more than the threshold 1.0. Therefore, the relay will be inhibited from issuing a trip signal in this situation.

4.3.2.2 Responses to Simultaneous Fault and Inrush Conditions

Switching on the transformer bank with no load often causes the inrush current of nonfault phases, which has been verified by a total of 52 cases with simultaneous inrush currents and internal fault currents. Figure 4.12 as an example shows this situation, which is obtained by switching on the transformer with no load and a 6.2% turn-to-turn internal fault in phase A. The differential currents of phases A and C are fault differential currents, but that of phase B is the differential current which only includes the inrush current.

Figure 4.13 shows the respective *hs* of three phases along with their WSFs outputs. As shown in Figure 4.13a, the calculated *hs* of the faulty phases keep almost a constant value and only have a little variation owing to the noises and disturbances. However, the calculated ρ of the nonfaulty phase shows drastic fluctuation. In Figure 4.13b, the WSF of the nonfaulty phase is very noticeable and much more than the threshold 1.0, whereas the WSFs of the faulty phases are all much less than the threshold 1.0. Therefore, the relay determines that it is an internal fault and trips.

In the 52 cases, identical results verify that the WSF-based method can be used to identify internal faults when the simultaneous inrush current and fault occur in the transformer bank.

4.3.2.3 Responses to Internal Fault Conditions Only

Data from a total of 54 different internal fault cases were used to verify the principle that the sinusoidal feature will be detected in the waveforms of faulty phases. An example is shown in Figures 4.14 and 4.15, where a 6.2% turn-to-turn internal fault occurs in phase A during the normal condition. It can be seen from Figure 4.14 that the differential currents of phases A and C are larger than the nominal value. Therefore, it is necessary to calculate the WSFs of these two faulty phases. The *hs* along with their WSFs outputs are shown in Figure 4.15.

The *hs* of phases A and C in Figure 4.15a are both smooth and stationary and only have small peaks and valleys due to the measurements and calculation errors. The WSFs of faulty phases are all less than the threshold 1.0 (Figure 4.15b). Therefore, the relay determines that it is an internal fault and lets the relay trip. These results prove the accuracy of the calculated WSFs and the sensitivity of the method to identify internal faults.

In addition, the WSFs of faulty phases during other internal faults (including grounding internal faults and phase-to-phase internal faults) are all close to zero, which is effectively used to distinguish the internal faults and inrush currents.

In summary, based on the high nonlinearity characteristic in exciting cores of transformers, a new scheme using WSF to extract singularity characteristics of transformer is proposed. The feature extraction with WSF is a sensitive and a computationally flexible way to conduct signal discrimination between internal faults and inrush currents. The technique can block the relay even under simultaneous fault and inrush conditions. The experimental results validate the proposed method and show that the method is sensitive for the identification of low-level internal faults.

4.4 A New Principle of Discrimination between Inrush Current and Internal Fault Current of Transformer Based on Self-Correlation Function

4.4.1 Basic Principle of Correlation Function Applied to Random Single Analysis

According to the theory of digital signal processing, a random signal is different from the deterministic signal, since it cannot be described by a given math formula and forecasted accurately. In order to detect, identify and extract a random signal, the similarity of two random signals or self-similarity of one random signal by means of statistics is usually used. Therefore, correlation function is a significant algorithm in analysing a random signal.

For two random signals $X(n)$, $Y(n)$, their cross-correlation function can be defined as:

$$r_{xy}(n_1, n_2) = E\{X^*(n_1)Y(n_2)\} \tag{4.14}$$

where $X^*(n_1)$ is the conjugate of $X(n_1)$.

If $X(n) = Y(n)$, the definition will be converted from cross-correlation function to self-correlation function as below:

$$r_{xx}(n_1, n_2) = E\{|X(n)|^2\} \tag{4.15}$$

The self-correlation function $r_{xx}(n_1,n_2)$ reflects the similarity of signal $X(n_1)$ and itself after some time delay. Practically, a random signal is the actual physical signal with causality, that is, when $n < 0$, $X(n) = 0$. $X(n)$ is a real variable signal, so its self-correlation function can be defined as:

$$r(m) = \lim_{N\to\infty} \frac{1}{N} \sum_{n=0}^{N-1} X(n)X(n+m) \tag{4.16}$$

The self-correlation function $r(m)$ can be estimated by detected values $X_N(0), X_N(1), \cdots, X_N(N-1)$.

If N in Equation (4.16) is a finite value, *r(m)* can be defined as:

$$\hat{r}(m) = \frac{1}{N} \sum_{n=0}^{N-1-|m|} X_N(n) X_N(n+m) \tag{4.17}$$

where the length of $\hat{r}(m)$ is $2N-1$.

4.4.2 Theory and Analysis of Waveform Similarity Based on Self-Correlation Function

4.4.2.1 Differential Currents between Phases

Differential current waveforms between phases act as the object to be analysed. Taking the 'A' – 'B' phase for instance, differential currents between primary and secondary currents of all phases are calculated and then are applied to form differential current waveform between phases by means of the formula:

$$\begin{cases} I_{\mathrm{a}} = I_{\mathrm{a1}} - I_{a2} \\ I_{\mathrm{b}} = I_{\mathrm{b1}} - I_{b2} \\ I_{\mathrm{abxj}} = I_{\mathrm{a}} - I_{\mathrm{b}} \end{cases} \tag{4.18}$$

where I_{a1}, I_{b1} and I_{c1} represents the primary currents, I_{a2}, I_{b2} and I_{c2} represent the secondary currents and I_{abxj} represents the differential current between phases A and B.

I_{a}, I_{b} and I_{abxj} of the symmetrical inrush current waveform derived from EPDL simulation are shown in Figure 4.16. Additionally, waveforms of an asymmetrical inrush current, transformer fault current when energized without load as well as an internal fault current are shown in Figures 4.17–4.19, respectively.

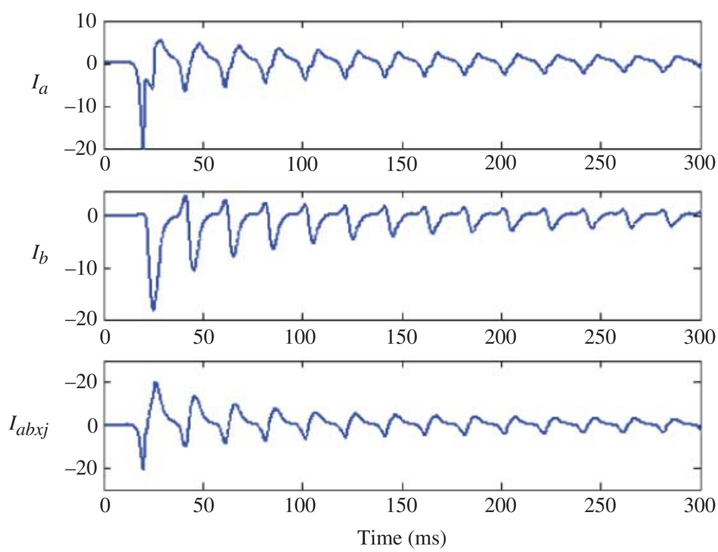

Figure 4.16 I_{a}, I_{b} and I_{abxj} of the symmetrical inrush current waveform

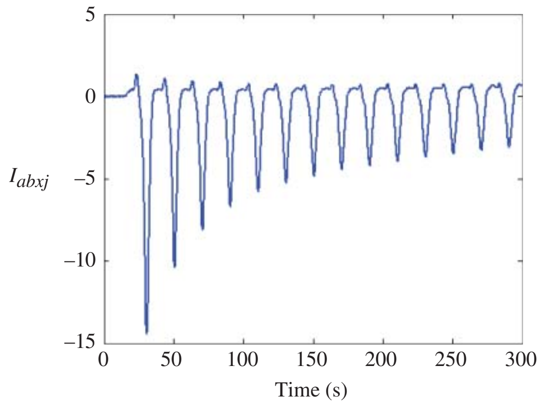

Figure 4.17 Asymmetrical inrush current waveform

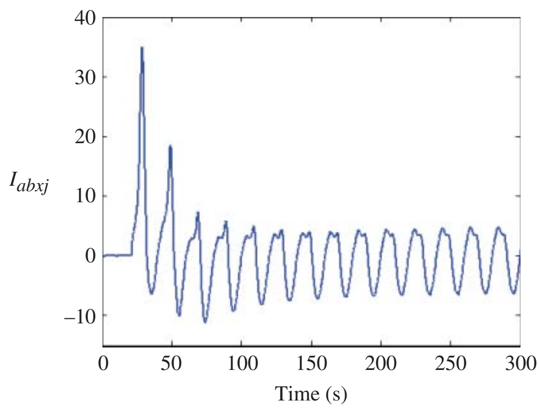

Figure 4.18 Transformer light fault current waveform when the switch is closed without load

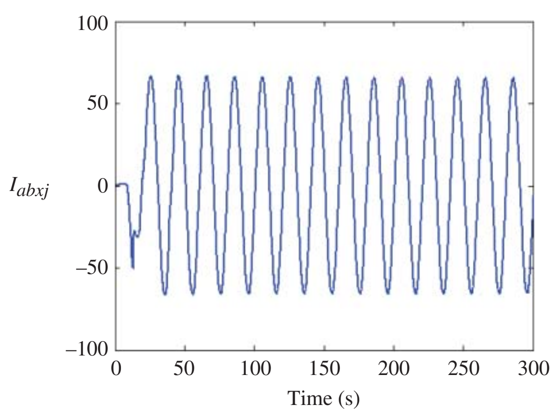

Figure 4.19 Internal fault current waveform

4.4.2.2 Starting Point of Protection

The differential currents then pass through filters where DC components are removed. Meanwhile, time range, which is always the range of the data window, should be selected to calculate the self-correlation function. 10 ms is selected as the range of the data window ($2N = 32$ sampled data in one-cycle). A half cycle integral window area value, S, is calculated by means of the absolute value sum of the current sampling in this time window and k of $S_{max}(k)$ is selected as the starting point of protection, which is:

$$S_{\max}(k) = \max\left(\sum_{j=k}^{k+N-1} |I(j)|\right) \tag{4.19}$$

4.4.2.3 Self-Correlation Function and Normalization

A running integral 10 ms window of the differential current waveform between phases is used to calculate $N/2 = 8$ groups of estimated values of self-correlation function after 3/4 cycle from the starting point of protection by using Equation (4.20). Meanwhile, another integral 10 ms window of sinusoidal current forms estimated values of the SCF by using Equation (4.23). Then, these values can be normalized by means of Equations (4.22) and (4.23):

$$\widehat{p}(m) = \frac{1}{N}\sum_{n=0}^{N-1-|m|} I_N(n)I_N(n+m) \tag{4.20}$$

$$\boldsymbol{p} = (p_1, p_2, \cdots, p_i, \cdots, p_{2N-1}) \tag{4.21}$$

$$\overline{p}_i = \frac{\text{abs}(p_i)}{\max\limits_i[\text{abs}(p_i)]} \tag{4.22}$$

$$\widehat{q}(m) = \frac{1}{N}\sum_{n=0}^{N-1-|m|} I_{\text{ZXN}}(n)I_{\text{ZXN}}(n+m) \tag{4.23}$$

$$\boldsymbol{q} = (q_1, q_2, \cdots, q_i, \cdots, q_{2N-1}) \tag{4.24}$$

$$\overline{q}_i = \frac{\text{abs}(q_i)}{\max\limits_i[\text{abs}(q_i)]} \tag{4.25}$$

where:

$I_N(n)$ and $I_{\text{ZXN}}(n)$ are the actual value of differential current between phases and fundamental current sampled data, respectively;

$\widehat{p}(m)$ and $\widehat{q}(m)$, the estimated values of self-correlation function of differential current between phases and SCF, can form a vector in $2N - 1$ dimensions; $\boldsymbol{p}$ and $\boldsymbol{q}$ respectively, then normalized values $\overline{p}_i$ and $\overline{q}_i$ can be obtained.

4.4.2.4 Minimum Similarity Coefficients

$N/2$ groups of minimum similarity coefficients can be computed through equations:

$$\rho_n = \frac{1}{1 + [\text{abs}(\overline{p}_i - \overline{q}_i)]^3} \tag{4.26}$$

$$\rho = \min(\rho_n) \tag{4.27}$$

$$J = \left(\frac{N}{2}\sum_{n=1}^{N/2}\rho\right)^2 \tag{4.28}$$

where ρ_n, ρ are similarity coefficients and its minimum value of each group, respectively.

4.4.3 EPDL Testing Results and Analysis

4.4.3.1 EPDL Testing System

To verify the feasibility of the proposed method, the author obtained a large number of actual data through EPDL simulation. Figure 4.20 shows the connection scheme of the EPDL testing system. The transformer is a Y/Δ-11 connection transformer consisting of three single-phase units. The parameters of each single-phase are: $S_{rated} = 10$ kVA, rated voltage ratio $U_{1N}/U_{2N} = 1$ kV/380 V, $I_{no\text{-}load} = 1.45\%$, $U_{shortcircuit} = 9.0–15.0\%$,losses of open circuit is 1%, losses of short circuit is 0.35%.

4.4.3.2 EPDL Testing Results and Analysis

N/2 groups of minimum similarity coefficients and their average values of transformer under several states are shown in Table 4.5. To be convenient, the faults in Table 4.5 are numbered to indicate the fault conditions. For instance, cases 0–6 are short-circuit internal faults, cases 7–13 are energizing with internal faults, cases 14 and 15 are energizing without faults. Moreover, case 0 is 'B'-earth fault, case 1 is 'A'-phase winding fault, case 2 is 'A'–'B' phase fault, case 3 is 'A'-earth fault, case 4 is 'B'-phase winding fault, case 5 is 'B'–'C' phase fault, case 6 is 'C'-phase winding fault, case 7 is energizing with 'A'-phase 9% winding fault, case 8 is energizing with 'A'-'B' phase fault, case 9 is energizing

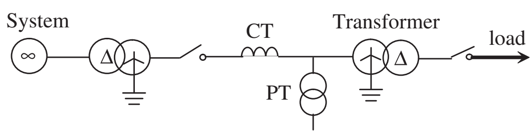

Figure 4.20 Connection scheme of the EPDL testing system

Table 4.5 N/2 groups of minimum similarity coefficients and values J of transformer under several states

Case	Minimum similarity coefficients								J
	First group	Second group	Third group	Forth group	Fifth group	Sixth group	Seventh group	Eighth group	
0	0.9861	0.9983	0.9999	1.0000	1.0000	1.0000	0.9999	0.9969	0.9952
1	0.9851	0.9981	1.0000	1.0000	0.9999	0.9999	0.9985	0.9910	0.9933
2	0.9852	0.9986	1.0000	0.9999	1.0000	1.0000	0.9992	0.9917	0.9936
3	0.9743	0.9955	0.9997	1.0000	0.9999	0.9999	1.0000	0.9995	0.9922
4	0.9947	0.9998	1.0000	0.9999	1.0000	0.9993	0.9955	0.9831	0.9932
5	0.9913	0.9994	1.0000	0.9998	0.9999	0.9999	0.9987	0.9903	0.9948
6	1.0000	0.9999	1.0000	0.9998	0.9976	0.9899	0.9685	0.9326	0.9720
7	0.9996	1.0000	0.9993	0.9957	0.9877	0.9751	0.9555	0.9192	0.9584
8	0.9022	0.9285	0.9634	0.9769	0.9967	0.9999	0.9998	0.9997	0.9428
9	0.9998	1.0000	0.9998	0.9999	1.0000	0.9994	0.9908	0.9643	0.9886
10	0.9271	0.9653	0.9892	0.9991	0.9999	0.9988	0.9990	0.9999	0.9698
11	0.9945	0.9992	0.9991	0.9982	0.9984	0.9996	0.9973	0.9565	0.9858
12	0.8783	0.8726	0.9037	0.9409	0.9689	0.9835	0.9834	0.9752	0.8804
13	0.9750	0.9959	0.9999	0.9999	0.9998	1.0000	0.9997	0.9969	0.9918
14	0.7672	0.7884	0.7873	0.7580	0.7391	0.7933	0.8171	0.7929	0.6090
15	0.8589	0.8900	0.9201	0.8361	0.6208	0.6821	0.6291	0.7067	0.5898

Table 4.6 Value J ranges of minimum similarity coefficients under energizing with or without internal faults of transformer

Fault type and conditions	Value J ranges	Case
Normal energizing	0.5175–0.6090	14.15
Energizing with 'A'-phase 9% winding fault	0.9162–0.9629	7
Energizing with 'B'-phase 18% winding fault	0.8949–0.9714	10
Energizing with 'C'-phase 18% winding fault	0.8671–0.8866	12
Energizing with 'A'-earth fault	0.9508–0.9914	9
Energizing with 'B'-earth fault	0.9017–0.9868	11
Energizing with 'A'–'B' phase fault	0.8828–0.9463	8
Energizing with 'B'–'C' phase fault	0.8701–0.9918	13

with 'A'-earth fault, case 10 is energizing with 'B'-phase 18% winding fault, case 11 is energizing with 'B'-earth fault, case 12 is energizing with 'C'-phase 18% winding fault, case 13 is energizing with 'B'–'C' phase fault, case 14 is symmetrical inrush current, case 15 is asymmetrical inrush current.

Theoretical analysis shows that, when a fault occurs during the operation of the transformer, the fault current is still a sine function after an instantaneous transient period, which is proved by the EPDL results in Table 4.5. Therefore, it is only necessary to distinguish energizing with or without internal faults. Each case in the EPDL simulation is measured 10 times, the results of which are shown here. In Table 4.6, the maximum value of J under normal energizing conditions is 0.6090, which is caused by symmetrical inrush current; on the other hand, the minimum value of J under energizing with internal fault conditions is 0.8671, which is caused by energizing with 'C'-phase fault. Additionally, more desirable results will be obtained when the 'B'–'C' or 'C'–'A' phase is also taken for consideration.

In summary, a new method to discriminate an inrush current and internal fault current of a transformer is proposed based on self-correlation function in DSP. With a proper threshold the method can block the relay even under symmetrical inrush currents conditions. The results in the EPDL show that this method is effective in distinguishing inrushes from various kinds of transformer internal faults.

4.5 Identifying Inrush Current Using Sinusoidal Proximity Factor

4.5.1 Sinusoidal Proximity Factor Based Algorithm

The sinusoidal waveform $f(t)$ as shown in Figure 4.21a can be expressed as:

$$f(t) = A\sin(\omega t + \theta) \tag{4.29}$$

where A is the amplitude of sinusoidal waveform, ω is the power angular frequency and θ is the initial phase angle.

Suppose that $f(t)$ has n (n is an even number) sampling points in one cycle. For the sampling point at t_k instant, $f(t_k)$ is given by:

$$f(t_k) = A\sin(wt_k + \theta) \tag{4.30}$$

The time interval of a quarter cycle Δt is $0.5\pi/\omega$ s, the $f(t)$ at $t_k + \Delta t$ instant is given by:

$$\begin{aligned} f(t_k + \Delta t) &= A\sin(\omega(t_k + \Delta t) + \theta) \\ &= A\sin(\omega(t_k + 0.5\pi/\omega) + \theta) \\ &= A\cos(\omega t_k + \theta) \end{aligned} \tag{4.31}$$

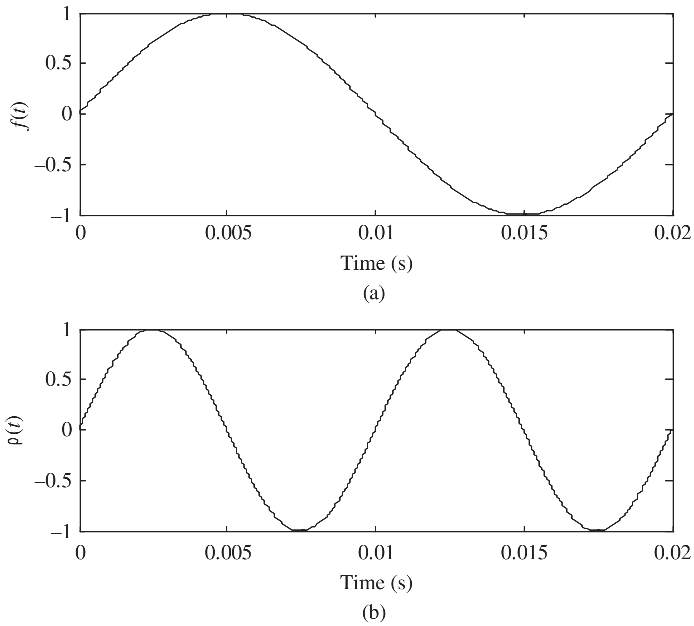

Figure 4.21 (a) The sinusoidal waveform $f(t)$ and (b) the multiplication ρ

Normalize $f(t)$ and then multiply $f(t_k)$ with $f(t_k + \Delta t)$:

$$\begin{aligned}\rho(t_k) &= 2f(t_k)f(t_k + \Delta t)\\ &= 2\sin(\omega t_k + \theta)\cos(\omega t_k + \theta)\\ &= \sin(2\omega t_k + 2\theta)\end{aligned} \tag{4.32}$$

For the sinusoidal waveform, ρ is on the curve of the pure sinusoidal as shown in Figure 4.21b. However, in the real world, the current waveform contains harmonics or noises and cannot be exactly the pure sinusoidal waveform. So the SPF is defined to calculate the difference between the actual current waveform and the pure sinusoidal waveform:

$$\eta(t_k) = abs(\rho(t_k) - \sin(2\omega t_k + 2\theta)) \tag{4.33}$$

where η is the SPF, *abs* means absolute difference between $\rho(t_k)$ and $\sin(2\omega t_k + 2\theta)$.

When an internal fault occurs, owing to its operation point in the linear area of the magnetizing characteristic, the waveform of the faulty phase presents an approximate pure sinusoidal feature. So the curve of the multiplication ρ in the faulty phase is very close to the curve of the pure sinusoidal. And by using Equation (4.33), η of the faulty phase is close to zero. On the other hand, when the magnetizing current is generated, the feature of ρ of the phase with the inrush current is the drastic variation, which is caused by the high nonlinearity characteristic exciting the core of the transformer. Therefore, η, also called SPF, is a favourable feature of discrimination between the inrush currents and internal faults. If the SPF of some phase is less than the threshold 0.5, the relay determines there is an internal fault and trips the fault. Otherwise, the relay determines that there is an inrush current and rejects the tripping.

4.5.2 Testing Results and Analysis

To verify the effectiveness of the proposed method, experimental tests have been carried out at the EPDL. The experimental system is one machine model with a two-winding three-phase Y/Δ-11 connected transformer bank (Figure 4.22). The parameters of the experimental system are given in Table 4.7. CTs with Y/Y connection are used as transducers to measure line currents of the transformer bank.

The experiments provide samples of line currents and terminal voltages in each phase when the transformer is energized or when a fault occurs or when both occur simultaneously. A total of 162 cases have been divided into four main categories: 56 cases for switching on the transformer with no load, 52 cases for simultaneous internal fault and inrush conditions, and 54 cases for faulty conditions only, to test the various features of the algorithm. Different switching and clearing instants for inrush current, as well as different faults and short circuit turn ratios for the internal fault are considered in the tests. The measured data are used as an input to the developed algorithm to identify its response. Figures 4.23–4.28 show some examples of the experimental test results: the line currents and the waveforms of the calculated SPFs along with the resulting analysis.

4.5.2.1 Responses to Inrush Conditions Only

A total of 56 cases were carried out in this situation. The inrush current waveform is a function of the different core residual magnetization and the switching instant. The same feature of the inrush current, just like the previous analysis, is extracted from the data of the 56 cases, although the inrush current waveforms are different from each other. An example taken from those cases is given in Figures 4.23 and 4.24, where the three differential currents present as asymmetrical and symmetrical inrush currents are shown in Figure 4.23.

The calculated ρs of three differential currents are shown in Figure 4.24a–c. The ρ of each phase presents a noticeable difference from the pure sinusoidal waveform. After calculation using Equation (4.33), the SPFs of three phases are obtained and shown in Figure 4.24d. The SPF of each

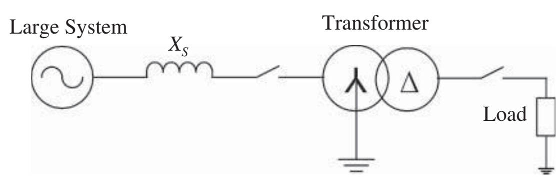

Figure 4.22 Experimental system

Table 4.7 Parameters of the transformer used in the test

Rated capacity (kVA)	30
Rated voltage ratio (V)	1732.05/380
Rated current ratio (A)	10/45.58
Rated frequency (Hz)	50
No load current (%)	1.45
No load loss (%)	1
Short-circuit voltage (%)	9.0–15.0
Short-circuit loss (%)	0.35
Load (kW)	0.9

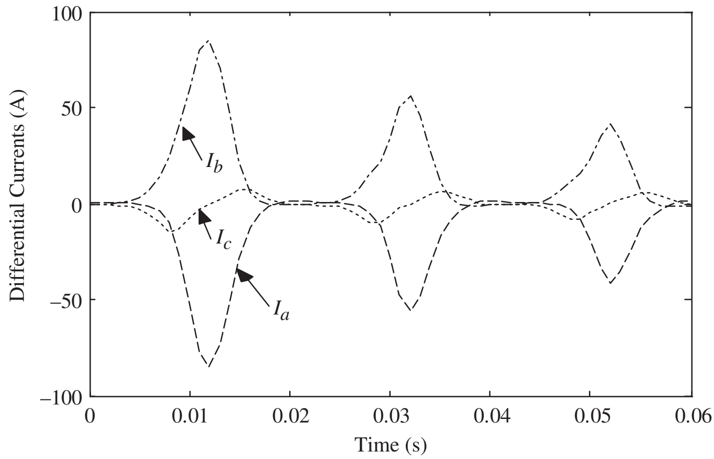

Figure 4.23 Differential currents when the transformer is energized

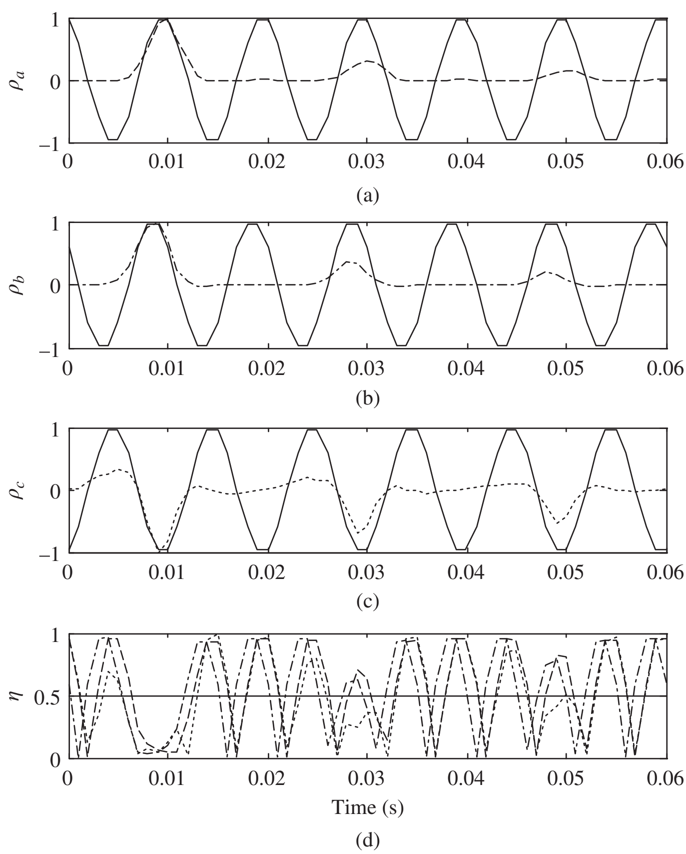

Figure 4.24 Experimental results when the transformer is energized: (a) the multiplication of differential current of phase A ρ_a; (b) the multiplication of differential current of phase B ρ_b; (c) the multiplication of differential current of phase C ρ_c; (d) the SPF of three phases

phase shows a drastic variation between 0 and 1. Furthermore, some sampling values of the SPF of each phase are more than the threshold 0.5. Therefore, the relay will be inhibited from issuing a trip signal in this situation.

4.5.2.2 Responses to Simultaneous Fault and Inrush Conditions

Switching on the transformer bank with no load often causes the inrush current of nonfault phases, which has been verified by a total of 52 cases with simultaneous inrush currents and internal fault currents. Figure 4.25 as an example shows this situation, which is obtained by switching on the transformer with no load and a 6.2% turn-to-turn internal fault in phase A. The differential currents of phases A and C are fault differential currents, but that of phase B is the differential current which only includes the inrush current.

Figure 4.26 shows the respective ρs of the three differential currents along with their SPFs outputs. As shown in Figure 4.26a and 4.26c, the calculated ρs of faulty phases present approximately sinusoidal waveforms and have negligible differences with the pure sinusoidal waveform. However, the calculated ρ of the nonfaulty phase shows a noticeable difference compared with the pure sinusoidal waveform, as shown in Figure 4.26b. The SPF of the nonfaulty phase shows drastic variation and some sampling values are more than the threshold, whereas the SPFs of the faulty phases are all less than the threshold 0.5. Therefore, the relay determines that it is an internal fault and trips.

In the total of 52 cases, the identical results verify that the SPF-based method can be used to identify internal faults when the simultaneous inrush current and fault occur in the transformer bank.

4.5.2.3 Responses to Internal Fault Conditions Only

Data from a total of 54 different internal fault cases are used to verify the principle that the sinusoidal feature will be detected in the waveforms of faulty phases. An example is shown in Figures 4.27 and 4.28, where a 6.2% turn-to-turn internal fault occurs in phase A during the normal condition.

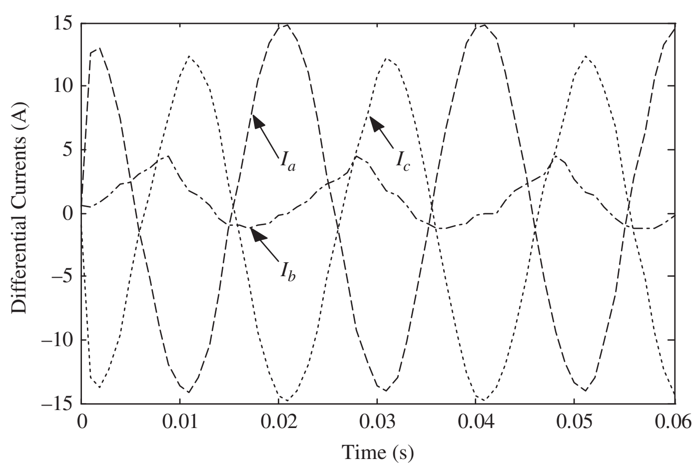

Figure 4.25 Differential currents when the transformer is energized with a 6.2% turn-to-turn internal fault

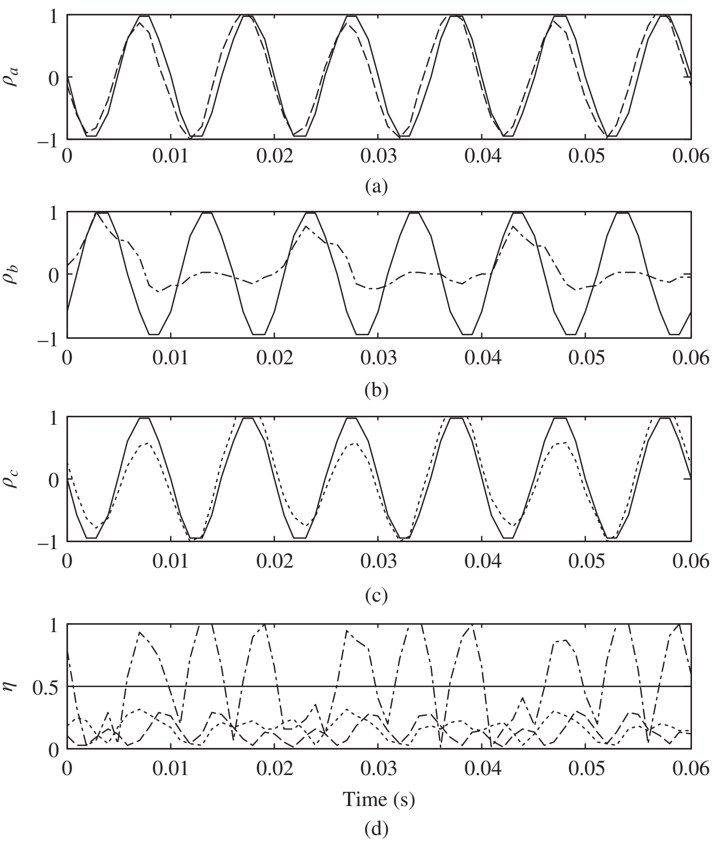

Figure 4.26 Experimental results when the transformer is energized with a 6.2% turn-to-turn internal fault: (a) the multiplication of differential current of phase A ρ_a; (b) the multiplication of differential current of phase B ρ_b; (c) the multiplication of differential current of phase C ρ_c; (d) the SPF of three phases

It can be seen from Figure 4.27 that the differential currents of phases A and C are larger than the nominal value. Therefore, it is necessary to calculate the SPFs of phases A and C. The ρs along with their SPFs outputs are shown in Figure 4.28.

The ρs of phases A and C in Figure 4.28a and 4.28b show the sinusoidal characteristics. The differences between the ρs of the two phases and the pure sinusoidal waveform are negligible. The SPFs of faulty phases are all less than the threshold 0.5 (Figure 4.28c). Therefore, the relay determines that it is an internal fault and lets the relay trip. These results prove the accuracy of the calculated SPFs and the sensitivity of the method to identify the internal faults.

In addition, the SPFs of faulty phases during other internal faults (including grounding internal faults and phase-to-phase internal faults) are all close to zero, which is effectively used to distinguish the internal faults and inrush currents.

In summary, based on the high nonlinearity characteristic in exciting cores of transformers, a new scheme using SPF to extract sinusoidal characteristics of a transformer is proposed. The feature extraction

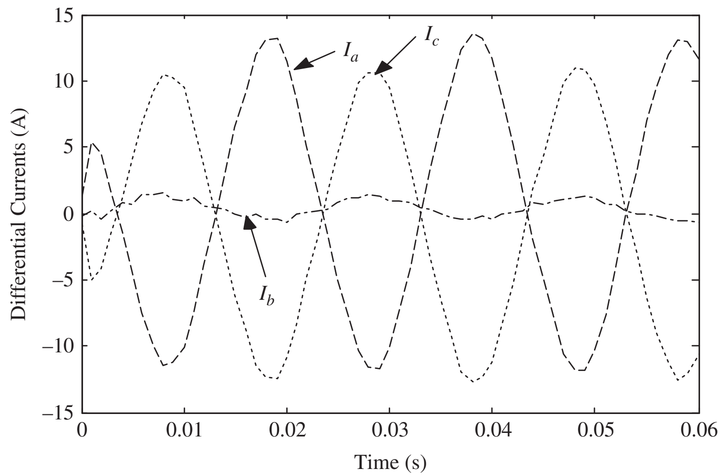

Figure 4.27 Differential currents when a 6.2% turn-to-turn internal fault occurs during normal conditions

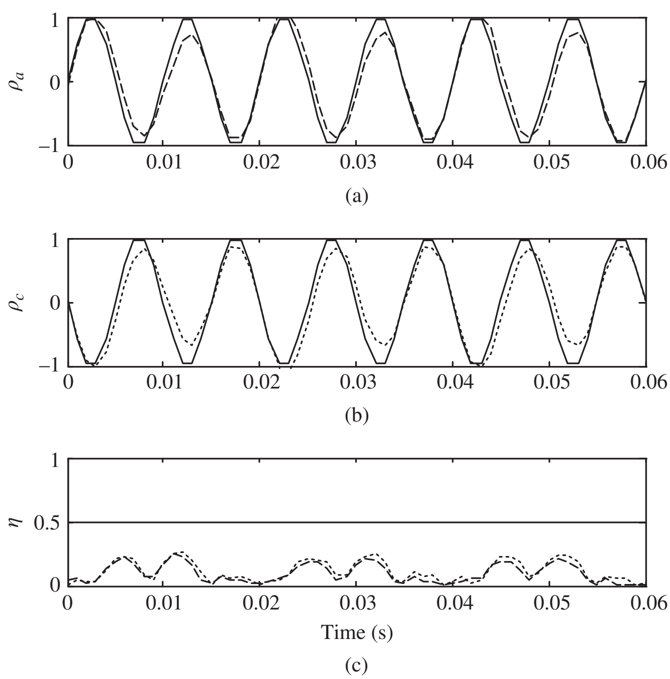

Figure 4.28 Experimental results when a 6.2% turn-to-turn internal fault occurs during normal conditions: (a) the multiplication of differential current of A phase ρ_a; (b) the multiplication of differential current of phase C ρ_c; (c) the SPF of three phases

with SPF is a sensitive and computationally flexible way to conduct signal discrimination between internal faults and inrush currents. The technique can block the relay even under symmetrical inrush current conditions. The experimental results validate the proposed method and show that the method is sensitive for the identification of low level internal faults.

4.6 A Wavelet Transform Based Scheme for Power Transformer Inrush Identification

4.6.1 Principle of Wavelet Transform

4.6.1.1 WT Model and Dyadic Wavelet

By using Fourier analysis, the sampled signals in terms of time domain can be treated in the frequency domain. Therefore, Fourier analysis has played and will continue to play an important role in signal processing. However, one of the most serious disadvantages of Fourier analysis is that it is difficult to deal with those problems in which it is necessary to the determine the precise frequency characteristics of a signal in a local time domain. For instance, signals of power system sampled at the moment when the fault occurs contain very rich important information about the fault. Effective use of such information can significantly improve the performance of the protective relay. Obviously, the Fourier transform is unable to handle this kind of problem. It is then necessary to develop an algorithm that combines the advantages of both the Fourier transform and its inverse transform with the property of time-window and frequency-window. The wavelet transform is exactly this type of transform.

For a finite energy function, $\psi(t) \in L^2(R)$, if the functions $\psi_{ab}(t)$ can be derived from $\psi(t)$, we have:

$$\psi_{ab}(t) = |a|^{-\frac{1}{2}}\psi\left(\frac{t-b}{a}\right) \tag{4.34}$$

where 'a' represents a time dilation and 'b' represents a time translation and function $\psi(t)$ satisfies the following admissibility condition:

$$C_\psi = \int_R \frac{|\hat{\psi}(\omega)|^2}{|\omega|} d\omega < \infty \tag{4.35}$$

where $\hat{\psi}(\omega)$ is the Fourier transform of $\psi(t)$, function $\psi(t)$ is called an admissive wavelet or 'mother wavelet'.

Then, the wavelet transform for a given function, $f(t) \in L^2(R)$, is defined by the equation:

$$(W_\psi f)(a,b) = |a|^{-\frac{1}{2}} \int_R f(t)\overline{\psi\left(\frac{t-b}{a}\right)}dt \quad a,b \in R, a \neq 0 \tag{4.36}$$

where '$\overline{x}$' represents the complex conjugate of 'x'. Parameters 'a' and 'b' can be used to specify the range of the frequency and the location of the time of the sampled signals.

Similar to the ideas of the Fourier series and the Fourier transform, it is desired to form a family of orthogonal functions in time-frequency space. Equation (4.37) gives a set of orthogonal dyadic wavelets:

$$\begin{cases} \psi_{jk}(t) = 2^{j/2}\psi(2^{j/2}t-k) & j,k \in Z \\ (\psi_{jk}(t), \psi_{il}(t))) = \delta_{ji}\delta_{kl} & i.l \in Z \end{cases} \tag{4.37}$$

Then, the wavelet series is given by:

$$\begin{cases} f(t) = \sum_{j,k \in Z} C_{jk}\psi_{jk}(t) \\ C_{jk} = (f(t), \psi_{jk}(t)) \end{cases} \tag{4.38}$$

4.6.1.2 Construction of the Wavelet

Y. Meyer proposed a concept for multiresolution analysis (MRA). With the proposed concept, it is easy to construct a wavelet and to understand the following theorem about the wavelet construction.

Let $\{\varphi(2t-n)\}$ be an ortho-normal basis. For $\{h_n\} \in l_2$:

$$\varphi(t) = \sum_{n \in Z} h_n \varphi(2t-n) \tag{4.39}$$

Defining

$$\psi(t) = \sum_{n \in Z} (-1)^n h_{1-n} \varphi(2t-n) = \sum_{n \in Z} g_n \varphi(2t-n) \tag{4.40}$$

where $g_n = (-1)^n \overline{h}_{1-n}$ represents the construction coefficients, the following two equations can be obtained:

$$\psi_{jn}(t) = 2^{j/2} \psi(2^j t - n) \tag{4.41}$$

$$\begin{cases} V_j = span\{\varphi_{jn}(t), n \in Z\} \\ W_j = span\{\psi_{jn}(t), n \in Z\} \end{cases} \tag{4.42}$$

where V_j is the subspace of the space spanned by φ and W_j is the subspace of the space spanned by ψ. The following two conclusions can be obtained:

$\{\psi_{jn}(t)\}$ is a set of orthogonal basis of W_j;

$$\begin{cases} W_j \perp V_l \,(j, l \in Z) & W_j \perp W_l (j \neq l) \\ W_j + V_j = V_{j+1} & L^2(R) = \bigoplus\limits_{j \in Z} W_j \end{cases} \tag{4.43}$$

In general, $\psi(t)$ is called 'mother wavelet' and W_j is a subspace of the wavelet. Equation (4.39) is called the two-scale equation.

$\{V_j\}_{0 \leq j \leq N}$ is a part of the sequence of MRA in the finite wavelet decomposition. $f_j \in V_j$ is given by:

$$\begin{cases} f_j = \sum\limits_k C_k^j \varphi_{jk}, 0 \leq j \leq N \\ C_k^j = \left(f_j, \varphi_{jk}\right) = (f, \varphi_{jk}) \end{cases} \tag{4.44}$$

where $\{C_k^j\}$ can be understood as the projection of the finite energy signal $f(t)$ on V_j. Information contained in the $f_j \in V_j$ increases with the increase of j. The other terms, $w_j \in W_j$, that contain the rest information of $f(t)$ can be written as:

$$\begin{cases} w_j = \sum\limits_k d_k^j \psi_{jk}, 0 \leq j \leq N-1 \\ d_k^j = \left(w_j, \psi_{jk}\right) = (f, \psi_{jk}) \end{cases} \tag{4.45}$$

where $\{d_k^j\}$ is the projection of $f(t)$ on W_j. This kind of transformation is actually a dyadic wavelet transformation, in which $w_j = f_{j+1} - f_j$ is referred to as the jth level orthogonal decomposition of the signal $f(t)$. The finite wavelet decomposition is given by:

$$f_N = f_M + w_M + w_{M+1} + \cdots + w_{N-1}, M < N-1 \tag{4.46}$$

For a sampling rate of 2^N per second, f_M is the lowest frequency component within the frequency band ranged from 0 to 2^M and $w_j(M \leq j \leq N-1)$ is the jth level orthogonal decomposition of the signal $f(t)$ within the frequency band ranged from 2^{j-1} to 2^j.

4.6.1.3 Wavelet Packet Transform (WPT)

It should be noted that the space localizability of a wavelet base function increases with the increase of j. This helps in improving the space resolving capability. However, it degenerates the localizability of spectrum. Therefore, the wavelet packet is proposed to address this problem by further splitting the spectrum window.

Assume that $h = \{h_n\}_{n \in Z}$ satisfies

$$\sum h_{n-2k} h_{n-2l} = \delta_{kl} \quad \sum h_n = \sqrt{2} \tag{4.47}$$

Let

$$g_n = (-1)^n \overline{h}_{1-n} \tag{4.48}$$

A set of the following recursive functions are defined for a fixed scale:

$$\begin{cases} W_{2n}(t) = \sqrt{2} \sum h_k W_n(2t-k) \\ W_{2n+1}(t) = \sqrt{2} \sum g_k W_n(2t-k) \end{cases} \tag{4.49}$$

where $W_0(t)$ is equal to the above-mentioned function $\varphi(t)$ and $W_1(t)$ corresponds to $\psi(t)$. As a result, $\{W_n(t)\}_{n \in N}$ defined by Equation (4.49) constitutes a wavelet packet determined by $W_0 = \varphi$.

The family of the functions $\{2^{j/2} W_n(2^j t - k) : n \in N, j, k \in Z\}$ derived by multiresolution productive element $\varphi(t)$ is a wavelet depot. A set of orthogonal basis of $L^2(R)$ extracted from the wavelet depot $\{2^{j/2} W_n(2^j t - k) : n \in N, j, k \in Z\}$ is called the wavelet packet basis of $L^2(R)$.

Define

$$\Omega_k = \overline{span\{W_k(t-l), l \in Z\}} \tag{4.50}$$

It has been proven that:

$$\begin{cases} \Omega_0 = V_0 = \overline{span\,\{\varphi\,(t-l)\,, l \in Z\}} \\ \delta^k \Omega_0 = V_k \end{cases} \tag{4.51}$$

Therefore, $\delta^k \Omega_0 \to L^2(R)$ in the case of $k \to \infty$.

Let $x = x(t) \in L^2(R)$; $\{x_p, p \in Z\}$ represent the projection coefficients of x located on $\delta^L \Omega_0$, that is:

$$x_p = \int 2^{L/2} W_0(2^L t - p) x(t) dt \tag{4.52}$$

and

$$\begin{cases} x_p^{2n,s-1} = F_0\,(x^{ns})\,(p) \\ x_p^{2n+1,s-1} = F_1(x^{ns})(p) \end{cases} \tag{4.53}$$

If $0 \le s \le L$ and $0 \le n < 2^{L-s}$, then:

$$x_p^{n,s} = F_{\varepsilon_1} \cdots F_{\varepsilon_{L-s}} \{x^{0L}\}(p) \tag{4.54}$$

Among them, ε_j is the coefficient of the jth term if n is represented by the sum of a series of dyadic terms:

$$\begin{cases} F_0\left\{S_k\right\}(j) = \sum_{k \in Z} S_k h_{k-2j} \\ F_1\{S_k\}(j) = \sum_{k \in Z} S_k g_{k-2j} \end{cases} \tag{4.55}$$

It is well known that wavelet depot is made of wavelet packets. Theoretically, the number of such wavelet packets should be infinite. However, only finite a number of wavelet packets trends uniformly toward the compact space when x^p approaches $\delta^L\Omega_0$.

The projection coefficients, when $2^{s/2}W_n(2^s t-p)$ locates on $\delta^L\Omega_0=\overline{span\{2^{L/2}W_0(2^L t-k),k\in Z\}}$, are given by:

$$x_j = F^*_{\varepsilon_{L-s}}\cdots F^*_{\varepsilon_1}\{1^p\}(j) \tag{4.56}$$

with

$$n=\sum\nolimits_{l=1}^{L-s}\varepsilon_l 2^{l-1}$$

where 1^p is such a sequence in which the only nonzero element, with the value of 1, is located at the position of p.

Consequently, $x_p^{n.s}$ can be obtained by processing the basic sequence $\{1^p,p\in Z\}$ with the operators F_0 and F_1, which are represented by S and D respectively in Figure 4.29. By means of this method, a sequence $\{2^{s/2}W_n(2^s t-p)\}$ consisting of a fast constructive wavelet depot can be easily obtained. The path of F_0 and F_1 forms a dyadic tree. The root of the tree is $\delta^L\Omega_0$ and the leaves of it are $\Omega_0,\ldots,\Omega_{2^{L-1}}$. The tree is graphically described in Figure 4.29.

Considering a function specified by eight sampling data of $\{x_1,\cdots,x_8\}\subset R^8$, and $\{x_i\}_{i=1}^8$ being the projection coefficient of $x(t)$ on $\delta^3\Omega_0$, the periodical wavelet packet coefficients of $x(t)$ are obtained and shown in Figure 4.29.

Obviously, processing one group of the items in one level with the operator F_0 or F_1 will result in two groups of the items in the next level. For each of this processing, the number of the group will be double and the number of the elements in each group will be half. This process continues until every group only contains one element. Each group mentioned above corresponds to a subspace that is represented in Figure 4.30. Those subspaces form Figure 4.29. Those completely covering the orthogonal basis of R^N can be selected to constitute a subset. Equation (4.57) gives an example of such selection.

$$\delta^3\Omega_0=\Omega_0\oplus\Omega_1\oplus\delta^1\Omega_1\oplus\delta^2\Omega_1 \tag{4.57}$$

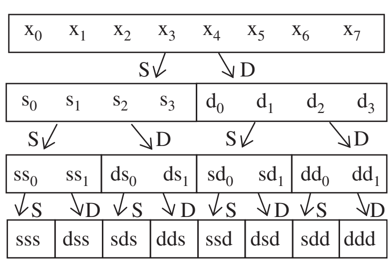

Figure 4.29 Wavelet packet coefficients decomposition

<table>
<tr><td colspan="4">$\delta^2\Omega_0$</td><td colspan="4">$\delta^2\Omega_1$</td></tr>
<tr><td colspan="2">$\delta^1\Omega_0$</td><td colspan="2">$\delta^1\Omega_1$</td><td colspan="2">$\delta^1\Omega_2$</td><td colspan="2">$\delta^1\Omega_3$</td></tr>
<tr><td>Ω_0</td><td>Ω_1</td><td>Ω_2</td><td>Ω_3</td><td>Ω_4</td><td>Ω_5</td><td>Ω_6</td><td>Ω_7</td></tr>
</table>

Figure 4.30 Extraction of orthogonal wavelet packet base

4.6.2 Inrush Identification with WPT

4.6.2.1 Basic Principle

Although both the inrush and the fault current resulting from transformer energizing or fault are of high peak values, inrush is characterized with the distinguished second harmonic component, considerable nonperiodical and transient components. The problem is whether a suitable wavelet transform that can effectively detect the most useful information can be found. Investigation carried out as below shows encouraging results. Differences existing in the higher frequency band of currents provide sufficient evidence to distinguish the inrush and the fault of the transformer. As a result, a new criterion based on the waveform identification is arrived.

It should be pointed out that the degree of smoothness of the compactly supported MRA productive element ϕ is not good enough. It means that the coherence between frequency bands is not ideal if the compactly supported orthogonal wavelet basis productive element ψ is used as a band-pass filter. However, improving the degree of smoothness of ϕ will result in an increase of the length of the subset.

Therefore, the frequency-dividing capability will be useful if $\hat{\psi}(\omega)$ is considered as a band-pass filter. However, with a prolonged subset of $\phi(t)$, the space localizability will be weakened. By comparing the currents of both transformer inrush and different kinds of internal faults and decomposing the sampling data, it is easy to develop an algorithm to find out the difference between the two kinds of waveforms if the normal orthogonal and wavelet algorithm is used.

4.6.2.2 Waveform Identification with the WPT

A complete wavelet packet is available based on the study of the wavelet transform and the multiresolution. A smoothened version and a detailed version are available after executing the mirror filtering on the current waveforms of both the inrush and the fault. Inputting the smooth version and detailed version into the mirror filter again will result in smoother and more detailed versions. This procedure continues until the decomposition finishes. All the versions should be saved in order to select the optimal wavelet packet basis. The optimal wavelet packet basis is selected such that a pre-selected information cost function is maximized. The following information entropy sequence, $x = \{x_j\}$, is used for the present application:

$$M(x) = -\sum_j p_j \log p_j \tag{4.58}$$

where $p_j = \frac{|x_j|^2}{\|x\|_2^2}$, $plogp = 0$ for $p = 0$ and $\|x\|_2^2$ denotes the square of the norm $x = \{x_j\}$.

4.6.2.3 Selection of the Mother Wavelet

Simulation results show that taking Daubechies five-order wavelet as the mother wavelet, the wavelet packet transform for the inrush shows quite different characters on the first scale wavelet decomposition. This means that the best frequency range used to distinguish the inrush and the internal fault of transformers is from 150 to 300 Hz. Therefore, it is used for the present studies.

4.6.3 Results and Analysis

The proposed method has been tested on a physical power system in the laboratory environment. The configuration of the system used is shown in Figure 4.31. Data for the wavelet analysis are sampled for different kinds of internal and external faults with and without inrushes. The sampling frequency is 600 Hz. The data window used for this application is 32 samplings, that is, 20 samplings for the pre-fault and 12 samplings (one cycle) for the post-fault.

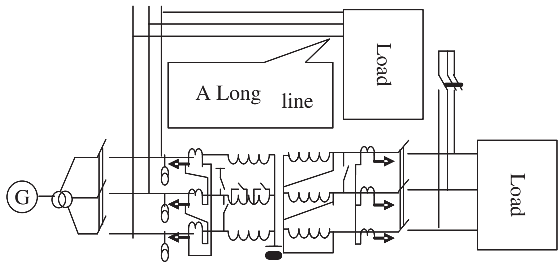

Figure 4.31 Power system model

Considerable number of tests has been carried out to compare the effectiveness of different kinds of wavelet transformation for the inrush identification. The WPT that gives the best results is used for the following tests.

Different kinds of transformer internal and external faults together with or without inrushes have been tested. Also, in order to investigate the influence of the transmission line on the inrush of the transformer, both cases, with and without transmission line connected, have been considered. Test results are given in Figures 4.31–4.37, which show the current waveforms sampled from the power system (called sampled waveform) and the results obtained from the wavelet transformation analysis (WTA) (called WPT results). In these figures, without special specification, the solid line is used for the inrush and the dotted line is for the other cases.

It can be seen from the figures that:

1. Although very few differences exist between the waveforms of the inrushes and the different kinds of transformer internal fault, the wavelet packet transformation results for faults and the inrushes present obvious differences (Figures 4.31–4.37). The waveform of the WPT results for transformer internal

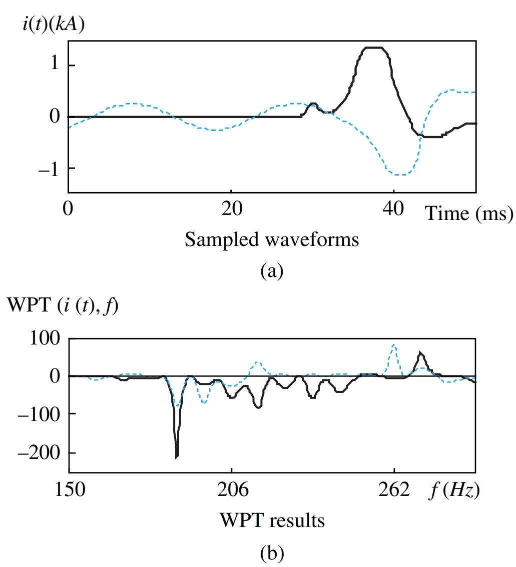

Figure 4.32 Waveforms of an inrush and a single-phase to ground fault without inrush

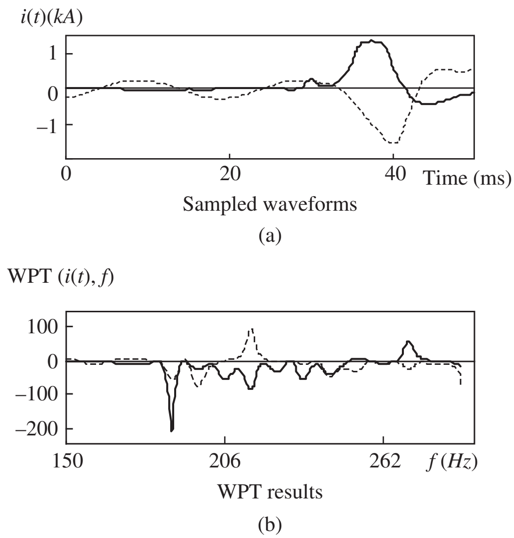

Figure 4.33 Waveforms of inrush with long transmission line and phase to phase internal fault without inrush

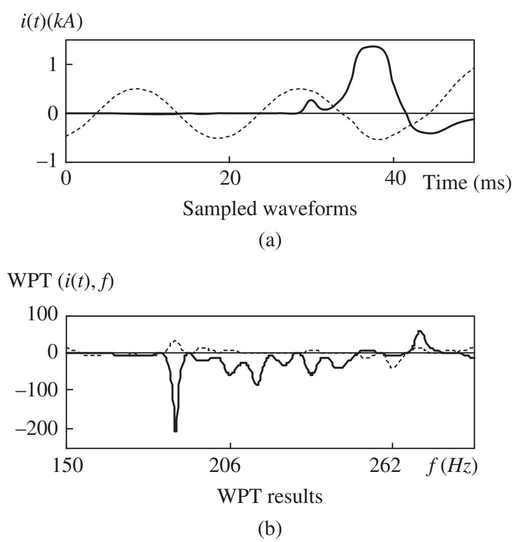

Figure 4.34 Waveforms of an inrush with long line and a winding short-circuit fault without inrush

faults seems quite smooth while that for inrushes presents a large sudden change. As a result, inrushes existing in the power systems can be identified easily.

2. The waveform for the transformer external fault without transmission line is more or less similar to that of inrush with a long transmission line (Figure 4.38). As the external fault can be easily detected by the other conventional protective relay devices, this does not cause any problem.

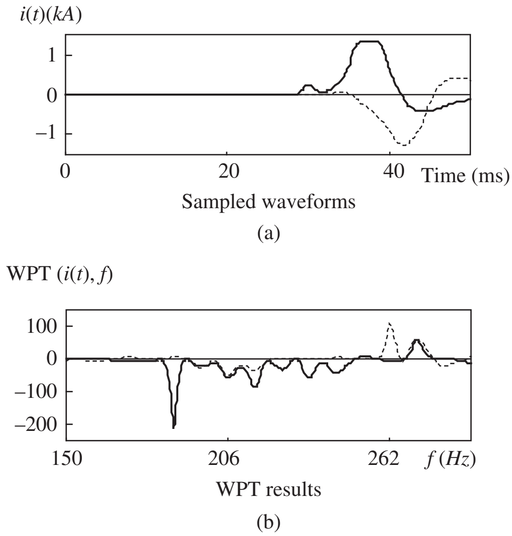

Figure 4.35 Waveforms of the inrush with long transmission line and a single-phase ground fault with inrush

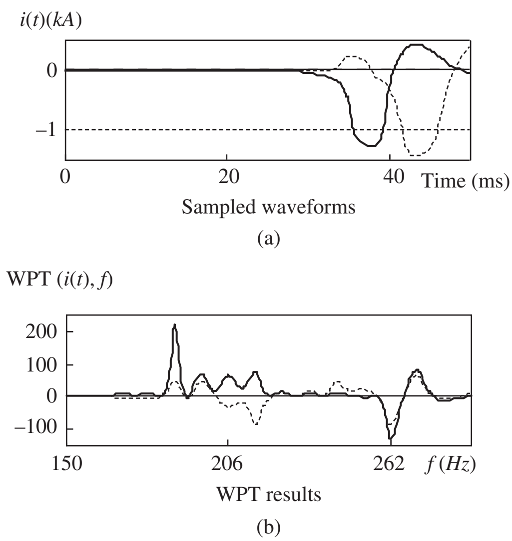

Figure 4.36 Waveforms of the inrush with long transmission line and phase-to-phase fault with inrush

3. The result of WPT for the inrush currents with or without the transmission line presents very few differences (Figure 4.39). However, this will not cause any problem for the correct inrush identification.

It is worth pointing out that all the other wavelet transformation based algorithms presently used are not realizable in real-time, because their data decomposition relies on the whole sampling data instead of a

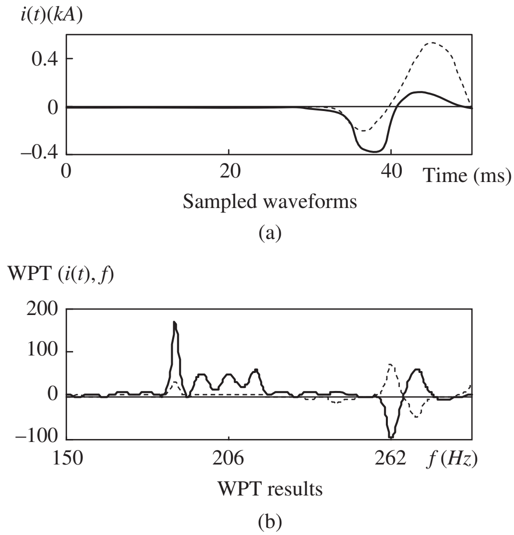

Figure 4.37 Waveforms of the inrush with long transmission line and winding short-circuit fault with inrush

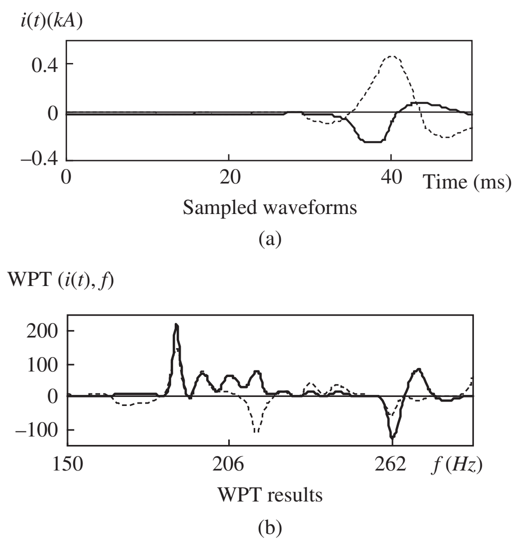

Figure 4.38 Waveforms of inrush with long transmission line and external fault

short data window. The proposed algorithm overcomes this. This is important for the practical application of the wavelet transformation in the power system protection and other applications.

In summary, a new algorithm used for the transformer inrush identification has been developed. The proposed algorithm is based on the wavelet packet transformation. As a relatively short data window is used in the algorithm, it can be realized in real-time applications, which is different from all the other currently used waveform identification based methods. Simulation results show that this algorithm is

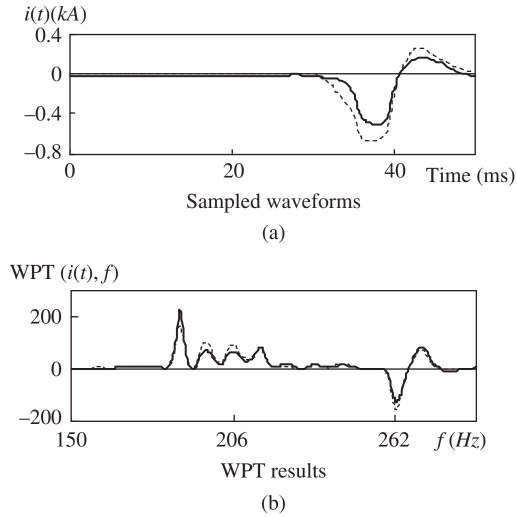

Figure 4.39 Waveforms of inrush without transmission line (solid line) and inrush with long transmission line (dotted line)

effective in distinguishing inrushes from different kinds of transformer internal faults with or without transmission lines.

4.7 A Novel Adaptive Scheme of Discrimination between Internal Faults and Inrush Currents of Transformer Using Mathematical Morphology

4.7.1 Mathematical Morphology

4.7.1.1 The Fundamental Concepts and Basic Operations of Mathematical Morphology

Mathematical Morphology (MM) is known as an image processing technique, where the key points of an image are described by transformations called the dilations and erosions. Dilation is the expansion of a particular shape into another bigger shape, while erosion is shrinking a shape into another shape. Let *f(x)* shown in Figure 4.40a and *g(x)* shown Figure 4.40b denote a one-dimension signal and a structure element (SE) respectively, whose domain of definition are D_f, D_g, $D_f = \{1, \ldots, M\}$, $D_g = \{1, \ldots, N\}$ and $M > N$. Dilation and erosion of *f(x)* by *g(x)* can be computed from the direct formulae:

$$(f \oplus g)(x) = \max\{f(x-y) + g(y) | (x-y) \in D_f; y \in D_g\} \tag{4.59}$$

$$(f \,\Theta\, g)(x) = \min\{f(x+y) - g(y) | (x+y) \in D_f; y \in D_g\} \tag{4.60}$$

where $\oplus$ and Θ denote morphological dilation shown in Figure 4.40c and erosion shown in Figure 4.40d, respectively.

Usually, dilation and erosion are not mutually inversed. They can be combined through cascade connection to form new transforms. If dilation is next to erosion, such cascade transform is an opening transform. The contrary is a closing transform. The transform can be computed using the following formulae respectively:

$$f \circ g = f \,\Theta\, g \oplus g \tag{4.61}$$

$$f \bullet g = f \oplus g \,\Theta\, g \tag{4.62}$$

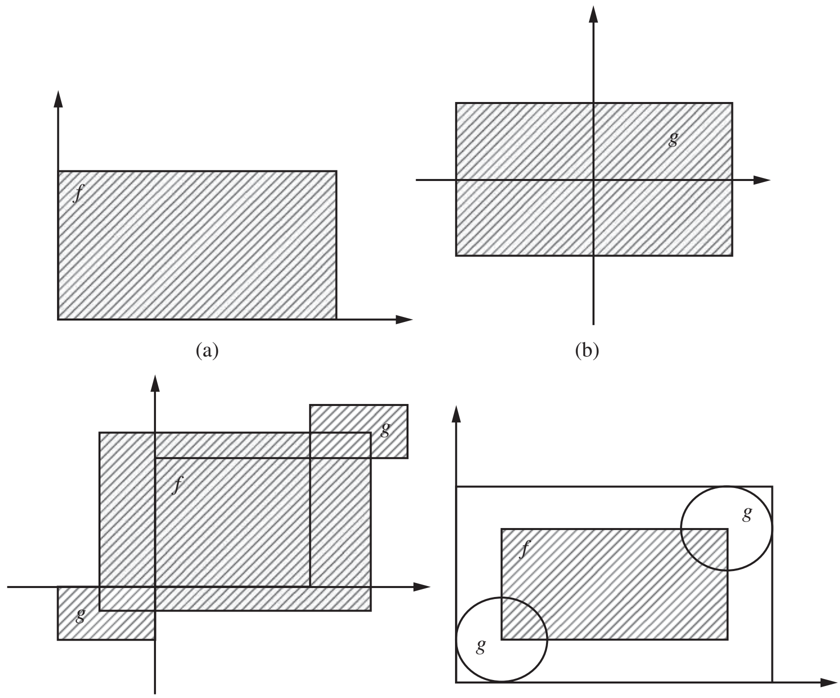

Figure 4.40 Morphological approach to signal using a flat structuring element: (a) original signal; (b) structure element; (c) dilation transformation; (d) erosion transformation

Due to the expansibility of the opening transform, it can be used to remove the peaks in the signal. Due to inverse expansibility of the closing transform, it can be used to fill the valleys in the signal. In order to reject both the positive noise and negative noise together and extract transient signals simultaneously, the differential operation between morphological opening and closing transform is proposed.

4.7.1.2 Novel Morphological Gradient

The basic morphological gradient (MG) is defined as the arithmetic difference between the dilated and eroded function *f(x)* by the SE *g(x)* of the considered grid; it is given by:

$$G_{grad} = (f \oplus g)(x) - (f \ \Theta \ g)(x) \tag{4.63}$$

There is a distinct difference in the meaning of MG from gradient in physics. Frequently, the MG is used for edge detection in image and signal processing.

Since the results of the opening transform and dilation preserve the negative sudden changes, while the results of the closing transform and erosion preserve the positive sudden changes, a novel morphological gradient (NMG) may be used to depress the steady components and, hence, enhance the sudden changes:

$$G_{nmg} = (f \circ g \oplus g)(x) - (f \bullet g \ \Theta \ g)(x) \tag{4.64}$$

The SE acts as a filtering window, in which the data are smoothed to have a similar morphological structure as the SE. The effectiveness and accuracy of the extraction depend on not only the combination mode of different transforms but also on the shapes and width of the SE. The SE with simple geometrical shape, such as a circle or triangle, is preferable; its shape should be selected according to the shape of the processed series. To extract the ascending and descending edges of sudden changes, a symmetrical triangle shape SE is preferable, defined as :{0, …, v, …, 0}. Meanwhile, only if the width of the SE is shorter than that of sudden changes, can all sudden changes be extracted. To obtain the width of the narrowest sudden change, the definition of Open is introduced and described as:

$$\text{Open}\ (i) = |n - j| \text{ when } |\ \text{Peak(j)} - \text{x(n)}| < \delta \tag{4.65}$$

where Open (i) is ith Open value, $I = 1, 2, \ldots, P_n - 1$, P_n is the sum of local maximum points, Peak(j) is the ith local maximum at jth point, x(n) is the value at nth point, n = 1, 2, … , N and δ is a very small predefined threshold.

Based on the above definition of Open, the width of the narrowest sudden change in the data, L_p, is the minimum of the Open values, that is:

$$\mathrm{L_p} = \min\ [\mathrm{Open}(i)], I = 1, 2, \ldots, P_n - 1 \tag{4.66}$$

To verify the effectiveness of the NMG with the Open value, a good example obtained by the EPDL is illustrated in Figure 4.41. Various kinds of white noise are added into the sampled signal. The noise data are shown in Figure 4.41a. Signal noise rate (SNR) is about 35 dB. The formula of SNR is defined as:

$$D_{SNR} = 20 \log(P_S/P_N) \tag{4.67}$$

where P_S is the variance of the original data and P_N is the variance of noises.

Figure 4.41b shows that the NMG has immunity from random noises, since the time-domain variation periods and, thus, the Open values of them differ from sudden changes greatly. The testing data

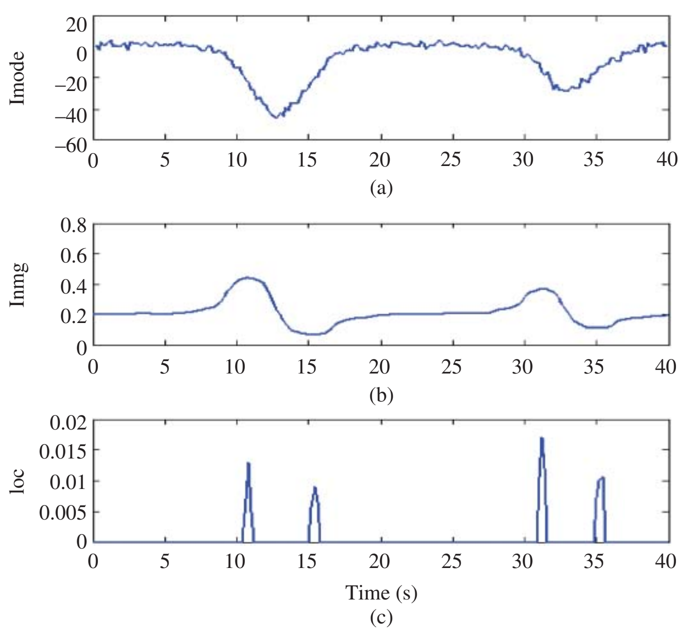

Figure 4.41 Processing results of the Electrical Power Dynamic Laboratory testing data by mathematical morphology method: (a) the SNR; (b) the NMR; (c) the eventually extracted transient signals

Table 4.8 Calculation speed of the mathematical morphology method and FFT

Parameters of sampling rate		Computation time (s)	
Periods	Frequency (Hz)	MM	FFT
10	1600	0.0028	0.0002
10	3200	0.0034	0.0041
30	6400	0.0043	0.0084

are then processed by the differential operation between morphological opening and closing transform. Figure 4.41c shows the transient signals eventually extracted. It is easy to be applied on-line with clear physical meaning and little computational cost.

The calculation speed of the morphology method and fast Fourier transform (FFT) are shown in Table 4.8. When dealing with the equivalent data, the MM method is slower than FFT. However, compared with FFT, the computational time of the MM method is stable, as the sampling rate and data size are increasing, whereas the computational time of FFT has increased significantly together with sampling rate and data size.

4.7.2 Principle and Scheme Design

4.7.2.1 Basic Principle

Inrush can be generated when a transformer is switched on in the transmission line or an external line fault is cleared. Due to the difference of the magnetic permeability in the iron core of the transformer between inrush currents and internal fault currents, the main magnetic flux varies alternately from nonsaturation to saturation in one cycle under the inrush currents, which means their waveforms are distorted. However, the transformer operates in the linear section of the magnetizing curve for internal fault conditions. Therefore 'sudden change' characteristics will not be observed in their waveforms apart from at a fault point.

Since the MM possesses great capability to characterize and recognize an unique feature in the waveforms, which is a series of sudden changes on the waveforms, the proposed principle to distinguish between the magnetizing inrush and internal fault is thus feasible.

4.7.2.2 Scheme Design

Differential current waveforms between phases are taken as the object to be analysed. Take the 'A' – 'B' phase for instance, differential currents between primary and secondary currents of all phases are calculated and are then applied to form three mode signals (I_{abxj}, I_{bcxj}, I_{caxj}) by the formulae:

$$\begin{cases} I_{\mathrm{a}} = I_{\mathrm{a}1} - I_{a2} \\ I_{\mathrm{b}} = I_{\mathrm{b}1} - I_{b2} \\ I_{\mathrm{abxj}} = I_{\mathrm{a}} - I_{\mathrm{b}} \end{cases} \tag{4.68}$$

where $I_{\mathrm{a}1}$, $I_{\mathrm{b}1}$ and $I_{\mathrm{c}1}$ are the primary currents, I_{a2}, I_{b2} and I_{c2} are the secondary currents, and I_{abxj} is the differential current between phases A and B.

The NMG of each current mode is calculated using Equation (4.64) and then is extracted by use of the differential operation between morphological opening and closing transform, through which a few random noises may still exist in the series after being processed and can be used as the detector of the starting point, as illustrated here.

Because of various types of actual transformers and various fault conditions, in order to improve the feasibility and practicability of the scheme, a floating threshold I_{fd} is proposed to evaluate whether or not it is the starting point of protection. I_{fd} is defined as:

$$I_{fd} > K_{k*} I_{ranmax} \tag{4.69}$$

where I_{ranmax} is the maximum value of random noises under normal conditions and is detected using a sliding data window in a half cycle (10 ms), whose value is much smaller than the value of fault-generated or inrush-generated transient signals. K_k is the proportion factor.

Then, N, the number of fault or inrush generated transient signals, is added from the starting point in one and a half cycles if $I_{ts} > k' \times I_{fd}$, where I_{ts} is the value of fault or inrush generated transient signals and k' is the attenuation factor.

If N of each mode is more than or equal to three, it indicates that there is a current inrush and the relay is inhibited from tripping. On the contrary, the relay gives the correct response since there is an internal fault. The transformer protection scheme block diagram is shown in Figure 4.42.

4.7.3 Testing Results and Analysis

4.7.3.1 Electrical Power Dynamic Laboratory Testing System

To verify the feasibility of the proposed method, the author obtained a large number of actual data through the EPDL simulation. Figure 4.43 shows the connection scheme of the EPDL testing system. The transformer is a Y/Δ-11 connection transformer consisting of three single-phase units. Parameters of each singlephase are: $S_{rated} = 10$ kVA; rated voltage ratio, $U_{1N}/U_{2N} = 1000$ V/380 V; $I_{no\text{-}load} = 1.45\%$; $U_{shortcircuit} = 9.0–15.0\%$; losses of open circuit 1%; losses of short circuit 0.35%. The sampling frequency used is 5 kHz.

4.7.3.2 Responses to Different Inrush Conditions

Figures 4.44a and 4.45a show the current modes obtained from the typical asymmetrical and symmetrical inrush conditions, respectively. Figures 4.44b and 4.45b show the corresponding signals from the NMG

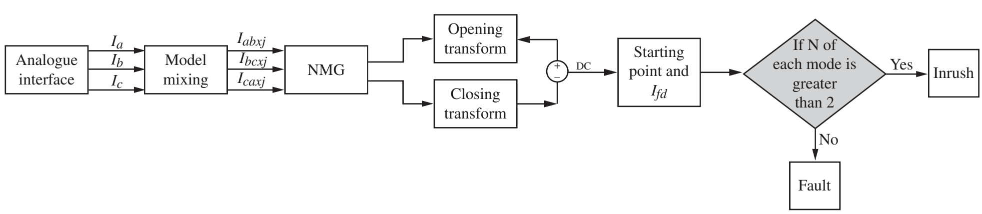

Figure 4.42 Block diagram of the transformer protection scheme

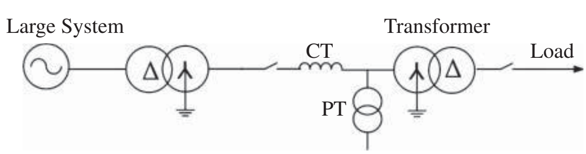

Figure 4.43 Connection scheme of the EPDL testing system

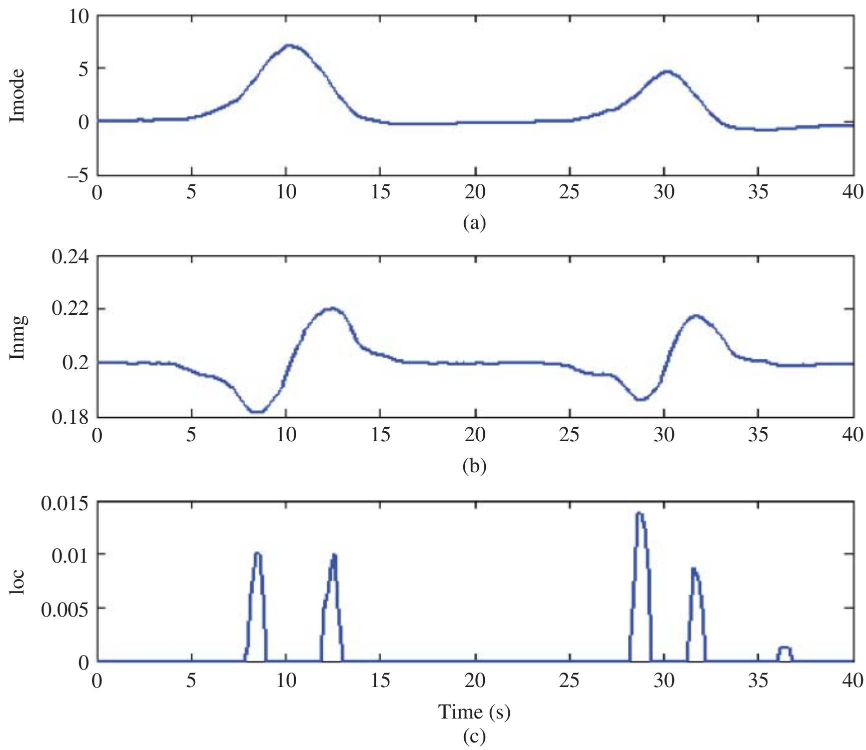

Figure 4.44 The case of asymmetrical inrush: (a) the current modes obtained from the typical asymmetrical inrush conditions; (b) the output of NMG; (c) the transient signals extracted by the differential operation between morphological opening and closing transform

outputs, respectively. As shown in figures, the variations in inrush wave shapes have resulted in variations in the NMG outputs.

Figures 4.44c and 4.45c show the transient signals extracted by the differential operation between the morphological opening and closing transforms, respectively. DC components are depressed by the differential operation, meanwhile peaks and valleys of sudden changes can be extracted effectively. According to the scheme introduced above, N is equal to four in the case of asymmetrical inrush and equal to five in the case of symmetrical inrush. Therefore, the relay will be inhibited from issuing a trip signal in both cases. Compared with this method, Fourier transform-based schemes have difficulties in filtering DC components if some disturbing signals are superimposed.

4.7.3.3 Responses to Internal Fault Conditions

Figure 4.46 shows the corresponding responses to a 9% turn-turn fault on phase ‘A.’ The NMG output in Figure 4.46b illustrates sudden changes of internal faults are much less severe compared with inrush currents. With the transient signals shown in Figure 4.46c fast decaying, internal fault currents can be discriminated from inrush currents since N, the number of fault-generated transient signals, is only equal to one. Though there are still a few random noises, their values are too small to be considered as I_{ts}. As a result, the relay operates.

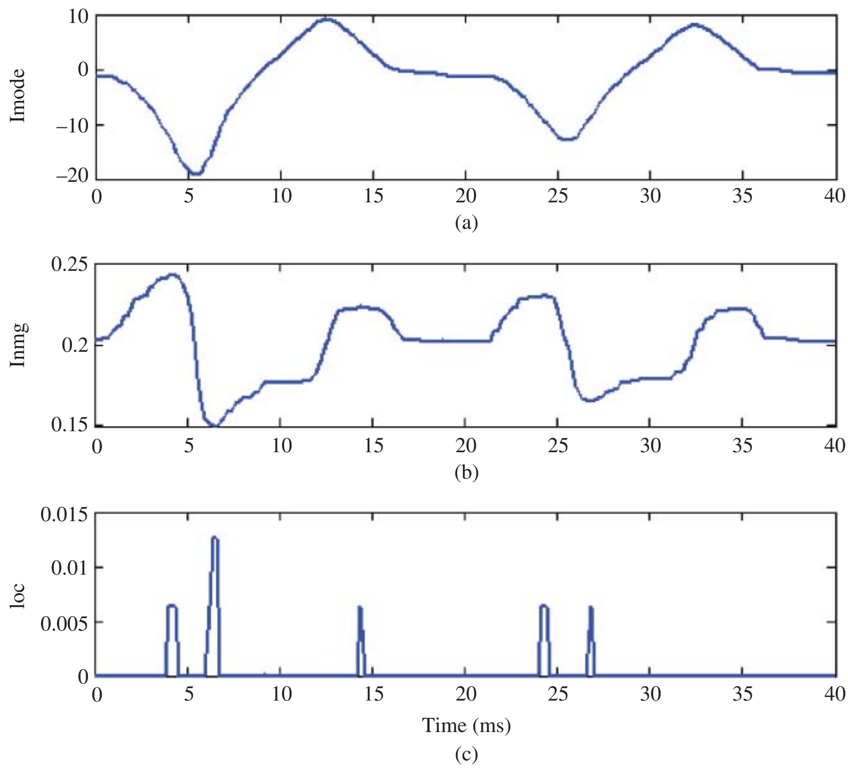

Figure 4.45 The case of symmetrical inrush: (a) the current modes obtained from the typical symmetrical inrush conditions; (b) the output of NMG; (c) the transient signals extracted by the differential operation between morphological opening and closing transform

4.7.3.4 Responses to Simultaneous Fault and Inrush Conditions

Figure 4.47 shows the corresponding responses of the inrush to a light internal fault. As shown in the figure, whose variation trends are similar to Figure 4.46, high frequency transient signals are decaying instantaneously right after the fault point. N is also equal to one in this case, which leads to the final decision that this is an internal fault as shown in Figure 4.47c.

The distortion degree in spite of inrush to an internal fault attenuates rapidly, while the waveforms of magnetizing inrush currents are distorted more severely due to enlargement of the dead angle.

4.7.3.5 Responses to CT Saturation Conditions

If the conditions are severe enough, it is possible that the distortion may be even worse and saturation can start to occur even sooner. The severe saturation can cause problems in the transformer differential relays. Figure 4.48a shows the responses obtained due to a simultaneous internal fault and CT (located at the low voltage side) saturation. As shown in Figure 4.48b, the variations in inrush waveforms due to CT saturation do not have any effect on the relay responses, since N is also equal to one and relay operates in this case. Compared with restraining algorithm based on second harmonics, the ratio of second harmonics

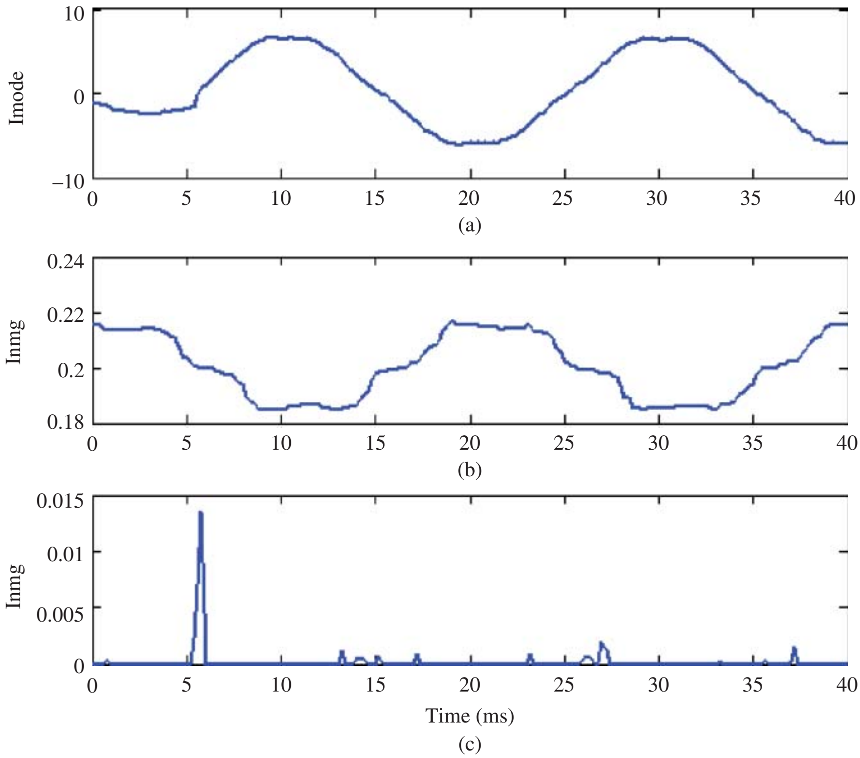

Figure 4.46 The case of internal fault current: (a) the corresponding responses to a 9% turn-turn fault on phase 'A'; (b) the output of NMG; (c) the transient signals

after CT saturation is 26.7% and exceeds the predefined threshold 15%, which makes the relay give an incorrect response.

Furthermore, due to the slowly decaying offset components of inrush currents, CTs can and do saturate during inrush with no internal fault. Due to a simultaneous asymmetrical inrush current and CT saturation, the waveform of asymmetrical inrush current is distorted more and more severely while the dead angle is extinct after about one power frequency cycle (Figure 4.49a). However, in this case, the output of N is equal to five (Figure 4.49b), so the relay will be inhibited from issuing a trip signal. Compared with the restraining algorithm based on second harmonics, the ratios of second harmonic to fundamental before and after CT saturation are 26.9 and 32.1%, respectively, which makes the relay give a correct response. In addition, compared with the WCS, the waveform coefficients are 0.17 before CT saturation and 0.43 after CT saturation. The relay can also be inhibited from tripping. However, the redundancy of this scheme is small.

4.7.3.6 Responses to Internal Faults with External Shunt Capacitance

Since the second harmonic components in fault currents are increased together with the capacitance in the power system, the proposed technique is used to avoid the needless relay blocking when a transformer has an internal failure. Figure 4.50 shows a waveform of differential current in the case of short-circuit fault

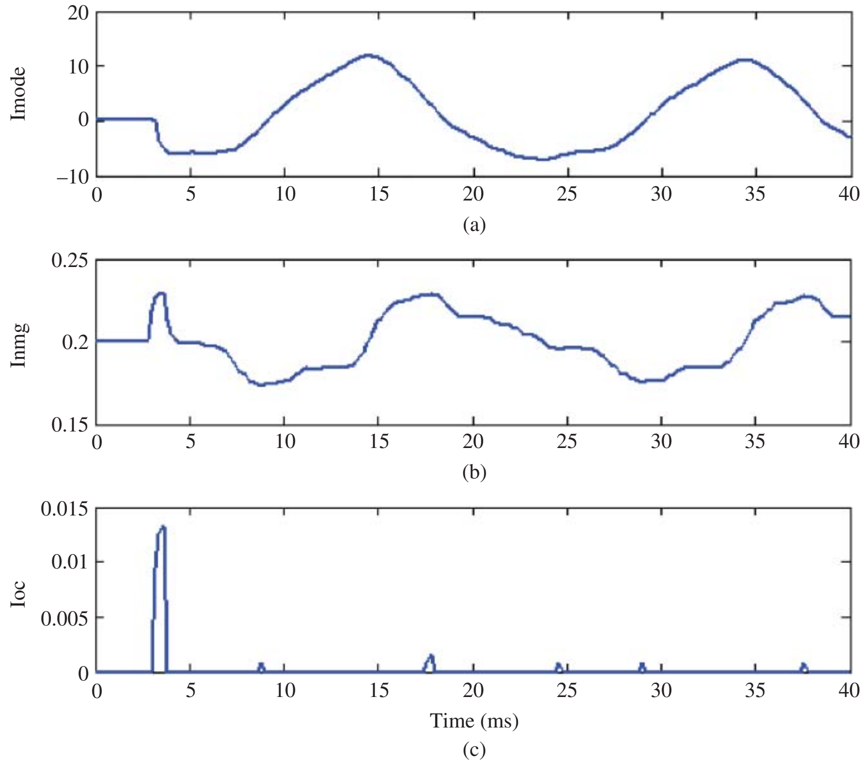

Figure 4.47 The case of inrush due to a light internal fault current: (a) the corresponding responses of the inrush; (b) the output of NMG; (c) the transient signals

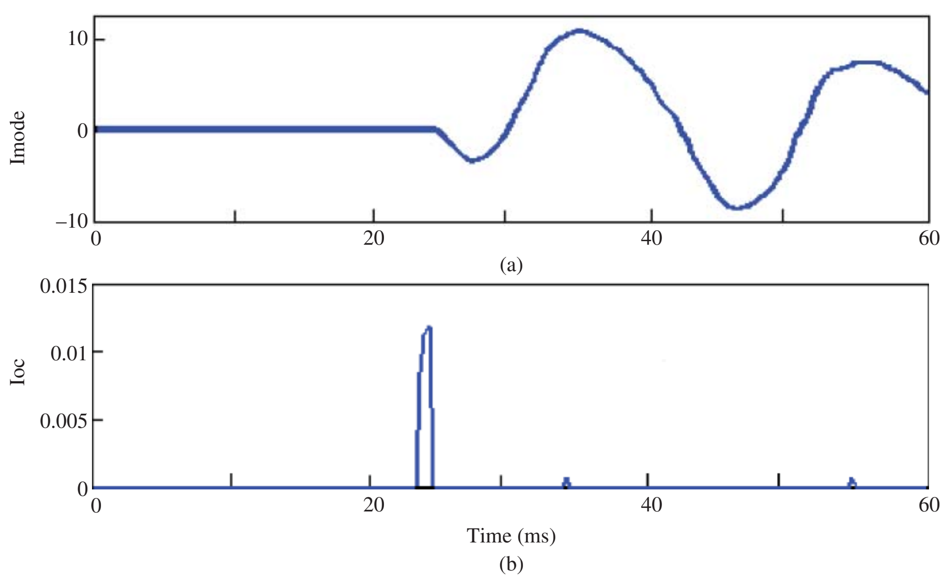

Figure 4.48 (a) The responses due to a simultaneous internal fault and CT saturation; (b) the output of N

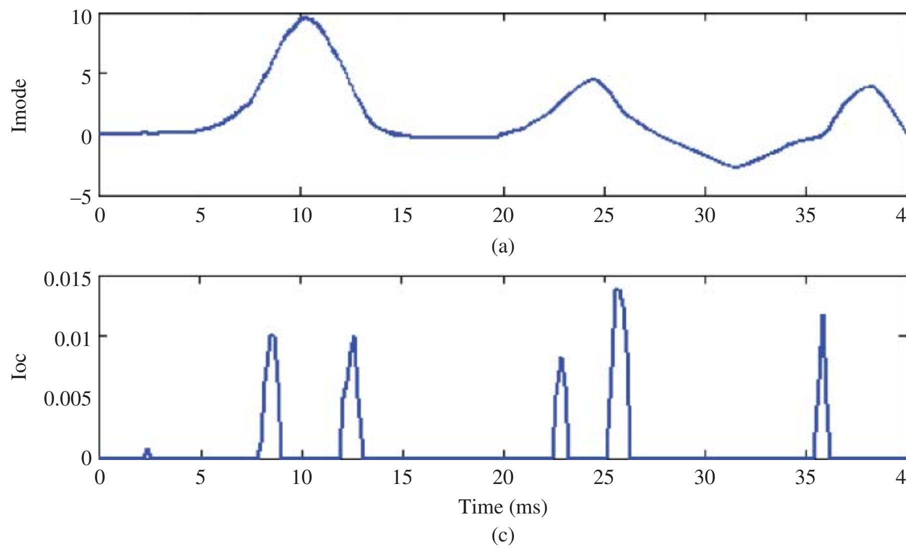

Figure 4.49 (a) The responses due to a simultaneous asymmetrical inrush current and CT saturation; (b) the output of N

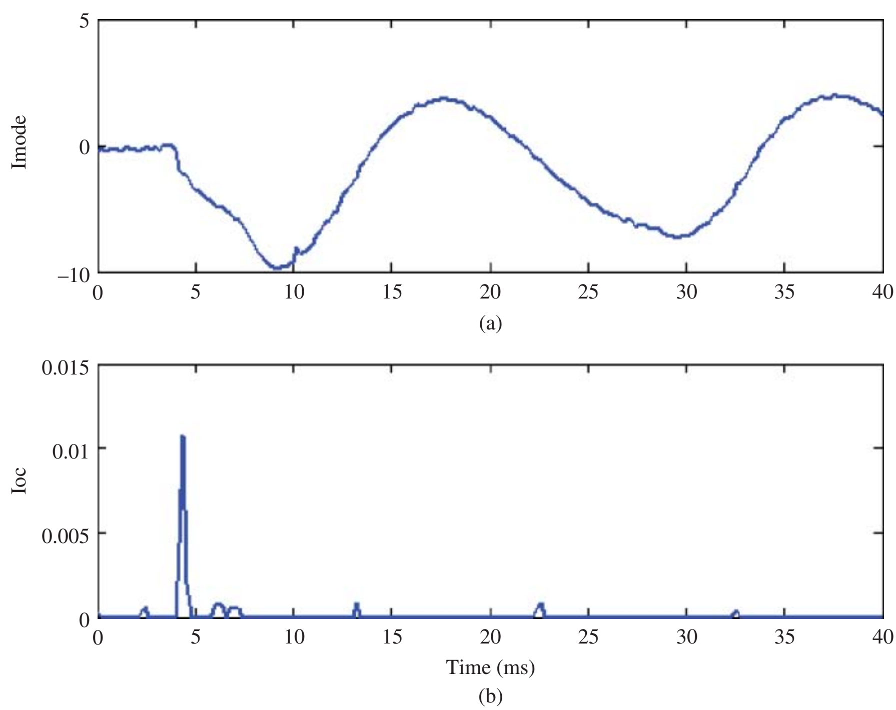

Figure 4.50 The case of an internal fault current with external shunt capacitance: (a) the differential current in the case of short-circuit fault on phase C of a 670 MVA transformer; (b) the output of N

Table 4.9 Parameters of the test transformer (internal faults with external shunt capacitance)

Transformer type	Three-phase, two-winding
Rated apparent power (MVA)	670
Rated voltage ratio (kV)	19/500
Connection style	Y/Δ-11
Short circuit reactance (%)	13.0
Rated frequency (Hz)	50

on phase ‘C’ of a 670 MVA transformer, the parameters of which are shown in Table 4.9. A 20.26 kA power source, a 257 km overhead 500 kV transmission line and the transformer mentioned above are simulated through EPDL. It includes nearly 33.9% second harmonic and conventional relays are locked. However, in this case, N is equal to one which indicates this is an internal fault and the relay operates correctly.

The results at the EPDL indicate that the proposed technique can distinguish the magnetizing inrush from internal faults in a power transformer and avoid the symmetrical inrush current and CT saturation.

It can also deal with the sampled data containing various kinds of noise and DC components and is stable during internal faults with external shunt capacitance in a long EHV transmission line.

4.7.3.7 Test Results and Analysis

For convenience, typical EPDL simulation cases are outlined in Table 4.10 and are numbered to indicate operation conditions. Cases 0–6 are different magnetizing inrush conditions. N of three model signals are all more than or equal to four.

Table 4.10 EPDL simulation cases

Case	Description	
1–6	Inrush currents only	
7	3% turn-turn fault in phase ‘A’	Internal fault only
8	5% turn-turn fault in phase ‘B’	
9	5% turn-turn fault in phase ‘C’	
10	Turn-to-earth fault in phase ‘A’	
11	Turn-to-earth fault in phase ‘B’	
12	‘A’–‘B’ phase fault	
13	‘B’–‘C’ phase fault	
14	3% turn-turn fault in phase ‘A’	Simultaneous fault and inrush
15	4% turn-turn fault in phase ‘B’	
16	4% turn-turn fault in phase ‘C’	
17	Turn-to-earth fault in phase ‘A’	
18	Turn-to-earth fault in phase ‘B’	
19	‘A’–‘B’ phase fault	
20	‘B’–‘C’ phase fault	

Case 7 is a 9% turn-turn fault on phase 'A'. Case 8 is an 18% turn-turn fault on phase 'B'. Case 9 is an 18% turn-turn fault on phase 'C'. Case 10 is a turn-to-earth fault on phase 'A'. Case 11 is a turn-to-earth fault on phase 'B'. Case 12 is an 'A' – 'B' phase fault. Case 13 is a 'B' – 'C' phase fault. N of three mode signals are all less than or equal to one.

Case 14 is the inrush to a 9% turn-turn fault on phase 'A'. Case 15 is the inrush to an 18% turn-turn fault on phase 'B'. Case 16 is the inrush to an 18% turn-turn fault on phase 'C'. Case 17 is the inrush to a turn-to-earth fault on phase 'A'. Case 18 is the inrush to a turn-to-earth fault on phase 'B'. Case 19 is the inrush to an 'A' – 'B' phase fault. Case 20 is the inrush to a 'B' – 'C' phase fault. Mainly due to the loose coupling between phases in the condition of inrush to light internal faults, partial mode signals in case 14–16 cannot meet the requirement that N is less than or equal to two; however, taking all three mode signals for comprehensive consideration, the relay operates correctly as a result. As shown in Table 4.10 inrush currents can be distinguished from internal fault currents by this scheme.

The performances of the proposed technique are evaluated for different types of internal faults and magnetizing inrush currents. Dynamic simulation results and N of three model signals under various states are shown in Table 4.11. In the results column, '0' indicates that the relay will be inhibited from issuing a trip signal, while '1' indicates that this is an internal fault and the relay operates.

4.7.3.8 Comparison between the MM and WT Methods

The comparison between the proposed MM technique and WT method has been undertaken. A 2B-spline wavelet is employed to process the input signal. The same alternate trend is also denoted in the 2B-spline wavelet transform. However, compared with the filtered series shown in Figure 4.44b, the

Table 4.11 Dynamic simulation results of three model signals under various states

Case	N of I_{abxj}	N of I_{bcxj}	N of I_{caxj}	Results
1	4	4	5	0
2	5	8	4	0
3	6	5	4	0
4	4	7	4	0
5	8	4	6	0
6	6	4	8	0
7	1	0	1	1
8	1	1	1	1
9	0	1	1	1
10	1	1	1	1
11	1	1	0	1
12	1	1	1	1
13	1	1	1	1
14	1	4	2	1
15	1	1	3	1
16	4	1	1	1
17	1	2	1	1
18	1	1	1	1
19	1	1	2	1
20	1	2	1	1

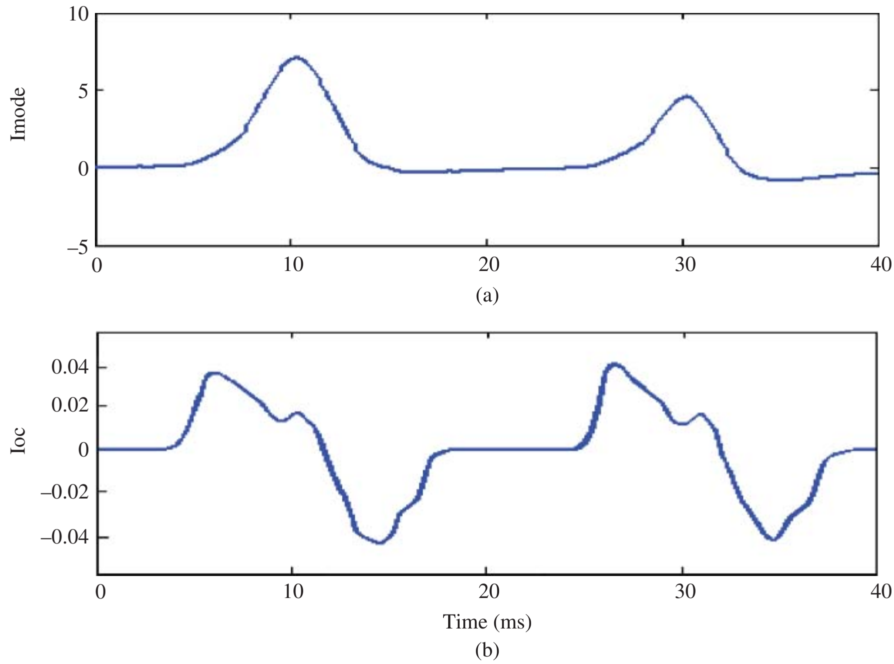

Figure 4.51 Waveform of the asymmetrical inrush current and its 2B-spline wavelet transform: (a) the response when a 2B-spline wavelet is employed; (b) the output of N

trend in Figure 4.51b is less stationary and smooth, with some small concave variations still existing in the series that may generate false transient signals and cause error in the number N. As a result, the relay will give an incorrect response.

In summary, a new scheme to extract the high frequency transient signals of the transformer is proposed based on the high nonlinearity characteristics in excited cores of transformers. The feature extraction with MM can be implemented in real time, since the MM requires only a small amount of computation. Meanwhile, DC components and various kinds of noises can be effectively depressed. The technique also includes a floating threshold to improve its flexibility and feasibility and blocks the relay even under symmetrical inrush current conditions. The proposed technique is stable and reliable during CT saturation and internal faults with external shunt capacitance in a long EHV transmission line. The results in the EPDL show that this scheme is effective and accurate in distinguishing between a current inrush and an internal fault.

4.8 Identifying Transformer Inrush Current Based on Normalized Grille Curve

4.8.1 Normalized Grille Curve

4.8.1.1 Introduction to Grille Curve

Here N_d is defined as the number of the square grids needed with the sampling time d as its side length, covering the differential current for a window of half cycle $[t_k - T/2, t_k]$ as shown in Figures 4.52 and 4.53.

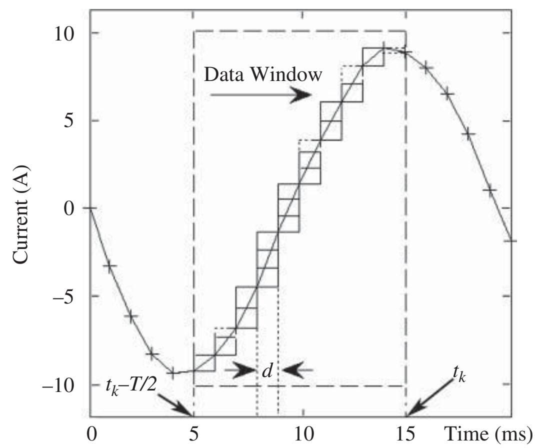

Figure 4.52 The needed square grids covering the differential current at a certain interval when an internal fault occurs

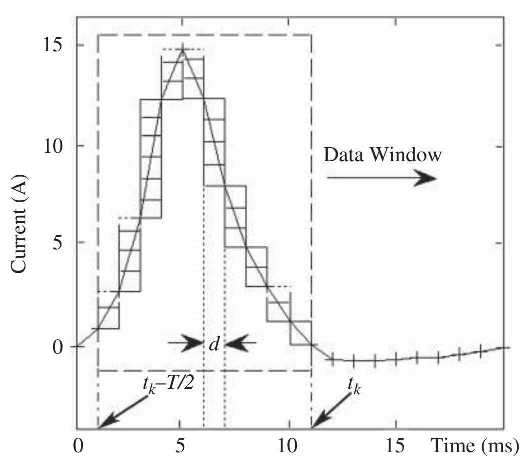

Figure 4.53 The needed square grids covering the differential current at a certain interval when the transformer is energized

The number of needed square grids between two sampling points is calculated by division between their vertical distance and the sampling time d. The grid with the real lines indicates that it is a full square grid, whereas the grid with the dashed lines indicates that it is a fractional square grid. Furthermore, N_d, the number of needed square grids for a window of half cycle, is calculated by adding all square grids (full square grids and fractional square grids) in a half cycle period. Suppose that the signal has $n+1$ sampling points at $(t_{i-n}, t_{i-n+1}, \ldots, t_i)$ within the data window $[t_k - T/2, t_k]$, then:

$$N_d(i) = \frac{1}{d} \sum_{j=i-n}^{j=i-1} |i(t_j) - i(t_{j+1})| \tag{4.70}$$

where d is the sampling time.

Two cases are given to illustrate conceptually the advantages of the grille curve method.

Figure 4.52 shows the internal fault case of power transformer. The iron core is not saturated and the magnetizing current is very small, which results in the approximate sine waveform due to the operation in the linear region of the magnetizing characteristic. If t is a half cycle, the N_d curve, which is also called the grille curve (Figure 4.54), is kept at an almost constant value during any t interval.

In the case of inrush current, the iron core will alternate between saturation and nonsaturation, which causes distortions and discontinuities (much different from the normal sine waveform) shown in Figure 4.53. In this instance, the grille curve, as shown in Figure 4.55, keeps on changing severely. Therefore, the variation of grille curve can be used to discriminate the inrush current from the internal fault current.

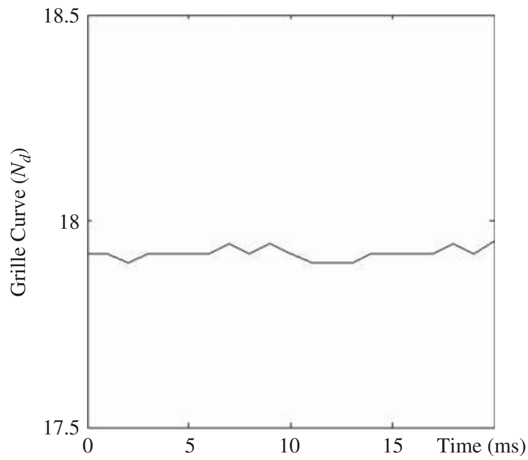

Figure 4.54 The grille curve (N_d) when an internal fault occurs

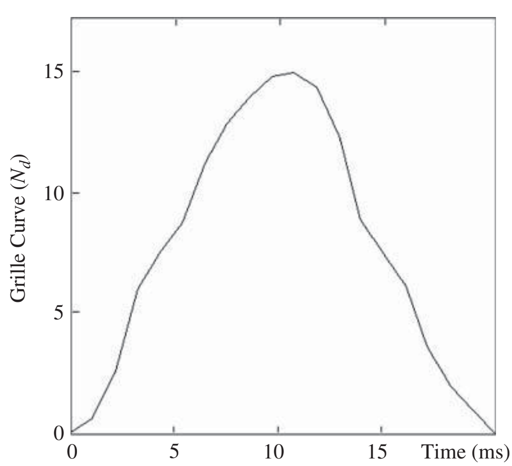

Figure 4.55 The grille curve (N_d) when the transformer is energized

Calculation of Normalized Grille Curves

The normalization of the grille curve is given by:

$$B_d(i) = N_d(i)/\max(N_d) \tag{4.71}$$

where $i = 1, \ldots, M$ and M is the number of the N_d. If $M = 1$, the maximum value of N_d is N_d (1). If $M = 2$, $\max(N_d)$ is the maximum value of N_d (1) and N_d (2). If N_d (1), … , N_d (M) are obtained, $\max(N_d)$ is the maximum value among N_d (1), … , N_d (M). $B_d(i)$ is the ith value in the NGC. The maximum value of the B_d is 1 and the range of the B_d is between 0 and 1.

NGC-Based Criteria to Identify the Inrush

Two criteria are proposed, in the time domain and in the frequency domain, respectively. The method in the time domain directly detects the variation of the NGC, while that in the frequency domain indirectly reflects the variation by using the ratio between the fundamental frequency component and the DC component.

1. *Time domain method*

   The variation of the NGC is directly calculated using the root mean square (RMS) amplitude given by:

$$E_d = \frac{1}{M}\sum_{i=1}^{M} B_d(i) \tag{4.72}$$

$$g = \frac{1}{E_d}\sqrt{\frac{1}{M}\sum_{i=1}^{M}(E_d - B_d(i))^2} \tag{4.73}$$

   g is employed to distinguish the inrush current from the internal fault according to following criterion: if g exceeds a threshold, the relay judges that there is an inrush current and rejects the tripping; otherwise, the relay judges that an internal fault occurs if g is less than the threshold. The threshold should be set to avoid the needless operation by the measurement error and the calculation error.

2. *Frequency domain method*

   The fundamental frequency component of the NGC is almost zero and the DC component of the NGC is noticeable during an internal fault. However, both the fundamental frequency and DC components of the NGC reveal different characteristics during the inrush current, for the reason that the NGC not only severely varies but also has a periodic interval between two minimum values. Therefore, the ratio p between the fundamental frequency and DC components can be used as the criterion for identifying the inrush: if p is larger than the threshold, then the decision is made of an inrush current in the transformer and the relay tripping of the differential protection blocked.; otherwise, the decision is of detection of an internal fault and the relay let trip. The ratio p can be calculated by using Fourier analysis.

3. *Analysis of NGCs in the time and frequency domains*

   The calculated NGCs of the two cases in Figures 4.54 and 4.55 are analysed in the time and frequency domains, respectively. For the case of the internal fault, both g and p are negligible and are less than 0.05, as shown in Figure 4.56. However, for the case of inrush current, both g and p are noticeable, as shown in Figure 4.57. g is more than 0.65 and p is more than 0.45.

4.8.2 Experimental System

To verify the effectiveness of the proposed method, experimental tests have been carried out at the EPDL. The experimental transformer is a three-phase, two-winding transformer bank with Y/Δ-11 connection,

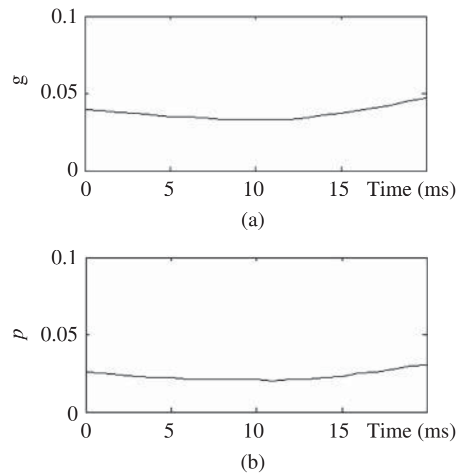

Figure 4.56 The *g* and *p* when an internal fault occurs: (a) analysis of the calculated NGCs in the time domain; (b) analysis of the calculated NGCs in the frequency domain

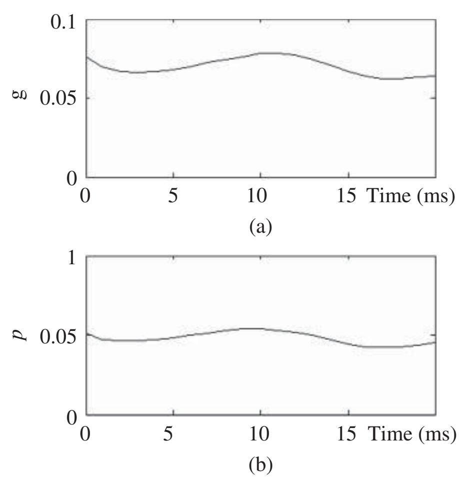

Figure 4.57 The *g* and *p* when the transformer is energized: (a) analysis of the calculated NGCs in the time domain; (b) analysis of the calculated NGCs in the frequency domain

which is fed by a low impedance source (Figure 4.58). The parameters of the two-winding transformer are given in Table 4.12. Three identical CTs are connected in Δ on the primary side, and another three identical CTs are connected in Y on the secondary side of the power transformer.

The experiments provide different switching and clearing instants for inrush currents, as well as different faults and a different number of turns for internal faults. A total of 268 cases have been tested and divided into five main categories: 56 cases for switching on the transformer with no load, 54 cases for faulty conditions only, 52 cases for simultaneous internal fault and inrush conditions, 54 cases for external faults with the CT in saturation conditions and 52 cases for internal faults with the CT in saturation conditions, to test the algorithm.

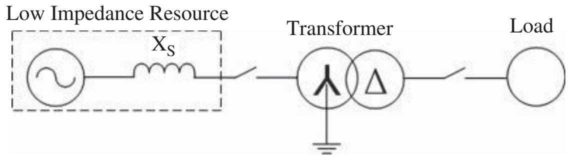

Figure 4.58 Experimental system at the EPDL

Table 4.12 Parameters of each single phase unit of the transformer used in the test

Rated power (kVA)	10
Rated voltage ratio (V)	1000/380
Rated frequency (Hz)	50
No load current (%)	1.45
No load loss (%)	1
Short circuit voltage (%)	9.0–15.0
Short circuit loss (%)	0.35

4.8.3 Testing Results and Analysis

Figures 4.59–4.61 show some examples of the experimental test results: the differential currents and the waveforms of the calculated NGC along with the resulting analysis. In addition, the threshold of g in the time domain is set at 0.25 and the threshold of p in the frequency domain is set at 0.15.

4.8.3.1 Responses to Different Inrush Conditions

A total of 56 tests were carried out in this situation. The inrush current waveform is a function of the different core residual magnetization and the switching instant, so the inrush current waveforms are different from each other. However, in each case, the calculated NGCs alternate between 0 and 1 with a period of one cycle and the maximum value of the NGCs is 1. An example taken from these cases is given in Figure 4.59a, where the differential currents of the three phases represent the inrush currents. The NGCs of the three phases along with their respective results in the time and frequency domains are shown in Figure 4.59b–d. It is found that the calculated NGCs present distorted oscillatory waveform, which is the key feature of the inrush current. Their analysis results in the frequency domain also show the noticeable ratio between the fundamental frequency and DC components in the calculated NGCs. These results indicate the severe variation of NGCs and the alternate saturation and exit-saturation of the transformer core during the inrush current period.

4.8.3.2 Responses to Internal Fault Conditions Only

Data from a total of 54 cases are used to calculate the NGCs. Their results have been analysed both in the time domain and in the frequency domain. An example is shown in Figure 4.60, where a 6.1% turn-to-turn internal fault occurs in phase A.

In Figure 4.60a, it can be seen that the differential currents i_{ab} and i_{ca} are larger than the nominal magnetizing current and contain a slowly decaying DC component, whereas i_{bc} is within the range of

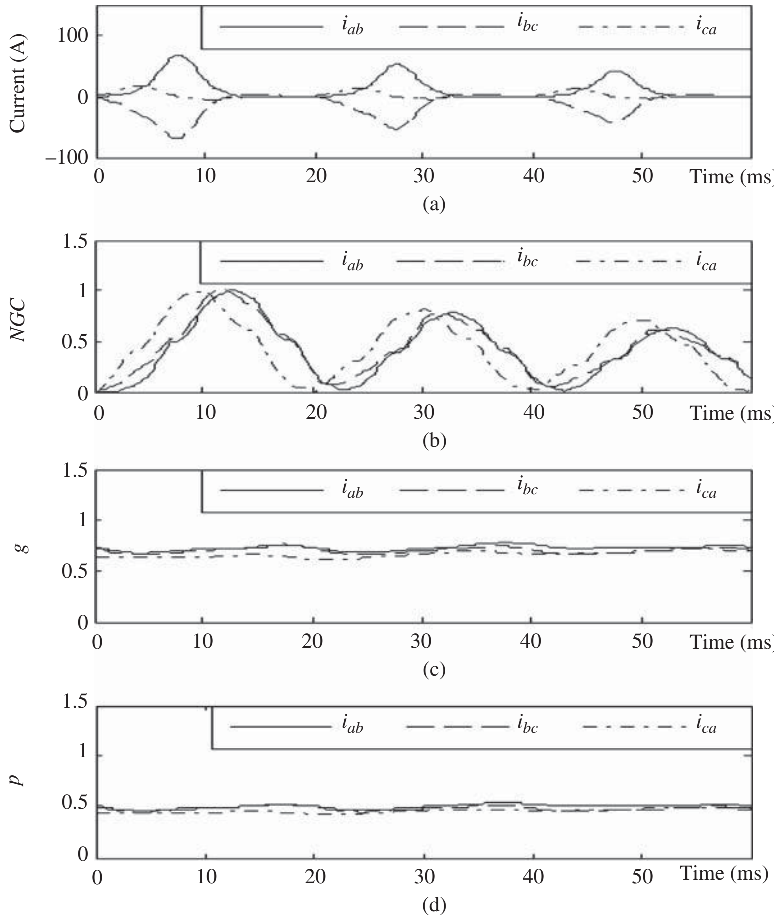

Figure 4.59 Differential currents and experimental results when the transformer is energized. (a) Differential currents, (b) calculated NGCs, (c) analysis of the calculated NGCs in the time domain, and (d) analysis of the calculated NGCs in the frequency domain

the nominal value. Therefore, it is necessary to calculate the NGCs of i_{ab} and i_{ca}, and further analyse them in the time and frequency domains. The calculated NGCs along with their analysis in the time and frequency domains are shown in Figure 4.60b–d. In the time domain, due to the slowly decaying DC component, the positive and the negative half cycles of i_{ab} and i_{ca} are not symmetrical while the DC component is significant. Accordingly, the variation of each NGC calculated by Equation (4.73) presents a higher amplitude in the first 30 ms compared with that in the next 30 ms. But even in the first 30 ms the amplitude of variation is still less than the threshold (Figure 4.60c). In the frequency domain, the calculated NGCs of both phases contain negligible ratios between the fundamental frequency and DC components (Figure 4.60d), which proves that i_{ab} and i_{ca} are both internal fault currents. In the total of 54 cases, it is found that the method is able to detect the internal fault current even with the decaying dc component.

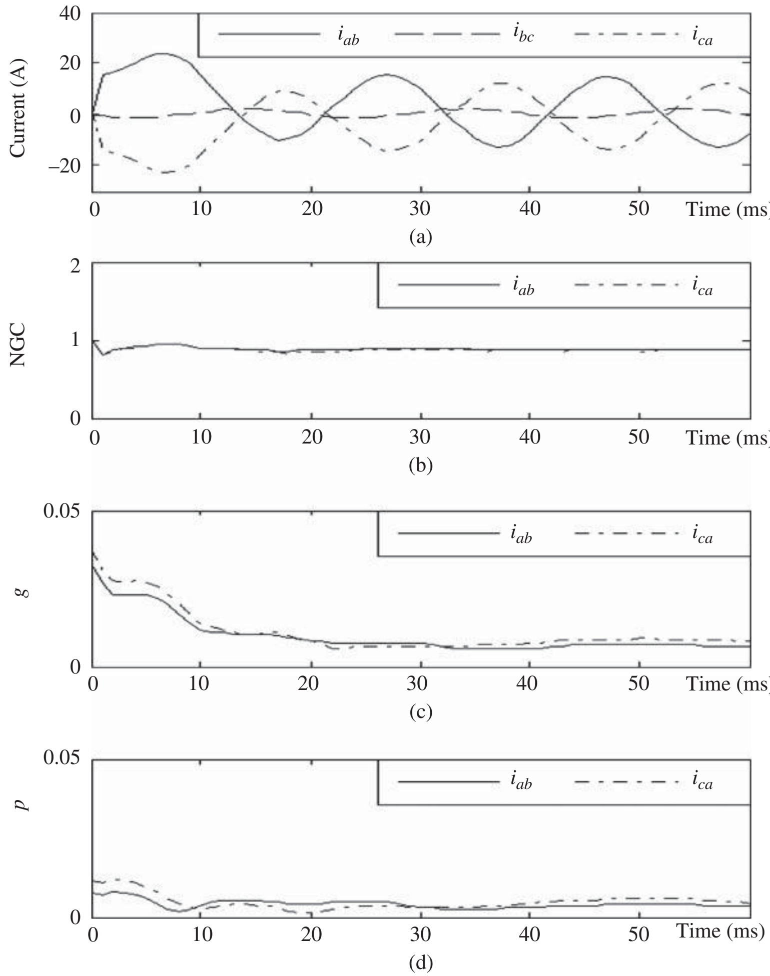

Figure 4.60 Differential currents and experimental results when a 6.1% turn-to-turn internal fault occurs. (a) Differential currents, (b) calculated NGCs, (c) analysis of the calculated NGCs in the time domain, and (d) analysis of the calculated NGCs in the frequency domain

4.8.3.3 Responses to Simultaneous Fault and Inrush Conditions

Switching on the transformer bank with no load often causes the inrush current of nonfault phases, which has been verified by a total of 52 cases with simultaneous inrush currents and internal faults. Figure 4.61 is an example showing this situation; it is obtained by switching on the transformer bank with no load and a 6.1% turn-to-turn internal fault in phase A. The differential currents of the three phases are all distorted severely (Figure 4.61a). After analysis in the frequency domain, it can be found that the magnitudes of the second harmonic in fault phases A and C are greater than that of some magnetizing inrush currents. Consequently, the commonly employed conventional differential protection technique based on the second harmonic will thus have difficulty in distinguishing between an internal fault and an inrush current.

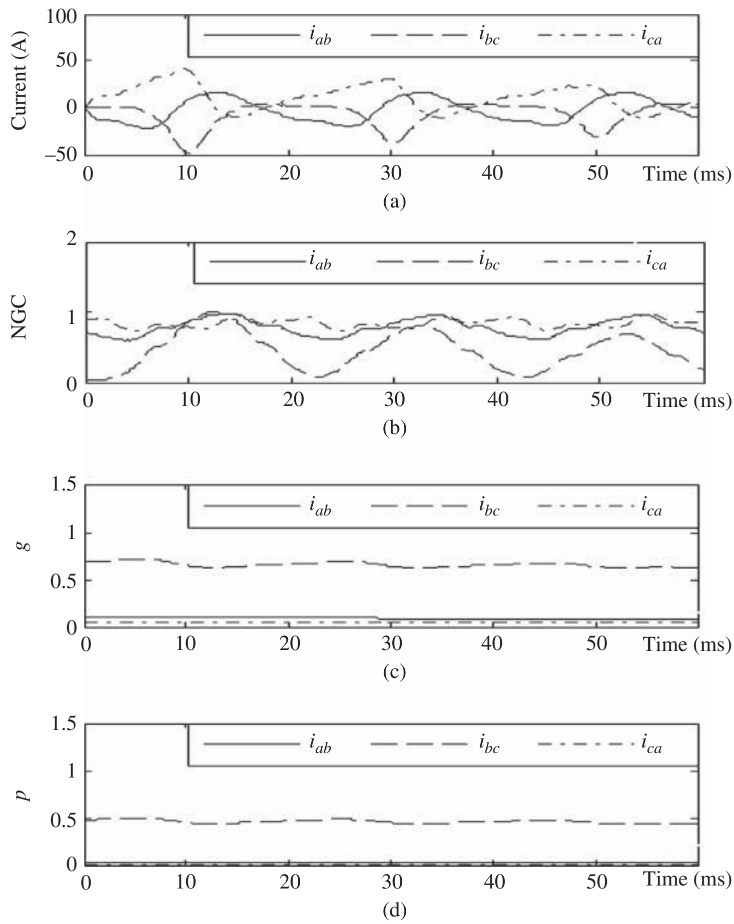

Figure 4.61 Differential currents and experimental results when the transformer is switched with no load and a 6.1% turn-to-turn internal fault. (a) Differential currents, (b) calculated NGCs, (c) analysis of the calculated NGCs in the time domain, and (d) analysis of the calculated NGCs in the frequency domain

The NGCs of three phases are calculated using Equation (4.71). Figure 4.61b–d show the respective calculated NGCs along with their analysis results in the time and frequency domains. In Figure 4.61b, the NGC of i_{bc} shows severe variation, whereas the NGCs of i_{ab} and i_{ca} are almost constant and only have a little variation resulting from harmonics in the internal fault currents. According to the proposed criterion in the time domain, it is apparent that i_{ab} and i_{ca} are both the internal fault currents and i_{bc} is the inrush current. The same result can be obtained from the frequency domain analysis. The NGCs of i_{ab} and i_{ca} contain negligible ratios between the fundamental frequency and DC components (Figure 4.61d). However, the NGC of i_{bc} is characterized by its noticeable ratio between two components. These results are in accordance with the practical state of the transformer. In the total of 52 cases, identical results verify that the proposed technique can be used to discriminate internal faults from inrush currents when the simultaneous inrush currents and faults occur in the transformer.

In summary, application of the NGC to discriminate the inrush current from the internal fault current of transformers is proposed. The NGC calculation method is firstly derived. Then, the criteria to extract features of the inrush current and the internal fault in the respective time and frequency domains are developed in detail. The iron core is not saturated and the magnetizing current is very small in the case of an internal fault, which results in the approximate sine waveform due to the operation in the linear region of the magnetizing characteristic. The NGC of the faulty phase is almost constant in the time domain and the ratio between the fundamental frequency and DC components in the frequency domain is negligible. On the other hand, the iron core will alternate between saturation and nonsaturation during the inrush current, which causes severe distortions in the differential current. The NGC of the phase with the inrush current is characterized by its severe variation in the time domain and a noticeable ratio between the fundamental frequency and DC components in the frequency domain. A large number of measurements were carried out to test the proposed method. The algorithm can take effect just after the protection has been started for one circle (20 ms), and the operating time is generally less than 23 ms, even for the slight turn-to-turn fault. The experimental results validate that the proposed method can effectively discriminate internal faults from inrush currents. The computational simplicity of the proposed method enables its implementation with low-cost microprocessors. Before the proposed method is applied to practical transformer protection products, several larger power transformer banks need to be tested.

4.9 A Novel Algorithm for Discrimination between Inrush Currents and Internal Faults Based on Equivalent Instantaneous Leakage Inductance

4.9.1 Basic Principle

4.9.1.1 Physical Theory

Consider a two-winding single-phase transformer as shown in Figure 4.62. The primary and secondary voltages can be expressed as:

$$u_1 = i_1 r_1 + L_1 \frac{di_1}{dt} + \frac{d\psi_m}{dt} \tag{4.74}$$

$$u_2 = i_2 r_2 + L_2 \frac{di_2}{dt} + \frac{d\psi_m}{dt} \tag{4.75}$$

where: u_1 and u_2 are the voltages of primary and secondary windings; i_1 and i_2 are the currents of primary and secondary windings; r_1 and r_2 are the resistances of primary and secondary windings; L_1 and L_2 are the leakage inductances of primary and secondary windings; and ψ_m is the mutual flux linkage. The equations consider that the transformation ratio is one.

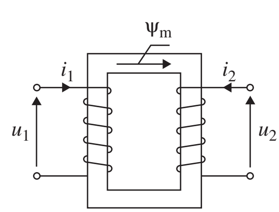

Figure 4.62 A two-winding single-phase transformer

The mutual flux linkage of the primary and secondary windings is equal and can be eliminated by using Equations (4.74) and (4.75) as follows:

$$u_{12} = L_1 \frac{di_1}{dt} - L_2 \frac{di_2}{dt} \tag{4.76}$$

with

$$u_{12} = u_1 - u_2 - i_1 r_1 + i_2 r_2 \tag{4.77}$$

Under the assumption that the parameters of the transformer L_1 and L_2 are given, it is then possible to calculate the right-hand side of Equation (4.76). The computed values of the right-hand side and the actual values of the left-hand side are equal during magnetizing inrush and normal operations. However, these values are not equal during internal faults. Therefore, this equation is an inherent feature of internal faults, which can be used to discriminate the inrush currents from internal faults.

4.9.1.2 Equivalent Instantaneous Leakage Inductance

In fact, it is very difficult to calculate the right-hand side of Equation (4.76) because it depends on the leakage inductances, which are determined by the size, shape and location of transformer windings. Furthermore, with the physical dimension varied, the internal faults make it hardly possible even if an approximation of the leakage inductances can be obtained from the transformer design data. This problem is evitable when the equivalent instantaneous leakage inductance (EILI) definition is employed as a solution.

The trapezoid principle is adopted in Equation (4.76) to transform the continuous differential equation into a discrete difference equation. The digital expressions at kT and $(k+1)T$ instants are given by:

$$u_{12}(k) = L_{1k} \frac{i_1(k+1) - i_1(k-1)}{2T} - L_{2k} \frac{i_2(k+1) - i_2(k-1)}{2T} \tag{4.78}$$

$$u_{12}(k+1) = L_{1k} \frac{i_1(k+2) - i_1(k)}{2T} - L_{2k} \frac{i_2(k+2) - i_2(k)}{2T} \tag{4.79}$$

where the T is the sampling cycle.

Each of L_{1k} and L_{2k} is defined as the EILI, which will be constant when there is an inrush current and during normal operation, but will be no longer constant when there is an internal fault. Therefore, the EILI that is equivalent to leakage inductances in the discrimination between internal fault and inrush current exactly presents the inherent status of the transformer.

Consider that the parameters of the transformer, r_1 and r_2 are known. The differential currents and voltages at kT and $(k+1)\,T$ instants are used and the calculated EILIs of primary and secondary windings at kT instant are written as:

$$\begin{aligned} L_{1k} = {} & 2T[u_{12}(k)i_2(k+2) - u_{12}(k)i_2(k) - u_{12}(k+1)i_2(k+1) + u_{12}(k+1)i_2(k-1)] \\ & \times [(i_1(k+1) - i_1(k-1)) \times (i_2(k+2) - i_2(k)) - (i_1(k+2) - i_1(k)) \times (i_2(k+1) - i_2(k-1))]^{-1} \end{aligned} \tag{4.80}$$

$$\begin{aligned} L_{2k} = {} & 2T[u_{12}(k)i_1(k+2) - u_{12}(k)i_1(k) - u_{12}(k+1)i_1(k+1) + u_{12}(k+1)i_1(k-1)] \\ & \times [(i_2(k+2) - i_2(k)) \times (i_1(k+1) - i_1(k-1)) - (i_2(k+1) - i_2(k-1)) \times (i_1(k+2) - i_1(k))]^{-1} \end{aligned} \tag{4.81}$$

4.9.1.3 Two-Winding Three-Phase Y/Δ Transformer

Figure 4.63 shows the connections of the primary and secondary windings of a Δ/Y transformer. The following equations express the delta and Y-connected windings as functions of the mutual flux linkages

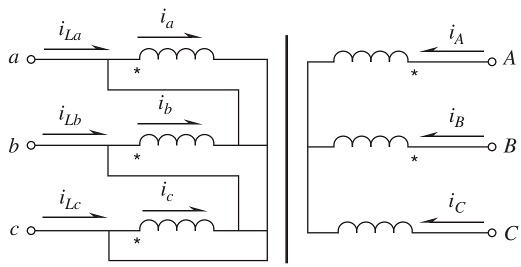

Figure 4.63 A two-winding three-phase Δ/Y transformer

and the currents of the windings:

$$u_a = i_a r + L_a \frac{di_a}{dt} + \frac{d\psi_{ma}}{dt} \tag{4.82}$$

$$u_b = i_b r + L_b \frac{di_b}{dt} + \frac{d\psi_{mb}}{dt} \tag{4.83}$$

$$u_c = i_c r + L_c \frac{di_c}{dt} + \frac{d\psi_{mc}}{dt} \tag{4.84}$$

$$u_A = i_A R + L_A \frac{di_A}{dt} + \frac{d\psi_{ma}}{dt} \tag{4.85}$$

$$u_B = i_B R + L_B \frac{di_B}{dt} + \frac{d\psi_{mb}}{dt} \tag{4.86}$$

$$u_C = i_C R + L_C \frac{di_C}{dt} + \frac{d\psi_{mc}}{dt} \tag{4.87}$$

where: the parameters of the secondary side have been converted to the primary side by the transformer ratio; u_a, u_b and u_c are the voltages of the primary windings a, b and c; i_a, i_b and i_c are the currents of the primary windings; L_a, L_b and L_c are the leakage inductances of the primary windings; r is the resistance of the primary windings; u_A, u_B and u_C are the voltages of the secondary windings A, B and C; i_A, i_B and i_C are the currents of the secondary windings; L_A, L_B and L_C are the leakage inductances of the secondary windings; R is the resistance of the secondary windings; and ψ_{ma}, ψ_{mb} and ψ_{mc} are the mutual flux linkages.

i_a, i_b and i_c are the currents of delta connected windings, which it is not possible to measure in many situations. In order not to position the CTs within the delta loop to get the exact phase current, the line currents as functions of the currents in the delta connected windings are expressed as:

$$i_{La} = i_a - i_b \tag{4.88}$$

$$i_{Lb} = i_b - i_c \tag{4.89}$$

$$i_{Lc} = i_c - i_a \tag{4.90}$$

Consider the leakage inductances to be constant and equal in the normal operation state and during the inrush current period: $L_a = L_b = L_c = L_1$, $L_A = L_B = L_C = L_2$. The equations of the primary and secondary sides can be written as:

$$u_a - u_b = i_{La} r + L_1 \frac{di_{La}}{dt} + \frac{d(\psi_{ma} - \psi_{mb})}{dt} \tag{4.91}$$

$$u_b - u_c = i_{Lb} r + L_1 \frac{di_{Lb}}{dt} + \frac{d(\psi_{mb} - \psi_{mc})}{dt} \tag{4.92}$$

$$u_c - u_a = i_{Lc}r + L_1\frac{di_{Lc}}{dt} + \frac{d(\psi_{mc} - \psi_{ma})}{dt} \tag{4.93}$$

$$u_A - u_B = (i_A - i_B)R + L_2\frac{d(i_A - i_B)}{dt} + \frac{d(\psi_{ma} - \psi_{mb})}{dt} \tag{4.94}$$

$$u_B - u_C = (i_B - i_C)R + L_2\frac{d(i_B - i_C)}{dt} + \frac{d(\psi_{mb} - \psi_{mc})}{dt} \tag{4.95}$$

$$u_C - u_A = (i_C - i_A)R + L_2\frac{d(i_C - i_A)}{dt} + \frac{d(\psi_{mc} - \psi_{ma})}{dt} \tag{4.96}$$

The flux linkages mutual to the primary and secondary windings of each phase are equal and can be eliminated by using Equations (4.97)–(4.102) as follows:

$$u_{AaBb} = L_1\frac{di_{La}}{dt} - L_2\frac{d(i_A - i_B)}{dt} \tag{4.97}$$

$$u_{BbCc} = L_1\frac{di_{Lb}}{dt} - L_2\frac{d(i_B - i_C)}{dt} \tag{4.98}$$

$$u_{CcAa} = L_1\frac{di_{Lc}}{dt} - L_2\frac{d(i_C - i_A)}{dt} \tag{4.99}$$

with

$$u_{AaBb} = u_a - u_b - u_A + u_B - i_{La}r + (i_A - i_B)R \tag{4.100}$$

$$u_{BbCc} = u_b - u_c - u_B + u_C - i_{Lb}r + (i_B - i_C)R \tag{4.101}$$

$$u_{CcAa} = u_c - u_a - u_C + u_A - i_{Lc}r + (i_C - i_A)R \tag{4.102}$$

The trapezoid principle is adopted in Equation (4.97) to transform the continuous differential equation into a discrete difference equation. The digital expressions at kT and $(k+1)T$ instants are given by:

$$u_{AaBb}(k) = L_{1k}\frac{i_{La}(k+1) - i_{La}(k-1)}{2T} - L_{2k}\frac{(i_A(k+1) - i_B(k+1)) - (i_A(k-1) - i_B(k-1))}{2T} \tag{4.103}$$

$$u_{AaBb}(k+1) = L_{1k}\frac{i_{La}(k+2) - i_{La}(k)}{2T} - L_{2k}\frac{(i_A(k+2) - i_B(k+2)) - (i_A(k) - i_B(k))}{2T} \tag{4.104}$$

The EILIs of L_{1k} and L_{2k} at kT instant can be calculated in real time by using Equations (4.103) and (4.104). A similar procedure provides the other two groups of L_{1k} and L_{2k} by using Equations (4.98) and (4.99), respectively.

4.9.1.4 Three-Winding Three-Phase Y_0/Y/Δ Transformer

Consider a three-winding three-phase transformer as shown in Figure 4.64, Y_0/Y/Δ connection, whose primary windings are A1, B1 and C1, secondary windings are A2, B2, and C2, and tertiary windings are A3, B3, and C3. The following equations express the voltages of the windings as functions of the mutual flux linkages and the currents of the windings:

$$u_{a1} = i_{a1}r_1 + L_1\frac{di_{a1}}{dt} + m_{21}\frac{di_{a2}}{dt} + m_{31}\frac{di_{a3}}{dt} + \frac{d\psi_{ma}}{dt} \tag{4.105}$$

$$u_{b1} = i_{b1}r_1 + L_1\frac{di_{b1}}{dt} + m_{21}\frac{di_{b2}}{dt} + m_{31}\frac{di_{b3}}{dt} + \frac{d\psi_{mb}}{dt} \tag{4.106}$$

$$u_{c1} = i_{c1} r_1 + L_1 \frac{di_{c1}}{dt} + m_{21} \frac{di_{c2}}{dt} + m_{31} \frac{di_{c3}}{dt} + \frac{d\psi_{mc}}{dt} \tag{4.107}$$

$$u_{a2} = i_{a2} r_2 + L_2 \frac{di_{a2}}{dt} + m_{12} \frac{di_{a1}}{dt} + m_{32} \frac{di_{a3}}{dt} + \frac{d\psi_{ma}}{dt} \tag{4.108}$$

$$u_{b2} = i_{b2} r_2 + L_2 \frac{di_{b2}}{dt} + m_{12} \frac{di_{b1}}{dt} + m_{32} \frac{di_{b3}}{dt} + \frac{d\psi_{mb}}{dt} \tag{4.109}$$

$$u_{c2} = i_{c2} r_2 + L_2 \frac{di_{c2}}{dt} + m_{12} \frac{di_{c1}}{dt} + m_{32} \frac{di_{c3}}{dt} + \frac{d\psi_{mc}}{dt} \tag{4.110}$$

$$u_{a3} = i_{a3} r_3 + L_3 \frac{di_{a3}}{dt} + m_{13} \frac{di_{a1}}{dt} + m_{23} \frac{di_{a2}}{dt} + \frac{d\psi_{ma}}{dt} \tag{4.111}$$

$$u_{b3} = i_{b3} r_3 + L_3 \frac{di_{b3}}{dt} + m_{13} \frac{di_{b1}}{dt} + m_{23} \frac{di_{b2}}{dt} + \frac{d\psi_{mb}}{dt} \tag{4.112}$$

$$u_{c3} = i_{c3} r_3 + L_3 \frac{di_{c3}}{dt} + m_{13} \frac{di_{c1}}{dt} + m_{23} \frac{di_{c2}}{dt} + \frac{d\psi_{mc}}{dt} \tag{4.113}$$

where: the parameters of the secondary and the tertiary sides have been converted to the primary side by the transformer ratio; u_{a1}, u_{b1} and u_{c1} are the voltages of the primary windings A1, B1 and C1; i_{a1}, i_{b1} and i_{c1} are the currents of the primary windings; i_{La1}, i_{Lb1} and i_{Lc1} are the line currents of the primary windings; r_1 is the resistance of the primary windings; L_1 is the self-leakage inductance of the primary windings; u_{a2}, u_{b2} and u_{c2} are the voltages of the secondary windings A2, B2 and C2; i_{a2}, i_{b2} and i_{c2} are the currents of the secondary windings; r_2 is the resistance of the secondary windings; L_2 is the self-leakage inductance of the secondary windings; u_{a3}, u_{b3} and u_{c3} are the voltages of the tertiary windings A3, B3 and C3; i_{a3}, i_{b3} and i_{c3} are the currents of the tertiary windings; r_3 is the resistance of the tertiary windings; L_3 is the self-leakage inductance of the tertiary windings; m_{12} and m_{21} are the mutual leakage inductances between the primary and secondary windings; m_{31} and m_{13} are the mutual leakage inductances between the primary and tertiary windings; m_{32} and m_{23} are the mutual leakage inductances between the secondary and tertiary windings; ψ_{ma}, ψ_{mb} and ψ_{mc} are the mutual flux linkages. Consider the mutual leakage inductances to be constant and equal during the normal operation conditions, the inrush currents and external faults: $m_{12} = m_{21}$, $m_{13} = m_{31}$, $m_{23} = m_{32}$.

The procedure described in the two-winding three-phase transformer provided Equation (4.97) from Equations (4.91) and (4.94). Processing Equations (4.105) and (4.106) and Equations (4.108) and

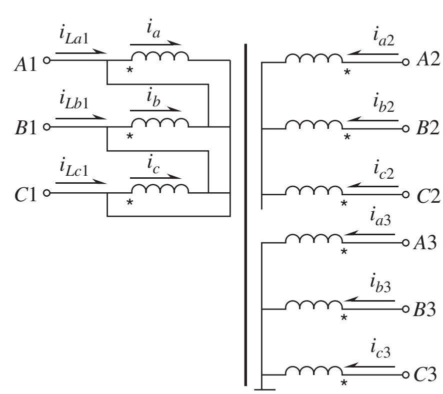

Figure 4.64 A three-winding three-phase Y_0/Y/Δ transformer

(4.109) in a similar manner provides Equation (4.114). A similar procedure provides Equations (4.115) and (4.116):

$$u_{ab12} = -(L_1 - m_{12})\frac{di_{La1}}{dt} + (L_2 - m_{21})\frac{d(i_{a2} - i_{b2})}{dt} + (m_{32} - m_{31})\frac{d(i_{a3} - i_{b3})}{dt} \tag{4.114}$$

$$u_{bc12} = -(L_1 - m_{12})\frac{di_{Lb1}}{dt} + (L_2 - m_{21})\frac{d(i_{b2} - i_{c2})}{dt} + (m_{32} - m_{31})\frac{d(i_{b3} - i_{c3})}{dt} \tag{4.115}$$

$$u_{ca12} = -(L_1 - m_{12})\frac{di_{Lc1}}{dt} + (L_2 - m_{21})\frac{d(i_{c2} - i_{a2})}{dt} + (m_{32} - m_{31})\frac{d(i_{c3} - i_{a3})}{dt} \tag{4.116}$$

with

$$u_{ab12} = u_{b1} - u_{a1} + u_{a2} - u_{b2} + i_{La1}r - (i_{a2} - i_{b2})r_2 \tag{4.117}$$

$$u_{bc12} = u_{c1} - u_{b1} + u_{b2} - u_{c2} + i_{Lb1}r_1 - (i_{b2} - i_{c2})r_2 \tag{4.118}$$

$$u_{ca12} = u_{a1} - u_{c1} + u_{c2} - u_{a2} + i_{Lc1}r_1 - (i_{c2} - i_{a2})r_2 \tag{4.119}$$

The parameters of the self and mutual leakage inductances cannot be obtained even from the no-load test and the steady-state short-circuit test, which is another obstacle for the existing algorithm. However, application of the EILI is a reasonable method to solve this problem. The trapezoid principle is adopted in Equation (4.114) to transform the continuous differential equation into three discrete difference equations at $(k-1)T$, kT and $(k+1)T$ instants:

$$\begin{aligned} u_{ab12}(k-1) = &-(L_{1k} - m_{12k})\frac{i_{La1}(k-2) - i_{La1}(k)}{2T} + (L_{2k} - m_{21k})\frac{i_{ab2}(k-2) - i_{ab2}(k)}{2T} \\ &+ (m_{32k} - m_{31k})\frac{i_{ab3}(k-2) - i_{ab3}(k)}{2T} \end{aligned} \tag{4.120}$$

$$\begin{aligned} u_{ab12}(k) = &-(L_{1k} - m_{12k})\frac{i_{La1}(k+1) - i_{La1}(k-1)}{2T} + (L_{2k} - m_{21k})\frac{i_{ab2}(k+1) - i_{ab2}(k-1)}{2T} \\ &+ (m_{32k} - m_{31k})\frac{i_{ab3}(k+1) - i_{ab3}(k-1)}{2T} \end{aligned} \tag{4.121}$$

$$\begin{aligned} u_{ab12}(k+1) = &-(L_{1k} - m_{12k})\frac{i_{La1}(k+2) - i_{La1}(k)}{2T} + (L_{2k} - m_{21k})\frac{i_{ab2}(k+2) - i_{ab2}(k)}{2T} \\ &+ (m_{32k} - m_{31k})\frac{i_{ab3}(k+2) - i_{ab3}(k)}{2T} \end{aligned} \tag{4.122}$$

The EILIs of $L_{1k} - m_{12k}$, $L_{2k} - m_{21k}$ and $m_{32k} - m_{31k}$ at instant kT can be calculated in real time by using Equations (4.120)–(4.122). A similar procedure is valid for Equations (4.115)–(4.117) to provide the other two groups of $L_{1k} - m_{12k}$, $L_{2k} - m_{21k}$ and $m_{32k} - m_{31k}$, respectively.

Similarly, Equations (4.108)–(4.110) and Equations (4.111)–(4.113) are used to calculate three groups of $L_{2k} - m_{23k}$, $L_{3k} - m_{32k}$ and $m_{12k} - m_{13k}$. Mean while, Equations (4.105)–(4.107) and Equations (4.111)–(4.113) are used to calculate three groups of $L_{3k} - m_{31k}$, $L_{1k} - m_{13k}$ and $m_{21k} - m_{23k}$.

Subtracting $L_{2k} - m_{21k}$ from $L_{1k} - m_{12k}$ provides Equation (4.123):

$$(L_{1k} - m_{12k}) - (L_{2k} - m_{21k}) = L_{1k} - L_{2k} \tag{4.123}$$

A similar procedure can be followed to obtain $L_{2k} - L_{3k}$ and $L_{1k} - L_{3k}$:

$$(L_{2k} - m_{23k}) - (L_{3k} - m_{32k}) = L_{2k} - L_{3k} \tag{4.124}$$

$$(L_{1k} - m_{13k}) - (L_{3k} - m_{31k}) = L_{1k} - L_{3k} \tag{4.125}$$

4.9.2 EILI-Based Criterion

Two criteria are proposed, one for dealing with the two-winding transformer and one for the three-winding transformer. Both of them cooperate with the differential relay to perform the protection task.

1. *The Criterion for the Two-Winding Transformer*: at instant kT, the difference of the EILIs among the three groups of primary windings can be expressed as

$$\Delta L_{1k} = \sqrt{\frac{1}{L_{\min 1}}((L_{1ka} - L_{1kb})^2 + (L_{1kb} - L_{1kc})^2 + (L_{1kc} - L_{1ka})^2)} \tag{4.126}$$

$$L_{\min 1} = \min(L_{1ka}, L_{1kb}, L_{1kc}) \tag{4.127}$$

where L_{1ka}, L_{1kb} and L_{1kc} are the EILIs of primary windings calculated by Equations (4.97)–(4.99), respectively.

A similar procedure applies to the EILIs of the secondary windings:

$$\Delta L_{2k} = \sqrt{\frac{1}{L_{\min 2}}((L_{2ka} - L_{2kb})^2 + (L_{2kb} - L_{2kc})^2 + (L_{2kc} - L_{2ka})^2)} \tag{4.128}$$

$$L_{\min 2} = \min(L_{2ka}, L_{2kb}, L_{2kc}) \tag{4.129}$$

ΔL_{1k} and ΔL_{2k} are employed to distinguish the inrush current from the internal fault according to the following criterion: if ΔL_{1k} or ΔL_{2k} exceeds a threshold, the relay judges that an internal fault occurs and lets the relay trip; or the relay judges that there is an inrush current and rejects the tripping if both ΔL_{1k} and ΔL_{2k} are less than the threshold. In theory, the threshold is close to zero.

2. *The Criterion for the Three-Winding Transformer*: the difference of three groups of the $L_{1k} - L_{2k}$ can be described as:

$$\Delta L'_{1k} = \sqrt{\frac{1}{L'_{\min 1}}((L_{1ka} - L_{2ka})^2 + (L_{1kb} - L_{2kb})^2 + (L_{1kc} - L_{2kc})^2)} \tag{4.130}$$

$$L'_{\min 1} = \min(L_{1ka}, L_{1kb}, L_{1kc}, L_{2ka}, L_{2kb}, L_{2kc}) \tag{4.131}$$

where $L_{1ka} - L_{2ka}$, $L_{1kb} - L_{2kb}$ and $L_{1kc} - L_{2kc}$ are the three groups of EILIs calculated by Equation (4.129).

Two similar procedures respectively provide the difference of three groups of the $L_{2k} - L_{3k}$ and the difference of three groups of the $L_{1k} - L_{3k}$:

$$\Delta L'_{2k} = \sqrt{\frac{1}{L'_{\min 2}}((L_{2ka} - L_{3ka})^2 + (L_{2kb} - L_{3kb})^2 + (L_{2kc} - L_{3kc})^2)} \tag{4.132}$$

$$\Delta L'_{3k} = \sqrt{\frac{1}{L'_{\min 3}}((L_{1ka} - L_{3ka})^2 + (L_{1kb} - L_{3kb})^2 + (L_{1kc} - L_{3kc})^2)} \tag{4.133}$$

$$L'_{\min 2} = \min(L_{2ka}, L_{2kb}, L_{2kc}, L_{3ka}, L_{3kb}, L_{3kc}) \tag{4.134}$$

$$L'_{\min 3} = \min(L_{1ka}, L_{1kb}, L_{1kc}, L_{3ka}, L_{3kb}, L_{3kc}) \tag{4.135}$$

where $L_{2ka} - L_{3ka}$, $L_{2kb} - L_{3kb}$ and $L_{2kc} - L_{3kc}$ are the three groups of EILIs calculated by Equation (4.124). $L_{1ka} - L_{3ka}$, $L_{1kb} - L_{3kb}$ and $L_{1kc} - L_{3kc}$ are the three groups of EILIs calculated by Equation (4.125).

If the amplitude of $\Delta L'_{1k}$, $\Delta L'_{2k}$ and $\Delta L'_{3k}$ are all less than a threshold, a decision is made either that an inrush current in the transformer has been detected and the relay tripping of the differential protection is blocked or that and an internal fault has been detected, in which case the relay is tripped. In theory, the threshold is close to zero.

4.9.3 Experimental Results and Analysis

To verify the effectiveness of the proposed method, experimental tests have been carried out at the Electric Power Research Institute (EPRI). The experimental system is one machine model with a two-winding three-phase Y/Δ-11 connected transformer bank as shown in Figure 4.65. The system includes two parallel lines. The system parameters are given in Table 4.13. CTs with Y/Y connection are used as transducers to measure the line currents of the transformer bank.

The experiments provide samples of line currents and terminal voltages in each phase when the transformer is energized or when a fault occurs or when both occur simultaneously. A total of 147 cases have been divided into four main categories: 27 cases for switching on the transformer with no load, 27 cases for clearing an external line fault, 49 cases for simultaneous internal fault and inrush conditions, and 44 cases for faulty conditions only, to test the various features of the algorithm. Different switching on and clearing instants for inrush current, as well as different faults and short-circuit turn ratios for the internal fault are considered in the tests. The measured data are used as an input to the developed algorithm to identify its response.

Figures 4.66–4.70 show some examples of the experimental test results: the line currents and the waveforms of the calculated EILIs along with the resulting analysis.

4.9.3.1 Responses to Different Inrush Conditions Only

The magnetizing inrush current is often generated when a transformer is energized or an external line fault is cleared. Data from a total of 54 cases were tested in both situations: 27 cases for switching on

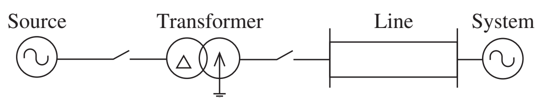

Figure 4.65 The EPRI experimental system

Table 4.13 Parameters of the test model

Source	
Rated power (MW)	600
Rated voltage (kV)	19
Rated current (kA)	20.26
Transformer	
Rated capacity (MVA)	670
Rated voltage ratio (kV)	19/550
Short circuit voltage (%)	13.0
Line	
Length (km)	257
Voltage class (kV)	500
System	
System capacity (MVA)	11 000
Rated frequency (Hz)	50

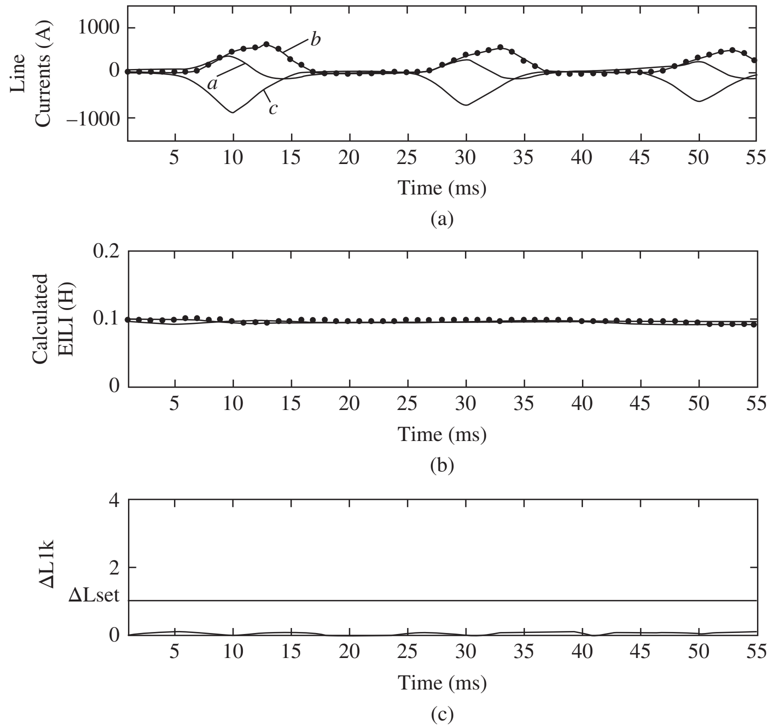

Figure 4.66 Experimental results when the transformer is energized: (a) line currents; (b) calculated EILIs; (c) analysis of the calculated EILIs

the transformer with no load and 27 cases for clearing the external line fault, respectively. Energizing at the primary side of the transformer is given in Figure 4.66, where the line currents and the EILIs of the primary windings calculated by using Equations (4.97)–(4.99) are shown along with the analysis result. It is found that the calculated EILIs of the three phases are almost kept constant and have only little variation resulting from the measurement and calculation errors (Figure 4.66b). The variation of the ΔL_{1k} based on both Equations (4.126) and (4.127) is close to zero and much less than the threshold ΔL_{set} (Figure 4.66c).

The same result can be obtained from the case of clearing an external line fault, as shown in Figure 4.67, where the EILIs of three phases only have slight difference at the fault clearing instant. According to the criterion for the two-winding transformer, the protection will be both blocked, although the EILIs of the secondary windings are not available because the line currents of the secondary side are zero in these situations. In the total of 54 cases, the same feature of the inrush current is presented in the calculated EILIs.

4.9.3.2 Responses to Simultaneous Fault and Inrush Conditions

Switching on the transformer bank with no load often causes the inrush current of nonfault phases, which has been verified by a total of 49 cases with simultaneous inrush currents and internal fault currents. Figure 4.68a as an example shows this situation, which is obtained by switching on the transformer bank with no load and a 2% turn-to-turn internal fault in phase C. The line current of phase A presents the nominal magnetizing current; however, the line current of phase B is larger than the nominal magnetizing

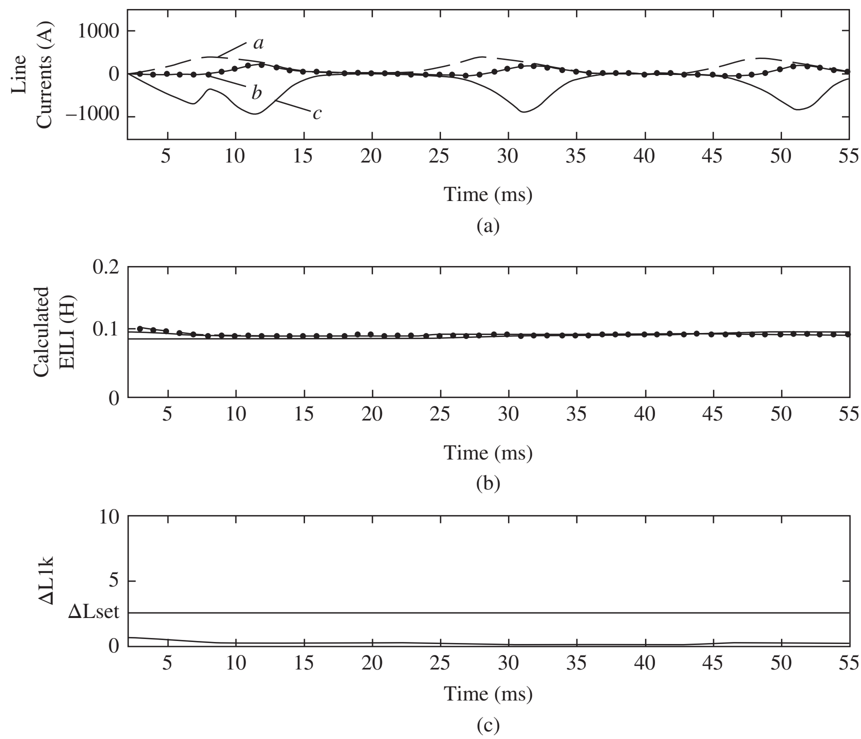

Figure 4.67 Experimental results when an external line fault is cleared: (a) line currents; (b) calculated EILIs; (c) analysis of the calculated EILIs

current. Therefore, the EILIs are calculated by using Equations (4.97)–(4.99). Figures 4.68b and 4.68c show the calculated EILIs and the analysis result, respectively. The difference is very noticeable in the calculated EILIs of the three phases. According to the proposed criterion, it is obvious that the protection will operate rapidly and correctly. These results are in accordance with the practical state of the transformer bank.

In the total of 49 cases, the identical results verify that the proposed techniques can be used to identify internal faults when a simultaneous inrush current and fault occur in the transformer bank. Moreover, it is difficult to discriminate low level (less than 9%) turn-to-turn internal faults from inrush currents when the algorithm proposed by M.S. Sachdev [13] is applied, which provides less accurate results than the method to calculate EILIs.

4.9.3.3 Responses to Internal Fault Conditions Only

Data from a total of 44 cases are used to calculate the EILIs based on Equations (4.97)–(4.99). In all of the 44 cases, the calculated EILIs are not constant, which results from the variation of physical dimension and the deformation of the windings during the internal fault. As shown in Figures 4.69a and 4.70a, a 3% turn-to-turn internal fault occurs in phase B at the secondary side during steady operation. The calculated EILI waveforms of the primary and secondary windings are shown in Figures 4.69b and 4.70b, respectively, which present different variations right after the fault occurrence. Their analysis results are shown in Figures 4.69c and 4.70c, respectively, which show that not only ΔL_{1k} but also ΔL_{2k} exceed the threshold ΔL_{set} soon after the fault occurs. The operating time is only about 8 ms.

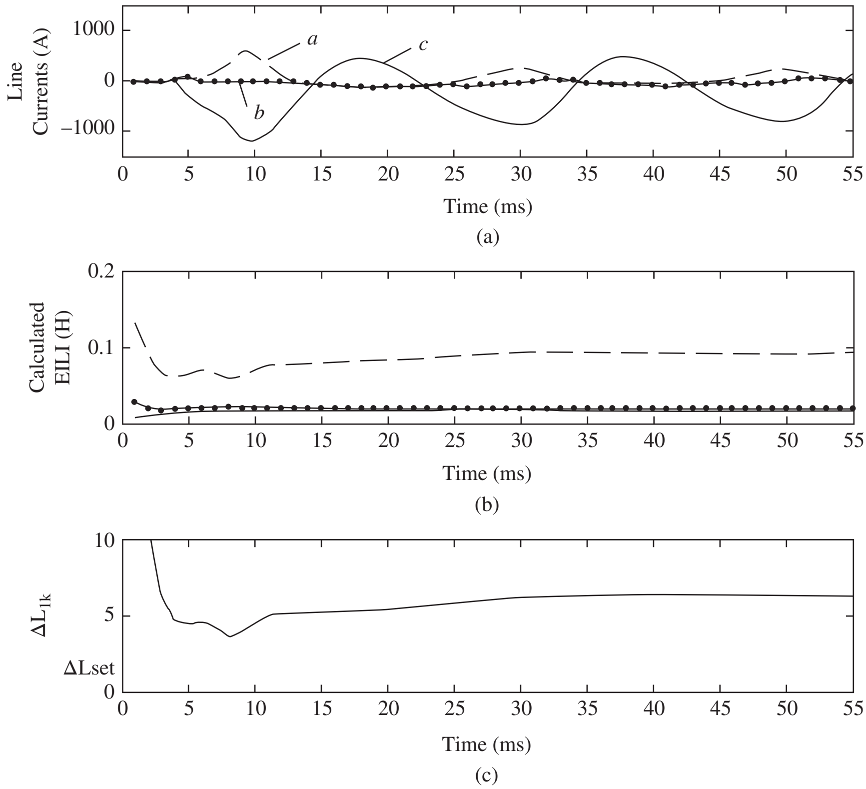

Figure 4.68 Experimental results when the transformer is energized with a 2% turn-to-turn internal fault: (a) line currents; (b) calculated EILIs; (c) analysis of the calculated EILIs

In addition, the EILIs during the other internal faults (such as grounding internal faults and phase-to-phase internal faults) do not have constant values, which can be effectively used to distinguish the internal faults and inrush currents without the parameters of the leakage inductances of the primary and secondary windings. Meanwhile, no problems are foreseen in applying the proposed technique with the impact of the CTs during internal faults. However, since a quite high false line current may emerge if the CT at one side saturates in depth, the effectiveness of the proposed technique when the CT is in heavy saturation is currently being studied.

In order to validate the proposed method more thoroughly, further practical studies will be continued in planned future work. Firstly, the proposed method will be tested on several three-winding three-phase transformer banks. Additionally, different transformers will be used in a large number of practical tests, in which the EILI during different types of internal faults and inrush currents will be analysed to verify the proposed method. These results will be useful for the application of the proposed method in the practical transformer products.

In summary, a novel EILI-based technique has been proposed for identification of magnetizing inrush and internal fault conditions in transformers. The EILI concept along with its calculation methods and criteria to extract features of the inrush current and the internal fault have been developed in detail. A large number of experiments have been carried out to test the proposed scheme. In all of the tests, the EILI is kept constant during magnetizing inrush and normal operating conditions. On the other hand, the EILI was characterized by its drastic variation during internal faults. The experimental results validate that the proposed method requires neither the data of the B–H curve nor the values of the leakage inductances.

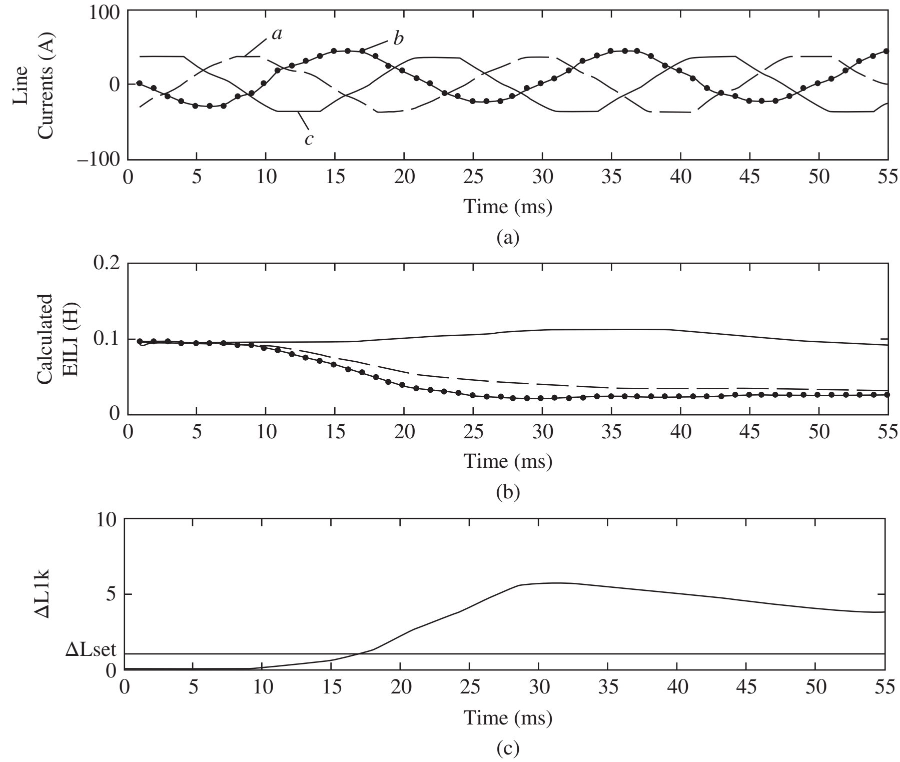

Figure 4.69 Experimental results when a 3% turn-to-turn internal fault occurs at the secondary side: (a) line currents at the primary side; (b) calculated EILIs of the primary windings; (c) analysis of the calculated EILIs

It has been demonstrated that the method is sensitive for the identification of low level internal faults at very high speed. Furthermore, this technique is also suitable for the protection of three-winding transformers.

4.10 A Two-Terminal Network-Based Method for Discrimination between Internal Faults and Inrush Currents

4.10.1 Basic Principle

4.10.1.1 The Two-Terminal Network of a Single-Phase Transformer

A two-winding single-phase transformer is shown in Figure 4.71. The primary and secondary voltages can be expressed as:

$$u_1 = i_1 r_1 + L_1 \frac{di_1}{dt} + \frac{d\psi_m}{dt} \tag{4.136}$$

$$u_2 = i_2 r_2 + L_2 \frac{di_2}{dt} + \frac{d\psi_m}{dt} \tag{4.137}$$

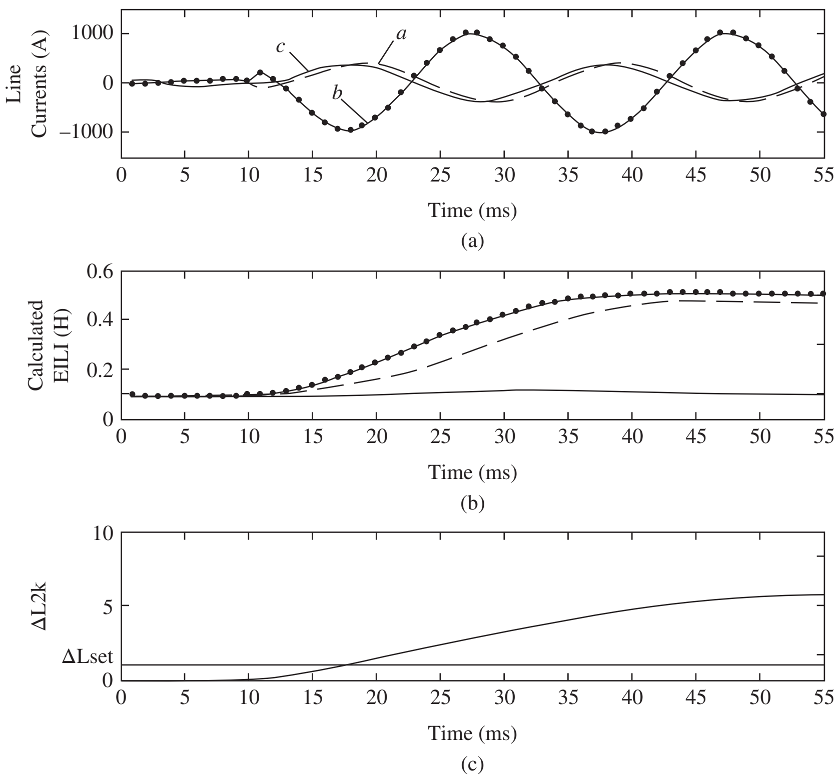

Figure 4.70 Experimental results when a 3% turn-to-turn internal fault occurs at the secondary side: (a) line currents at the secondary side; (b) calculated EILIs of the secondary windings; (c) analysis of the calculated EILIs

where the parameters of the secondary side have been converted to the primary side by the transformer ratio. u_1 and u_2 are the voltages of primary and secondary windings; i_1 and i_2 are the currents of primary and secondary windings; r_1 and r_2 are the resistances of primary and secondary windings; L_1 and L_2 are the leakage inductances of primary and secondary windings; ψ_m is the mutual flux linkage.

The mutual flux linkage of the primary and secondary windings is equal and can be eliminated using Equations (4.136) and (4.137) as follows:

$$u_d = i_d r_1 + L_1 \frac{di_d}{dt} \tag{4.138}$$

with

$$u_d = u_1 - u_2 + i_2 r_k + \frac{x_k}{\omega}\frac{di_2}{dt} \tag{4.139}$$

$$i_d = i_1 + i_2 \tag{4.140}$$

$$r_k = r_1 + r_2 \tag{4.141}$$

$$x_k = \omega(L_1 + L_2) \tag{4.142}$$

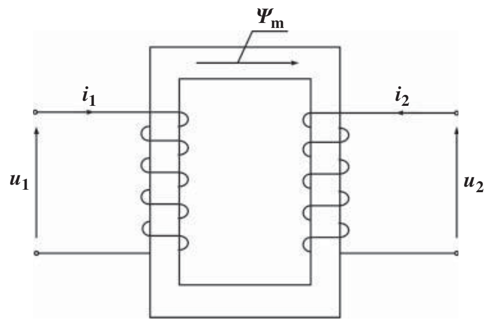

Figure 4.71 A two-winding single-phase transformer

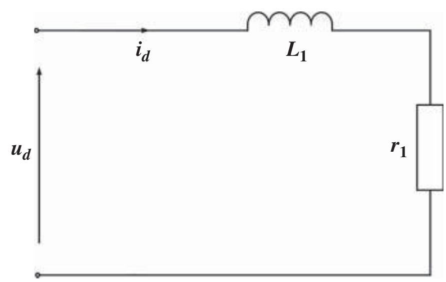

Figure 4.72 A two-terminal network

where i_d and u_d are the differential current and virtual differential voltage between the primary and secondary windings, respectively, and r_k and x_k are the winding resistance and the short-circuit reactance, respectively.

Using Equation (4.138), a two-terminal network containing only the winding resistance and the leakage inductance can be obtained (Figure 4.72).

Here, P_f and P_c are defined as the active powers flowing into and consumed by the two-terminal network, respectively. They can be expressed as:

$$P_f = \frac{1}{T}\int_0^T (u_d(t)i_d(t))dt \tag{4.143}$$

$$P_c = \frac{1}{T}\int_0^T (i_d^2(t)r_1)dt \tag{4.144}$$

where T is one cycle data window.

In the magnetizing inrush and normal operation cases of the power transformer, P_f is very close to P_c. However, when an internal fault occurs, P_f and P_c are both affected and P_f is no longer close to P_c owing to the arcing discharge.

$$P = |P_f - P_c| \tag{4.145}$$

P is defined as the absolute difference of active power (ADOAP) between P_f and P_c. If ADOAP is less than a threshold, the relay determines that there is an inrush current and rejects the tripping. Otherwise, the relay determines that an internal fault has occurred. The threshold should be set to avoid the needless operation by the measurement error and the calculation error. In theory, the threshold is close to zero.

Due to the elimination of the mutual flux linkage, the technique does not require data on the B–H curve or knowledge of iron losses. Also, from Equations (4.143) and (4.144), it is found that ADOAP does not make use of the leakage inductances of the primary and secondary windings to distinguish the internal fault from the inrush current.

4.10.1.2 The ADOAPs of a Two-Winding Three-Phase Transformer

Figure 4.73 shows the connections of the primary and secondary windings of a Δ/Y transformer.

The following equations express the Δ and Y-connected windings as functions of the mutual flux linkages and the currents of the windings:

$$u_a = i_a r + L_a \frac{di_a}{dt} + \frac{d\psi_{ma}}{dt} \tag{4.146}$$

$$u_b = i_b r + L_b \frac{di_b}{dt} + \frac{d\psi_{mb}}{dt} \tag{4.147}$$

$$u_c = i_c r + L_c \frac{di_c}{dt} + \frac{d\psi_{mc}}{dt} \tag{4.148}$$

$$u_A = i_A R + L_A \frac{di_A}{dt} + \frac{d\psi_{ma}}{dt} \tag{4.149}$$

$$u_B = i_B R + L_B \frac{di_B}{dt} + \frac{d\psi_{mb}}{dt} \tag{4.150}$$

$$u_C = i_C R + L_C \frac{di_C}{dt} + \frac{d\psi_{mc}}{dt} \tag{4.151}$$

where the parameters of the secondary side have been converted to the primary side by the transformer ratio. u_a, u_b and u_c are the voltages of primary windings a, b and c; i_a, i_b and i_c are the currents of primary windings; L_a, L_b and L_c are the leakage inductances of primary windings; r is the resistance of primary windings; u_A, u_B and u_C are the voltages of secondary windings; i_A, i_B and i_C are the currents of secondary windings; L_A, L_B and L_C are the leakage inductances of secondary windings; R is the resistance of secondary windings; ψ_{ma}, ψ_{mb} and ψ_{mc} are the mutual flux linkages.

The line currents in the Δ-connected windings are obtained as follows:

$$i_{La} = i_a - i_b \tag{4.152}$$

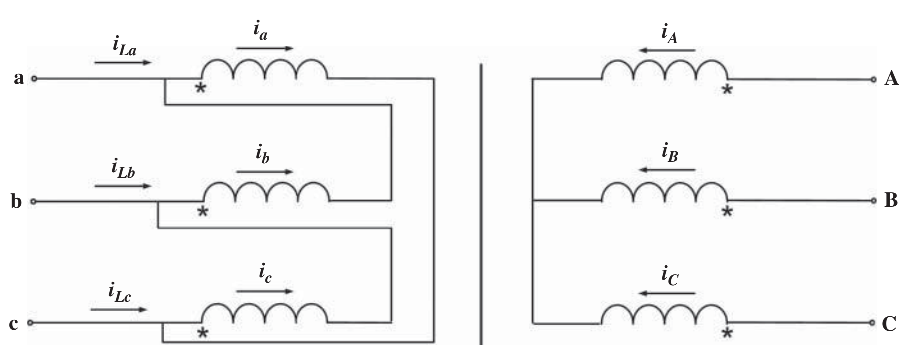

Figure 4.73 A two-winding three-phase Δ/Y transformer

$$i_{Lb} = i_b - i_c \tag{4.153}$$

$$i_{Lc} = i_c - i_a \tag{4.154}$$

Consider the leakage inductances to be constant and equal in the normal operation state and during the inrush current period. $L_a = L_b = L_c = L_1$, $L_A = L_B = L_C = L_2$. The equations of the primary and secondary sides can be written as:

$$u_a - u_b = i_{La}r + L_1\frac{di_{La}}{dt} + \frac{d(\psi_{ma} - \psi_{mb})}{dt} \tag{4.155}$$

$$u_b - u_c = i_{Lb}r + L_1\frac{di_{Lb}}{dt} + \frac{d(\psi_{mb} - \psi_{mc})}{dt} \tag{4.156}$$

$$u_c - u_a = i_{Lc}r + L_1\frac{di_{Lc}}{dt} + \frac{d(\psi_{mc} - \psi_{ma})}{dt} \tag{4.157}$$

$$u_A - u_B = (i_A - i_B)R + L_2\frac{d(i_A - i_B)}{dt} + \frac{d(\psi_{ma} - \psi_{mb})}{dt} \tag{4.158}$$

$$u_B - u_C = (i_B - i_C)R + L_2\frac{d(i_B - i_C)}{dt} + \frac{d(\psi_{mb} - \psi_{mc})}{dt} \tag{4.159}$$

$$u_C - u_A = (i_C - i_A)R + L_2\frac{d(i_C - i_A)}{dt} + \frac{d(\psi_{mc} - \psi_{ma})}{dt} \tag{4.160}$$

The flux linkages mutual to the primary and secondary windings of each phase are equal and can be eliminated using Equations (4.155)–(4.160) as follows:

$$\begin{cases} u_{dA} = i_{dA}r_2 + L_2\dfrac{di_{dA}}{dt} \\ u_{dB} = i_{dB}r_2 + L_2\dfrac{di_{dB}}{dt} \\ u_{dC} = i_{dC}r_2 + L_2\dfrac{di_{dC}}{dt} \end{cases} \tag{4.161}$$

with

$$\begin{cases} u_{dA} = u_a - u_b - u_A + u_B - i_{La}r_k - \dfrac{x_k}{\omega}\dfrac{di_{La}}{dt} \\ u_{dB} = u_b - u_c - u_B + u_C - i_{Lb}r_k - \dfrac{x_k}{\omega}\dfrac{di_{Lb}}{dt} \\ u_{dC} = u_c - u_a - u_C + u_A - i_{Lc}r_k - \dfrac{x_k}{\omega}\dfrac{di_{Lc}}{dt} \end{cases} \tag{4.162}$$

$$\begin{cases} i_{dA} = -\left(i_{La} + i_A - i_B\right) \\ i_{dB} = -(i_{Lb} + i_B - i_C) \\ i_{dC} = -(i_{Lc} + i_C - i_A) \end{cases} \tag{4.163}$$

$$\begin{cases} r_k = r_1 + r_2 \\ x_k = \omega\left(L_1 + L_2\right) \end{cases} \tag{4.164}$$

Using Equation (4.161), three groups of two-terminal networks containing winding resistances and leakage inductances can beobtained. Then, a procedure similar to the single-phase transformer provides

P_1, P_2 and P_3, which are all defined as the ADOAPs.

$$\begin{cases} P_1 = \dfrac{1}{T}\left|\displaystyle\int_0^T \left(u_{dA}(t)\, i_{dA}(t) - i_{dA}^2(t) r_2\right) dt\right| \\ P_2 = \dfrac{1}{T}\left|\displaystyle\int_0^T \left(u_{dB}(t)\, i_{dB}(t) - i_{dB}^2(t) r_2\right) dt\right| \\ P_3 = \dfrac{1}{T}\left|\displaystyle\int_0^T \left(u_{dC}(t)\, i_{dC}(t) - i_{dC}^2(t) r_2\right) dt\right| \end{cases} \tag{4.165}$$

If the ADOAPs of three phases are all less than the threshold, the relay determines there is an inrush current and rejects the tripping. Otherwise, the relay determines that there is an internal fault.

4.10.1.3 The ADOAPs of a Three-Winding Three-Phase Transformer

A three-winding three-phase transformer with $\Delta/Y/Y_0$ connection is shown in Figure 4.74.

The following equations express the voltages of the windings as functions of the mutual flux linkages and the currents of the windings:

$$u_{a1} = i_{a1} r_1 + L_1 \frac{di_{a1}}{dt} + m_{21} \frac{di_{a2}}{dt} + m_{31} \frac{di_{a3}}{dt} + \frac{d\psi_{ma}}{dt} \tag{4.166}$$

$$u_{b1} = i_{b1} r_1 + L_1 \frac{di_{b1}}{dt} + m_{21} \frac{di_{b2}}{dt} + m_{31} \frac{di_{b3}}{dt} + \frac{d\psi_{mb}}{dt} \tag{4.167}$$

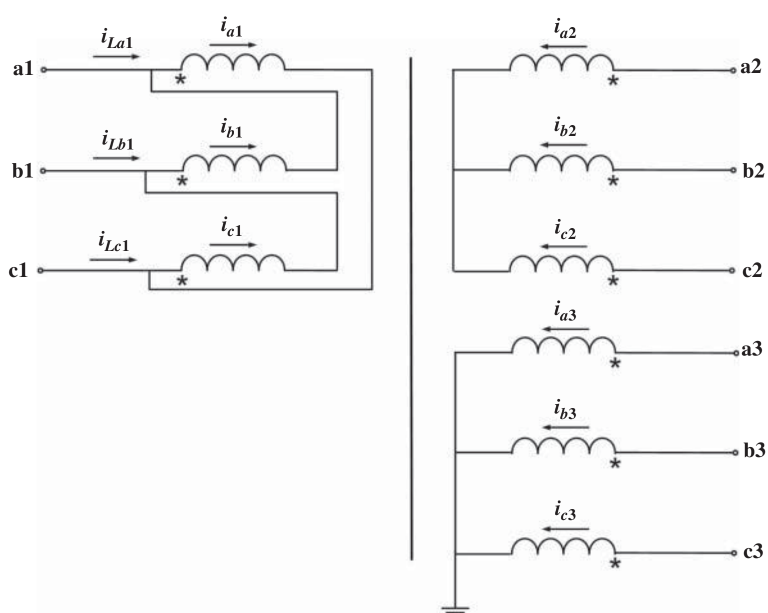

Figure 4.74 A three-winding three-phase $\Delta/Y/Y_0$ transformer

$$u_{c1} = i_{c1}r_1 + L_1\frac{di_{c1}}{dt} + m_{21}\frac{di_{c2}}{dt} + m_{31}\frac{di_{c3}}{dt} + \frac{d\psi_{mc}}{dt} \tag{4.168}$$

$$u_{a2} = i_{a2}r_2 + L_2\frac{di_{a2}}{dt} + m_{12}\frac{di_{a1}}{dt} + m_{32}\frac{di_{a3}}{dt} + \frac{d\psi_{ma}}{dt} \tag{4.169}$$

$$u_{b2} = i_{b2}r_2 + L_2\frac{di_{b2}}{dt} + m_{12}\frac{di_{b1}}{dt} + m_{32}\frac{di_{b3}}{dt} + \frac{d\psi_{mb}}{dt} \tag{4.170}$$

$$u_{c2} = i_{c2}r_2 + L_2\frac{di_{c2}}{dt} + m_{12}\frac{di_{c1}}{dt} + m_{32}\frac{di_{c3}}{dt} + \frac{d\psi_{mc}}{dt} \tag{4.171}$$

$$u_{a3} = i_{a3}r_3 + L_3\frac{di_{a3}}{dt} + m_{13}\frac{di_{a1}}{dt} + m_{23}\frac{di_{a2}}{dt} + \frac{d\psi_{ma}}{dt} \tag{4.172}$$

$$u_{b3} = i_{b3}r_3 + L_3\frac{di_{b3}}{dt} + m_{13}\frac{di_{b1}}{dt} + m_{23}\frac{di_{b2}}{dt} + \frac{d\psi_{mb}}{dt} \tag{4.173}$$

$$u_{c3} = i_{c3}r_3 + L_3\frac{di_{c3}}{dt} + m_{13}\frac{di_{c1}}{dt} + m_{23}\frac{di_{c2}}{dt} + \frac{d\psi_{mc}}{dt} \tag{4.174}$$

where the parameters of the secondary and the tertiary sides have been converted to the primary side by the transformer ratio. u_{a1}, u_{b1} and u_{c1} are the voltages of the primary windings; i_{a1}, i_{b1} and i_{c1} are the currents of the primary windings; i_{La1}, i_{Lb1} and i_{Lc1} are the line currents of the primary windings; r_1 is the resistance of primary the windings; L_1 is the self-leakage inductance of the primary windings; u_{a2}, u_{b2} and u_{c2} are the voltages of the secondary windings; i_{a2}, i_{b2} and i_{c2} are the currents of the secondary windings; r_2 is the resistance of the secondary windings; L_2 is the self-leakage inductance of the secondary windings. u_{a3}, u_{b3} and u_{c3} are the voltages of tertiary windings; i_{a3}, i_{b3} and i_{c3} are the currents of the tertiary windings; r_3 is the resistance of the tertiary windings; L_3 is the self-leakage inductance of the tertiary windings; m_{12} and m_{21} are the mutual leakage inductances between the primary and secondary windings; m_{31} and m_{13} are the mutual leakage inductances between the primary and tertiary windings; m_{32} and m_{23} are the mutual leakage inductances between the secondary and tertiary windings; ψ_{ma}, ψ_{mb} and ψ_{mc} are the mutual flux linkages.

Assume the mutual leakage inductances to be constant and equal during normal operation conditions and the inrush currents: $m_{12} = m_{21}$, $m_{13} = m_{31}$, $m_{23} = m_{32}$. A procedure similar to the two-winding transformer provides three groups of the ADOAPs:

$$\begin{cases} P_1 = \dfrac{1}{T}\left|\displaystyle\int_0^T \left(u_{ab12}(t)\, i_{da}(t) - i_{da}^2(t) r_1\right) dt\right| \\ P_2 = \dfrac{1}{T}\left|\displaystyle\int_0^T \left(u_{bc12}(t)\, i_{db}(t) - i_{db}^2(t) r_1\right) dt\right| \\ P_3 = \dfrac{1}{T}\left|\displaystyle\int_0^T \left(u_{ca12}(t)\, i_{dc}(t) - i_{dc}^2(t) r_1\right) dt\right| \end{cases} \tag{4.175}$$

$$\begin{cases} P_4 = \dfrac{1}{T}\left|\displaystyle\int_0^T \left(u_{ab23}(t)\, i_{da}(t) - i_{da}^2(t) r_2\right) dt\right| \\ P_5 = \dfrac{1}{T}\left|\displaystyle\int_0^T \left(u_{bc23}(t)\, i_{db}(t) - i_{db}^2(t) r_2\right) dt\right| \\ P_6 = \dfrac{1}{T}\left|\displaystyle\int_0^T \left(u_{ca23}(t)\, i_{dc}(t) - i_{dc}^2(t) r_2\right) dt\right| \end{cases} \tag{4.176}$$

$$\begin{cases} P_7 = \dfrac{1}{T}\left|\displaystyle\int_0^T \left(u_{ab31}(t)\, i_{da}(t) - i_{da}^2(t) r_3\right) dt\right| \\ P_8 = \dfrac{1}{T}\left|\displaystyle\int_0^T \left(u_{bc31}(t)\, i_{db}(t) - i_{db}^2(t) r_3\right) dt\right| \\ P_9 = \dfrac{1}{T}\left|\displaystyle\int_0^T \left(u_{ca31}(t)\, i_{dc}(t) - i_{dc}^2(t) r_3\right) dt\right| \end{cases} \tag{4.177}$$

with

$$\begin{cases} i_{da} = i_{La1} + i_{a2} - i_{b2} + i_{a3} - i_{b3} \\ i_{db} = i_{Lb1} + i_{b2} - i_{c2} + i_{b3} - i_{c3} \\ i_{dc} = i_{Lc1} + i_{c2} - i_{a2} + i_{c3} - i_{a3} \end{cases} \tag{4.178}$$

$$\begin{cases} u_{ab12} = u_{b2} - u_{a2} + u_{a1} - u_{b1} + \left(i_{a2} - i_{b2}\right)(r_1 + r_2) \\ \qquad + \dfrac{x_1 + x_2}{\omega}\dfrac{d(i_{a2} - i_{b2})}{dt} + (i_{a3} - i_{b3}) r_1 + \dfrac{x_1}{\omega}\dfrac{d(i_{a3} - i_{b3})}{dt} \\ u_{bc12} = u_{c2} - u_{b2} + u_{b1} - u_{c1} + (i_{b2} - i_{c2})(r_1 + r_2) \\ \qquad + \dfrac{x_1 + x_2}{\omega}\dfrac{d(i_{b2} - i_{c2})}{dt} + (i_{b3} - i_{c3}) r_1 + \dfrac{x_1}{\omega}\dfrac{d(i_{b3} - i_{c3})}{dt} \\ u_{ca12} = u_{a2} - u_{c2} + u_{c1} - u_{a1} + (i_{c2} - i_{a2})(r_1 + r_2) \\ \qquad + \dfrac{x_1 + x_2}{\omega}\dfrac{d(i_{c2} - i_{a2})}{dt} + (i_{c3} - i_{a3}) r_1 + \dfrac{x_1}{\omega}\dfrac{d(i_{c3} - i_{a3})}{dt} \end{cases} \tag{4.179}$$

$$\begin{cases} u_{ab23} = u_{b3} - u_{a3} + u_{a2} - u_{b2} + \left(i_{a3} - i_{b3}\right)(r_2 + r_3) \\ \qquad + \dfrac{x_2 + x_3}{\omega}\dfrac{d(i_{a3} - i_{b3})}{dt} + i_{La1} r_2 + \dfrac{x_2}{\omega}\dfrac{di_{La1}}{dt} \\ u_{bc23} = u_{c3} - u_{b3} + u_{b2} - u_{c2} + (i_{b3} - i_{c3})(r_2 + r_3) \\ \qquad + \dfrac{x_2 + x_3}{\omega}\dfrac{d(i_{b3} - i_{c3})}{dt} + i_{Lb1} r_2 + \dfrac{x_2}{\omega}\dfrac{di_{Lb1}}{dt} \\ u_{ca23} = u_{a3} - u_{c3} + u_{c2} - u_{a2} + (i_{c3} - i_{a3})(r_2 + r_3) \\ \qquad + \dfrac{x_2 + x_3}{\omega}\dfrac{d(i_{c3} - i_{a3})}{dt} + i_{Lc1} r_2 + \dfrac{x_2}{\omega}\dfrac{di_{Lc1}}{dt} \end{cases} \tag{4.180}$$

$$\begin{cases} u_{ab31} = u_{b1} - u_{a1} + u_{a3} - u_{b3} + i_{La1}\left(r_1 + r_3\right) \\ \qquad + \dfrac{x_1 + x_3}{\omega}\dfrac{di_{La1}}{dt} + (i_{a2} - i_{b2}) r_3 + \dfrac{x_3}{\omega}\dfrac{d(i_{a2} - i_{b2})}{dt} \\ u_{bc31} = u_{c1} - u_{b1} + u_{b3} - u_{c3} + i_{Lb1}(r_1 + r_3) \\ \qquad + \dfrac{x_1 + x_3}{\omega}\dfrac{di_{Lb1}}{dt} + (i_{b2} - i_{c2}) r_3 + \dfrac{x_3}{\omega}\dfrac{d(i_{b2} - i_{c2})}{dt} \\ u_{ca31} = u_{a1} - u_{c1} + u_{c3} - u_{a3} + i_{Lc1}(r_1 + r_3) \\ \qquad + \dfrac{x_1 + x_3}{\omega}\dfrac{di_{Lc1}}{dt} + (i_{c2} - i_{a2}) r_3 + \dfrac{x_3}{\omega}\dfrac{d(i_{c2} - i_{a2})}{dt} \end{cases} \tag{4.181}$$

where x_1, x_2 and x_3 are the short-circuit reactances of the primary, secondary and tertiary windings, respectively. These values can be obtained from the transformer manufacturer.

$$\begin{cases} x_1 = \omega\left(L_1 - m_{12} - m_{13} + m_{23}\right) \\ x_2 = \omega(L_2 - m_{12} - m_{23} + m_{13}) \\ x_3 = \omega(L_3 - m_{13} - m_{23} + m_{12}) \end{cases} \tag{4.182}$$

If three groups of the ADOAPs are all less than a pre-set threshold, the relay determines that there is an inrush current and rejects the tripping. Otherwise, the relay determines that an internal fault has occurred.

4.10.2 Experimental System

To verify the effectiveness of the proposed method, the experimental tests have been carried out at the EPDL. The experimental transformer is a three-phase, two-winding transformer bank with Y_0/Δ-11 connection fed by a large power system grid (Figure 4.75). The parameters of the two-winding transformers are given in Table 4.14. Three identical CTs are connected in Δ on the primary side and another three identical CTs are connected in Y on the secondary side of the power transformer.

The experiments provide samples of three phase voltages and differential currents when the transformer is energized or when a fault occurs or when both occur simultaneously. To test various features of the algorithm, a total of 162 cases have been divided into three main categories: 56 cases for inrush conditions only, 52 cases for simultaneous internal fault and inrush conditions, and 54 cases for faulty conditions only. Different switching on and clearing instants for inrush currents, as well as different faults and short-circuit turn ratios for internal faults, are considered in the tests. The measured data are used as inputs to the developed algorithm to identify its response.

Figures 4.76–4.80 show some examples of the experimental test results: the differential currents and the resulting analysis. The ADOAPs are calculated just after the relay starts up for one cycle. In addition, the threshold is set to be 5 W (represented with the dashed line in the diagrams) and fairly good results have been obtained in all 162 cases.

4.10.3 Testing Results and Analysis

4.10.3.1 Responses to Different Inrush Conditions

A total of 56 test cases were carried out in this situation. The inrush current waveform is a function of the different core residual magnetization and the switching on instant, so the waveforms of the inrush current are different from each other. However, the ADOAPs calculated using Equation (4.165) present identical

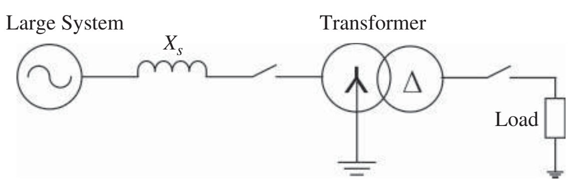

Figure 4.75 The EPDL experimental system

Table 4.14 Parameters of the transformer used in the test

Rated capacity (kVA)	30
Rated voltage ratio (V)	1732.05/380
Rated current ratio (A)	10/45.58
Rated frequency (Hz)	50
No-load current (%)	1.45
No-load loss (%)	1
Short-circuit voltage (%)	9.0–15.0
Short-circuit loss (%)	0.35
Load (kW)	0.9

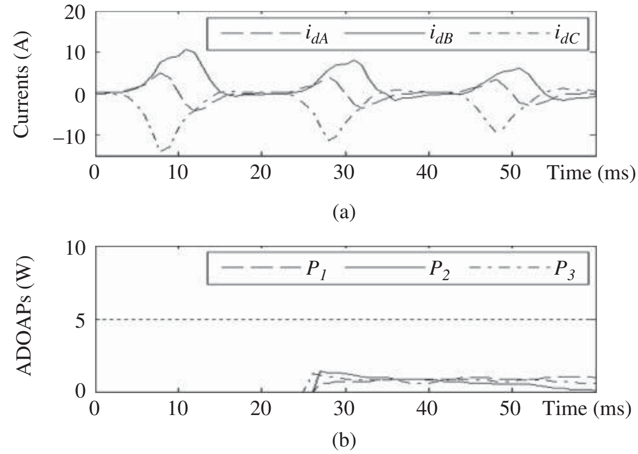

Figure 4.76 Differential currents and experimental results when the transformer is energized: (a) differential currents; (b) ADOAPs

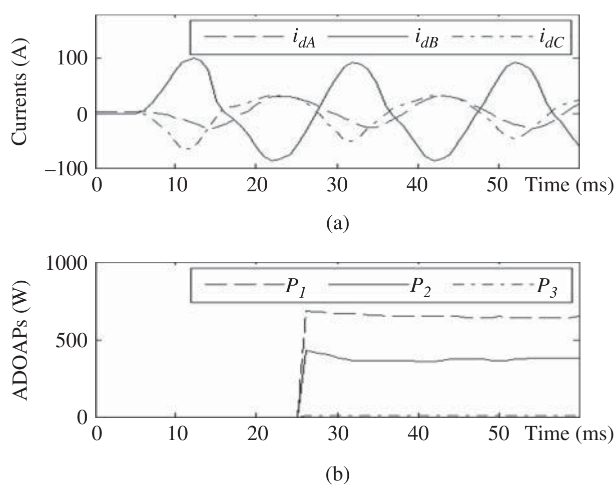

Figure 4.77 Differential currents and experimental results when the transformer is switched on with no load and a turn-to-ground fault in phase B: (a) differential currents; (b) ADOAPs

results due to elimination of flux linkages. An example taken from these cases is given in Figure 4.76, where the differential currents of the three phases and their ADOAPs are shown in Figures 4.76a and 4.76b, respectively. It is found that the calculated ADOAPs of the three phases are negligible and only have little variation resulting from the measurement and calculation errors (Figure 4.76b). According to the criterion of the two-winding three-phase transformer, the protection will be blocked.

4.10.3.2 Responses to a Simultaneous Fault and Inrush Conditions

When the transformer is energized with an internal fault, the inrush current may occur and will affect the differential current waveforms of fault phases. This has been verified by a total of 52 cases with simultaneous inrush currents and internal fault currents.

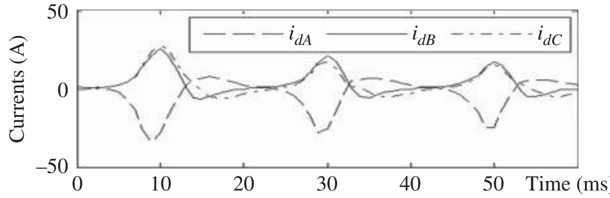

(a)

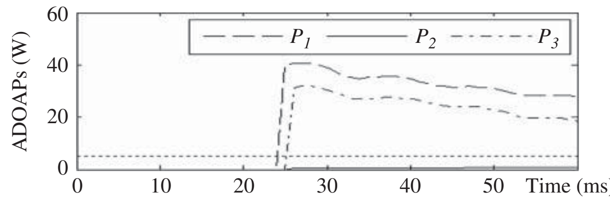

(b)

Figure 4.78 Differential currents and experimental results when the transformer is energized with a 2.4% turn-to-turn fault in phase A: (a) differential currents; (b) ADOAPs

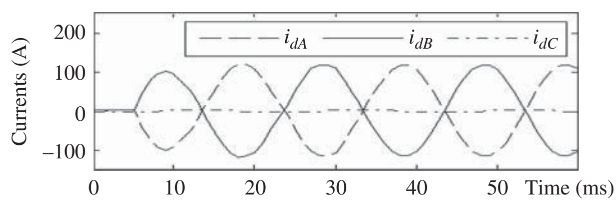

(a)

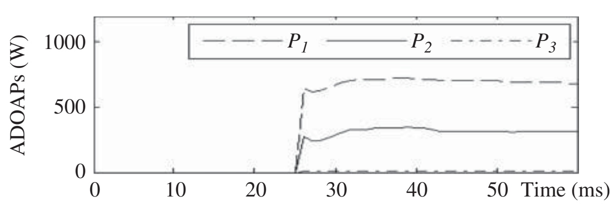

(b)

Figure 4.79 Differential currents and experimental results when a turn-to-ground internal fault occurs in phase B: (a) differential currents; (b) ADOAPs

Figure 4.77a as an example shows this condition, which is obtained by switching on the transformer bank with no load and a turn-to-ground fault in phase B. Nonfault phase C presents the magnetizing current and fault phases A and B show little distortion. Using Equation (4.165), the ADOAPs of the three phases can be calculated (Figure 4.77b). The ADOAP of phase C is close to zero, whereas the ADOAPs of phases A and B are very noticeable.

Compared with Figure 4.77a, Figure 4.78a shows differential currents with more severe distortion, where the transformer bank is energized with no load and a 2.4% turn-to-turn fault (minimum ratio of turns provided by the experimental transformer) occurs in phase A.

After analysis in the frequency domain, it is found that the magnitudes of the second harmonic in fault phases A and C are greater than that of some magnetizing inrush currents. Consequently, the commonly employed conventional differential protection technique based on the second harmonic will thus have difficulty in distinguishing between an internal fault and an inrush current. However, the ADOAPs of fault phases show much higher amplitudes than the threshold in Figure 4.78b, which means that the relay determines there is an internal fault and lets the relay trip.

These results are in accordance with the practical state of the transformer bank. In the total of the 52 cases, the identical results verify that the proposed technique is sensitive and reliable to discriminate internal faults from inrush currents when the simultaneous inrush currents and faults occur in the transformer.

4.10.3.3 Responses to Internal Fault Conditions Only

Data from a total of 54 cases are used to calculate the ADOAPs based on Equation (4.165). In all of the 54 cases, the ADOAPs of the faulty phases are noticeable, whereas the ADOAPs of nonfaulty phases are negligible. Two examples are shown in Figures 4.79 and 4.80, respectively. One is a turn-to-ground fault in the phase B (the same fault location as the example shown in Figure 4.77) and the other one is a 2.4% turn-to-turn internal fault in the phase A (the same fault location as the example shown in Figure 4.78), where the differential currents of the faulty phases become sufficiently small to be comparable with the nominal value.

In Figures 4.79b and 4.80b, it is found that the ADOAPs of nonfault phases are close to zero but the ADOAPs of fault phases are all larger than the threshold. Moreover, the ADOAPs in Figures 4.79b

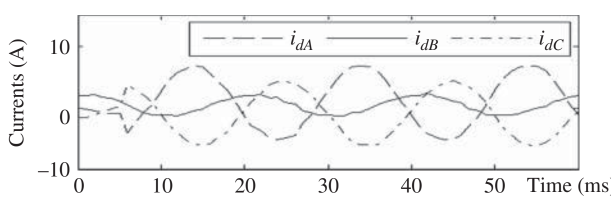

(a)

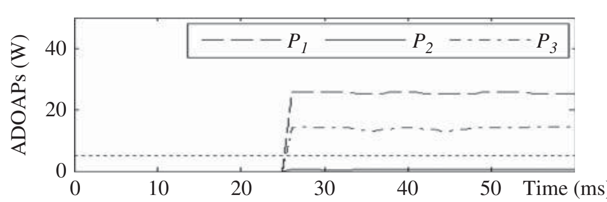

(b)

Figure 4.80 Differential currents and experimental results when a 2.4% turn-to-turn fault occurs in phase A: (a) differential currents; (b) ADOAPs and 4.80b present similar results to those in Figures 4.77b and 4.78b, respectively. These results prove the accuracy of the calculated ADOAPs and the sensitivity of the method to identify the internal faults.

In summary, application of the two-terminal network to discriminate the inrush current from the internal fault current of a transformer is proposed. The basic theory about the two-terminal network was derived first. Then, the criteria of the single-phase transformer, the two-winding three-phase transformer and the three-winding three-phase transformer were developed in detail. A large number of experiments were carried out to test the proposed techniques. In all of the 162 cases, the ADOAPs of the nonfault phases are close to zero. On the other hand, the ADOAPs of phases with the internal faults are noticeable and faults are all determined within one and a quarter cycle. The method is suitable whether it is possible to measure the winding currents or not. Also, the method does not require the presence of harmonic currents to restrain the protection system during magnetizing inrush. Furthermore, the proposed method is independent of the B–H curve, the leakage inductances and iron losses. The experimental results verify the reliability, sensitivity and computational simplicity of the method.

4.11 Summary

Inrush can be generated when a loaded transformer is switched on the transmission line or an external line fault is cleared, which may result in mal-operation of differential protection. Several schemes have been proposed to distinguish between inrush and fault currents in this chapter, which is the key to improve the reliability of the differential protection of power transformer. Experimental cases have been tested and the results show that the proposed method is able to reliably and accurately discriminate internal faults from inrush currents.

References

[1] Sharp, R.L. and Glassburn, W.E. (1958) A transformer differential relay with second-harmonic restraint. *AIEE Transactions, Part III: Power Apparatus and Systems*, **77** (3), 913–918.

[2] Thorp, J.S. and Phadke, A.G. (1982) A microprocessor based three-phase transformer differential relay. *IEEE Transactions on Power Apparatus and Systems*, **2**, 426–432.

[3] Phadke, A.G. and Thorp, J.S. (1983) A new computer-based flux-restrained current-differential relay for power transformer protection. *IEEE Transactions on Power Apparatus and Systems*, **11**, 3624–3629.

[4] Sidhu, T.S. and Sachdev, M.S. (1992) Online identification of magnetizing inrush and internal faults in three-phase transformers. *IEEE Transactions on Power Delivery*, **7** (4), 1885–1891.

[5] Liu, P., Malik, O.P., Chen, D. *et al.* (1992) Improved operation of differential protection of power transformers for internal faults. *IEEE Transactions on Power Delivery*, **7** (4), 1912–1919.

[6] Rahman, M.A. and Jeyasurya, B. (1988) A state-of-the-art review of transformer protection algorithms. *IEEE Transactions on Power Delivery*, **3** (2), 534–544.

[7] Youssef, O.A. (2003) A wavelet-based technique for discrimination between faults and magnetizing inrush currents in transformers. *IEEE Transactions on Power Delivery*, **18** (1), 170–176.

[8] Lin, X.N., Liu, P. and Malik, O.P. (2002) Studies for identification of the inrush based on improved correlation algorithm. *IEEE Transactions on Power Delivery*, **17** (4), 901–907.

[9] Zaman, M.R. and Rahman, M.A. (1998) Experimental testing of the artificial neural network based protection of power transformers. *IEEE Transactions on Power Delivery*, **13** (2), 510–517.

[10] Wiszniewski, A. and Kasztenny, B. (1995) A multi-criteria differential transformer relay based on fuzzy logic. *IEEE Transactions on Power Delivery*, **10** (4), 1786–1792.

[11] Yabe, K. (1997) Power differential method for discrimination between fault and magnetizing inrush current in transformers. *IEEE Transactions on Power Delivery*, **12** (3), 1109–1118.

[12] Ge, B.M., de Almeida, A.T., Zheng, Q.L. *et al.* (2005) An equivalent instantaneous inductance-based technique for discrimination between inrush current and internal faults in power transformers. *IEEE Transactions on Power Delivery*, **20** (4), 2473–2482.
[13] Sachdev, M.S., Sidhu, T.S. and Wood, H.C. (1989) A digital relaying algorithm for detecting transformer winding faults. *IEEE Power Engineering Review*, **9** (7), 49–50.

5

Comprehensive Countermeasures for Improving the Performance of Transformer Differential Protection

5.1 Introduction

Under certain conditions, a considerable magnetizing inrush will occur when the transformer is switched on. Magnetizing inrush is harmful to a power grid in many aspects: magnetizing inrush is a kind of shock current. The mechanical stiffness of the transformer coil may be completely changed by the mechanical force generated by the operation of switching on. In the worst case, it will produce a shift of the transformer in the fuel tank, which may destroy the coupling between the coils and the links between the coils and the terminals. It eventually leads to the winding open. Meanwhile, the existence of the magnetizing inrush will be regarded as an internal fault by the differential protection, causing the malfunction of the relay. Rich harmonic components within the magnetizing inrush may cause resonance under a certain frequency, which results in a negative impact on the power quality of the power grid. The DC component of the magnetizing inrush produces a mechanical torque of an oscillating nature on the motor and will increase the oscillation of the motor, thereby affecting its life. For the power transformers in the transmission system and distribution system, the magnetizing inrush will not occur until the operation of the routine switching on or re-closing after fault removal. However, it is different for a traction transformer, which is widely used in electrified railways. Because of the existence of intermediate links (dead zone) in the overhead transmission lines, the power-up and power-down operation will occur 50 times in each 1000 km distance, and these will frequently induce magnetizing inrush of the transformer.

The main research interests in the field of transformer inrush suppression include the following two aspects: one is to control the inception angles of the transformer or switch large resistance to suppress the inrush; the other is to eliminate the adverse effects of inrush on the transformer differential protection by identifying the characteristics of magnetizing inrush. Both strategies have obvious shortcomings. Firstly, the control accuracy of the inception angle needs high hardware requirements. The optimal closing time may be missed due to a very short delay. In a power-frequency cycle, only two voltage inception angles without magnetic bias can be captured, that is, the two peaks of the sinusoidal voltage (90° or 270°). If these two points deviate, the magnetic bias will occur, which requires that all operation mechanisms (including circuit breakers) of the switching-on operation must have an accurate and stable operating time. In order to completely eliminate the three-phase magnetizing inrush, the three phases of the breaker

Electromagnetic Transient Analysis and Novel Protective Relaying Techniques for Power Transformer, First Edition. Xiangning Lin, Jing Ma, Qing Tian and Hanli Weng.

must be switched on in terms of time-sharing and split-phase. However, some existing electricity operating codes prohibit such time-sharing and split-phase operation in that it will lead to non-wholly-phase operation. In addition, some breakers structurally cannot be split-phase operated. On the other hand, the identification error is affected by many factors and it is rather difficult to identify the magnetizing inrush by means of physical and mathematical methods because the characteristics of the magnetizing inrush are related to many factors, such as the inception angle, the electromagnetic parameters of the transformer. Therefore, there exists remarkable action discreteness. Universally valid identification and avoidance strategies 'to avoid inrush occurrence' have not yet been found although there have been decades of unremitting efforts. Another Achilles' heel 'to avoid inrush occurrence' is to tolerate the appearance of the magnetizing inrush. Its pollution of the power grid and the destructive force to the electrical equipment still exist.

To solve the above problem, a so-called 'Magnetizing Inrush Suppresser' (MIS) based on second-order underdamped circuit are designed to directly eliminate magnetizing inrush. Incorporating the MIS, it imposes the source voltage on the tertiary winding of the three-winding transformer, which has the same phase with the excitation voltage and its amplitude can slowly change according to a specific time constant. As the voltage amplitude is gradually increased to the rated voltage, there will be no magnetizing inrush caused by the transient process. When the main winding is switched on, the main magnetic flux is first established through the tertiary winding. Because of the seamless connection of the boundary conditions, it will not stimulate the magnetizing inrush at the moment of switching on. An MIS ceases operation when the energizing process is completed. The simulation tests for the function of magnetizing inrush suppression are carried out based on PSCAD/EMTDC software, and the simulation results show the correctness and effectiveness of the proposed method.

Differential protection, having a simple principle and reliable performance, is one of the key protections of mainstream electric equipment. When applied to protecting transformers, two important problems need to be resolved – how to ensure the stability of the differential protection during occurrences of magnetizing inrush and how to ensure stability during current transformer (CT) saturation [1, 2]. With regard to the inrush restraint, a variety of solutions have been proposed [3–6]. In contrast, solutions for the latter have yet to be studied in depth. The definition of the problem resulting from CT saturation can be illustrated by Figure 5.1 and is elaborated further here

Figure 5.1 shows the comparison of the primary, secondary and magnetizing currents during CT saturation due to a heavy external fault. In this case, the short-circuited current with great amplitude, especially with the aperiodic component of the current, probably means that the CT enters into the saturation quickly. In this case, a proportion of the primary current of the CT is forced to flow through the magnetizing branch. If supposing that CTs on the other side of the protected equipment, such as the power transformer or busbar, can still transform linearly, the differential protection can detect the false differential current with observable amplitude. Actually, this differential current is the magnetizing current of the saturated CT. The mal-operation of the differential protection possibly occurs if this current exceeds the operating threshold.

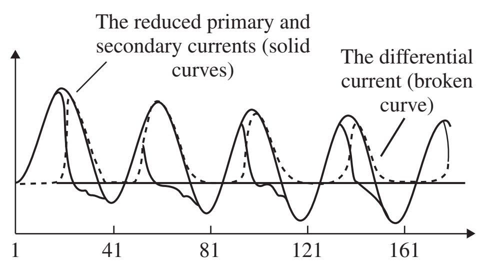

Figure 5.1 Currents during CT saturation

The percentage restraint criterion and the method using operation time difference between start-up element and the differential protection element [7] are two typical solutions.

The characteristic of the percentage restraint principle is that the operation current will increase with respect to the increase of the through current. Therefore, mal-operation due to CT saturation caused by an external fault can be avoided to some extent. However, in the event of extreme saturation of the CT, this method will fail to restrain the differential protection. To deal with this scenario, an alternative method emerges in terms of the facts outlined in the following paragraph.

In the initial stage of an external fault (1/4.1/2 cycle), even if an extreme one, CTs are commonly in the unsaturated state and the false differential current is quite low, as CTs transform linearly. Therefore, in the event of external fault, the differential element will operate a little bit slower than the start-up element; but for an internal fault, the start-up element and the differential protection operate simultaneously no matter whether the CT saturates or not. Therefore, the operating time difference between the start-up element operation and differential protection operation can be used to discriminate between internal and external faults effectively. In this way, the differential protection will be blocked for a period of time to avoid mal-operation when an external fault is determined. Adopting this method can basically ensure the security of the differential protection experiencing an external fault. To implement a complete protection scheme, the scenario of a cross-country fault should be dealt with. A cross-country fault is one where there are two faults affecting the same circuit, but in different locations and, possibly, involving different phases. Among a variety of cross-country faults, the one in which an external fault develops to become an internal fault is the concern of the protection engineer. There are two methods for dealing with the problem of a cross-country fault. One ignores the cross-country fault's existence, that is, the blocking process of the protection lasts until the differential element reclaims and then the protection can be unblocked. In this case, if the external fault develops to an internal fault, the protection will fail to trip for a long time. The other method is to detect the waveform of the differential current continuously to check if the CT is still saturated. In this case, the cross-country fault will be regarded as nonexistence if the CT still saturated; otherwise, it is determined that the external fault develops to an internal fault and the protection is unblocked. Some methods identifying CT saturation have been proposed, such as the one based on waveform identification, the one based on wavelet analysis, the one based on harmonic detection and so on. All these methods are established with a potential premise, that is, the CT saturation will vanish when the external fault develops to an internal fault, and this assumption is basically correct for busbar protections.

For busbar protection, when a fault occurs at the near-end of one line, short-circuited currents supplied by each power supply all flow through the CT on the faulty line. As type selections of CTs are identical under the same voltage level, the short-circuited current on the faulty line far exceeds the short-circuited currents on other lines, which lead CTs on the faulty line to enter an extreme saturated state while the CTs on other lines remain unsaturated. In this case, false differential current occurs. When the external fault develops to an internal fault of the busbar, the short-circuited current carried by the CT of the heaviest burden will turn to a much lower value, since it is fed only by a certain source. Herein, the saturation of the CT will disappear. In this case, the waveform of the differential current will present the characteristic of an unsaturated one. Therefore, it is correct to unblock the busbar differential operation according that whether the saturation characteristic of differential current waveform exists or not.

However, the situation for the transformer protection is different. As the voltage level of each side of the transformer is different under normal operating condition, load currents flowing through both sides are different. The differential current should not exist under normal operating conditions. Therefore, the linearity degrees of the CTs on both sides should be identical. However, it is a difficult task due to different load currents. In this scenario, when an external short-circuit fault occurs, the through current always enables the CT on one side to saturate more easily. If an external fault occurs on the external side of the unsaturated CT and then develops to an internal one, the differential current consequentially contains the current flowing through the saturated CT. The worst scenario occurs in the case of single-end power supply. In this case, the differential current only consists of the secondary current of the saturated CT. Under this circumstance, varied criteria unblocking the protection based on the vanishing of the saturation characteristic of differential current will fail to unblock the differential protection. Obviously, it does not meet the requirement for fast operation of differential protection.

To deal with the above problem, a new criterion was sought for the fast unblocking of the differential protection when experiencing a cross-country fault. During our investigations, it was noticed that the locus of the variation of the saturated secondary current with respect to the differential current can be used to dynamically identify the cross-country fault. Therefore, the blocked protection during CT saturation due to an external fault can be unblocked as soon as possible. The detail of this method is given below.

The differential protection is a widely-applied main protection of power transformers. Due to the influence of the saturation of the iron core of the transformers, the sensitivity and reliability of the relay are not always harmonized in terms of identifying between the inrushes and fault currents.

Up to now, many solutions have been proposed, for example, multipiecewise based percentage differential protection, second harmonic restraint and so on. These methods have been successfully applied on site. However, there are also some disadvantages to be overcome. To improve the use ratio of ferromagnetic materials, the point of saturation is designed at a relatively low value, which leads to challenges to a category of criteria based on the characteristic of the differential currents, such as second harmonic based ones and the so-called waveform symmetry based ones. Actually, the average correct operation ratio of the differential protection of transformers of 220 kV and above is only up to 76% approximately according to the statistics of relay operation.

The faults of transformers can be classified as ones inside the tank and ones outside the tank. The usual faults outside the tank include the phase–phase faults and the earth faults, and so on. These serious faults will result in the heavy short-circuit current, leading to serious impact on the transformers. Even the tank-in faults, which include the inter-turn faults and turn-to-ground faults, also lead to the overheating of the transformer, damaging the winding or the core if they are not cleared in time. On the other hand, the sensitivity of the protection is often lowered deliberately to avoid mal-operation resulting from the false differential current, such as magnetizing inrushes. To effectively protect the transformer, the sensitivity of the protection in terms of discrimination between false differential currents and inter-turn fault currents must be significantly improved.

Besides, the differential protection will be blocked by the restraint element when the false current results from transformer energizing or voltage recovery. In this case, if the cross-country fault occurs during this period, some existing criteria are incapable of identifying the developing fault and lead to the long-time fail-to-trip of the protection. Although it is perhaps a small-probability event, it has been reported several times previously. A well-designed protection should not ignore this defect. Therefore, a good criterion will have the ability to identify the developing fault even in the existence of false differential current and allow the protection to operate rapidly.

Furthermore, most conventional criteria based on the harmonic or waveform characteristics to identify the magnetizing inrush current usually need one cycle post-fault current data, which limits the operation speed. However, the benefit of reliable and high-speed main protection of the transformer is self-evident if the speed of identifying the fault can be increased.

Aimed at solving the problems above, the characteristic of the time interval between the sudden change of phase voltage and the emergence of differential current has been investigated and a new time-interval based relay criterion for differential protections is proposed. An EMTDC-based model, which covers various fault situations, taking the Y/Δ-connected transformer as an example, is established to verify this criterion. The test results confirm that the criterion is effective and practical. Furthermore, a comprehensive protection scheme is designed on the basis of time-difference based method, together with second harmonic restraint criterion and cross-country fault identification criterion to deal with a variety of complicated energizing and fault scenarios. This scheme is also validated with extensive simulation tests.

Differential protection is widely used to protect generators, transformers, busbars and the transmission lines [8]. Therefore, the reliability of the differential protection, especially when experiencing a variety of disturbances, becomes the main concern. CT saturation is the greatest challenge to the stability of the differential protection. A false differential current will occur if the transforming characteristic of the CT on one side differs from that of the CT on the other side. A significantly high false differential current may emerge if the CT at one side saturates in depth, while the one at the other side completely transforms the primary current. In this case, the differential protection possibly mal-operates. Such scenarios must be taken into account and prevented.

Studies have disclosed that the CT output at each side will not saturate immediately, even when experiencing a heavy through fault. Suppose that the differential protection is equipped with two CTs, one can transform the primary current all over the transient process while the other one saturates during this process. It should be noticed that both CTs operate in the linear region for at least 3.5 ms before one attains saturation. This phenomenon results from the fact that the reactance of the core of the CT is an energy-storage element and follows the law the conversation of energy. Therefore, the current through it cannot change suddenly. Therefore, both CTs can truly transform the primary current during this period of time, and the differential current will not emerge in this period. Afterwards, a false differential current may occur if one of the CTs begins to saturate. In this case, a time difference (TD) between the fault occurrence and the emergence of a false differential current will exist. As for any internal fault, even accompanied by the subsequent CT saturation, this TD is nearly equal to zero in that both CTs can transform the primary currents truly in the initial stage of the fault, and the authentic differential current can be obtained instantaneously when the phase currents change. Therefore, there will not be such a TD in the event of any internal fault. As a result, this TD can be used as a criterion for allowing the differential protection to operate instantaneously. However, the TD is possibly too small to be identified in the event of very fast CT saturation. An effective algorithm to locate this TD is still worth studying. A new scheme of CT saturation blocking using mathematical morphology (MM) is introduced to accurately discern this TD between the fault occurrence instant and differential current emergence instant.

As the theoretical fundamental of the proposed criterion, MM is introduced briefly below. Then a novel TD detection criterion using series multiresolution morphological gradient (SMMG) is put forward. To evaluate the effect of the proposed method, the EMTDC-based simulations were carried out and the performance of this scheme evaluated.

Differential protection is the main protection of primary electrical equipment from internal faults, the application of which is very successful on generators. But there are some problems when it is applied to transformers. There are two or three voltage grades in conventional transformers. Because the voltage level, the transformation ratio, capacity and iron core saturation as well as three-phase wiring of CT used by differential protection are different, the magnitude of the stable and transient unbalanced current of the differential circuit is very large. Especially when an external short-circuit fault occurs, the magnitude of the unbalanced current is much larger. The characteristic of the internal fault may be shown in a differential circuit, which inevitably leads to protection mal-operation without any measurements. The ability to avoid the unbalanced current can be improved by selecting reasonable braking characteristics of the differential relay ratio. On this basis, different countermeasures are proposed according to the characteristics of the waveform of the unbalanced current, such as the Time Difference Method, Harmonic Detection Method, DC Latching Method and so on. The internal and external faults are distinguished by detecting whether the faults and the moment when the differential current occurs are synchronized using the Time Different Method. Because the CT may be saturated in a very short time when an external fault occurs, accurate judgments will not be made if a tiny deviation of positioning occurs at that time. For the Harmonic Detection Method, because the harmonics in the transient current cannot be accurately quantified, the setting value is determined by experience, as well as filter parameters and algorithms, the sensitivity of which needs to be improved. The significant feature of the imbalanced current is that the maximal value of the DC component is greater than that of the AC component, so the phenomena that the waveform of the current is biased to the timeline occur. That is, the instantaneous value of the current is unipolar; the insulation of winding only breaks down when the voltage is close to peak, so the instantaneous value of the short-circuit current is bipolar when a fault occurs in a transformer. If a regional fault occurs outside the protected transformer and it is a threat to system stability that requires rapid removal, a differential current quick break protection can be added to constitute a DC lockout program of CT transient saturation.

Traditional relays, based on the DC component of the velocity saturation principle, often mal-operate because of failure to avoid an inrush current when the transformer is closed with no load. So, based on the analysis of the CT transient saturation behaviour, a new method using grille fractal algorithms to fully excavate the singularity information of the current waveform is proposed. The protection mal-operation caused by CT saturation can be avoided when an external fault occurs, and inrush current can be latched by the method. The grille fractal curve can be denoised and smoothed by means of a generalized morphological filter combined with an adaptive algorithm. Finally, the correctness and feasibility of the method is verified by dynamic simulation tests.

5.2 A Method to Eliminate the Magnetizing Inrush Current of Energized Transformers

5.2.1 Principles and Modelling of the Inrush Suppressor and Parameter Design

5.2.1.1 Factors Influencing the Magnetizing Inrush

The magnitude of the magnetizing inrush depends on the value of the magnetizing inductance, L_μ, and also on whether the transformer core is saturated. The transformer core is not saturated during normal operation and external faults. When the voltage is restored after no-load transformer energizing and removal of external fault, the transformer voltage will rise to the operating voltage from zero or a very small value suddenly. During the electromagnetic transient process of the voltage rising, the transformer may be severely saturated, leading to a magnetizing inrush of great magnitude. Its peak value can be up to 4–8 times the rated current. Remanence and inception angle are the most critical factors affecting the inrush magnitude.

Magnetizing inrushes caused by transformer energizing under conditions of different inception angles are shown in Figures 5.2–5.5. The peak values of the inrushes and the times to steady state for various switching angles are summarized in Table 5.1.

The simulation uses the benchmark model of the single-phase transformer in PSCAD/EMTDC, the fundamental parameters are:

Normal capacity: $S_N = 100.0$ MVA

Normal voltage (RMS): $U_{1N}/U_{2N} = 230.0\ \mathrm{kV}/115.0\ \mathrm{kV}$

(Note: The following data are p.u.)

Leakage inductance: $L_\sigma = 0.10$

Air gap core mutual impedance: $L_m = 0.20$

Core magnetization curve knee point: $\Phi_{sat} = 1.25$

Excitation current: $I_\mu = 0.3\%$

Remanence: $\Psi_r = 0.7$

Owing to the existence the core remanence, the inrush value is not 0 in the case when the inception angle, $\alpha, = 90°$ and $270°$. However, compared with other cases, the magnitude of the inrush is lower and the transitional time to normal operation is also greatly reduced. In fact, there always exists a certain inception condition that corresponds to each of the remanence leading to the synthesis of DC magnetic bias being equal to zero. For instance, in the case of remanence $\psi = 0.7$ (per unit), the magnetic flux of the core after transformer switch-on is:

$$\Psi = -\Phi_m \cos(\omega t + \alpha) + (\Phi_m \cos \alpha + \Psi_r) \tag{5.1}$$

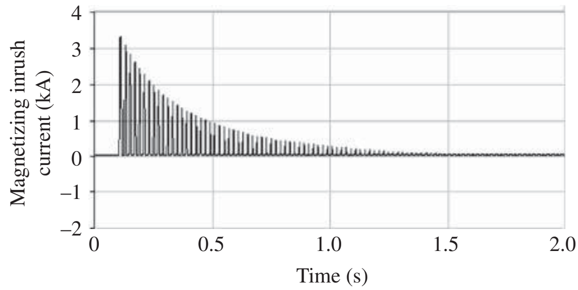

Figure 5.2 Magnetizing inrush when $\alpha = 0°$

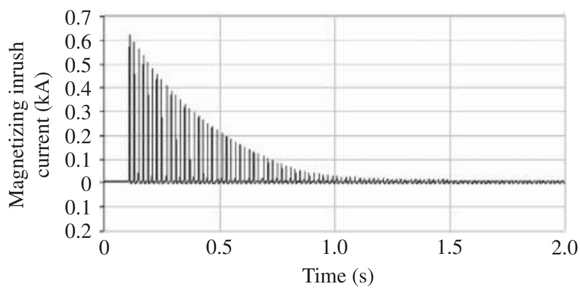

Figure 5.3 Magnetizing inrush when $\alpha = 90°$

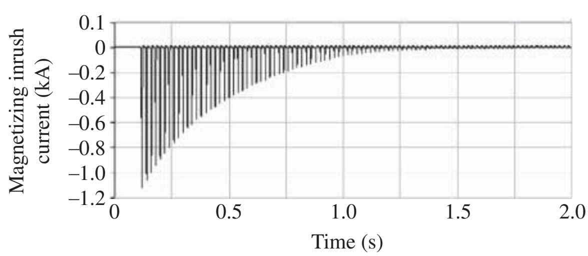

Figure 5.4 Magnetizing inrush when $\alpha = 180°$

The magnetic bias of the core (i.e. transient nonperiodic) is:

$$\Psi_{res} = (\Phi_m \cos\alpha + \Psi_r) \tag{5.2}$$

Substituting $\psi_r = 0.7$ p.u. into Equation (5.2) and letting Equation (5.2) equal 0, the ideal inception angle should be:

$$\alpha_{best} = \arccos\left(-\frac{\Psi_r}{\Phi_m}\right) = \arccos(-0.7) = 2.3462\ \text{rad} \tag{5.3}$$

If the inception angle is α_{best}, the transient process of the flux does not appear at the inception moment and the magnetizing inrush will no longer appear. In this case, the transformer will directly enter the steady-state operation.

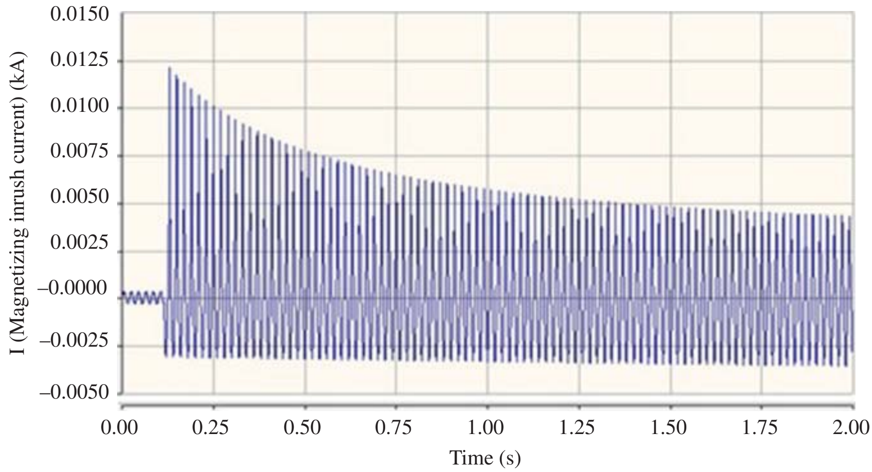

Figure 5.5 Magnetizing inrush when $\alpha = 270^\circ$

Table 5.1 The peak value of the inrush and the time to steady state for various switching instants

Inception angle, α (°)	Peak value of the inrush (kA)	Duration of the transient process (s)
0	3.0354	1.7
90	0.618	1.1
180	−1.1376	1.5
270	0.01121	0.9

As seen, the inception angle of the transformer has great impact on the generation of magnetizing inrush. If the inception angle can be effectively controlled, the appearance of the magnetizing inrush will be fundamentally suppressed. There exist two scenarios for the transformer from its switching-off to re-energizing. The first is that the protection will disconnect the transformer when a transient fault occurs on transformer. The transformer will then be commissioned again through the re-closing operation when the detected fault is eliminated. Secondly, after outage for a long period due to routine maintenance, the transformer is commissioned again through the energizing operation. For the former case, the core flux of the transformer at the exiting moment can be obtained indirectly by recording its current value before the transformer was switched off. According to the ferromagnetic material aging characteristics of the transformer iron core, the magnetic flux can be calculated when the transformer is re-closed again after a relatively short period of time. However, at present, a recognized model to calculate the remanence of the core is still not available. Most existing models are theoretical ones. For the second case, determining the remanence of the core during transformer energizing is more difficult. In summary, it is quite difficult to accurately determine the remanence of the transformer. Even if the remanence is given, it is still not feasible to catch the best time and successfully switch on by means of inception-angle control as mentioned earlier. Therefore, elimination the magnetizing inrush by relying on inception-angle control cannot be guaranteed.

In view of this problem, a process to inhibit the magnetizing inrush that does not depend on detecting the core residual flux or controlling the inception angle is presented.

In this method, the tertiary winding is connected to a self-designed Inrush Current Suppresser (or magnetizing inrush suppressor, MIS). Firstly, the tertiary winding side is switched on until the main flux is stable. Then, the primary winding side is switched on. Finally, the tertiary winding is switched off and the transformer operates in the normal state. The input voltage of the MIS comes from the primary winding side, so no extra power is needed and the phase of the output is the same as the primary one. With the above design, the magnitude of the voltage applied to the tertiary winding can rise gradually up to the rated voltage based on the specific time constant. No magnetizing inrush will occur, since the voltage increases smoothly. Theoretically, with the coordinate of the MIS and the order of switch-on, the transient nonperiodical components (biasing magnetism) generated by the combination of inception order and residual flux can be eliminated completely.

5.2.1.2 Principle and Modelling of MIS

The MIS is located at between the tertiary winding of the three-circuit transformer and power supply.

Firstly, the tertiary winding is charged by the MIS before the primary winding is energized, which establishes the steady-state alternating magnetic flux:

$$\Psi_2 = -\Phi_{\mathrm{m}} \cos(\omega t + \alpha) \tag{5.4}$$

Then, the primary winding is switched on the grid. Neglecting the active power loss of the transformer (that is, ignoring the resistance in the equivalent circuit) gives:

$$\begin{cases} u = \sqrt{2}U_m \sin(\omega t + \alpha) \\ u = \dfrac{d\Psi}{dt} \end{cases} \tag{5.5}$$

Therefore:

$$\Psi = -\Phi_m \cos(\omega t + \alpha) + C \tag{5.6}$$

When the primary winding is switched on, according to the core flux linkage conservation:

$$-\Phi_m \cos(\omega t + \alpha)|_{t=t_0} + C = -\Phi_m \cos(\omega t + \alpha)|_{t=t_0} \tag{5.7}$$

Thus the bias magnetism is given by Equation (5.8) when the transformer is switched on:

$$\Psi_{res} = C = 0 \tag{5.8}$$

Under such circumstances, the transformer can directly enter into steady state. After the transformer has been successfully switched on, disconnecting the tertiary winding at any time will not lead to a transient process, since it has no influence on the main magnetic circuit. Therefore, with the help of the suppressing design and the coordination between switching on and switching off, the big voltage step that results in biasing magnetism, and thus causes saturation and magnetizing inrush, can be avoided. A simulation instance which illustrates the process of transformer switching on and switching off to implement the core magnetic flux seamless connection is shown in Figure 5.6.

In this case, the tertiary winding voltage has been increased to the steady state gradually. Then, the simultaneous switching-on and switching-off operations are executed at the time of t = 0.1 s. The corresponding current and potential waveforms are shown in Figure 5.6. This figure shows that the current of the tertiary winding is very small before t = 0.1 s and the current through the primary winding is zero. After t = 0.1 s, the tertiary current turns into zero because of switch off while the primary winding enters directly into steady state. The simulation indicates that no inrush occurs on the primary winding.

Therefore, the key point to solve the problem rests with designing an appropriate inrush suppresser that inhibits the possible magnetizing inrush when the tertiary winding is switched on in advance.

The inrush suppresser should consist of a voltage divider and a second order underdamped system. The MIS should exit when the transformer is running in a steady state, since it is a series element that

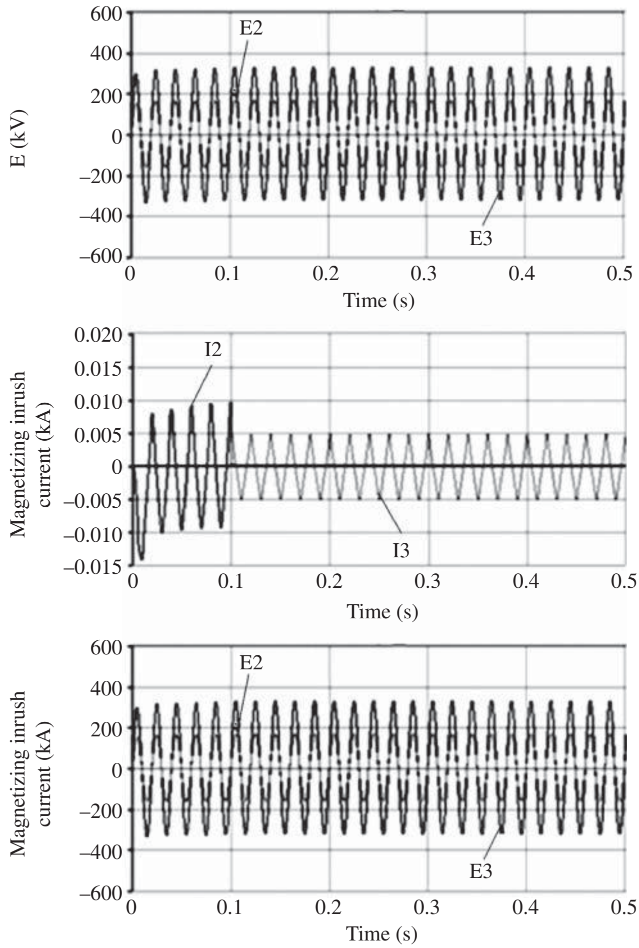

Figure 5.6 Magnetizing current and the electromotive force (EMF) waveform in the main winding and the tertiary winding in the case of synchronized switch-on accompanied by switch-off

contains energy dissipating elements such as resistance. Taking this factor into consideration, it is better to operate by means of the tertiary winding instead of by the primary loop. When the power supply is charging the transformer through the MIS and the tertiary winding, the voltage can change according to the step response and the specific time constant. The voltage magnitude rises gradually to the rated value, and the voltage frequency and phase are in accordance with the primary winding.

The model of the MIS between winding #2 and the power supply on a three-circuit transformer is shown in Figure 5.7. (#2 stands for the circuit of the tertiary winding and #3 denotes the primary one.)

When energizing the transformer, the tertiary winding is firstly energized by the MIS. Then, the circuit breaker of the primary winding is closed when the tertiary winding voltage reaches the stable value; the MIS is disconnected subsequently. Finally, the transformer runs in the normal operation state.

As mentioned previously, the MIS is realized based on second-order underdamped system. The characteristic roots of the transfer function of the second-order underdamped system are a pair of conjugate complex roots. With reasonable design of the damping ratio of the second-order underdamped system,

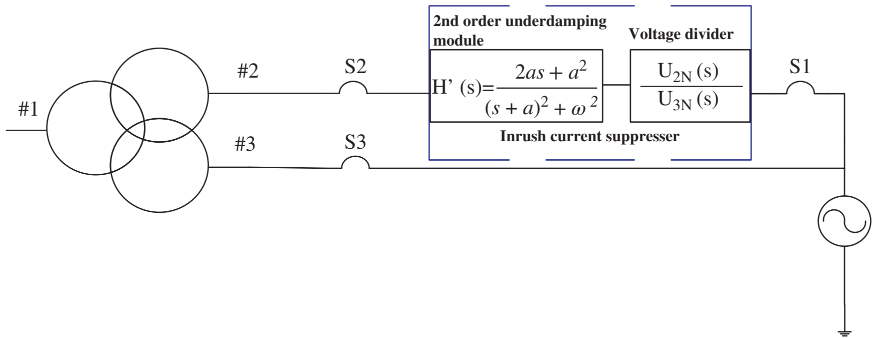

Figure 5.7 Connection of the magnetizing inrush suppresser

it is fully capable of tracking the frequency and phase of sinusoidal input voltage, to achieve the purpose of restraining inrush. The specific design is described here.

Assume the input voltage source of the tertiary winding is given by:

$$u_i = \sqrt{2}U_m \sin(\omega t + \alpha) \tag{5.9}$$

The expected output voltage of the second-order system is:

$$u_o = \sqrt{2}U_m(1 - \exp(-t/T)) \sin(\omega t + \alpha) \tag{5.10}$$

Using the Laplace transform to deal with the input signal and output signal, gives:

$$\begin{cases} U_i(s) = \sqrt{2}U_m \omega e^{\frac{\alpha}{\omega}s} \dfrac{1}{s^2+\omega^2} \\ U_o(s) = \sqrt{2}U_m \omega e^{\frac{\alpha}{\varpi}s} \left(\dfrac{1}{s^2+\omega^2} - \dfrac{1}{\left(s+\frac{1}{T}\right)^2+\omega^2} \mathrm{e}^{\frac{\alpha}{\omega T}} \right) \end{cases} \tag{5.11}$$

The system transfer function is:

$$H(s) = \frac{U_o(s)}{U_i(s)} = \frac{\sqrt{2}U_m \omega e^{\frac{\alpha}{\omega}s} \left(\dfrac{1}{s^2+\omega^2} - \dfrac{1}{\left(s+\frac{1}{T}\right)^2+\omega^2} \mathrm{e}^{\frac{\alpha}{\omega T}} \right)}{\sqrt{2}U_m \omega e^{\frac{\alpha}{\omega}s} \dfrac{1}{s^2+\omega^2}} = \left(1 - \frac{s^2+\omega^2}{\left(s+\frac{1}{T}\right)^2+\omega^2} \mathrm{e}^{\frac{\alpha}{\omega T}} \right) \tag{5.12}$$

According to Equation (5.12), the system transfer function is a function of the initial fault current angle, α, and time constant, T. Where, the initial fault current angle, α, is considered as:

$$\begin{cases} \alpha_{\min} \le \alpha \le \alpha_{\max} \\ \alpha_{\min} = 0 \\ \alpha_{\max} = 2\pi \end{cases} \tag{5.13}$$

Time constant, T, can characterize the tracking speed of the output voltage with respect to the input voltage. Based on the following two considerations, the value of time constant, T, should be increased appropriately: Firstly, the large time constant, T, can minimize the impact of the initial fault current angle, α, because $e^{\frac{\alpha}{\omega T}} \approx 1$ when T is large enough. The above system can be approximately equivalent to a second-order system, which is easily designed and low cost. Secondly, increasing the time constant, T, can ensure that the amplitude of the voltage applied to the tertiary winding rises smoothly. In this case, the possibility of core flux change due to changes in voltage amplitude, and the corresponding inducing of a high-amplitude magnetizing inrush, can be reduced.

Based on the above assumption, that is:

$$e^{\frac{\alpha}{\omega T}} \approx 1 \tag{5.14}$$

Then the system transfer function becomes:

$$H'(s) = \frac{U_o(s)}{U_i(s)} = \left(1 - \frac{s^2 + \omega^2}{\left(s + \frac{1}{T}\right)^2 + \omega^2} \right) \tag{5.15}$$

Letting $\frac{1}{T} = a$, gives:

$$H'(s) = \left(1 - \frac{s^2 + \omega^2}{(s + a)^2 + \omega^2} \right) = \frac{2as + a^2}{(s + a)^2 + \omega^2} \tag{5.16}$$

According to the denominator of the system transfer function:

$$(s + a)^2 + \omega^2 = s^2 + 2as + (a^2 + \omega^2) = s^2 + 2\frac{a}{\sqrt{a^2 + \omega^2}}\sqrt{a^2 + \omega^2}s + (\sqrt{a^2 + \omega^2})^2 \tag{5.17}$$

Achieving the damping ratio of the system:

$$\xi = \frac{a}{\sqrt{a^2 + \omega^2}} \tag{5.18}$$

It is obviously that:

$$0 < \xi < 1 \tag{5.19}$$

This system is a typical second-order underdamped system.

5.2.1.3 Parameter Design of the MIS

According to the parameters of the above transfer function, this function can be simplified as:

$$\begin{aligned} H'(s) &= \left(1 - \frac{s^2 + \omega^2}{(s + a)^2 + \omega^2} \right) \\ &= \frac{2as + a^2}{(s + a)^2 + \omega^2} \\ &= \frac{2as}{(s + a)^2 + \omega^2} \end{aligned} \tag{5.20}$$

According to the design method of the MIS shown in Equation (5.20), the circuit diagram of the MIS is illustrated in Figure 5.8.

Its transfer function is given by:

$$H(s) = \frac{\frac{R_2}{L}s}{s^2 + \frac{R_1 + R_2}{L}s + \frac{1}{LC}} \tag{5.21}$$

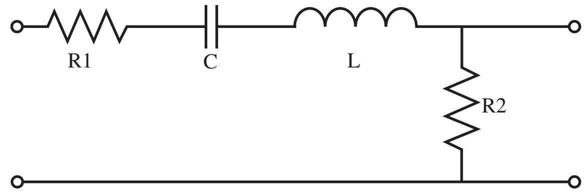

Figure 5.8 Design map of the magnetizing inrush suppresser

Letting $T = 2.0$ seconds:

$$\begin{cases} \dfrac{R_2}{L} = \dfrac{2}{T} * \dfrac{U_{2N}}{U_{3N}} \\ \dfrac{R_1 + R_2}{L} = \dfrac{2}{T} = 1 \\ \dfrac{1}{LC} = \left(\dfrac{1}{T}\right)^2 + \omega^2 \approx \omega^2 = (2\pi f)^2 \end{cases} \tag{5.22}$$

In accordance with Equation (5.22), the appropriate capacitors, inductors and resistors can be selected. In this case, the controlled characteristics mentioned above can be realized. Adopting the parameters:

$$\begin{cases} R_1 = R_2 = R = 50.0\ \Omega \\ L = 10H = 100 \times 0.1H \\ C = 1\ \mu\text{F} \end{cases} \tag{5.23}$$

The output voltage of the system mentioned above is $u_o = \sqrt{2}U_m(1 - \exp(-t/T))\sin(\omega t + \alpha)$, which is directly imposed on the tertiary winding of the three-winding transformer; Equation (5.24) is available:

$$\begin{cases} u_o = \sqrt{2}U_m\,(1 - \exp\,(-t/T))\sin(\omega t + \alpha) \\ u_o = \dfrac{d\Psi}{dt} \end{cases} \tag{5.24}$$

The solution of Equation (5.24) is given by:

$$\Psi = -\,\Phi_m \cos(\omega t + \alpha) + \Phi_m \frac{(\omega T)^2}{(\omega T)^2 + 1} e^{-\frac{t}{T}} (\cos(\omega t + \alpha) + \frac{1}{\omega T}\sin(\omega t + \alpha)) + C \tag{5.25}$$

Equation (5.25) shows that the core flux in the main magnetic circuit is able to rise smoothly with respect to the terminal voltage, and gradually increased to the steady-state flux of the transformer. In this case, the high-amplitude magnetizing inrush can be eliminated.

5.2.2 Simulation Validation and Results Analysis

Firstly, the input and output characteristics of the MIS are simulated. Figure 5.9 shows the variation of the output voltage with respect to the time in the second-order underdamped system under the condition of different time constants, T.

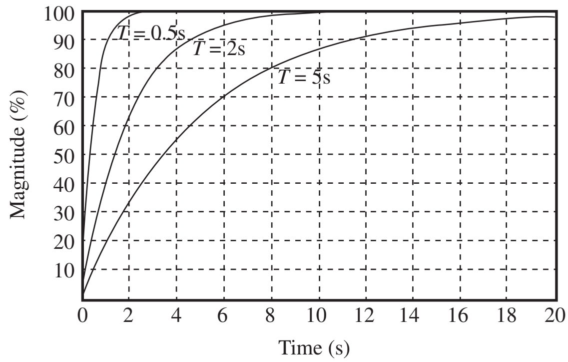

Figure 5.9 Output voltage amplitude waveform of the two-order system with different time constant, T

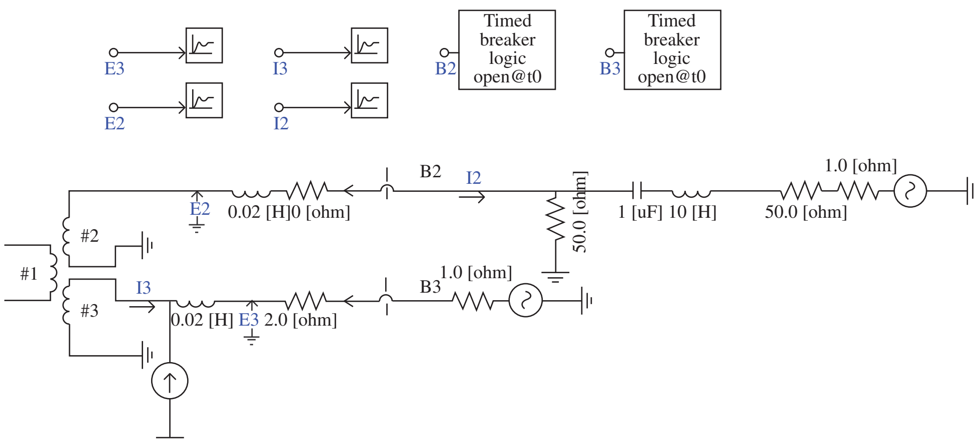

Figure 5.10 Circuit used to simulate the magnetizing inrush incorporating the MIS

The simulation circuit incorporating the MIS is established based on the platform of the PSCAD/EMTDC. The simulation circuit is shown in Figure 5.10.

Coupling group: Y/D11/Y

Rated capacity: $S_N = 100.0$ MVA

Rated voltage(RMS): $U_{1N}/U_{2N}/U_{3N} = 230.0\ \text{kV}/115.0\ \text{kV}/35.0\ \text{kV}$

(Note: The following data are denoted in terms of p.u.)

Leak inductance: $L_{\sigma 12} = L_{\sigma 23} = L_{\sigma 13} = 0.10$

Air gap core mutual impedance: $L_m = 0.20$

Core magnetization curve knee point: $\Phi_{sat} = 1.25$

Excitation current: $I_\mu = 0.3\%$

Remanence: $\Psi_r = 0.7$

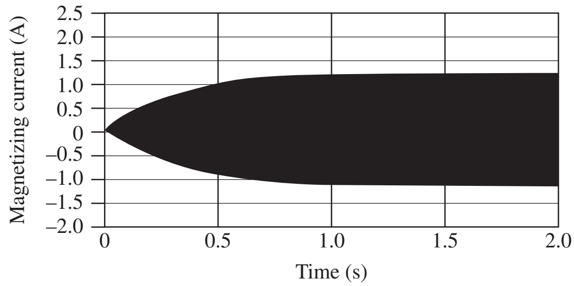

Figure 5.11 The magnetizing current waveform in the tertiary winding when $T = 2$ seconds

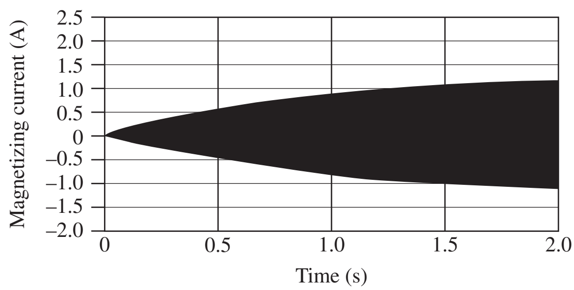

Figure 5.12 The magnetizing current waveform in the tertiary winding when $T = 5$ seconds

Among them, winding #2 is the tertiary winding of the three-winding transformer and winding #3 is the main circuit for the purpose of energizing. Winding #1 is not loaded.

Figures 5.11 and 5.12 show the magnetizing current waveforms in the tertiary winding in the case of $T = 2$ s and $T = 5$ s, respectively. The peak values of the induced magnetizing inrush in the above cases are shown and compared in Table 5.2.

However, taking the speed of the transformer switching on process into account, the time constant of the MIS output voltage amplitude rise can be smaller. For example, no obvious inrushes will occur if $T = 0.5$ s. The simulation results when $T = 0.5$ s are shown in Figure 5.13.

The above analyses show that magnetizing current will gradually rise with the increase of incentive voltage amplitude. However, the phenomenon of the inrush with high amplitude never occurs. Therefore, MIS can eliminate the inrush successfully.

The following simulation analyses are respectively carried out based on the simultaneous switching-on and switching-off operations and the asynchronous switching-on and switching-off operations between the primary winding and the tertiary winding of the three-phase three-winding transformer.

Table 5.2 The peak values of the magnetizing inrush for different time constants

Time constant, T (s)	Peak inrush (A)	Time steady state (s)
2	1.2	10.0
5	1.1	20.0

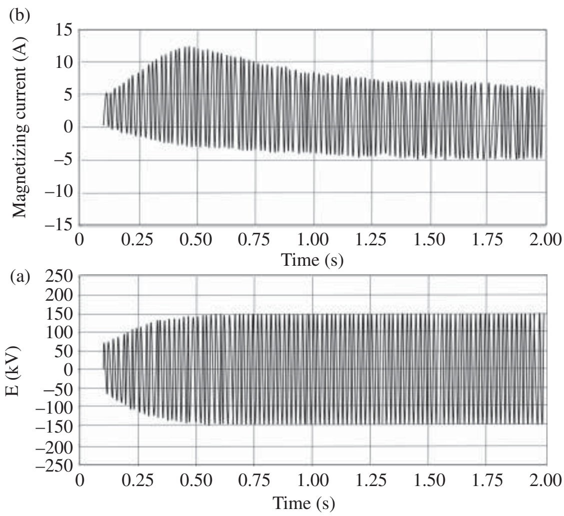

Figure 5.13 (a) Magnetizing inrush and (b) the EMF waveform in the tertiary winding

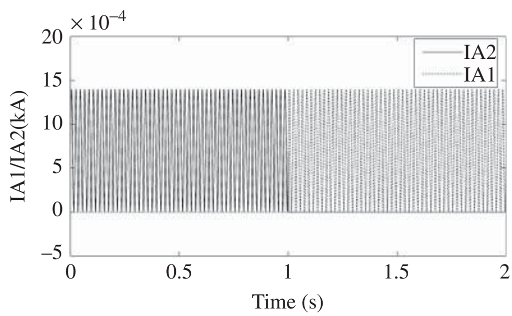

Figure 5.14 Magnetizing inrush in phase A both in the main winding and the tertiary winding in the case of synchronized switch-on accompanied by switch-off

Case 1: The tertiary winding is switched on at $t = 0$ s. The tertiary winding is switched off at $t = 1.0$ s and meanwhile the main winding is switched on.

Figures 5.14–5.16 show the actual waveforms of such a scenario when the primary winding of the three-phase three-winding transformer is switched on and the tertiary winding is switched off simultaneously at time $t = 1.0$ s. In this case, no obvious inrush transient process occurs. Instead, it appears as the normal magnetizing current.

The requirement to switch on the primary winding at the moment the tertiary winding is switched off is not easily realized in engineering applications. Two circuit breakers will receive the synchronous instruction from the protection to connect the MIS into the system. Meanwhile, another circuit breaker also receives the instruction to cut off the current stably. However, there exists the dispersion in the time between these two operations.

Therefore, the scenario that the main winding is switched on firstly and then the tertiary winding is switched off has been investigated. Due to the electric power of the two windings coming from the same power source, during the short period of switching on simultaneously the two windings, no circulation

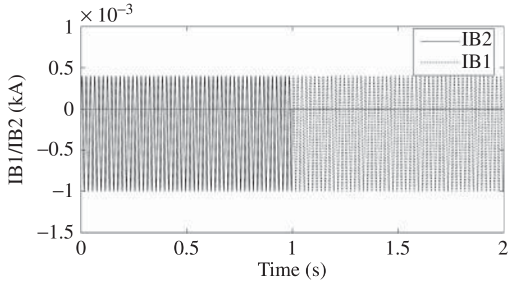

Figure 5.15 Magnetizing inrush in phase B both in the main winding and the tertiary winding in the case of synchronized switch-on accompanied by switch-off

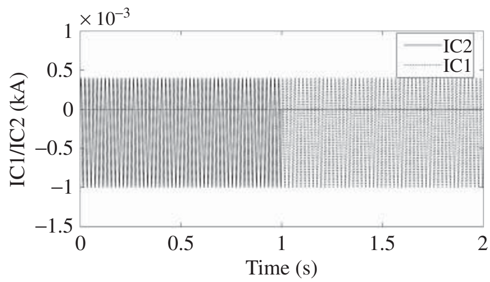

Figure 5.16 Magnetizing inrush in phase C both in the main winding and the tertiary winding in the case of synchronized switch-on accompanied by switch-off

current occurs. Once the primary winding is stably switched on, the switching-on circuit of the tertiary winding can be disconnected. Case 2 shows the simulation results for this case.

Case 2: the tertiary winding switch-on at t = 0.0 s; the main winding switch-on at t = 1.0 s; the tertiary winding switch-off at t = 1.5 s.

Figures 5.17–5.19 show the actual waveforms of such a scenario in which the primary winding of the three-phase three-winding transformer is switched on at time t = 1.0 s and the tertiary winding is switched off at time t = 1.5 s. In this case, too, no obvious inrush transient process occurs.

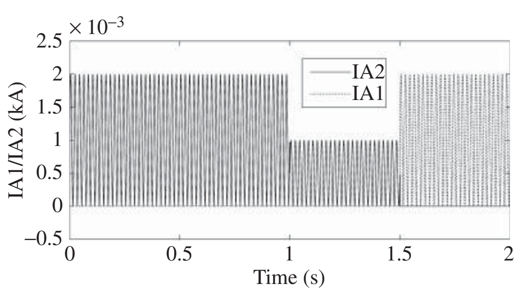

Figure 5.17 Magnetizing inrush in phase A both in the main winding and the tertiary winding in the case of unsynchronized switch-on accompanied by switch-off

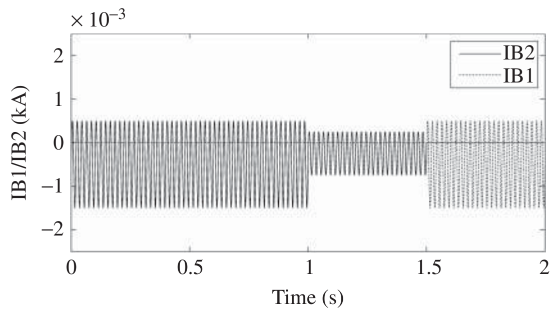

Figure 5.18 Magnetizing inrush in phase B both in the main winding and the tertiary winding in the case of unsynchronized switch-on accompanied by switch-off

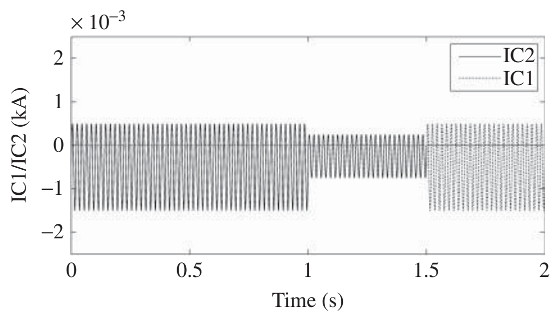

Figure 5.19 Magnetizing inrush in phase C both in the main winding and the tertiary winding in the case of unsynchronized switch-on accompanied by switch-off

The two cases above are the simulation results under the action of the MIS. Case 1 shows the inrush waveforms of the main winding and the tertiary winding under the condition that the transformer's main winding and the tertiary winding close and trip at the same time. Case 2 shows the inrush waveforms of the main winding and the tertiary winding under the condition that the transformer's main winding and the tertiary winding close and trip asynchronously. The difference between the two examples rests with the transition process caused by closing and tripping asynchronously in the transformer's excitation branch. However, this transition process does not cause magnetizing inrush. The current waveform and magnitude still indicate that this is a normal excitation current.

In conclusion, if the condition that the three-phase winding transformer's main winding and the tertiary winding close and tripp at the same time can be satisfied, the generated magnetizing current would be smaller than the value caused by the asynchronous operations, and the magnetizing current does not exceed 20 A. The synchronization between the two winding is better, the effect to inhibit the inrush will be better. However, even if the closing and tripping operations are unsynchronized, the suppression effect of the inrush is also satisfactory. The restrained inrush will not cause mal-operation of the transformer differential protection.

As a consequence, in a variety of energizing scenarios, the transformer with any winding connection type will not encounter a magnetizing inrush. Simulation results show that the inrush suppression effect is also good without requiring that the breakers in the two windings act simultaneously. The proposed control strategy can be widely used in three-phase transformer, without the restrictions of the regulations that the phase-separated closing is not allowed. This is significantly better than inception angle control strategy.

In summary, a new method to restrain the inrush in the case of the transformer energizing has been presented in this section. An inrush current suppressor composed of a second-order underdamped system and voltage divider is designed. This MIS can be connected to the original primary power source through the tertiary winding of the three-winding transformer. The time constant of the flux rise can be freely designed and regulated. In this case, the suppression of magnetizing inrush can be realized entirely. The simulation tests have been carried out based on PSCAD/EMTDC software and the simulation results have shown the correctness, effectiveness and feasibility of the proposed method.

In power systems, the three-winding transformer is widespread, and the tertiary winding is used to implement the functions of monitoring and measuring in many cases. After the proposed function to inhibit the magnetizing inrush is achieved, the common functions still can be executed by quitting the MIS. Therefore, there are favourable conditions to implement the proposed method.

As a consequence, the proposed MIS provides a feasible method in theory to achieve the inhibition of magnetizing inrush. With the rapid development of power electronics technology and a low cost to realize it is expected that the proposed control characteristic will be implemented.

5.3 Identification of the Cross-Country Fault of a Power Transformer for Fast Unblocking of Differential Protection

5.3.1 Criterion for Identifying Cross-Country Faults Using the Variation of the Saturated Secondary Current with Respect to the Differential Current

To describe the fundamental of the proposed method, it is acceptable to use the protection of a two-winding power transformer as an example. For convenience of analysis, it is assumed that the secondary currents of the unsaturated and saturated CTs are i_1 and i_2, respectively, and that the false differential current is $\mathrm{i_d}$. The transforming characteristic of the saturated CT are as in Figure 5.1.

Under normal operating condition, the CTs on both sides of the transformer can transform linearly, hence the differential current is zero.

In the event of a heavy external fault, it is assumed that the CT on one side of the transformer saturates, as shown in Figure 5.19. If the CT on the other side of the transformer can be regarded as transforming linearly in this case, the two currents forming the bias current will actually be the primary and secondary currents of the saturated CT, and the differential current is actually the magnetizing current of the saturated CT. According to the analyses in Figure 5.19, in the initial post-fault period, the saturated CT can basically transform linearly. Herein, the primary and secondary currents are basically equal and the differential current is close to 0. After a while, the CT enters the saturation state, the secondary current decreases rapidly and the magnetizing current increases correspondingly. When the instantaneous value of the primary current is close to the maximum, the differential current also approaches its maximum and the corresponding amplitude of the secondary current is quite small. When the primary current decreases from the maximum to the part around zero, the CT also returns to its linear transforming section gradually; and, correspondingly, the secondary current increases and the magnetizing current decreases accordingly. When the instantaneous value of the primary current lies entirely within the linear section, the magnetizing current is close to 0 and the primary and secondary currents are basically equal again. Afterwards, when the instantaneous value of the primary current increases and exceeds the saturation point once again, the magnetizing current accordingly increases and, meanwhile, the secondary current begins to deviate from the primary current again and decreases gradually. It should be pointed out that the above-mentioned law comes into existence only when samplings are in terms of absolute values.

According to the above analyses, the variation of the secondary current of the saturated CT is inversely proportional to the variation of the differential current for an external fault accompanied by the CT saturation, that is, $\frac{|i_d(n)|-|i_d(n-1)|}{|i_2(n)|-|i_2(n-1)|} < 0$. To simplify the depiction, let $\frac{dI_d}{dI_R} = \frac{|i_d(n)|-|i_d(n-1)|}{|i_2(n)|-|i_2(n-1)|}$. For the internal fault, under the ideal condition, assume that the sources of both sides supplying the short-circuit current are in-phase; the angle of the impedance of the fault loop is in-phase as well. In this scenario, the secondary currents of both CTs and the differential current are all in-phase. From the point of view of sampling values, the differential current varies directly proportional to the secondary current of the CT on any side during any cycle. Supposing that the secondary current with the smaller amplitude is i_2, $\frac{dI_d}{dI_R} > 0$ comes into existence. When the sources of both sides are not in-phase, the points of $\frac{dI_d}{dI_R} < 0$ begin to appear among the sampling values within one cycle. However, the points of $\frac{dI_d}{dI_R} > 0$ still dominate when the phase angle between the two power supplies is relatively small. In the case that the phase angle between the two systems connected by the transformer does not exceed 45°, the phase angle between the differential current and the secondary current with smaller amplitude is less than 45°, even if the amplitudes of the currents flowing through the CTs on both sides differ widely from each other, which makes the angle of the composed differential current deflect to the secondary current with greater amplitude. It is noticed that if adopting the absolute values of the sampling values, the changing trends of the two currents are the same for half the sampling points within one cycle (that is, $\frac{dI_d}{dI_R} > 0$) and opposite for the other half sampling points (that is, $\frac{dI_d}{dI_R} < 0$) (Figure 5.20). In Figure 5.20, the variation of $\frac{dI_d}{dI_R}$ within one cycle of post-fault period during an internal fault in the case of a two-end power supply with a big power angle difference is presented, where the sampling rate is 40 points/cycle. As seen, the points on the line section of positive slope amount to 20 and the points on the line section of negative slope amount to 20 as well. Therefore, the above claim about the scenario of an internal fault is verified.

For the overwhelming majority of internal faults, the phase angle between the differential current and the secondary current with the smaller amplitude is far smaller than 45°, which means that the sampling points satisfying $\frac{dI_d}{dI_R} < 0$ are far less than those satisfying $\frac{dI_d}{dI_R} > 0$ within any cycle. In addition, all the sampling points should satisfy $\frac{dI_d}{dI_R} < 0$ theoretically during an external fault. To this end, discriminating internal and external faults according to the sign of $\frac{dI_d}{dI_R}$ will be quite accurate. In terms of real application, an appreciate threshold can be set when designing the criterion. That is, when the number of the points satisfying $\frac{dI_d}{dI_R} < 0$ exceeds the threshold within one cycle, the fault can be regarded as an external fault, otherwise it is an internal fault. In this case, the discrimination of internal and external faults can be obtained. This criterion is referred to as variation rate criterion. It should be pointed out that, in the case of a single-end power supply, if the CT on the source side of the transformer saturates and the external short-circuit fault on the load side of the transformer develops to an internal fault, the differential current will be completely the secondary current of the saturated CT. This cross-country fault cannot be identified by virtue of the criterion identifying the waveform of the saturated current. In comparison, the condition

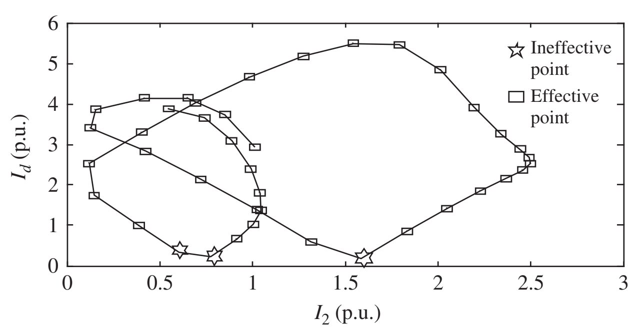

Figure 5.20 The variation of $\frac{dI_d}{dI_R}$ within one cycle of post-fault period during an internal fault in the case of two-end power supplies of big power angle difference

$\frac{dI_d}{dI_R} > 0$ is always satisfied, since i_2 and i_d are the same current. Herein, the cross-country fault can be identified and the differential protection can be unblocked rapidly. This view of point can be testified by the simulation results in Section 5.3.2.

It should be admitted that above conclusion is valid regardless of the precision of acquisition system. However, the amplitude of i_2 is quite small when the CT is highly saturated and the amplitude of i_d is quite low when the CT transforms linearly. In this instance, as the precision of acquisition system in the microcomputer-based protection is finite, the variation characteristics of currents are difficult to identify. However, it is fortunate that above-mentioned phenomena all correspond to the saturation characteristics of the CT during external faults and the corresponding points should be identified as the points expressing external faults. In this case, an appropriate threshold can be set, for example $0.5I_n$ (I_n is the rated current of the power transformer); when the sampling values of i_2 and i_d are less than this threshold, the points of the corresponding variation rates are regarded as ineffective points. If the ratio of effective points to total points participating in identification is less than a certain number, for example 40%, the corresponding fault can be directly identified as an external fault. As the amplitudes of i_2 and i_d are relatively great for internal faults, and the ratio corresponding to their sampling values exceeding $0.5I_n$ will be far greater than 40%, this criterion will work correctly. This assumption can also be testified by the simulation results in Section 5.3.2.

Therefore, the variation rate criterion can be started up only if the number of effective points satisfying the variation rate criterion exceeds the threshold. The sign of $\frac{dI_d}{dI_R}$ can be recorded at each time; when the number of points satisfying $\frac{dI_d}{dI_R} < 0$ exceeds a certain threshold, for example 70–80%, the fault is identified as external fault, otherwise it is an internal fault. It should be pointed out that the thresholds mentioned above are all set according to theoretical analyses and simulation tests. In practice, they can be adjusted within a respectively wide range to satisfy the different requirement to the operation stability and speed of the protection.

As analysed above, adopting the identification criterion based on the threshold of effective points may fail to unblock the differential protection during some slight faults, such as inter-turn short-circuit faults. Therefore, the proposed criterion is not suitable to serve as the main criterion but can be used to serve as the criterion of fast unblocking the protection in the event of a cross-country fault. In other words, after a fault has been identified as an external fault by some other method, such as the one using operation time difference, it will choose the current with smaller amplitude of both sides of the differential protection as i_2. Then it compares the variation trends of i_d and i_2 continuously. With above criterion, the cross-country fault can be identified if it occurs.

Figure 5.21 shows the basic flow of the proposed method. In the figure, K_1 and K_2 are the thresholds of the ratio of effective points and the ratio of negative variation rate respectively; the two thresholds can both be set.

5.3.2 Simulation Analyses and Test Verification

The simulation model is a 220 kV power transmission system established with EMTDC software (Figure 5.22). The system consists of a generator, a power transformer, a 10 km transmission line and an infinite system. EMTDC provides a benchmark CT model. To let one CT saturate and the other remain unsaturated, the CT parameters are shown in Table 5.3; the through current is adjusted appropriately.

To ensure that the variation rate criterion can still be effective when the ratio of effective points within one cycle is low (40%), the sampling frequency should not be too low; 40 points/cycle is adopted here. This model is used to simulate internal and external faults of the transformer accompanied by the CT saturation and to verify the validity of proposed the method. When simulating an external fault, the short-circuit point can be set at the terminal of the transformer (F_2 in Figure 5.22) to give rise to a current high enough to result in CT saturation. When simulating a single-end power supply system, the infinite system can be replaced with a load with fixed equivalent impedance. When the external fault

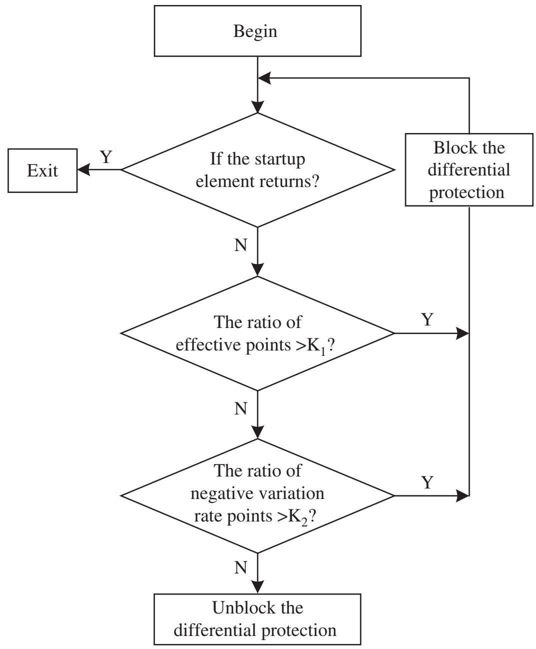

Figure 5.21 Flow chart of the variation rate criterion

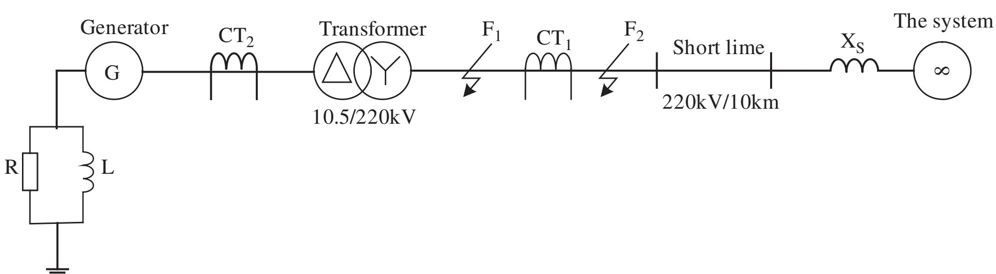

Figure 5.22 Power transmission simulation system

develops to the internal fault, the fault point can be switched from F_2 to F_1. By virtue of adjusting the parameters of the system and CTs, hundreds of cases of external faults accompanied by CT saturation and external faults developing to internal faults under varied operating conditions can be simulated. On this basis, the security and sensitivity of the proposed criterion were studied. Only a few simulation results corresponding to several scenarios are outlined here due to the space limitation (Scenarios 5.1–5.5).

Scenario 5.1 External fault exists persistently and one CT saturates

Figure 5.23 shows currents transformed by CTs and the differential current during an external fault. Here $K_1 = 40\%$ is adopted for the threshold of effective points. It means that if the number of effective points within one cycle exceeds 16, the variation rate criterion should be adopted according to the flow chart in Figure 5.21, otherwise the fault is directly identified as an external fault. For the threshold of variation

Table 5.3 CT parameters for a 220kV power transmission system

Parameters	CT1	CT2
Current transformer ratio (A)	120/5	2400/5
Mean core length (m)	0.8	0.5
Core cross-section (cm^2)	23.2	41.2
Burden, R (ohm)	3.0	1.0
Knee point	(0.1 A. 1.6 T)	(0.1 A. 1.6 T)

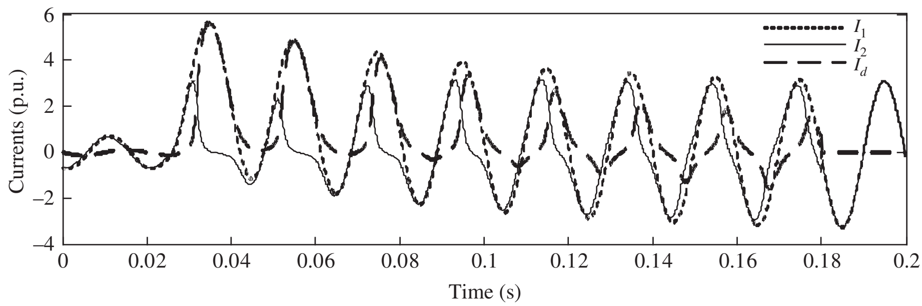

Figure 5.23 Currents transformed by CTs and the false differential current during an external fault (one CT saturates)

rate, $K_2 = 75\%$ is adopted. For example, in the case of the number of effective points exceeding 16, if the number of the points of negative variation rate is equal to or exceeds 12, the corresponding fault is identified as an external fault, otherwise it is an internal fault.

The variation rule of $\frac{dI_d}{dI_R}$ within one cycle of pre-fault period and one cycle post-fault is shown in Figure 5.24. As the concern in not with the real value of $\frac{dI_d}{dI_R}$ but its sign, when i_2 and i_d both lie within the range of effective points, it is unnecessary to show the actual value of $\frac{dI_d}{dI_R}$. For the sake of clear expression, $\frac{dI_d}{dI_R}$ can be shown in terms of per unit 1 (when the sign is positive) or −1 (when the sign is negative). It can be seen from Figure 5.24 that the differential current is smaller than $0.5I_n$ within one cycle of the pre-fault period, and hence the corresponding points of $\frac{dI_d}{dI_R}$ are all regarded as ineffective. The number of effective points within one cycle of the post-fault period is 29, which means the ratio of effective points to total sampling points is 72.5%. Meanwhile, the ratio of points of negative variation rate to total effective points is 92%. As a consequence, the fault is identified as an external fault according to the variation rate criterion. Figure 5.24b shows the locus of $(|i_2|, |i_d|)$ in $|i_2|-|i_d|$ plane corresponding to variations of currents after fault occurs. The variation rule of $|i_2|$ with respect to $|i_d|$ can be simply comprehended by virtue of this figure. The variation rule of $\frac{dI_d}{dI_R}$ within the fourth cycle of the post-fault period is shown in Figure 5.25.

According to Figure 5.25a, the number of effective points is 19, the corresponding ratio within one cycle is 47.5%. Then adopting the variation rate criterion, the ratio of points of negative variation rate to effective points is 89.4%, which proves a correct identification. Figure 5.25b shows the corresponding locus of the variations of currents in the $|i_2|-|i_d|$ plane. Because of the sufficient decay of the DC component within the ninth cycle of the post-fault period, the false differential current decreases. Correspondingly, the number of effective points is 4, accounting for 10% of the sampling points within one cycle. As a consequence, the fault can be identified as an external fault according to the threshold of effective points. The relative figures are not listed here for lack of space.

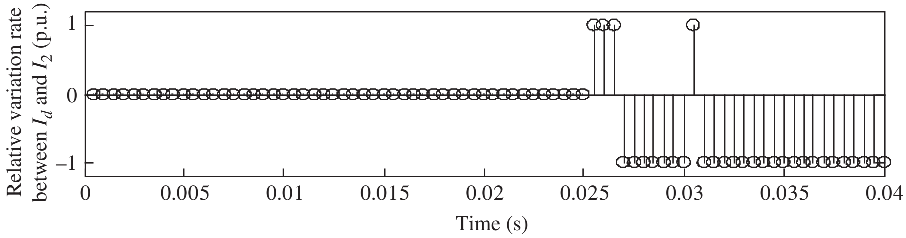

(a)

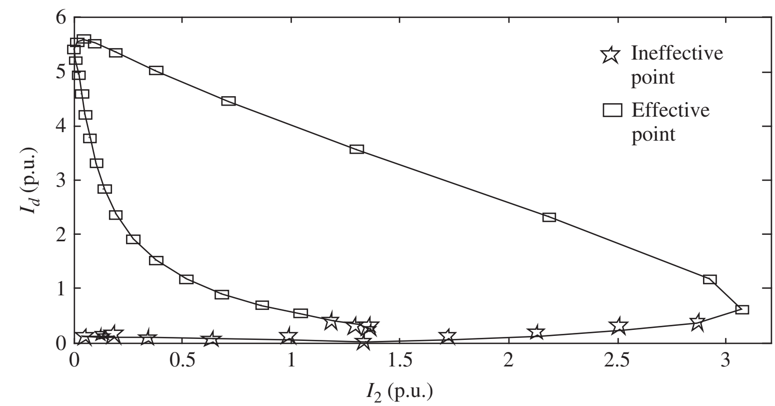

(b)

Figure 5.24 The variation rate of $\frac{dI_d}{dI_R}$ within one cycle of the pre-fault period and one cycle post-fault during an external fault: (a) relative variation rate between I_d and I_2 in terms of time series; (b) locus of I_d with respect I_2

Scenario 5.2 External fault exists persistently and both CTs saturate (the saturation degrees are different)

In Scenario 5.1, the primary current of the saturated CT can be considered as an enveloping line of the corresponding secondary current, as illustrated in Figure 5.23. Therefore, the gap between the primary current and the secondary current will form the different current. Different from Scenario 5.1, in this scenario the CTs of both sides saturate; one saturates mildly and the other saturates deeply. Correspondingly, when forming the differential current, the secondary current of the mildly saturated CT, instead of the primary current, will be considered as an enveloping line of the secondary current of the deeply saturated CT. Compared with Scenario 5.1, as the secondary current of the mildly saturated CT is just a proportion of the primary current, the area that the secondary current of the mildly saturated CT covers is smaller than that which the primary current covers. As a result, the pulse width of the differential current formed by the two saturated secondary currents is narrower than that of the differential current in the case of only one CT saturating. Correspondingly, the ratio of the effective points decreases. At the same time, the points satisfying $\frac{dI_d}{dI_R} < 0$ still account for the majority of the effective points. In order to contrast with Scenario 5.1, the load of CT_1 in Figure 5.22 is adjusted to make the CT saturate mildly. The secondary currents of both CTs and the differential current are shown in Figure 5.26. In this case, the secondary current, i_{22}, of the deeply saturated CT is regarded as i_2 in the criterion and the secondary current i_{21} of the mildly saturated CT is regarded as i_1 in the criterion. It can be seen from Figure 5.26, the law of $|i_d|$ varying inversely proportional to $|i_{22}|$ basically still comes into existence.

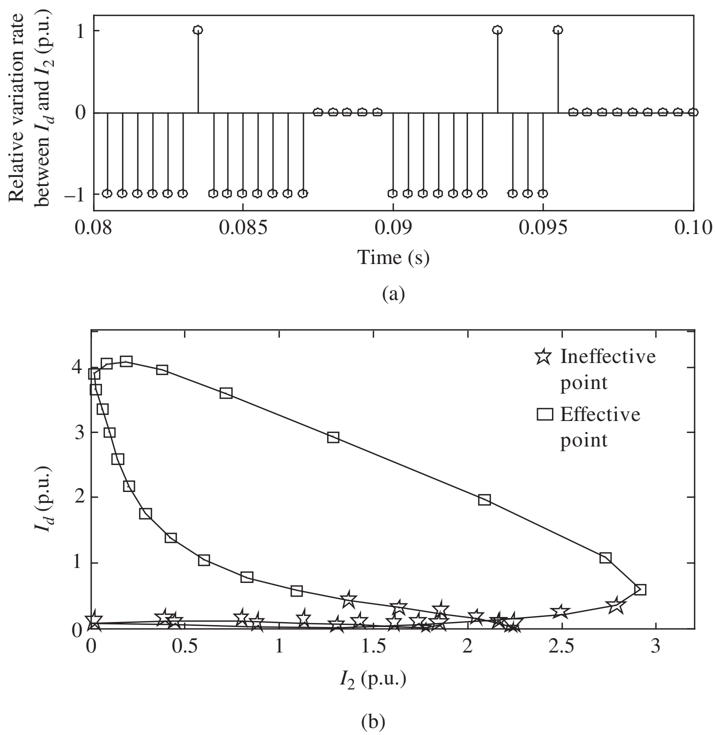

Figure 5.25 The variation rate of $\frac{dI_d}{dI_R}$ within the fourth cycle of the post-fault period during an external fault: (a) relative variation rate between I_d and I_2 in terms of time series; (b) locus of I_d with respect I_2

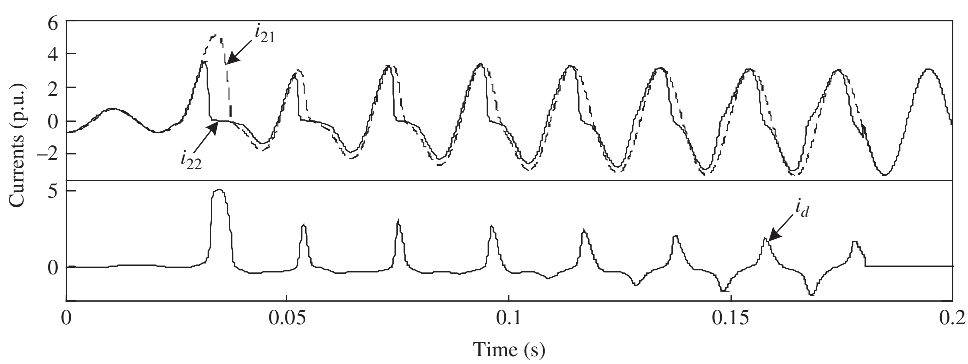

Figure 5.26 Currents transformed by CTs and the false differential current during an external fault (both CTs saturate)

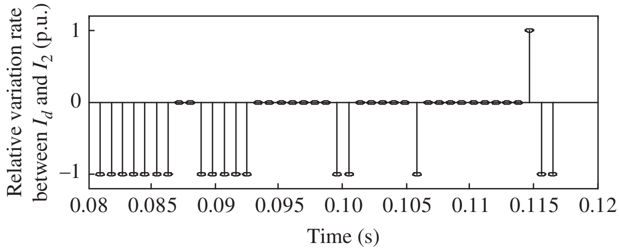

Figure 5.27 The variation rate of $\frac{dI_d}{dI_R}$ within the fourth cycle of the post-fault period during an external fault (both CTs saturate)

To analyse the overall process,the data within the fourth cycle of the post-fault period are used to study the variation rule of effective points of $\frac{dI_d}{dI_R}$ (Figure 5.27). By virtue of Figure 5.27, the number of effective points is 17, accounting for 42.5% of sampling points within one cycle. Further, according to the variation rate criterion, the ratio of points of negative variation rate to effective points is 94% (16/17). Obviously, the identification is correct. For other stages of the post-fault period, reliable identifications can be ensured by combining the threshold of effective points with the variation rate criterion.

Therefore, even though CT saturation exists (or both CTs saturate) during an external fault, adopting the threshold of effective points together with the variation rate criterion can block the differential protection reliably.

Scenario 5.3 An external fault develops into an internal fault in the case of a two-end power supply (the phase difference of the two power supplies being equal to 10°).

Figure 5.28 shows the current waveforms corresponding to the cross-country fault in this scenario; Figure 5.28a shows the waveforms of the secondary currents of both CTs and Figure 5.28b is the waveform of the differential current. Figure 5.29 illustrates the variation locus between $|i_2|$ and $|i_d|$ when experiencing a developing fault; Figure 5.29a corresponds to the case of the fault staying as an external fault and Figure 5.29b corresponds to the situation after the external fault has developed into an internal fault. Figure 5.30 shows the variation rate of $\frac{dI_d}{dI_R}$ corresponding to Figure 5.29. It can be seen from Figures 5.28–5.30 that the ratio of effective points to total sampling points is 37.5% when the fault stays as an external fault. Therefore, the fault can be directly identified as an external fault according to the threshold of effective points. As soon as the fault develops into an internal fault, the effective point ratio increases to 92.5% within one cycle, then the variation rate criterion is activated. To this end, the ratio of points of negative variation rate to effective points is only 10.8%, which satisfies the unblocking condition, and hence the protection is unblocked and operates correctly.

Scenario 5.4 An external fault develops into an internal fault in the case of a two-end power supply (the phase difference of the two power supplies is equal to 60°)

This scenario can be regarded as an extreme case when testing the criterion being used to identify a cross-country fault. It is because the phase difference of the two power supplies is quite large, leading to a large phase difference between two corresponding short-circuit currents. This large phase difference can be used to effectively test the sensitivity of the variation rate criterion after an external fault has developed into an internal fault.

Figure 5.31 shows the current waveforms corresponding to the cross-country fault mentioned in Scenario 5.4, in which Figure 5.31a shows the waveforms of the secondary currents of both CTs and Figure 5.31b denotes the waveform of the differential current. Corresponding to Figure 5.31, Figure 5.32

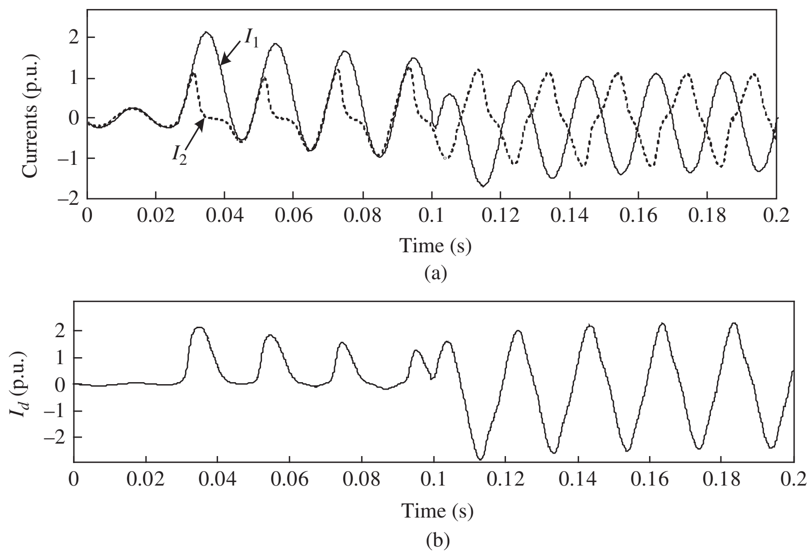

Figure 5.28 The current waveforms corresponding to a developing fault (the phase difference of the two-end power supplies is equal to 10°): (a) the waveforms of the secondary currents of both CTs; (b) the waveform of the differential current

illustrates the variation rate of $\frac{dI_d}{dI_R}$ after the external fault has developed to an internal fault, which contains one-cycle data before the fault develops and one-cycle data after the fault has developed. It can be seen from Figure 5.32 that the ratio of effective points to total sampling points is 37.5% before the external fault develops into an internal fault. Therefore, the fault can be directly identified as an external fault according to the threshold of effective points. The effective point ratio increases to 95% within one cycle after the fault develops. Correspondingly, the ratio of points of negative variation rate to effective points is only 36.83%, which satisfies the unblocking condition. Therefore, the protection is unblocked and operates correctly.

Scenario 5.5 An external fault develops into an internal fault in the case of a one-end power supply
This scenario can more clearly verify that the proposed criterion is superior to the criterion based on identifying the waveform of the saturated current in identifying cross-country faults. As the external fault develops from the external side to the internal side of the unsaturated CT, the differential current is actually the secondary current of the saturated CT after the fault has developed into an internal fault.

Figure 5.33 shows the current waveforms corresponding to the cross-country fault mentioned in Scenario 5.5, in which Figure 5.33a shows the waveforms of the secondary currents of both CTs and Figure 5.33b is the waveform of the differential current. It can be seen from Figure 5.33b that the saturated characteristic of the differential current is still obvious within five cycles after the fault has developed into an internal fault. As a consequence, the unblocking controlled by the criterion based on identification of waveform characteristic of saturated current will be delayed for a long time. Corresponding to Figure 5.33, Figure 5.34 illustrates the variation rate of $\frac{dI_d}{dI_R}$ within one-cycle before and one-cycle after the external fault has developed into an internal fault. It can be seen from Figure 5.34 that the ratio of effective points to total sampling points is 47.5% and the ratio of points of negative variation rate to effective points is 84.2% before the external fault develops into an internal fault. Therefore, the fault can be correctly identified as an external fault according to the variation rate criterion. The ratio

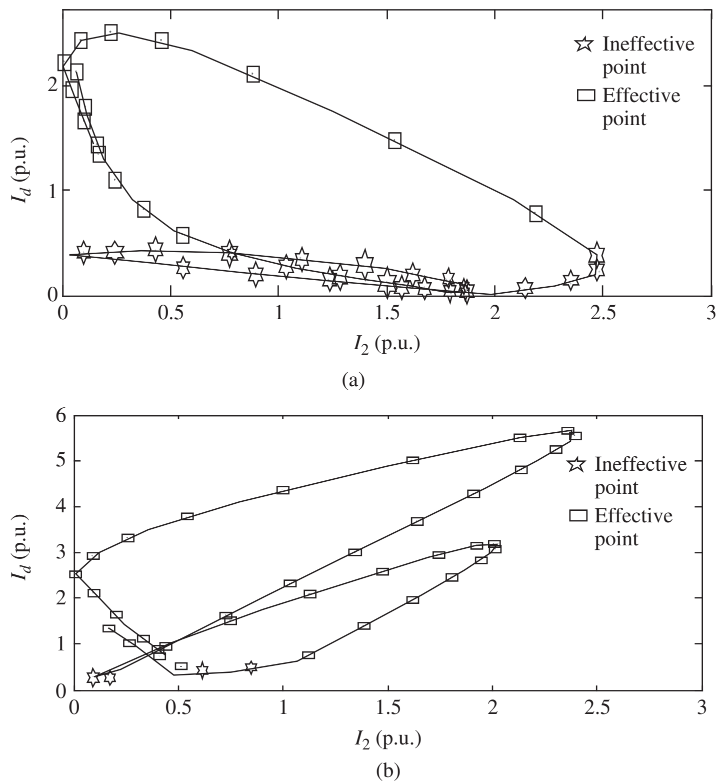

Figure 5.29 The variation between $|i_2|$ and $|i_d|$ when experiencing a developing fault: (a) locus of I_d with respect I_2 when a fault stays as an external fault; (b) locus of I_d with respect I_2 after an external fault has developed into an internal fault

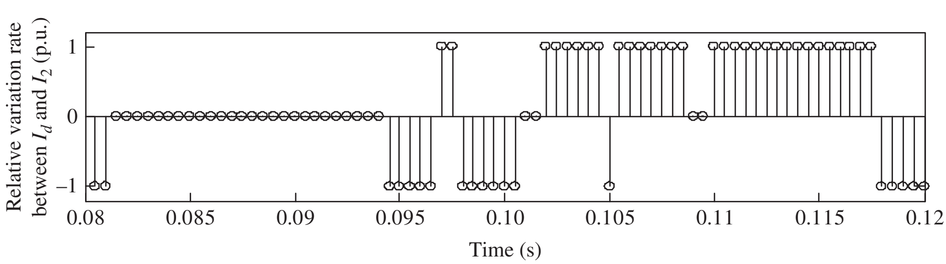

Figure 5.30 The variation rate of $\frac{dI_d}{dI_R}$ when experiencing a developing fault corresponding to Scenario 3

of effective points increases to 72.5% within one cycle after the fault has developed into an internal fault. Meanwhile, the ratio of points of negative variation rate to effective points decreases to only 6.9%, which satisfies the unblocking condition. Therefore, the protection is unblocked and operates correctly.

Figure 5.35 illustrates the ratio of second harmonic to fundamental of the differential current when an external fault develops into an internal fault in the case of a single-end power supply. It can be seen from

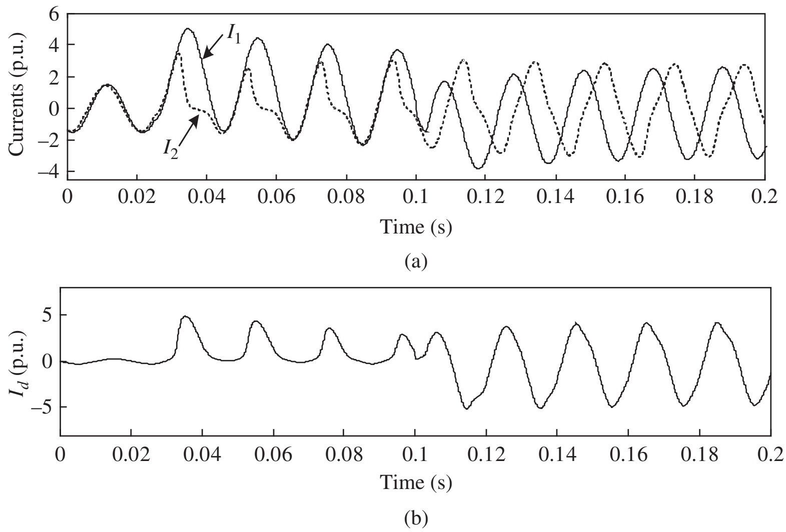

Figure 5.31 The current waveforms corresponding to a developing fault (the phase difference of the two-end power supplies being equal to 60°): (a) the waveforms of the secondary currents of both CTs; (b) the waveform of the differential current

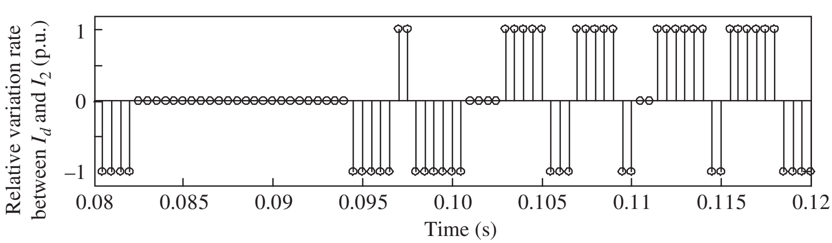

Figure 5.32 The variation rate of $\frac{dI_d}{dI_R}$ when experiencing a developing fault corresponding to Scenario 4

this figure that the ratio of second harmonic far exceeds 15% after the external fault occurs, even after the fault has developed into an internal fault. According to the criterion based on the ratio of the second harmonic, although the protection can be blocked during the external fault, it cannot be unblocked after the fault has developed into an internal fault.

These test results manifest that the proposed criterion can reliably restraint the protection during a pure external fault with CT saturation. When an external fault develops into an internal fault, the proposed criterion can correctly identify the fault and unblock the protection within one cycle after the fault has developed.

Furthermore, a dynamic simulation test was conducted to verify the validity of the proposed criterion. The test data come from the disturbance recorder of the dynamic simulation test laboratory of the Huazhong University of Science and Technology. The relative data acquired are as follows: an external fault of phase A to ground on the high voltage side of the transformer develops to an internal grounded fault of the same phase; the fault results in the saturation of the CT on the low voltage side; the single-phase to ground fault on the high voltage side is transformed into a phase–phase short-circuit

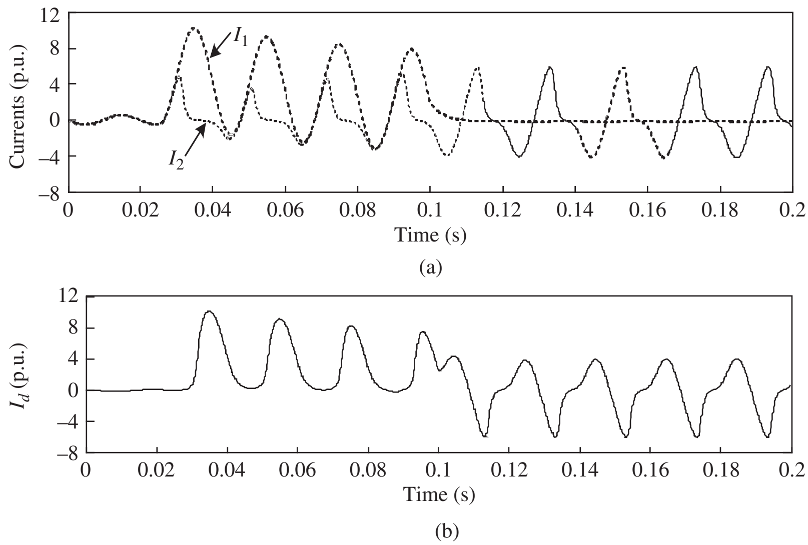

Figure 5.33 The currents waveforms corresponding to a developing fault (single-end power supply): (a) the waveforms of the secondary currents of both CTs; (b) the waveform of the differential current

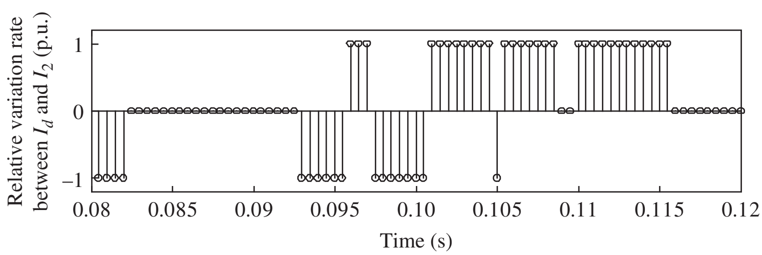

Figure 5.34 The variation rate of $\frac{dI_d}{dI_R}$ when experiencing a developing fault corresponding to Scenario 5.5

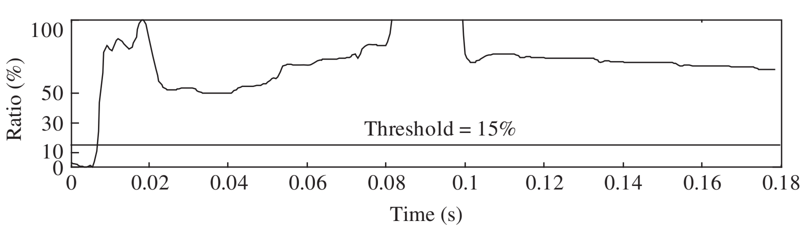

Figure 5.35 The ratio of second harmonic to fundamental of the differential current when an external fault develops into an internal fault in the case of a single-end power supply

fault on the low voltage side due to the Y/Δ-11 connection of the power transformer. As the types of CTs on one side are the same, CTs of two phases on the low voltage side both saturate. The currents of three phases on both sides of the transformer are all recorded. The differential currents of phases A and C both occur after their angle transformation and waveforms are similar. Here only the operating status of phase A ($i_a - i_b$) is discussed; the currents of both sides and the differential current are shown in Figure 5.36.

Because the sampling frequency of the protection is quite low (12 points/cycle), the recorded data cannot be directly used to verify the proposed criterion. The sampling frequency increases to 36 points/cycle by means of linear interpolation. The corresponding output of the variation rate using the proposed criterion is shown in Figure 5.37.

The number of effective points is 16, accounting for 44% of sampling points within one cycle before the external fault develops into an internal fault. Meanwhile, the number of points of negative variation is 14, accounting for 88% of total effective points. Therefore, the protection is blocked reliably. After the fault has developed into an internal fault, the number of effective points is 25 and the number of points of negative variation is 1, only accounting for 4% of total effective points. As a result, the protection can be unblocked according to the variation rate criterion.

In summary, on the basis of the different mechanisms giving rise to differential currents during external and internal faults, a novel method to unblock the differential protection in the case of cross-country fault has been proposed based on the variation rate criterion and the threshold of effective points of sampling. Some disadvantages of the existing criteria can, therefore, be compensated for to some extent.

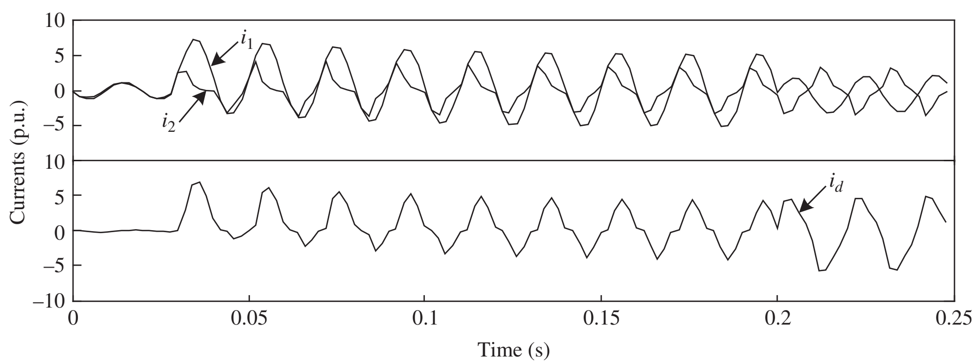

Figure 5.36 The currents waveforms corresponding to a developing fault (disturbance record)

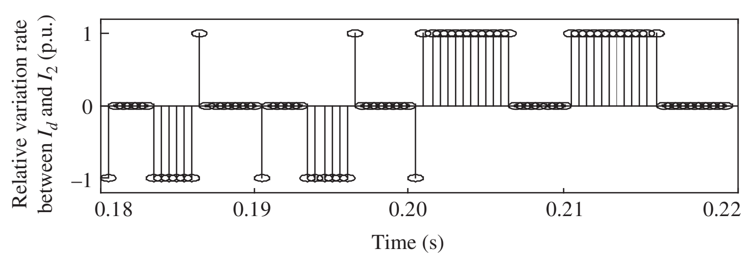

Figure 5.37 The variation rate of $\frac{dI_d}{dI_R}$ when experiencing a developing fault corresponding to the fault in Figure 5.36

This method needs few computations and is easy to realize in existing microprocessor-based protection. Simulation tests have verified the validity of the proposed criterion.

5.4 Adaptive Scheme in the Transformer Main Protection

5.4.1 The Fundamental of the Time Difference Based Method to Discriminate between the Fault Current and the Inrush of the Transformer

At present, the time difference based methods have been widely applied to detecting the saturation of CTs; this is based on the fact that the CTs on the two sides of the transformer will not saturate immediately as soon as a severe fault has emerged. The change of the phase current and the real fault differential current will be detected at the same time in the case of the internal fault even if the CT ultimately enters into saturation, as long as the CTs on the two sides of the transformer can transfer as normal during the beginning period of the fault occurring. In this case, theoretically there will be no time difference.

By virtue of the characteristic above, a MM based method to detect the time difference between the emergence of the fault and the emergence of the differential current is put forward; it can effectively prevent mal-operation of the differential relay protection resulting from the high through current. In the scheme, the time difference of the sudden change of the line current at one side and the time when the differential current occurs is used to decide whether there is sympathetic inrush current. Furthermore, whether there is an external or internal fault in the existence of the sympathetic inrush current can be detected. The two time difference based methods above both take the line current at the Y-side and the differential current of the CTs on two sides of the transformer as the reference.

However, when the transformer is energized under no-load conditions, such a time difference will not exist in that the differential current is actually the line current at the switching side. Therefore, the above criteria based on the time difference all mal-operate.

When the transformer is energized under no-load condition or when the transformer terminal voltage recovers, as the core of the transformer will not saturate immediately, the false differential current caused by the magnetizing inrush current will lag behind the applied voltage for 3.5 ms. This phenomenon is the fundamental of the time difference based method.

When the normal transformer is switched on under no-load condition, the differential current is the magnetizing current caused by the core saturation, but the emergence of the magnetizing current lags behind the terminal voltage. The time interval between the voltage occurrence and the changing of the differential current can be detected. In this case, the differential current is also the magnetizing current at the switching side. If this time interval is bigger than a specific threshold, the differential current should be the magnetizing inrush and the differential protection will be blocked. In the case of internal faults, whenever it occurs during normal operations or transformer energizing, the time interval between the change of the applied voltage and the emergence of the differential current is very small, which should theoretically be zero. In this case, the differential current can be recognized as the fault current. Especially when the transformer is switched on accompanied by a slight inter-turn fault, the fault current is mixed with the magnetizing inrush current, leading the traditional differential protection based on the second harmonic restraint to be blocked for a period of time. In contrast, the time interval corresponding to the fault current still satisfies the characteristic of simultaneity. According to on-site experiences and various simulation test result analysis, the threshold value of this time interval can be set as 3 ms.

Therefore, a new criterion using the time interval between the sudden change of the phase voltage and the sudden change of the differential current is proposed; this overcomes the deficiencies that the existing time difference based methods cannot identify the scenario of no-load energizing. Meanwhile, this new method guarantees the correct operation of the differential protection of the transformer during normal operation.

The superimposed components of the phase voltage and the differential current are extracted firstly; this is implemented with the so-called the one-cycle subtracting algorithm. The change of the current sampling with respect to the sampling one-cycle ago is calculated in real time. The time instants that the superimposed voltage and superimposed differential current exceed the normal fluctuation range are detected and recorded. Then, the time difference between these two time instants is calculated and whether an internal fault occurs is determined according to the threshold of the criterion.

This criterion not only provides differential protection for the internal and external faults of the transformer when the transformer is switched on under no-load conditions, but also detects the fault quickly and accurately when the transformer operates with load. This criterion is based on the fast calculation of the simultaneous value, of which the logic is simple and reliable. The criterion flow diagram is shown in Figure 5.38.

5.4.2 *Preset Filter*

The signals sampled from the secondary side of the real PT (potential transformer) and the CT in the power systems usually contain some electromagnetic interference noises. This criterion makes use of transient component resulting from the change of the power frequency component. In some scenarios, the magnitude of the superimposed component may be weak, which results in the low signal-to-noise ratio. It is difficult to extract the real electrical information if reliable countermeasures are not adopted.

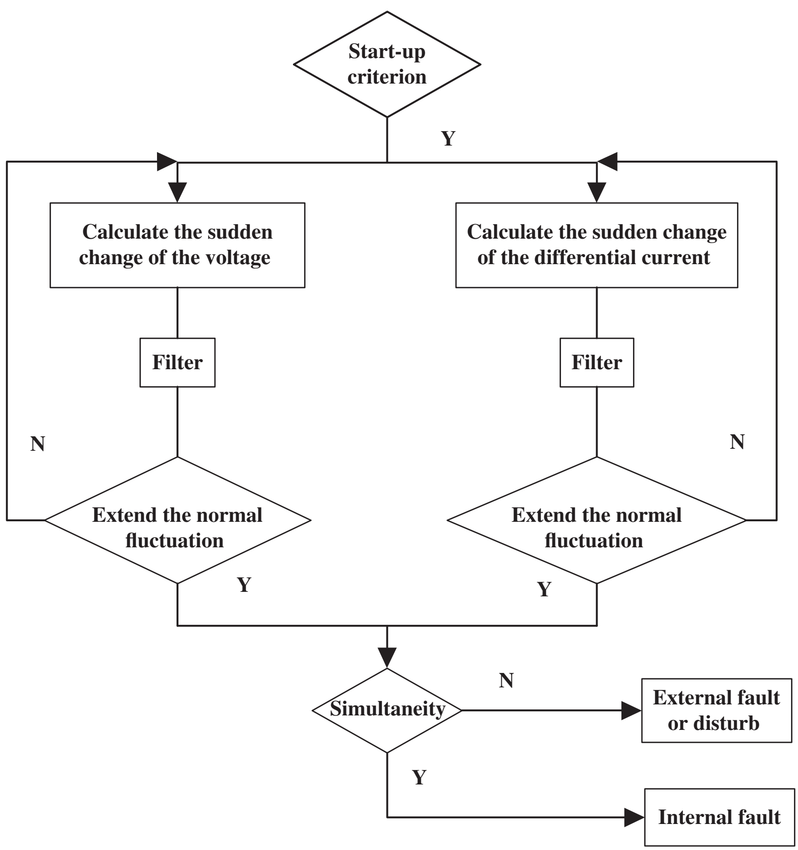

Figure 5.38 Criterion flow diagram

Therefore, it is necessary to remove the noise component by virtue of some appropriate filters. In this case, the sensitivity and reliability can be improved.

The superimposed signal series gained by the method of one-cycle subtraction often contains some high frequency interference like burrs. Usually, the useful electrical quantity is the power frequency component used by the power system protection, while the noise is usually the higher harmonics of the power frequency. As for this criterion, the main interference is the burr with high magnitude, which may result in the wrong decision with respect to the time instant the superimposed component occurs. It is necessary to design the filtering method with regard to this kind of noise characteristic. Different from the traditional least square algorithm and Kalman filtering algorithm to gain the precise information of the frequency and phase, this criterion focuses on the superimposed component in the time domain, and it is a filtering algorithm based on discriminant:

$$y(n)=\begin{cases}\dfrac{1}{2}\left[x(n-1)+x(n+1)\right] & \text{(if discriminant is tenable)}\\ x(n) & \text{(if not)}\end{cases} \tag{5.26}$$

in which, the discriminant is (K is the adjustment coefficient):

$$\left|\left(\frac{x(n-1)+x(n+1)}{2}\right)-x(n)\right|>K \tag{5.27}$$

In theory, the purpose of this filtering algorithm rests with the judgment whether the value of a certain point is far different from the average value of the two adjacent samplings by virtue of the discriminant (controls the sensitivity, the detection of the discriminant is controlled by the parameter K). If the discriminant comes into existence, the changes of this point will be regarded as beyond the normal range and recognized as the high frequency interference of 'burr singular point' caused by the noise. Therefore, the value the point is reset to is the average value of the two adjacent samplings, which is equivalent to interpolate between the two adjacent samplings. However, if the discriminant does not come into existence, the value of this point is normal and should be maintained, no filtering is necessary.

The comparison between the unfiltered series and filtered series is shown in Figures 5.39 and 5.40, respectively. This superimposed voltage series experiences the 'switching on under no-load condition' and 'inter-turn short-circuit fault' respectively at the time of 1.0 and 1.1 s, so two sudden changes occur accordingly.

Figure 5.39 shows the unfiltered superimposed voltage series and the moments corresponding to the sudden change of this series. It can be seen that the burr interference in this series lets the discriminant detect many false sudden changes. In contrast, Figure 5.40 shows that the discriminant will be

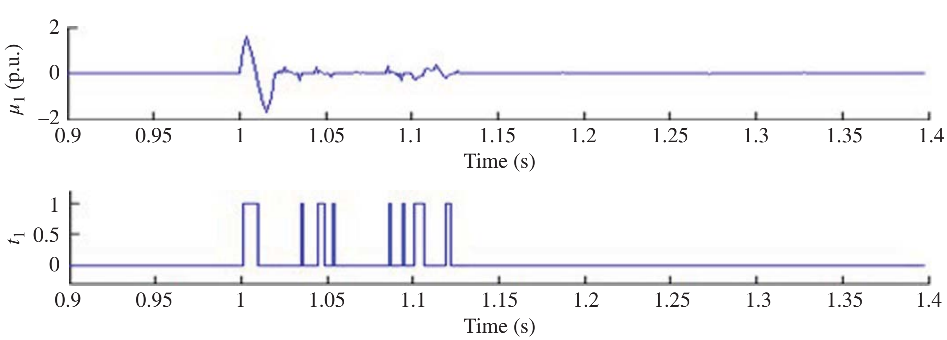

Figure 5.39 Component and its occurrence time (unfiltered)

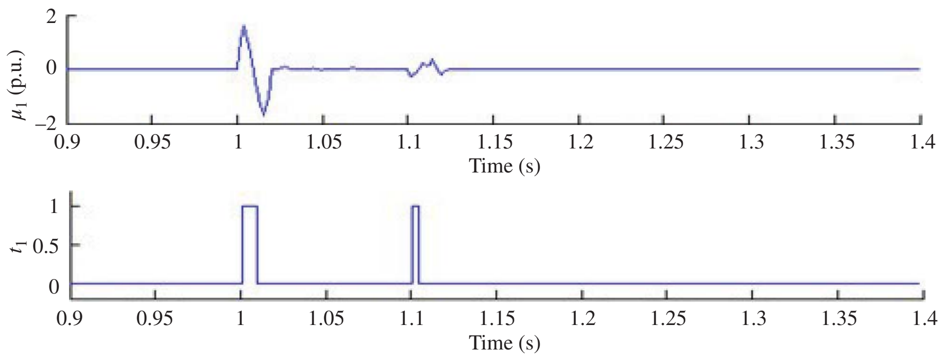

Figure 5.40 Component and its occurrence time (filtered)

immune to the burr interference by means of the above-mentioned filtering. In this case, the time instant corresponding to the sudden change can be detected correctly.

Therefore, this filtering algorithm not only removes multiburr interference but also maintains all the transient information on the change of the superimposed component during no-load switching-on and inter-turn short-circuited fault, which is a very necessary countermeasure to guarantee the reliability of this criterion.

According to the design, the time difference based method is not influenced by the voltage measurement mode. This is because it is only necessary to capture the voltage change of a certain phase that leads to such a change. If three phase-phase voltage measurement elements are all used, this phase must be included. Therefore, the time difference will always be captured in any case.

However, it is difficult to use the time difference based method only to make a decision whether the event is determined not to be an internal fault and the protection logic is switched to the successive judgment processes. In this case, a comprehensive protection scheme should be designed deliberately. The phase–phase measurement mode possibly has some potential impacts on the successive judgments. Investigations on these issues are analysed here.

5.4.3 Comprehensive Protection Scheme

To deal with a variety of complex scenarios, it is proposed that the time difference based criterion is combined with existing second harmonic restraint criterion in terms of cross-phase blocking. If the operating conditions of the power system and the transformer parameters allow the effective detection of the voltage change, the time difference criterion will be enabled. Any internal fault can be detected and removed very quickly. In contrast, the false differential current resulting from transforming switching-on or CT saturation can be identified according to the time difference compared with the change of voltage and the protection is blocked reliably. If the voltage change is minor and cannot be detected while the differential current is high enough to trigger the percentage differential protection, the time difference based criterion will not be enabled, while the second harmonic restraint criterion will be enabled instead. For these scenarios, the protection scheme is able to achieve the same operating performance as the existing schemes. Therefore, among the total disturbance set, quite a lot of internal faults can be tripped faster than before, quite a lot of extreme external faults and inrushes leading to the mal-operation of second harmonic restraint based criterions can be identified and the protection can be blocked correspondingly. For other scenarios, the protection exhibits the same performance as that of the existing schemes.

Based on above analyses, a comprehensive decision making process is designed. The time difference based method is not a one-shot decision process that is kept enabled for a period of time. Actually, two possible results can be reached according to the decision of the time difference based method. For instance, the decision result could be an internal fault. In this scenario, the protection will trip and the judgment process finished. The other result of the decision should be ‘not internal fault’. In this scenario, the judgment may go to one of two branches according to the residual voltage level. If the voltage is relatively low, it should be determined that this scenario results from a through fault, and the judgment go to the branch 1. If the voltage is relatively high, this scenario should result from the transformer energizing, and the judgment should go to the branch 2.

In branch 1, a cross-country fault identification method is introduced. With the aid of this method, any developing faults,from an external fault to a multi-external fault, or from an external fault to internal fault, can be identified and appropriate treatment adopted. As for the recovery inrush due to removing an external fault, a cross-phase blocking second harmonic restraint criterion is introduced to deal with it. For most successive scenarios, this scheme has satisfactory performance except for two scenarios. In the first, the second harmonic contents of three differential currents (due to inrushes or CT ratio mismatch) are all below the threshold like 15%, which will lead to mal-operation. In the second scenario, the removal of external fault results in recovery inrush (which is not very usual due to the residual voltage level and the residual flux of the transformer core) and, in the meantime, an internal fault occurs exactly during the period of inrush existence. This second scenario will lead to the protection tripping with a possible time delay. However, according to the above analysis and common sense, these two scenarios are quite rare. Therefore, the risk due to these scenarios can be taken.

In branch 2, the differential current is monitored continuously. If it always exists, the second change of the voltage will be monitored. If a second change of the voltage is detected, a phase-separated second harmonic restraint criterion will be enabled. Otherwise, the protection will be blocked for five cycles and then the protection logic quits this branch and goes to the cross-phase blocking based second harmonic restraint criterion. In this case, as for the internal fault occurring after the transformer is switched on, the phase-separated second harmonic restraint criterion can be enabled to trigger the protection if this fault is not too slight to trigger the voltage change. In this case, the possible existing inrushes on other phases will not block the protection. If this voltage change is due to an external fault, two possible mal-operation scenarios may occur. The first scenario is such an extreme case that inrush does not decrease to the value below the threshold, while the second harmonic content of at least one phase of inrush is below the threshold, such as 15%, and, at the same time, an external fault occurs during this period (exactly within a five-cycle duration after the transformer switches on). As seen, the probability of this case is quite low. The second scenario is a case such that inrush does not decrease to the value below the threshold, while the CT extremely and rapidly saturates, leading the second harmonic content of the false differential current to being below the threshold, such as 15%, and, at the same time, an external fault occurs during this period. As seen, the probability of this case is also quite low. Actually, the criterion of cross-phase blocking based second harmonic restraint can solve above problems by means of the help of existing inrushes on the healthy phase(s). However, this countermeasure may lead to a long time delay if an internal fault occurs during this period due to the impact of the existing inrushes on the healthy phase(s). From the view of engineering application, internal faults of the electric apparatus should be protected as much as possible. Therefore, it is preferred to adopt the phase-separated second harmonic restraint criterion and to take the risk of mal-operation due to the two rare scenarios outlined above. In this branch, the protection keeps blocked for five cycles if the successive faults do not lead to a detectable voltage change. If it is an external fault, this action exactly meets the requirement of blocking the protection. If it is an internal fault, it must be a slight fault in most cases. Therefore, a five-cycle operating time delay should be acceptable from the viewpoint of engineering applications. Figures 5.41 and 5.42 illustrate the above comprehensive protection logic with flowcharts.

As for evolving multiphase external faults, especially when the disturbance detector for a differential current is sensitive and may trigger external faults when the standing differential signal (due to ratio mismatch) changes even without CT saturation, this problem can also be solved by the operating logic design of the cross-country fault identification method. Assume a phase A external fault developing to a phase A-to-phase B external fault, and that a false differential current occurs on phase B due to a ratio mismatch other than saturation. In this case, the waveform shape of the phase B false differential current

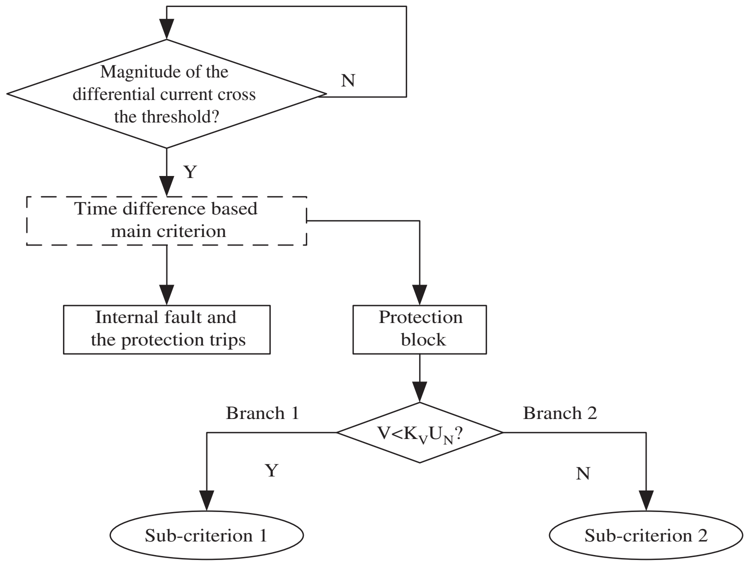

Figure 5.41 Main flowchart of the integrated protection logic

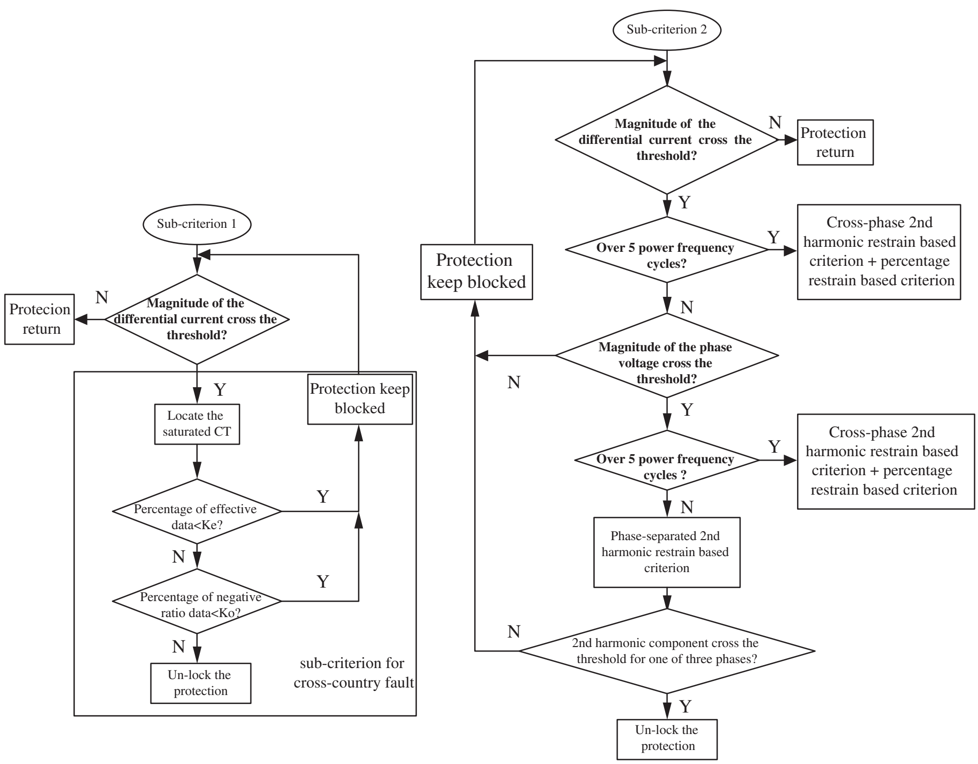

Figure 5.42 Flowchart of the two subcriteria

is relative regular and possibly does not satisfy the criterion of above cross-country fault identification criterion. However, this criterion is able to be designed as a cross-phase blocking scheme. The possible mal-operation of phase B differential protection can be blocked by the decision of phase A, since the false differential current in phase A still satisfies the criterion of the above cross-country fault identification criterion. The cross-phase blocking scheme will not result in the fail-to-trip of a developing fault from the one-phase external fault to the same phase internal fault, such as from a phase A external fault to a phase A internal fault. Only in the following very rare scenario it may bring some operation time delay for a complicated multifault: phase A external fault developing to a multiple fault, that is, -phase A external fault combined with phase B internal fault. In this case, the differential protection is perhaps blocked by the phase A criterion until the false differential current due to saturation decay below the threshold. From the view point of the engineering, this operation with some time delay should be acceptable.

As described above, the low voltage criterion is used at the exit of the main process and within the branch 2. If the phase–phase voltage measurement mode is adopted, the operating sensitivity will become lower because the zero-sequence components are not included. Therefore, the operating threshold of the low voltage element should be set more sensitive in the real application with respect to the phase-separated measurement mode.

5.4.4 Simulation Tests and Analysis

Based on the EMTDC software, the system simulation model of the 110/35 kV transformer is established. In the model, the source is at the 110 kV side. The transformer uses Y/Δ-11 connections and the high voltage side was Y-connected. The rated capacity of the 110/35 kV transformer is 100 MVA. Its leakage reactance is 0.1 (p.u.) and the source impedance on the 110 kV side of the transformer is 2.0 Ω resistance cascading with 0.02H reactance (Figure 5.43).

To ensure the effectiveness of the time difference based method, the sampling frequency of the simulation is set as 1 kHz, which means sampling 20 points in one cycle. The phase correction is done according to the connection of the transformer before forming the differential current. The u_1 represents the voltage of the side of Y-connection and i_d represents the corresponding differential current. u_1' represents the corresponding a one-cycle superimposed component of the phase voltage u_1, and i_d' represents the corresponding one-cycle superimposed component of the differential current i_d in one cycle. t_1 and t_2 represent the states of the sudden change of the voltage and the differential current. The value '1' represents that the sudden change occurs and '0' represents that no sudden change is detected.

By virtue of this model, various scenarios of energizing and different types of faults of the transformers are simulated. Some representative cases are illustrated here (Scenarios 5.6–5.18) for the purpose of validation.

Scenario 5.6 Energizing of a healthy no-load transformer

This case presents the scenario of switching-on the transformer at the high voltage side. Figure 5.44 shows the waveforms of the phase voltage and the differential current (taking phase A of the Y-side for reference). This scenario presents the switching-on of the normal transformer. The phase A residual flux of the iron core of the transformer is 40%, the inception angle is 0° and the transformer is switched on at 1.0 s. The voltage and magnetizing inrush current after switching-on would lead to the superimposed

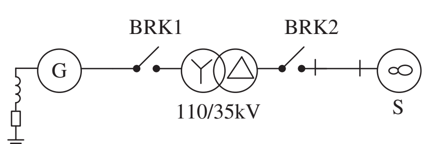

Figure 5.43 Simulation system model of the 110/35kV transformer

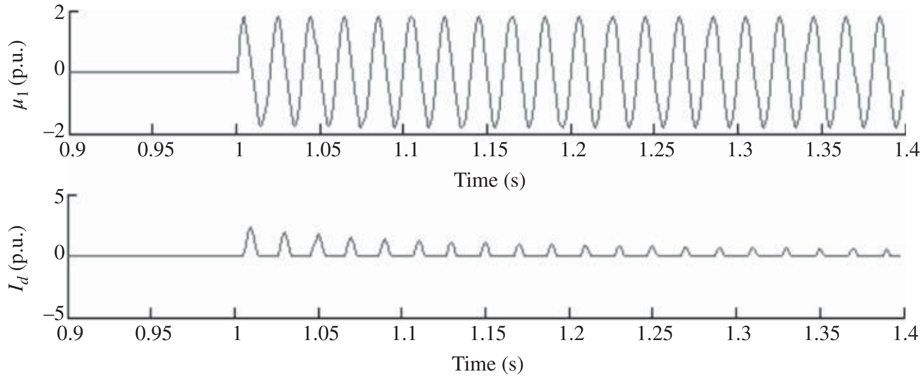

Figure 5.44 Voltage and differential current (Scenario 5.6)

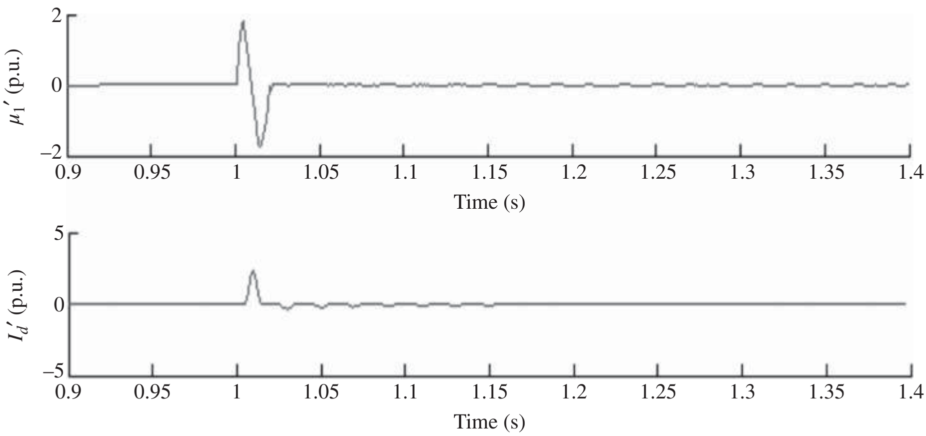

Figure 5.45 Component of voltage and differential current (Scenario 5.6)

components of the voltage and the differential current. The filtered superimposed series of the voltage and the differential current are shown in Figure 5.45. Furthermore, time corresponding to the sudden change could be obtained (Figure 5.46). According to Figure 5.46, the time difference between the sudden change of the voltage and the differential current is 4 ms, which exceeds the threshold set above. In this case, the protection would be blocked correctly. Afterwards, no matter what the voltage or the current, no successive change occurs. Therefore, the protection would be blocked reliably in the whole process.

Scenario 5.7 Energizing of a faulty no-load transformer

This case provides the simulations of the switching-on of the no-load transformer with an internal turn-to-turn short-circuit fault. Figure 5.47 shows the waveforms of the voltage and the differential current and Figure 5.48 shows the superimposed components of the voltage and the differential current. Figure 5.49 shows the comparison between the occurrences of superimposed voltage and superimposed

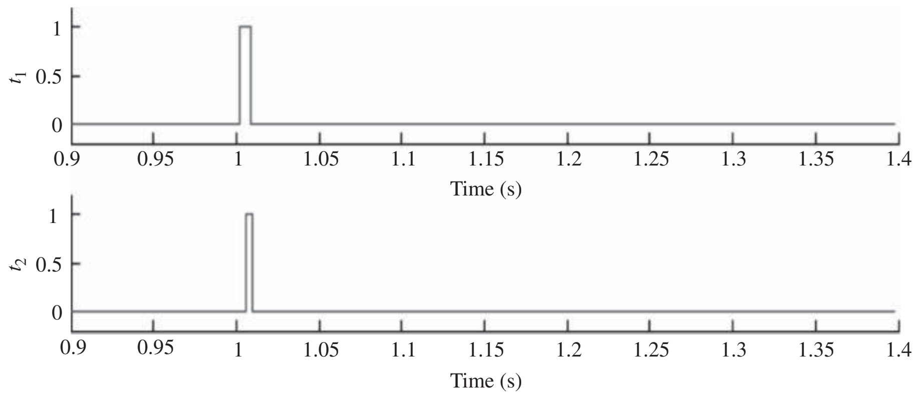

Figure 5.46 Occurrence time of component of voltage and differential current (Scenario 5.6)

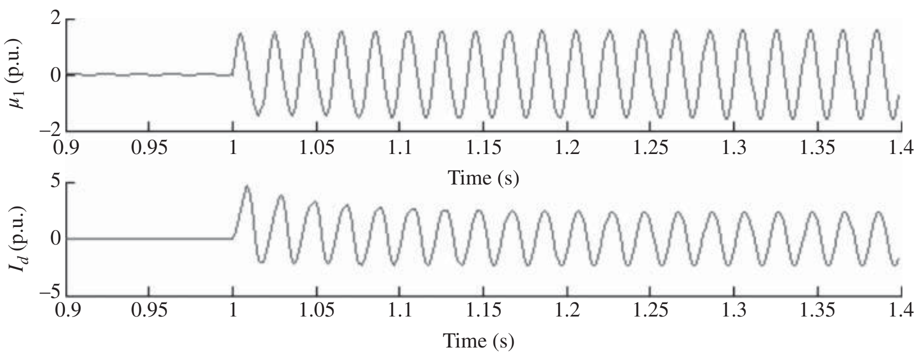

Figure 5.47 Voltage and differential current (Scenario 5.7)

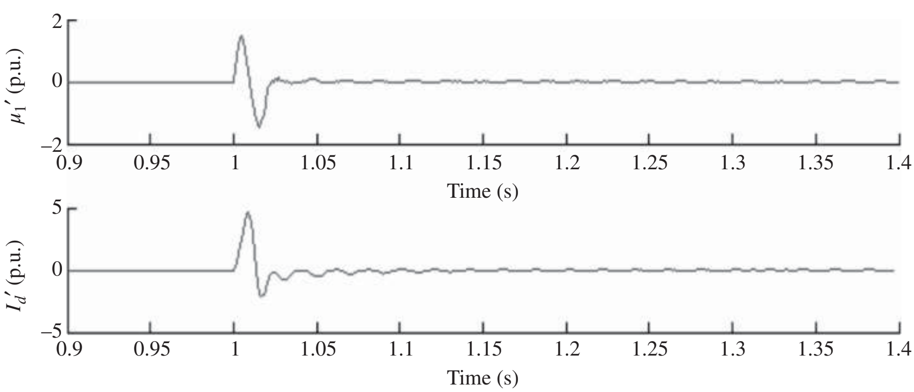

Figure 5.48 Component of voltage and differential current (Scenario 5.7)

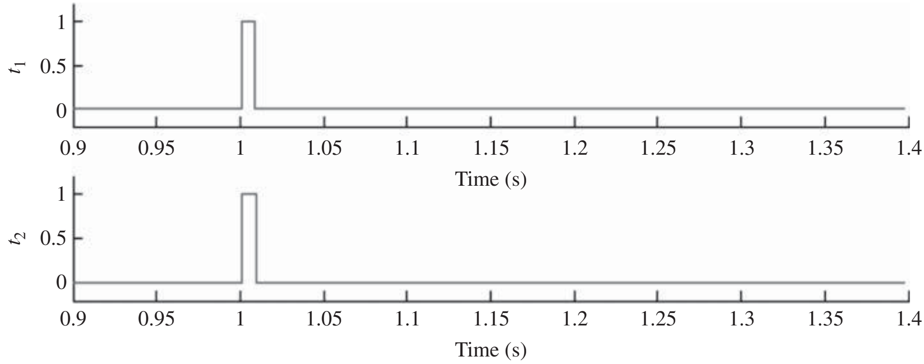

Figure 5.49 Occurrence time of component of voltage and differential current (Scenario 5.7)

differential currents. The time difference between the superimposed voltage occurrence and the differential current occurrence is identified as 0 s by this criterion. Therefore, the fault is recognized as an internal one and the protection should trip reliably. This criterion does not rely on the whole characteristic of the waveform of the differential current but on the time difference of the superimposed series. Therefore, it will not have to gain the whole characteristic by virtue of a long data window and it will operate more quickly. It can avoid the mal-operation due to the low second harmonic content in some conditions.

Scenario 5.8 A developing fault occurring during energizing of a no-load transformer
A developing fault is a special type of fault. In this case, the transformer was switched on under no-load (switching angle is 18° and the residual flux is 30%) and the transformer experienced the internal fault (turn-to-turn short-circuit) at 1.1 s. Figure 5.50 shows the waveforms of the voltage and the differential current and Figure 5.51 shows the waveform of the superimposed component of the voltage and differential current. Figure 5.52 presents the comparison between their superimposed components. As seen, this criterion detected that the time difference between the sudden changes of the superimposed components of the voltage and differential currents was 5 ms at approximately 1.0 s. Therefore, this scenario should not be an internal fault and the protection should be blocked. When an internal fault occurs at

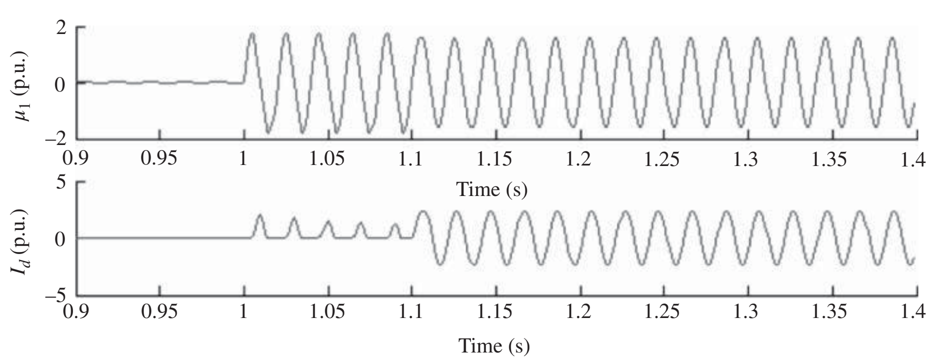

Figure 5.50 Voltage and differential current (Scenario 5.8)

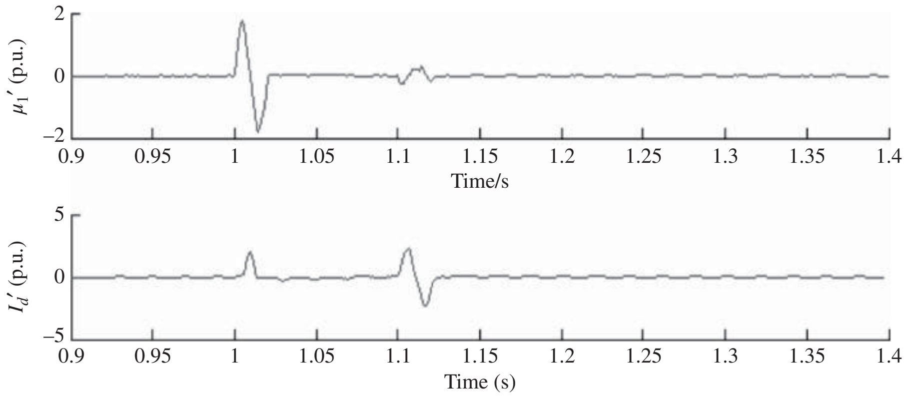

Figure 5.51 Component of voltage and differential current (Scenario 5.8)

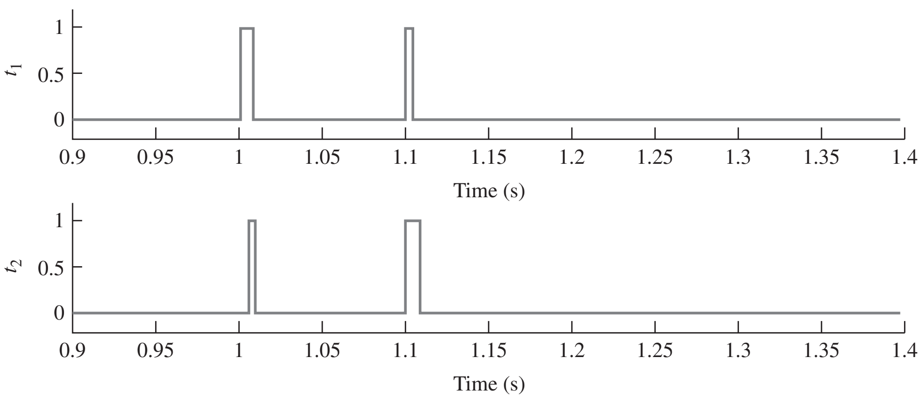

Figure 5.52 Occurrence time of superimposed component of voltage and differential current (Scenario 5.8)

1.1 s, as shown in Figure 5.51, the time difference between the sudden changes of the superimposed components of the voltage and the differential current is identified as 0 s. In this case, it is recognized as a developing fault and the blocking logic of the protection should be released to allow the protection to trip correctly. It can be seen that this criterion will still maintain the accuracy and the speed of operation with respect to the developing fault during the period when the protection is being blocked due to the magnetizing inrush.

Scenario 5.9 Phase-to-phase fault during the operation of the no-load transformer

In this case, the internal phase-to-phase short-circuit fault under no-load is simulated. The fault occurs at 4.0 s. The faulty phase voltage sags very quickly while the differential current rises very fast (Figure 5.53). Figure 5.54 presents the transient characteristic more clearly by means of the superimposed components of the voltage and the current. Figure 5.55 indicates the time when the superimposed components corresponding to the waveforms in Figure 5.54 emerge. From Figure 5.55 it can been seen that the time

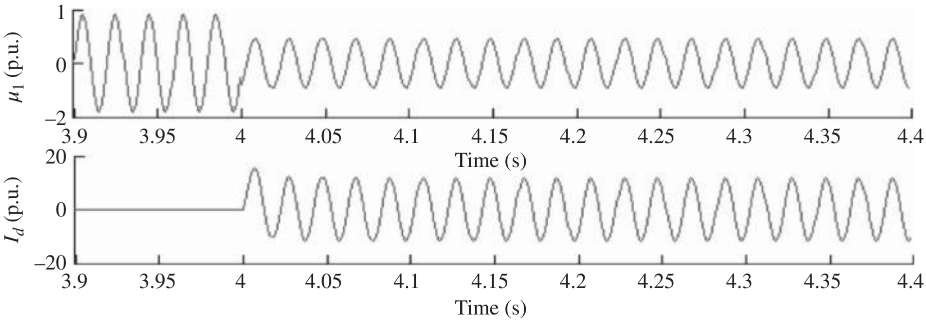

Figure 5.53 Voltage and differential current (Scenario 5.9)

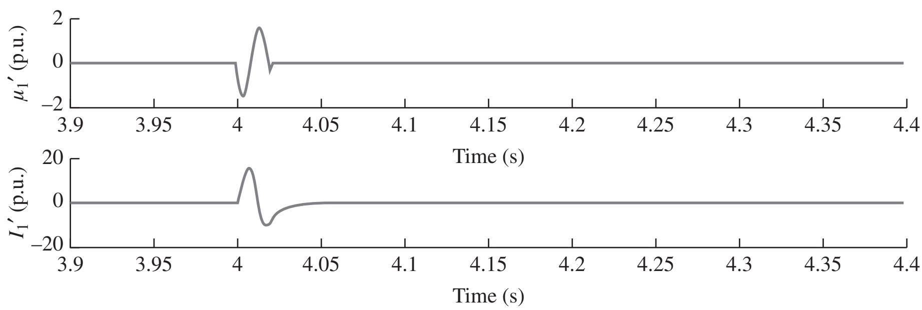

Figure 5.54 Component of voltage and differential current (Scenario 5.9)

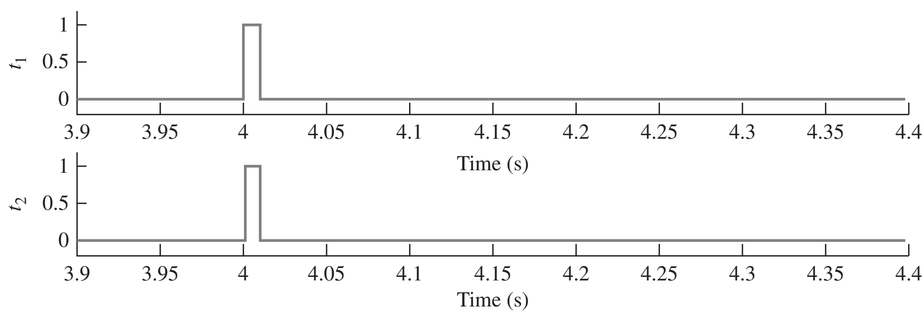

Figure 5.55 Occurrence time of superimposed component of voltage and differential current (Scenario 5.9)

difference between the emergence of the superimposed component of the voltage and that of the differential current was 0 s, and the protection should operate instantaneously.

Scenario 5.10 Phase-to-phase fault during the operation of the loaded transformer
An internal phase-to-phase short-circuit fault of a loaded transformer is simulated in this case. Figure 5.56 shows the waveform of the voltage and the differential current and Figure 5.57 shows the waveforms of

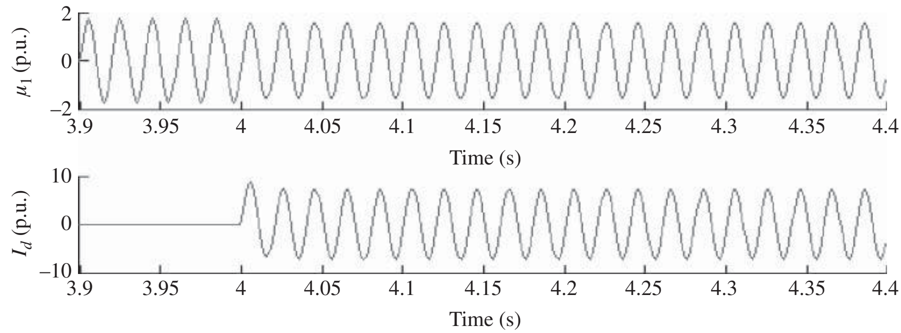

Figure 5.56 Voltage and differential current (Scenario 5.10)

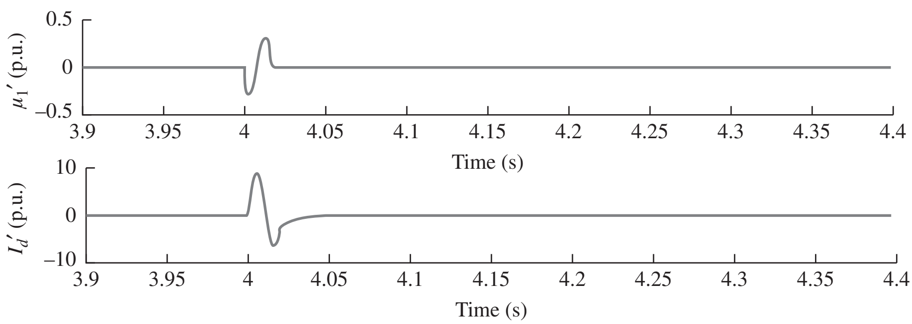

Figure 5.57 Component of voltage and differential current (Scenario 5.10)

the superimposed components of the voltage and the differential current. Figure 5.58 presents the comparison between their superimposed components. The fault occurs at 4.0 s and the faulty phase voltage sags very quickly while the differential current rises to several times the rated value (Figure 5.56). Figure 5.57 shows the transient characteristic more clearly by means of the superimposed components of the voltage and the current. As seen, according to this criterion, the time difference between the superimposed component of the voltage and that of the differential current was 0 s. In this case, the protection should operate instantaneously.

Scenario 5.11 Inter-turn fault during the operation of the loaded transformer

An internal turn-to-turn short-circuit fault of a loaded transformer is simulated in this scenario. The simulation module for designing the internal fault in the EMTDC software has no specifications for setting the turns of short-circuit winding, total turns of the faulted winding the total turns of the un-faulted winding. Therefore, the auto-transformer module is used to simulate the inter-turn fault. The short-circuit ratio depends on the voltage ratio of the corresponding winding. In this scenario, we design a 9.1% inter-turn fault occurring on the 110 kV side of the transformer. Figure 5.59 shows the waveforms of the voltage and the differential current and Figure 5.60 shows the waveforms of the superimposed component of the voltage and differential current. Figure 5.61 presents the comparison between their superimposed components. At 4.0 s, the faulty phase voltage sags very quickly while the differential current rises suddenly (Figure 5.59). Figure 5.60 shows the transient characteristic more clearly by means of the superimposed

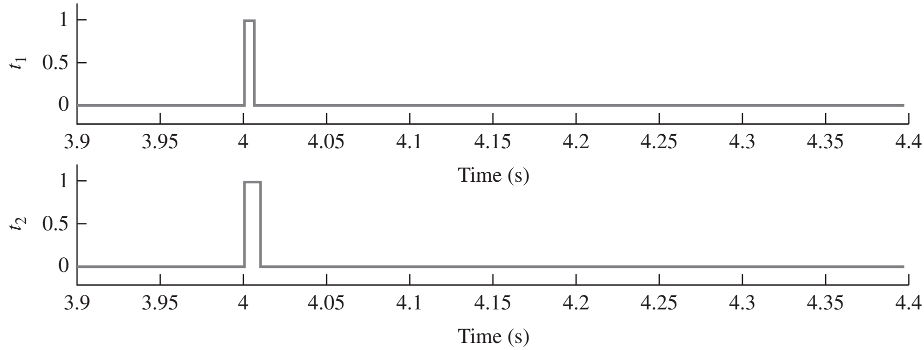

Figure 5.58 Occurrence time of superimposed component of voltage and differential current (Scenario 5.10)

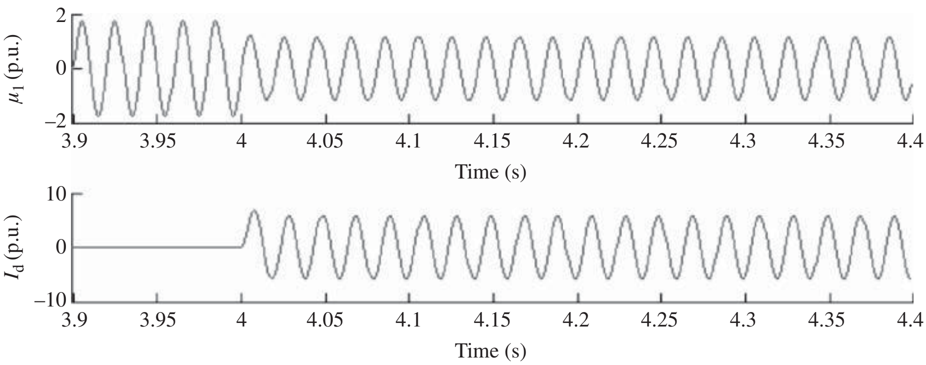

Figure 5.59 Voltage and differential current (Scenario 5.11)

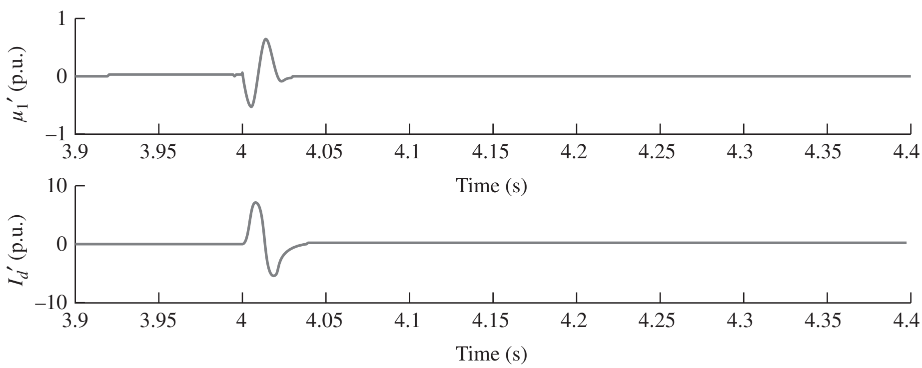

Figure 5.60 Component of voltage and differential current (Scenario 5.11)

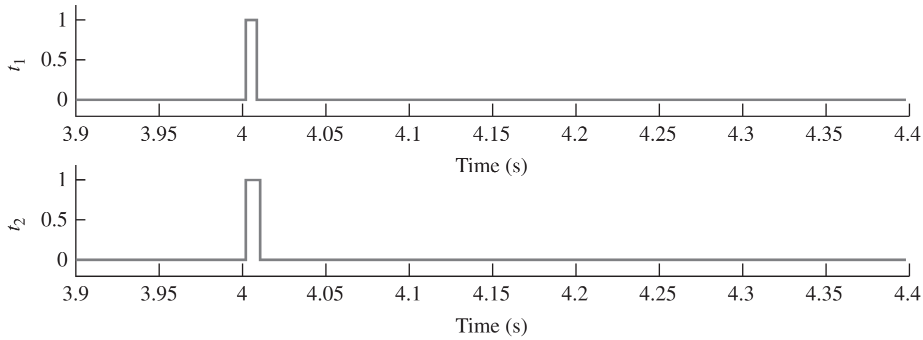

Figure 5.61 Occurrence time of superimposed component of voltage and differential current (Scenario 5.11)

component of the voltage and the current. According to this criterion, the time difference between the emergence of the superimposed component of the voltage and that of differential current was 0 s. The protection should operate instantaneously.

Numerous of different typical types of 'switching on under no-load condition' and internal faults are simulated to verify the proposed criterion, and the results prove that this criterion is effective and fast.

Scenario 5.12 Energizing the no-load transformer connecting with a stiff system

Scenario 5.12.1: $x_s/x_T = 1 : 10$, where x_s represents the internal reactance of the stiff system and x_T represents the positive sequence leakage reactance of the transformer.

This case presents the scenario of switching on a transformer at the Y-side (high voltage side). The PTs are installed on the voltage bus. The phase A residual flux of the transformer core is 40% and the inception angle is 0°. The transformer is switched on at 0.3 s. The voltage and magnetizing inrush current after switching on are also able to lead to the detectable superimposed components of the voltage and the differential current in this scenario. Figure 5.62 shows the waveforms of the differential current and the corresponding superimposed component (taking phase A of the Y-side for reference).

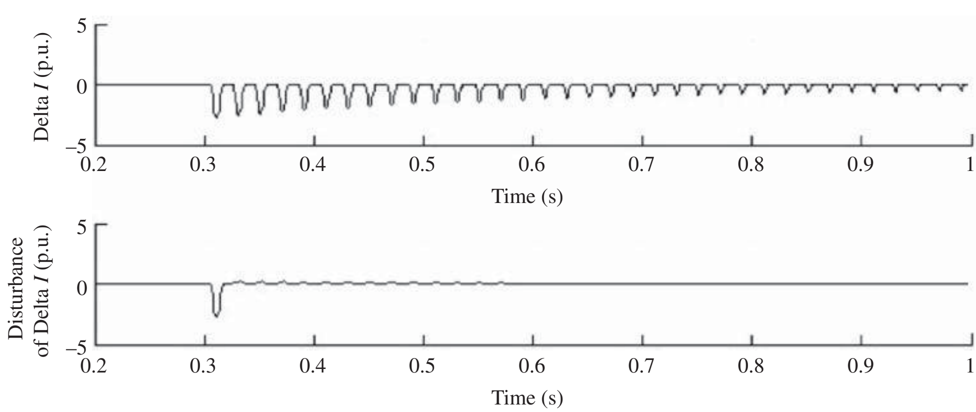

Figure 5.62 Differential current and the component (Scenario 5.12.1)

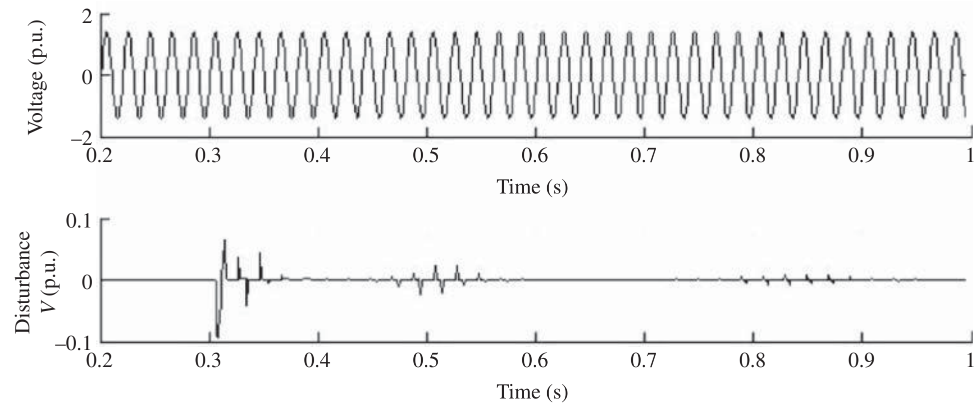

Figure 5.63 Voltage and the component (Scenario 5.12.1)

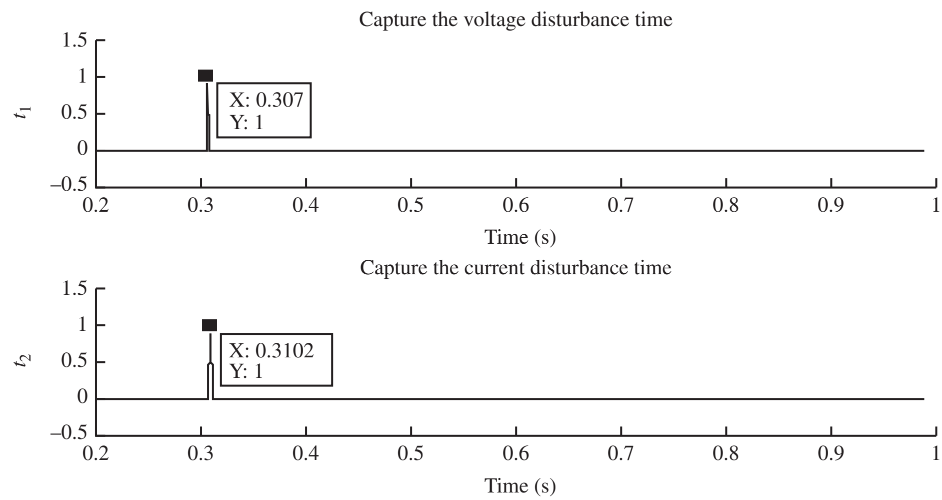

Figure 5.64 Occurrence time of component of voltage and differential current (Scenario 5.12.1)

The voltage and the filtered superimposed series of it are shown in Figure 5.63. According to Figure 5.63, the superimposed component of the voltage is 0.067 (p.u.), greater than 0.05 (p.u.). Furthermore, the time corresponding to the sudden change could be obtained (Figure 5.64). According to Figure 5.64, the time difference between the sudden change of the voltage and the differential current is 3.2 ms, which exceeds the threshold set above. In this case, the protection would be blocked correctly.

Scenario 5.12.2: $x_s/x_T = 1 : 15$, where x_s represents the internal reactance of a very stiff system and x_T represents the positive sequence leakage reactance of the transformer.

This case presents the scenario of switching on the transformer at the high voltage side. The PTs are installed on the voltage bus. The phase A residual flux of the iron core of the transformer is 40%, the inception angle is 0° and the transformer is switched on at 0.3 s. The voltage and magnetizing inrush current after switching on also lead to the superimposed components of the voltage and the differential current. Figure 5.65 shows the waveforms of the differential current and the superimposed component

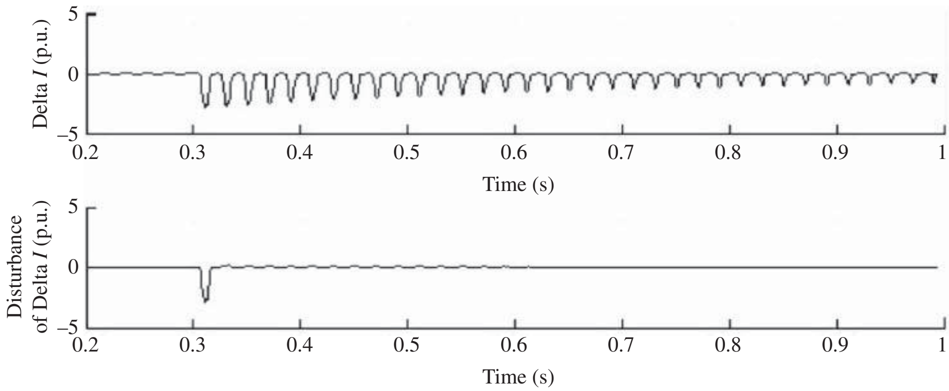

Figure 5.65 Differential current and the superimposed component (Scenario 5.12.2)

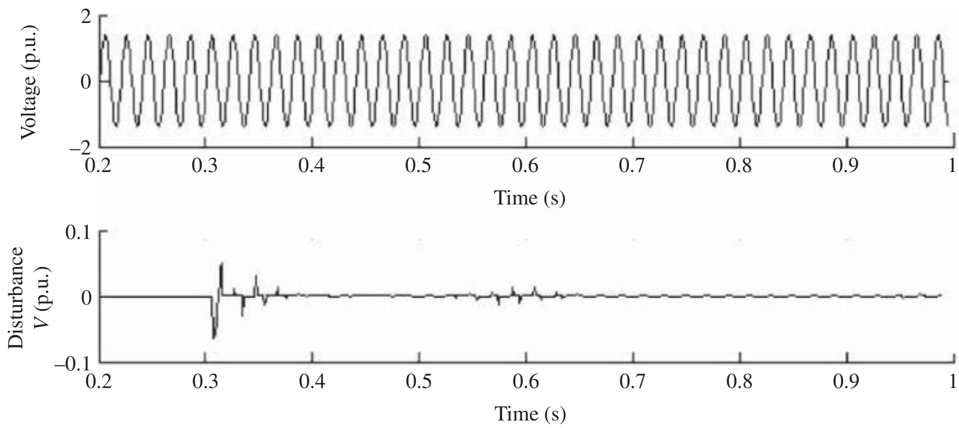

Figure 5.66 Voltage and the superimposed component (Scenario 5.12.2)

of it (taking phase A of the Y-side for reference). The voltage and the filtered superimposed series of it are shown in Figure 5.66. According to Figure 5.66, the superimposed component of the voltage is 0.0457 (p.u.), less than 0.05 (p.u.). Therefore, it should be considered that there is no sudden change on the voltage. Furthermore, the time corresponding to the sudden change could be obtained (Figure 5.67). According to Figure 5.67, no time difference between the sudden change of the voltage and the differential current needs to be calculated due to the condition that the voltage change is not satisfied.

According to Scenarios 5.12.1 and 5.12.2, the voltage change decreases with respect to the increase of the degree of stiffness of the connected system when the PT is installed on the voltage bus. Therefore, it is possible that the superimposed component of the voltage cannot be detected if the connected system is very stiff.

The value 0.05 (p.u.) for the voltage change can be set as a threshold in terms of engineering applications. In this case, the voltage change in Scenario 5.12.1 is greater than 0.05 (p.u.) and can be detected correspondingly. The time difference based method is still valid for this case. In contrast, the

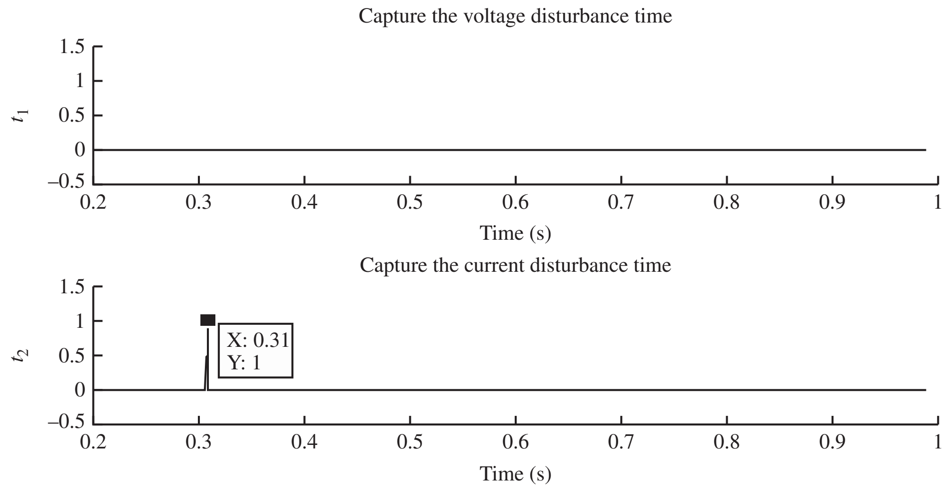

Figure 5.67 Occurrence time of the superimposed component of voltage and differential current (Scenario 5.12.2)

voltage change in Scenario 5.12.2 is less than 0.05 (p.u.) and cannot be detected correspondingly. The time difference based method will fail for this case. Instead, the second harmonic restraint scheme will be enabled.

Scenario 5.13 Turn-to-turn fault during operation of the loaded transformer

In this scenario, the aim is to find out the relationship of the severity of the fault to the detectable voltage change when the transformer is connected to a stiff system. Therefore, still assume that $x_s/x_T = 1 : 10$. An internal turn-to-turn (20%) short-circuit fault of a loaded transformer is simulated in this scenario. PTs are installed on the voltage bus. In this case the disturbance of the voltage is 0.0557 (p.u.), greater than the threshold 0.05 (p.u.). Figure 5.68 shows the waveforms of the differential current and superimposed

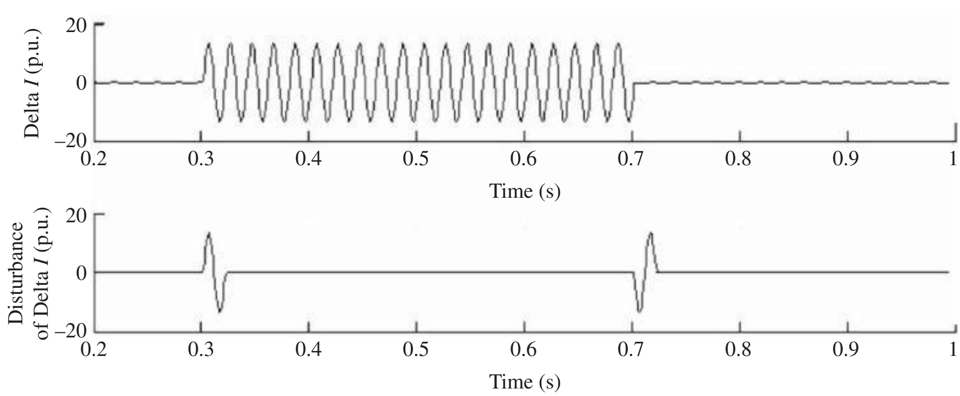

Figure 5.68 Differential current and the component (Scenario 5.13)

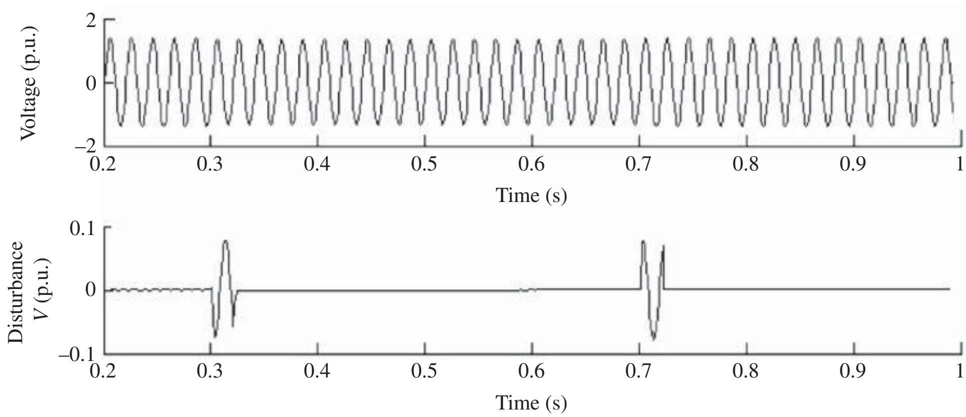

Figure 5.69 Voltage and the component (Scenario 5.13)

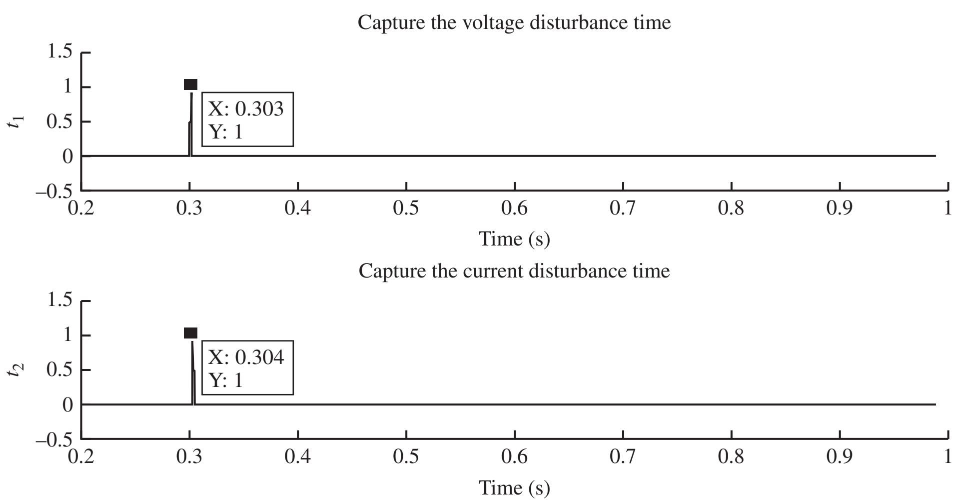

Figure 5.70 Occurrence time of superimposed component of voltage and differential current (Scenario 5.13)

component of it. Figure 5.69 shows the waveforms of the voltage and the superimposed component of it. Figure 5.70 presents the comparison between their superimposed components. At 0.3 s, the faulty phase voltage sags very quickly while the differential current rises suddenly (Figures 5.68 and 5.69). According to Figure 5.70, the time difference between the emergence of the superimposed component of the voltage and that of the differential current was 1 ms, less than the threshold (3 ms). In this case, the time difference based criterion will be enabled and the protection should operate instantaneously.

If the severity of the fault decreases further, for example 10% turn-to-turn fault, the voltage change due to fault occurrence will not be detected in the case of 5% operating threshold. In this case, the second harmonic restraint criterion will be enabled and this fault also can be cleared in time. Of course, the protection using the second harmonic restraint criterion will trip with some time delay if a transformer with a slight internal fault is switched to a stiff system. However, it is the inherent problem of this type of criterion. It should be pointed out that the time difference based method can work in a variety of internal fault scenarios as long as the voltage change due to the fault occurrence can be detected, which corresponds to most internal fault scenarios.

Scenario 5.14 Clearing the external fault to probe the inrush current

This case presents the scenario of clearing the external fault to probe the magnetizing inrush current. The external fault was applied at 0.5 s. The differential current keeps low and the faulty voltage drops greatly. In this case, the differential current cannot be detected since it is an external fault. The external fault is cleared at 0.9 s. As a result of voltage recovery, the magnetizing inrush current is probed. Figure 5.71 shows the differential current and the superimposed component of it. Figure 5.72 shows the voltage and the superimposed component of it. According to Figure 5.73, the time difference between the voltage disturbance and the inrush current is 16 ms, much greater than the threshold. In this case, the time difference based criterion will be enabled and the protection will be blocked reliably.

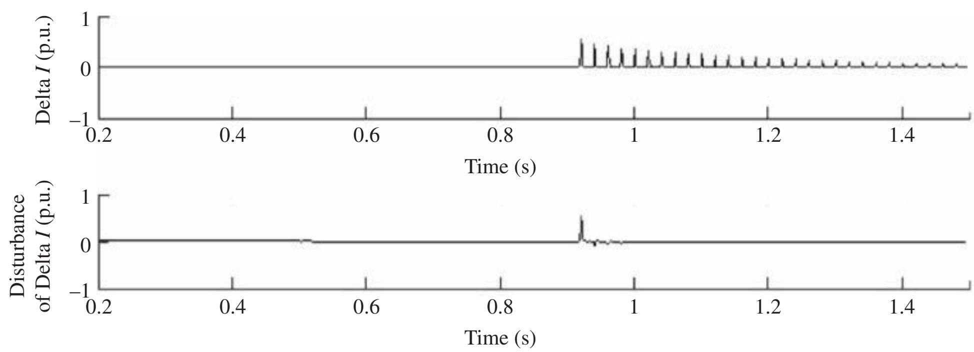

Figure 5.71 Differential current and the superimposed component (Scenario 5.14)

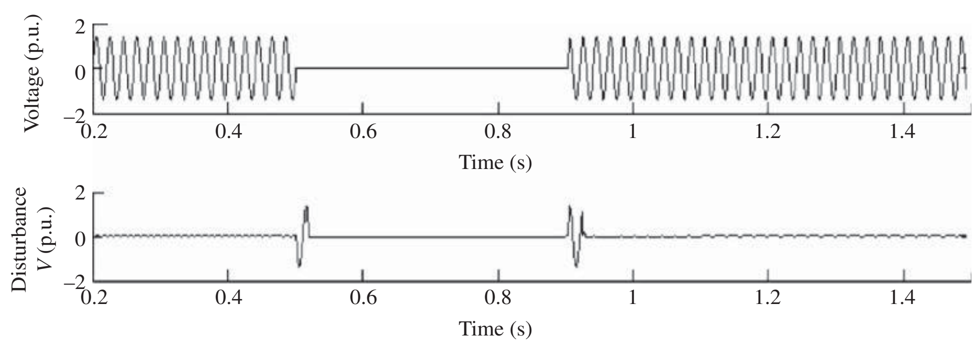

Figure 5.72 Voltage and the superimposed component (Scenario 5.14)

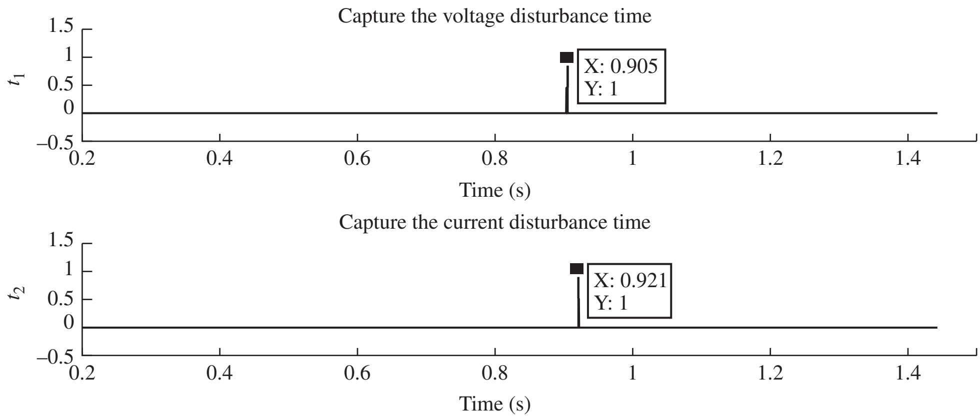

Figure 5.73 Occurrence time of superimposed component of voltage and differential current (Scenario 5.14)

Scenario 5.15 Non-zero differential current changes due to the CT ratio mismatch when voltage recovers

This case presents the scenario of non-zero differential current changing due to voltage recovery after an external fault is cleared. Figure 5.74 shows the differential current and the superimposed component of it. Figure 5.75 shows the voltage and the superimposed component of it. The external fault is applied at 0.5 s. The differential current keeps low and the faulty voltage drops greatly. The external fault is cleared at 0.9 s. As a result of voltage recovery, the differential current grows because of the CT ratio mismatch. According to Figure 5.76, the second harmonic of the differential current is less than 10%, which may lead to the mal-operation of the second harmonic restraint based differential protection with a 15% restraint threshold. However, according to Figures 5.77 and 5.78, the second harmonic of the differential current of another phase (phase B) is always greater than 18%. The protection will be blocked by the cross-phase blocking scheme.

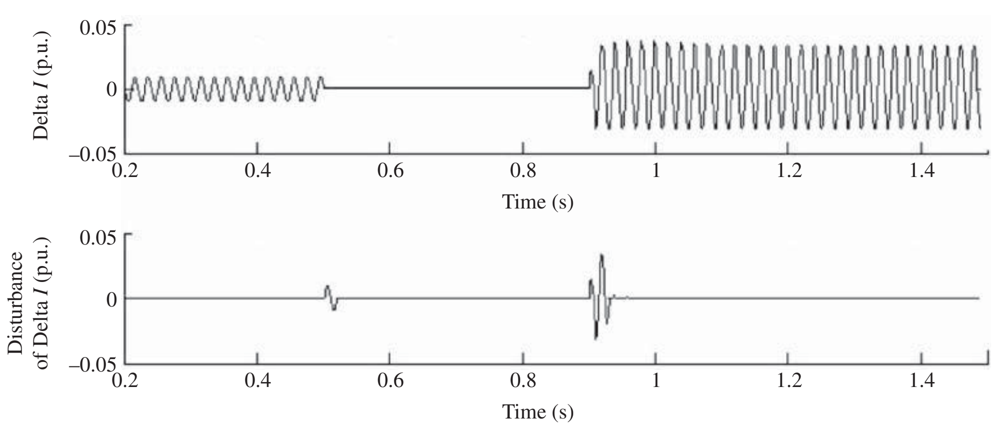

Figure 5.74 Differential current and the superimposed component (Scenario 5.15)

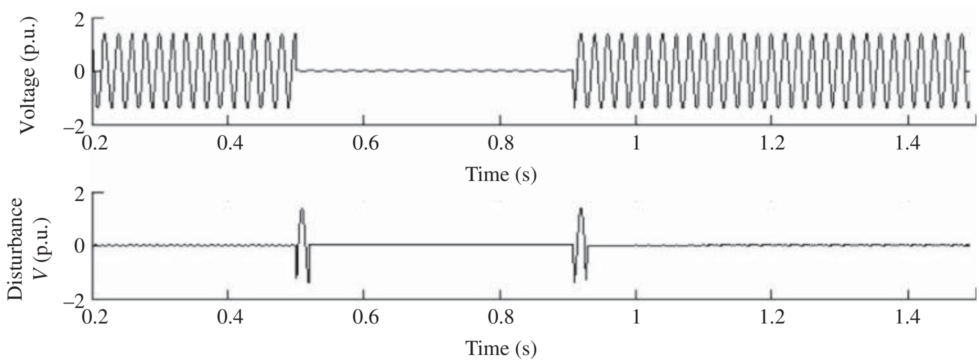

Figure 5.75 Voltage and the superimposed component (Scenario 5.15)

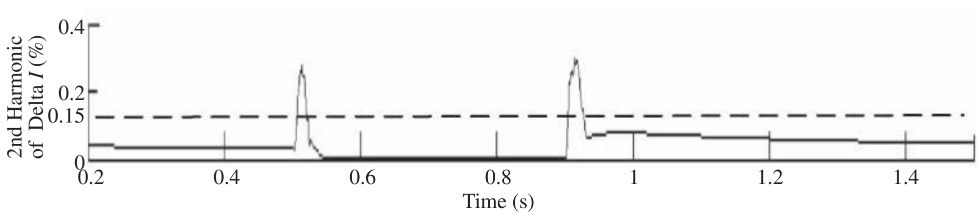

Figure 5.76 Second harmonic of the differential current (Scenario 5.15)

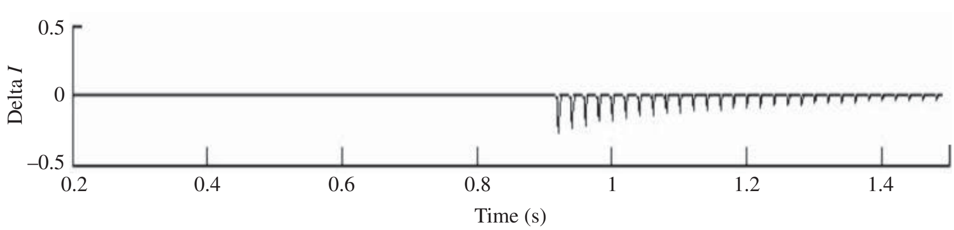

Figure 5.77 Differential current of phase B (Scenario 5.15)

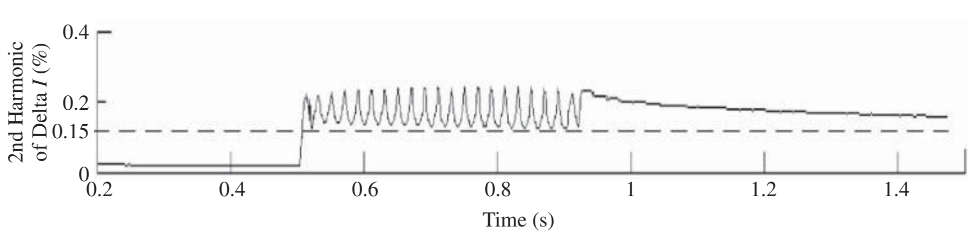

Figure 5.78 Second harmonic of the differential current of phase B (Scenario 5.15)

Scenario 5.16 Energizing a healthy no-load transformer from the delta side (low voltage side)
This case presents the scenario of the switching on the transformer at the delta side (low voltage side). The PTs are installed on the low voltage bus. The phase A residual flux of the iron core of the transformer is 20%, the inception angle is 0° and the transformer is switched on at 0.3 s. The voltage and magnetizing inrush current after switching on would lead to the superimposed components of the voltage and the differential current. Figure 5.79 shows the waveforms of the differential current and the superimposed component of it (taking phase A of the Y-side for reference). The voltage and the filtered superimposed series of it are shown in Figure 5.80. According to Figure 5.80, the superimposed component of the voltage is 0.15 (p.u.), greater than 0.05 (p.u.). Furthermore, the time corresponding to the sudden change could be obtained (Figure 5.81). According to Figure 5.81, the time difference between the sudden change of the voltage and the differential current is 6 ms, which exceeds the threshold set above. In this case, the protection would be blocked.

Scenario 5.17 Three phases of the no-load transformer are energized separately
This case presents the scenario of switching on the transformer at the Y-side (high voltage side) and three phases energized separately. The PTs are installed on the transformer side of the breaker used for energizing. The phase A residual flux of the iron core of the transformer is 30%, the inception angle is 0° and pole A is switched on at 0.3 s. The phase B residual flux of the iron core of the transformer is 20%, the inception angle is 0° and pole B is switched on at 0.308 s. The voltage and magnetizing

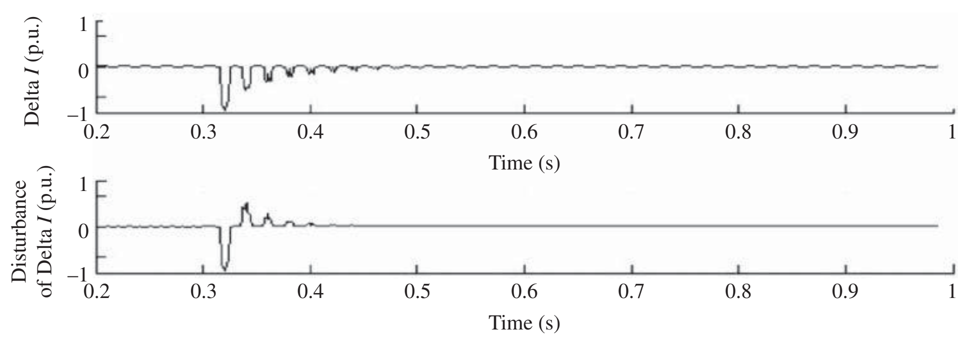

Figure 5.79 Differential current and the superimposed component (Scenario 5.16)

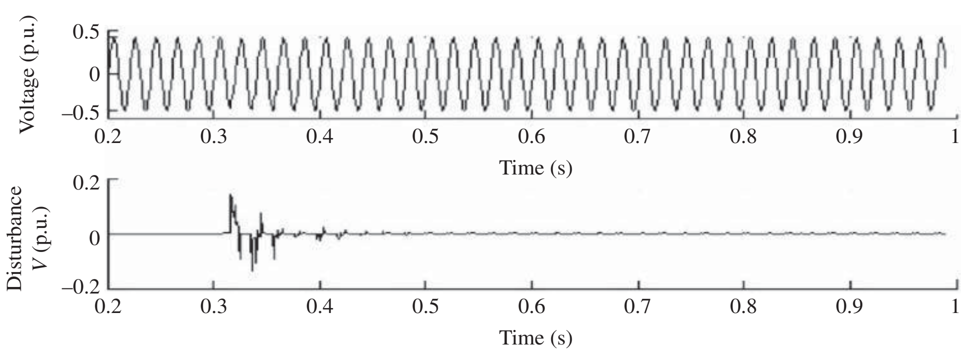

Figure 5.80 Voltage and the superimposed component (Scenario 5.16)

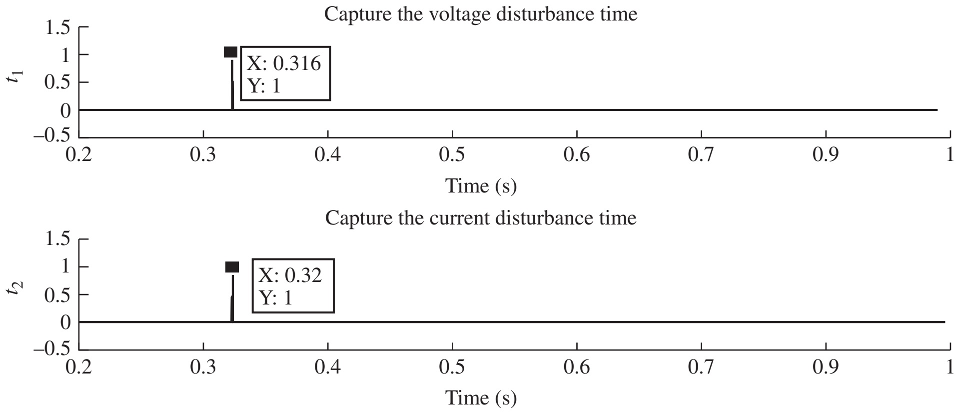

Figure 5.81 Occurrence time of superimposed component of voltage and differential current (Scenario 5.16)

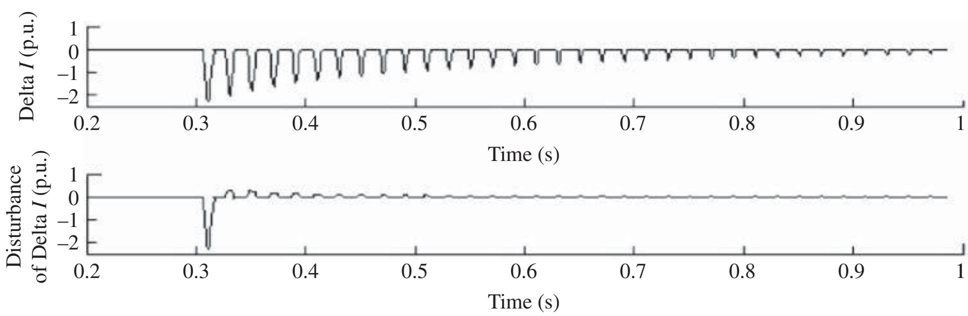

Figure 5.82 Differential current and the superimposed component (Scenario 5.17)

inrush current after switching on would lead to the superimposed components of the voltage and the differential current. Figure 5.82 shows the waveforms of the differential current of phase A and the superimposed component of it. The voltages of phase A and B and their filtered superimposed series are shown in Figures 5.83 and 5.84 respectively. Furthermore, the time corresponding to the sudden change of voltage of phase A and phase B could be obtained, as could the time of the first occurrence of differential current (Figures 5.85–5.87). According to Figures 5.85–5.87, the first occurrence of the differential current is at 0.308 s, lagging 8 ms behind the occurrence of the voltage disturbance of pole A, and lagging only 1 ms behind the occurrence of the voltage disturbance of pole B. According to the design of the time difference based criterion, only the first disturbance time is taken into account. Therefore, the time difference between the sudden change of the voltage and the differential current should be 8 ms, which exceeds the threshold set above. In this case, the protection would be blocked correctly.

Scenario 5.18 Transformer over-excitation

This case presents the scenario of transformer over-excitation by increasing the bus voltage to 1.7 (p.u.); this is actually impossible in real applications. Figure 5.88 shows the waveforms of the differential current and the voltage. As a result of the 1.7 (p.u.) voltage, the differential current of the transformer is

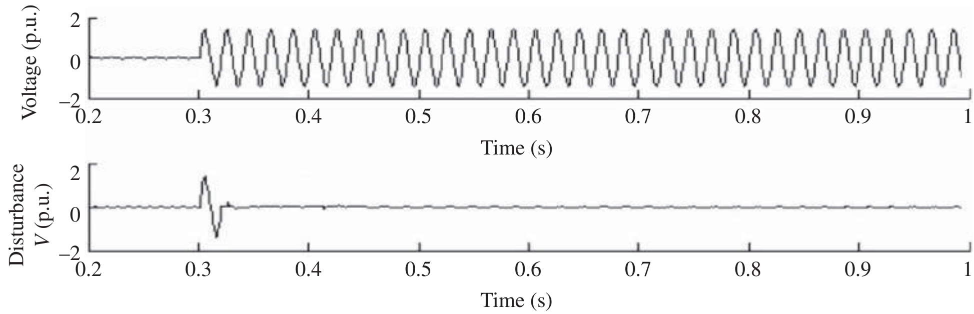

Figure 5.83 Voltage and the superimposed component of phase A (Scenario 5.17)

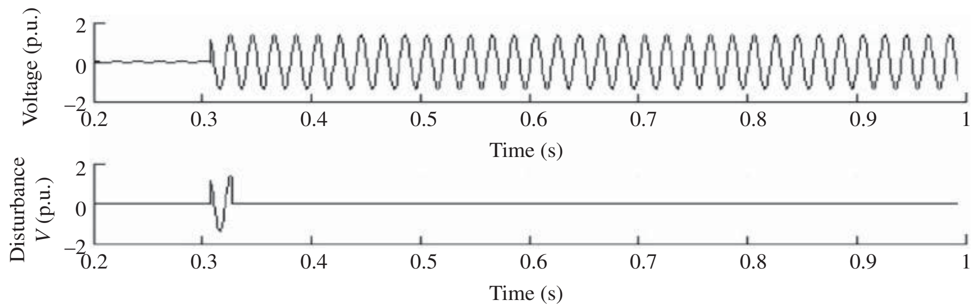

Figure 5.84 Voltage and the superimposed component of phase B (Scenario 5.17)

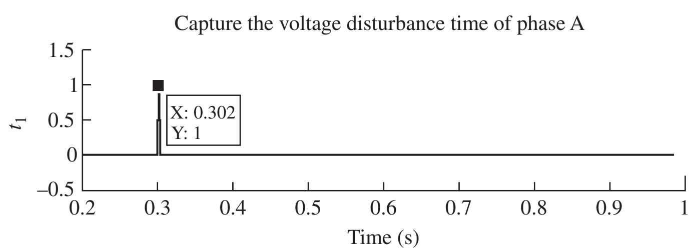

Figure 5.85 The occurrence time of superimposed component of voltage of phase A (Scenario 5.17)

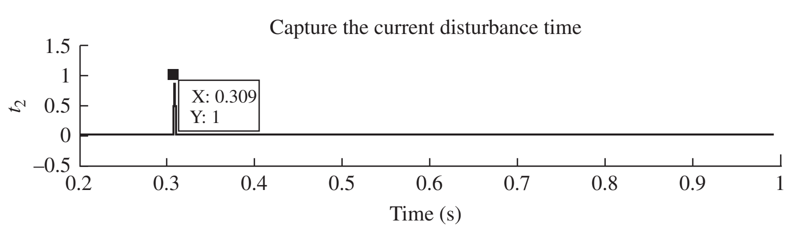

Figure 5.86 The occurrence time of superimposed component of voltage of phase B (Scenario 5.17)

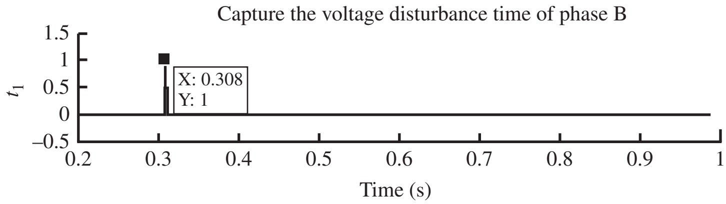

Figure 5.87 The occurrence time of the first superimposed component of differential current (Scenario 5.17)

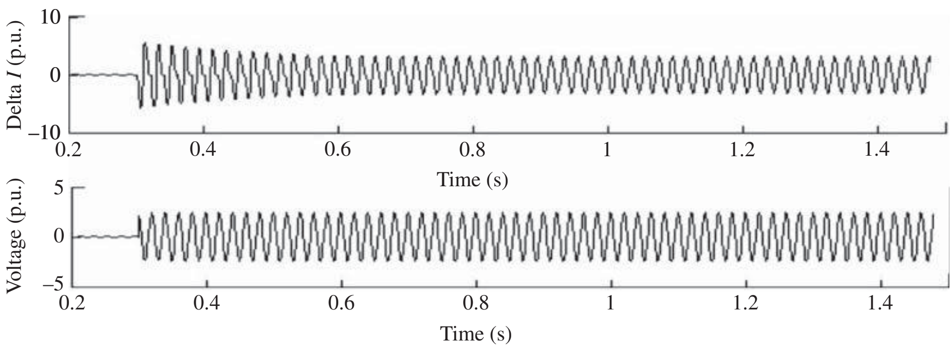

Figure 5.88 Waveforms of the differential current and the voltage (Scenario 5.18)

symmetrical. This scenario leads to extreme over-excitation of the transformer. In this case, the time difference is 6 ms (Figure 5.89), enough to block the differential protection. In this case, the protection would be blocked correctly.

In summary, by virtue of the phenomenon that the false differential current caused by saturation of the transformer iron core lags behind the fault current caused by the internal fault for a period of time, a

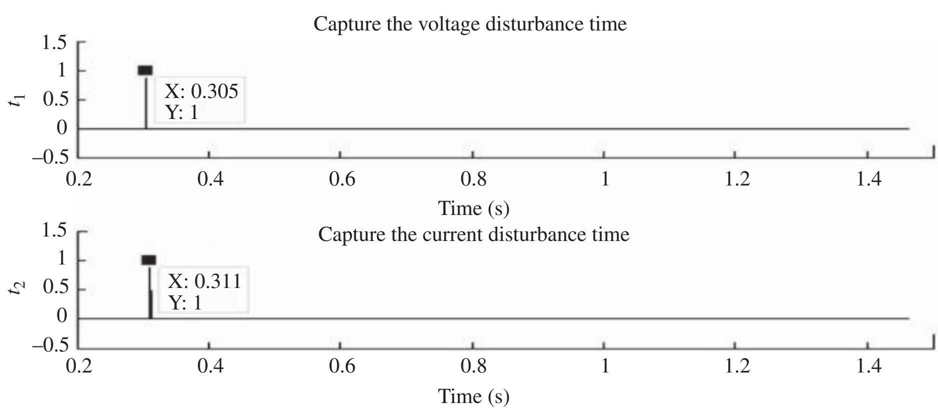

Figure 5.89 Occurrence time of superimposed component of voltage and differential current (Scenario 5.18)

new time-difference based criterion for differential protection is proposed. The false differential current resulting from the magnetizing inrush current of the transformer can be identified. Meanwhile, even if the differential current obviously contains the interference or the magnetizing inrush current, various internal faults can be identified reliably and the protection will trip instantaneously. Furthermore, the criterion can discriminate the developing fault very quickly. No matter what kind of fault occurs, it can be identified at a very high speed. Conservatively, the time for the protection to operate is within a half cycle. The effectiveness of this criterion has been verified with simulation tests. Furthermore, a comprehensive protection scheme is designed to deal with a variety of complicated scenarios, including switching on or a fault of a transformer to a stiff system, asynchronous switching on of a transformer, multiple phases developing external or internal faults, inrushes due to voltage recovery or nonzero differential current due to CT mismatch and so on. The corresponding countermeasures are proposed in this comprehensive scheme and the limitations of each individual criterion are analysed. Finally, the analyses on the above scenarios are testified with the corresponding simulation tests.

5.5 A Series Multiresolution Morphological Gradient Based Criterion to Identify CT Saturation

5.5.1 Time Difference Extraction Criterion Using Mathematical Morphology

5.5.1.1 Mathematical Morphology Fundamentals

Mathematical morphology, originally introduced by Matheron and Serra as a tool for investigating geometric structure in binary images, is a nonlinear theory for signal processing and analysis. Unlike most filtering methodologies emphasizing the response of the frequency domain, MM prefers to depict the profile of signal waveform in the pure time domain. The underlying basis of the morphological filtering technique is to process signals by a function, known generally as the structuring element (SE) or the structuring function. When operating upon a signal of complicated shapes, MM operations are capable of decomposing a signal into certain parts with specific characteristics and highlighting them from the background.

As known, most applications of power system analysis are the processing of a 1D signal. A superimposed transient signal is normally taken to represent foreground regions, while the steady-state signal, no matter if it is pre-fault or post-fault, acts as the background.

Suppose that the original samplings is expressed by the function *X(x)*, whose domain is *Dx*, and the structure function is given by *G(y)*, whose domain is *Dg*. Therefore, two basic morphological operators can be specified as erosion and dilation, defined as:

$$X \oplus G(x) = \min_{y \in D_g}[X(x+y) - G(y)], \forall x \in D_x \tag{5.28}$$

$$X \oplus G(x) = \max_{y \in D_g}[X(x-y) + G(y)], \forall x \in D_x \tag{5.29}$$

among which Equation (5.26) denotes erosion and Equation (5.27) specifies dilation. For instance, suppose that the length of *Dg* is h. For arbitrary $x_0 \in Dx$, $X \oplus G(x_0)$ is equal to the maximum of $\{X(\mathrm{x}_0 - 1) + G(1), X(\mathrm{x}_0 - 2) + G(2), \ldots, X(\mathrm{x}_0 - \mathrm{h}) + G(\mathrm{h})\}$. Note that the domain of the sampling *Dx* is from negative infinity to positive infinity. Hence $(x+y)$ and $(x-y)$ are still contained in *Dx*. Erosion is an anti-extensive operator that suppresses the peak pulses. As the dual of erosion, dilation is an extensive operator that suppresses bottom pulses. According to the definition of erosion and dilation, the edge of the signal, no matter whether it is a positive-going edge or negative edge, will be shifted by erosion and dilation operators but in reverse directions. This characteristic is used to design an improved edge detection algorithm.

5.5.1.2 MMG

A gradient operator is an effective tool to highlight the edge (sudden change) information and, thus, is applicable to detect the transient superimposed on a steady-state signal. However, it is sensitive to most noises as well. In contrast, the morphological filter has excellent de-noise ability. Thereby, the combination of morphological filter and arithmetic differential operation naturally results in the appearance of a morphological gradient (MG). The basic MG is defined as the arithmetic difference between the dilated and the eroded original sampling function *f(x)* by g, the elementary SE. The definition of MG is given by:

$$MG = (f \oplus g)(x) - (f \oplus g)(x) \tag{5.30}$$

The MG is actually more than the gradient in mathematical fundamentals. Along the successive sampled signal, the MG is determined by the difference between maxima and minima obtained within the domain of the flat SE.

Similar to the wavelet analysis, the concept of multiresolution analysis is introduced to MM. Multiresolution morphological filtering can repress various noises effectively. Combined with the concept of MG, the goal of highlighting singularity information together with depressing noise can be achieved. Accordingly, multi-resolution morphological gradient (MMG) is proposed. The technique is introduced here to recognize and characterize the moments of transient change, such as fault occurrence and CT saturation. To extract the ascending and descending edges of the transient signal, the MMG is designed to possess scalable flat lines SE g^+ and g^- with different origins defined as:

$$g^+ = \{g_1, g_2, \dots, g_{l-1}, \underline{g_l}\} \tag{5.31}$$

$$g^- = \{\underline{g_1}, g_2, \dots, g_{l-1}, g_l\} \tag{5.32}$$

where g^+ is the SE used for extracting the ascending edges and g^- is for the identifying the descending edges. Here scalable flat lines mean the member of g^+ and g^- are all zero. $l = 2^{1-\alpha} l_1$, where α indicates the level of MMG to be processed; l_1 is the primary length of g at level 1. The underlined samples, $\underline{g}$, in g^+ and g^- show their origins.

With g^+ and g^-, two MG outputs at level n, ρ_n^+ and ρ_n^-, will be available according to Equations (5.33) and (5.34):

$$\rho_n^+ = (\rho_{n-1} \oplus g^+)(x) - (\rho_{n-1} \oplus g^+)(x) \tag{5.33}$$

$$\rho_n^- = (\rho_{n-1} \oplus g^-)(x) - (\rho_{n-1} \oplus g^-)(x) \tag{5.34}$$

Based on the definition of the MMG, ρ_n, the ultimate result of MMG filter on level n, can be given by Equation (5.35):

$$\rho_n = \rho_{n-1}^+ + \rho_{n-1}^- \tag{5.35}$$

5.5.1.3 SMMG

As mentioned above, the MMG may be used to depress the steady-state components of a signal and extract the transient features. However, an elementary MMG filter has failed to detect faint slow signal changes in some cases, as shown in Figure 5.90. Considering fine characteristics of MMG of transient component extraction, a n-order MMG transform in series by n same or different SEs is expected to be able to magnify inconspicuous transient features and detect faint signal changes in short period.

Let a signal g denote a flat line SE, $l = 2^\alpha$ or $l = \beta \times 2^{\alpha-1}$ (β is an odd number greater than 1) is the length of g, arithmetic operator MMG_l is defined as the dyadic MMG transform by g with level α. Correspondingly, let a set of signals $\{g_i\}$, $i = 1, 2, 3, \dots, n$, denote a set of flat lines SEs; $l_i = 2^{\alpha_i}$ is the

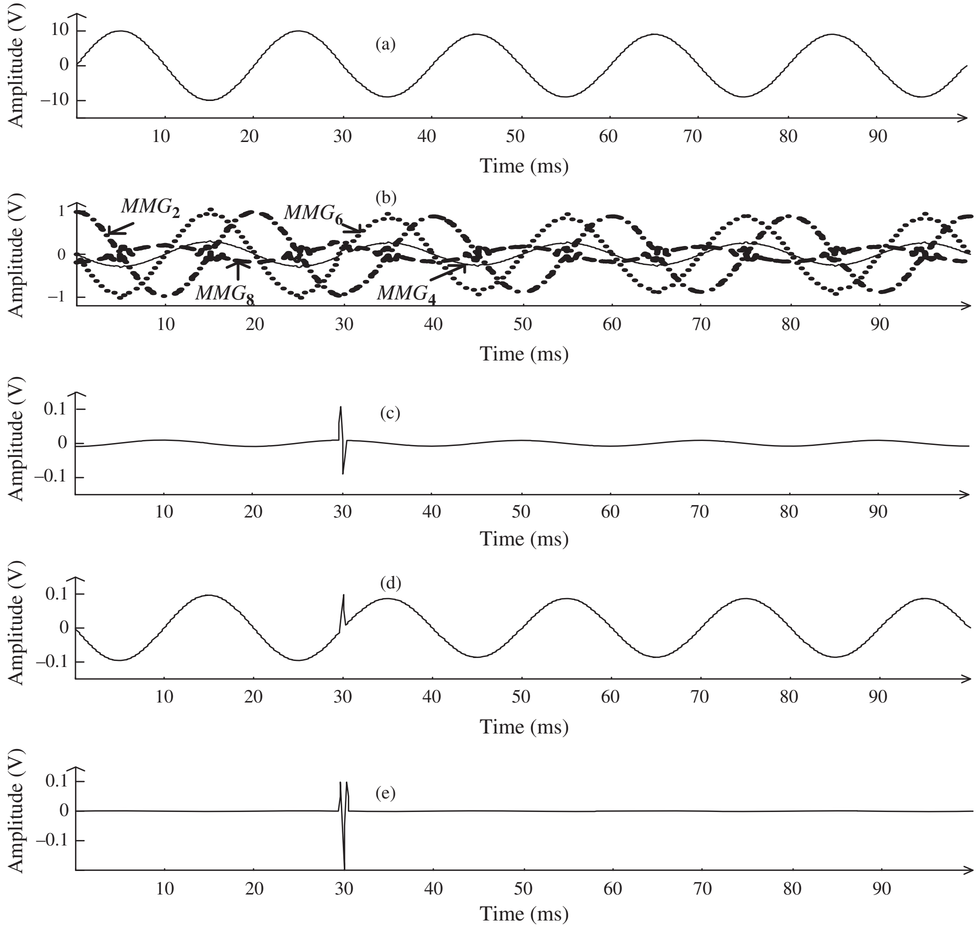

Figure 5.90 MMG and SMMG of a voltage sag signal: (a) a voltage sag signal; (b) MMG_2, MMG_4, MMG_6 and MMG_8 of the voltage sag; (c) $SMMG_2^3$ of the voltage sag; (d) $SMMG_2^2$ of the voltage sag; (e) $SMMG_2^4$ of the voltage sag

length of g_i; the arithmetic operator $\prod_{i=1}^{n} SMMG_{l_i}$ is defined as n-order eeries dyadic MMG transform by g_i with level α_i respectively. Specially, $SMMG_L^n$ if $l_i = L$, that is to say, n SEs have the same length L. As a special case, the MMG can be regarded as a one-order SMMG transform.

Figure 5.90a gives a 10% voltage sag wave occurring at 30 ms; the sampling frequency is 2 kHz. Its MMG_8 (dashed line), MMG_6 (dotted line), MMG_4 (solid line), MMG_2 (dash-dotted line) and $SMMG_2^3$, $SMMG_2^2$, $SMMG_2^4$ results are given in Figure 5.90b–e. In this case, it is hard for a simple MMG transform to locate the starting point of the voltage sag as shown in Figure 5.90b. In contrast, a large spike detected by $SMMG_2^3$ exactly indicates the starting point of the voltage sag, as demonstrated in Figure 5.90c. It can be seen from Figure 5.90d that $SMMG_2^2$ cannot provide a satisfactory result. According to Figure 5.90e, $SMMG_2^4$ is also capable of detecting the sag signal. Because the filter length of $SMMG_2^4$ is larger than that of $SMMG_2^3$, the latter is adopted to perform CT saturation identification.

The combination and sequence of SEs vary with the diverse features of the original signal to be extracted. Theoretically, any faint signal change can be detected by SMMG as long as the appropriate combination and sequence of SEs are chosen. The SMMG filter length is determined by the lengths of SEs, l_i and order n. The MMG_l filter length can be calculated from the following formula:

$$d_{MMG_l} = \sum_{i=1}^{\alpha} (2^{1-i} l - 1) \tag{5.36}$$

Based on Equation (5.36), the SMMG filter length can be calculated by:

$$d_{SMMG} = \sum_{i=1}^{n} d_{MMG_l} \tag{5.37}$$

Moreover, it should be noticed that the computational burden of limited order SMMG can be quite light-this is good for protection relays.

5.5.2 Simulation Study and Results Analysis

The EMTDC based 400 kV transmission system was used to evaluate the above scheme, which consists of a generator, a transformer, a 10 km transmission line and an infinite system, as shown in Figure 5.91.

All components in the power system come from the standard element library of EMTDC. Two CTs are equipped for the differential protection of the transformer.

A rational CT model is very important for the purpose of saturation study. Fortunately, the Lucas Model of a CT is available [9] in the EMTDC element library as well. The Lucas Model is quite adequate for many studies except where it is necessary to simulate successive faults due to reclosing onto a permanent fault [10]. In this sense, this model is suitable for the CT saturation study here. The CT parameters are presented in Table 5.4. With appropriate arrangement of the basic magnetizing curves and the residual fluxes of the CT, CT1 can transform the primary current exactly in the event of the any type of faults, whereas CT2 may saturate when experiencing a high primary current. In this case, the CT saturation can be simulated and used to evaluate the proposed scheme. The current signals observed at the second side of both CTs together with the differential current are used as the inputs of the SMMG. $SMMG_2^3$ is designed to fulfil the task of time difference identification. The time difference between fault occurrence and emergence of differential current can be obtained by observing the outputs of $SMMG_2^3$. The sampling rate in the simulation is 2 kHz. The proposed method is an instantaneous value-based algorithm.

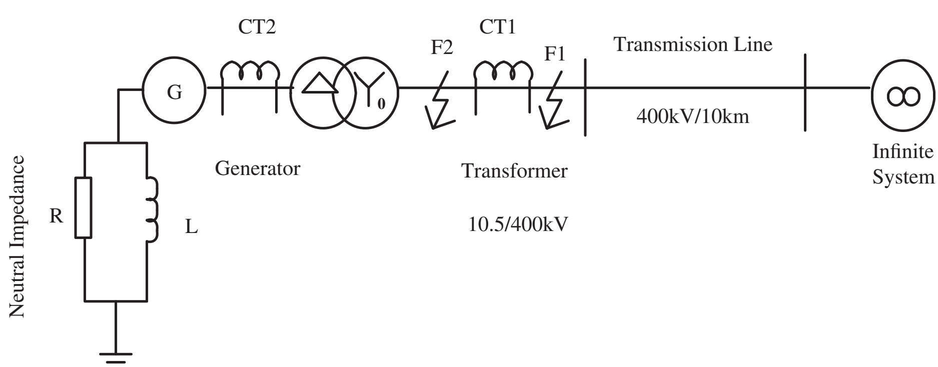

Figure 5.91 Simulated system (EMTDC based 400kV transmission system)

Table 5.4 CT parameters for a 400 kV transmission system

Parameters	CT1	CT2
Current transformer ratio (A)	120/5	2400/5
Mean core length (m)	0.8	0.5
Core cross-section (cm^2)	23.2	41.2
Burden, R (Ω)	3.0	1.0
Knee point	(0.1 A, 1.6 T)	(0.1 A, 1.6 T)

Therefore, the time delay of the criterion is exactly the length of the time window of $SMMG_2^3$. According to Equations (5.36) and (5.37) in the revision together with the sampling rate of 2 kHz, the actual time delay of the criterion is 1.5 ms.

5.5.2.1 CT Saturation due to an External Fault

Suppose an external three-phase fault of the transformer occurs with an inception angle of 0° at point F1 in Figure 5.91. In this circumstance, the fault occurrence, the emergence of the false differential current and the moment that the CT commences saturating are detected for the purpose of fault identification. The

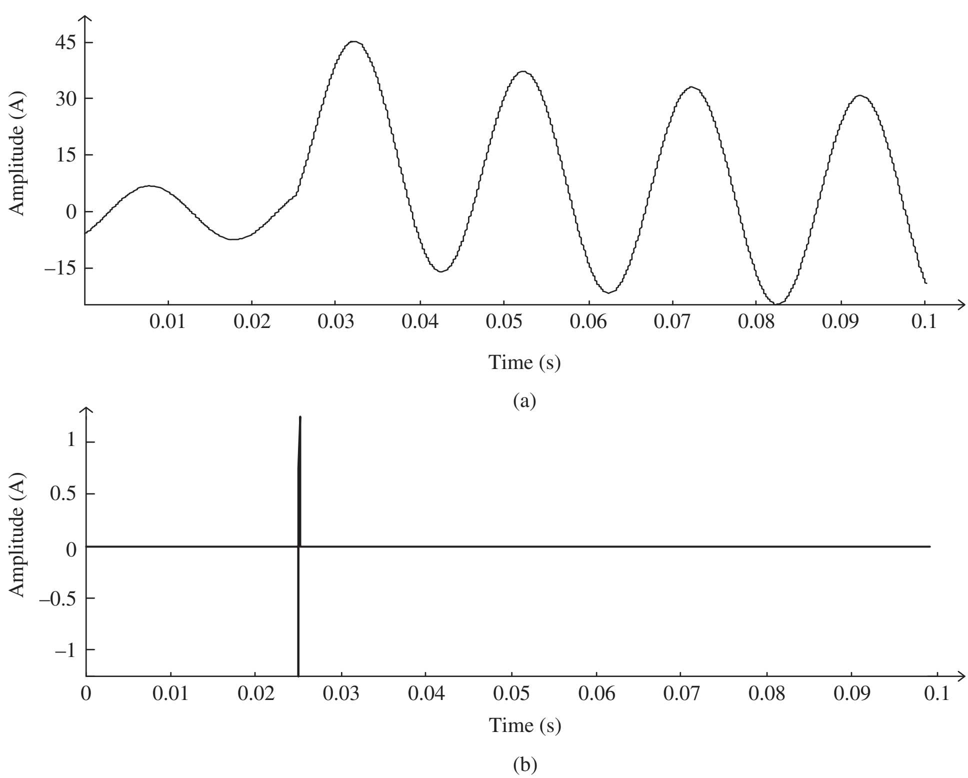

Figure 5.92 (a) The secondary current of CT1 and (b) its $SMMG_2^3$ output in the case of an external fault

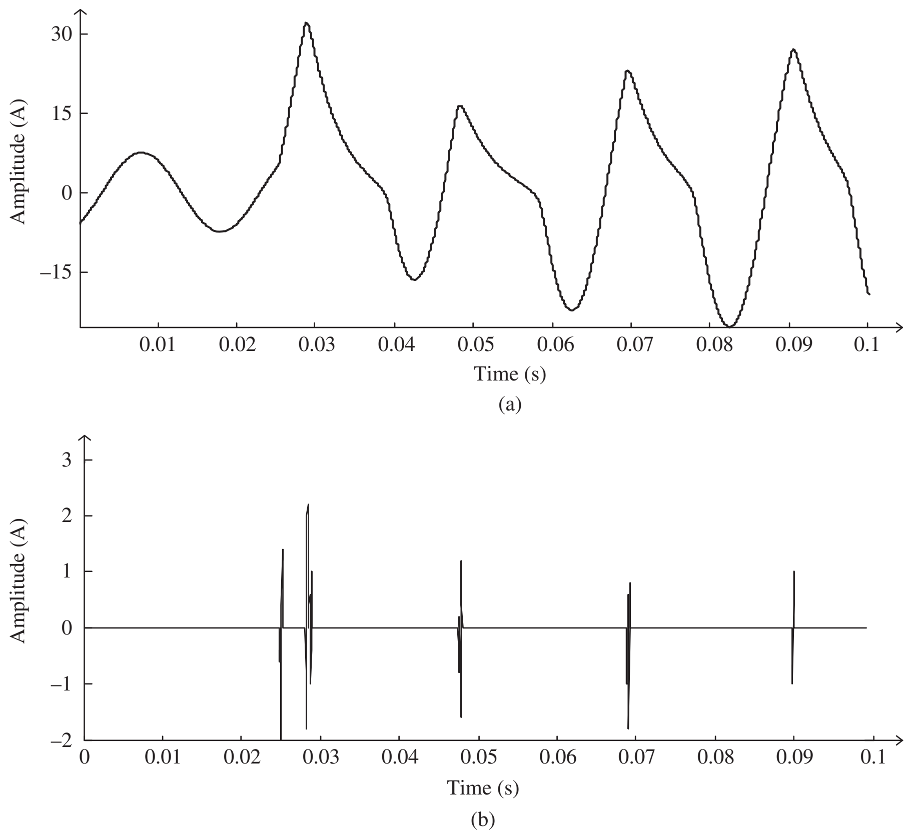

Figure 5.93 (a) The secondary current of CT2 and (b) its $SMMG_2^3$ output in the case of an external fault

secondary currents of CT1 and CT2 are shown in Figures 5.92a and 5.93a. As seen, CT1 can completely transform the primary current whereas CT2 saturates. Therefore, a false differential current occurs, as shown in Figure 5.94a. In this case the differential protection may mal-operate if appropriate blocking logic is not used.

The sampled current based TD method using SMMG is therefore proposed to address the aforesaid problem. The $SMMG_2^3$ outputs of the currents are shown in Figures 5.92b and 5.93b. As seen, the time instants of the sudden changes of the currents coming from both CTs can be captured with high sensitivity. Thereafter, the instant of fault occurrence can be determined as 0.025 s, since time instants of the first sudden change of the currents of CT1 and CT2 are both at 0.025 s.

As seen in Figure 5.94b, the time instant of sudden change of differential current is at 0.028 s, which corresponds to the second sudden change of the $SMMG_2^3$ output of the saturated current, as shown in Figure 5.93b. In this case, this small TD, namely 3 ms, can be detected and confirmed with the information available in Figures 5.92b and 5.94b. Therefore, this disturbance can be determined as an external fault and the protection can be blocked correctly. With a conventional TD method it is very difficult to detect such a minor time difference. It should be noted that only one sudden change is detected for the unsaturated CT (Figure 5.93b), which proves that the SMMG can focus on the significant singularity information and depress other undesired interference that possibly confuses the correct decision.

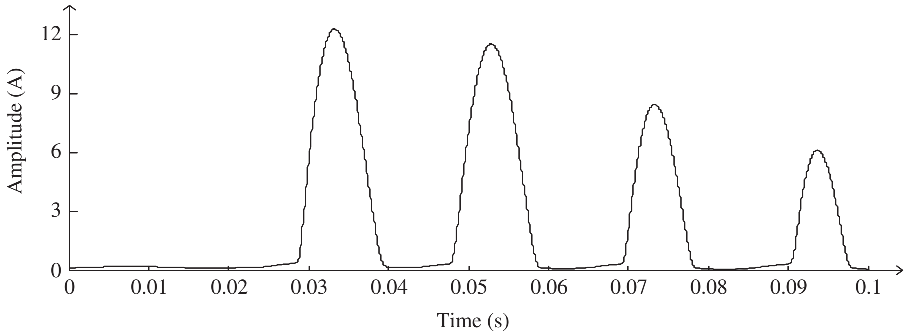

(a)

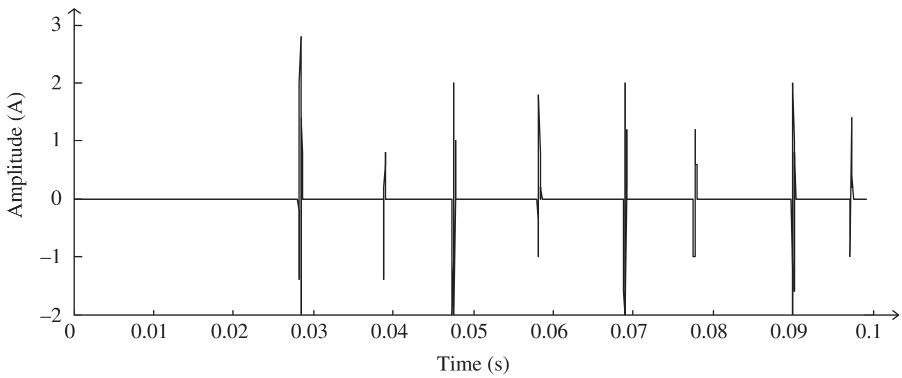

(b)

Figure 5.94 (a) The differential current and (b) its $SMMG_2^3$ output in the case of an external fault

A variety of serious external fault simulations have been carried out to validate the SMMG based TD method and this method always gives a correct response.

5.5.2.2 CT Saturation due to an Internal Fault

Suppose that an internal fault of the transformer occurs at point F2 in Figure 5.91. The secondary currents coming from CT1 and CT2 are shown in Figures 5.95a and 5.96a.

As illustrated, CT1 can completely transform the primary current whereas CT2 saturates. The differential current presents the feature of saturation, as shown in Figure 5.97a. Based on the $SMMG_2^3$ outputs of the currents in Figures 5.95a–5.97a, as shown in Figures 5.94b–5.97b, the time instants of the first sudden changes of the currents are all exactly at 0.025 s. As mentioned earlier, the time instant of the first sudden change of the currents coming from CT1 and CT2 can be used to detect the fault occurrence, and the time instant of the emergence of the differential current can be used for the purpose of distinguishing between an external fault and an internal fault. In this case, the internal fault can be identified easily since the time differences between any two signal sudden changes are all zero. Therefore, the protection can issue the trip command immediately without being subject to the possibly adverse impact of subsequent CT saturation.

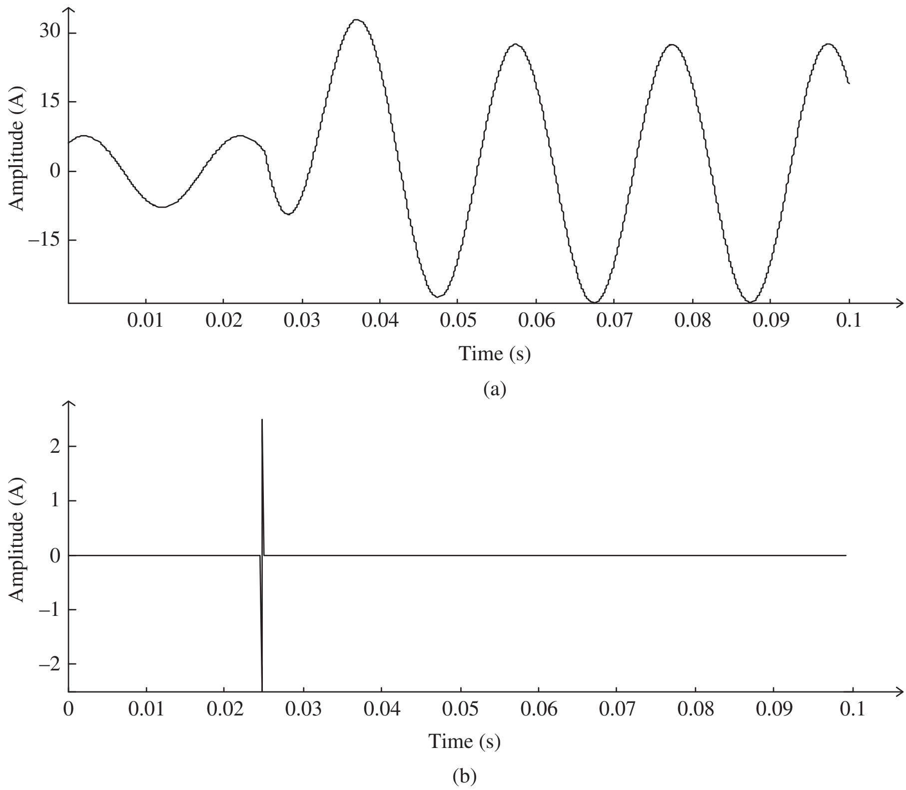

Figure 5.95 (a) The secondary current of CT1 and (b) its $SMMG_2^3$ output in the case of an internal fault

5.5.2.3 Results for the Case of both CTs being Saturated

By means of adjusting the burden, both CTs may be saturated, with different rates of saturation. Figure 5.98 shows the secondary currents of the CTs and theirs SMMG outputs in the case of both CTs being saturated. Among these, Figure 5.98a shows the secondary currents of CT1 and CT2. Their SMMG outputs are presented in Figure 5.98b and 5.98c. CT1 is in light saturation and CT2 in heavy saturation. Therefore, a false differential current occurs (Figure 5.99a). The instant of fault occurrence can be determined as 0.025 s, since the time instants of the first sudden change of the currents of CT1 and CT2 are both at 0.025 s. It can be seen from Figures 5.98c and 5.99b that the time instant of the sudden change of differential current is at 0.031 s, which corresponds to the second sudden change of the SMMG output of the CT2 saturated current and the second sudden change of the differential current SMMG output. The TD, therefore, is determined by the secondary currents of the CT saturated first.

5.5.2.4 Impacts of Fault Resistance, Fault Type, Fault Inception Angle and Noise Interference

Figures 5.100 and 5.101 give the case of an external single phase to ground fault through a fault resistance of 20 Ω. Figures 5.102–5.104 present the case of an external three-phase fault with an inception

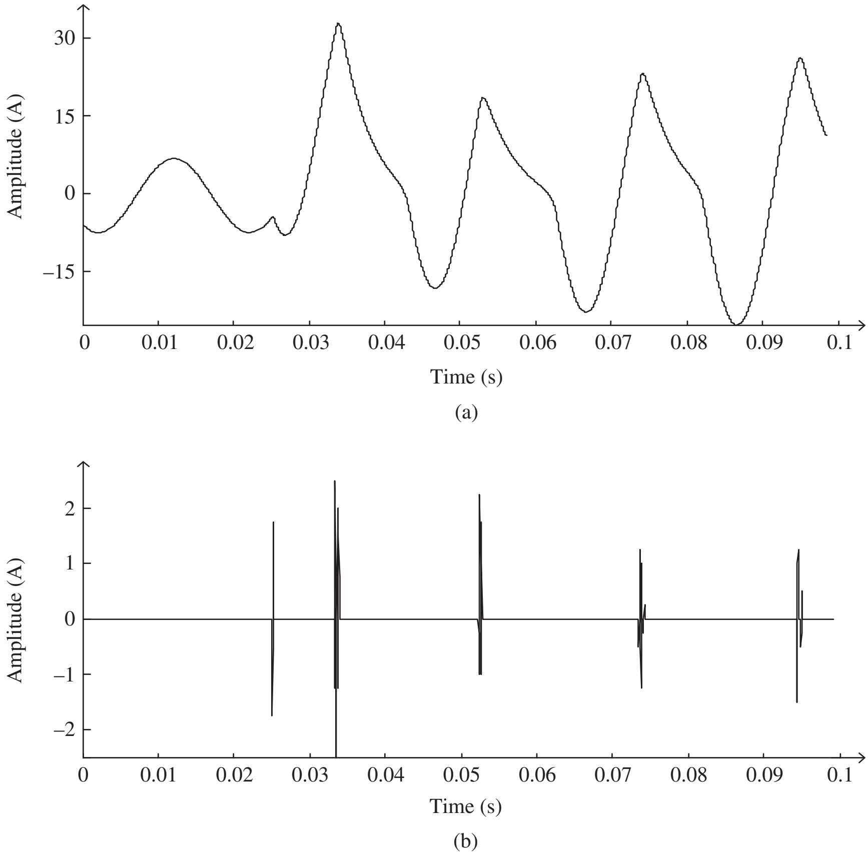

Figure 5.96 (a) The secondary current of CT2 and (b) its $SMMG_2^3$ output in the case of an internal fault

angle of approximate 30°. In order to verify the performance under noise condition, the waveforms in Figures 5.102a–5.104a are mingled with white noise and the signal noise rate (SNR) is 20 db. As seen from the results, the TD varies with the fault types, fault resistances, and inception angles. According to the simulation results, the proposed technique is adequate for detecting a small TD, even as small as 3 ms. Hence, these factors have little influence on the proposed method. Also, the algorithm can provide satisfactory result under moderate noise conditions.

5.5.3 Performance Verification with On-site Data

The practical data come from disturbance recorder of a two-winding transformer protection when this transformer experienced an external fault. The transformer is located in a substation in Shanxi province, China. The sampling rate of the field data is 600 Hz. The currents of both sides of the transformer are shown in Figure 5.105a. As seen, one was nearly transformed linearly and one is in the saturation state.

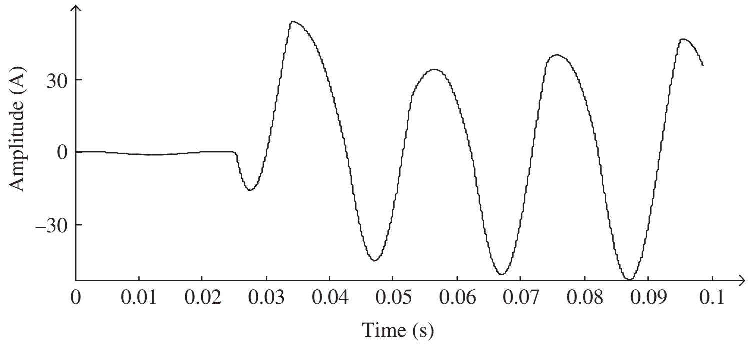

(a)

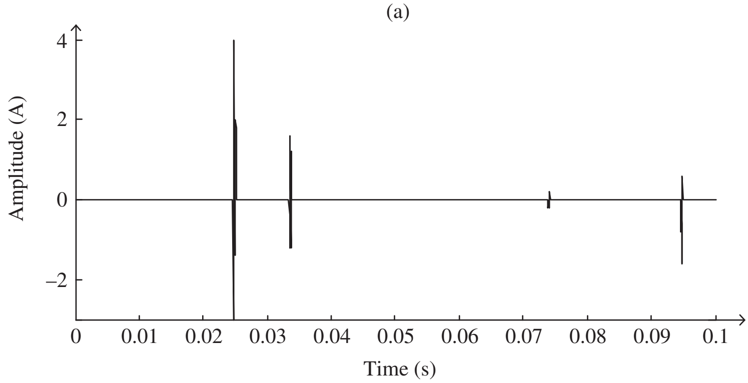

(b)

Figure 5.97 (a) The differential current and (b) its $SMMG_2^3$ output in the case of an internal fault

The samples in such a low sampling rate cannot be processed directly using the SMMG technique. For the purpose of the validation of the proposed method using the practical data, an interpolation processing is used to increase the sampling rate of the data to 1.8 kHz. Then, the differential current in Figure 5.106a can be formed. The SMMG output for the phase currents and differential current are shown in Figures 5.105b, 5.105c and 5.106b. Based on these outputs, the TD in 6 ms can be sensitively captured and the CT saturation is identified accordingly.

In summary, a SMMG technique was applied to implement the CT saturation blocking scheme for the differential protection. The singularity information of the transient current can be identified clearly and localized accurately by virtue of this technique no matter what the fault occurrence, differential current emergence or CT saturation. Therefore, the time difference between the fault occurrence and differential current emergence can be obtained with high accuracy. With the time difference, the saturation of the CT can be detected and an appropriate blocking scheme can thus be applied to prevent the differential protection from mal-operation. With this novel scheme, the differential protection can operate instantaneously in the event of a serious internal fault. Meanwhile, the stability of the operation can be ensured even if one of the CT saturates in depth due to a heavy external fault. The effectiveness of this scheme was proven with the EMTDC based simulation tests and practical data.

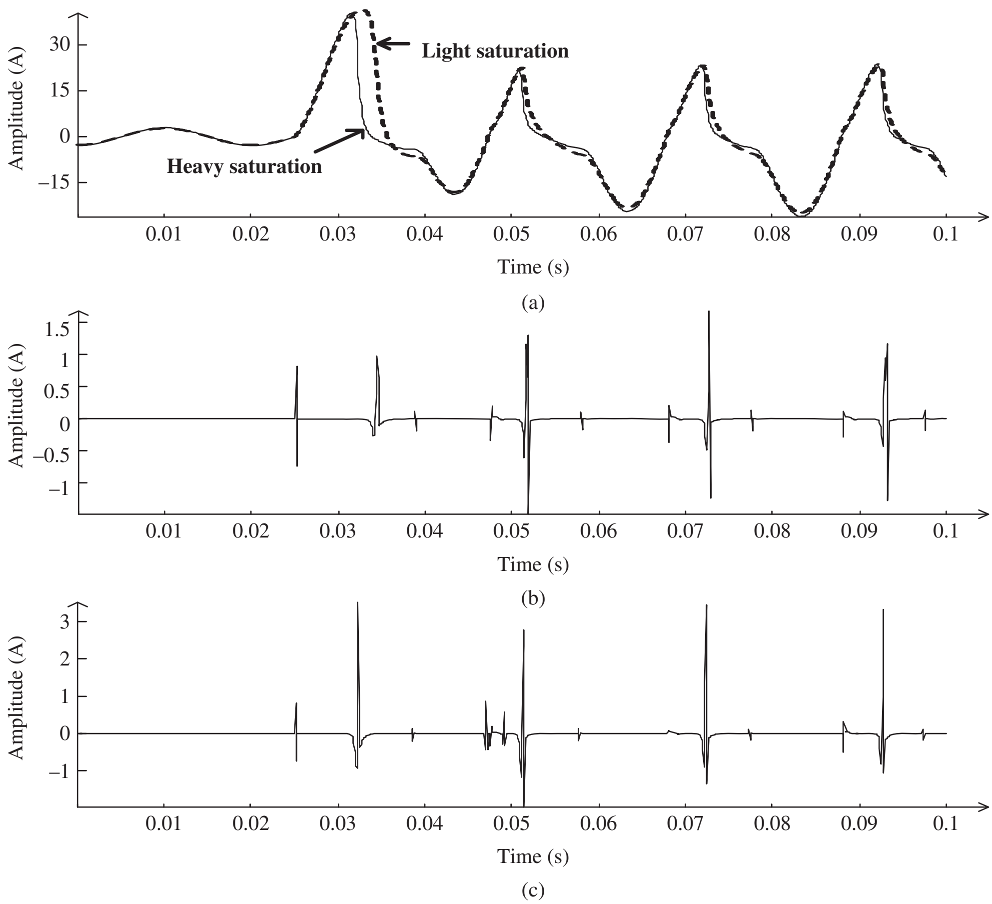

Figure 5.98 The secondary currents of the CTs and their SMMG outputs in the case of both CTs being saturated: (a) secondary currents of CT1 and CT2; (b) SMMG output of CT1; (c) SMMG output of CT2

5.6 A New Adaptive Method to Identify CT Saturation Using a Grille Fractal

5.6.1 Analysis of the Behaviour of CT Transient Saturation

CT saturation is divided into steady-state saturation and transient saturation: steady-state saturation is the saturation of the CT iron core when the primary current is in the steady state. For a low voltage grid, it is not difficult for general protection devices to adapt to CT steady-state saturation. But there will always be a transient process after an actual line fault during which the DC component is greater than the AC component in the excitation circuit. So the CT transient error increases, the performance of which is quite different compared to the steady-state case. At this point, the CT saturation is called transient saturation. The influence, when CT is transient saturated, on transfer characteristics is discussed here.

Supposing that external fault occurs and the CT is not saturated, the primary current of the CT is:

$$i_1 = I_{1m}(A - \cos \omega t) \tag{5.38}$$

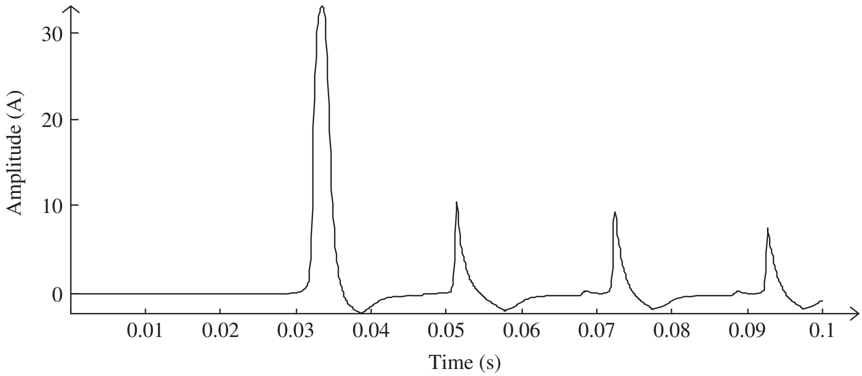

(a)

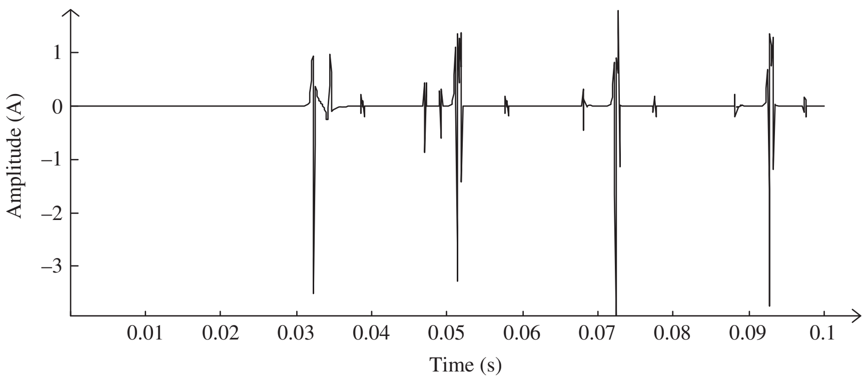

(b)

Figure 5.99 (a) The differential current and (b) its $SMMG_2^3$ output in the case of both CTs being saturated

where I_{1m} is maximal value of short-circuit current of primary side, $A = e^{-t/T}$ is attenuation DC component, and T is time constant of the primary system. The excitation current is very small when the CT is not saturated, namely $i_\mu = 0$. During the initial stage of the fault, the primary current i_1 is transmitted to the secondary side without any distortion. The transient current of secondary side is:

$$i_2 = I_{2m}(A - \cos \omega t) \tag{5.39}$$

where I_{2m} is maximal value of the short-circuit current of the secondary side.

It can be obtained from the equivalent circuit that:

$$W_2 \frac{d\phi'}{dt} = i_2 r_2 \tag{5.40}$$

$$\Delta\phi' = \frac{1}{W_2} \int_{t_1}^{t_2} i_2 r_2 dt \tag{5.41}$$

where W_2 is the number of turns on the secondary side, $\Delta\Phi'$ is the increment of iron core flux Φ' within one cycle, and r_2 is the secondary load of instrument transformer, only resistance accounted and reactance

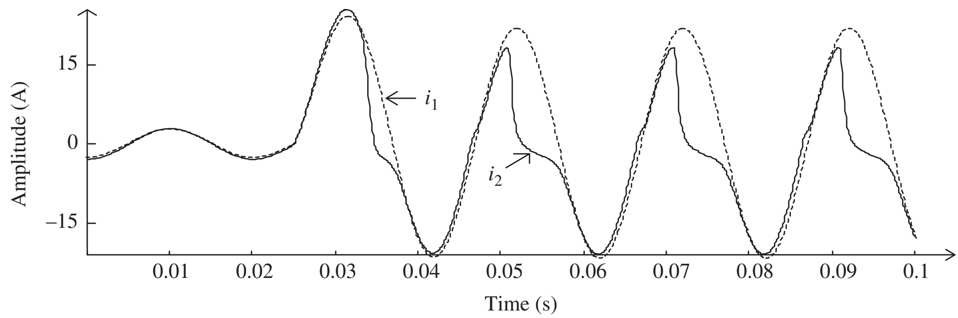

(a)

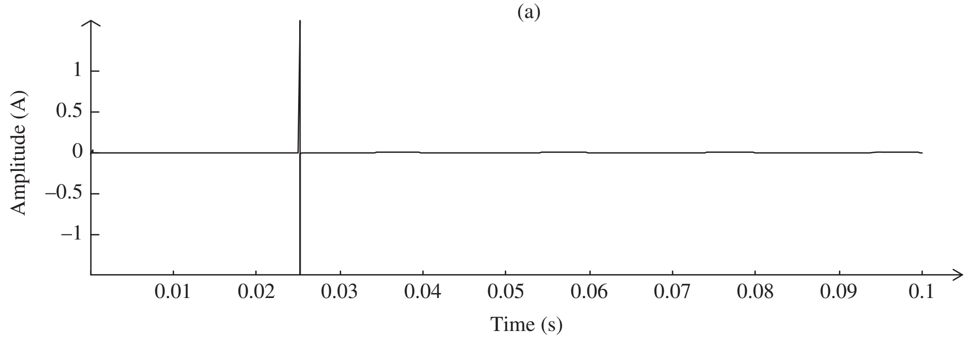

(b)

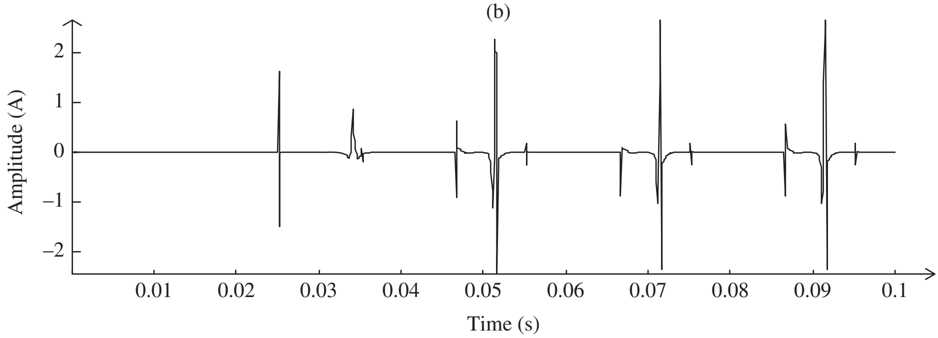

(c)

Figure 5.100 The secondary currents of the CTs and theirs SMMG outputs in the case of external single phase to ground fault through a fault resistance: (a) secondary currents of CT1 and CT2; (b) SMMG output of CT1; (c) SMMG output of CT2

excluded. Equation (5.39) substituted into Equation (5.41) then gives:

$$\Delta\phi' = \frac{2I_{2\mathrm{m}}r_2}{\omega W_2}[A(\pi - \arccos A) + \sqrt{1 - A^2}] \tag{5.42}$$

Continuously after n cycles, the iron core flux reaches the saturation value of the CT and the value is:

$$\phi_{\mathrm{r}}' + n\Delta\phi' = \phi_{\mathrm{s}}' \tag{5.43}$$

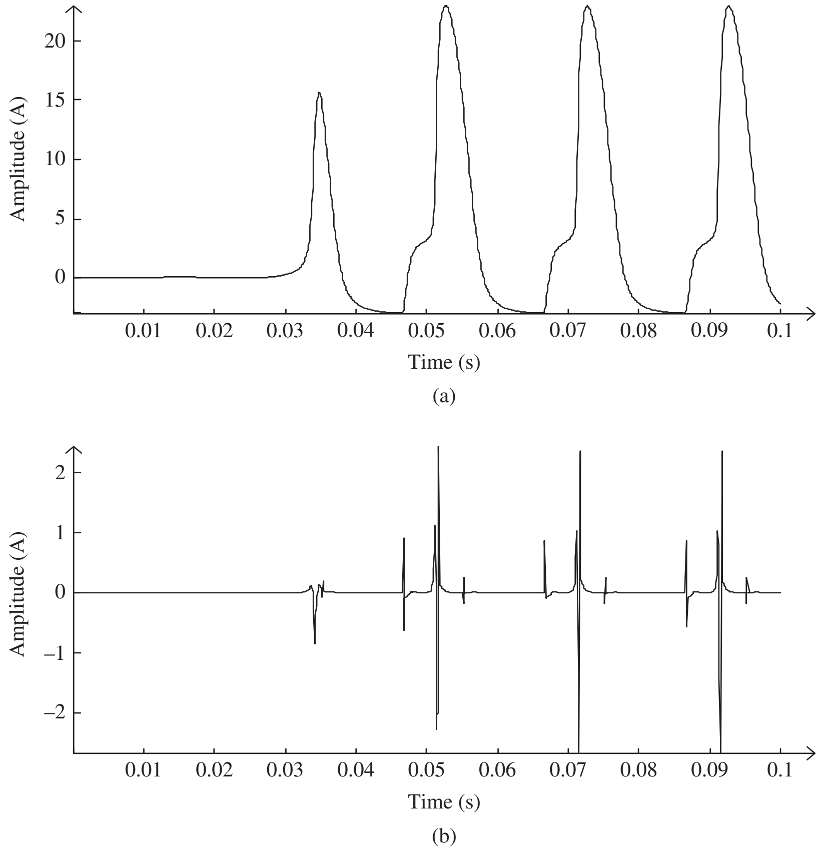

Figure 5.101 (a) The differential current and (b) its SMMG output in the case of external single phase to ground fault through a fault resistance

where Φ_r' is the iron core remanence of the CT. The number of cycles at which the saturation of CT begins saturation is:

$$n = \frac{\omega W_2(\phi_s' - \phi_r')}{2I_{2m}r_2[A(\pi - \arccos A) + \sqrt{1 - A^2}]} \tag{5.44}$$

By Equation (5.42), it can be found that although the CT will not be saturated immediately, there is a region of linear transmission, the size of which, however, is constrained by many factors: (i) the size and the degree of deviation of primary side short-circuit current; (ii) the time constant of the primary side system; (iii) the magnitude of the load on the secondary side; and (iv) the magnitude and direction of the remanence of the CT, the saturation value and so on. When an external fault occurs, and the magnitude and direction of remanence is close to that of the saturation value, the CT is likely to be saturated in a very short time, which brings some difficulties to the Time Difference Method.

In the preceding analysis, it has been shown that for the two kinds of cases of CT saturation when the inrush current and external fault occur, the iron core will periodically enter and exit the saturation region. There will be singular points when iron core iron core enters and exits the saturation region.

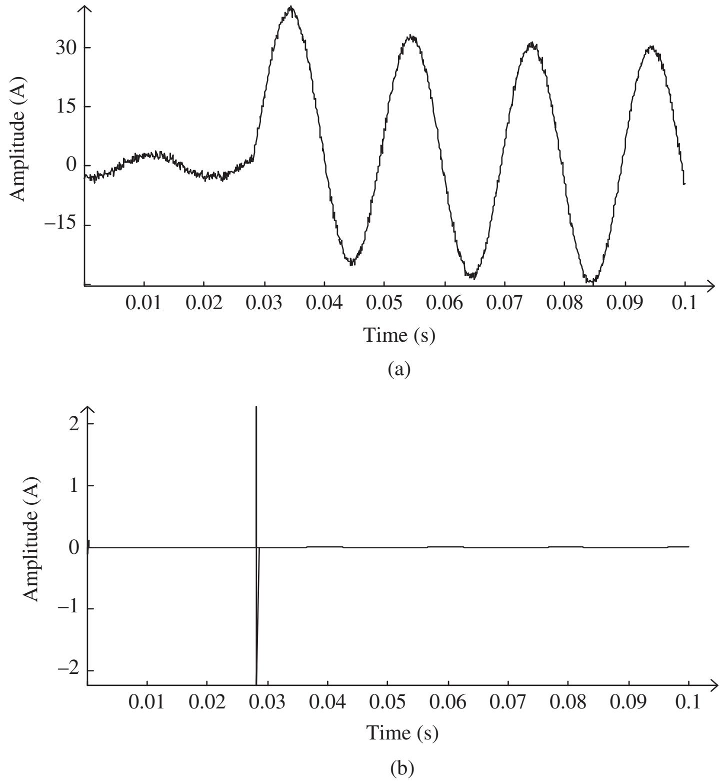

Figure 5.102 (a) The secondary current of CT1 and (b) its SMMG output in the case of external three-phase fault with an inception angle of approximate 30°

The symmetry of the inrush current is no exception. When the fault occurs inside transformers, due to the iron core in the linear region, there will be singular points only in fault time. Although the number of high-frequency details of the fault current increases by CT saturation, there are not obvious singular points near the time of fault occurrence. So the fault inside transformer is recognized by singular characteristics of current waveform.

5.6.2 The Basic Principle and Algorithm of Grille Fractal

Fractal is a general of self-similar graphics and structure with no characteristic length but certain sense, the typical nature of which is local similarity shown in small scale. A singular signal has self-similarity. The theory of fractals has been successfully applied in singular signal detection in many fields in power system. Because sampling frequency is not required for grille fractal algorithm, and there is no need to divide the band, it is suitable for real-time signal processing, favoured by more and more researchers. The definition of grille is referenced in grille fractal, and a brief and fast criterion of signal singularity detection is proposed. The description of the theory is: for signal X, suppose are is $n+1$ (n is even)

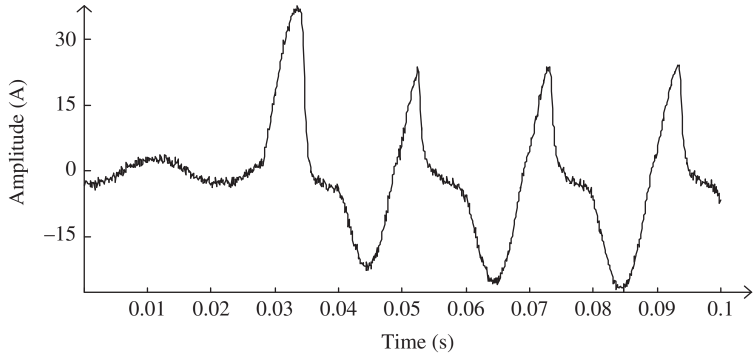

(a)

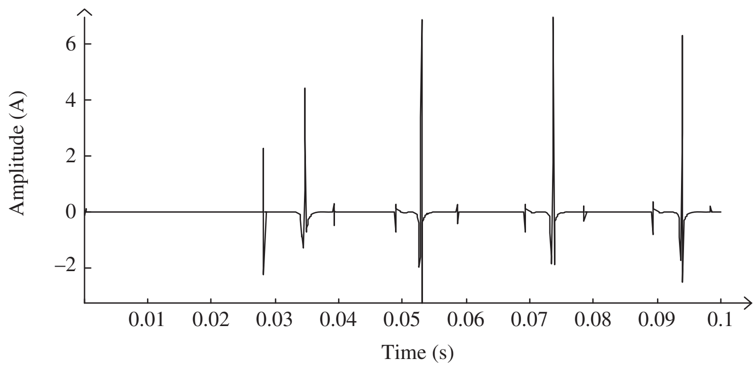

(b)

Figure 5.103 (a) The secondary current of CT2 and (b) its SMMG output in the case of external three-phase fault with an inception angle of approximate 30°

sampling points ($x_1, x_2, \ldots, x_{n+1}$) in a period $[t_k - \Delta t, t_k]$. Make $\delta = \Delta t/n$, then:

$$N_\delta = \frac{1}{\delta}\sum_{j=1}^{n}|x_j - x_{j+1}| \tag{5.45}$$

where δ is time difference of two sampling points, N_δ is the required number of grid lattice square grid and δ is the side length. The overlay signal in the period of $[t_k - \Delta t, t_k]$ is shown in Figure 5.107.

The differential current of the transformer during normal operation is approximate to a pure sinusoidal signal. Suppose Δt is one half cycle, the N_δ of any signal is the same for any period, Δt. If a fault occurs outside the transformer, due to the DC components in the short-circuit current during transient processing, the error of the DC components transmission of the CT is so large that the CT will be saturated and the induced electromotive force (EMF) of the secondary side will down to zero immediately. During that period, i_2 is also zero. Along with the instantaneous value of current decrease and CT exit saturation, the induced electromotive force of the secondary side increases and i_2 begins to increase again. It is

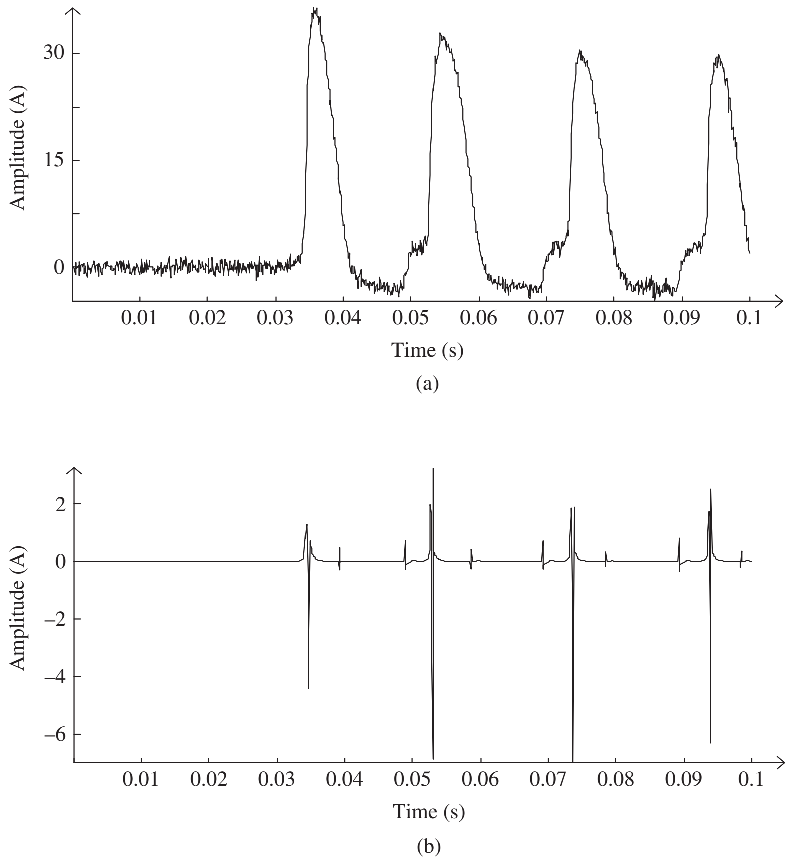

Figure 5.104 (a) The differential current and (b) its SMMG output in the case of an external three-phase fault with an inception angle of approximate 30°

shown that with entry and exit saturation of the CT, the waveform of i_2 will distort seriously and N_δ will change exclusively with the distortion points. Similarly, due to the highly nonlinear characteristics of the iron core, there must be a large number of high-frequency details in the inrush current along with the time when CT enters and exits saturation. Performed in the grille curve, the trend of increasing and then decreasing will be caught by both of them.

When a fault occurs inside a transformer, the high-frequency singular signal in the fault current will be generated in the fault point. N_δ will change exclusively until the waveform is restored to a sinusoidal waveform. Performed in the grille curve, Performed in the grille curve, N_δ has a trend of increasing at first and then remaining as a steady-state signal.

Form the analysis above, it can be shown that internal and external faults of transformers can be effectively recognized when the CT is saturated using grille curve variation, which will not be influenced by inrush current. In practice, the data of the transformer computer protection device sampled from the primary side of the power system are easily polluted by interference and noise. Reaction to grille curve, N_δ may fluctuate, which leads to an increase in the number of external points of curves. If an internal fault occurs and the CT is saturated, there will be a trend of increasing and then decreasing for the grille curve,

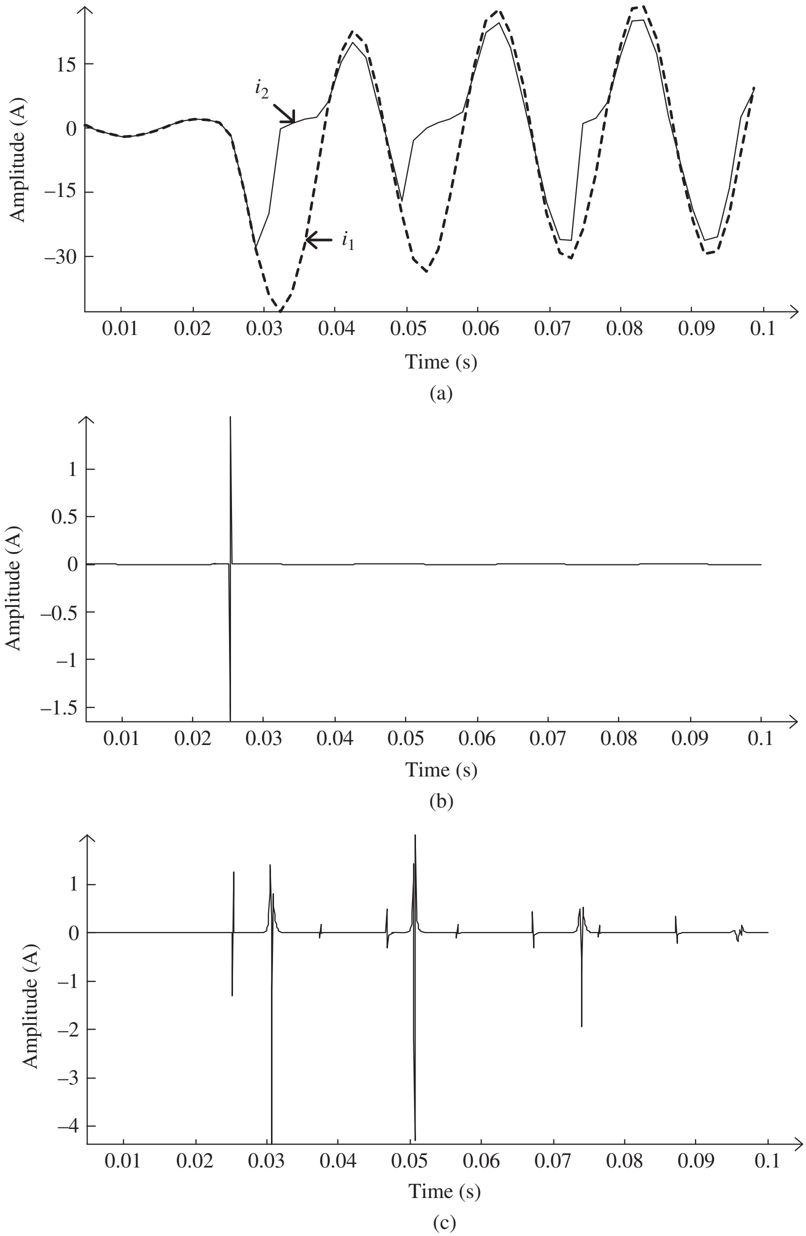

Figure 5.105 Practical recordings of the secondary currents of two CTs installed at either side of a two-winding transformer and their SMMG outputs: (a) currents of two sides of the transformer; (b) SMMG output of CT1; (c) SMMG output of CT2

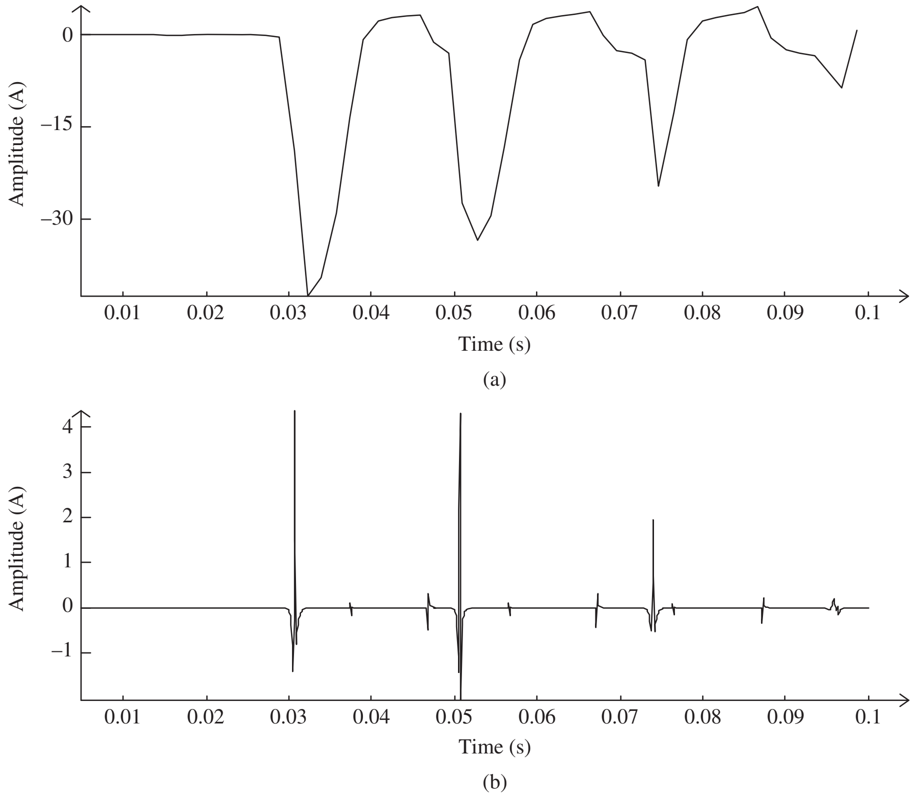

Figure 5.106 (a) The differential current and (b) its SMMG output for the practical recordings

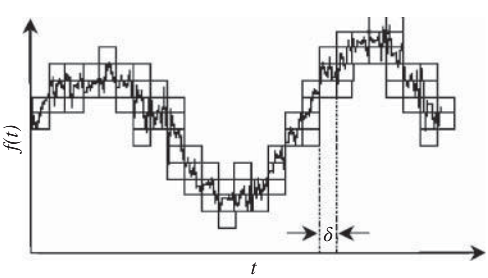

Figure 5.107 Grille definition

it may lead to protection mal-operation that only grille fractal is analysed. So a self-adaptive generalized morphological filter is proposed. The singular signal is sampled and the noise and interference restrained.

5.6.3 Self-Adaptive Generalized Morphological Filter

In recent years, the filtering method based on MM has been applied increasingly due to its clear physical meaning, efficiency and practicality. The algorithm is mainly concentrated on the morphological opening and closing operation, morphological closing and opening operation and their average formal combination. The structural elements of different sizes B_1 and B_2 are selected to removal noise and interference signal effectively. Suppose the width of post-structural element B_2 is twice that of fore-structural element B_1. Based on the morphological opening and closing operation, a kind of generalized morphological opening–closing and closing–opening filter, the definition of which respectively is:

$$y_1(n) = \mathrm{GOC}(x(n)) = (x \circ B_1 \bullet B_2)(n) \tag{5.46}$$

$$y_2(n) = \mathrm{GCO}(x(n)) = (x \bullet B_1 \circ B_2)(n) \tag{5.47}$$

Because there is still a statistical bias phenomenon in the two kinds of filters, it is difficult to obtain the best filtering effect used alone. Therefore, the average combination of the two kinds of generalized filter is adopted. The filtered output signal $y(n)$ is:

$$y(n) = 0.5 * (y_1(n) + y_2(n)) \tag{5.48}$$

The shape and size of the structure element is another important factor in determining the effect of morphological filtering. Taking into account the characteristics of the computation and grille curve variation, it is decided that flat structure elements, which are most suitable for smoothing, should be selected for analysis. In addition, the opening operation can guarantee that the width of the structure element is greater than the width of the maximal of noise. In order to maximize noise suppression, the width of the structure elements B1 must be greater than the maximal opening.

5.6.4 The Design of Protection Program and the Verification of Results

5.6.4.1 Dynamic Simulation System

According to the above analysis, a protection criterion is formulated to recognize the fault inside transformers when the CT is saturated. The extreme phenomenon that the CT of one side is deeply saturated and the CT of the other side transmits correctly is considered. At that time, the differential value of the secondary current of the CT is very large, which is likely to cause differential protection mal-operation. The practicality and feasibility of the criteria is tested by a dynamic simulation system. The wiring of the dynamic simulation system and the parameters of electrical components are shown in Figure 5.108. In Figure 5.108, the transformer is a two-winding three-phase transformer, and the wiring of transformer is YNd11, variable ratio 19/550 kV, rated volume $S_{\text{rated}} = 670$ MVA, short-circuit reactance $X_{\text{short-circuit}} = 13\%$; the parameters of the power source are $P_{\text{rated}} = 600$ MW, $U_{\text{rated}} = 19$ kV, $I_{\text{rated}} = 20.26$ kA; the input capacity of the system is $S_{\text{system}} = 11\,000$ MVA; the length of line is 257 km, parameter $Z_1 = 0.01808 + j0.27747\ \Omega/\text{km}$, $C_1 = 0.012917\ \mu\text{F/km}$, $Z_0 = 0.23084 + j0.9728\ \Omega/\text{km}$, $C_0 = 0.0081161\ \mu\text{F/km}$.

5.6.4.2 Analysis of External Fault and CT Saturation

The waveform of the differential current in the case of an external fault and CT saturation is shown in Figure 5.109a. Compared with the grille variation curve, it is shown that the fluctuation of the differential

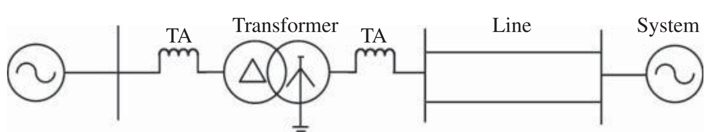

Figure 5.108 Electrical Power Dynamic Laboratory test model and parameters

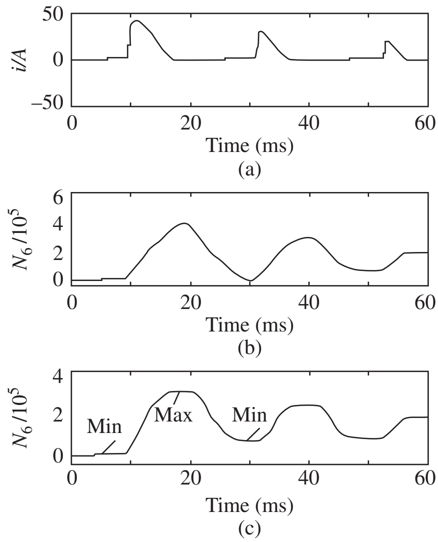

Figure 5.109 The differential current waveform and its results under CT saturation at out-zone fault: (a) differential current; (b) grille variation curve; (c) processed grille variation curve

current is small and N_δ remains at a low level before the fault. After the fault, N_δ varies with the increase and decrease of the degree of distortion of the current waveform, and the singular points of the waveform corresponding to maximal value or minimal value of N_δ. It is clear that the grille curve retains bumps or pits formed by disturbance or noise signal; these are easily confused with the extreme points, which singular points correspond to. Because flat structure elements are applied in morphological filters, bumps and pits are smoothed and small pieces of smooth region near extreme points can be caught, as shown in Figure 5.109c. Even though the noise or interference signal is not completely covered, transformer protection can be blocked, by the waveform characteristics of the minimal value smoothing domain–maximal value the smooth domain–minimal value of smoothing domain.

5.6.4.3 Analysis on Inrush Current

The symmetry inrush current in the case of a no-load transformer closing is shown in Figure 5.110a. As the waveform is no longer biased to the timeline side, the differential relay of pattern BCH-1 blocked by DC current components will mal-operate. From the grille variation curve shown in Figure 5.110b, it can be seen that the singular points formed by the transformer iron core enter and exit saturation correspond to the extreme points of N_δ. Smoothed by a filter, the waveform shown in Figure 5.110c also shows the characteristic of the minimal value smoothing domain – maximal value the smooth domain – minimal value of smoothing domain. The differential protection restraint can be achieved by this characteristic.

5.6.4.4 Analysis of Internal Fault and CT Saturation

The waveform in the case of an internal fault and CT saturation is shown in Figure 5.111a. From Figure 5.111b, it can be seen that N_δ varies exclusively with the distortion of differential current and the grille curve flattens with the reduced degree of waveform distortion. There are still small fluctuations

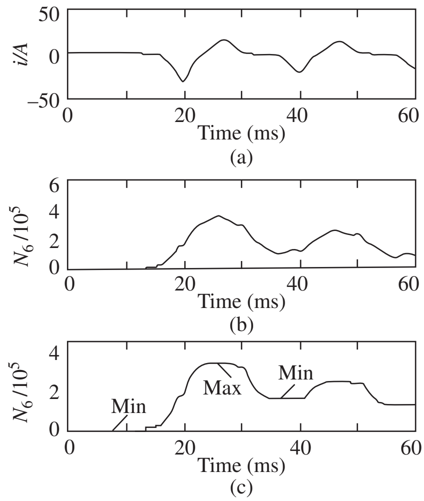

Figure 5.110 The symmetrical inrush current and its results: (a) inrush current; (b) grille variation curve; (c) processed grille variation curve

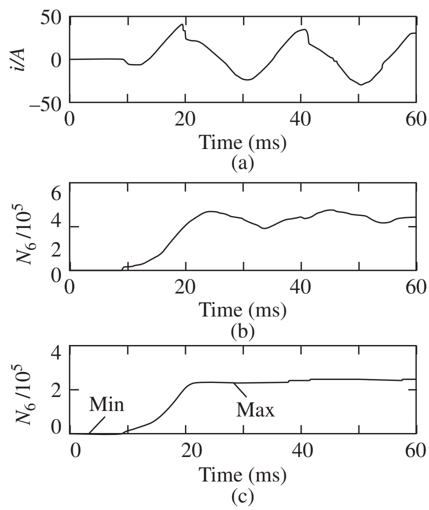

Figure 5.111 The differential current waveform and its results under CT saturation in the case of an internal fault: (a) differential current; (b) grille variation curve; (c) processed grille variation curve

on the curve due to CT saturation and the influences of interference. The variation trend of rising before becoming steady is not clear. The noise and disturbance signals are effectively restrained by generalized self-adaptive filters, and the singular characteristics near fault points will not be fuzzy. Shown in Figure 5.111c, only the waveform characteristic of minimal value smoothing domain – maximal value the smooth domain is retained after processing. Compared with Figures 5.109c and 5.110c, the waveform in Figure 5.111c has lack of variation trend from minimal value domain to maximal value domain. So it is important to recognize the maximal value domain for the reliable action of the protection. After the transformer differential protection starts, the N_δ of the differential current at time t_k and N_δ at time 1 ms before t_k should be measured in real time. If they are equal and five points taken sequentially are also equal, it is determined that the points after the time of $(t_k - 1)$ ms fall in the maximal smooth domain.

After the maximal value smooth domain is determined, the average of grille variation can be calculated using Equation (5.49) from $(t_k - 1)$ms, M = 10 points.

$$B_e = \left| \frac{1}{M} \sum_{i=0}^{M-1} \frac{N_\delta^2(i)}{N_\delta^2(i+S)} - 1 \right| \tag{5.49}$$

where $N_\delta(0)$ is the number of grille at the time of $(t_k - 1)$ms and S is the number of sampling points during one half cycle.

The results of three kinds of case, measured after 15 dynamic simulation tests, are listed in Table 5.5. The transformer internal short-circuit faults can be recognized by setting the threshold value at 0.5.

5.6.4.5 Analysis of Special Situation

Considering an external fault when the CT does not immediately saturate, it should be distinguished with the conversion of the fault zone. Protection is blocked by the ratio restraint characteristic when an external fault occurs and the CT is not saturated. When the CT is saturated after several cycles, protection is blocked by the above methods. Then, after several cycles, a developing fault may occur, which belongs to a complex fault. The external fault current, superimposed with the internal fault current waveform, attenuating after several cycles, shows the characteristics of the internal faults. Namely there will not be an obvious singular signal near differential current zero-crossing point, so the protection can reliably act.

In summary, the use of grid fractal theory and adaptive generalized morphological filtering technology to identify CT saturation method has the following characteristics:

(a) Signal singular feature does not become fuzzy by adaptive generalized morphological filtering technology; the noise and interference signals can be effectively filtered; DC component is restrained very well.
(b) Using the relative size of grille curve maximal value and minimal value smoothing domain, transformer faults and CT saturation can be correctly recognized by setting a reasonable threshold.

Table 5.5 Calculation results of B_e in various kinds of states

	CT saturation		Symmetry inrush current
	Internal fault	External fault	
Half cycle before $N_\delta/10^5$	5.7997–6.6973	2.7816–3.4374	2.7655–3.2906
Half cycle after $N_\delta/10^5$	5.7369–6.6492	0.7988–1.2859	1.1852–1.6547
$B_e/10^5$	0.019–0.034	4.5936–12.1857	2.7481–5.3794

(c) The disadvantages of DC speed saturation relay are overcome, not affected by inrush current. The characteristics are obvious and it is easy to achieve. The effectiveness and feasibility of this algorithm are verified by dynamic simulation data.

5.7 Summary

The differential relay may possibly mal-operate during occurrences of magnetizing inrush and CT saturation. With regard to the inrush restraint, a method to eliminate the magnetizing inrush current is proposed; it can ensure the voltages on both sides have the same phase but different magnitudes. The simulation results show the correctness and effectiveness of the proposed method. As for the CT saturation, new methods for identifying the phenomenon are put forward, with which the ability of the differential protection immune to cross-country faults can be improved further. The effectiveness of the proposed methods has been verified with the simulation tests.

References

[1] Liu, J., Yang, Q., Ren, B. *et al.* (1998) Analysis and discussion on several issues for application of digital transformer protective relays. *Power Systems Technology*, **22**, 18–21.
[2] Zhou, Y. and Cao, L. (2001) Inspection and analysis of a maloperation of transformer differential protection and its preventive measures. *Power Systems Technology*, **25** (12), 71–74.
[3] Jiao, S.H. and Liu, W.S. (1999) A novel scheme to discriminate inrush current and fault current based on integrating the waveform. *Proceedings of the CSEE*, **8**, 007.
[4] He, B.T., Zhang, X.S. and Bo, Z.Q. (2006) A new method to identify inrush current based on error estimation. *IEEE Transactions on Power Delivery*, **21** (3), 1163–1168.
[5] Faiz, J. and Lotfi-Fard, S. (2006) A novel wavelet-based algorithm for discrimination of internal faults from magnetizing inrush currents in power transformers. *IEEE Transactions on Power Delivery*, **21** (4), 1989–1996.
[6] Ge, B.M., de Almeida, A.T., Zheng, Q.L. *et al.* (2005) An equivalent instantaneous inductance-based technique for discrimination between inrush current and internal faults in power transformers. *IEEE Transactions on Power Delivery*, **20** (4), 2473–2482.
[7] Lin, X.N., Zou, L., Tian, Q. *et al.* (2006) A series multiresolution morphological gradient-based criterion to identify CT saturation. *IEEE Transactions on Power Delivery*, **21** (3), 1169–1175.
[8] Phadke, A.G. and Thorp, J.S. (2009) *Computer Relaying for Power Systems*, John Wiley & Sons, Inc., Hoboken.
[9] Lucas, J.R., McLaren, P.G., Keerthipala, W.W.L. *et al.* (1992) Improved simulation models for current and voltage transformers in relay studies. *IEEE Transactions on Power Delivery*, **7** (1), 152–159.
[10] Annakkage, U.D., McLaren, P.G., Dirks, E. *et al.* (2000) A current transformer model based on the Jiles–Atherton theory of ferromagnetic hysteresis. *IEEE Transactions on Power Delivery*, **15** (1), 57–61.

Index

Electromagnetic Transient Analysis and Novel Protective Relaying Techniques for Power Transformer,
First Edition. Xiangning Lin, Jing Ma, Qing Tian and Hanli Weng.